An Investigation of the Corrosion Behaviour of a Range of Engineering Materials in Marine Environments

Vol. II

A Thesis

Submitted in Fulfilment of the Requirements for the Degree of Doctor of Philosophy (Ph.D.)

by Anne Neville

Department of Mechanical Engineering,
University of Glasgow,
September 1995

Chapter 6

An Investigation of the Effect of Laser Treatment and Shot-Peening on Duplex and Austenitic Stainless Steels and the Co-base Stellite 6

Introduction

This chapter addresses an area of increasing importance : surface treatment. As a means of improving the mechanical properties of a material to resist wear by abrasion, erosion or other mechanisms, a number of processes are available.

Two processes are under investigation in this study, namely laser surface treatment and shot-peening. The objective of the study is to investigate the effect of laser treatment parameters on the mechanical and metallurgical properties of the material and ultimately on it's seawater corrosion resistance. Three shot-peening processes were investigated. Surface analysis was performed using microhardness techniques and microscopy. The corrosion resistance of each treated surface in elevated static and high velocity seawater was monitored using electrochemical techniques.

Literature Review

The demands made on engineering components today are often so exacting that it is not possible to meet them with conventional alloys. Materials' development has progressed significantly in recent years in the direction of surface engineering which describes a wide field of material processing, aimed solely at enhancing the properties (physical, mechanical or metallurgical) of a surface to closer meet with design requirements.

Surface engineering was borne out of a need to address the severe limitations of traditional materials with respect to wear resistance, corrosion, fatigue strength and fretting resistance. The use of the more exotic state-of-the-art materials such as ceramics or metal matrix composites is often unsuitable due to economic constraints or the inability to mechanically form the material. Surface engineering processes have the potential advantage of cost reduction by limiting the treatment to only the most susceptible areas. Also in some applications, the performance of less expensive substrate materials can be enhanced to give performance comparable with higher grade materials.

Laser Surface Modification

Since it's development in the 1960s, the Laser has found application in a range of materials processing environments. Significant developments have been made in the laser cutting of components, to obtain a near-cut area, free from heat affected zone effects [1,2]. Laser techniques are currently being developed to cut ceramic materials without detrimental brittle damage in the cut region. Laser welding has been extensively used in replacement of traditional techniques [3] in a number of industrial sectors [4] for example in the car industry because if it's suitability for automation and the potential to increase production output.

In the field of surface engineering, there is much activity in industry and academia focusing on techniques such as laser cladding, surface melting surface alloying, transformation hardening and coating consolidation [5,6].

Laser cladding involves supplying sufficient heat input to a powder which then forms a metallurgical bond between the solidified material and the base metal surface [4,7]. Laser cladding is often used to apply hard facing to a material surface to resist wear degradation [8,9]. Traditionally cobalt-based alloys have been applied as a hard facing in the form of wire, using manual tungsten inert gas techniques (TIG). Laser application uses a multi-pass technique to apply the material in powder form. This has

reduced the major problem which was often associated with the TIG process : dilution from the substrate [10]. Application of cobalt based layers can now be successfully achieved on nickel based superalloys for aero-engine applications without significant nickel dilution [11]. Layers of Ni-Cr and Ni-Cr-W have been applied by a laser on low alloy steel substrates and successfully improve the wear resistance [12].

Application of surface coatings consisting of a ceramic-metal matrix or pure ceramic, often results in gross porosity and a lack of adherence at the coating/substrate interface. Techniques under the description of laser consolidation have been attempted [13,14] to reduce detrimental porosity without causing a HAZ effect in the substrate. The porosity of Cr_2O_3 plasma sprayed coating could be reduced significantly reduced by laser post treatment [13].

Laser surface melting has mainly been performed with the intention of increasing the surface hardness of the material. Under an inert shrouding gas, several studies have reported an enhanced hardness on cast iron [15] and on Al-Si alloys [16]. Laser surface melting, when conducted in a gaseous atmosphere can also be termed laser surface alloying if the gas can diffuse sufficiently into the substrate. Laser surface alloying of titanium has successfully been achieved in a nitrogen atmosphere to produce a hard, wear resistant layer of TiN [17]. Further applications for the laser carbo-nitriding of titanium are being investigated.

Laser surface irradiation of Fe-based alloys, including stainless steels, involves local heating of the surface into the austenitic temperature region. The resulting cooling leads to an austenite-martensite transformation which is the cause of the increased hardness. The rate of cooling determines the microstructural changes during the transformation (i.e. the formation of precipitates etc).

The beneficial effects of nitrogen as an alloying element in stainless steels have been recognised by several authors. Nitrogen has been reported to increase the resistance of stainless steels to stress corrosion cracking (SSC) [18], to decrease the risk of intermetallic phase formation in duplex stainless steels [19] and to increase the pitting potential of austenitic stainless steels [18]. There have been several methods attempted to increase the nitrogen content of the surface of a material, the most common of these being plasma nitriding and ion nitriding [20]. However the use of laser surface melting in a nitrogen atmosphere on stainless steels represents a logical method of increasing locally the level of nitrogen and hence the mechanical and corrosion properties.

Shot-peening process and applications

Shot-peening as a surface treatment is reported to increase the materials' resistance to fatigue, stress corrosion cracking [21], fretting, galling and erosion. The cold working process involves repeated bombardment with small spherical media called shot. Each piece of shot hitting the surface acts like a tiny peening hammer, imparting to the surface a small indentation or dimple. In order for a dimple to be created, the surface fibres of the material must be yielded in tension. Below the surface the fibres try to revert the surface to it's original shape, thereby producing below the dimple, a hemispherical region of cold worked material in residual compressive stress.

Unlike shot-blasting which is mainly used as a surface texturing or cleaning treatment, controlled shot-peening can impose a given residual compressive stress at a certain depth depending on the process parameters : shot size, type and intensity of impingement. Shot peening residual stress is proportional to it's life cycle under fatigue loading [22].

The attributes of the process are manifested in the fact that cracks will not propagate unless there is a tensile force ahead of the crack tip. Therefore the resistance to mechanical fatigue is increased. However, there is only limited reported data on the corrosion behaviour of shot-peened surfaces in the absence of a mechanical effect. Controlled shot peening is claimed to prevent the incidence of corrosion fatigue by negating the cyclic applied loading [22,23]. Of all the engineering components to which shot-peening has been utilised, the most common are those most susceptible to stress corrosion cracking (SCC). Incidences of SCC have been reported in almost every industry, ranging from petrochemical to brewing and electronics [24]. In the chemical industry, SCC has been reported in austenitic 304, 316 and 321 stainless steel process and storage vessels [24]. In the nuclear industry, there have been incidences of SCC in sensitised type 304 stainless steel piping in boiler water reactors.

Experimental Methods

Laser treatment

Surface irradiation was carried out using a CO_2 laser with nitrogen as the shrouding gas. The gas pressure was kept constant at 5 bar. Figure 6.1 is a schematic representation of the laser treatment equipment. From previous work, it had been established that defocussing the laser beam gave a better penetration of the surface and so in all tests, the workpiece was positioned 0.3mm above the focal point as shown.

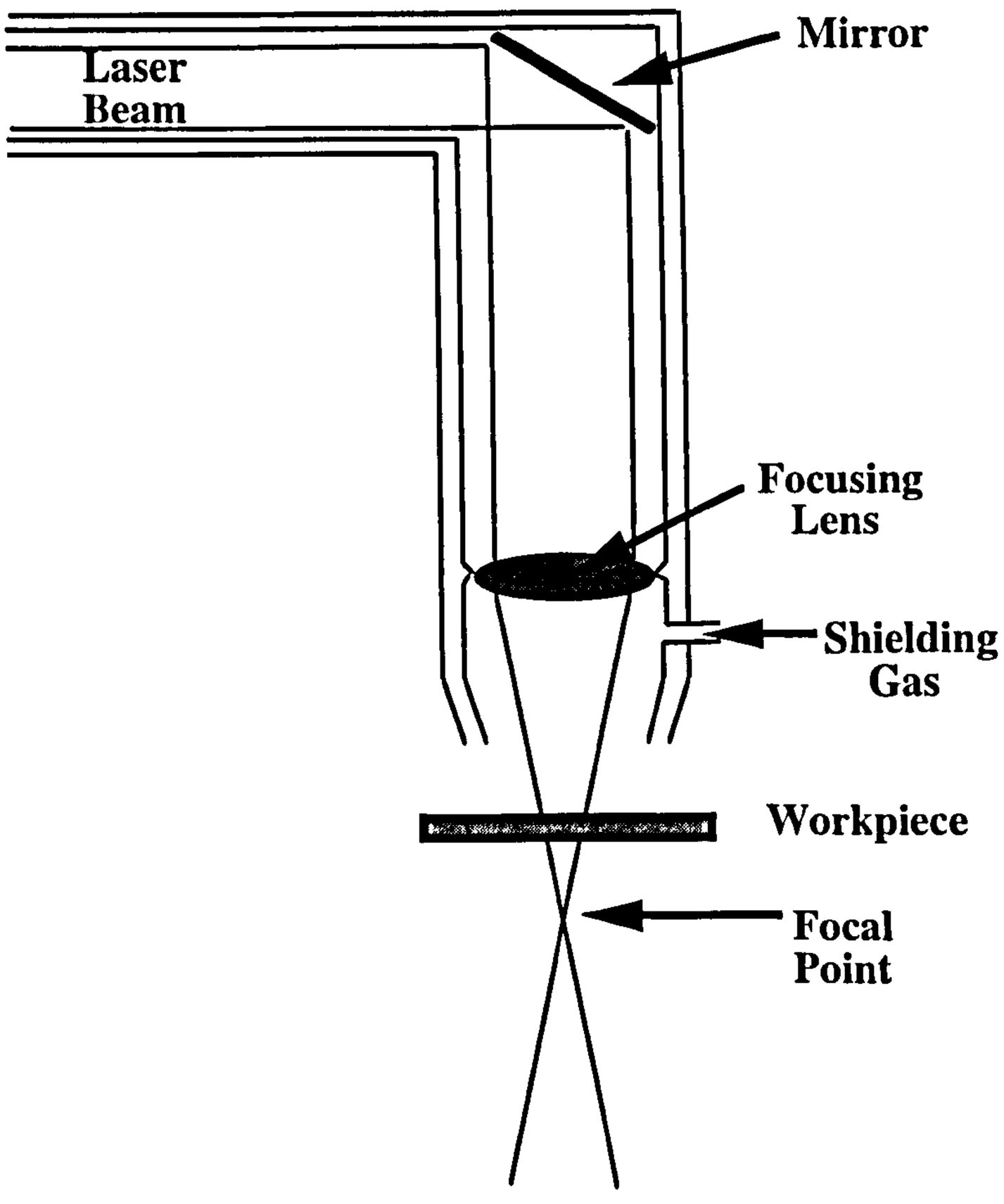

Fig. 6.1. CO_2 laser configuration for surface treatment of stainless steels

A constant sample feed rate of 1000mm/min was used for al the surface treatment, again determined from a series of tests done prior to this work. Preliminary tests were performed using continuous power (CW) but the bulk of the work was done on a pulsed power cycle of 200×10^{-5} seconds on and 100×10^{-5} seconds off. The power of the laser was 1kW. The degree of transverse overlap was varied according to the results of microscopical examination and corrosion tests. Primarily laser treatment was concentrated on duplex stainless steels (UNS S32760 and SAF 2205) but to conclude the study, two austenitic stainless steels (UNS 31603 and UNS S31254) were treated.

After laser treatment the specimens were cut in cross section in a line parallel to the run direction and transverse to it. In cross section, a microhardness profile was built up, the results quoted in Vickers hardness. Specimens were etched in a solution of chromic and oxalic acid and also in 40% potassium hydroxide depending on the metallurgical features of interest. This was done electrolytically at approximately 2V for 15-20s. In 40% KOH, the ferrite phase is darkened and precipitated phases of nitrides glow under dark field illumination [25]. The cross section was subsequently examined to determine the thickness of the laser layer, the uniformity of the layer and the microstructure compared to the substrate material.

Each laser treated material was tested in seawater using anodic polarisation techniques at ambient temperature (18°C) and at 50°C. Comparisons were made between the performance of the laser treated layer and the substrate based on electrochemical behaviour and on the corrosion characteristics. Each polarisation test was repeated three times on each material.

In the analysis of the compositional changes occurring during laser irradiation, EPMA techniques were utilised to try to detect nitrogen in the laser layer. In addition, X-ray diffraction was used in an attempt to identify the components of the metallurgically altered layer.

Shot-peening

The shot peening process was carried out by the Metal Improvement Company, Inc.. Three materials were treated : UNS S31603, UNS S32760 and Stellite 6. Samples of Stellite 6 were shot-peened using steel shot only. The stainless steels were treated by three different methods :

- using steel shot only

- using glass beads only

- using steel shot followed by glass beads.

The intention of using glass beads is that it eliminates any potential problems due to iron contamination when embedded shot corrodes on the surface. Before corrosion tests were performed, a test to detect 'free iron' (i.e. embedded shot) was conducted on all the samples. This involved using a solution as follows:

1000ml of distilled water
30g of Potassium Ferricyanide
20ml of Nitric Acid (60-67%).

The solution was used to saturate filter paper and than pressed on a degreased surface of the shot-peened material. The appearance of a blue stain occurs after 15 seconds and indicates the presence of free iron.

As with laser treated surfaces, the shot-peened surfaces were examined prior to testing to determine the hardness profile and the morphology of the as-treated surface. Electrochemical corrosion tests in static and high velocity impinging flow were conducted.

Results - Shot-Peened Specimens

Microhardness and Pre-test examination

On both stainless steels, a significant increase in hardness was detected in a layer of approximately 50-150μm thickness. On both stainless steels, the increase was greater when treated by steel shot compared to glass and steel then glass, but the margin was small. On Stellite 6, a significantly smaller increase in hardness was measured, only in the outer 50μm layer. Figure 6.2 shows the microhardness versus depth plots for the three materials, the stainless steels having been treated by three different peening media. Figure 6.3a and b shows the microhardness indentations on UNS S31603 and UNS S32760 across the profile. On UNS S31603, the microstructure seemed to have changed at the outer layer to clearly indicate the presence of Luders' bands, characteristic of a work hardened surface.

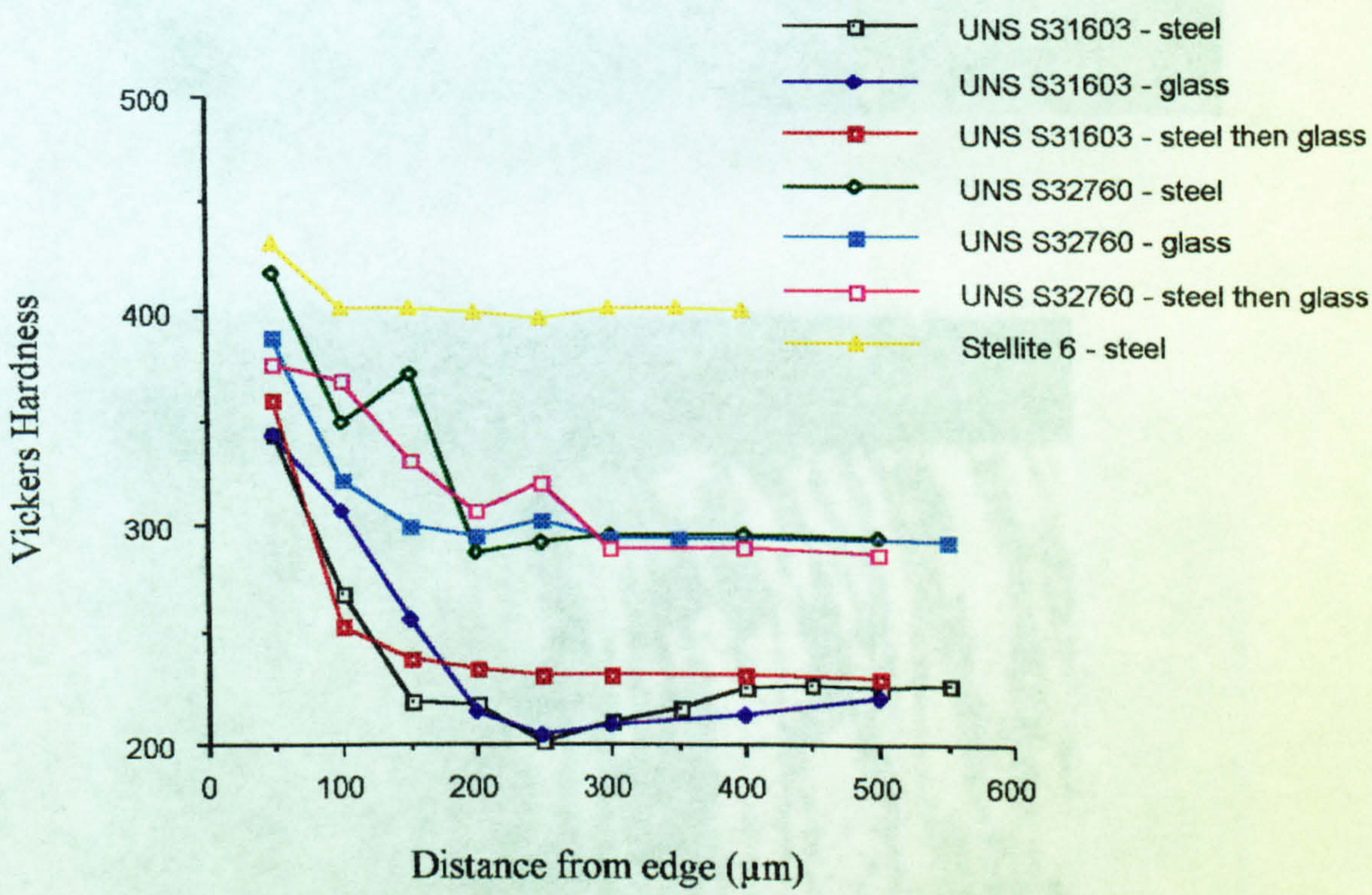

Fig. 6.2. Hardness profiles on shot-peened surface profiles

The shot peened surface using steel could clearly be seen to differ from the surfaces when glass was involved. Figure 6.4 shows a low magnification micrograph of a steel shot peened surface which has a rough but rounded surface in contrast to the glass and steel then glass surfaces (Figs. 6.5 and 6.6 respectively) which are sharper and more coarse. Much more acutely angled indentations are visible on the glass peened and steel then glass peened surfaces.

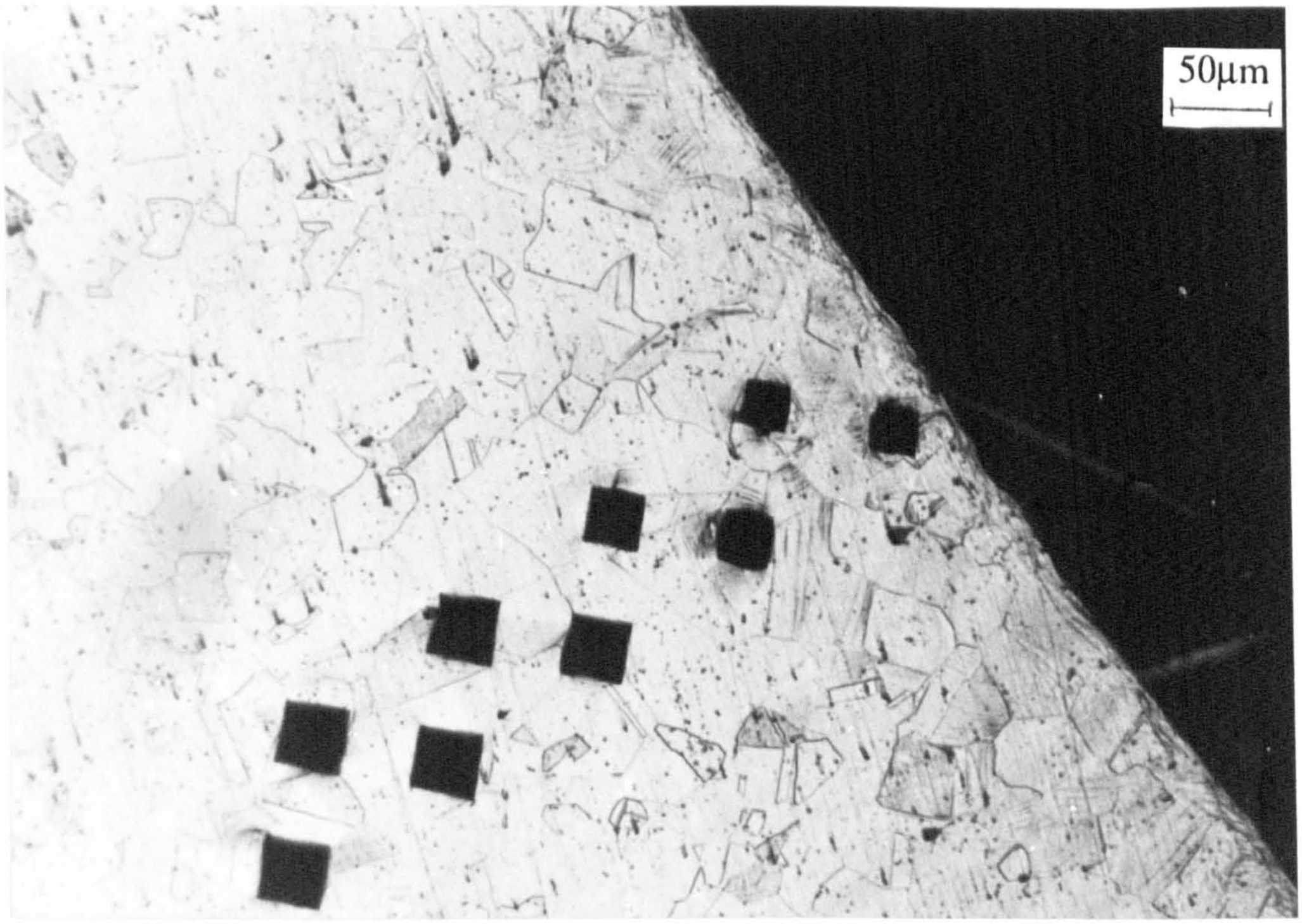

(a)

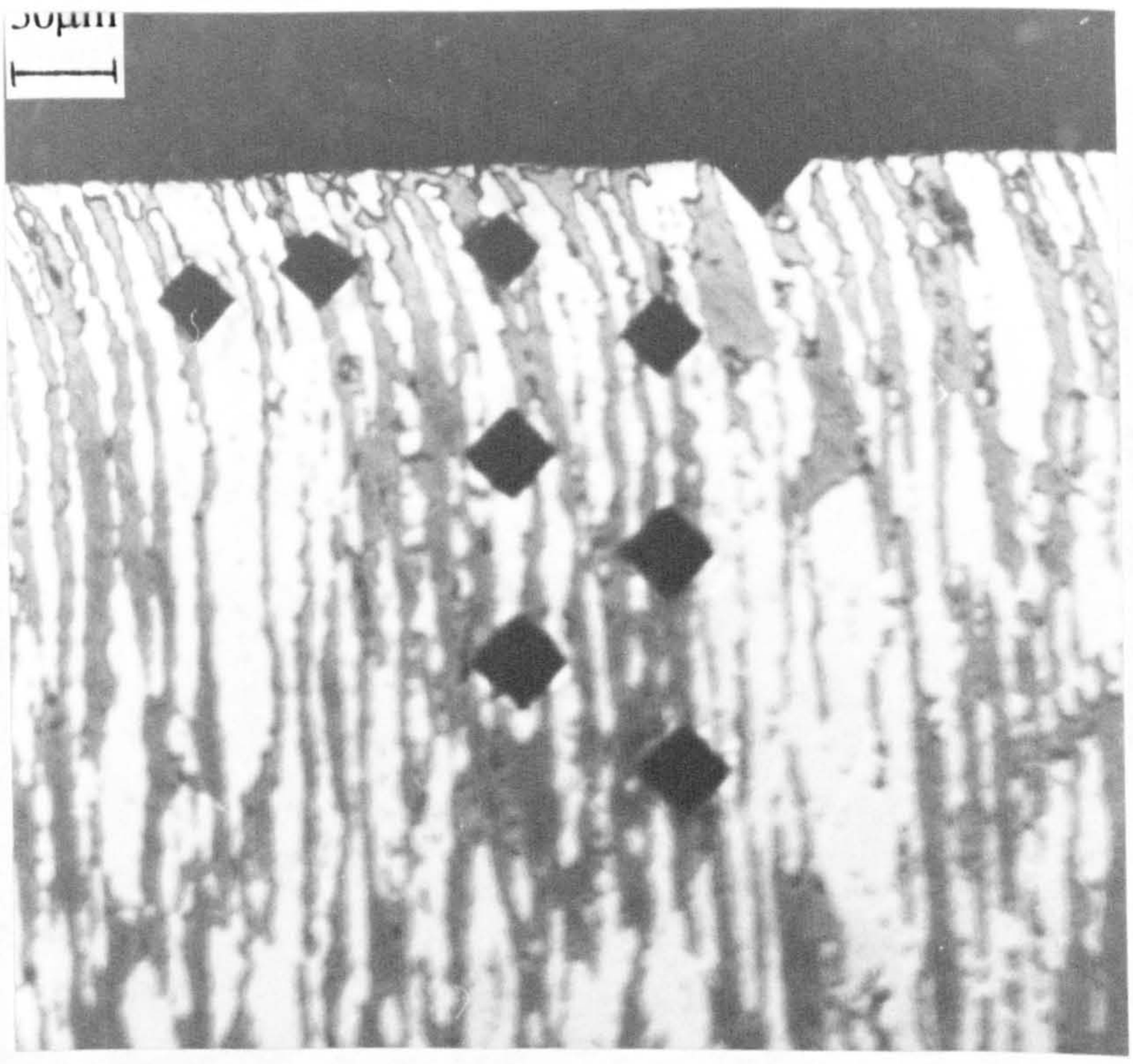

(b)

Fig. 6.3 Hardness indentation on profile of steel shot peened (a) UNS S31603 and (b) UNS S32760

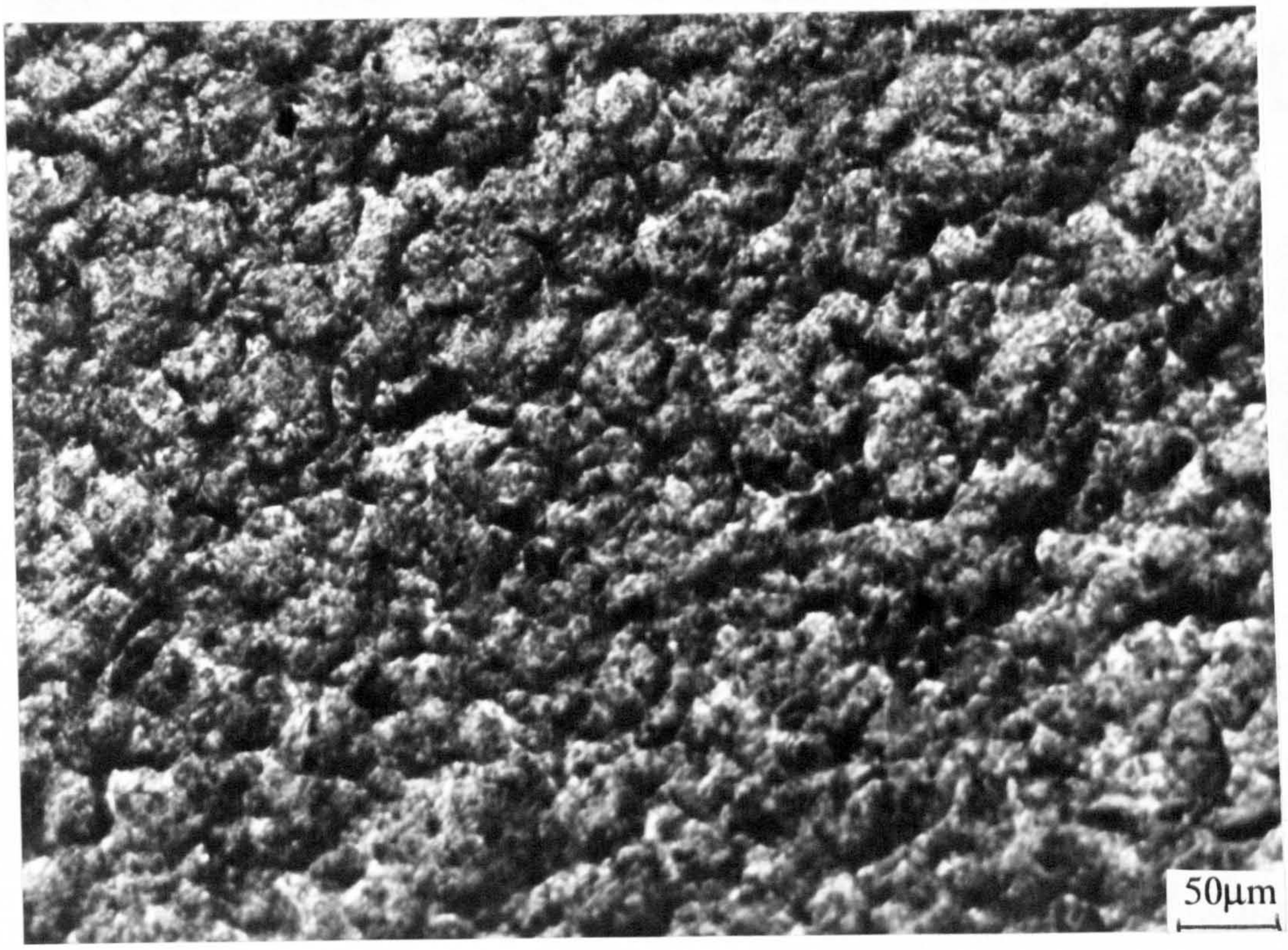

Fig. 6.4. As-produced steel shot peened surface on UNS S31603

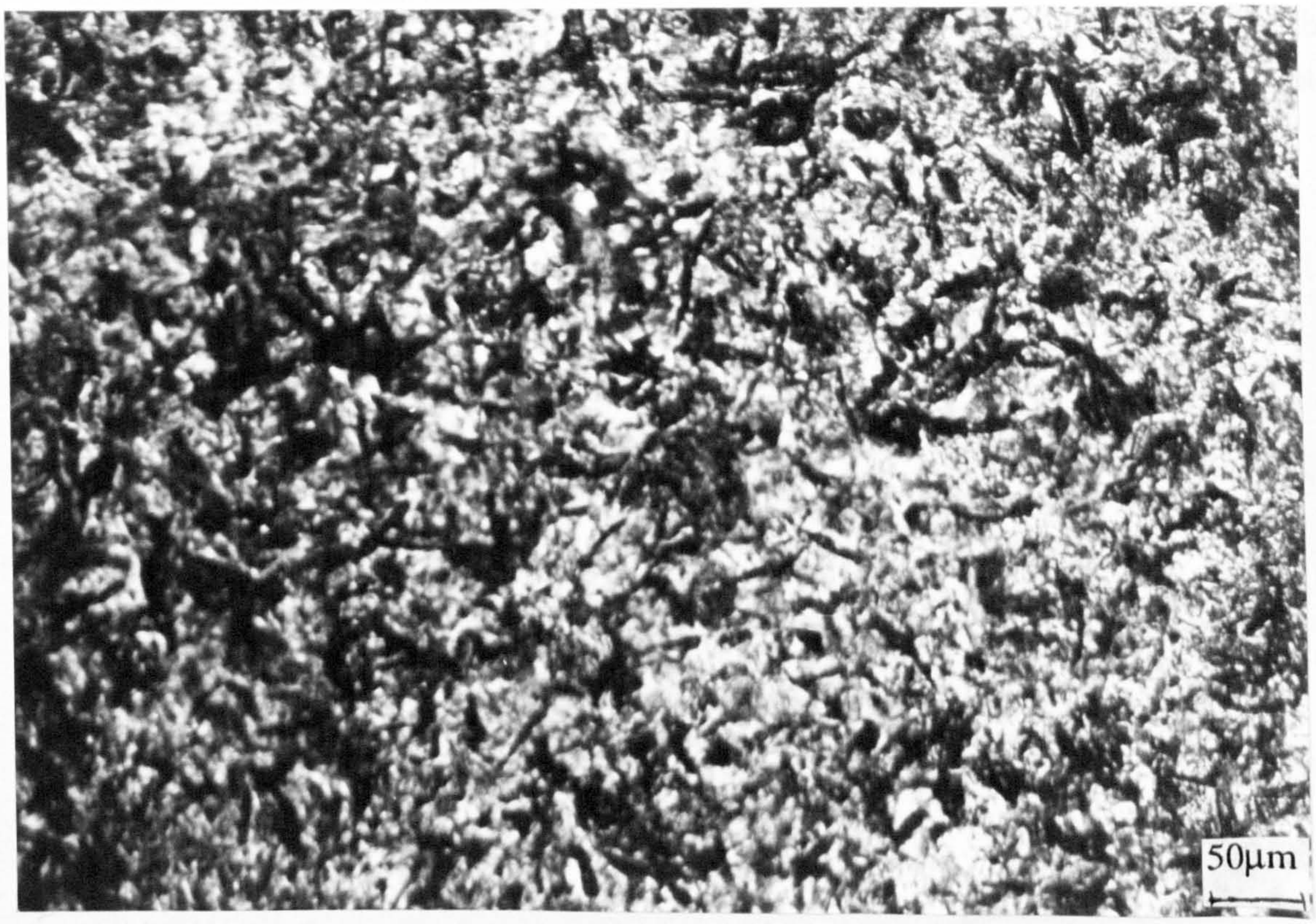

Fig. 6.5. As-produced glass shot-peened surface on UNS S31603

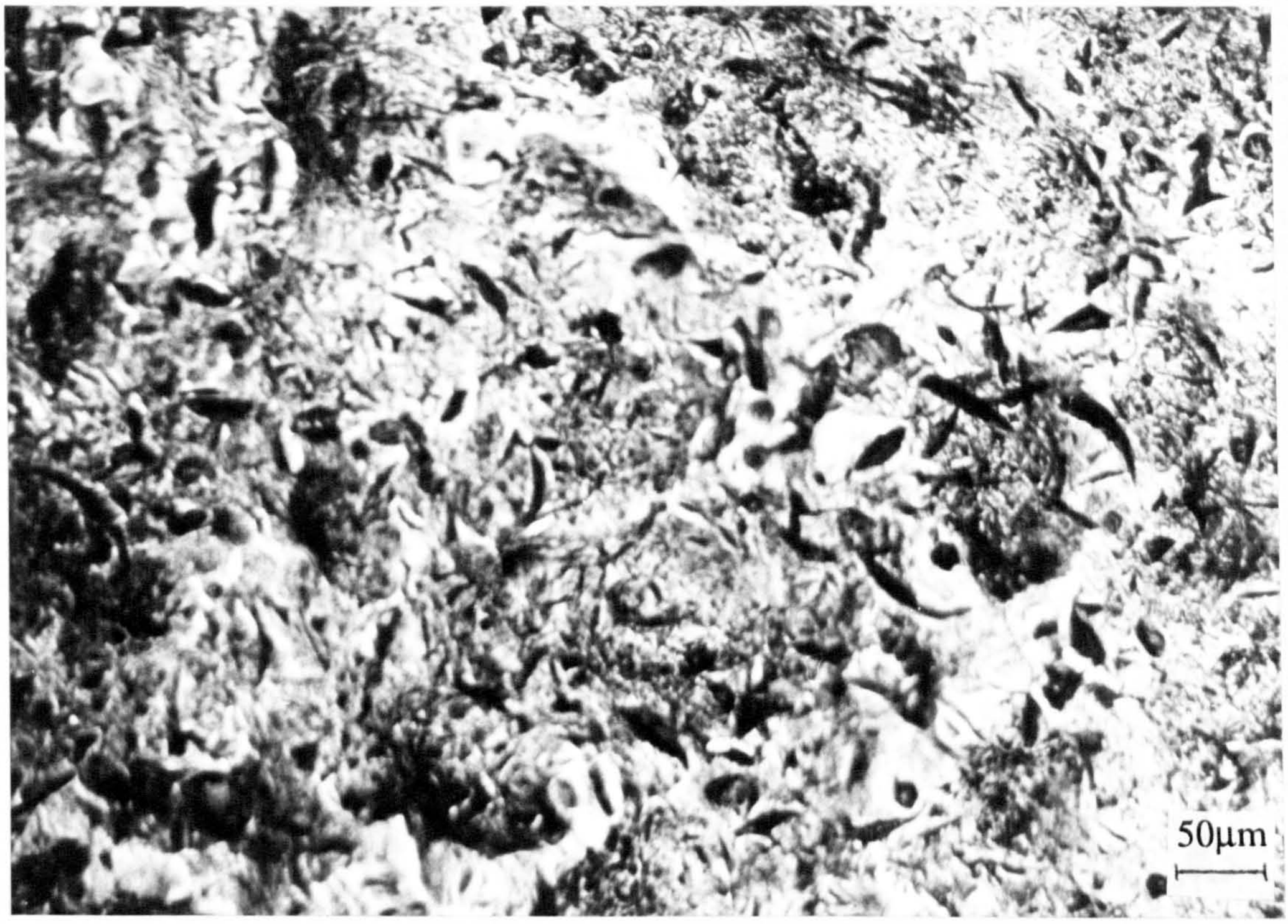

Fig. 6.6. As-produced steel then glass shot-peened surface

Closer examination of the as-produced shot-peened surfaces showed an indented, rippled surface with uniformly dispersed cracks as shown in the SEM micrograph (Fig. 6.7) for UNS S31603 after steel shot-peening. These cracks were also visible under the light microscope as shown in Fig. 6.8 on the glass shot-peened surface of UNS S32760.

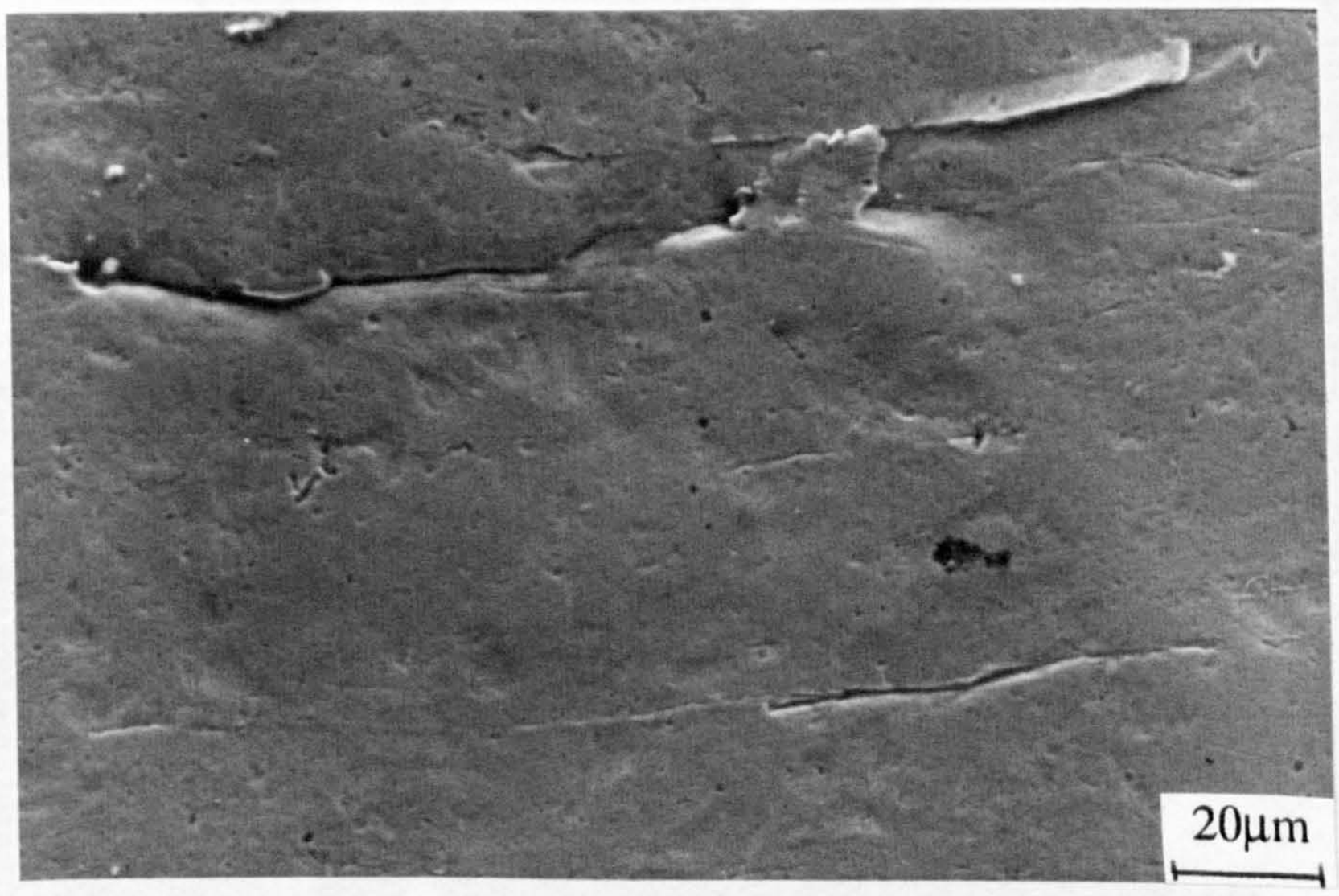

Fig. 6.7. SEM micrograph of cracks on UNS S31603 after steel shot-peening

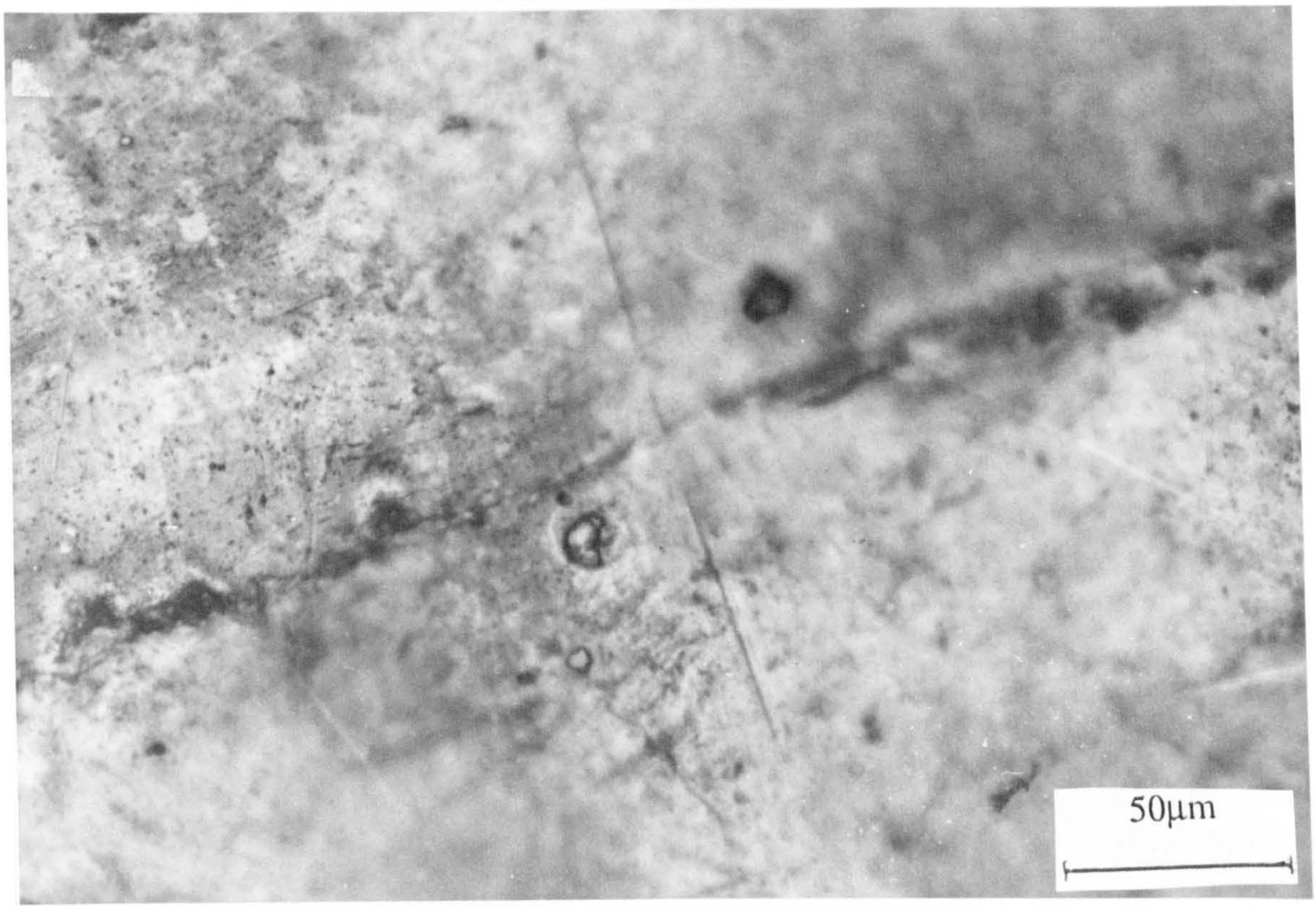

Fig. 6.8. Cracks visible on the surface of glass shot-peened UNS S32760.

The inherently harder alloy, Stellite 6 showed the same characteristics in the shot-peened surface (steel only). The indentations were rounded as on the stainless steels and cracks were clearly visible over the surface (Figs. 6.9, 6.10)

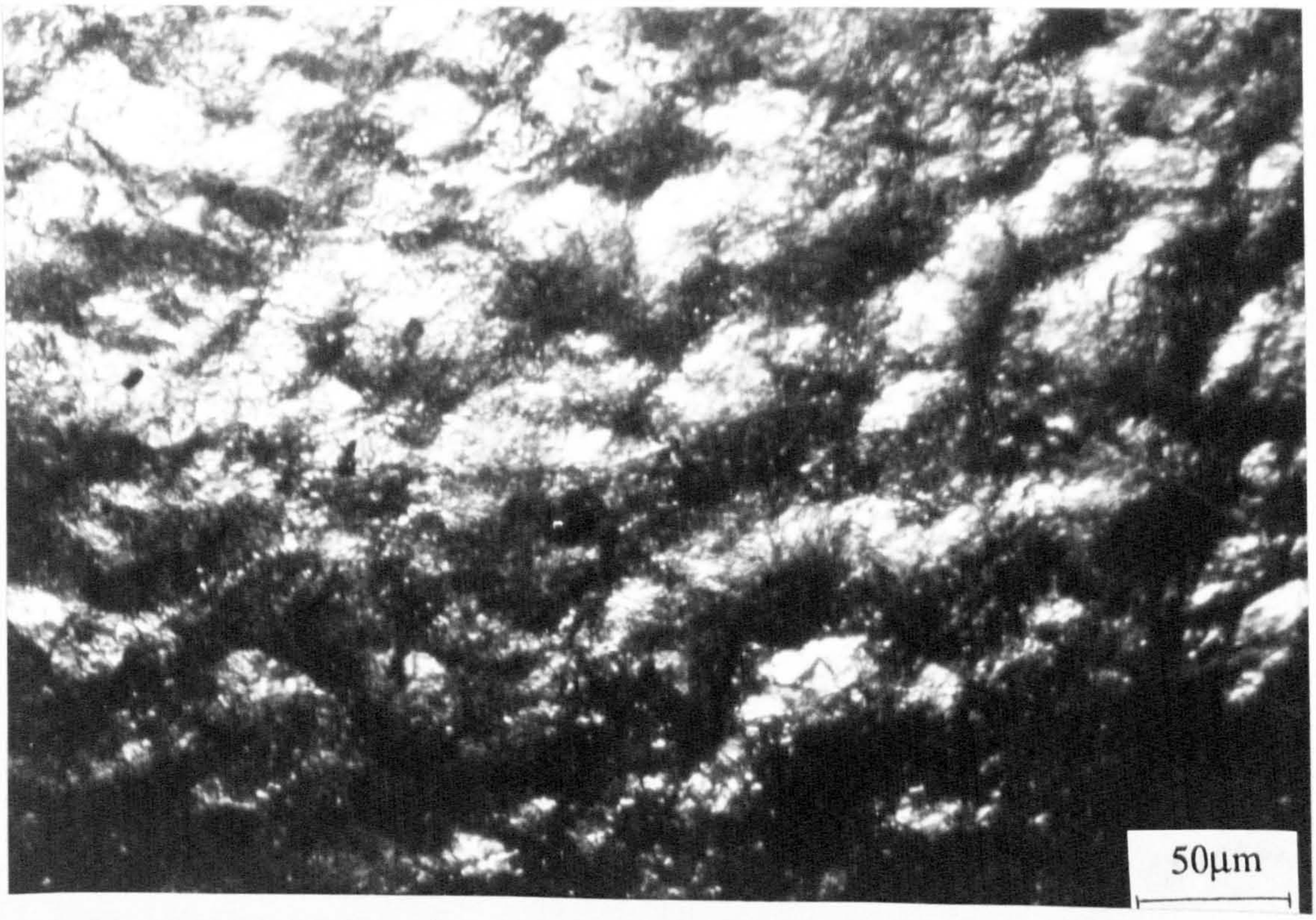

Fig. 6.9. Rounded indentations on the surface of steel shot-peened Stellite 6.

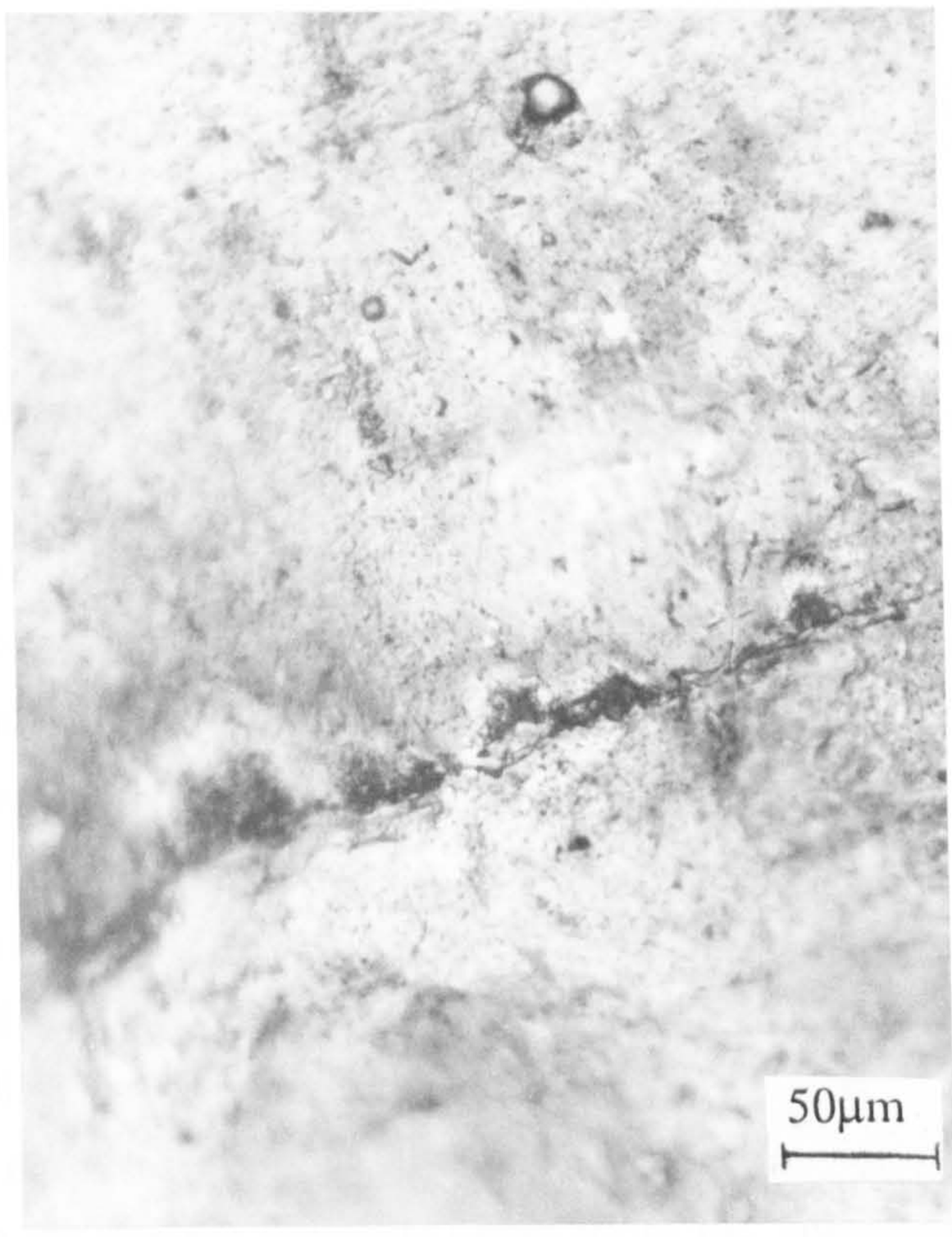

Fig. 6.10. Cracks visible on the surface of steel shot-peened Stellite 6.

As expected the result of tests using potassium ferricyanide to detect free iron (and therefore quantify the residual shot embedded in the surface) showed that on the steel shot specimens, there were significantly more traces and hence the post-treatment with glass shot appeared to be effective in removing the embedded shot on both stainless steels. As shown in Fig. 6.11 there was more free iron on UNS S31603 than on UNS S32760 and compared to the stainless steels, there was significantly less still on the Stellite 6.

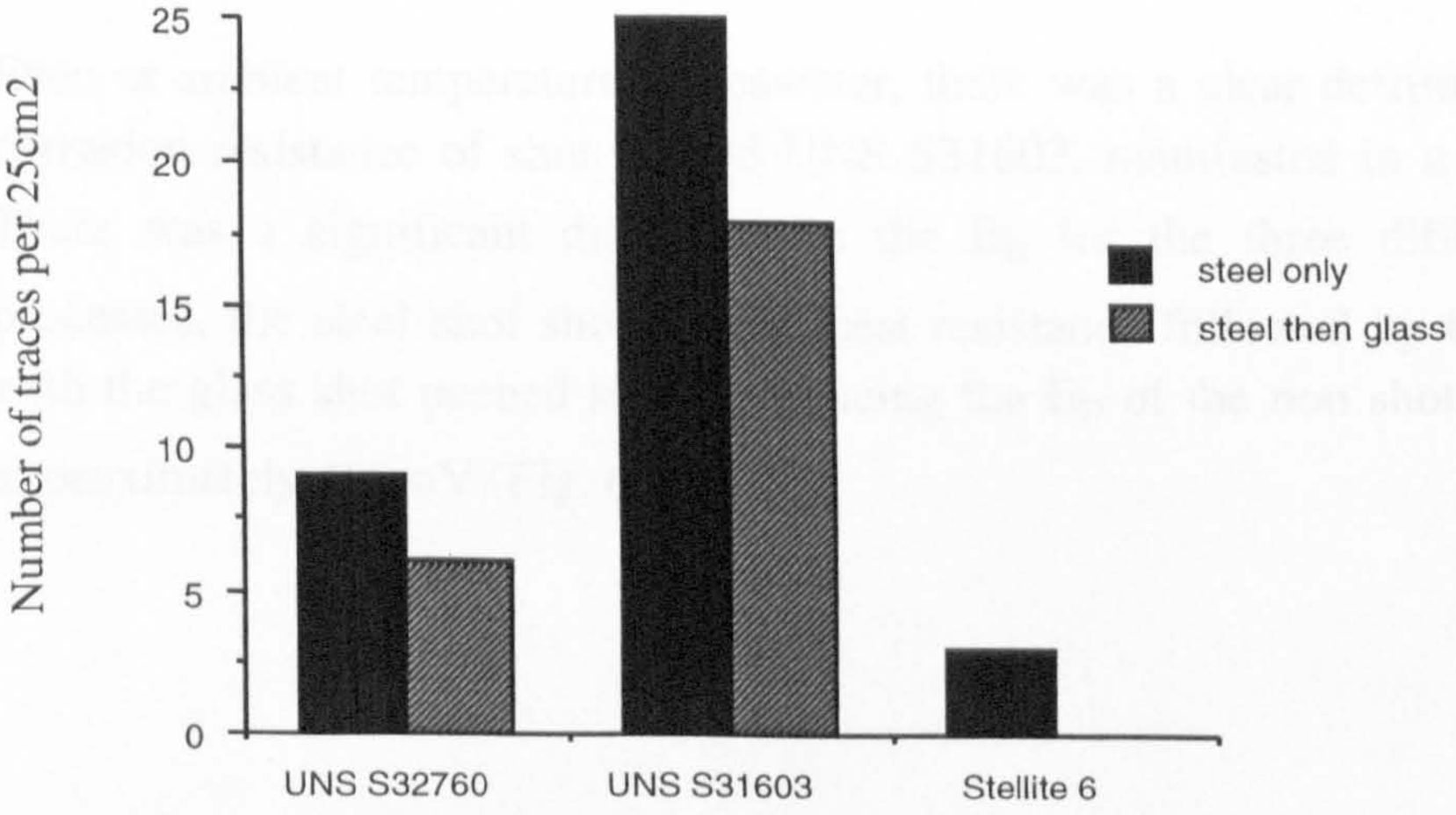

Fig 6.11. Free iron test to quantify residual embedded iron after shot peening

Corrosion Tests

Electrochemical accelerated anodic polarisation tests were carried out on the shot-peened materials and the resulting electrochemical characteristics and the extent and mechanisms of attack were compared with the non shot-peened substrate. It should be emphasised that although the beneficial characteristics of the shot-peening process are documented as being the resistance to stress corrosion cracking (SCC) and fatigue, the focus in this study is the pure corrosion resistance in a chloride containing environment on unstressed components, in static and liquid impingement conditions.

Shot-peening by either of the methods, on the superduplex stainless steel UNS S32760, did not significantly change the potential E_b at which the passivity breaks down in seawater at 18°C as shown in Fig. 6.12. However, a slight decrease in E_b was evident compared to the non shot-peened material. The shot-peened material exhibited small currents in the passive potential range up to E_b, comparable with the non shot-peened surface. The only significant difference on the steel shot-peened specimens of UNS S32760 compared to the substrate were the more noble free potentials exhibited (-20mV compared to -220mV), and therefore the actual magnitude of the potential range, over which the material was passive was reduced. Similarly on Stellite 6 and UNS S31603, more noble free corrosion potentials on the shot-peened surface were exhibited. Stellite 6 which already showed much less resistance to passivity breakdown in seawater than the superduplex stainless steel did not exhibit enhanced susceptibility to corrosion initiation after shot-peening, as is demonstrated in Fig. 6.13. There is perhaps evidence to suggest that passivity breakdown occurs at a slightly more noble potential for the shot-peened specimens.

Even at ambient temperature in seawater, there was a clear detrimental effect on the corrosion resistance of shot-peened UNS S31603, manifested in a much reduced E_b. There was a significant difference in the E_b for the three different shot-peening processes, the steel shot showing the best resistance followed by the steel then glass with the glass shot peened surface reducing the E_b of the non shot-peened surface by approximately 400mV (Fig. 6.14).

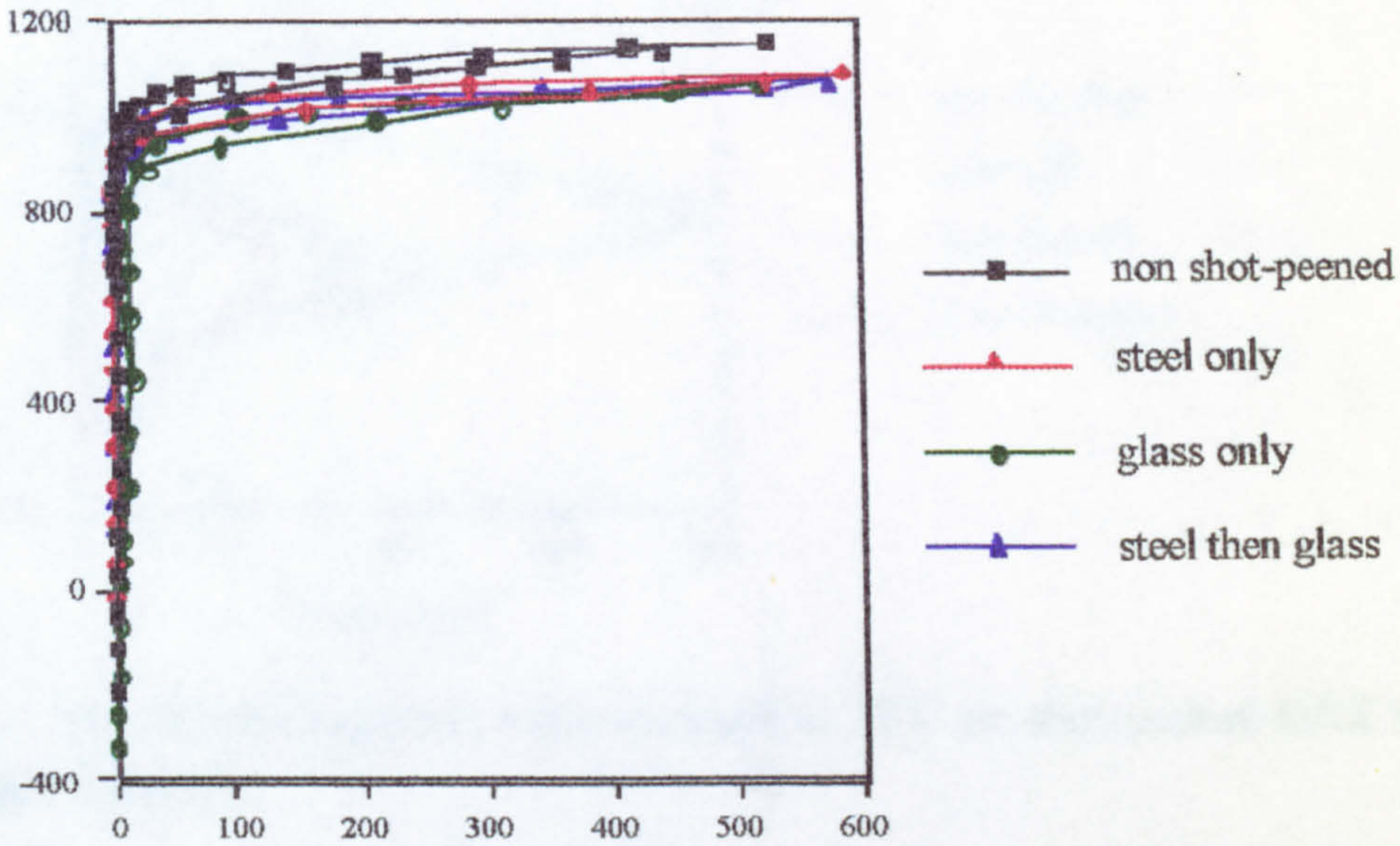

Fig. 6.12. Anodic polarisation on shot-peened and non shot-peened UNS S32760 in static seawater at 18°C

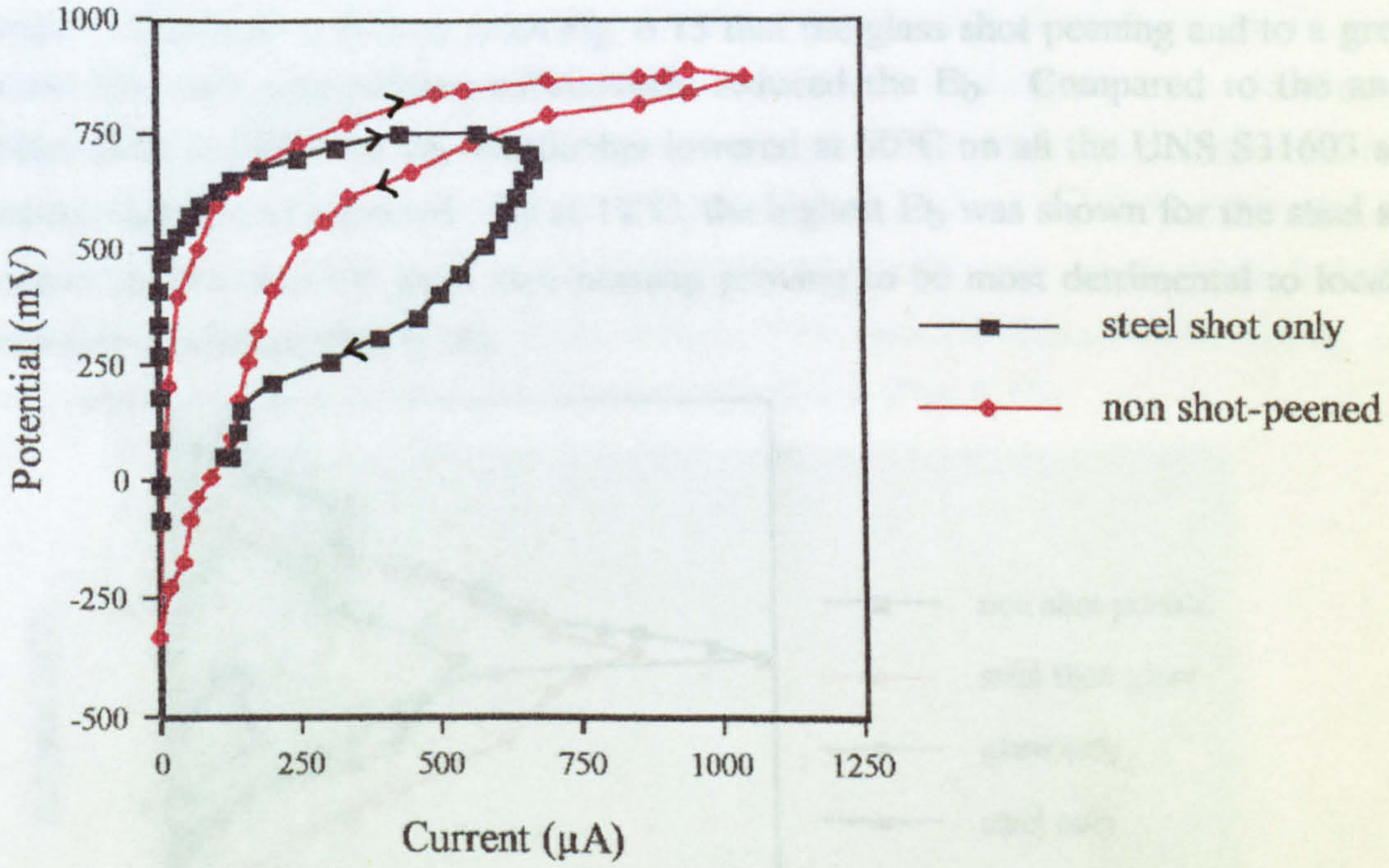

Fig. 6.13. Anodic polarisation on Stellite 6 shot-peened and non shot-peened surface at 18°C in static seawater

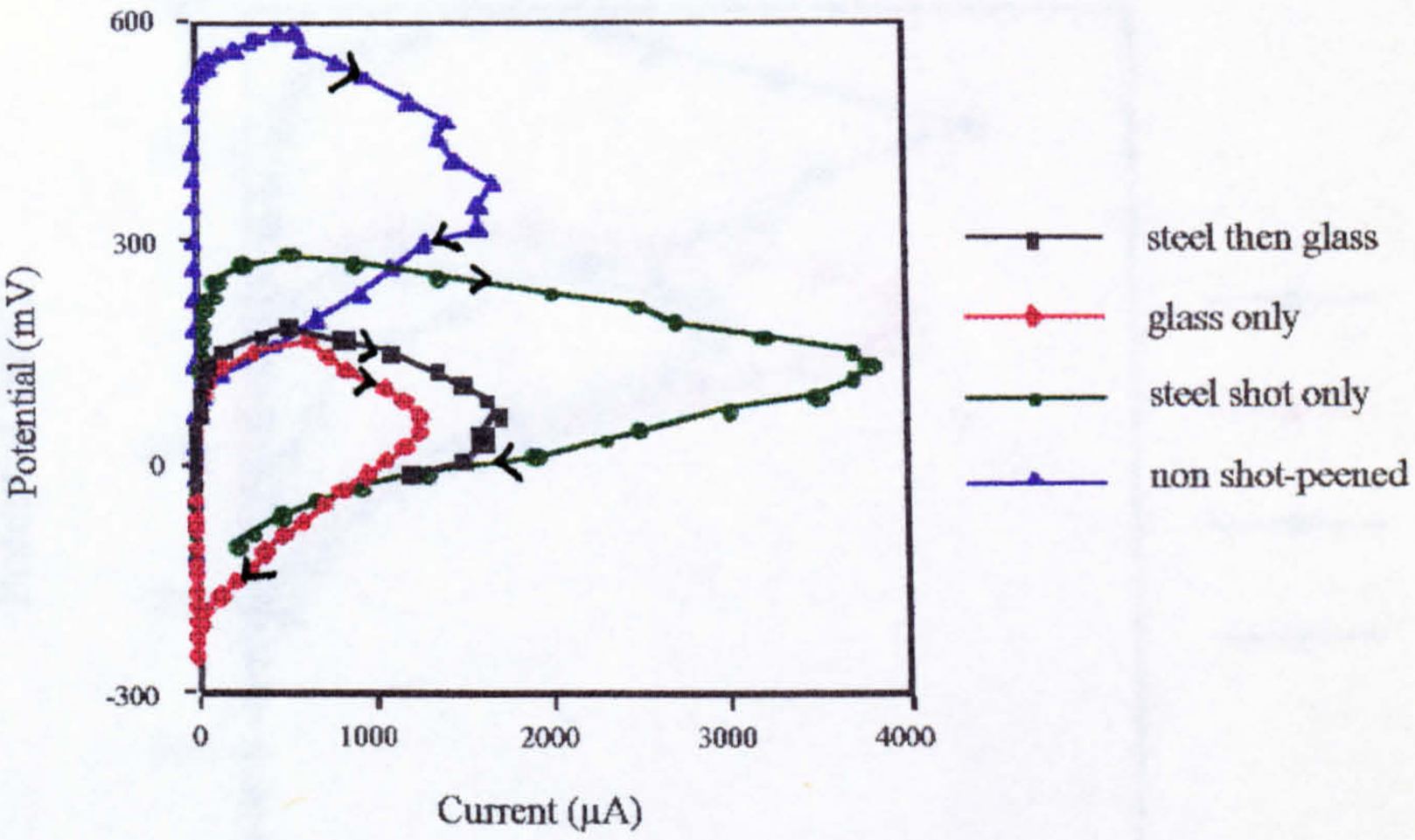

Fig. 6.14. Anodic polarisation in static seawater at 18°C on shot-peened UNS S31603 surface and substrate

The effect of increasing the temperature of the seawater to 50°C was to reveal the lower resistance to passivity loss on shot-peened UNS S32760. Of the three treatments, the steel then glass shot peening retained its resistance to localised corrosion the best and only a small decrease in E_b between that sample and the non shot-peened sample existed. However, it is clear from Fig. 6.15 that the glass shot peening and to a greater extent the steel shot-peening substantially reduced the E_b. Compared to the anodic polarisation at 18°C, the E_b was further lowered at 50°C on all the UNS S31603 shot-peened samples, as expected. As at 18°C, the highest E_b was shown for the steel shot-peened sample with the glass shot-peening proving to be most detrimental to localised corrosion resistance (Fig 6.16).

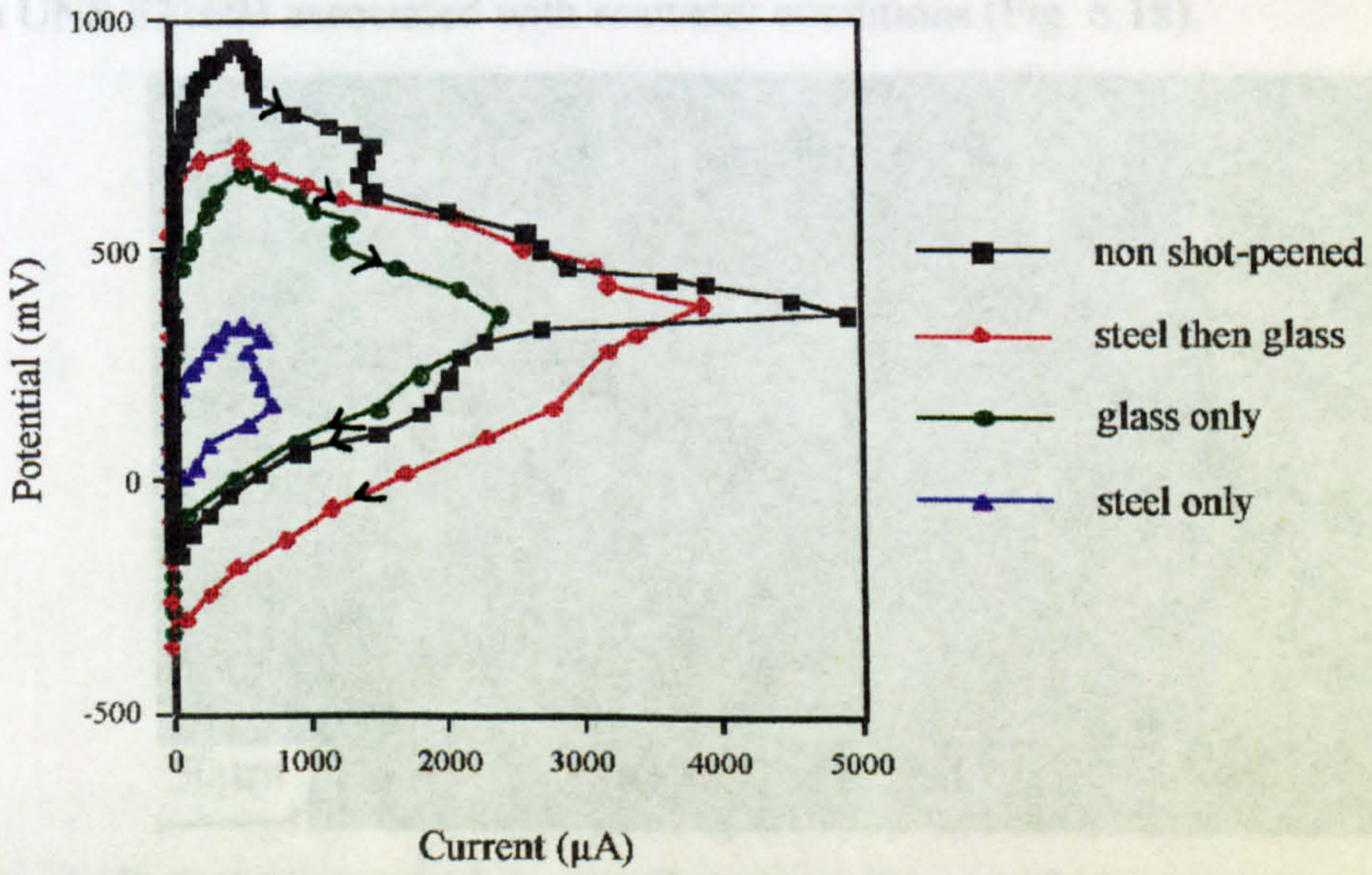

Fig. 6.15. Decreased resistance to corrosion initiation due to shot-peening on UNS S32760 super duplex stainless steel at 50°C

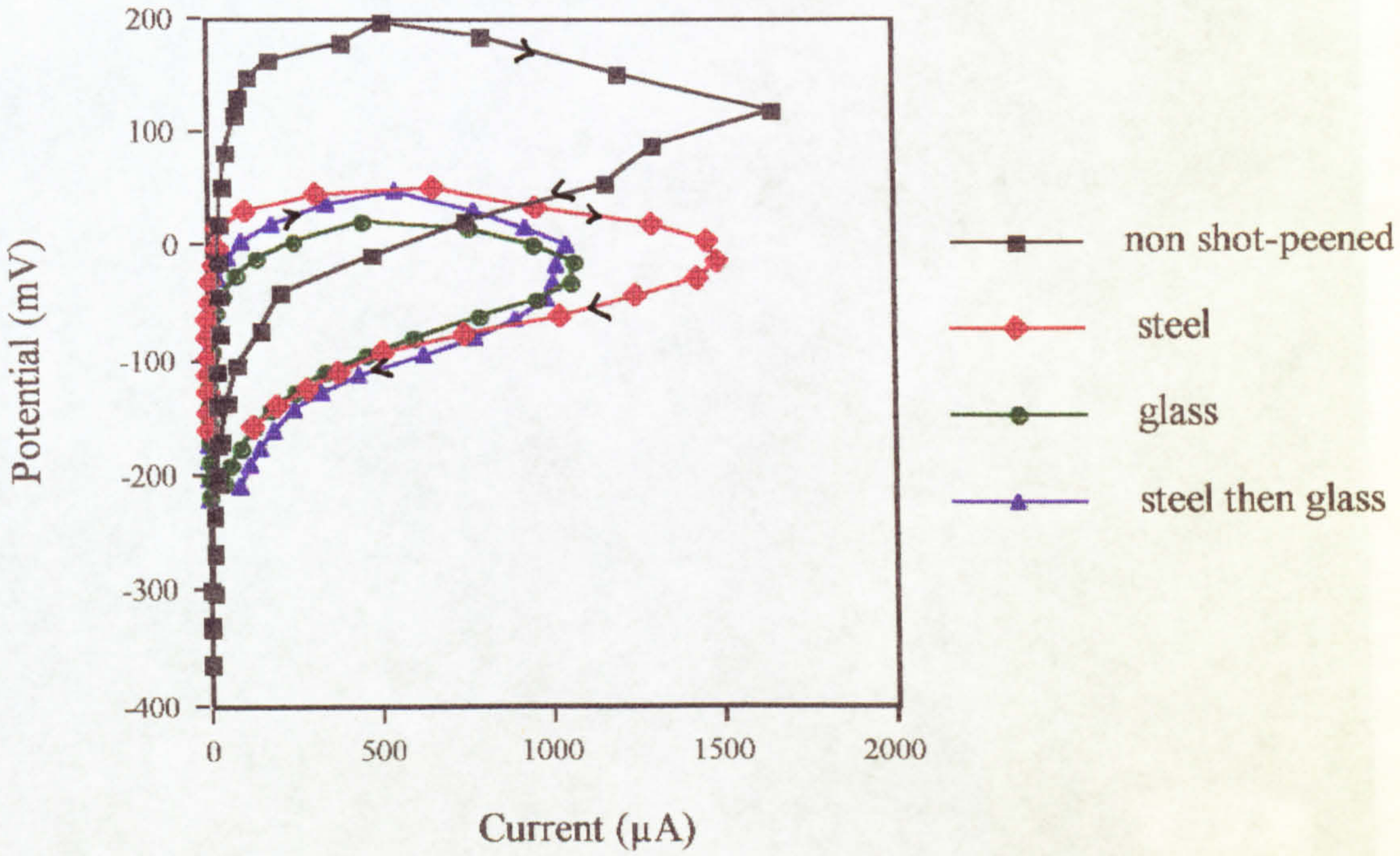

Fig. 6.16. Anodic polarisation curves for 50°C on UNS S31603 showing the same trend in shot peened surface corrosion resistance as at 18°C

On examination of the specimens after anodic polarisation, there was found to be a feature common to the stainless steels. As demonstrated previously, on all the as-produced shot-peened surfaces, there existed a network of surface cracks. In this work, these have been shown to provide sites for localised corrosion on the stainless steels. Although there was some evidence of this effect at 18°C on UNS S32760, the effect was much enhanced at 50°C on UNS S32760 (Fig. 6.17) and on the UNS S31603 at both temperatures. In addition to this attack, there was the characteristic pitting attack on UNS S31603 associated with seawater conditions (Fig. 6.18).

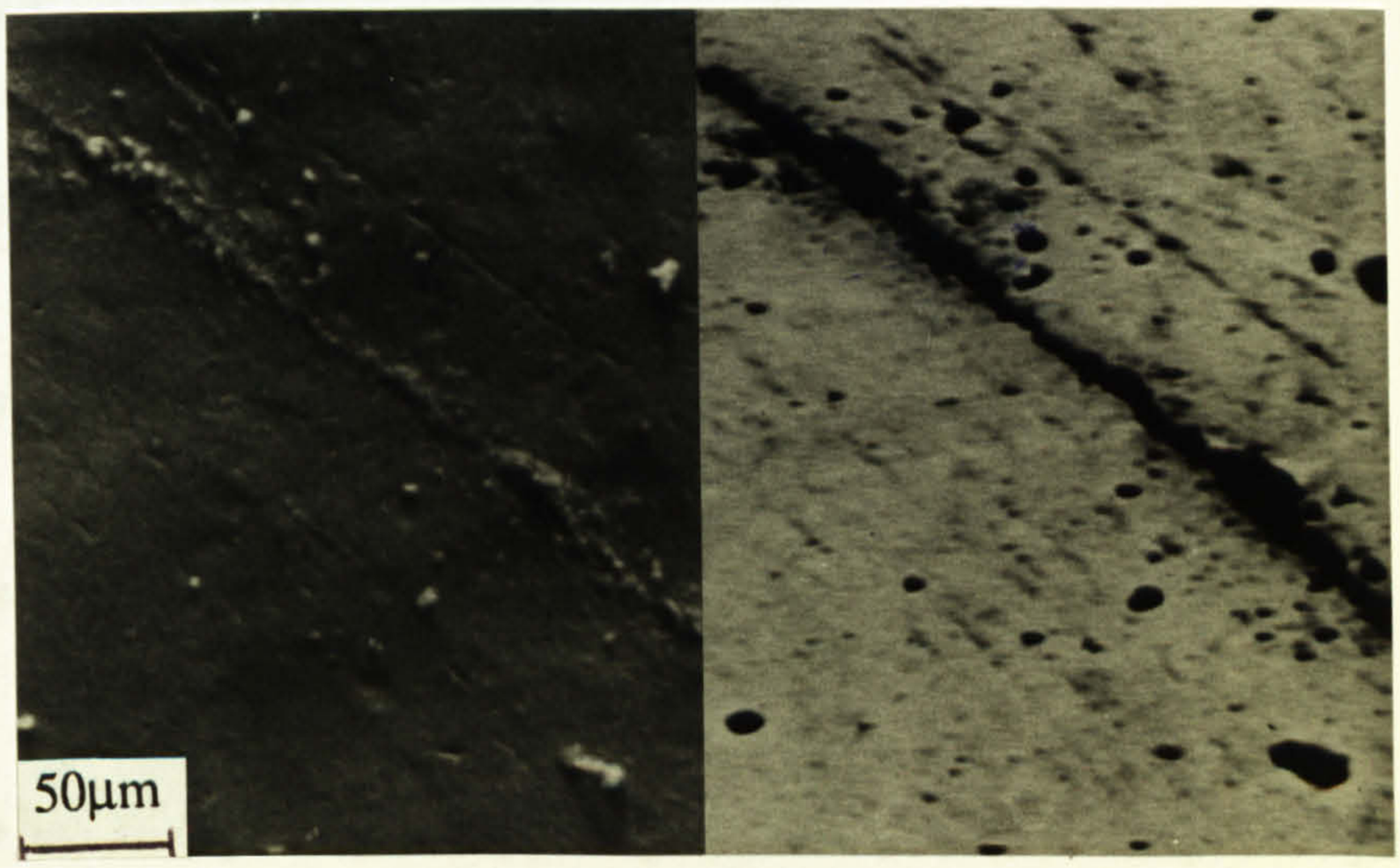

Fig. 6.17. Corrosion attack localised at the surface cracking on steel shot-peened UNS S32760 at 50°C (secondary and backscattered SEM micrograph)

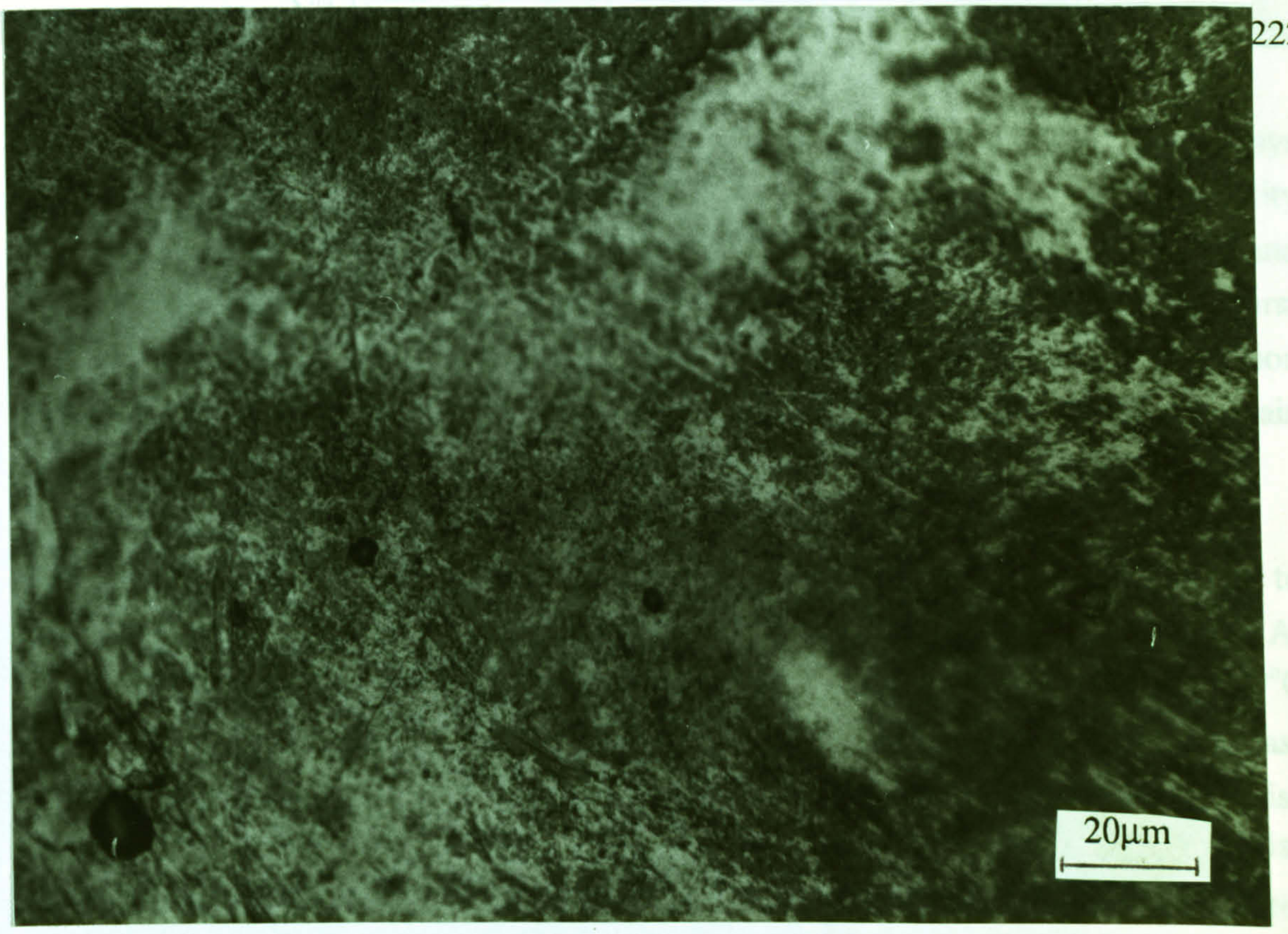

Fig. 6.18. Pitting on UNS S31603 steel shot-peened stainless steel after anodic polarisation at 18°C

No localised attack on shot-peened Stellite 6, could be identified at either temperature but a clear coloured film was evident on the entire specimen surface. The electrochemical anodic polarisation curve indicated that there is significant benefit to the corrosion resistance at elevated temperature to be obtained through shot-peening Stellite 6 (Fig. 6.19).

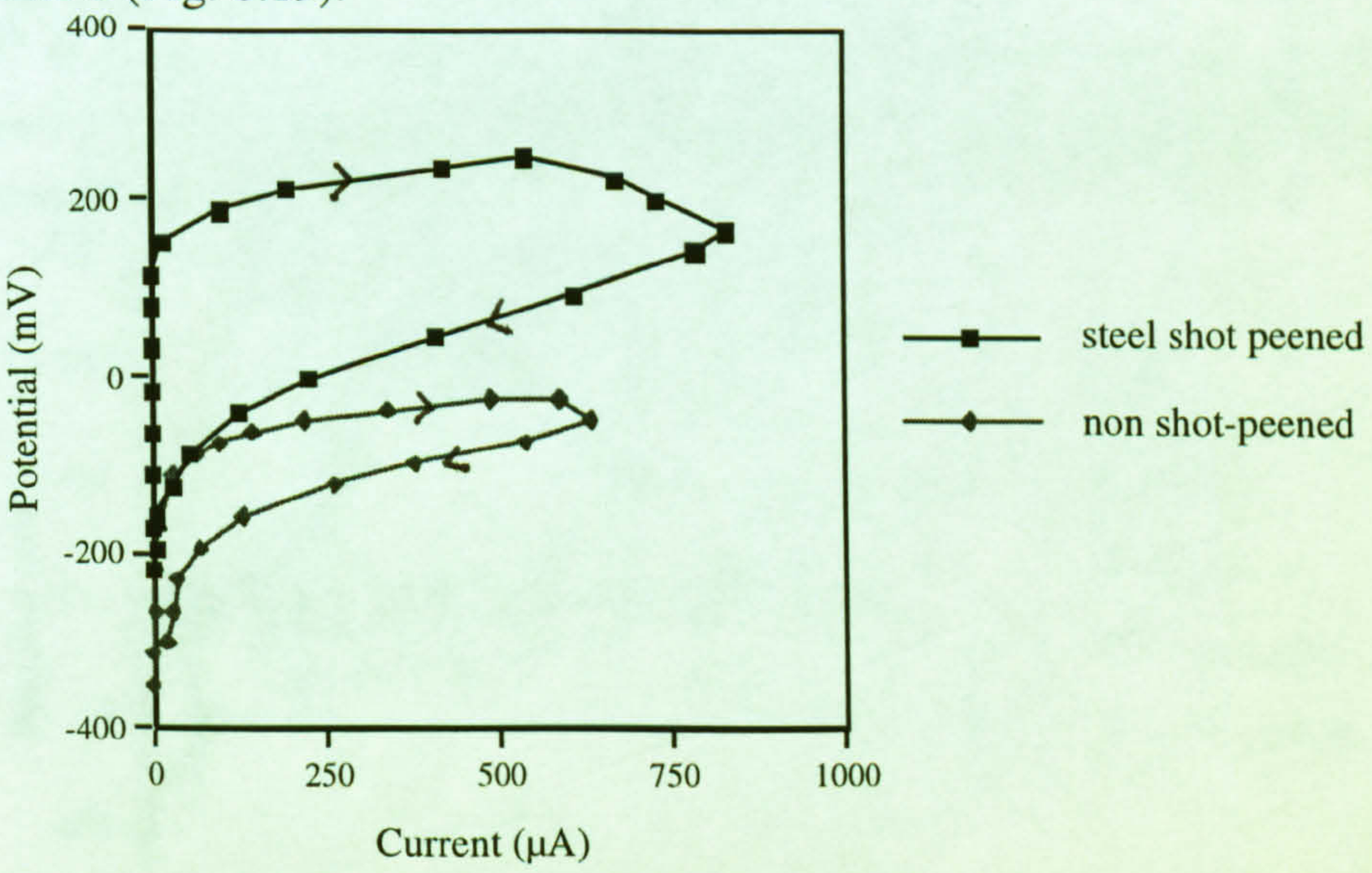

Fig. 6.19. Anodic polarisation showing improved resistance to passivity breakdown on Stellite 6 on shot-peened surface compared to the non shot-peened surface

at 50°C.

The results from tests conducted under liquid impingement of non shot-peened alloys are reported in chapter 2. It was shown that an impinging flow incident at high velocity on the surface detrimentally affected the resistance to localised corrosion initiation and led to the formation of a surface film on stainless steels. Stellite 6 was the worst affected alloy under the 100m/s flow and electrochemically it showed active corrosion behaviour where high corrosion currents were associated with intense attack at the grain boundaries.

The effect of shot-peening on the stainless steels and Stellite 6 was, on the whole, to render the surface more resistant to attack under liquid impingement conditions. At 18°C, on UNS S32760 there was no substantial difference in E_b detected but at 50°C there was a significant improvement in the resistance of the glass and steel and glass shot-peened surface over the untreated alloy (Fig 6.20a and b). The characteristic rise in current at the point E_p as reported in chapter 4 was present but the extent of the rise was much less than associated with the formation of a thick coloured film as in chapter 4. Indeed there was evidence of a surface film present on both stainless steels (Fig. 6.21) but the thickness was not comparable with the films formed on the untreated alloys. The steel shot-peened surface showed very poor resistance and was perhaps due to the corrosion of embedded iron shot. On the lower grade UNS S31603 at 18°C, there was a marked improvement in the resistance of all the shot-peened surface over the substrate (Fig 6.22) but no such benefit was observed as the temperature was increased to 50°C (Fig 6.23). It is interesting to note that in agreement with the results in static conditions, the resistance to the steel shot-peened surface on UNS S31603 at 18°C exceeds that of the steel than glass and the glass shot-peening confers the least resistance. There is no such trend in the ranking of the performance of the shot-peening processes on UNS S32760.

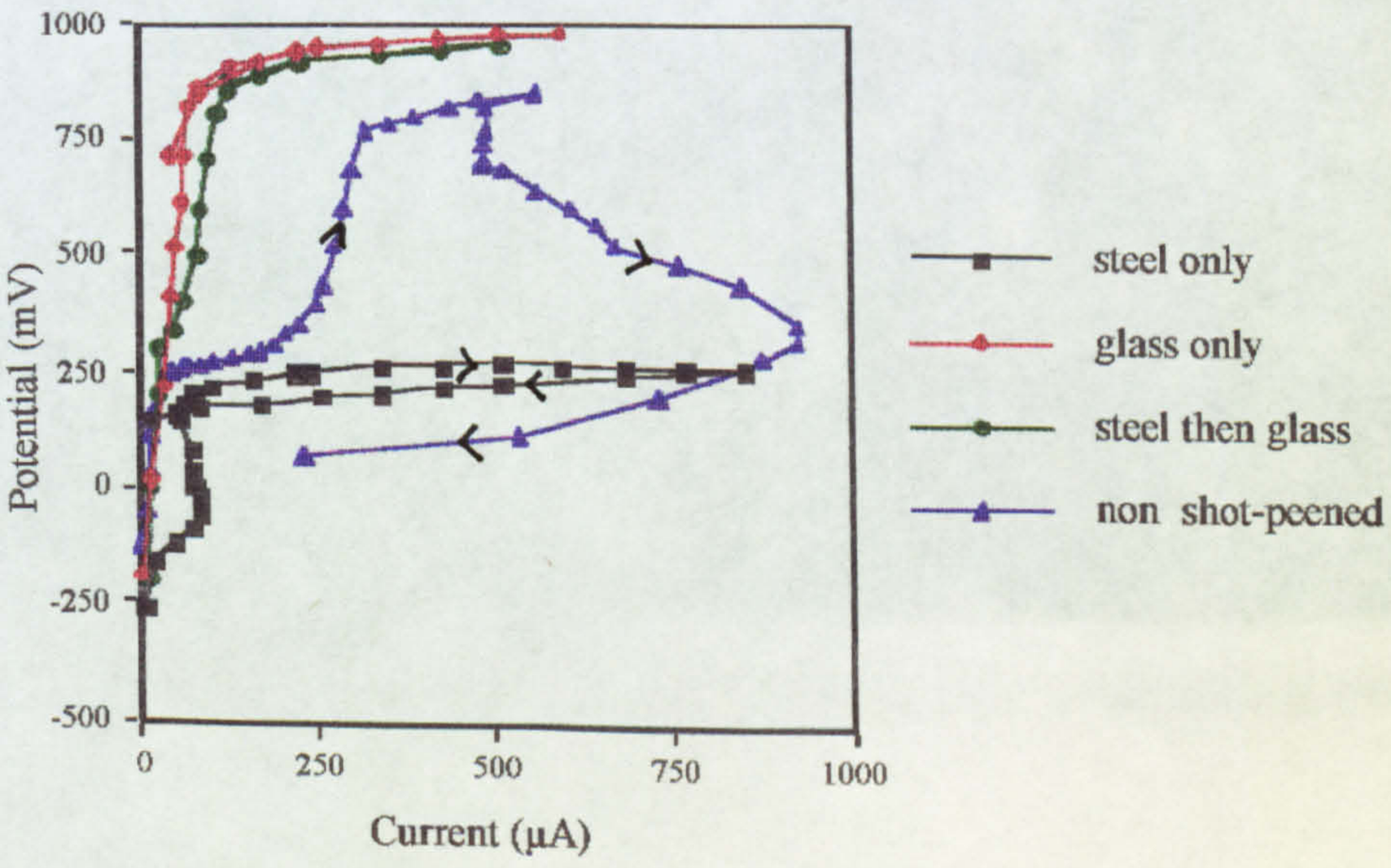

(a)

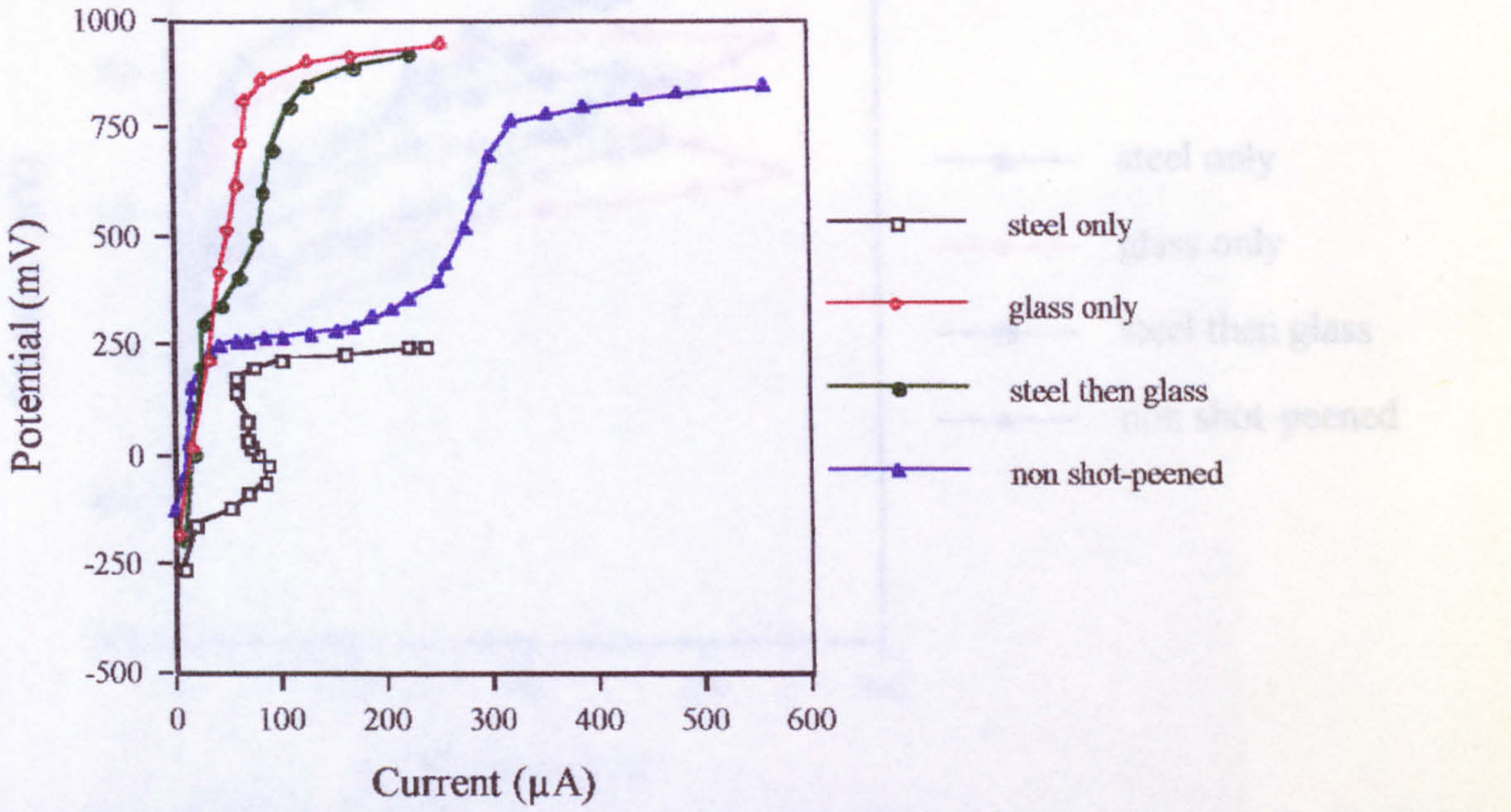

(b)

Fig.6.20. Anodic polarisation on UNS S32760 under impingement conditions at 50°C : shot-peened and non shot-peened (a) full polarisation curve (b) showing passive region

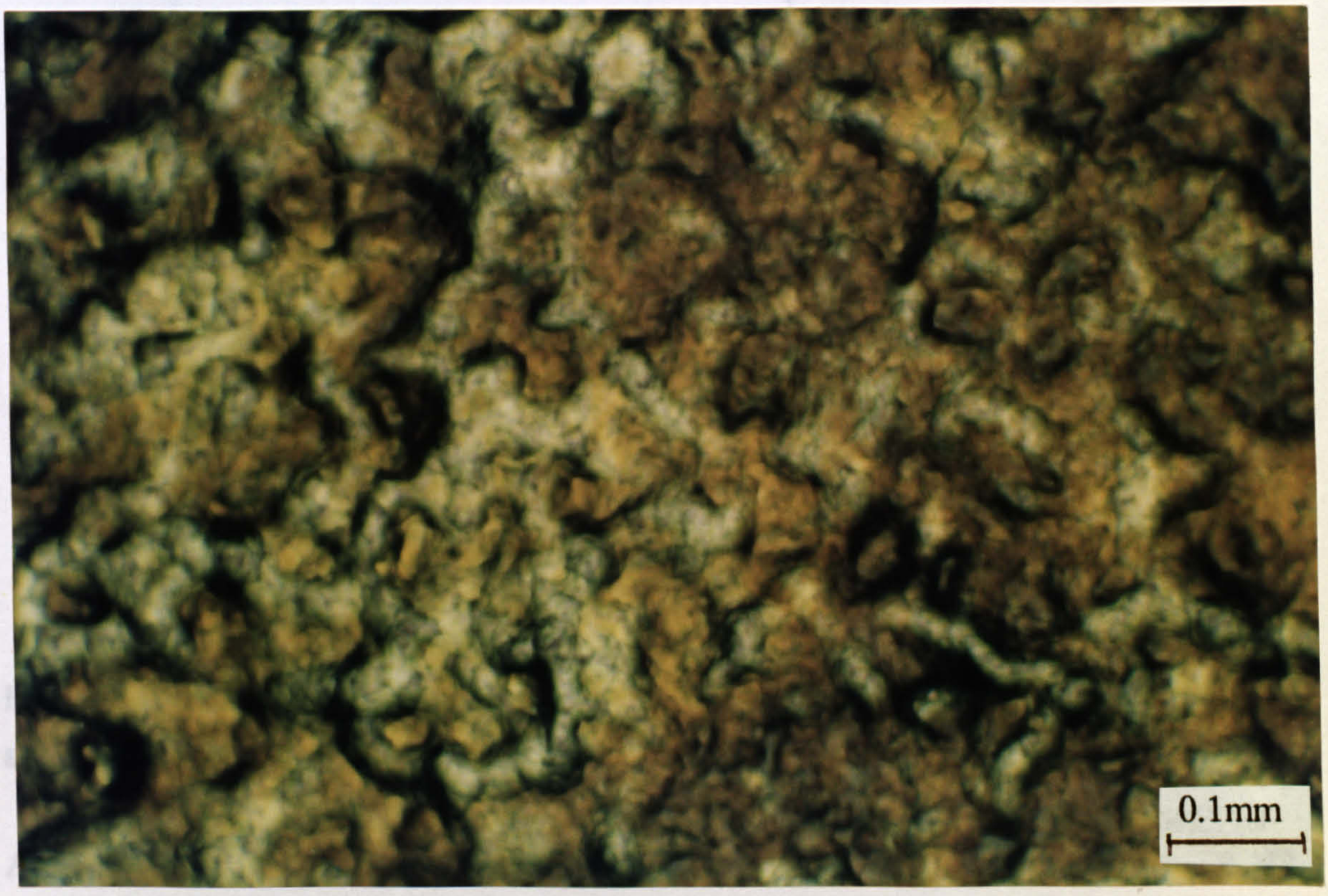

Fig. 6.21. Coloured film on UNS S31603 after anodic polarisation at 18°C under liquid impingement conditions.

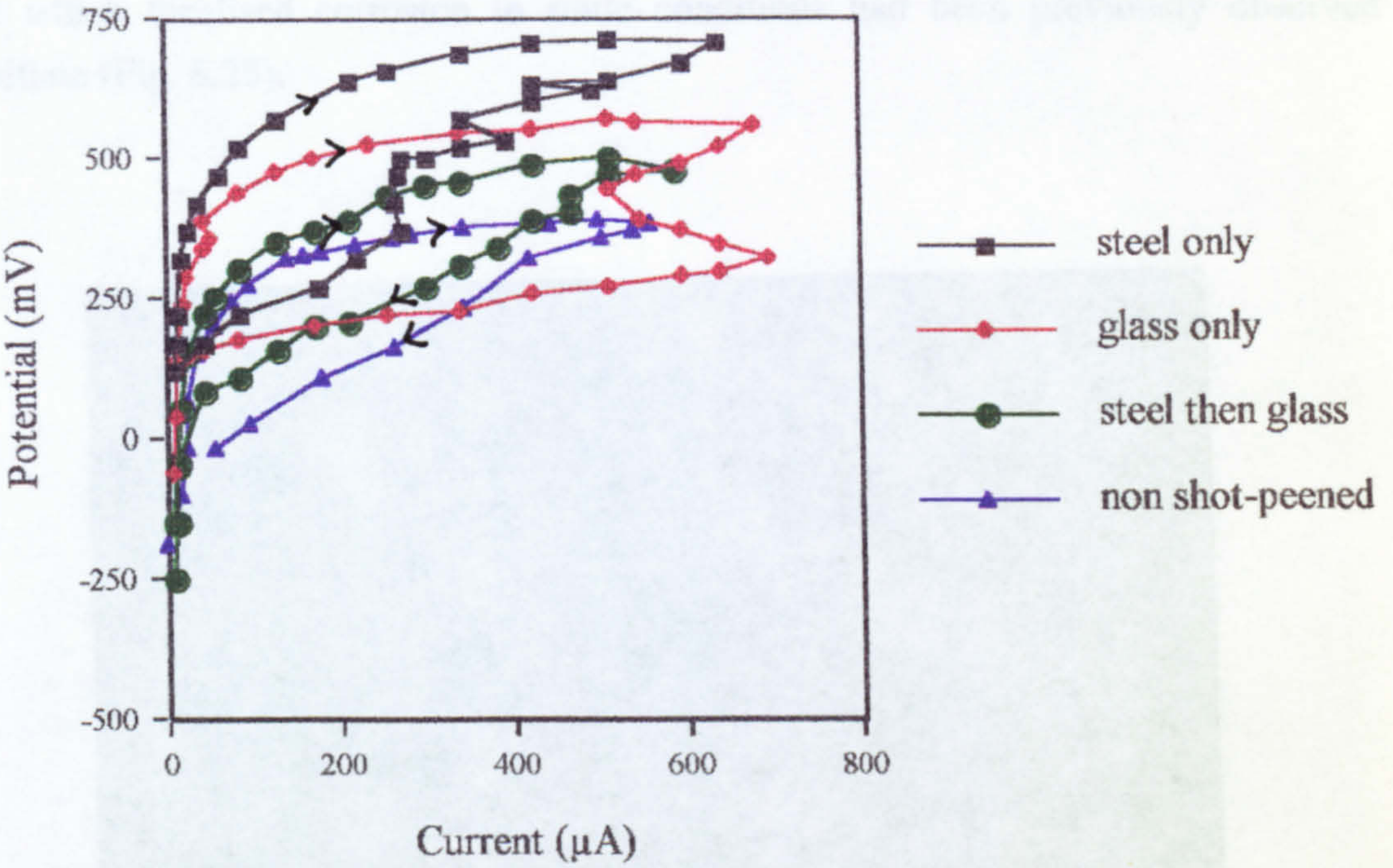

Fig. 6.22. Superior resistance to corrosion initiation of shot-peened UNS S31603 stainless steel at 18°C under liquid impingement conditions

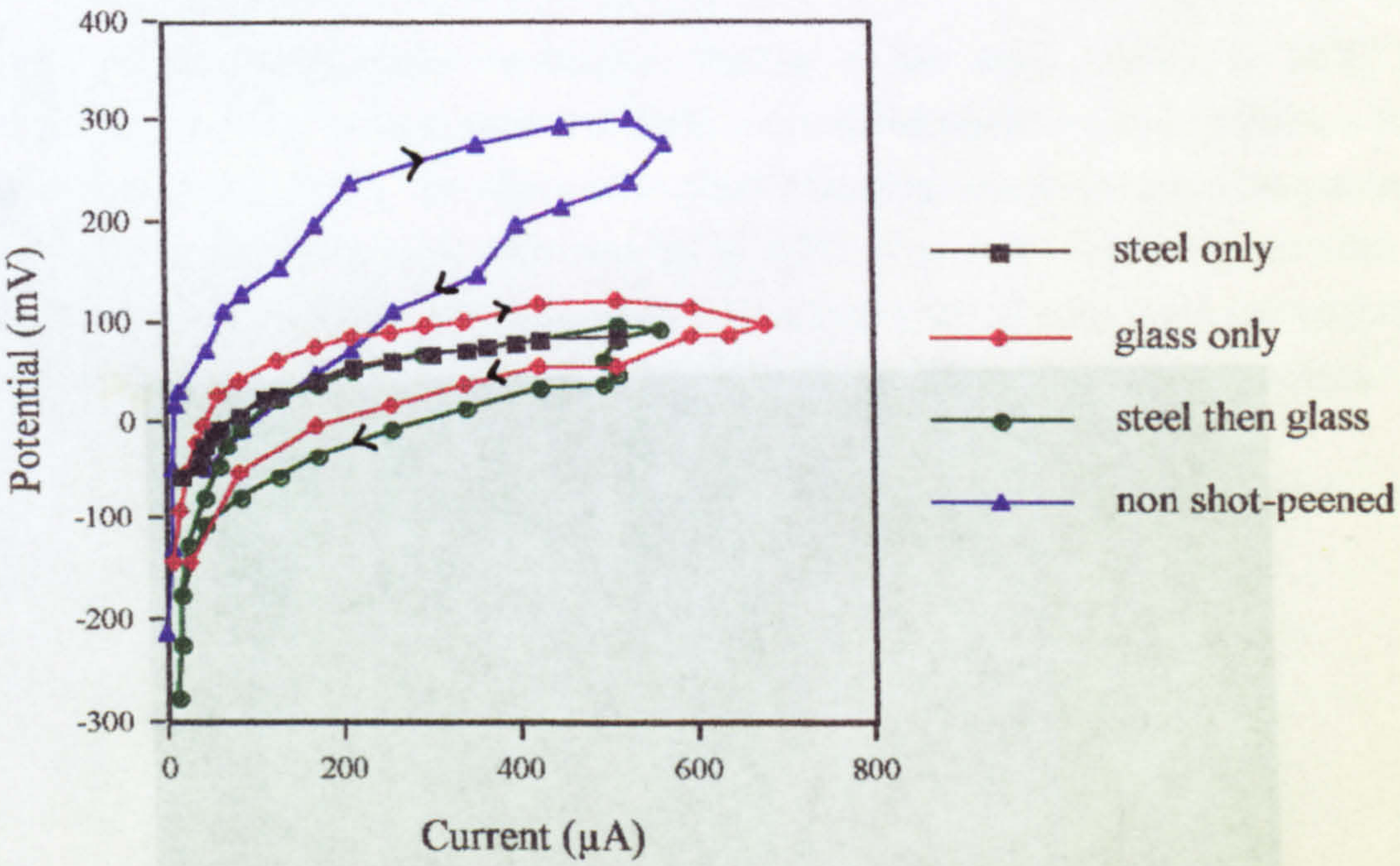

Fig.6.23. Anodic polarisation on UNS S31603 shot-peened and non shot-peened surfaces at 50°C in impingement conditions

After testing in liquid impingement conditions, the most notable distinction from the attack under static conditions was the formation of what were described in chapter 2 as comet pits. As shown in Fig. 6.24a, the comet pits consisted of a cluster of corrosion products at the head of the pit, and a distinct pit underneath (Fig 6.24b). The distinction in the shot-peened material was that they initiated at the surface crack sites at which

at which localised corrosion in static conditions had been previously observed to initiate (Fig. 6.25).

(a)

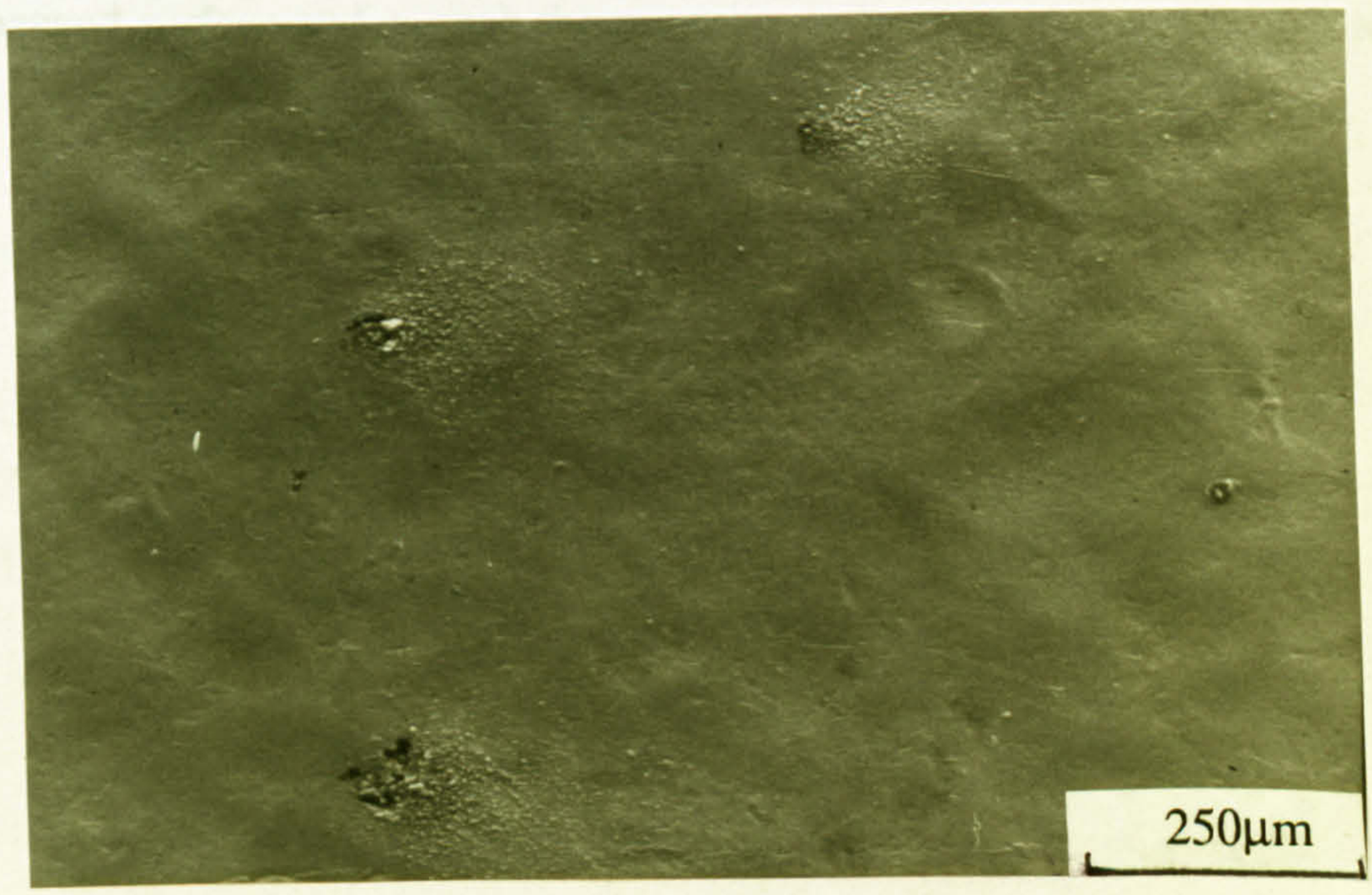

(b)

Fig. 6.24. Comet pitting on UNS S31603 under impingement conditions at 18°C (a) cluster of corrosion products and (b) pitting under corrosion products

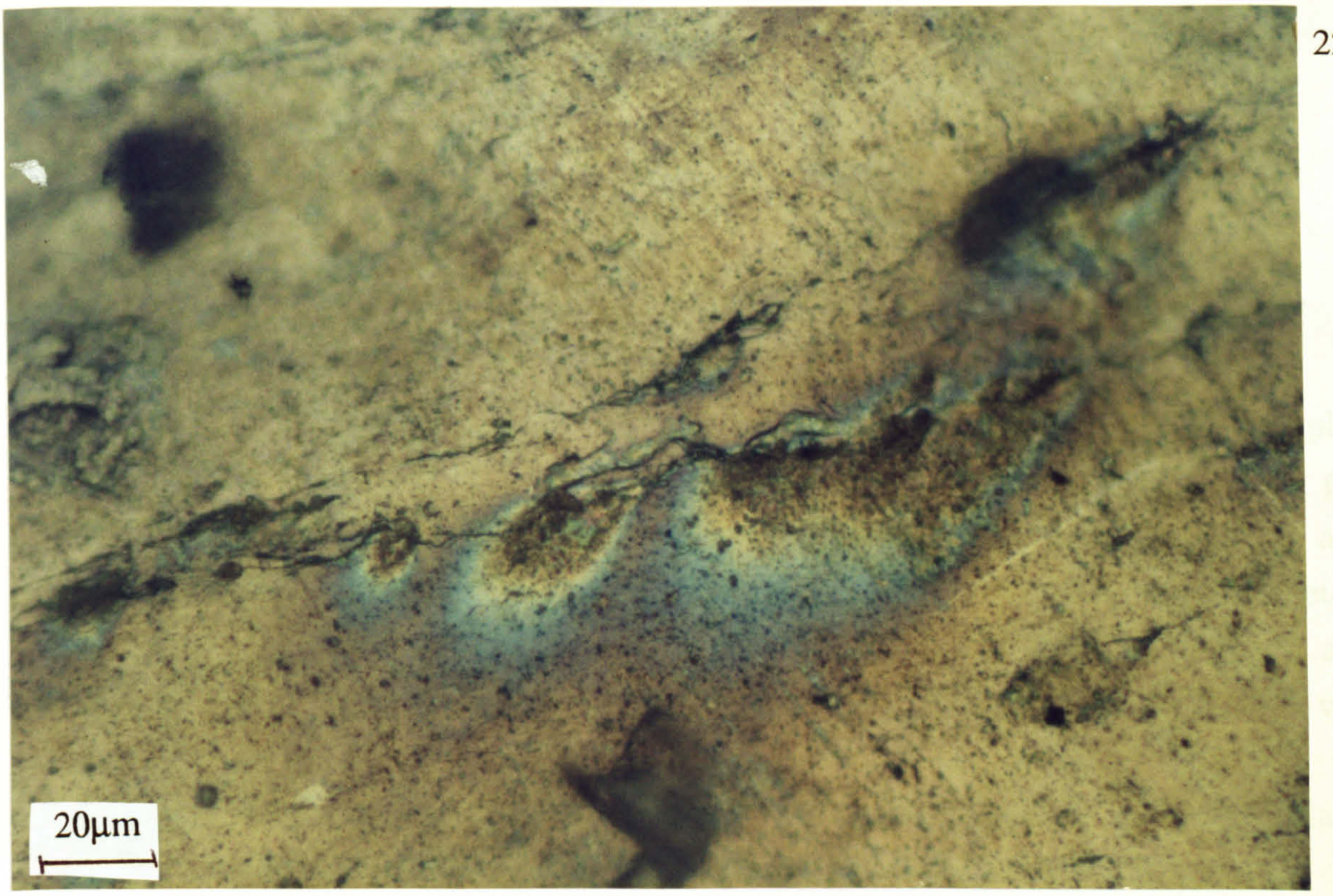

Fig. 6.25. Comet pitting initiated at surface cracks on steel shot peened UNS S32760 under impingement conditions at 18°C.

Under liquid impingement conditions, Stellite 6 has been shown at 18°C and particularly at 50°C to have poor resistance to localised corrosion and exhibits a small passive potential range. The effect of steel shot peening was to improve the corrosion resistance at 18°C but more substantially at 50°C (Fig. 6.26) which agrees with the trend in static conditions. The susceptible grain boundary regions were not visible on the shot-peened surface and as such there was no indication of intergranular attack.

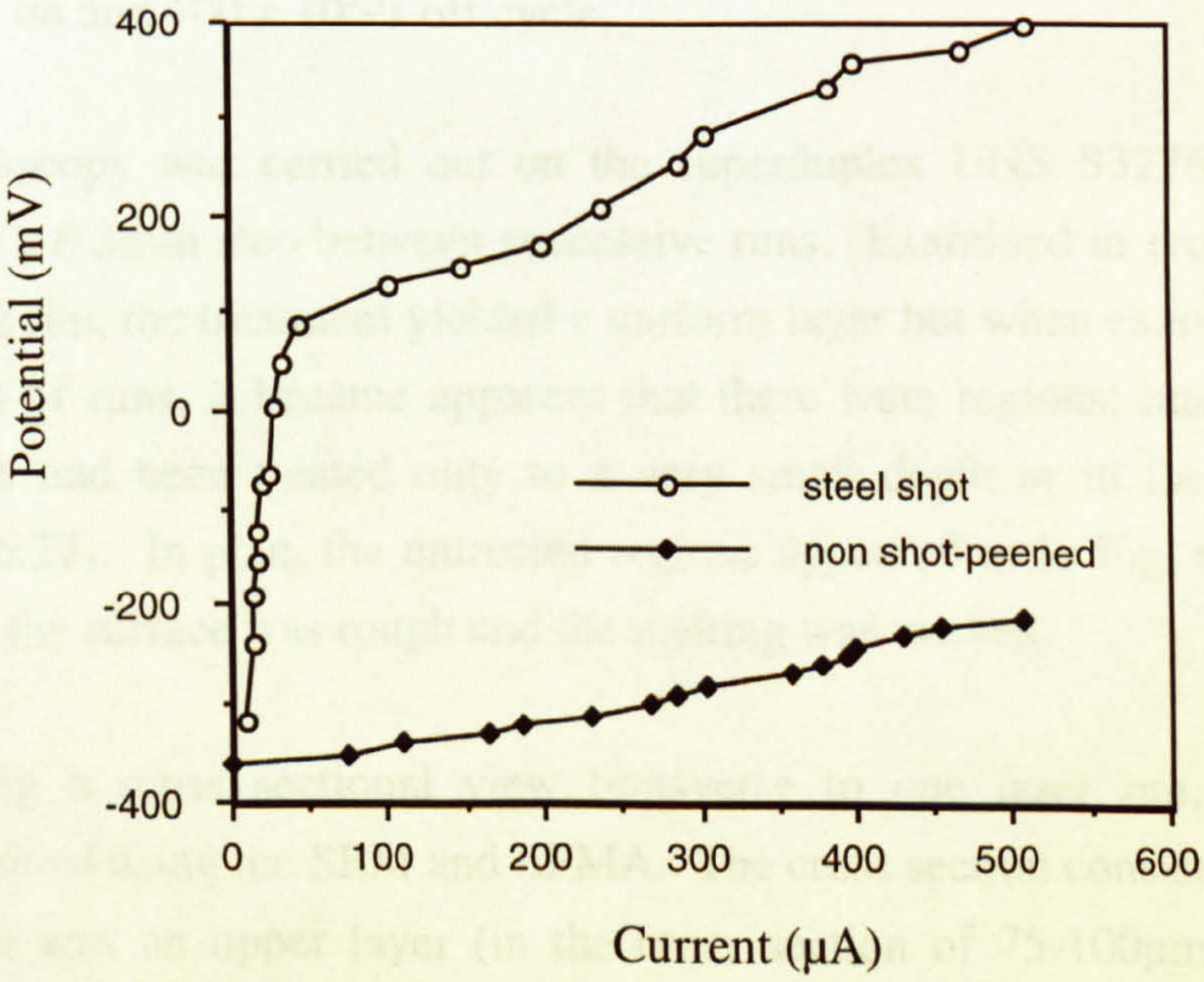

Fig. 6.26. Stellite 6 shot-peened and non shot-peened surface anodic polarisation under liquid impingement conditions at 50°C

Laser Treatment

Microhardness and Pre-test examination

Performance testing of the laser treated specimens began concentrating on the duplex stainless steels UNS S32760 and SAF 2205. As described earlier, the shrouding gas was nitrogen, the pressure was 5 bar, the feed rate of the laser was 1000mm/min and the beam was defocussed at 0.3mm above the focal point. The remaining parameters (laser power and heat input characteristics, degree of overlap) were not established and as such the procedure for testing followed an iterative process whereby the sample was treated, examined in plan, etched and examined in cross section, tested via electrochemical techniques in seawater and using the results from all the tests, the laser parameters were varied accordingly.

The first batch of laser treatment was carried out using continuous power and after each laser run the beam was automatically stepped 0.3mm perpendicular to the run direction to form an adjacent parallel run.

Although the treatment gave a surface section which appeared uniform, at each termination point there was a large bead of solidified metal and the heat input had been sufficiently intense to penetrate the 6mm thick plate causing distortion. Therefore for the remainder of the study the power input was used in pulsed mode following a 200 x 10^{-5}s on and 100 x 10^{-5}s off cycle.

Microscopy was carried out on the superduplex UNS S32760 after laser treatment using a 0.3mm step between successive runs. Examined in cross-section, parallel to a single run, the treatment yielded a uniform layer but when examined perpendicular to a series of runs, it became apparent that there were regions, intermediate between runs which had been treated only to a very small depth or in the worst cases not at all (Fig.6.27). In plan, the untreated regions appeared as in Fig. 6.28 where between the runs, the surface was rough and the melting was uneven.

Taking a cross sectional view transverse to one laser run, the treated layer was examined using the SEM and EPMA. The cross section consisted of three components. There was an upper layer (in the cross section of 75-100μm thick) the structure of which was not comparable with the untreated duplex structure. Fig. 6.29 shows the backscattered SEM micrograph with the upper layer which as shown in Fig. 6.30 appeared as primarily a single phase.

Fig. 6.27. Untreated regions between laser runs on UNS S32760

Fig. 6.28. Plan view of the laser treated surface showing rough regions between runs

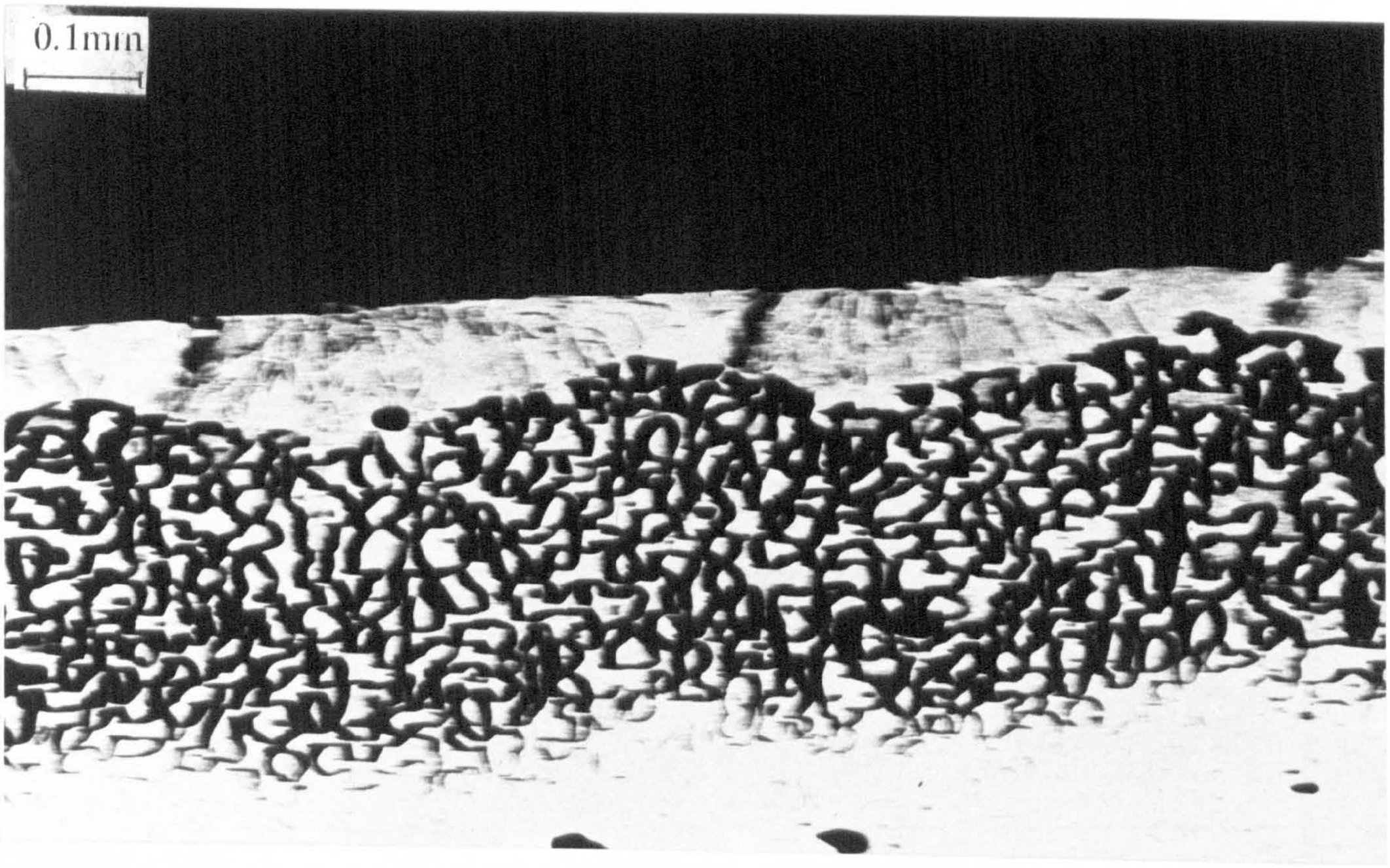

Fig. 6.29. Three layers of the UNS S32760 laser treated surface

Fig. 6.30. Inside the laser layer of UNS S32760 showing the microstructure.

The composition of this layer was between that of the austenite and the ferrite phases as shown over in Fig. 6.31.

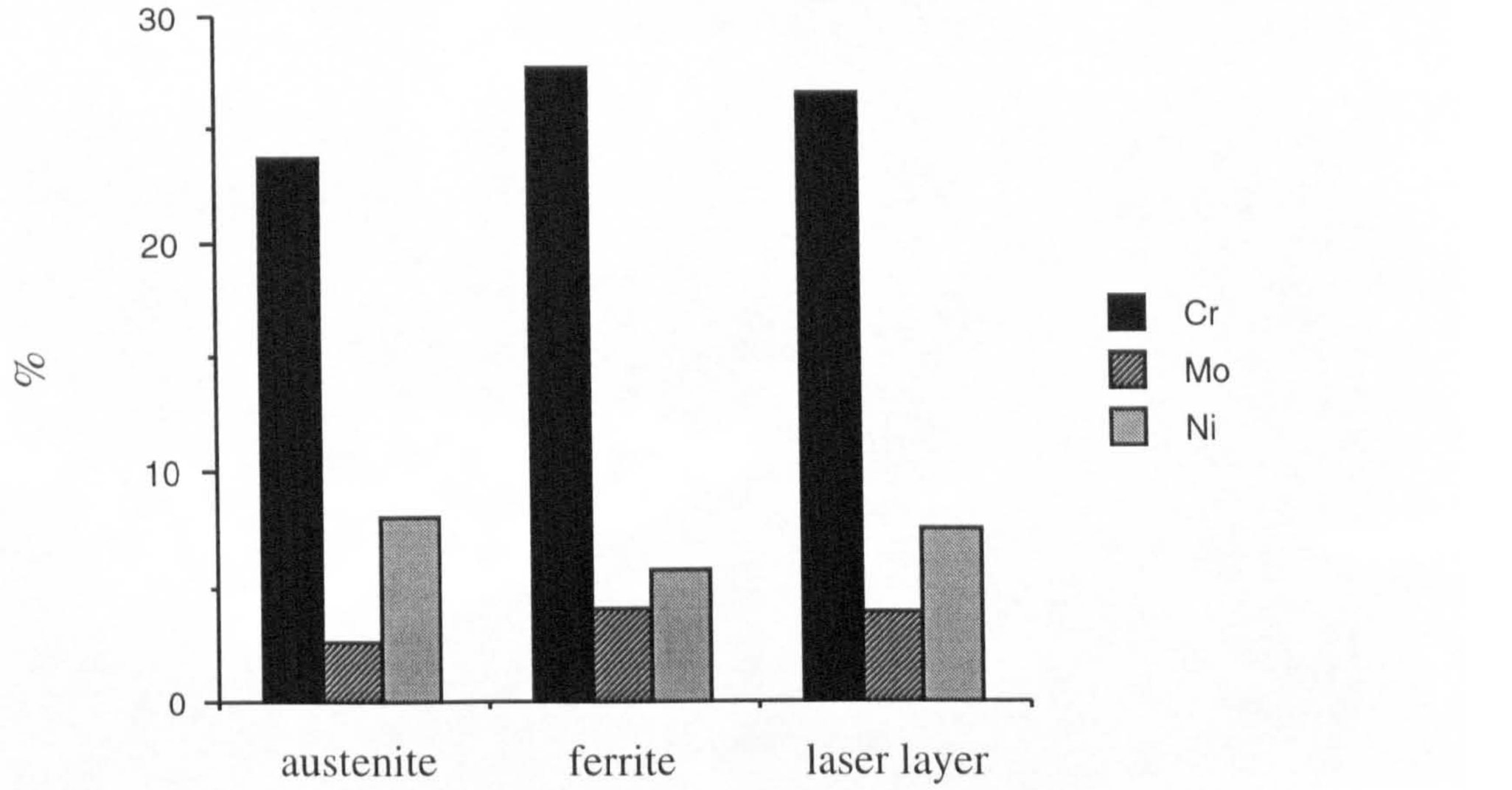

Fig. 6.31. Composition of the laser treated layer compared to the austenite and ferrite

Under this layer was a second layer, about two times the thickness of the upper layer in which the duplex structure and composition was apparent (Fig. 6.32) but in which there were precipitates at the grain boundaries (areas 1 and 2 in Fig. 6.33). Chemical analysis showed an enrichment of Cr at the grain boundary. Areas 1 and 2 in Fig. 6.33 contained 31.5% and 32.1%Cr respectively. An unaffected superduplex stainless steel, equal in composition and microstructure to the untreated material was found under the two layers.

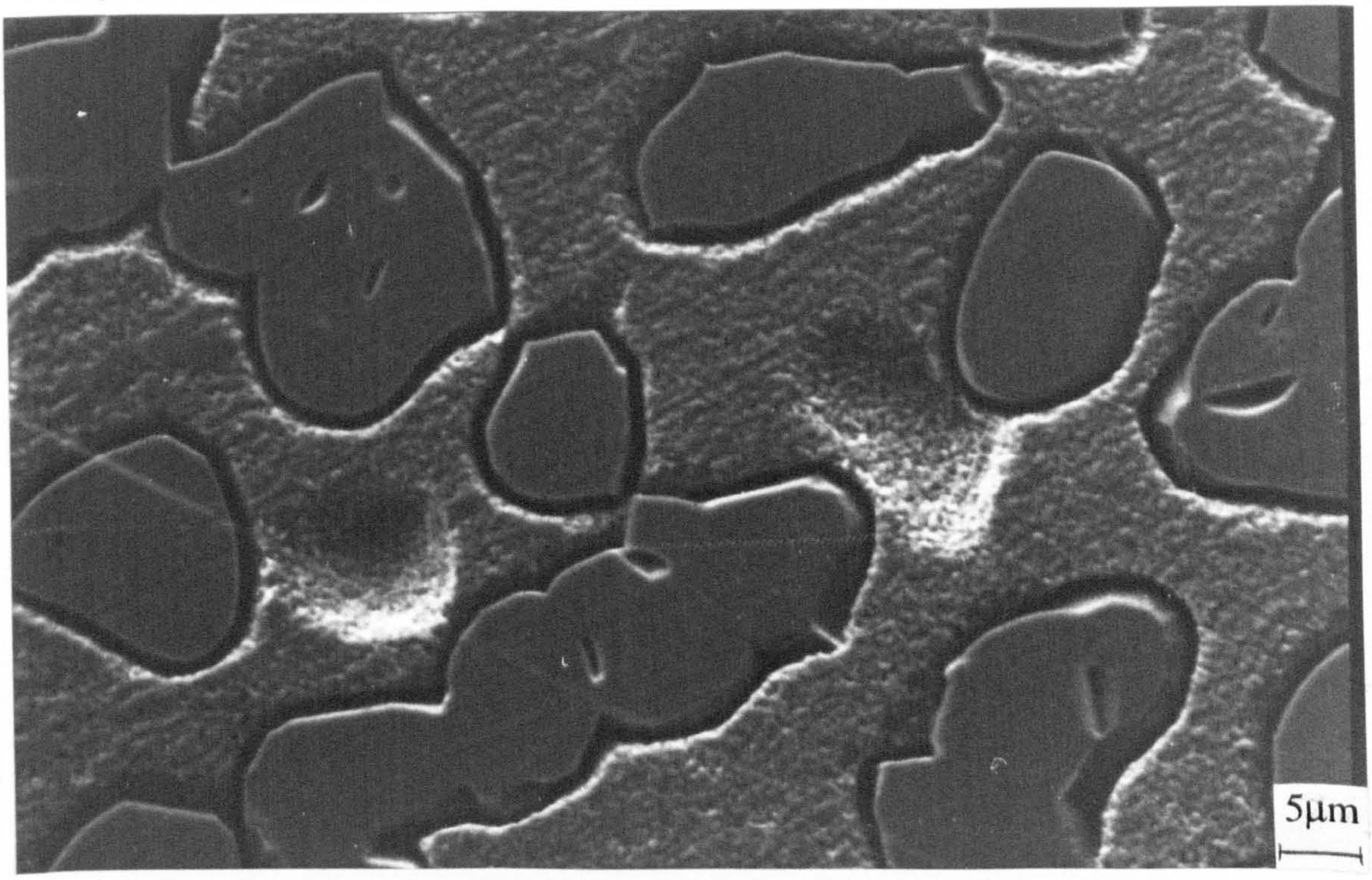

Fig. 6.32. Duplex structure in the second layer formed after laser treatment

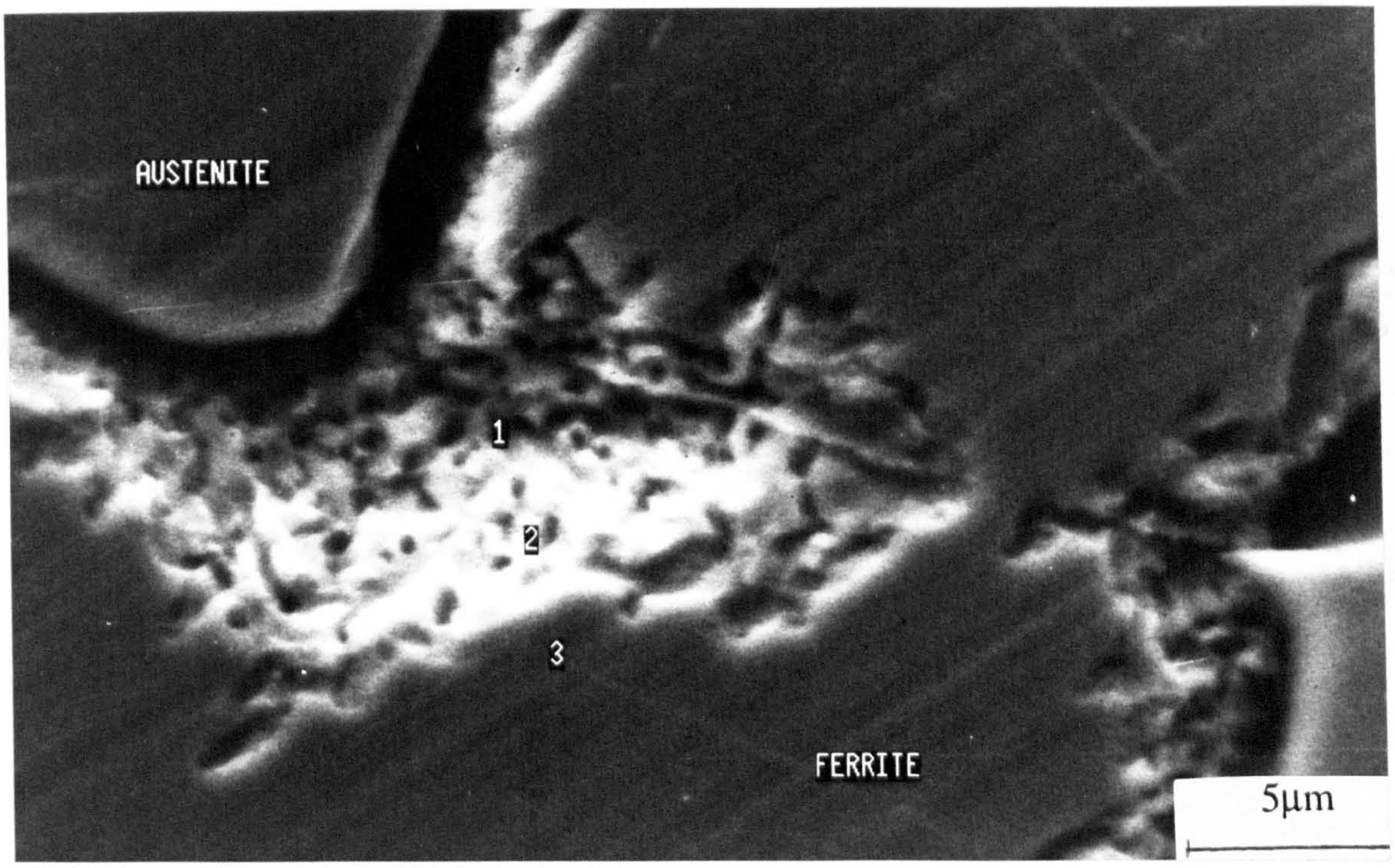

Fig. 6.33. Analysis regions at the grain boundaries where precipitates were evident

A microhardness profile was built up across the complete cross section and showed a significant hardening in the outer layer of almost 66% of the substrate. However, there was a loss of hardness across the layer immediately below (Fig. 6.34).

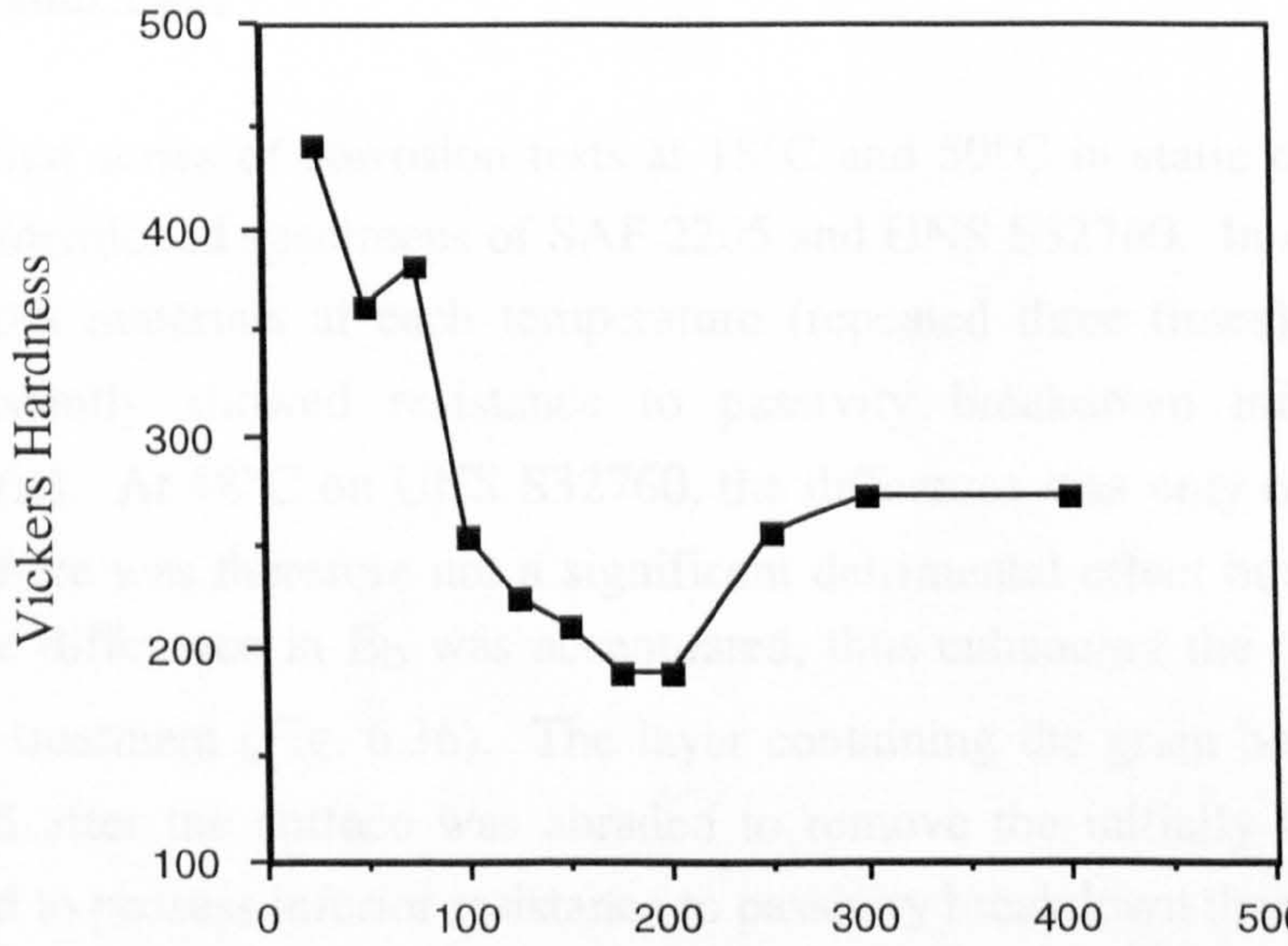

Fig. 6.34. Microhardness profile across the laser treated layer on UNS S32760

On SAF 2205 the same effect, showing the untreated areas was observed, shown in Fig. 6.35. The analysis on SAF 2205 (SEM, EPMA and microhardness) was not taken

further using these parameters - corrosion tests were performed (results shown in next section).

Fig. 6.35. Lack of sufficient overlap on SAF 2205 after laser treatment

Corrosion Tests

The first series of corrosion tests at 18°C and 50°C in static conditions involving the aforementioned specimens of SAF 2205 and UNS S32760. In anodic polarisation tests on both materials at each temperature (repeated three times) the laser treated layer consistently showed resistance to passivity breakdown inferior to the untreated material. At 18°C on UNS S32760, the difference was only of the order of 60-70mV and there was therefore not a significant detrimental effect but at 50°C the magnitude of the difference in E_b was accentuated, thus enhancing the detrimental effect of the laser treatment (Fig. 6.36). The layer containing the grain boundary precipitates was tested after the surface was abraded to remove the initially treated layer and it was found to possess inferior resistance to passivity breakdown than the upper layer.

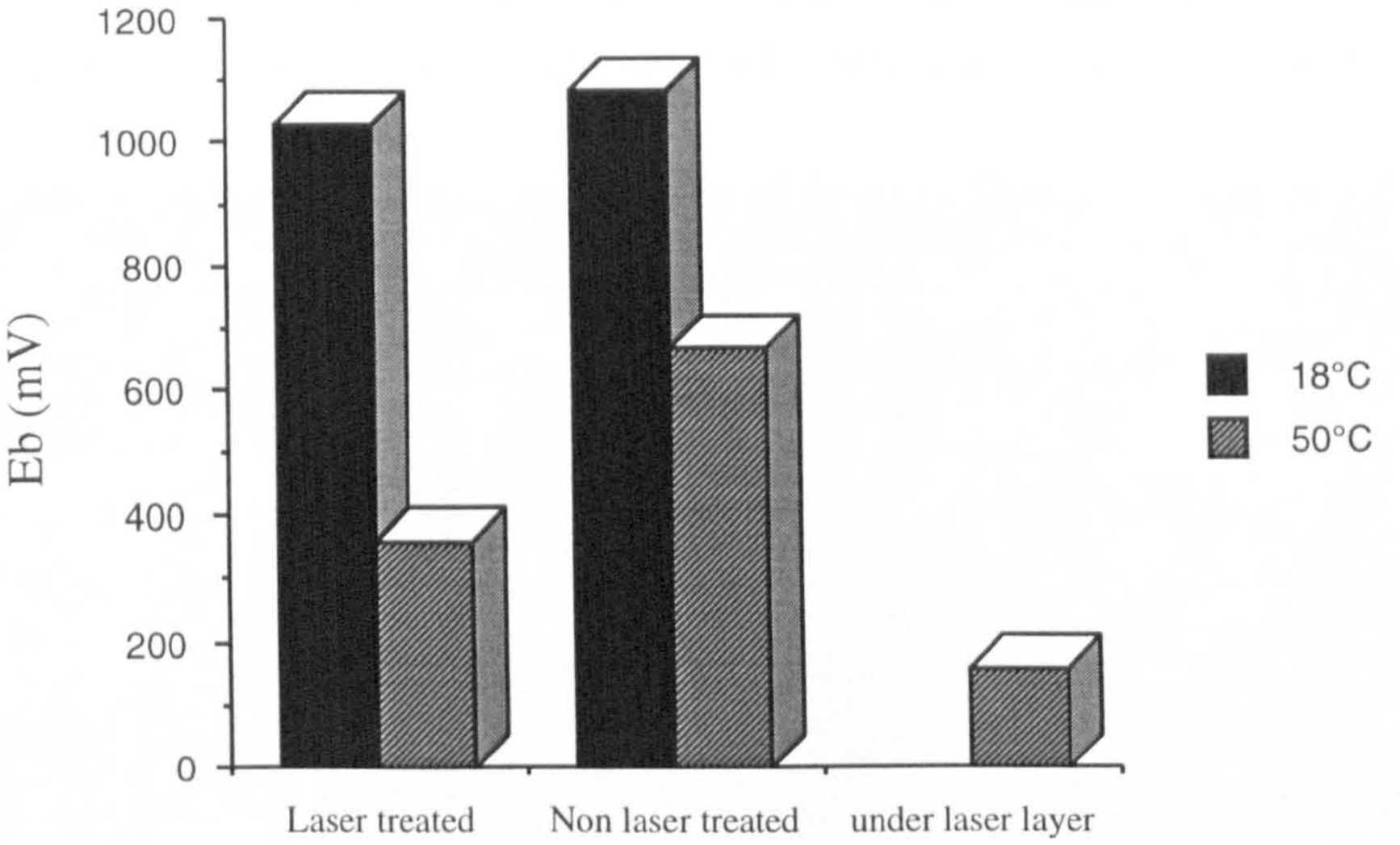

Fig. 6.36. Fall in E_b on UNS S32760 due to laser surface treatment using a transverse shift of 0.3mm between adjacent laser runs.

The lower Cr, SAF 2205 at 18°C showed a significant decrease in the E_b value after laser treatment which was enhanced at 50°C (Fig. 6.37).

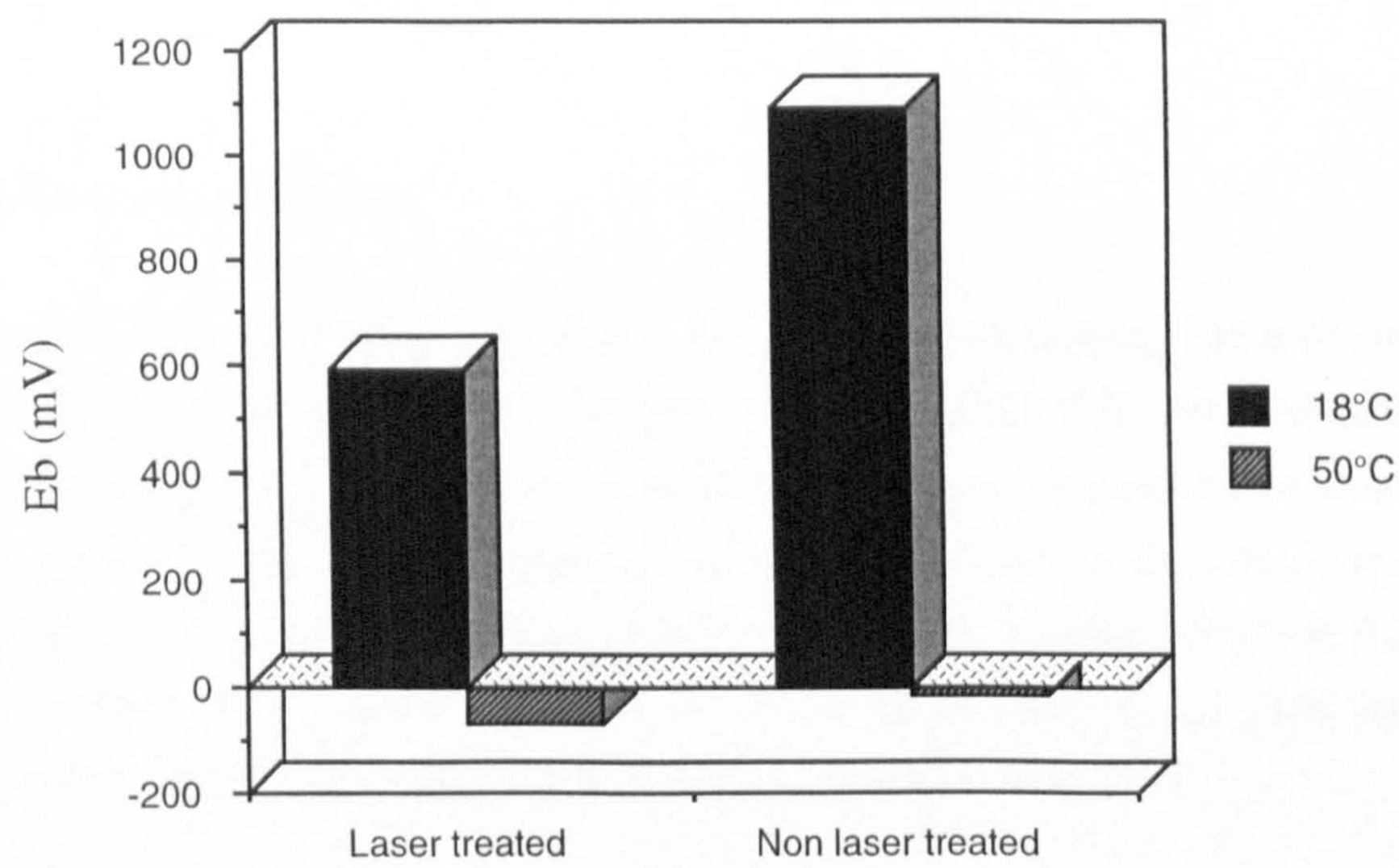

Fig. 6.37. Fall in E_b due to laser surface treatment using a transverse shift of 0.3mm between adjacent laser runs on SAF 2205.

As may have been anticipated the susceptible areas to localised attack were shown to be the areas in between the adjacent runs and it can be seen in Fig. 6.38, on UNS S32760 that after anodic polarisation at 50°C there was a significant accumulation of corrosion products at these areas.

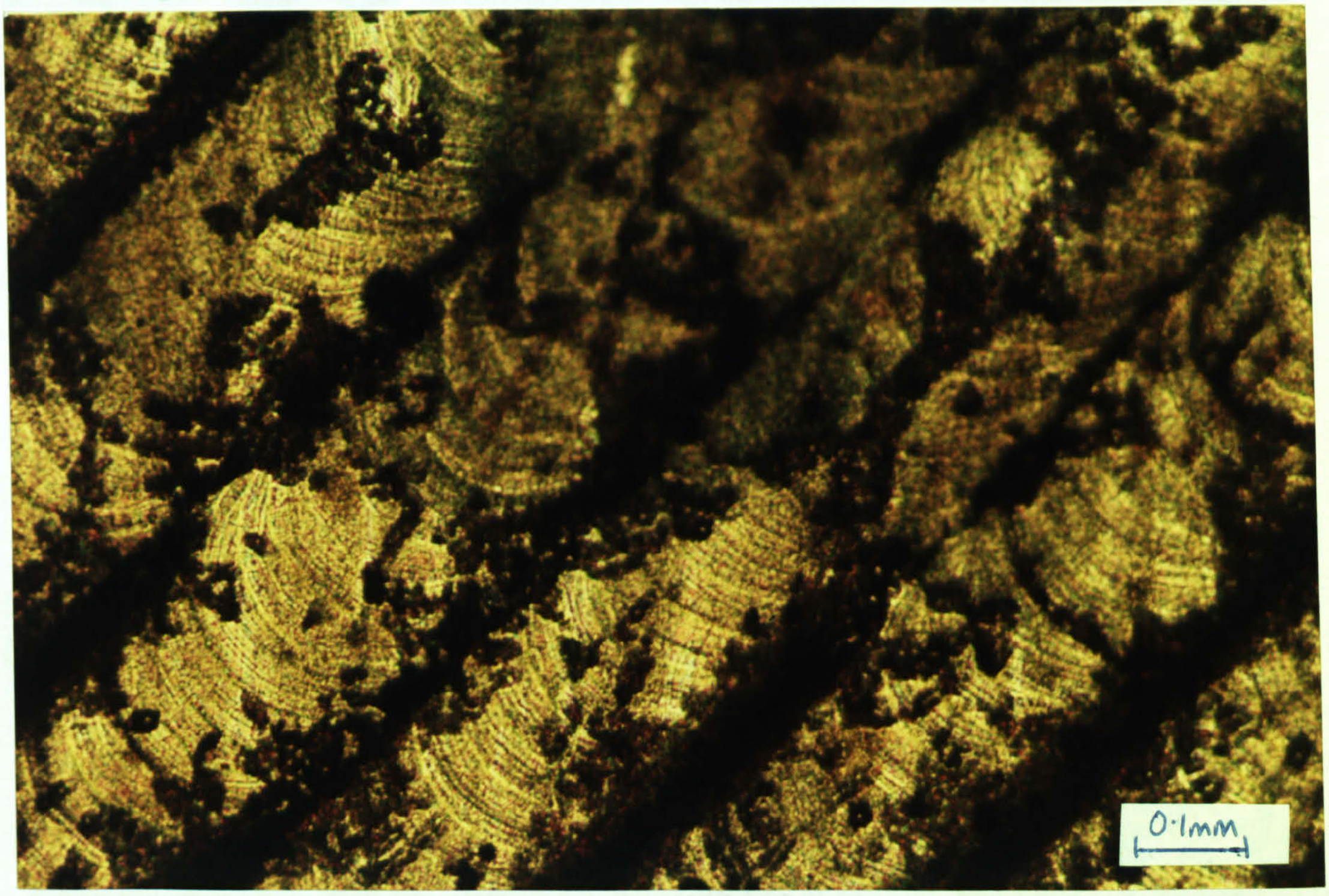

Fig. 6.38. Corrosion between laser runs on UNS S32760 after anodic polarisation at 50°C

Modified Laser Treatment

In the second batch of laser treatment, the parameter governing the amount of overlap between adjacent laser runs was changed. The amount of shift perpendicular to the run just completed was reduced from 0.3mm to 0.175mm. In plan there was an obvious improvement in the homogeneity of the treated surface, in that there were no areas between the runs which appeared to be insufficiently melted. Figures 6.39 and 6.40 show a low and a higher magnification view of the surface in plan which can be compared to the surface when the previous parameters were used.

The overlap proved to be sufficient to produce a layer of uniform thickness both along the weld (Fig. 6.41) and, more importantly, across several welds (Fig. 6.42).

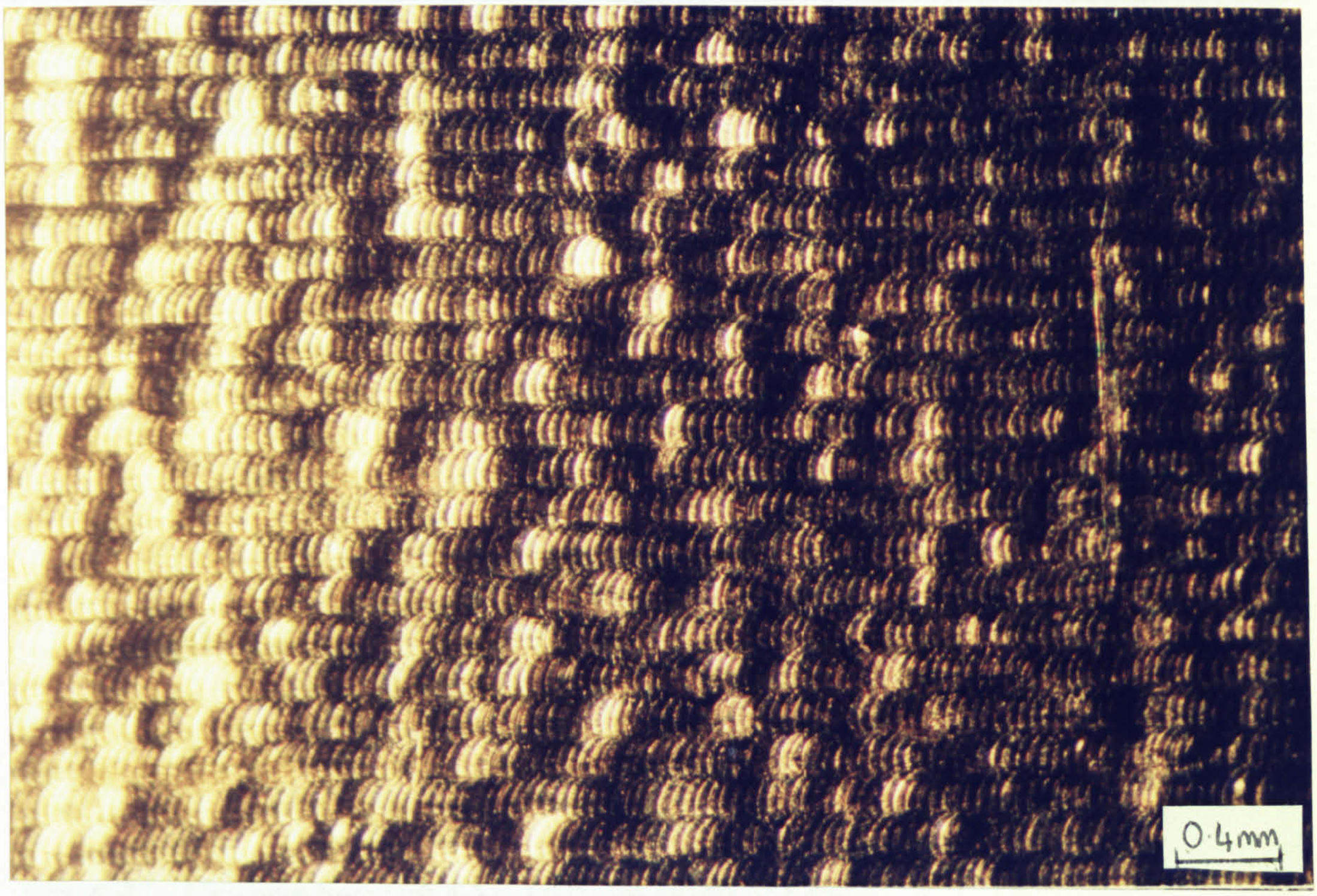

Fig. 6.39. Plan view of surface of SAF 2205 after laser treatment increasing the amount of overlap

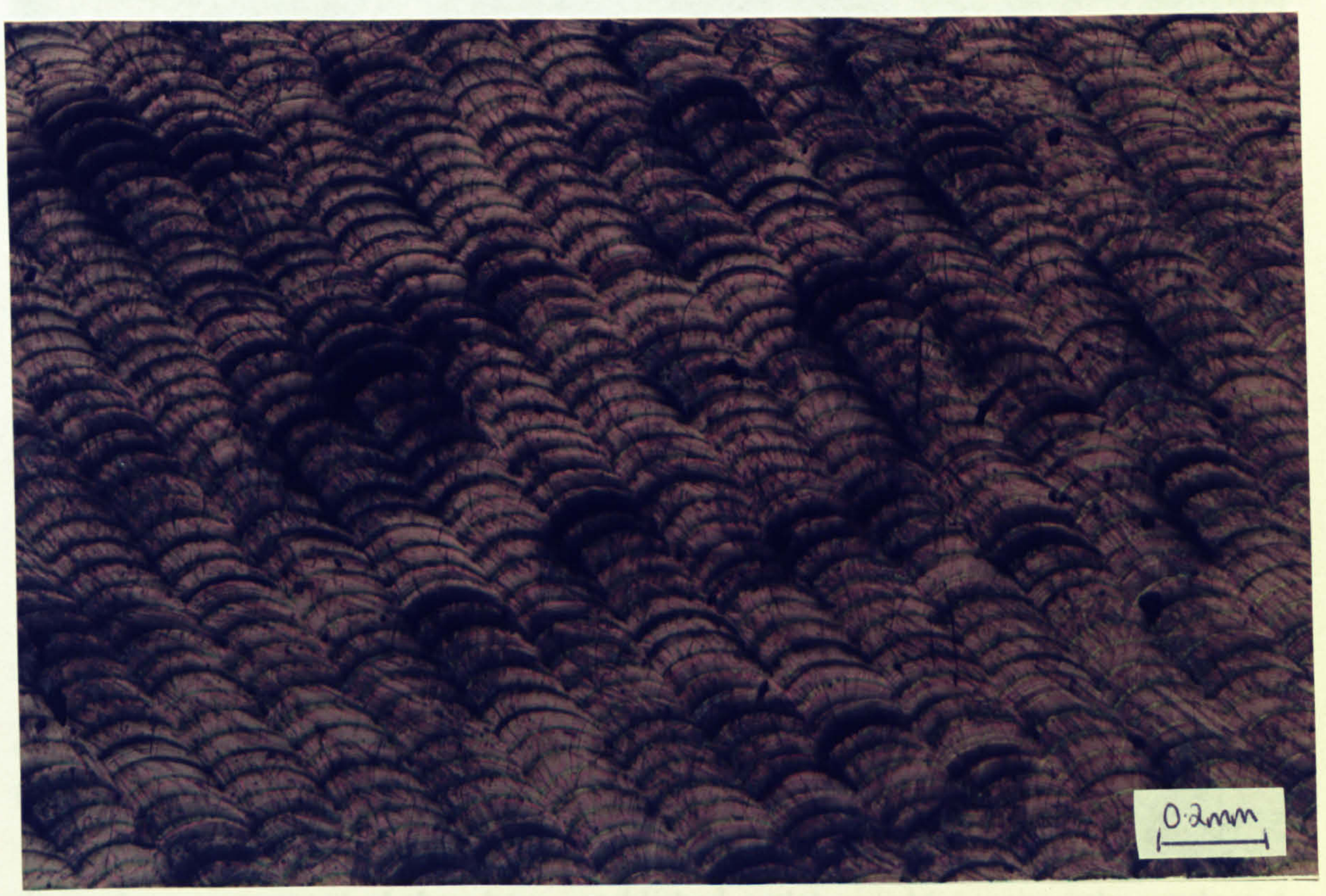

Fig. 6.40. Higher magnification of plan view of surface of SAF 2205 after laser treatment increasing the amount of overlap.

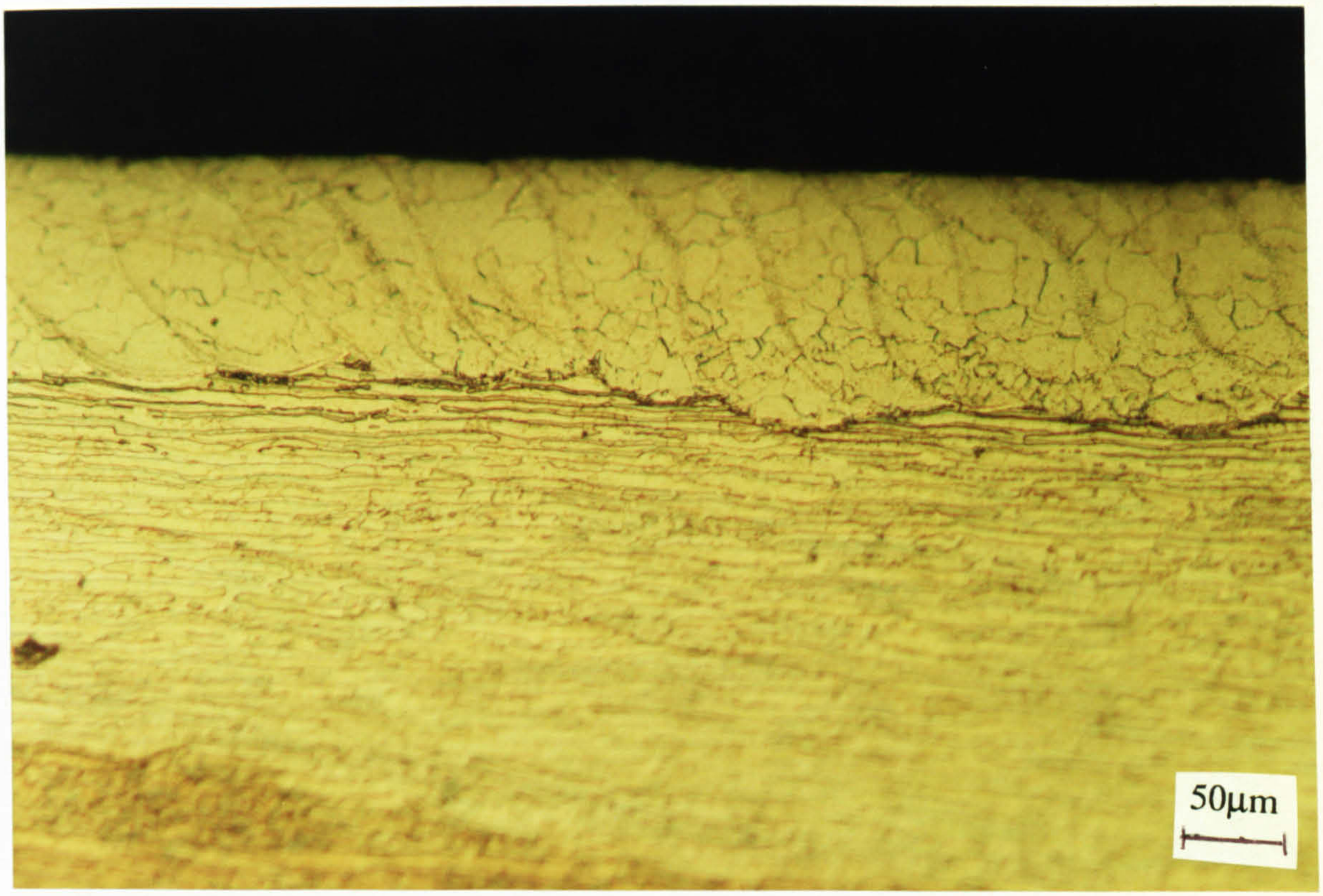

Fig. 6.41. Uniform layer on SAF 2205 cut along one run

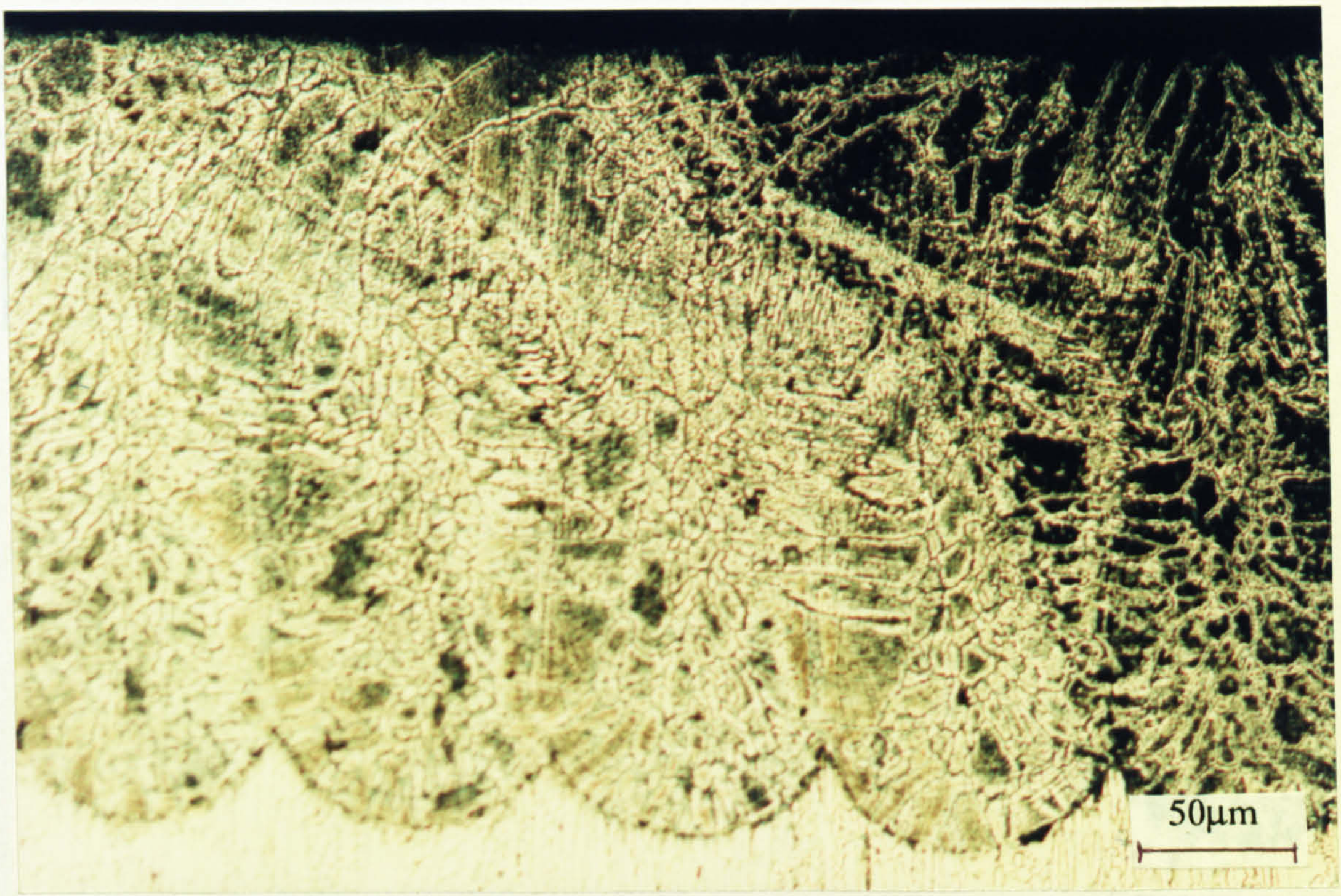

Fig. 6.42. Uniform thickness of laser treatment across several runs on UNS S32760 on increasing the overlap.

Since the parameters had then been established which would consistently produce a homogenous layer, the austenitic stainless steels were treated using the same conditions, for comparative purposes. It was found that the degree of overlap gave a

layer uniform when sectioned in both directions as shown for along the run on UNS S31254 in Fig. 6.43 and across the runs in Fig. 6.44.

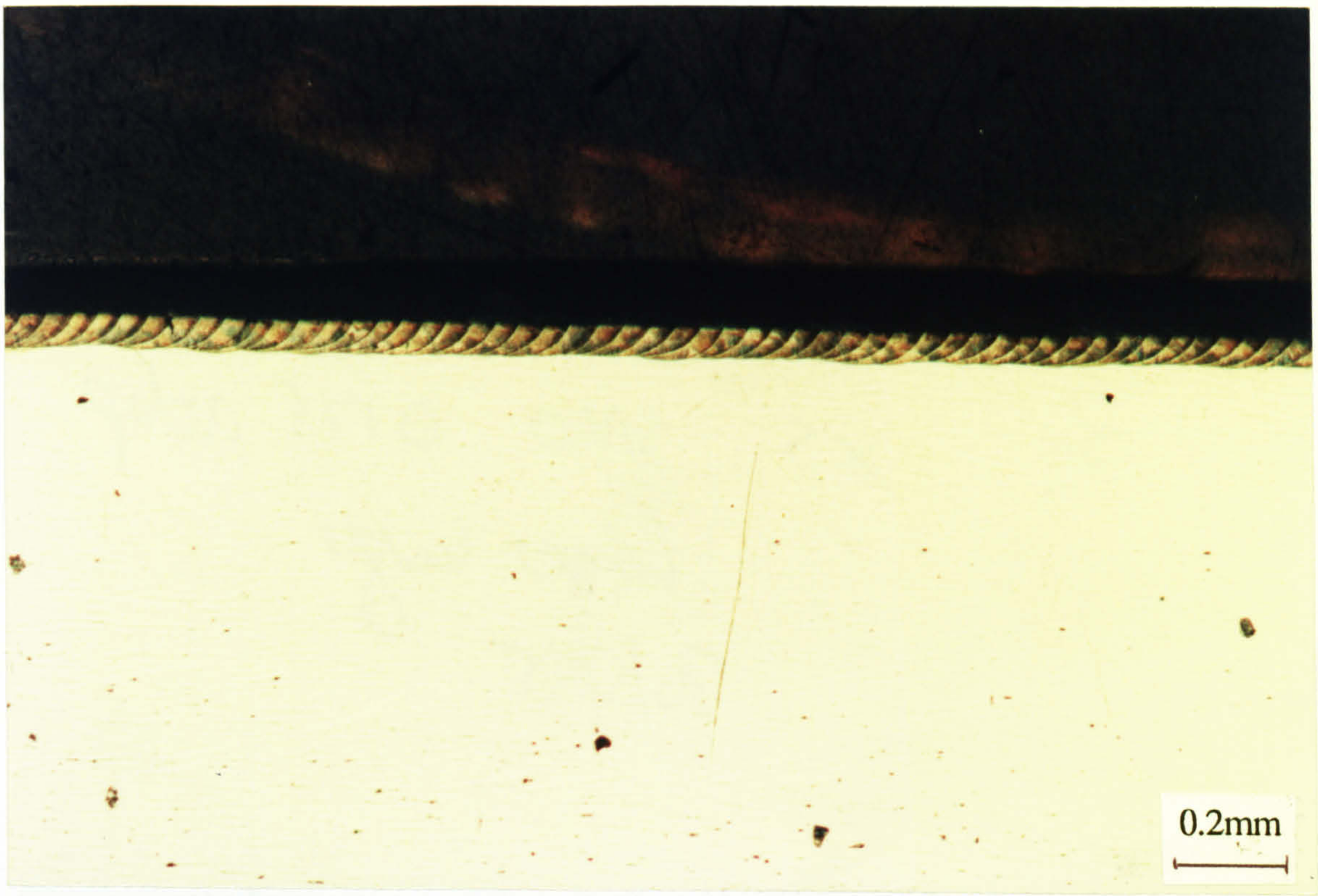

Fig. 6.43. Uniform thickness of laser treatment along one run on UNS S31254 on increasing the overlap

Fig. 6.44. Uniform thickness of laser treatment across several runs on UNS S31254 on increasing the overlap

The two duplex stainless steel showed a significant increase in hardness, in agreement with the results using the previous treatment parameters. There was no evidence of an intermediate layer between the substrate and the laser treated layer and as such there was no layer of significantly reduced hardness. However, as shown in Fig. 6.45, here was no such increase on the austenitic stainless steels, even though there was a considerable change in the surface microstructure.

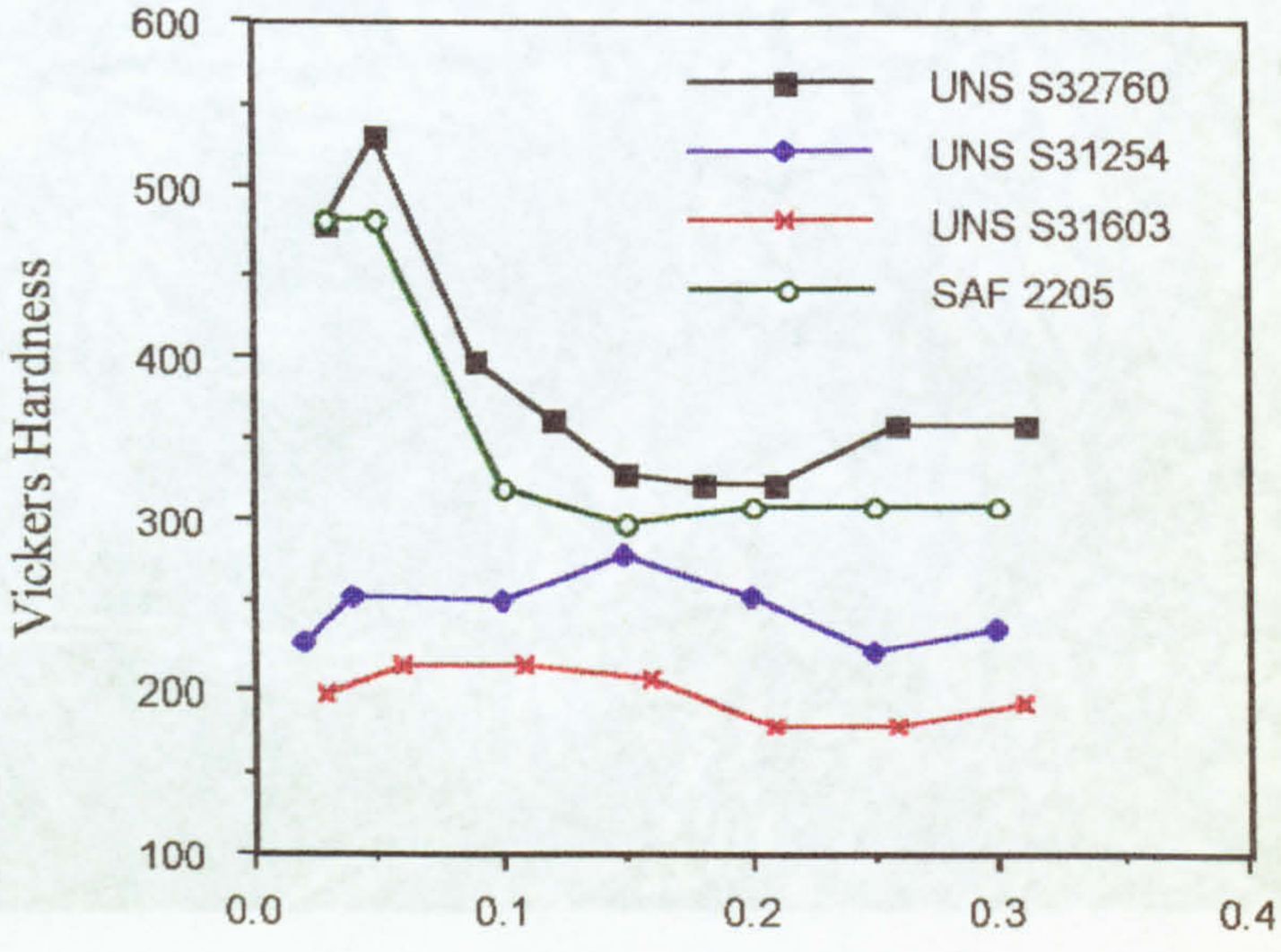

Fig. 6.45. Measured microhardnesses on the duplex and austenitic stainless steels after laser treatment in a nitrogen atmosphere

The microstructure of the duplex laser treated layer on both SAF 2205 and UNS S32760 differed significantly from a duplex stainless steel structure. Inside the laser layer there was a clear formation of precipitates or a secondary phase (Figs. 6.46 and 6.47). The laser treated surface of the austenitic stainless steels appeared in the form of rods or dendrites, forming a complex multi-directional array. The overall structure appeared to be porous since spaces between the individual dendrites were identified (Figs 6.48 and 6.49).

Since the shielding gas used was nitrogen, detection of nitrogen was attempted on the duplex stainless steels via two separate techniques : X-Ray Diffraction (XRD) and wavelength dispersive EPMA. The formation of nitrides in the laser layer could be used to explain the measured hardness increase. It is appreciated that there are inherent difficulties in detecting light elements using standard EPMA techniques but the equipment was capable of detecting elements down to the atomic weight of Boron. No nitrogen was detected by EPMA, even the residual content in the material which is

within the stated sensitivity of the equipment. Hence no conclusive information could be drawn from this.

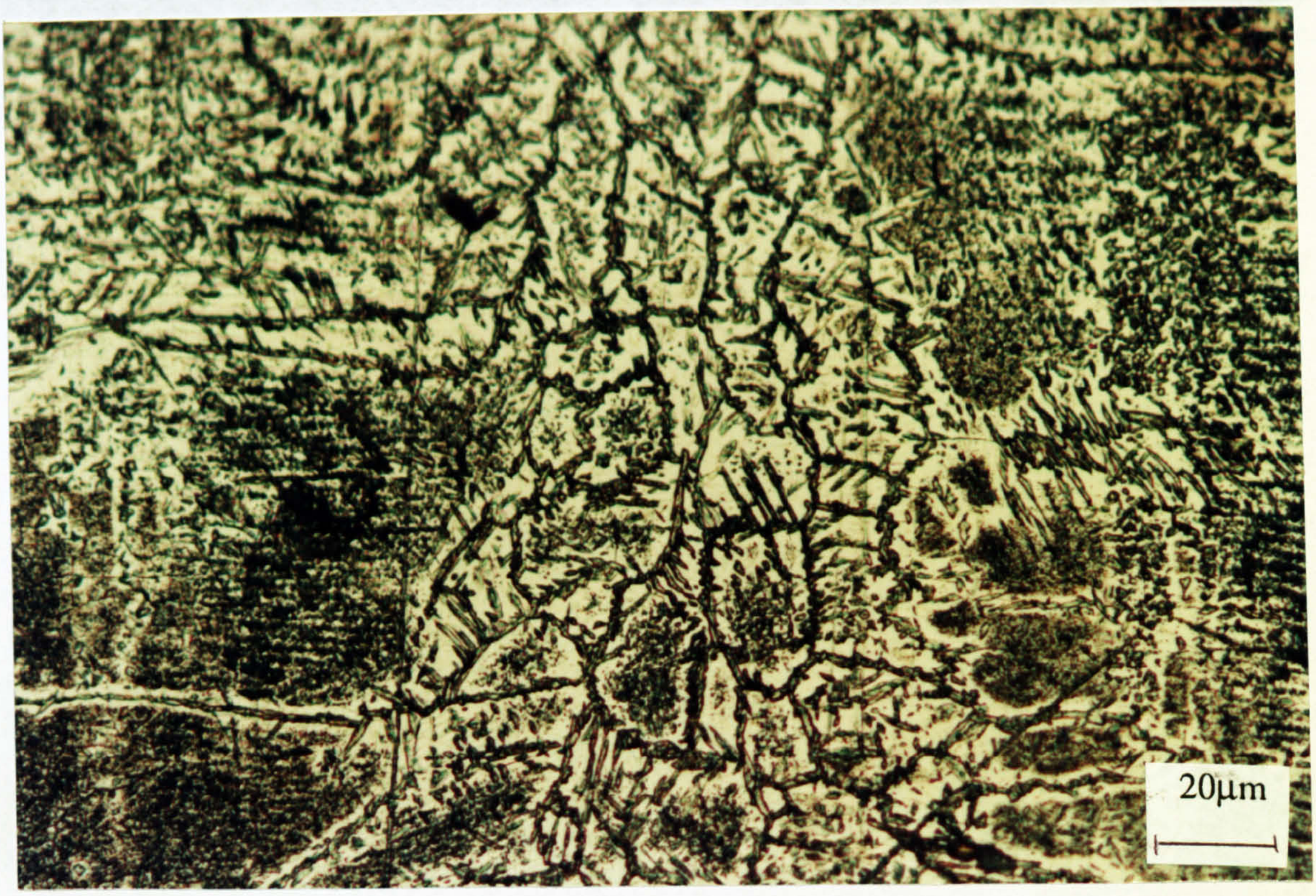

Fig. 6.46. Microstructure within the laser layer on UNS S32760

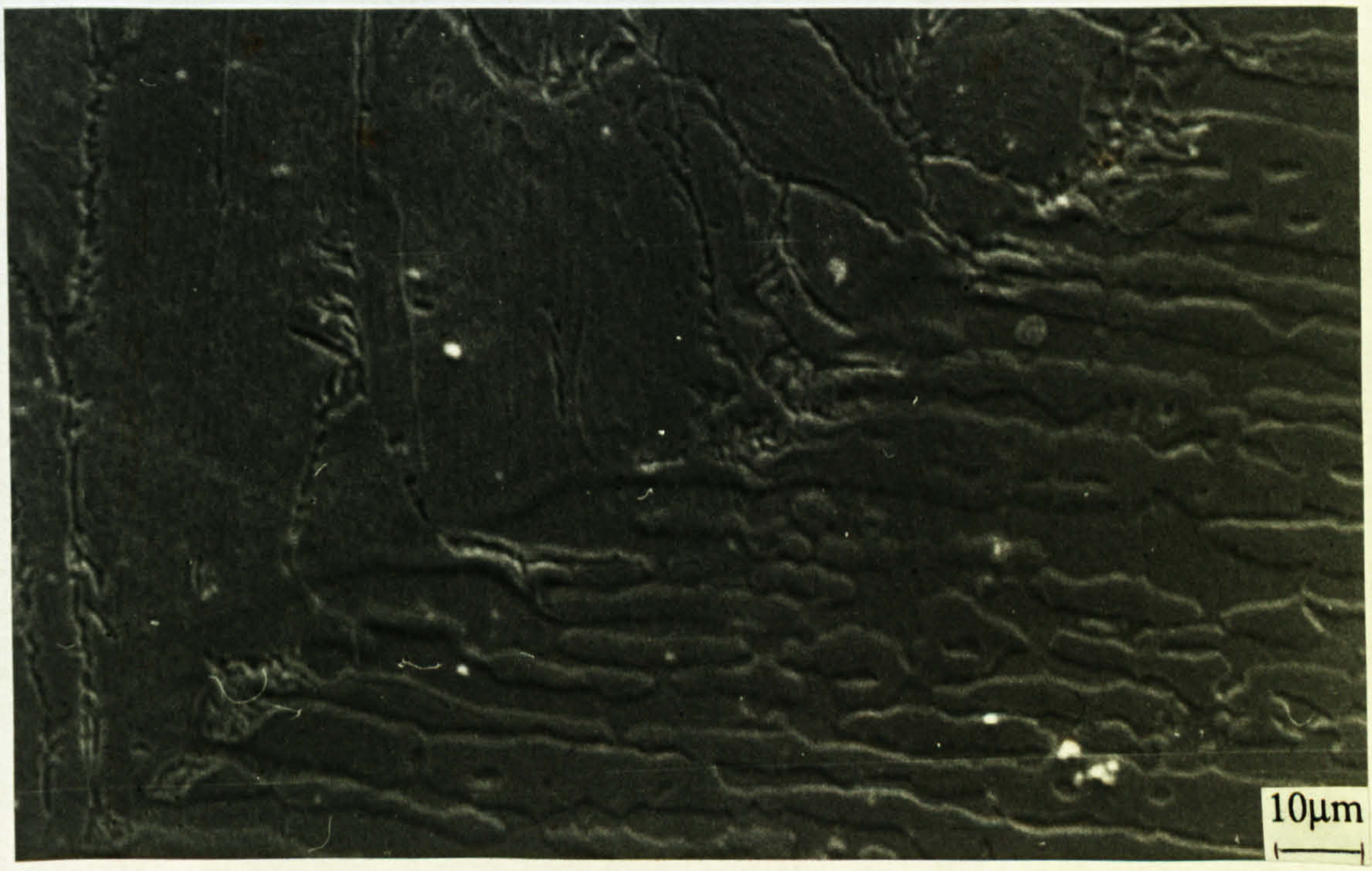

Fig. 6.47 Interface between duplex microstructure and the laser treated layer on SAF 2205

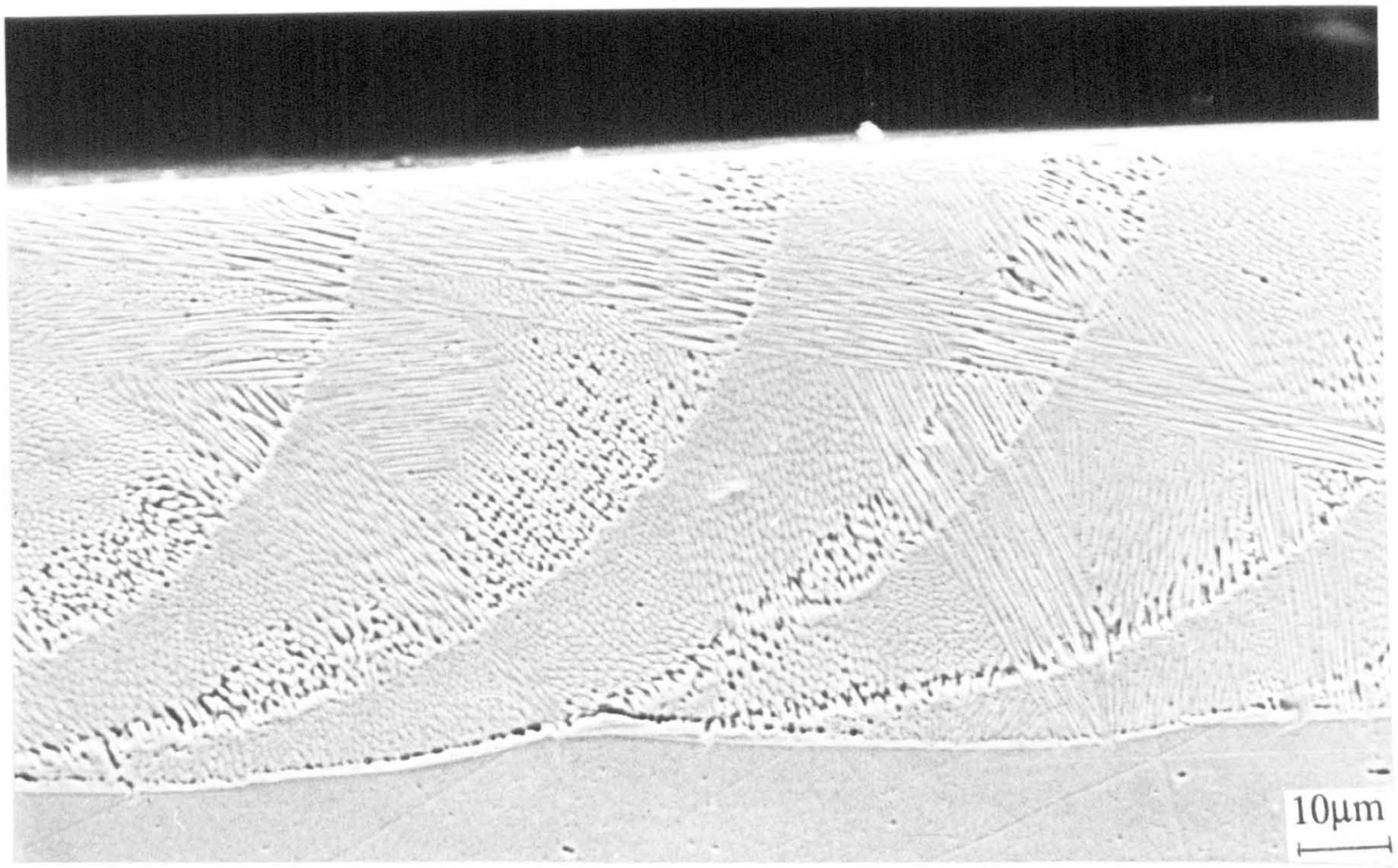

Fig. 6.48. Microstructure of the laser layer on UNS S31254

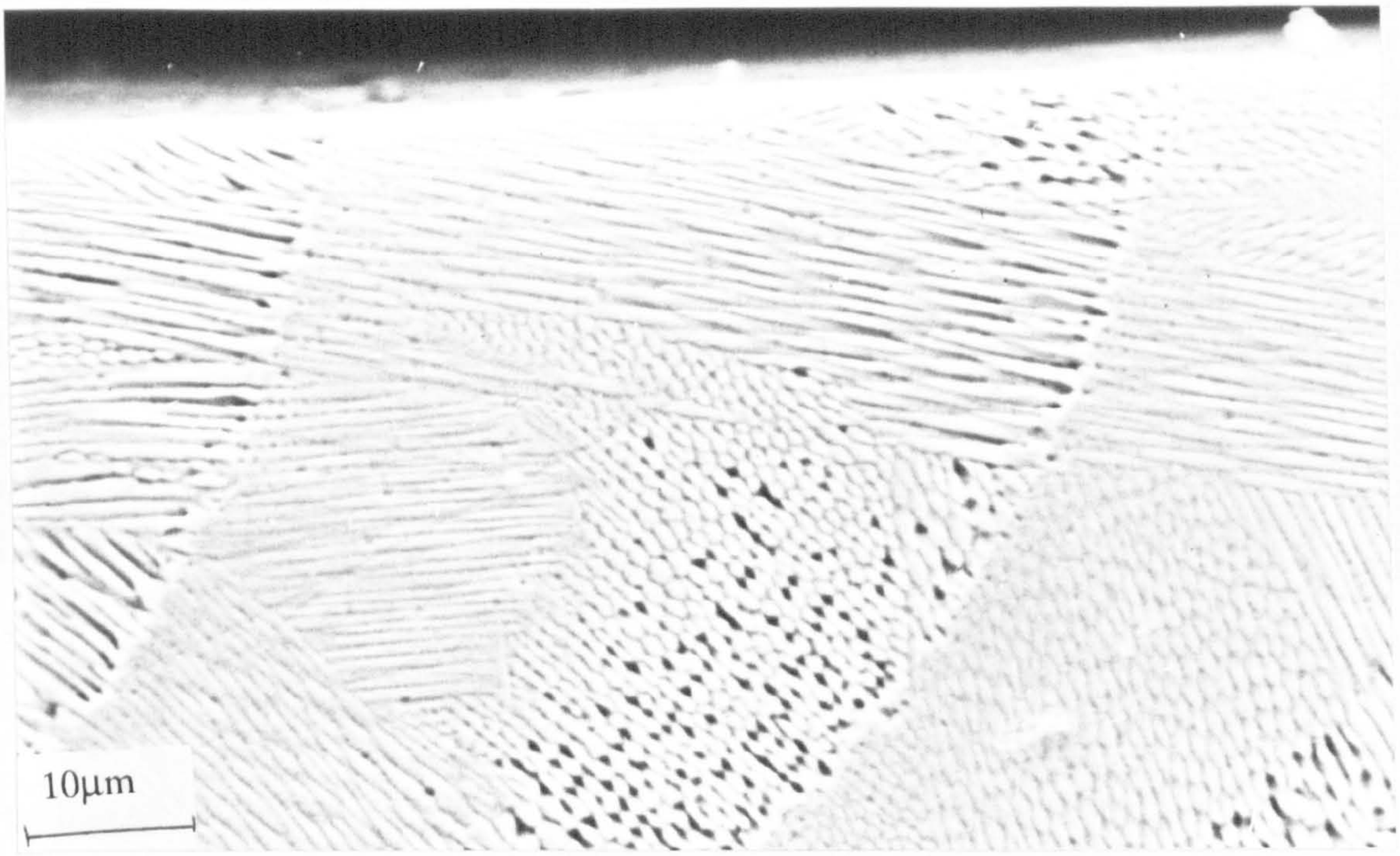

Fig. 6.49. Laser layer on UNS S31254 showing the porous structure

The effect of the shielding gas was confirmed when the same laser treatment parameters were used under an argon atmosphere. No increase in hardness was recorded, nor was the structure comparable to the N-treated specimen. In fact, the grain size was very small such that no clear structure could be seen.

XRD traces of powder samples taken from the laser treated surface and also directly from the surface yielded peaks at Bragg angles corresponding to Fe but gave no indication of the presence of nitrides in the form of either chromium or iron nitride and the nature of the precipitate could therefore not be elucidated by this method.

When etched in 40%KOH, the laser treated layer did not appear as brown and white regions corresponding to ferrite and austenite. Instead very little detail could be seen in the laser layer. Using dark field illumination, small acicular precipitates were shown to glow and were strongly suspected to be nitrides (Fig. 6.50)

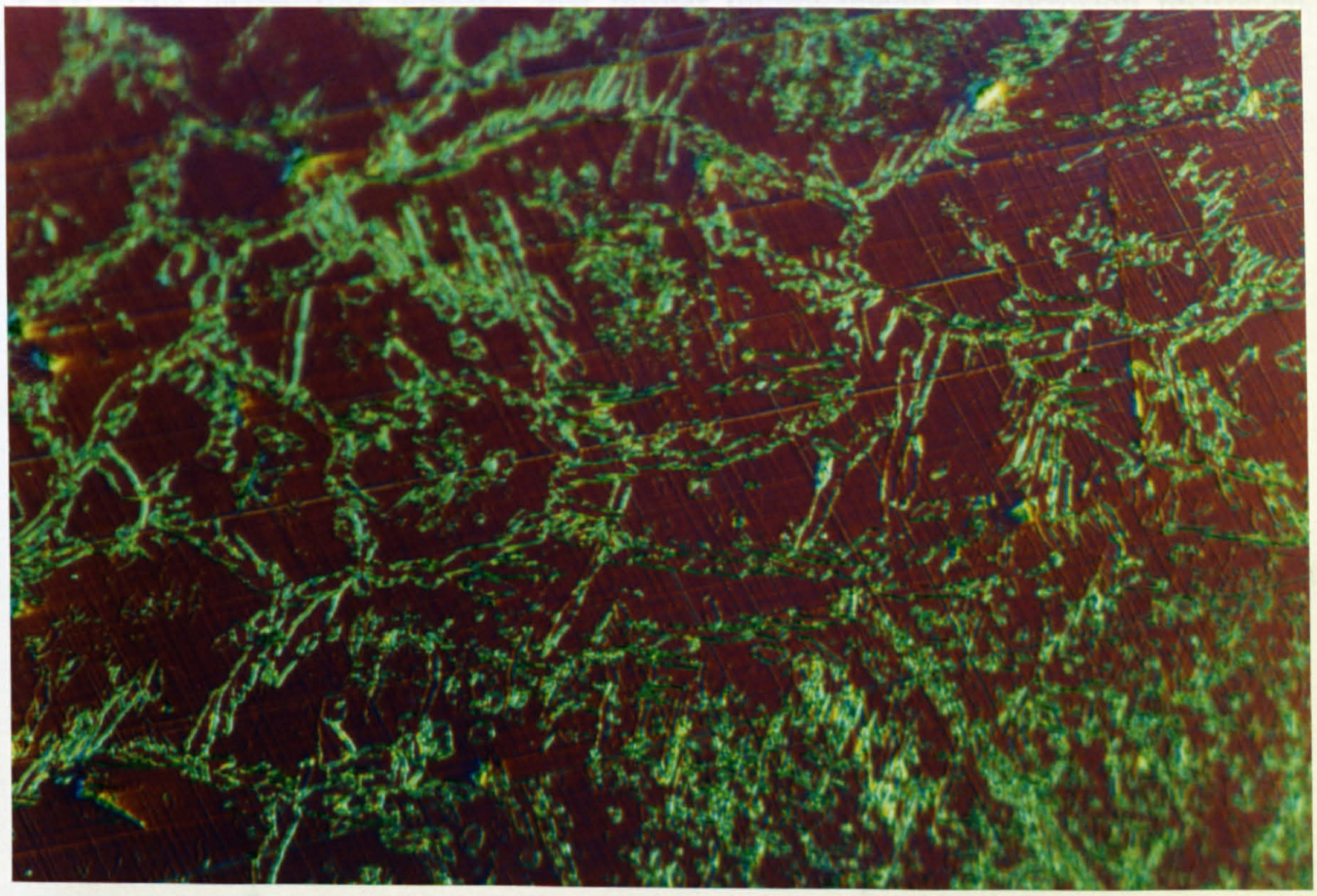

Fig. 6.50. Dark field illumination of the laser treated layer showing the fine precipitates. Etched electrolytically in 40%KOH

Corrosion Performance

Interesting results were obtained which showed that duplex stainless steels are amenable to an increase in resistance to corrosion initiation when irradiated under a nitrogen atmosphere. There is therefore a double benefit to be obtained in increased

microhardness and electrochemical corrosion resistance. SAF 2205 exhibited the most beneficial effect of the laser treatment in that, at 50°C, the E_b was substantially ennobled by approximately 400mV (Fig. 6.51). At 18°C, SAF 2205 already possesses good resistance to localised corrosion initiation and E_b is in the vicinity of +1000mV. This good resistance was maintained after laser treatment which was not the case when areas of the surface between the runs were left untreated. As with SAF 2205, the superduplex UNS S32760 retained it's passive potential range of in excess of 1200mV, in seawater at 18°C, after laser treatment. Where UNS S32760 is particularly susceptible to localised corrosion is at elevated temperature (shown in chapter 2) and the effect of laser treatment under nitrogen has been to increase E_b, and hence retard the corrosion initiation (Fig. 6.52). At elevated temperature, the current I_{max} on the laser treated surface exceeded that on the untreated UNS S32760. On examination, it was found that as under the previous parameters, the susceptible area of the surface was the line between the runs and in this case pitting corrosion had been sustained (Fig. 6.53). This observation indicates that further improvements in corrosion resistance could be attained by further reduction in overlap between runs. Alternatively, finishing of the surface by machining or grinding could possibly provide a more uniform surface and erradicate the potential sites for corrosion initiation.

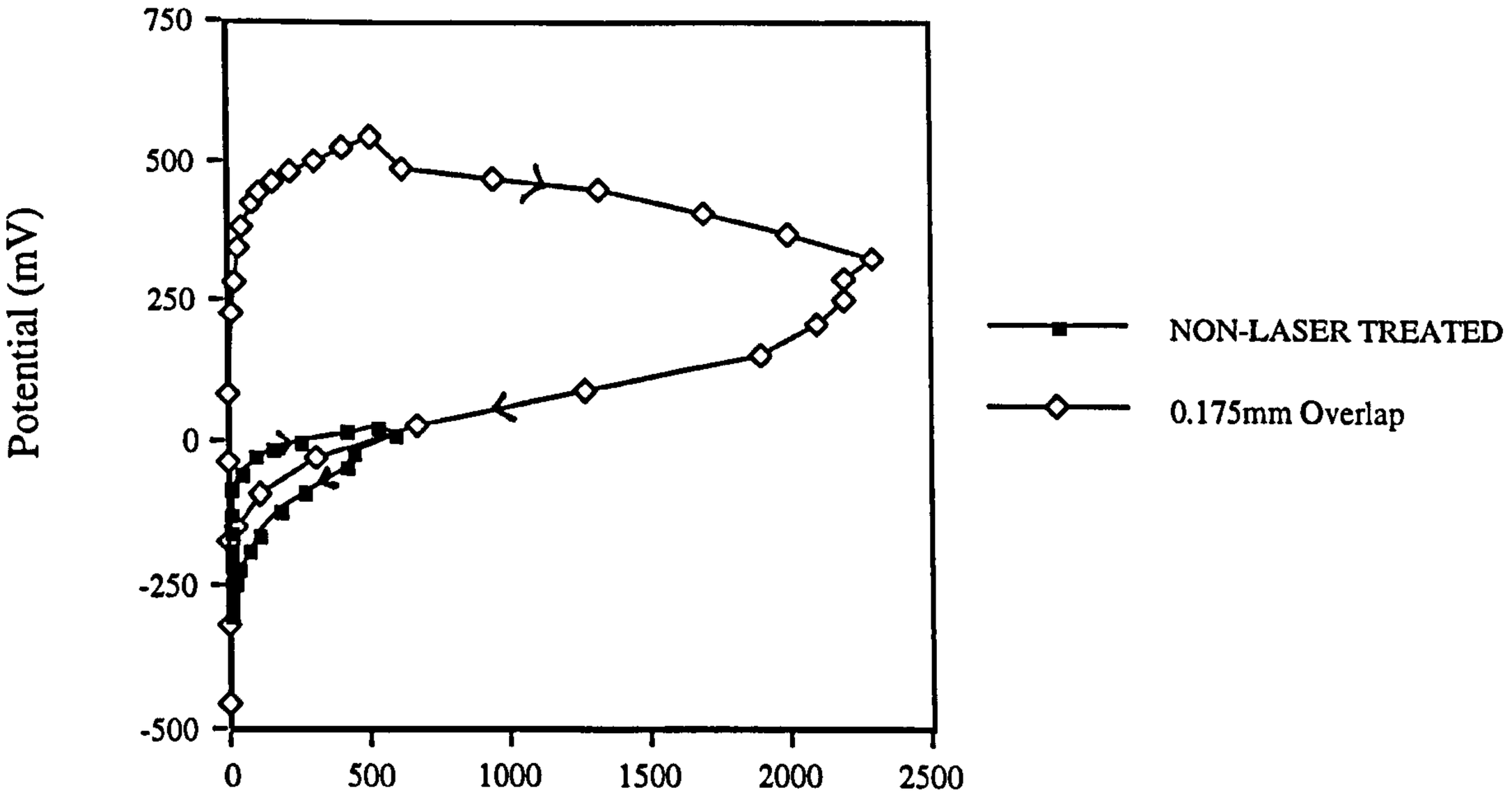

Fig. 6.51. Increased E_b on SAF 2205 after laser treatment in seawater at 50°C

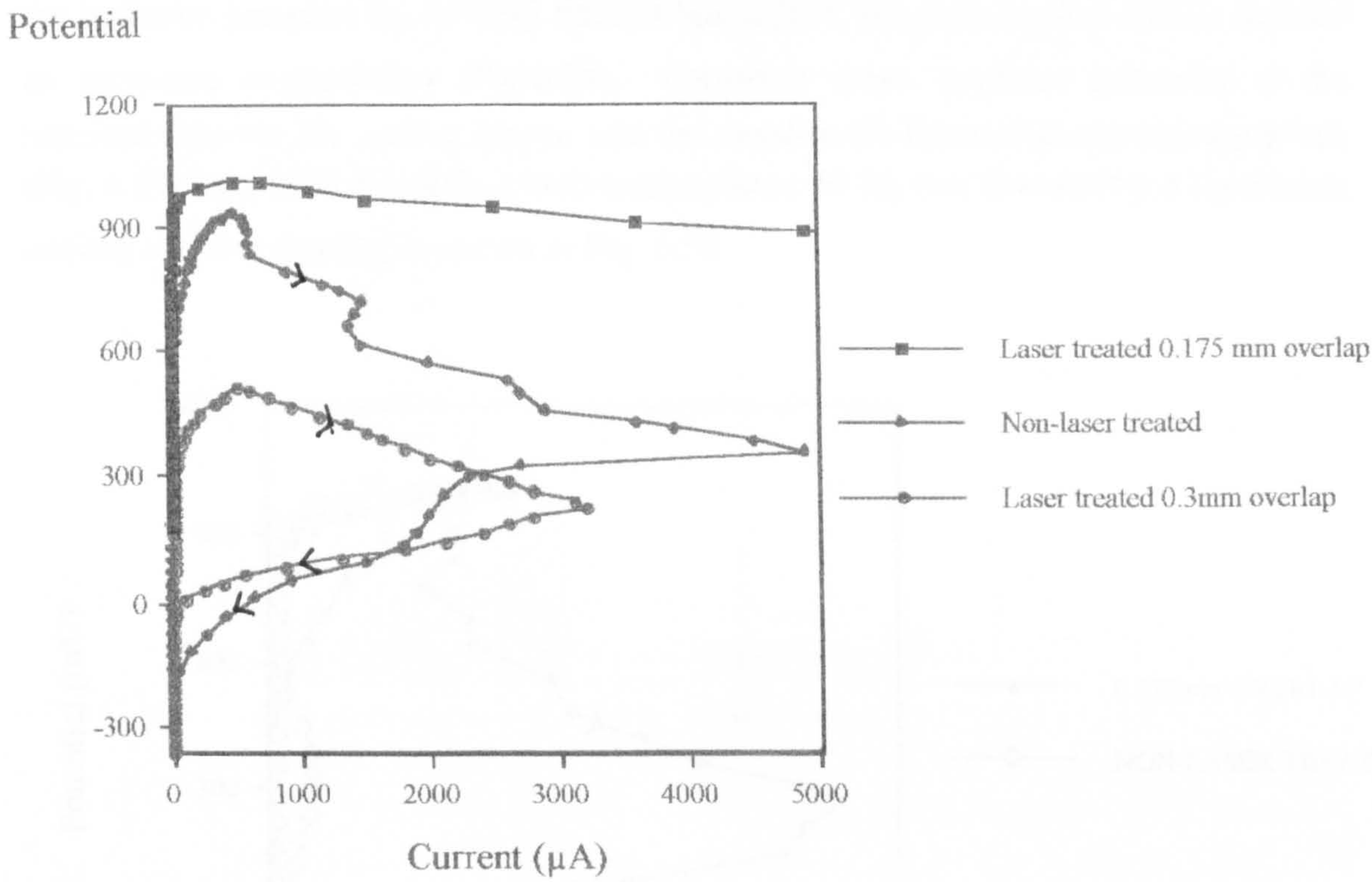

Fig. 6.52. Increased E_b on UNS S32760 after laser treatment in seawater at 50°C

Fig. 6.53. Pitting at the boundary between laser runs on UNS S32760 after anodic polarisation in seawater at 50°C

The benefits observed on duplex stainless steels manifested in increased hardness and corrosion resistance were not conferred to austenitic stainless steels when subjected to the same surface treatment. At ambient temperature, there was no detrimental effect on

the initiation potential E_b on UNS S31254 but at 50°C the laser treated surface showed an increased susceptibility (Fig.6.54). Corrosion attack occurred primarily at the interface between the sealing lacquer and the metal in the form of severe crevice attack (Fig. 6.55). On UNS S31603, at both temperatures the E_b was lowered by a significant amount on laser treating as shown in Fig. 6.56.

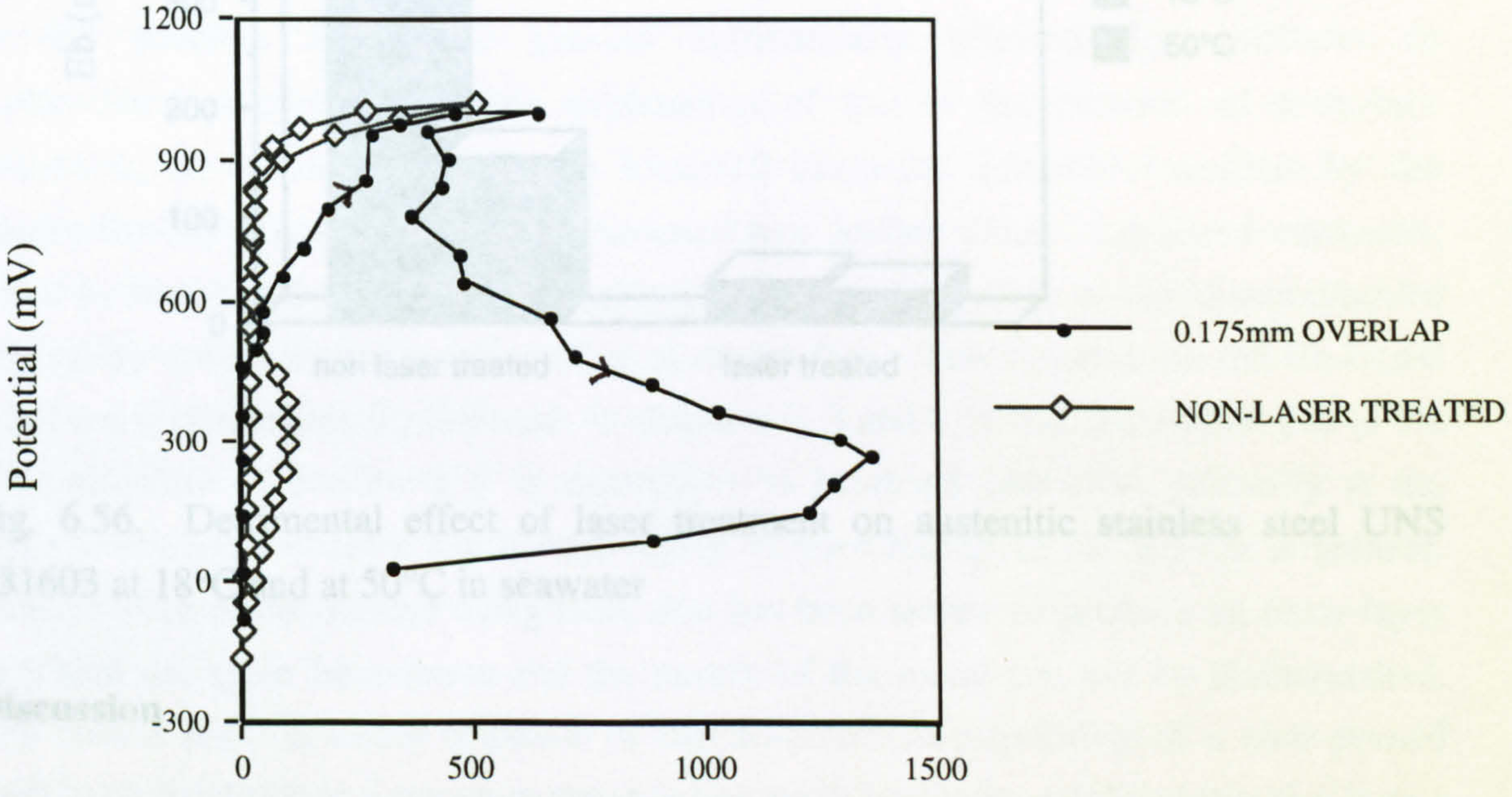

Fig. 6.54. Decreased resistance to the onset of localised corrosion in seawater at 50°C on laser treated UNS S31254

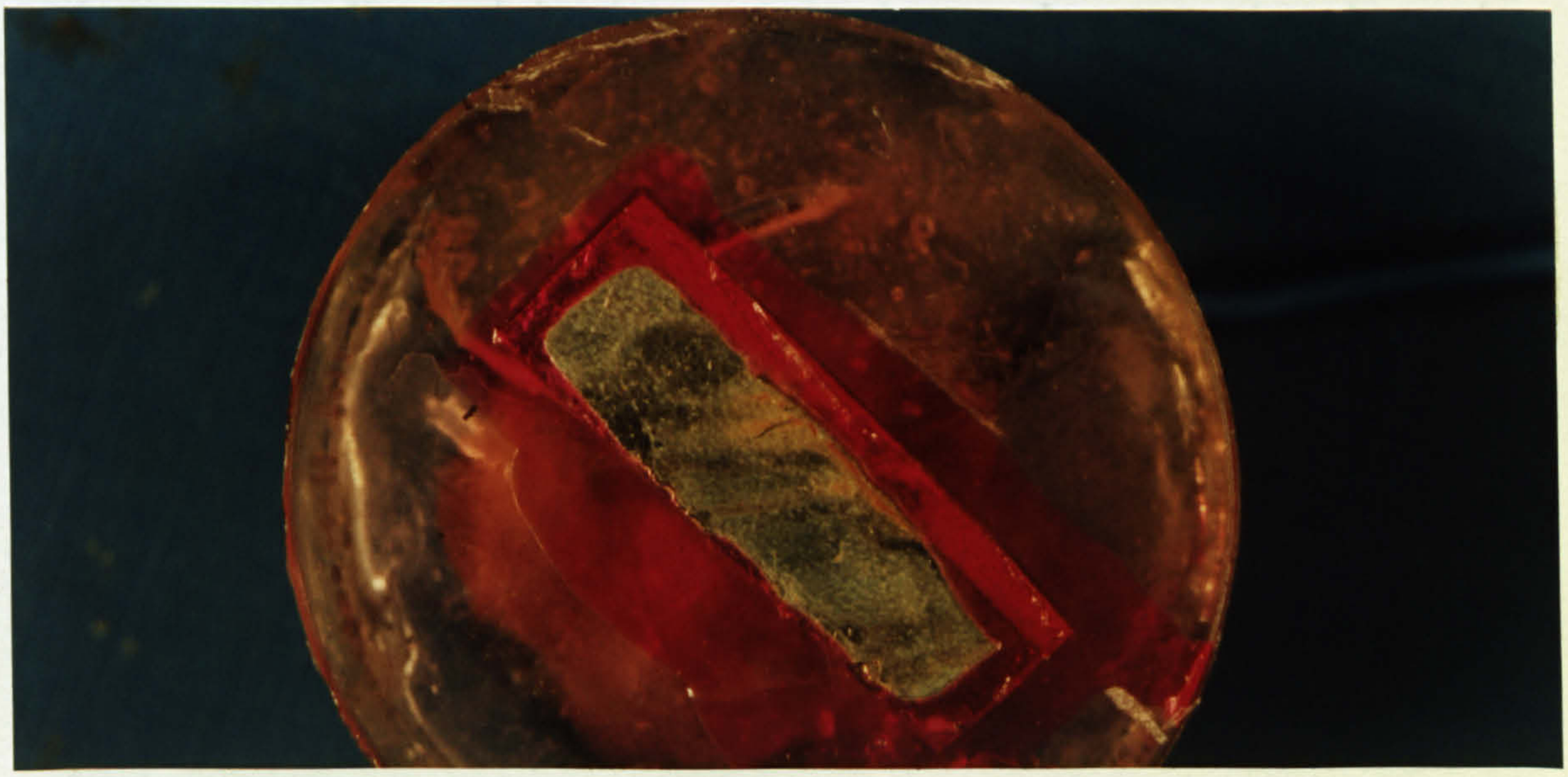

Fig. 6.55. Crevice attack at the metal/sealing lacquer boundary on UNS S31254 after anodic polarisation in seawater at 50°C

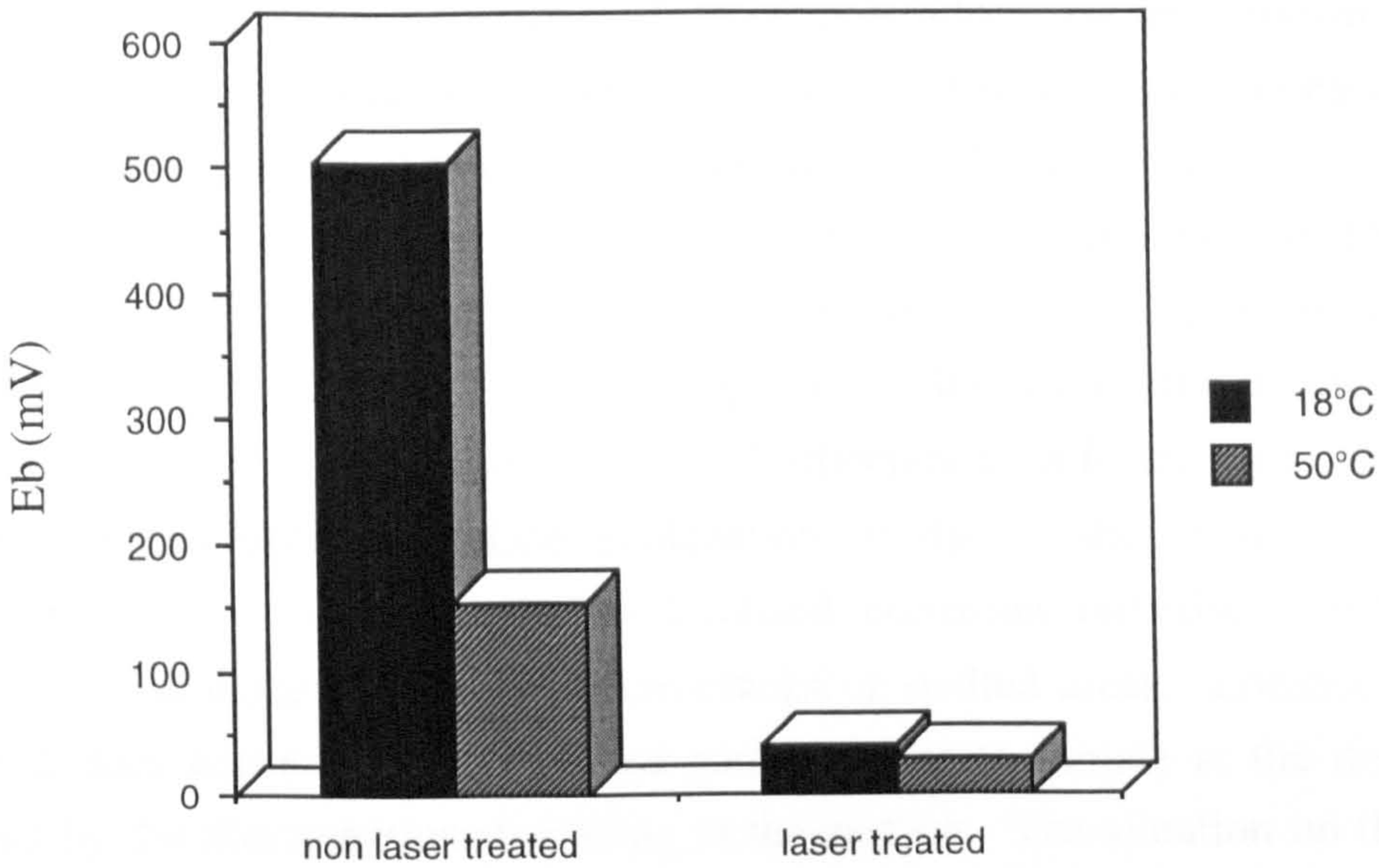

Fig. 6.56. Detrimental effect of laser treatment on austenitic stainless steel UNS S31603 at 18°C and at 50°C in seawater

Discussion

Within any engineering system, the principal aim is to optimise the properties of a material with respect to the potential application. Unavoidably, in every circumstance, there are interacting parameters which dictate to what extent it is possible to optimise each of the important material properties. For instance in an erosion-corrosion environment, as discussed in the previous chapter, there are clear interacting mechanical and electrochemical effects which makes effective material selection difficult. With respect to erosion-corrosion, the objectives are to produce a material resistant to mechanical wear but which can withstand corrosion effects. In much of recent research, the focus has been on surface engineering to optimise wear resistance of materials. There is currently a dearth of data relating to the performance of surface engineering options (whether it be thermal sprayed coatings, HVOF coatings, laser treated surface etc.) in a corrosion environment. There are two issues to be addressed, namely, how the component performs in an erosion environment in a corrosive aqueous fluid, the relevance of which is obvious. The second issue is the static corrosion behaviour, the importance of which is realised in components which can be subjected to periodic shutdown. This work has facilitated the determination of the relative corrosion resistance of two types of surface treatment in static seawater at ambient and elevated temperature and has also assessed the efficiency of shot-peening as a method of improving liquid erosion-corrosion resistance.

Application of shot-peening to the surface of three alloys has been shown to improve the material hardness in an outer layer, the thickness of which seems independent of the shot used. While it is realised that there are factors, other than hardness, which dictate the material performance in a wear environment, it is commonly assumed that an increase in hardness is one component which contributes to a enhanced wear resistance. Although beneficial to the mechanical properties of the surface, the results suggest that on the stainless steels, the process detrimentally affected the resistance to electrochemical corrosion. One explanation of this is the creation of a surface containing more sites amenable to localised corrosion initiation, verified by the observation of extensive surface micro-cracks or spalled areas. Localised corrosion, when it does occur on a shot peened surface tends to initiate at the discontinuities formed by the aforementioned spalling at the surface. The situation on the Co-based Stellite 6 is fundamentally different. In chapters 2, 3 and 4, it was shown that due to the microstructure of Stellite 6, it is susceptible to localised corrosion, primarily at the grain boundaries where a significant degree of partitioning of Cr and Co is present. Shot-peening of the surface using steel shot has been shown to produce an outer layer in which the grain boundaries and the matrix of the metal can not be distinguished. The results provide direct evidence of the decreased susceptibility of a shot-peened surface on Stellite 6 in contrast to the stainless steels and it is postulated that this is due to the removal of a surface in which a network of grain boundaries can provide sites for localised corrosion initiation.

There is some evidence in this study to suggest that there is benefit to be gained by shot-peening in the resitance to attack by liquid impingement. This is an important observation in two respects. Firstly shot-peening could therefore represent a viable means of reducing material degradation due to hydrodynamic effects. Secondly and from a more fundamental point of view, the increased resistance to attack by the shot-peened samples could relate directly to the findings in chapter 4 in which it was suggested that the appearance of a current increase during anodic polarisation at E_p, was due to pit intiation, possibly at sites of non metallic inclusions. It is postulated that the effect of the shot-peening is to pull out non-metallic inclusions and therefore reduce the number of susceptible sites for pit initiation. This would also link with the observation that a thick coloured film was not observed. Hence it can be seen that there are different mechanism of attack which prevail in static and liquid erosion conditions and it seems that there is a beneficial effect of shot-peening which can combat initiation mechanisms in liquid erosion.

Laser irradiation of a surface involves consideration of numerous parameters, each of which can alter the heat input rate, the degree of overlap and other critical process conditions. The assessment of laser treatment in this work has therefore relied on an iterative procedure of treatment, followed by examination of the treated surface and then feedback to the laser parameters. This work has shown that the localised corrosion initiation resistance of the duplex stainless steels (SAF 2205 and UNS S32760) can be improved, particularly at elevated temperature. The greatest effect was observed in the lower alloyed SAF 2205 which is in agreement with Jonsson et al. [26] regarding the effect of nitrogen in welding of duplex stainless steels. Quite apart from the significant hardness increase, this represents an important finding from both a practical and a fundamental aspect since it is at elevated temperature that the superduplex shows limitations in resisting localised (especially crevice) attack. An important aspect of surface treatment is the ability to reproduce a uniform surface layer and laser treatment using the laser parameters in this study has been shown to do this. The laser layer appeared relatively smooth which is important from the point of view of mechanical properties where a significantly roughened surface could introduce stress concentration points.

Consideration of the metallurgy and the compositional variations in the laser treated layer have focused on three possibilities. Increased hardness could be due to alloying with nitrogen which, on rapid cooling, precipitates a hard phase of perhaps CrN or could be primarily due to a metallurgical transformation on rapid cooling, independent of the shielding gas. Thirdly the nitrogen could be retained in solid solution.

The significant increase in hardness of the duplex stainless steel surfaces under a nitrogen atmosphere was not conferred to the duplex stainless steels under an argon atmosphere. Hence the notion that the effect of rapid solidification alone, independent of shielding gas, confers the increased hardness and corrosion resistance is not valid.

Welding in a nitrogen atmosphere has been studied by several workers [26,27] and in this work rapid cooling is considered to try and draw analogies to laser welding under a nitrogen shielding gas. The work by Fourie et al. [28] states that the Cr and Ni equivalent ratio (from the Schaeffler diagram) can give information on the solidification of the alloy. For $Cr_{eq}/Ni_{eq}>1.95$ (in the case for UNS S32760 $Cr_{eq}/Ni_{eq}=4.62$) the weldment solidifies as a fully ferritic single phase structure. The austenite is later formed in the solid state by a Widmanstatten mechanism.

Precipitation of Cr_2N has been reported during rapid cooling or quenching for annealing temperatures. Fine precipitates of Cr_2N have been detected on rapid cooling

of duplex stainless steels by Herbsleb and Schwaab [29]. Since nitrogen is less soluble in ferrite than in austenite, the Cr_2N formed preferentially in the ferrite phase. In our study, Cr_2N has not been detected and therefore another explanation for the precipitated phase is sought.

In the work by Fourie et al. [28], *laser* welding of SAF 2205 was shown to produce an almost fully ferritic structure with acicular austenite at the grain boundaries. No mention of N additions was made but the author did observe copious Cr_2N precipitation (the N coming from the alloy) within the ferrite grains with a precipitate free region near the reformed austenite. The microstructure of the laser layer in the present study was found to be similar to that reported by Fourie et al. (Fig. 6.46) where it can be seen that there appears to be a base ferritic structure with perhaps what could be austenite at the grain boundaries. Within the ferrite, fine precipitates are evident which, due to the evidence obtained during examination under dark field illumination, could perhaps be assumed to be the nitrides mentioned by Fourie et al.. However, since nitrides were not detected using XRD, the precise nature of these precipitates is not known. It could be that their fine nature renders them undetectable in the bulk analysis XRD trace.

Conclusions

This study has shown that although shot-peening of stainless steels could be useful for resisting attack due to wear processes, the structure of as-treated surface provides sites for localised corrosion initiation and as such, service in static conditions would be limited. However, some substantial benefits in corrosion performance, particularly in high velocity impinging seawater were observed, particularly at ambient temperature and this could possibly be due to removal of non-metallic inclusions.

Laser irradiation provides a complex system of metallurgical changes which within a duplex stainless steel have not been clearly elucidated. However, as a preliminary study, the results have shown that there is potential to increase the hardness and the localised corrosion initiation of even the superduplex stainless steels. There was some evidence to suggest that propagation might be enhanced. This could have been due to the form of the surface which because of it's increased roughness proved to be more amenable to corrosion propagation through formation of local electrochemical cells and, as such, refinement of the finishing process could be important.

Nevertheless the indication of increased resistance to initiation of corrosion, especially at elevated temperature where the duplex stainless steels are susceptible, is a promising

situation. Although no such improvements have been found on austenitic stainless steels in this work, there has been work reported on austenitic stainless steels which suggests that a post treatment of carefully polishing the surface has a beneficial effect on corrosion initiation on 304 stainless steel [30].

References

1. J. Huber, W. Marx, Production laser cutting, in *Applications of Lasers in Materials Processing*, ed. E. A. Metzbower, American Society For Metals, 1979

2. A. C. Lingenfelter, C. D. Anglin, C. N. Westrich, J. R. Murchie, Precision cutting and drilling with the Nd:YAG laser, in *The Changing Frontiers of Laser Materials Processing*, eds. C. M. Banas, G. L. Whitney, 1986

3. E. A. Metzbower, D. W. Moon, Mechanical properties, fracture toughnesses and microstructures of laser welds in high strength alloys, in *Applications of Lasers in Materials Processing*, ed. E. A. Metzbower, American Society For Metals, 1979

4. U. I. Chan, K. W. Casey, Laser welding of exhaust gas oxygen sensor, in *Applications of Lasers in Materials Processing*, ed. E. A. Metzbower, American Society For Metals, 1979

5. B. L. Mordike, H. W. Bergmann, *Rapidly solidified amorphous and crystalline alloys*, ed. Kear, Giessen, Cohen, North Holland Publishing Co. No. 8, 1982, 463

6. W. Gruhl, B. Grzemba, G. Ibe, W. Hiller, *Metal*, 1978, Vol.32, p549

7. S. Kosuge, M. Ono, K. Nakada, I. Watanabe, Advanced Laser materials processing, in *The Changing Frontiers of Laser Materials Processing*, eds. C. M. Banas, G. L. Whitney, 1986

8. B. L. Mordike, State of the art of surface engineering with high energy beams, in *Surface Engineering With High Energy Beams*, eds. A. P. Loureiro, O. Conde, L. Guerra-Rosa, R. Vilar, Trans Tech Publications, 1990

9. H. W. Bergmann, E. Schubert, Modification of metal surfaces by excimer laser treatment - state of the art, in *Surface Engineering With High Energy Beams*, eds. A. P. Loureiro, O. Conde, L. Guerra-Rosa, R. Vilar, Trans Tech Publications, 1990

10. W. M. Steen, Laser surface cladding, in *Laser Surface Treatment of Metals*, eds. C. W. Draper, P. Mazzoldi, NATO ASI series 1986

11. R. M. Macintyre, The use of lasers in Rolls-Royce, in *Laser Surface Treatment of Metals*, eds. C. W. Draper, P. Mazzoldi, NATO ASI series 1986

12. R. Padmanabhan, Improved wear resistance through laser alloying and transformation hardening, in *The Changing Frontiers of Laser Materials Processing*, eds. C. M. Banas, G. L. Whitney, 1986

13. L. N. Moskowitz, Application of HVOF thermal sprayng to solve corrosion problems in the petroleum industry, *Proc. of the Int. Thermal Spray Conference and Exposition*, Orlando, Florida, USA, 1992

14. F. Uchiyama, K. Tsukamoto, Y. Kaga, T. Okuo, S. Yamaoka, Y. Ohno, Y. Takahagi, T. Kamoshida, Ceramic coating technique using laser spray process for solid oxide fuel cells, *Proc. of the Int. Thermal Spray Conference and Exposition*, Orlando, Florida, USA, 1992

15. Z. D. Chen, D. R. F. West, W. M. Steen, Laser melting of alloy cast iron, in *The Changing Frontiers of Laser Materials Processing*, eds. C. M. Banas, G. L. Whitney, 1986

16. G. Coquerelle, J. L. Fachinetti, Friction and wear of laser treated aluminium-silicon alloys, in *The Changing Frontiers of Laser Materials Processing*, eds. C. M. Banas, G. L. Whitney, 1986

17. J. Folkes, D. R. F. West, W. M. Steen, Laser surface melting and alloying of titanium, in *Laser Surface Treatment of Metals*, eds. C. W. Draper, P. Mazzoldi, NATO ASI series 1986

18. A. J. Sedriks, Effects of alloy composition and microstructure on the passivity of stainless steels, *Corrosion*, Vol. 42, No. 7, 1986

19. M. Verneau, B. Bonnefois, Effects of alloying elements on the pitting corrosion resistance of duplex welded joints, *Proc. of Duplex Stainless Steels'91 Int. Conf.*, Vol II, eds. J. Charles, S. Bernhardsson, Bourgogne, 1991

20. B. de Bendetti, E. Angelini, P. Bianco, F. Rosalbino, Ion nitriding of duplex stainless steels : preferential dissolution phenomena in chloride media, *Proc. of Duplex Stainless Steels'91 Int. Conf.*, Vol II, eds. J. Charles, S. Bernhardsson, Bourgogne, 1991

21. Anon., Shot-peening applications, *Metal Improvement Company*, Inc, 7th Edition

22. D. McIntyre, J. Daly, How to prevent stress cracking in stainless steels I and II, *Chemical Engineering*, April 1980, McGraw-Hill

23. S. T. S. Al-Hassini, New advances in shot peening applications for surface treatment, *Presented at the Surface Engineering Conf.*, 1985

24. Anon, The application of controlled shot-peening for the prevention of stress corrosion cracking : A technical review, *Metal Improvement Co. Ltd*, 1991

25. R. Francis, *Private communication*

26. O. Jonsson, M. Liljas, P. Stenvall, The role of nitrogen in longitudinal welding of tubing in duplex stainless steels, *Avesta Corrosion Management*, No. 2, 1994

27. R. Doyen, R. Niset, Welding of duplex and superduplex stainless steels, *Proc. of Duplex Stainless Steels'91 Int. Conf.*, Vol II, eds. J. Charles, S. Bernhardsson, Bourgogne, 1991

28. J. W. Fourie, F. P. A. Robinson, Literature review on the influence of weld heat inputs o the mechanical and corroson proerties of duplex stainless steels, *Journal of the South African Institute of Mining and Metallurgy*, March, 1990, p59

29. G. Herbsleb, P. Schwaab, in R. A. Lula (ed), *Duplex Stainless Steels*, ASM, 1983, p15-40

30. J. Stewart, D. E. Williams, The initiation of pitting corrosion on austenitic stainless steel : on the role and importance of sulphide inclusions, *Corros. Sci.*, Vol. 33, No. 3, p457-474, 1992

Chapter 7

A Study of the Effect of Marine Aerobic Bacteria and Anaerobic Sulphate-Reducing Bacteria on the Corrosion of Duplex and Austenitic Stainless Steels

Introduction

This chapter investigate the effects of the anaerobic sulphate-reducing bacteria (SRB) and an aerobic strain of bacteria, *vibrio alginolyticus,* on the corrosion behaviour of high grade alloys.

In the SRB study, the materials were immersed in an active culture of SRB for varying periods from 1 hour to six months. After different periods of immersion and at different H_2S partial pressures, polarisation curves and potentiostatic tests were performed.

A culture of aerobic bacteria, commonly found in marine environments, was sustained and the electrochemical behaviour of the alloys monitored after different immersion times. The main aim of the work was to ascertain whether this strain of bacteria could significantly affect the electrochemical characteristics of the material and if so, whether bacterial settlement could be the most important factor in causing E_{corr} ennoblement in marine systems (see Chapter 8).

Literature Review

Microbiologically Induced Corrosion (MIC) has been used to explain engineering failures since the beginning of the century. However, the processes which link the metabolic behaviour of biological organisms to electrochemical corrosion phenomena have increasingly received attention over the past two decades to an extent associated with expanding activities in North Sea oil and gas production.

One class of organism which has been the focus of numerous studies is the Sulphate-Reducing Bacteria (SRB). The activity of SRB is inferred by the presence of hydrogen sulphide (H_2S) formed as a bacterial metabolic product. As early as 1910, when a high sulphur content was discovered in corrosion products from the Catsgill aqueduct in the USA [1] SRB were identified as the aggressive species, prevalent in anaerobic clays or wet soils. Although they are commonly referred to as anaerobes, problems due to their proliferation are by no means restricted to large scale anaerobic areas. On a much smaller scale, in the photic zone of the sea, encrustation due to macrofouling can lead to local areas of depleted oxygen and in such areas there is increased tendency for SRB activity.

Most acute problems due to SRB proliferation are encountered when large scale 'souring' of oil reservoirs occurs. Instances of reservoir souring have increased steadily in the last 10 years, as reported by Hill et al. [2] in the Alaskan Kupanik field. Concentrations of H_2S of up to 200ppm have frequently been recorded but Edyvean recently reported H_2S levels in excess of 2000ppm resulting from microbial activity [3].

Sulphate-Reducing Bacteria Characteristics

Sulphate-reducing bacteria are unique in that they perform dissimilatory reduction often called 'sulphate-reduction'. The process is often described as a type of anaerobic respiration [4]. SRB constitute an assemblage of morphologically different types of anaerobic bacteria, which all have the ability to reduce sulphate to sulphide.

Exclusion of oxygen alone is insufficient to initiate and sustain growth of an SRB population. They require an environment of low redox potential (-100mV SHE or lower) which in the laboratory is normally achieved by addition of sodium thioglycolate as a reducing agent [4]. A source of nutrient must be available (normally lactate based) to sustain growth.

SRB have been located in sub-zero temperature environments in Antarctica and in contrast, thermophilic strains can grow at temperatures in excess of 80°C and survive temperatures of 150°C and pressures of up to 150psi for over 24 hours [5]. They are found in fresh and saline environments and have been isolated at depths of 71m in clay and 500m in the sea [6].

Enumeration of SRB has been performed by dilution techniques (RP-38, described later), by 'agar deep' methods [7] and by various other culture techniques. Biochemical assays, not requiring culture growth, utilise measurement of constitutive properties such as adenosine-5 phosphosulphate (APS) reductase, hydrogenase and DNA [8] and have been proposed as accurate sampling methods for field analysis. Rosser and Hamilton [9] concluded that sulphate-reduction by SRB could not accurately be measured in the bulk phase and developed a ^{35}S sulphate radiorespirometric assay to measure SRB metabolic activity which has subsequently been adapted to enable the technique to be used to study biofilms on the surface of coupons in potentially corrosive environments [10]. To date, the results from this technique have not been compared to culture techniques.

Mechanisms of SRB corrosion

The concept of corrosion by SRB was introduced by Beijerinck in 1895 [11] but the first attempt at providing a detailed explanation of it's electrochemical mechanisms was made by Von Wolzogen Kuhr and Van Der Vlugt [12] in 1934 associated with underground corrosion [4]. The cathodic depolarisation theory (CDT), which was an advance of the work by Stephenson and Strickland in 1931, proposed a mechanism by which the SRB could remove adsorbed hydrogen from cathodic iron and subsequently oxidation of the cathodic hydrogen would occur [4]. The complete system of reactions to explain, in electrochemical terms, SRB corrosion of ferrous materials was developed as

anodic reaction	$Fe \rightarrow Fe^{2+} + 2e$
cathodic reaction	$8H^{+} + 8e \rightarrow 8H$
bacterial cathodic depolarisation	$SO_4^{2-} + 8H \rightarrow S^{2-} + 4H_2O$
corrosion product	$Fe^{2+} + S^{2-} \rightarrow FeS$ $2Fe^{2+} + 6OH^{-} \rightarrow 3Fe(OH)_2$

The enzyme hydrogenase was stated to stimulate the removal and oxidation of atomic hydrogen but since then, several workers have discredited this. Krasna [13] stated that the hydrogenase enzyme can catalyse heterolytic cleavage of H_2. However, in order for the enzyme to assist in the removal of atomic hydrogen in SRB corrosion, it would have to cleave H_2 by a homolytic reaction which is not possible.

An alternative CDT now stands, based on the early theory of Von Wolzogen Kuhr and Van der Vlugt and proposed by Costello [14] in which the alternative cathodic reaction,

$$H_2S + e \rightarrow HS^- + 1/2H_2$$

is depolarised by the removal of *molecular* hydrogen via hydrogenase. In this work, the action of iron/iron sulphide galvanic cells was also ascribed to give weight to the findings of King and Miller [15] in which higher corrosion rates were recorded in hydrogenase and sulphide than in hydrogenase alone. Galvanic couples set up in an active SRB environment between an FeS cathode and a bare iron electrode were studied by Daumos et al. [16]. Whereas this theory to date is still valid for iron and carbon steels, the current knowledge on the MIC of passive materials is more ambiguous.

On stainless steels, accelerated localised attack began to be reported in the early 1970's [6,17-20]. In the last few years, there have been incidences of premature failure of heat exchangers in Middle East refineries, which, when examined, were attributed to MIC [21-23].

Intermediate compounds formed by the SRB have been the focus of work by several groups who proposed that reduced sulphur compounds (probably S^o_{ads}) [24,25] are the aggressive species in a sulphate reducing system [26-29]. Microbial pitting on stainless steel in conditions where SRB are active has been correlated to the premature pitting observed in the pulp and paper process where thiosulphate ions are produced as a result of reactions with the paper brightening agent [30]. Pit initiation can occur at much lower potentials in the presence of thiosulphate and it is the concentration ratio of sulphate/thiosulphate which defines the aggressiveness of a solution with respect to pitting. Newman et al. showed [31] that corrosion of stainless steels can not occur in conventional SRB media even at high chloride content due to the low corrosion potential of <-500mV SCE. An effective oxygen cathode is required to drive the

corrosion cell with typically an anaerobic deposit acting as the anode. S^{o}_{ads} catalyses anodic dissolution at the anode and hinders passivation in the pit or crevice vicinity.

Gouda et al. [32] studied the electrochemical corrosion characteristics of stainless steels in SRB and after 26 days did not find any trace of corrosion on samples freely corroding. However, anodic polarisation yielded what was defined as an active-passive transition which was associated with pitting attack under bacterial colonies. The active-passive regime was found to emerge after an initial incubation period and the extent of the rise in current was dependent on material type and immersion time. Moreno et al. [33] found a similar active-passive transition but with a double loop, the first of which is supposed to be due to the formation of a ferrous sulphide film and the second to electro-oxidation of the film to elemental sulphur. The source of the ferrous sulphide film is not clear (whether due to pitting or general corrosion etc.) but the extent of the loop was determined by the level of sulphide.

The literature consistently returns to the theory that elemental sulphur, S^{o}, is often the causative species in MIC. Saschal performed experiments [34] in dissolved elemental sulphur and concluded that there is creation of a concentration cell analogous to the oxygen concentration cell where sulphur acts as the cathode reactant in a reaction of the form

$$\mathbf{S^{o} + H_2O + 2e \rightarrow HS^{-} + OH^{-}.}$$

In this work, the origin of the S^{o} was not confirmed but consideration of more recent work [24,25,32,33] may provide that solution.

Aerobic Marine Bacteria

The action of biofilm formation in marine systems has been widely studied (see chapter 8), however, it is still not well understood what the causative organism is in the ennoblement of the free corrosion potential as observed by several authors. Indeed it has not been established beyond doubt that the over riding factor is biological. The most widely accepted hypothesis is that of a cathodic depolarisation caused by bacterial settlement and in this study the effect of a strain of aerobic bacteria has been investigated.

Experimental Methods

Corrosion monitoring techniques used were electrochemically based, this chapter as a whole involving a series of DC-potentiodynamic (anodic and cathodic), potentiostatic and galvanic-type tests performed in the presence of an active culture of SRB and aerobic, *vibrio alginolyticus*. To complement the electrochemistry, light and scanning-electron microscopy were used on both polarised and freely-corroded specimens to determine the types of attack which predominated and the extent of attack after different immersion periods up to 6 months. In addition, Electron Probe Micro-Analysis (EPMA) enabled chemical analysis to be undertaken on local regions of the corroded samples. Integration of the microscopical observations into the findings from electrochemical monitoring enables mechanisms of attack to be linked to electrochemical features and hence the accelerated test methods can be utilised to predict the types and extent of attack which will prevail in real-time situations. Control tests in sterile seawater (aerated and deaerated) and in nutrient-only seawater were also conducted. In both long and short term experiments, duplicate specimens were used. The exposed surface area of all specimens was $1cm^2$.

This chapter concentrated on the behaviour of five stainless steels and some tests were performed on commercially pure titanium for comparative purposes. The stainless steels included the two duplex (SAF 2205 and 25Cr duplex), one superduplex (UNS S32760), standard austenitic (UNS S31603) and superausteinitc (UNS S31254) previously described in chapter 1.

SRB Culture

Laboratory conditions were set up to initiate and sustain growth of an SRB culture on a batch culture basis. The medium used in the culturing process was a minimal-iron, lactate-based variation of Postgates' B medium [35], the contents of which are given in Table 7.1 below.

ASCORBIC ACID	0.1g
THIOGLYCOLLIC ACID	0.4g
FERROUS SULPHATE HEPTAHYDRATE	0.004g
POTASSIUM DIHYDROGEN PHOSPHATE	0.5g
AMMONIUM CHLORIDE	1g
YEAST EXTRACT	1g
SODIUM LACTATE	14ml
ARTIFICIAL SEAWATER	1 Litre

Table 7.1. Composition of culturing medium based on Postgate's C.

Once the nutrients were prepared in synthetic seawater, the pH was adjusted to 7.5 using 0.1 M NaOH. The medium was then autoclaved at 121°C for 15 minutes. Checks were made on the pH of the cooled medium which was always between 7.4 and 7.5.

The SRB were cultured from a source of estuarine mud, extracted from the Clyde Estuary (at a depth of 17-20m) on the West Coast of Scotland. 30 ml of the culture medium was then added to a litre of synthetic seawater and, after inoculation with 25-30ml of the core sediment, the solution was deaerated using Nitrogen gas.

The vessel shown in Fig. 7.1 contained several metal specimens (10mm x 10mm) set in a non-conducting resin. Electrical wires attached to the rear emerged through bungs coated with pyragallol (an oxygen scavenger) and were sealed with silicone grease. The saturated calomel reference electrode (SCE) was connected via a salt bridge and a platinum auxiliary electrode was inserted prior to electrochemical tests.

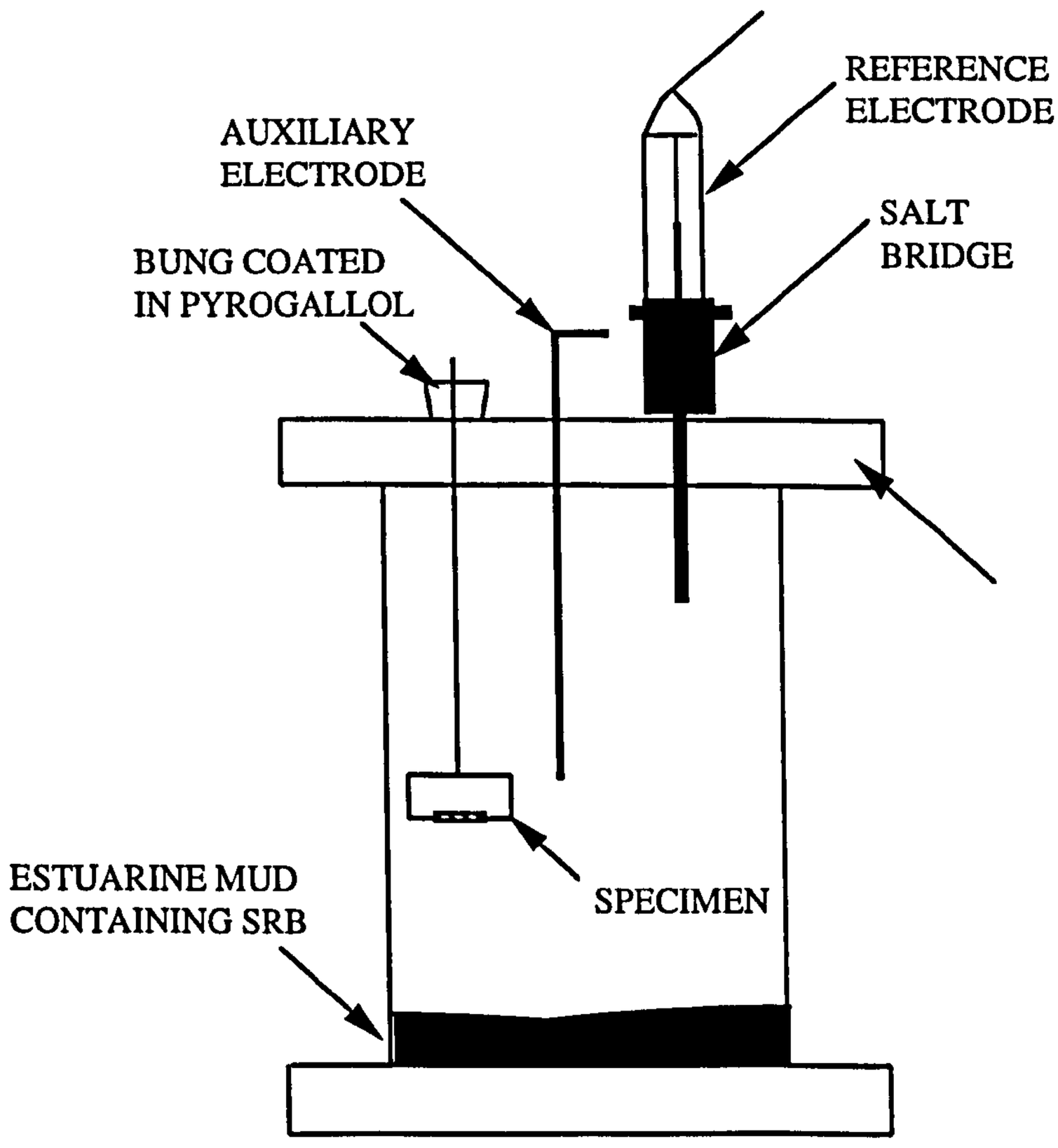

Fig. 7.1. Vessel used for anaerobic SRB culturing

Periodic analyses of the Hydrogen Sulphide content in each solution (via a gas detection unit) were made. The partial pressure of H_2S was measured in the gas above the solution and, via Henry's Law [36], the concentration of dissolved H_2S in the solution was obtained. H_2S levels quoted are in all cases as dissolved H_2S in solution. Control of the H_2S levels was virtually impossible and it is appreciated that, as such, the conditions in each vessel varied. However, regular monitoring of the conditions (H_2S levels, pH and redox potential) allowed interpretation of the electrochemistry and comparisons of the corrosion behaviour of each material to be made.

Growth of the SRB culture was accompanied by a characteristic blackening of the solution due to the precipitation of FeS. This was followed by a rapid increase in the measured partial pressure of H_2S, pH_2S, inferring that sulphate-reduction was proceeding.

Aerobic Bacteria - *Vibrio Alginolyticus*

The pure strain of *Vibrio Alginolyticus* was supplied by NCIMB, Aberdeen. The ampoule was opened in sterile conditions and several 30ml cultures of the bacteria were initiated in a medium consisting of the following ingredients:

Beef Extract	10mg
Peptone	10mg
Filtered (0.2μm), aged seawater	750ml
Distilled water	250ml.

The ingredients were dissolved and boiled for 3-5 minutes. After cooling the mixture was filtered and the pH was checked and read 7.8. The solution was then autoclaved at 121°C for 15 minutes prior to adding the bacteria.

Results - Sulphate-Reducing Bacteria

Trends in free-corrosion potential

Over the longest immersion period of six months, negative shifts in the free corrosion potential (E_{corr}) were recorded on all materials once an active culture of SRB was achieved and H_2S was detected. During the period in which the H_2S started to rise (i.e. first two days), the E_{corr} of the materials varied but tended to be more negative than in SRB-free seawater. During the six month period, the dissolved H_2S level and the E_{corr} of the materials varied as in Fig. 7.2.

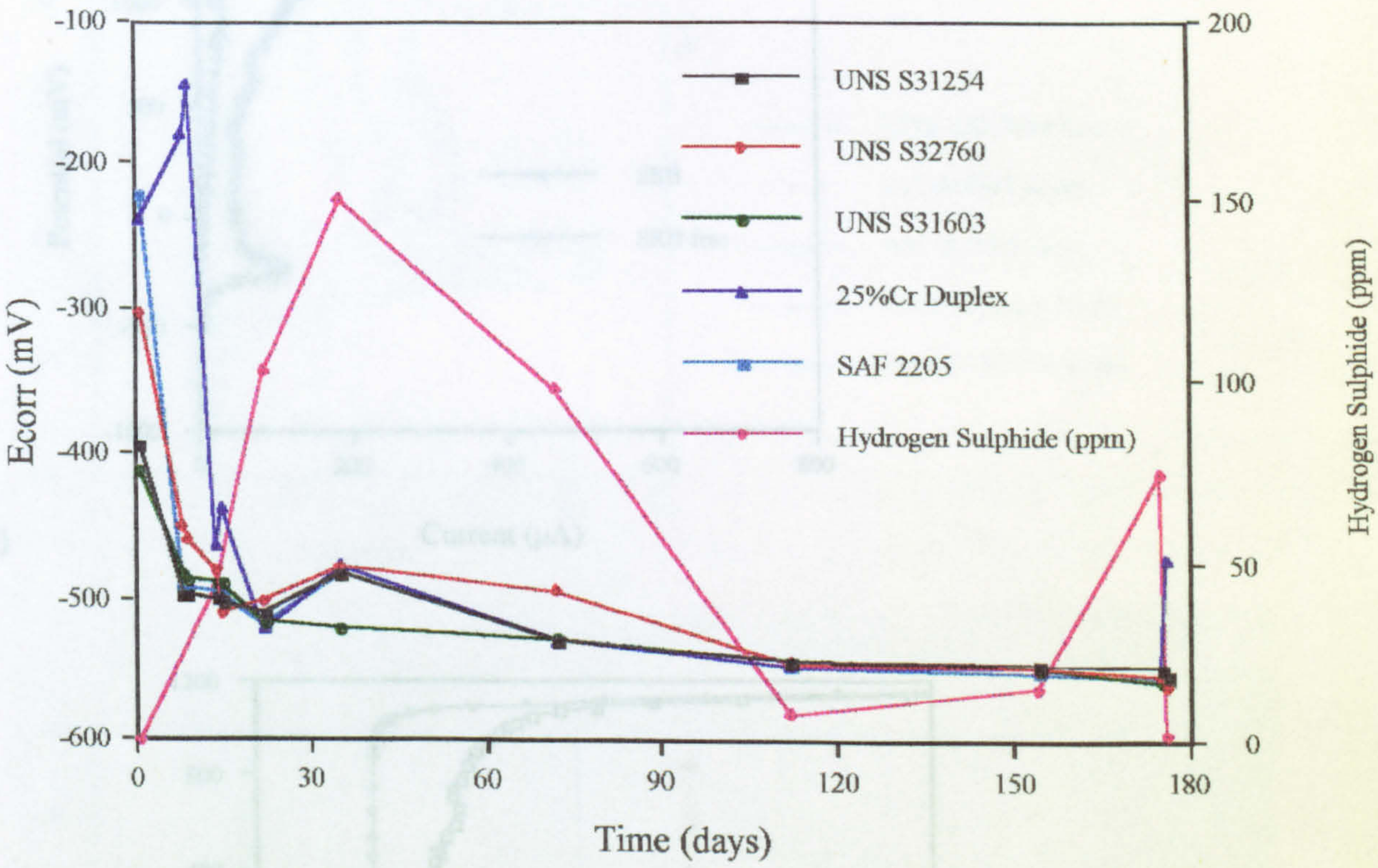

Fig. 7.2. Trends in free corrosion potential and hydrogen sulphide level over longest immersion period in SRB

Similar trends were observed on the specimens over shorter immersion periods, showing no correlation between the E_{corr} and the level of sulphide after the initial shift in the active direction.

Anodic polarisation after <1 week immersion

After even a relatively short immersion period of 4 hours, there was a significant difference in the anodic polarisation curve on all of the alloys tested, as can be seen in

Fig.7.3a on SAF 2205. In contrast to the anodic polarisation in 'SRB-free' seawater, the potential range above E_{corr} where low passive currents are normally observed was very short and was followed by a transient rise in current (to a value denoted by I_a, shown after 4 days on UNS S32760 in Fig. 7.3b). This feature was also documented by Moreno et al. [33] On further increasing the potential from that corresponding to I_a, the monitored current was observed to fall to a stable value (I_S) which was, however, several times greater than the passive currents (I_p) recorded in SRB-free seawater and could have been due to the oxidation of H_2S.

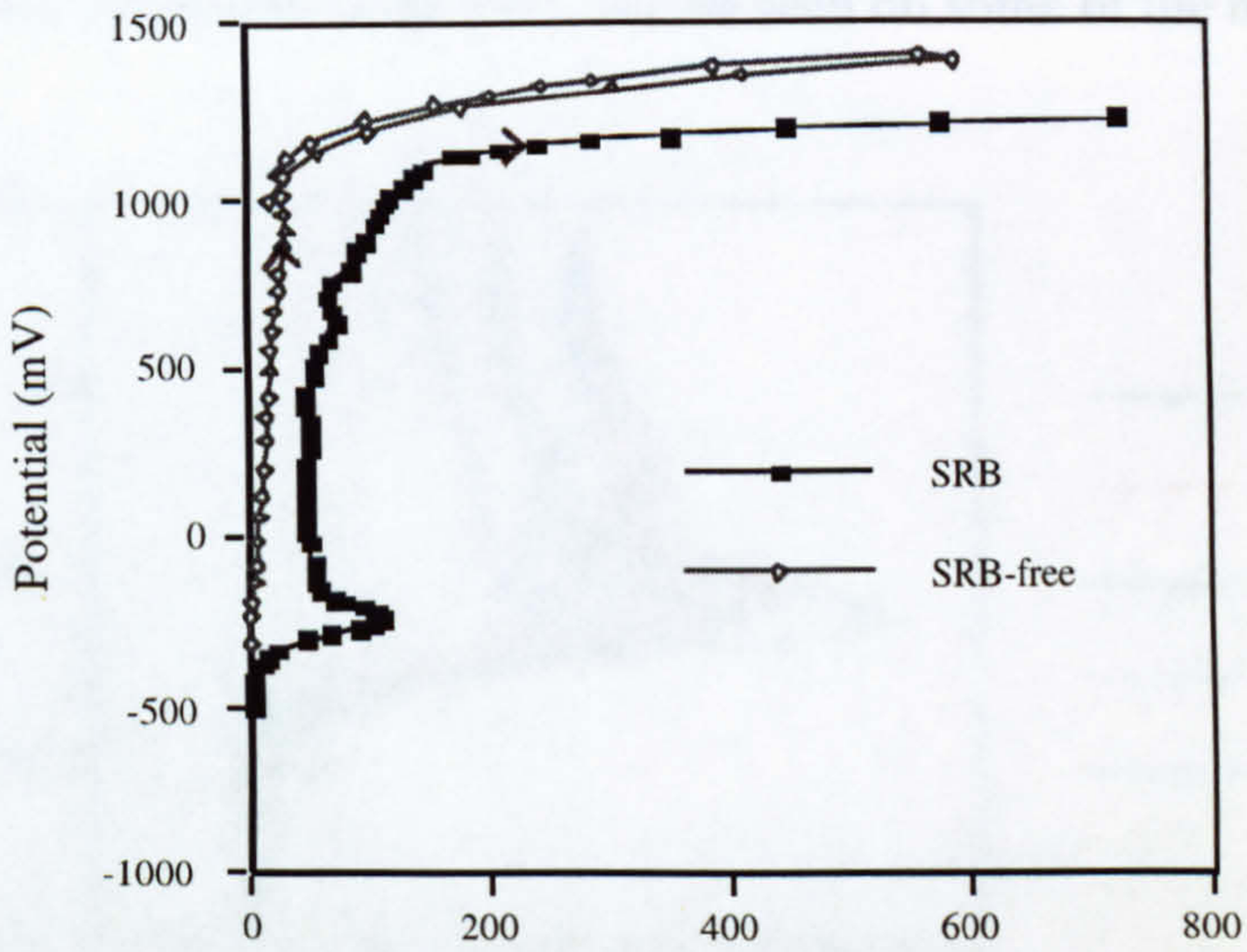

(a)

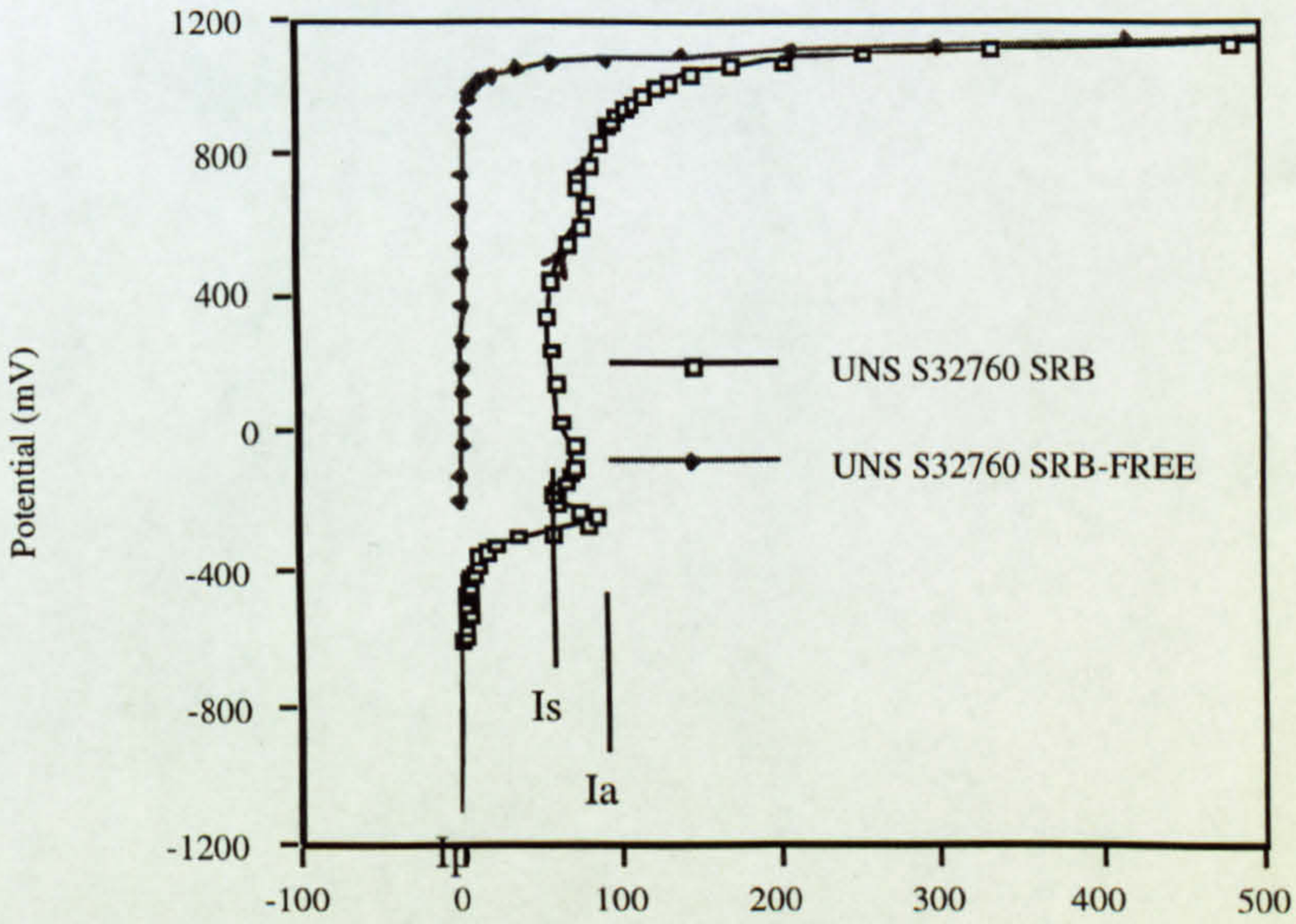

(b)

Fig. 7.3. Anodic polarisation contrasting characteristics on (a) SAF 2205 after 4 hours immersion and (b) on UNS S32760 after 4 days immersion in SRB-containing seawater and SRB-free seawater

Anodic polarisation on specimens immersed for <1 week showed a different magnitude of I_a on each material. At the time of polarisation the H_2S level was constant for each material at 15-20ppm in the solution. During the immersion period the H_2S concentration had ranged from 0-45ppm. An additional test on titanium in SRB for the same length of time also exhibited a current transient but to a much lower current transient peak of 5μA, compared to the 70-110μA recorded on the stainless steel specimens. Figure 7.4a shows the progression of the anodic polarisation scan to reach the peak of the current transient on all the stainless steels and Fig. 7.4b shows the corresponding graph obtained on titanium. A second small increase in current, as described by Moreno et al. [33], can be seen on some of the materials.

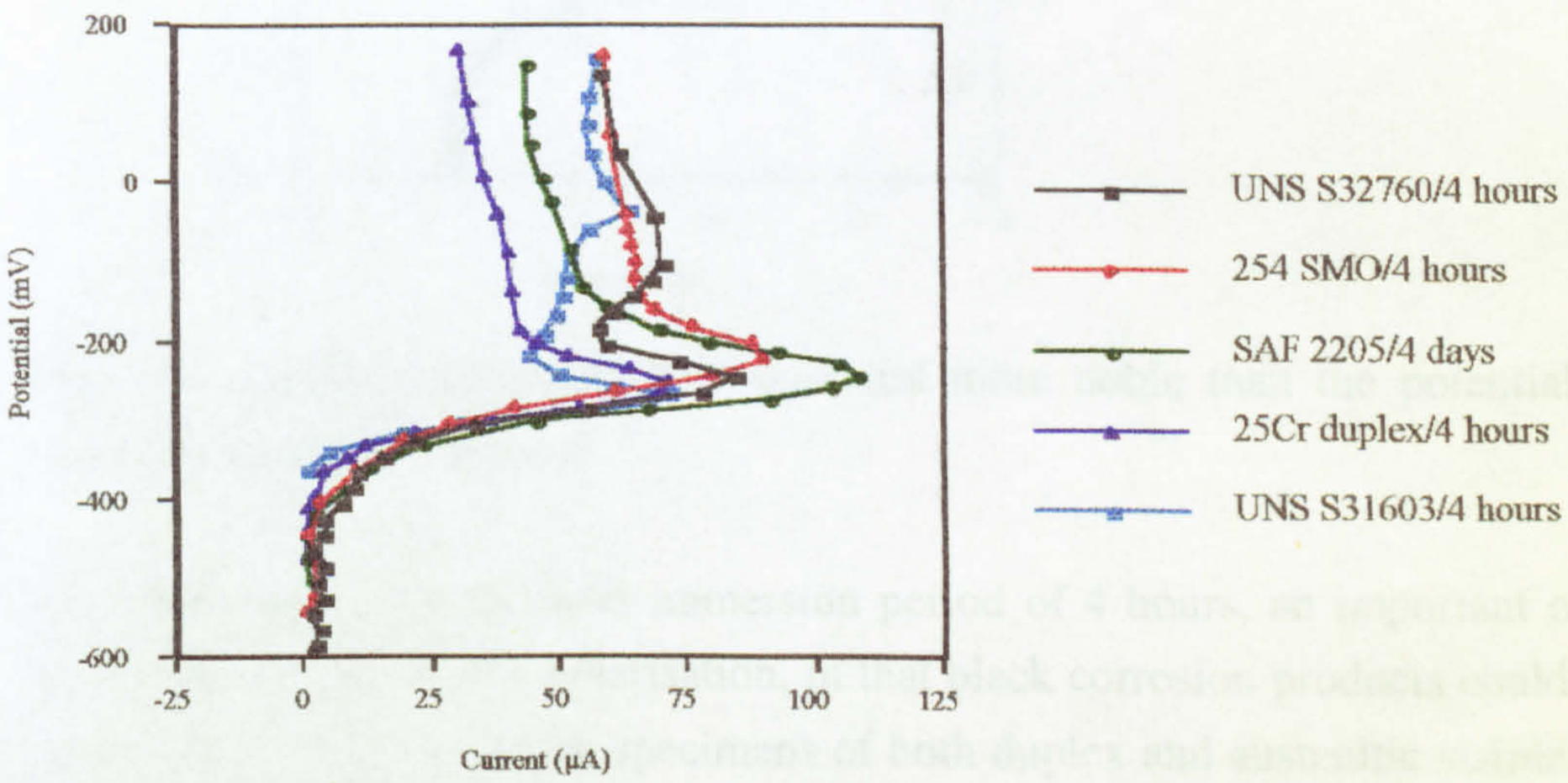

(a)

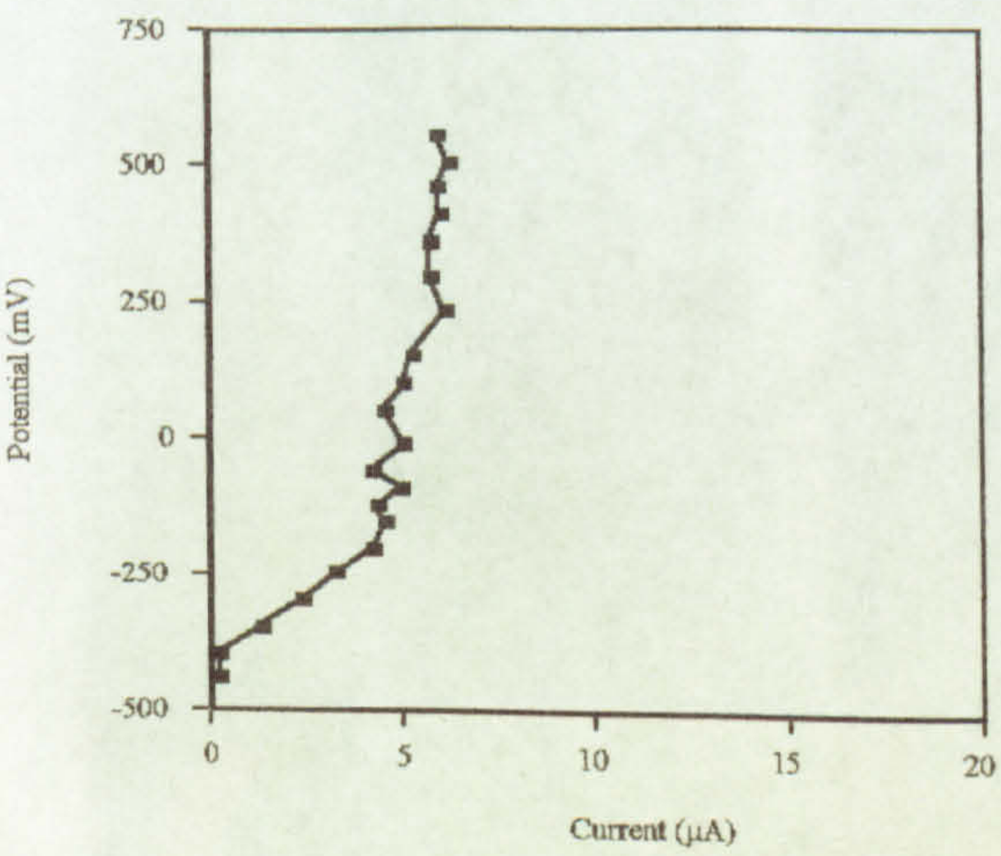

(b)

Fig. 7.4 (a) Progression of current up to the current transient peak, I_a, on the stainless steels and (b) much lower current at a similar transient peak on titanium after 4 days immersion in SRB

Control experiments in seawater containing the culturing medium and no SRB were carried out and on anodic polarisation, no current transient loop was observed (Fig. 7.5). The free corrosion potential was noticeably more noble than in the presence of the SRB.

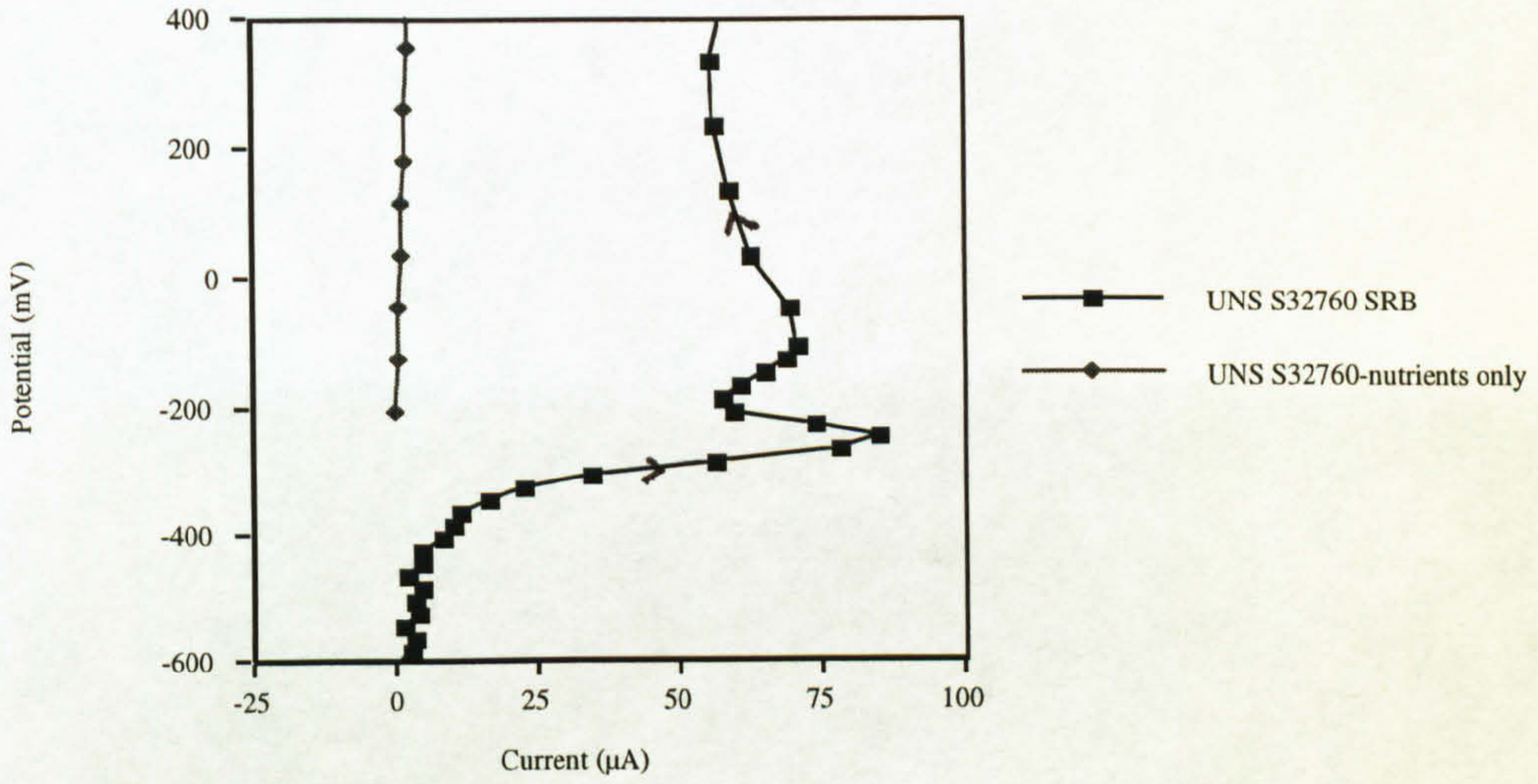

Fig. 7.5. Anodic polarisation to a potential more noble than the potential at which current transient is observed

Also after the relatively short immersion period of 4 hours, an important observation was made, during anodic polarisation, in that black corrosion products could be clearly seen emanating from certain specimens of both duplex and austenitic stainless steels at the point of passivity breakdown, E_b (Fig. 7.6).

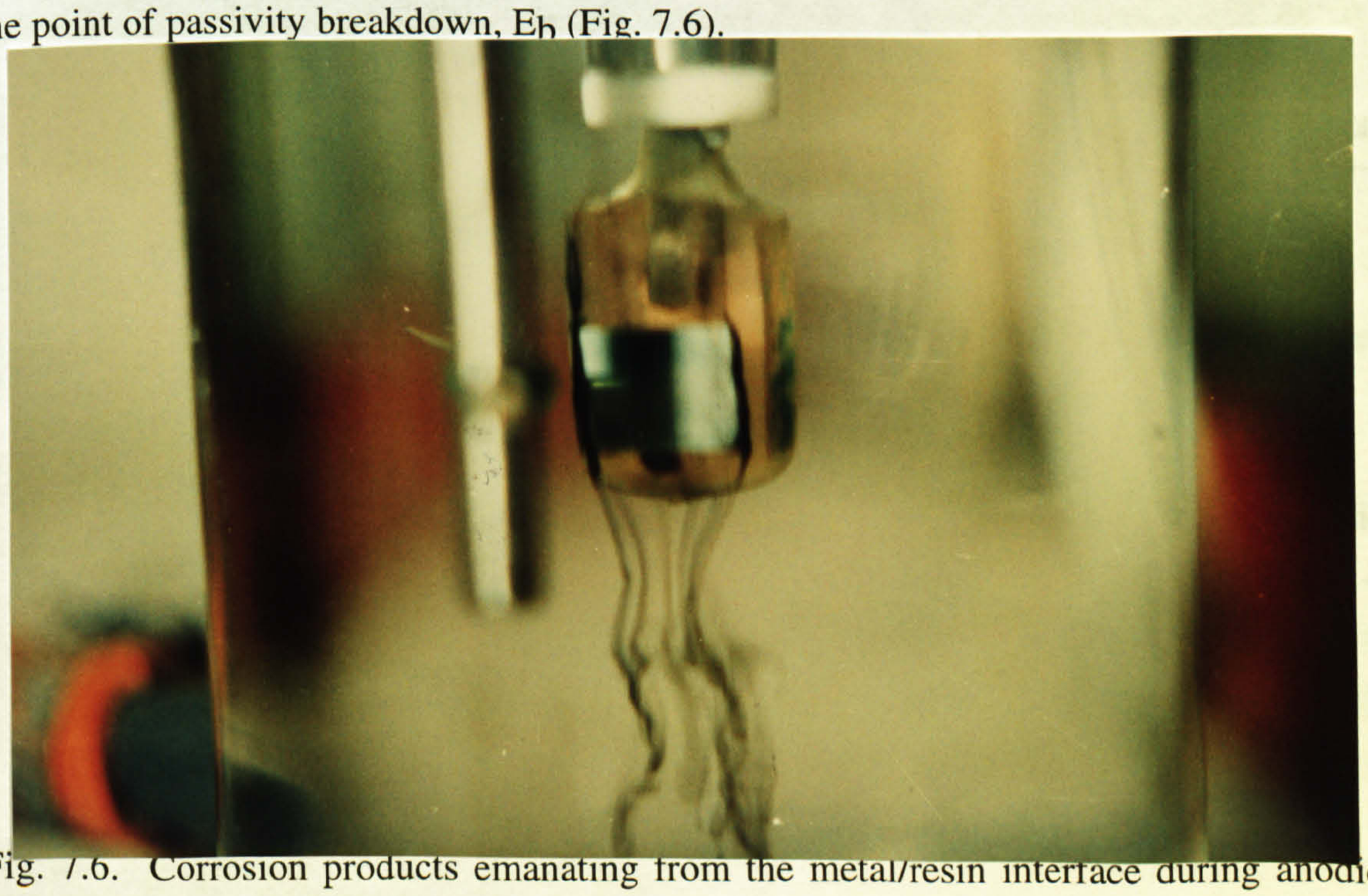

Fig. 7.6. Corrosion products emanating from the metal/resin interface during anodic polarisation on UNS S31254

This feature which occurred mainly at the metal/resin interface, commenced as E_b was reached and continued until the anodic polarisation scan had reached the repassivation potential (E_r). On examination of the specimens, a clear residue of corrosion products could be seen in the crevice which was later found to be rich in sulphur (probably as FeS). A concentration gradient of sulphur in the corrosion products at a site of crevice attack on UNS S31254 alloy was determined by EPMA with a maximum 7.4% at the specimen edge (point 1 on Fig.7.7) to a concentration of 0.6% (point 4 on Fig. 7.7) at a distance of 460μm from the specimen edge.

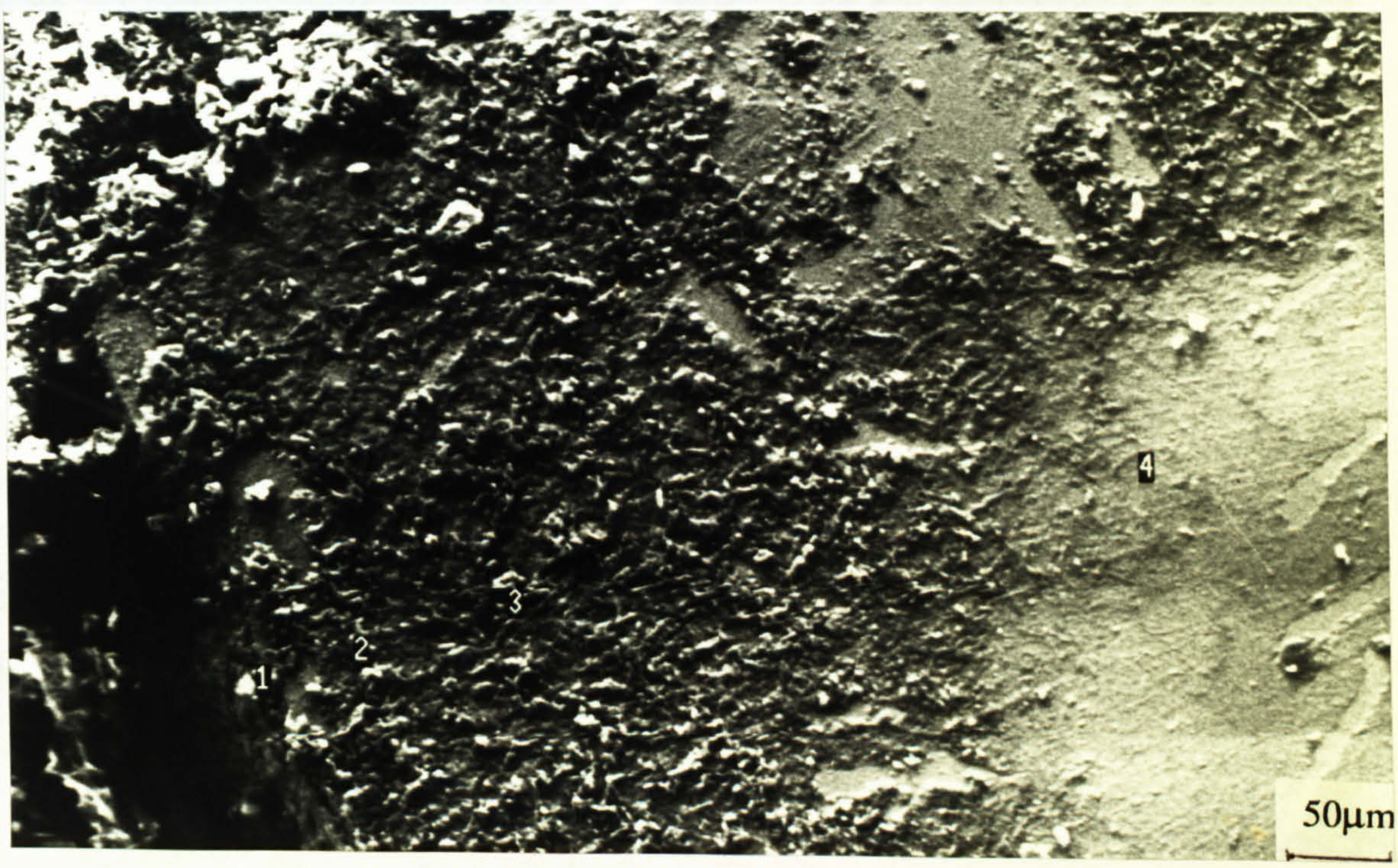

Fig. 7.7. Sulphide-containing corrosion products at the crevice of UNS S31254 after anodic polarisation in SRB

The visible streaming of corrosion products was not observed, during anodic polarisation, on the 25%Cr duplex stainless steel or UNS S32760 after 4 hours and 4 days immersion and on examination afterwards no crevice attack was found. However, pitting attack was detected in a short period of 4 hours, after anodic polarisation, with small pits evident under clusters of black corrosion products (Fig. 7.8) which were identified by EPMA as sulphur-containing.

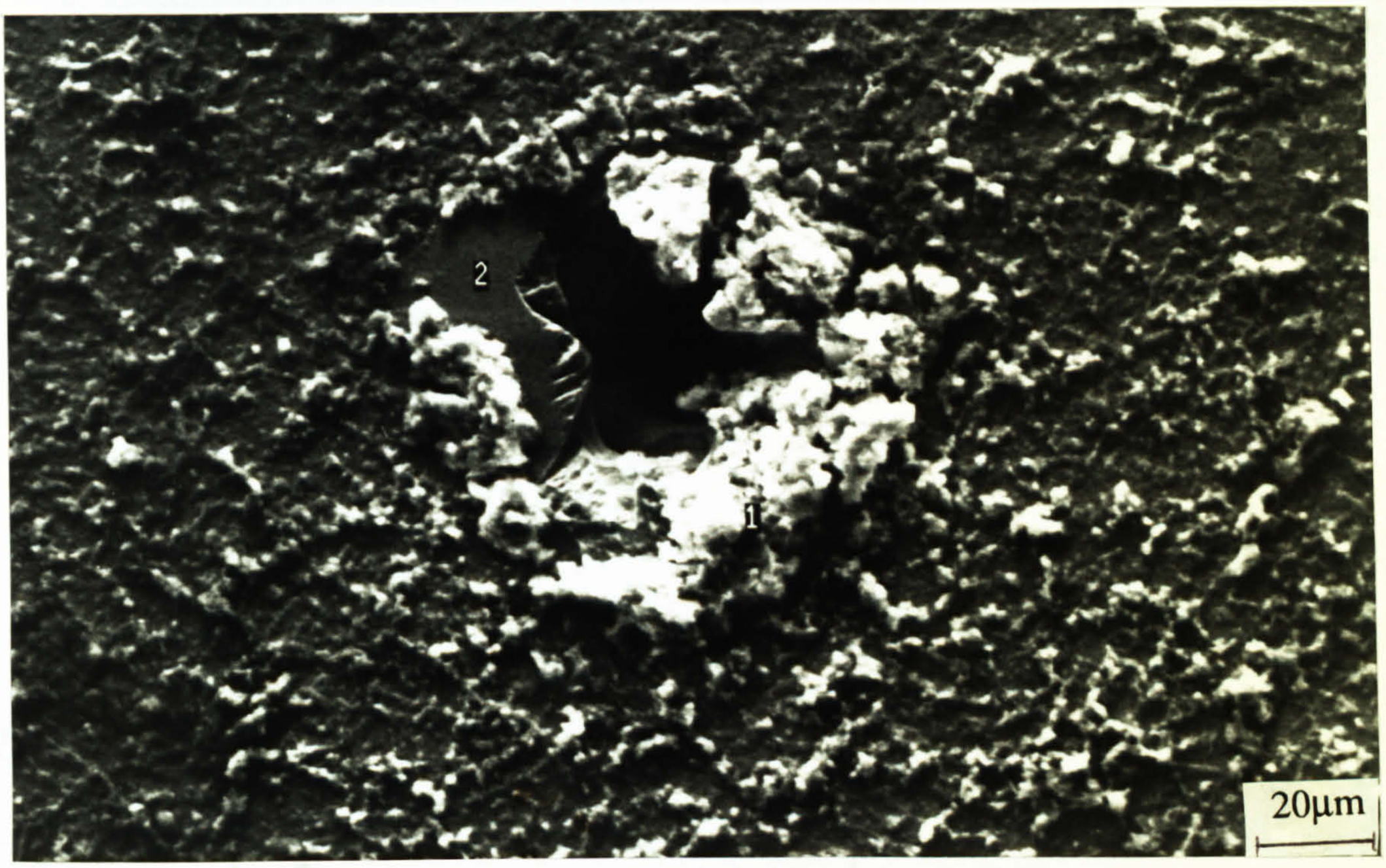

Fig. 7.8. Pitting under a cluster of sulphide-containing corrosion products on UNS S32760 after 4 days immersion and anodic polarisation

On the high-grade alloys, there was no obvious effect on the breakdown potential (E_b) after the short immersion period in SRB compared to SRB-free conditions but conversely on UNS S31603, a significant reduction of 200mV in the E_b value was recorded (Fig.7.9).

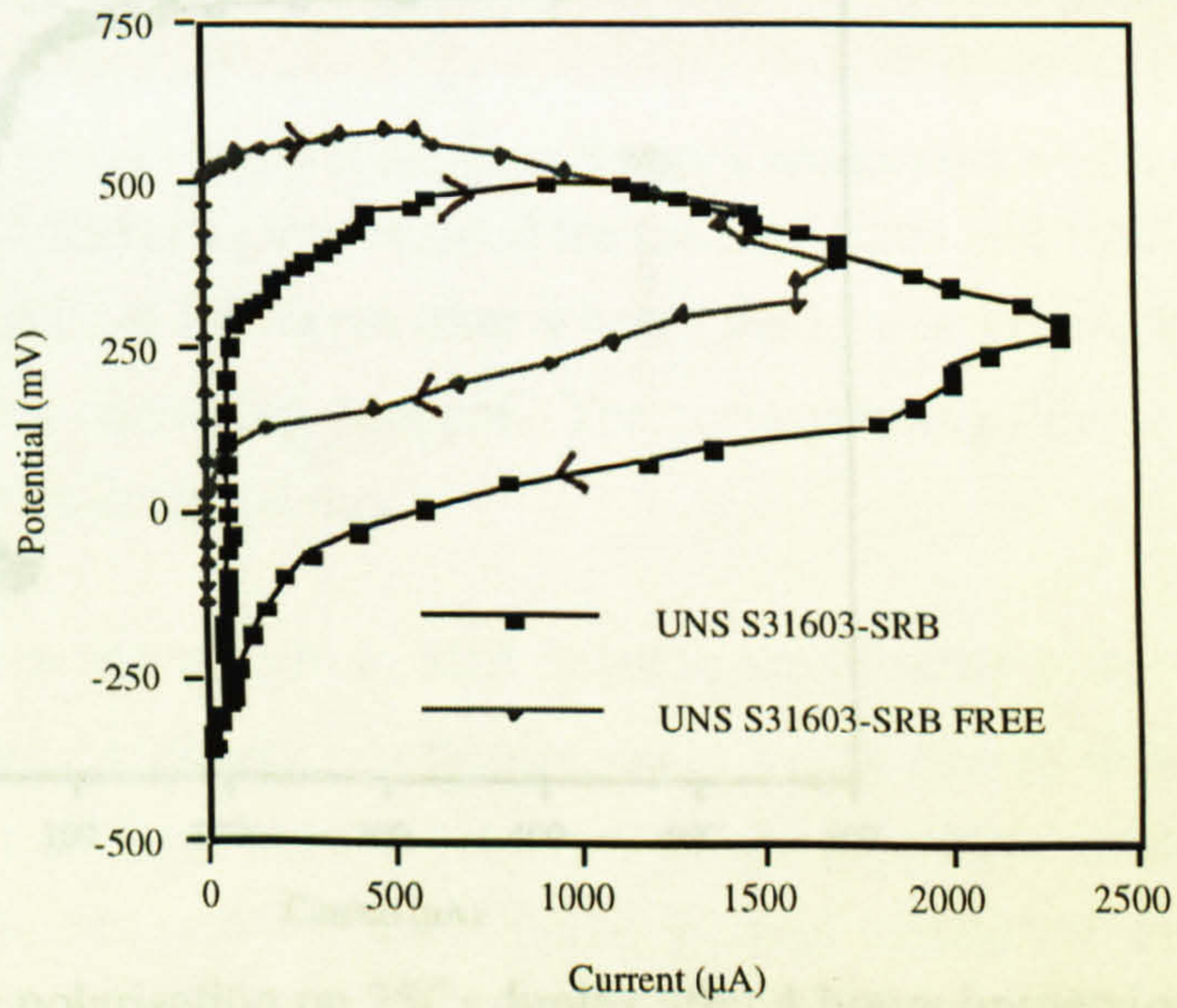

Fig.7.9. Comparison of anodic polarisation curves after 4 hours immersion in SRB-containing and SRB-free seawater

The repassivation characteristics in SRB-containing seawater could be assessed in electrochemical terms by considering two factors. Firstly, the width of the hysteresis loop and secondly the maximum current attained once the potential was reversed. It was clear that the short (4 hours, 4 days) immersion period did not detrimentally affect the repassivation potential E_r of the high-grade alloys (Figs. 7.10 and 7.11) but on the lower-alloyed UNS S31603, Er was significantly less positive (see Fig. 7.9).

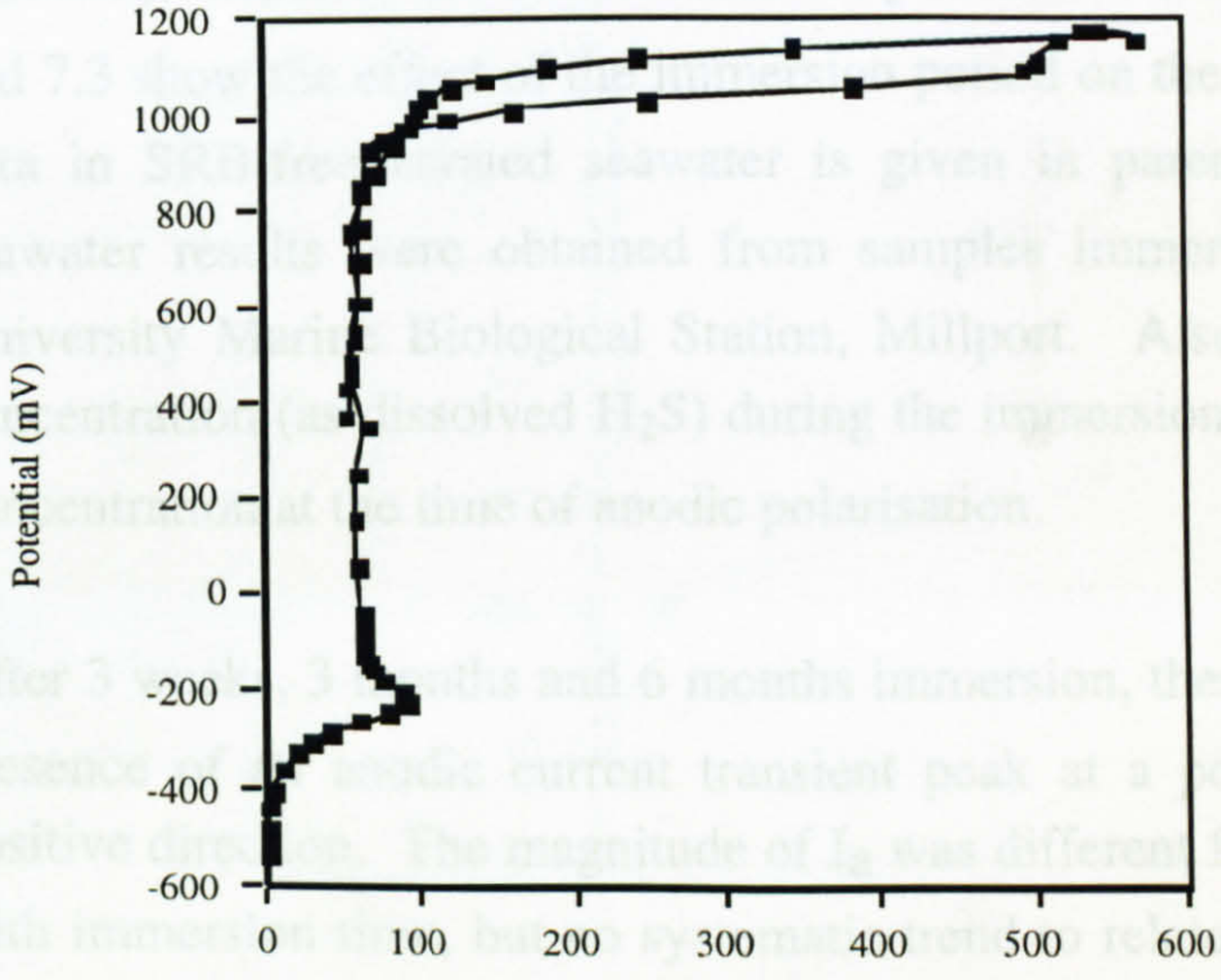

Fig. 7.10. Anodic polarisation on UNS S31254 after 4 days immersion

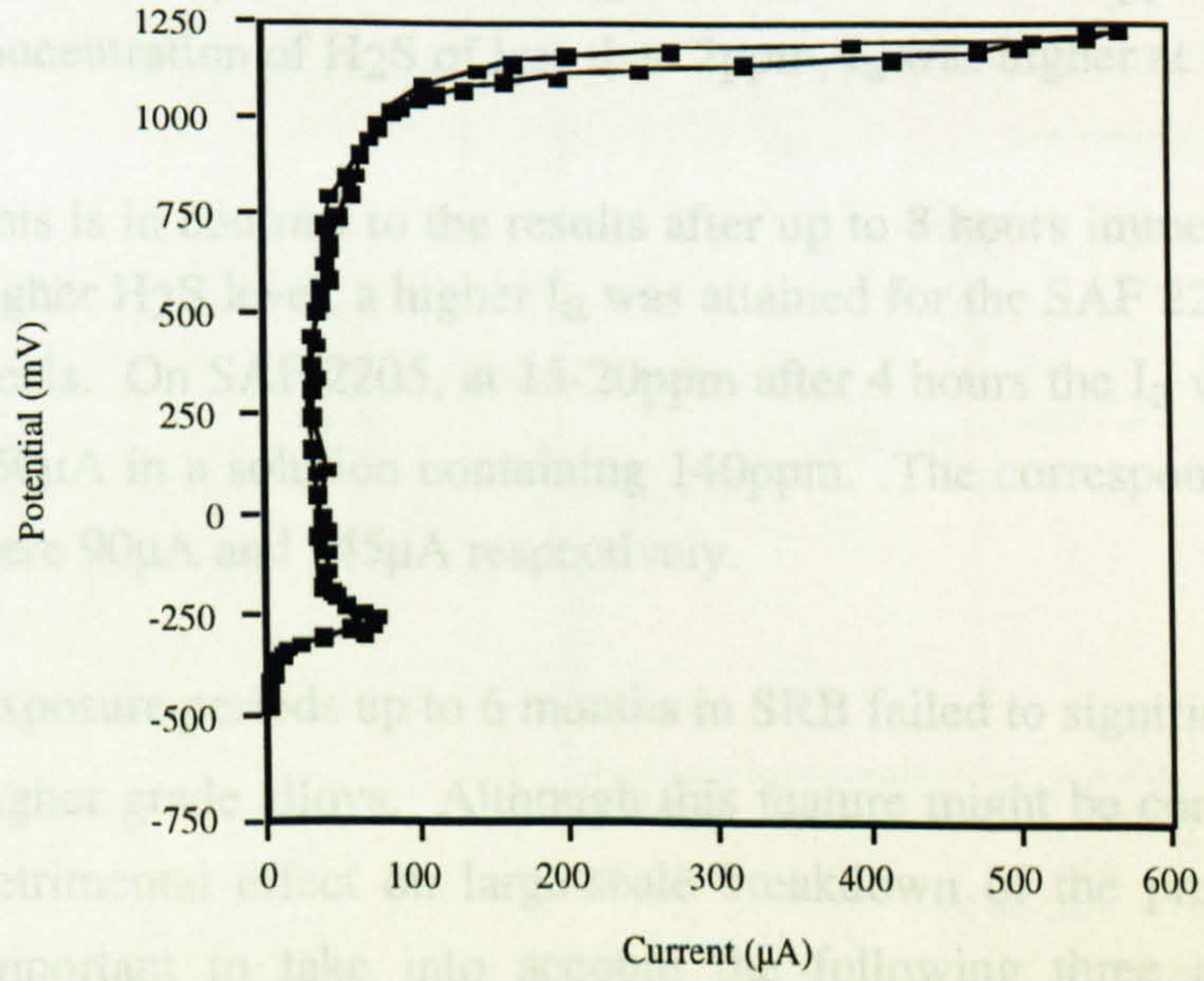

Fig. 7.11. Anodic polarisation on 25Cr duplex after 4 hours immersion

Also, it must be stressed that "repassivation" here involved reverting to anodic currents several times larger than in the passive state in SRB-free conditions. Again with the

exception of UNS S31603, the current did not proceed to high values after the reversal current of 500μA.

Longer exposure

Prolonged exposure to SRB did not result in any further fundamental changes in the form of the anodic polarisation curve, although there were distinct changes in the numerical values of the electrochemical parameters (i.e E_b, E_r, I_b, I_s etc.). Tables 7.2 and 7.3 show the effect of the immersion period on the parameters and the comparable data in SRB-free aerated seawater is given in parentheses. The 6-month aerated seawater results were obtained from samples immersed in natural seawater at the University Marine Biological Station, Millport. Also the tables show the sulphide concentration (as dissolved H_2S) during the immersion period and an indication of the concentration at the time of anodic polarisation.

After 3 weeks, 3 months and 6 months immersion, there was still, on all materials, the presence of an anodic current transient peak at a potential modestly shifted in the positive direction. The magnitude of I_a was different for each material and also varied with immersion time, but no systematic trend to relate I_a to the level of dissolve H_2S was determined. This is illustrated in Fig. 7.12 for UNS S32760, on which after 3 months, I_a attained the 500μA reversal current. After 3 weeks but with a higher H_2S content, I_a was only 30μA. Similarly on UNS S31254, after <1 week in SRB, I_a attained 90μA when the H_2S content was 15-20ppm but after 6 months and a concentration of H_2S of less than 2ppm, I_a was higher at 130μA (Fig. 7.13).

This is in contrast to the results after up to 8 hours immersion which showed that for a higher H_2S level, a higher I_a was attained for the SAF 2205 and UNS S31254 stainless steels. On SAF 2205, at 15-20ppm after 4 hours the I_a was 110μA which increased to 250μA in a solution containing 140ppm. The corresponding figures for UNS S31254 were 90μA and 145μA respectively.

Exposure periods up to 6 months in SRB failed to significantly lower the E_b of the four higher grade alloys. Although this feature might be considered to be indicative of no detrimental effect on large-scale breakdown of the protective oxide film, it is very important to take into account the following three additional factors. First, the evidence of transient anodic activity (denoted by I_a) at potentials much less positive than E_b. Second, the fact that the currents (I_s) at potentials more positive than the occurrence of the anodic peak were several times greater than the passive currents (I_p) in SRB-free seawater. Third, evidence of current instability at potentials between the

anodic peak and 1000mV; that is current increasing at significant rates prior to the very rapid increase normally associated with the breakdown potential, E_b. As an example of the third feature, anodic polarisation on SAF 2205, after 3 months showed the relatively rapid increase in current in the potential range 60-880mV which could be interpreted as passivity breakdown. Figure 7.14 compares this with the anodic polarisation after 4 hours on which there is less ambiguity about the E_b point.

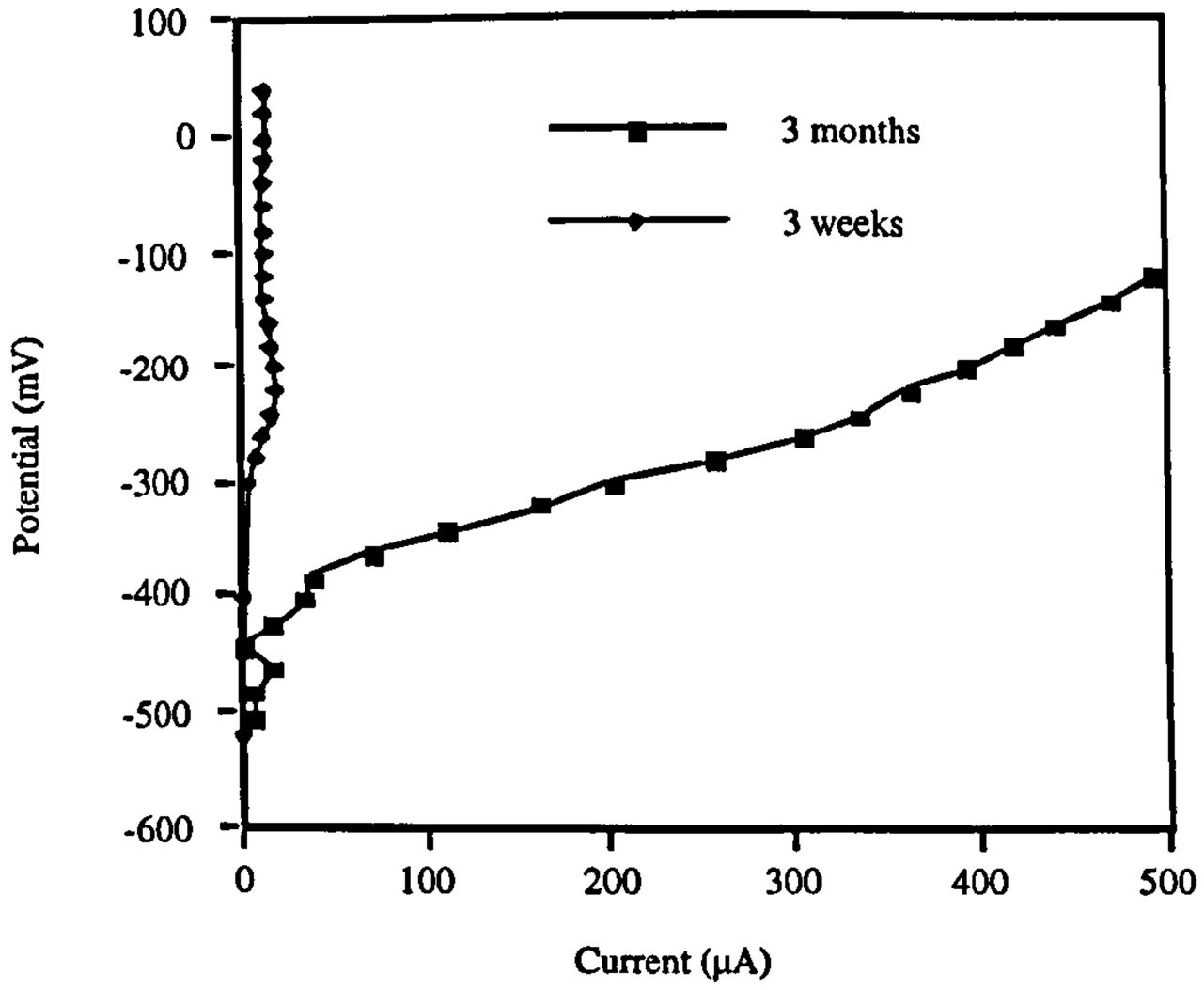

Fig. 7.12. Current transient after 3 weeks and 3 months immersion on UNS S32760

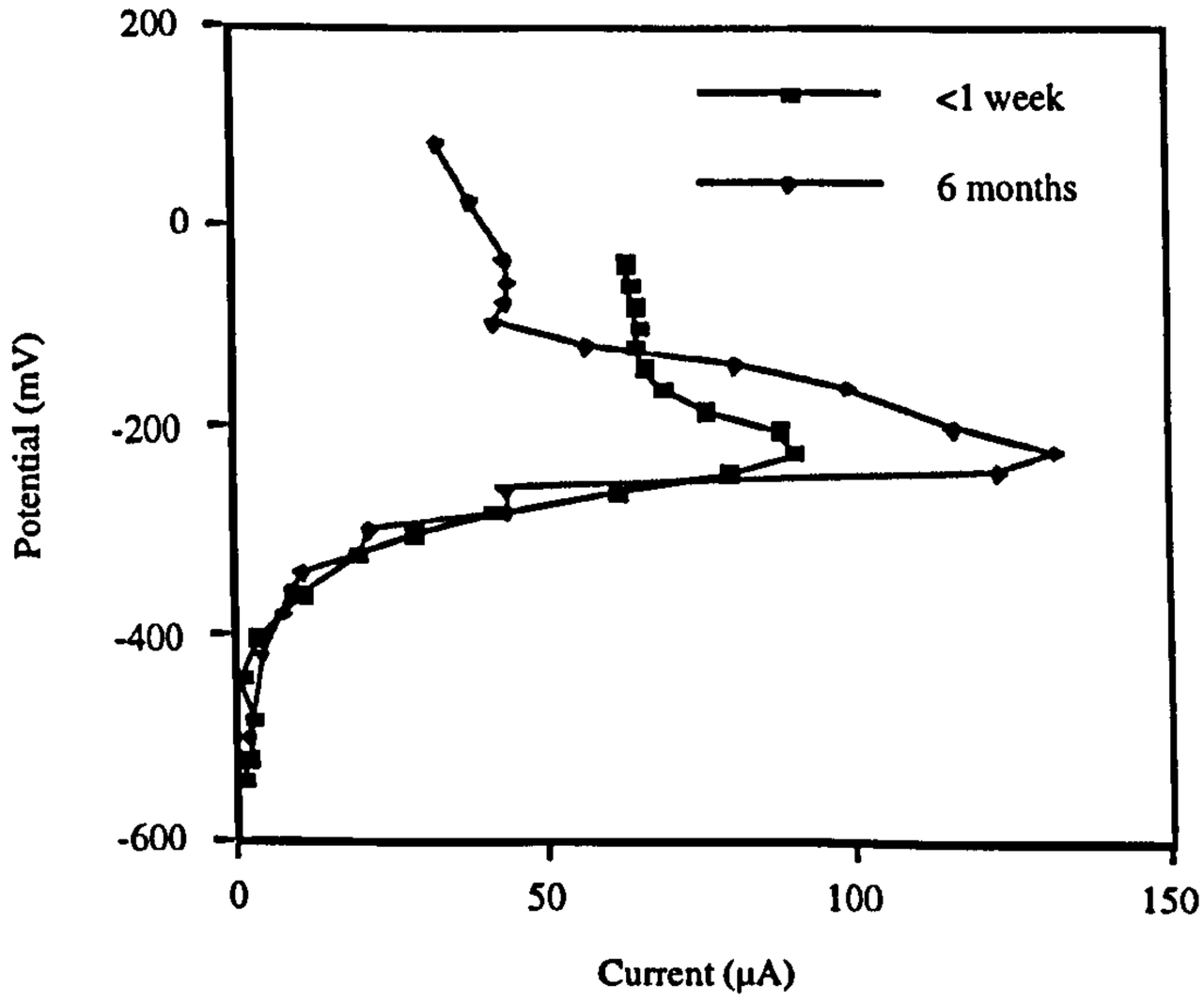

Fig. 7.13. Anodic current transient after <1 week and 6 months immersion on UNS S31254

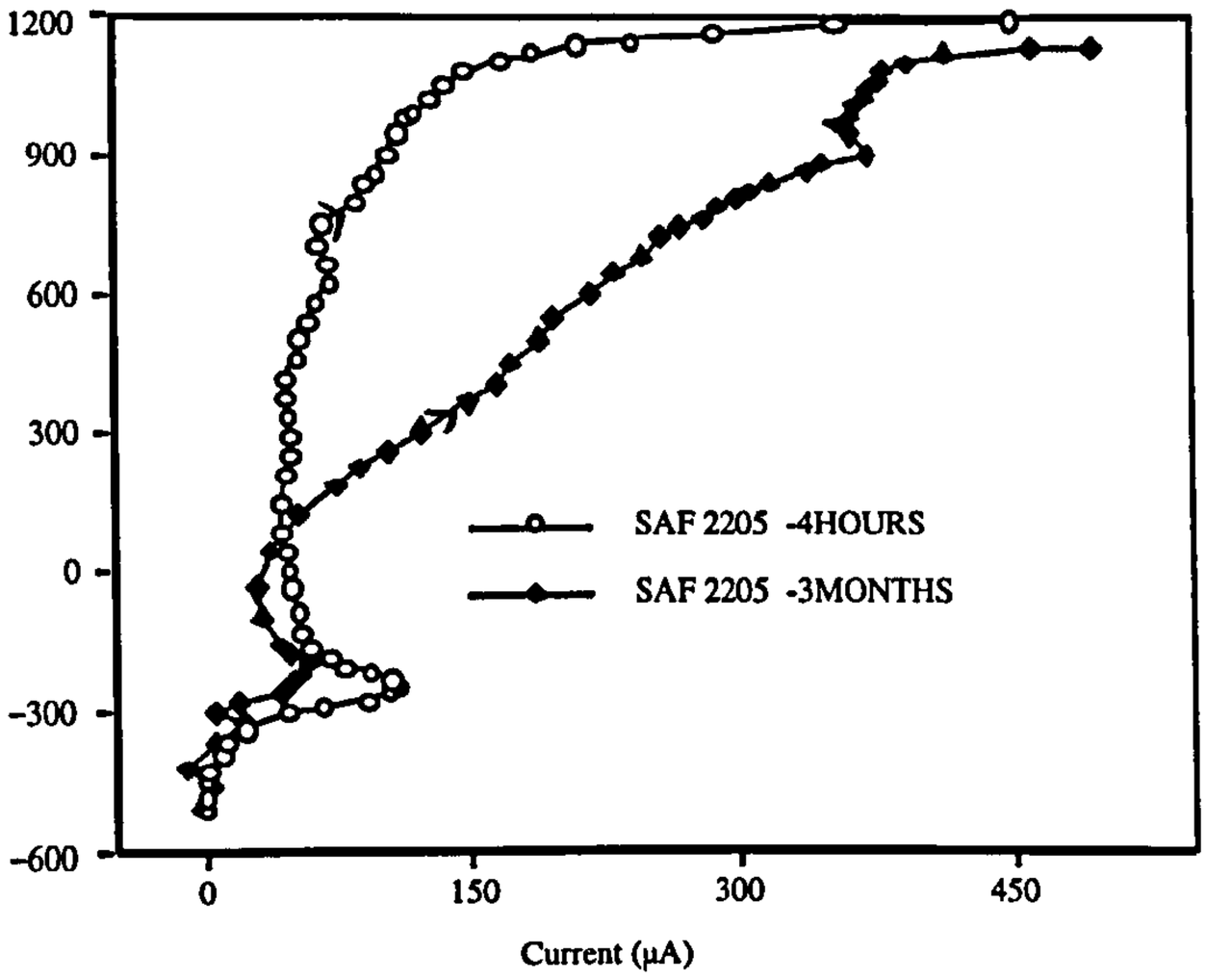

Fig. 7.14. Anodic polarisation on SAF 2205 after 4 hours and 3 months immersion

This feature of increasing current was also observed on the higher grade superduplex stainless steel and on the superaustenitic UNS S31254 after 3 weeks in the SRB-containing seawater. Figure 7.15 shows on UNS S31254 the anodic polarisation forward sweep after 3 weeks immersion where high currents are observed in what is normally referred to as the passive region.

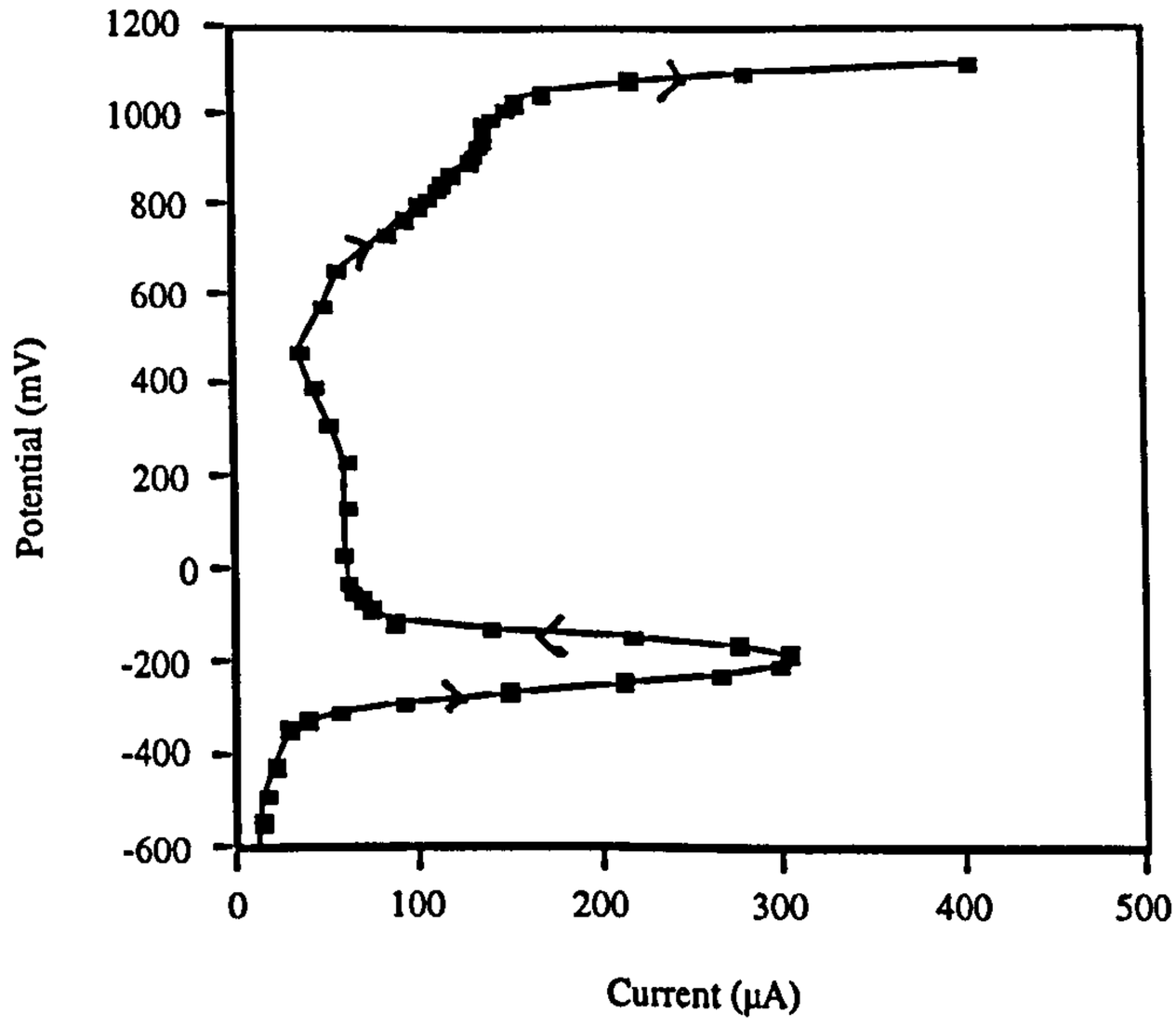

Fig. 7.15. Anodic polarisation on UNS S31254 after 3 weeks immersion

In Tables 7.2 and 7.3, the presence of an * beside the electrochemical data in SRB denotes that because of this effect, the E_b value could be taken to be less positive. On UNS S31603, it was shown previously that immersion in SRB significantly lowered the E_b even after very short immersion periods and higher currents are attained after

scan reversal, corresponding to a higher I_{max}. Longer immersion (up to 6 months) seemed to facilitate a slight ennobling of E_b (Fig. 7.16). There was no further increase in the maximum current attained after potential scan reversal.

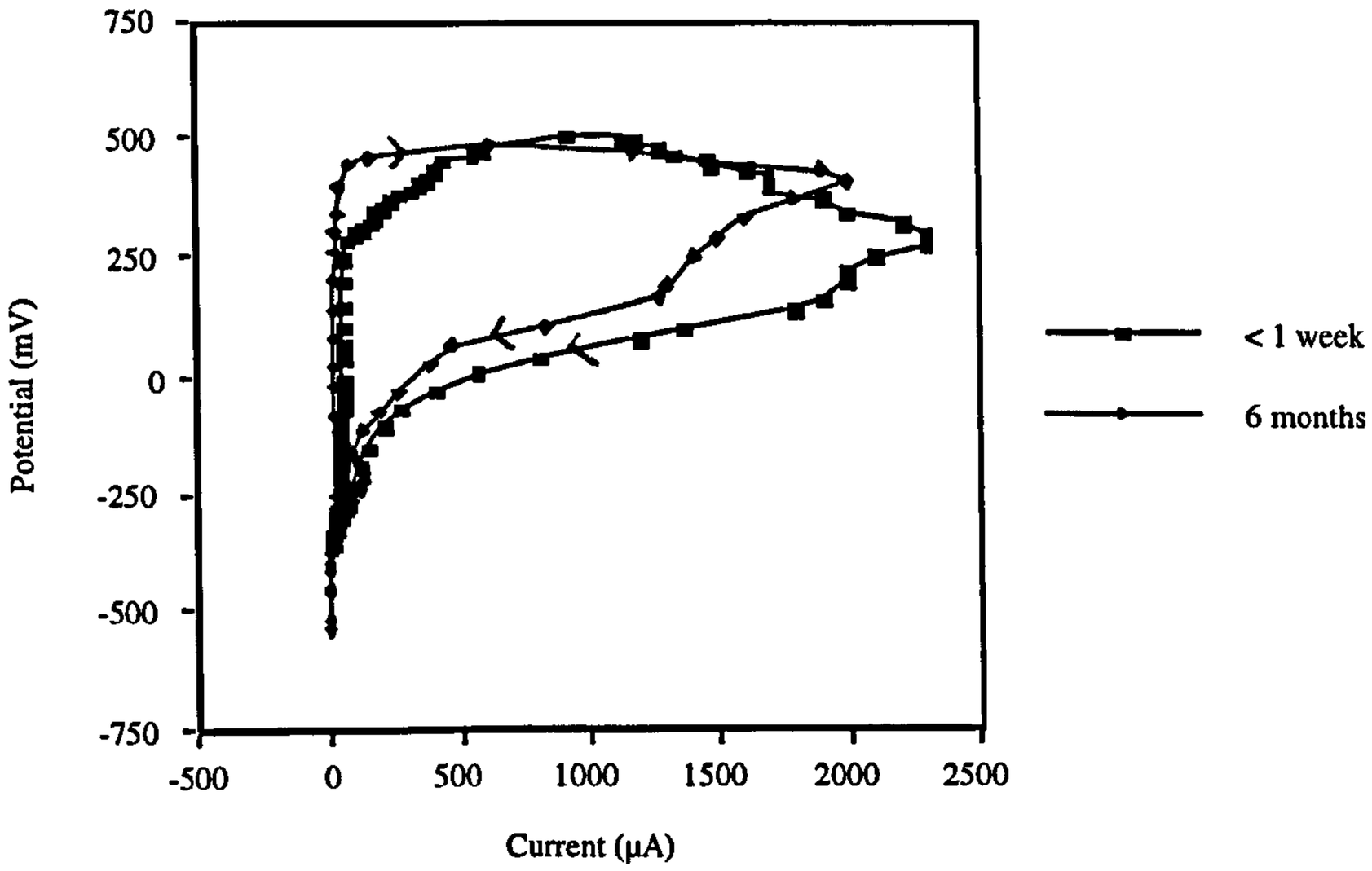

Fig. 7.16. Anodic polarisation and slight ennoblement of E_b after 6 months immersion

In one experiment, specimens of SAF 2205 were immersed in SRB-containing seawater for 8 days, after which specimens were anodically polarised and other specimens were removed to aerated seawater and subsequently anodically polarised. The characteristic current transient was observed in the presence of SRB whereas in contrast there was no current increase on the specimen in the aerated solution (Fig. 7.17)

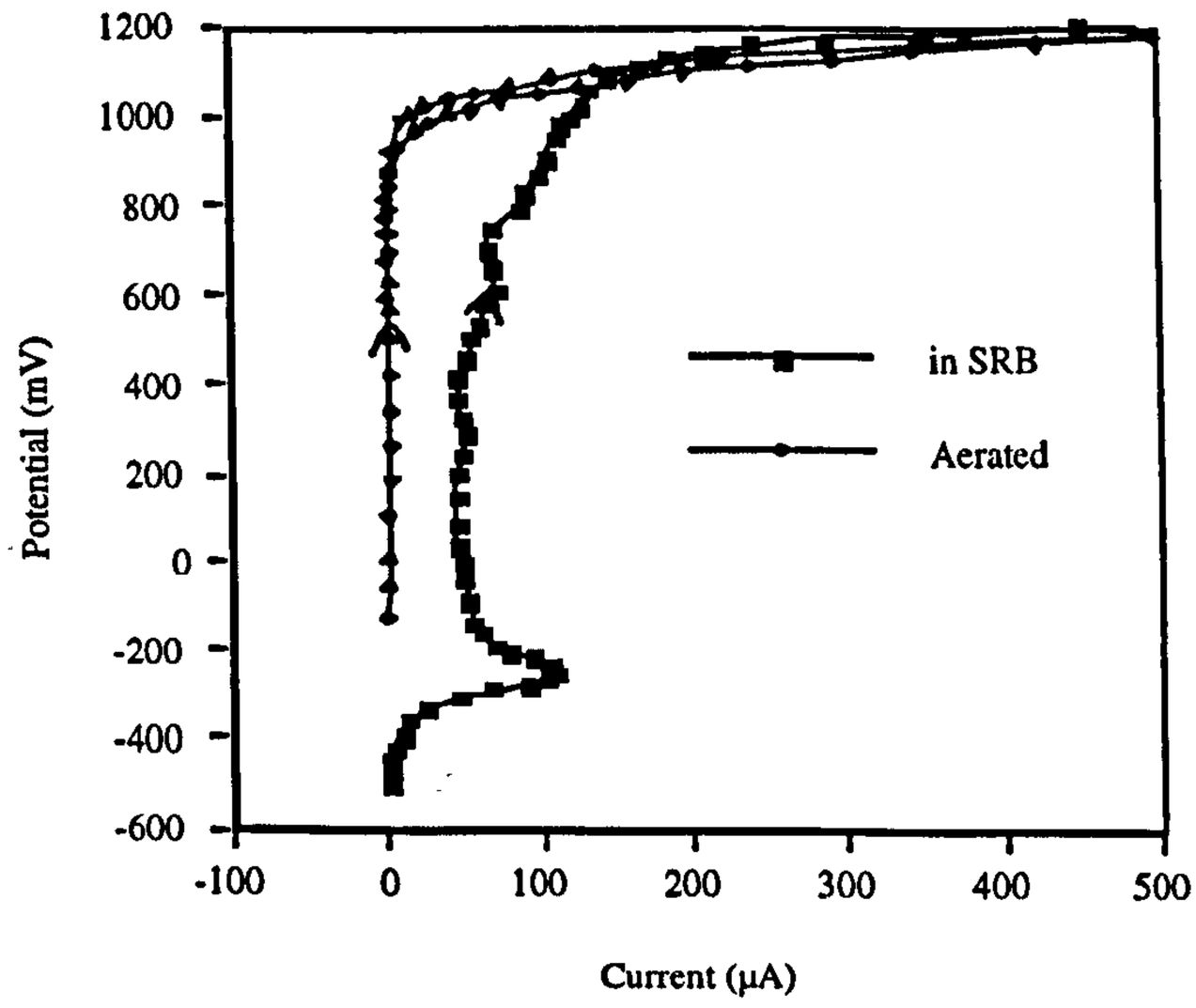

Fig. 7.17. Anodic polarisation on SAF 2205 after 8 days in SRB

Attack mechanisms

Details of the type of attack defined by microscopical analysis after each anodic polarisation test are given in Table 7.4. The data in Table 7.5 represent the attack observed after a period at the free-corrosion potential (i.e no polarisation).

Attack on a general level, manifested in an etching of the duplex structure, was observed on each duplex alloy after <1week immersion and anodic polarisation in SRB. Confirmation of the validity of accelerated test methods as a tool for predicting and defining the relevant mechanisms of attack was obtained when the same type of attack was observed on freely corroded specimens of 25%Cr and SAF 2205 after longer immersion. Figure 7.18 shows the general etching of 25Cr duplex stainless steel as a result of anodic polarisation after 4 days immersion and in agreement with the accelerated test. Figure 7.19 shows similar etching attack under a sulphide film formed after prolonged exposure for 6 months in SRB at the free corrosion potential. After an immersion period of 6 months at the free corrosion potential, no general attack was detected on UNS S32760, confirming its superior resistance to the onset of general attack.

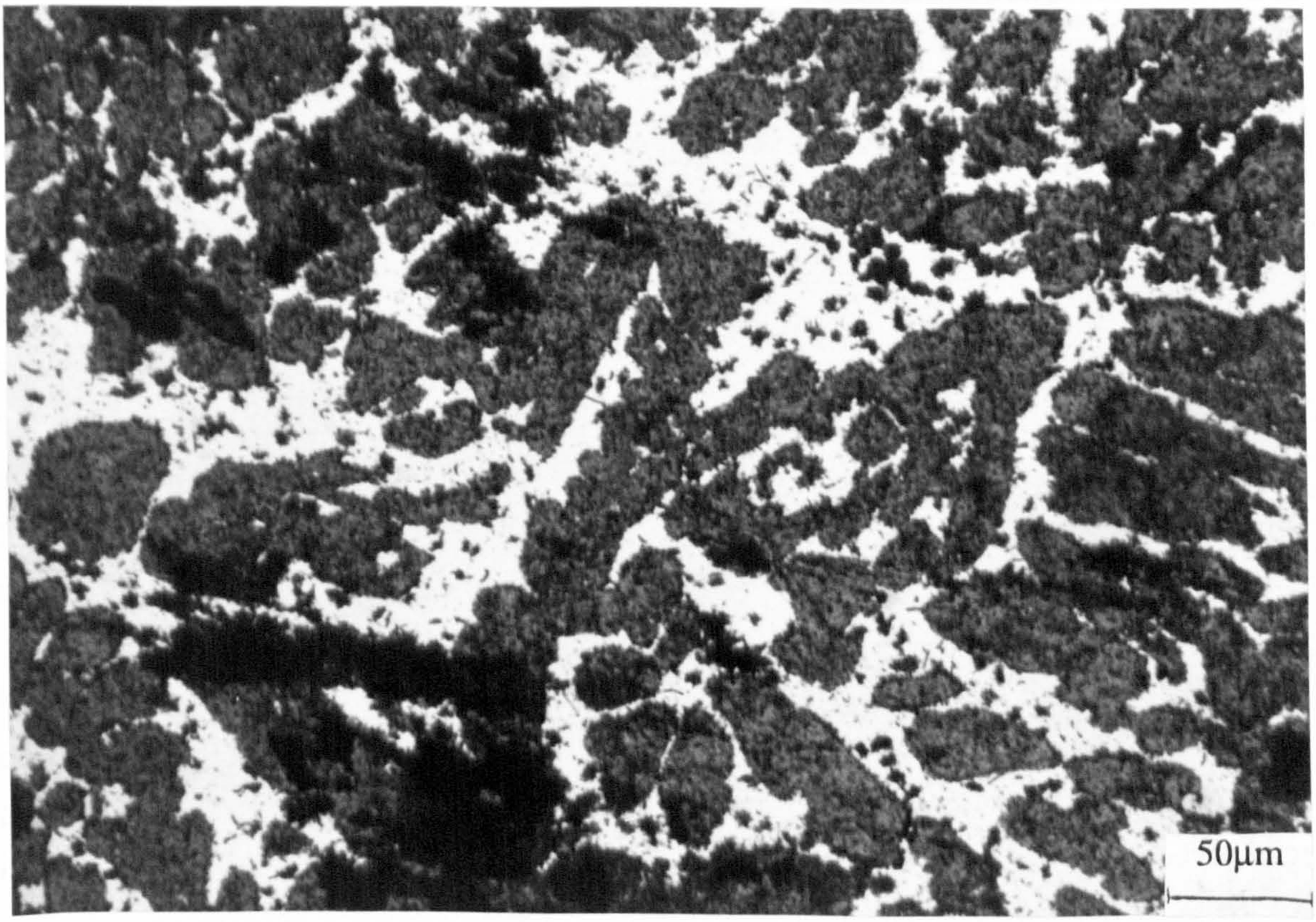

Fig. 7.18. Etching of the duplex structure and formation of sulphide film on the austenite phase of 25Cr duplex after anodic polarisation

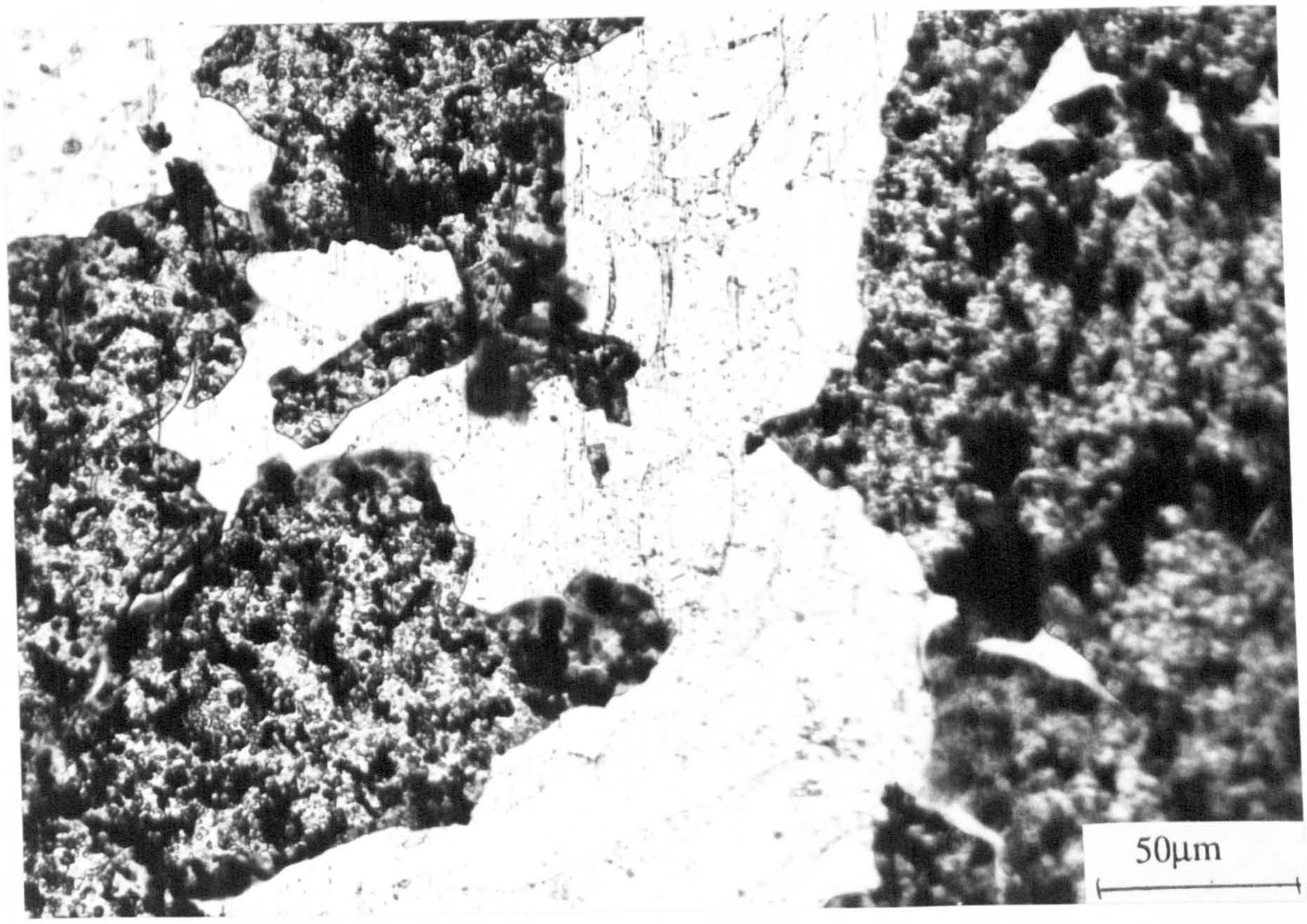

Fig. 7.19. Etching under sulphide film formed after immersion in SRB-containing seawater for 6 months at the free corrosion potential on 25Cr duplex

An important feature of the localised corrosion mechanisms in SRB was the extent of crevice attack, observed on every material, after anodic polarisation, even the shortest immersion periods, and which, when severe attack was observed, occurred in conjunction with a streaming of black corrosion products from the metal/resin interface as shown previously for UNS S31254 after a short period of <1 week in SRB. On the SAF 2205 specimen, the crevice attack extended around the complete perimeter of the specimen at the resin interface.

Under free-corrosion conditions, minor crevice attack was observed on only the 25%Cr duplex after <1 week immersion but after 6 months, all materials suffered crevice attack to some extent (Table 7.5). Figure 7.20 shows the only small area of crevice corrosion on 25Cr duplex after <1 week in SRB at the free corrosion potential.

On most materials after removal from SRB-containing seawater, a discontinuous black sulphide film was present. This loosely adherent film could be easily removed and

since it was present on the moulding resin, as well as on the specimen surface, it was assumed to be deposited (FeS) from the medium. However, on specific specimens as denoted by **F** in Tables 7.4 & 7.5, a dense, adherent, basal film formed after prolonged exposure and sometimes after anodic polarisation which could not easily be removed. Figure 7.21 shows the double layered film on UNS S31254 after 3 months exposure and anodic polarisation. The dark areas are the adherent film and the more widespread lighter areas are the loosely adherent film which is deposited from the medium.

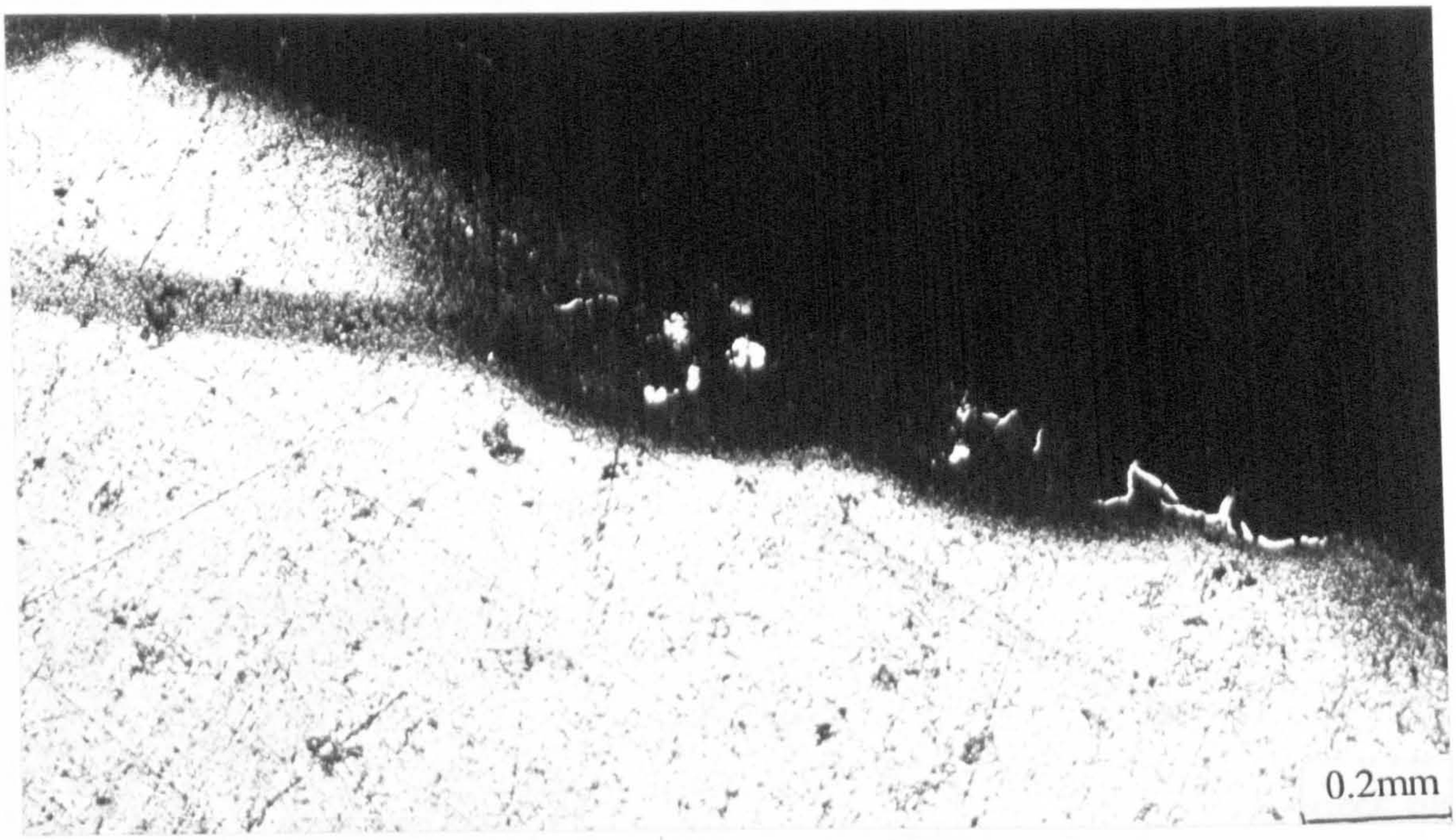

Fig. 7.20. Small area of crevice corrosion at the metal/resin interface of 25Cr duplex after <1 week in SRB

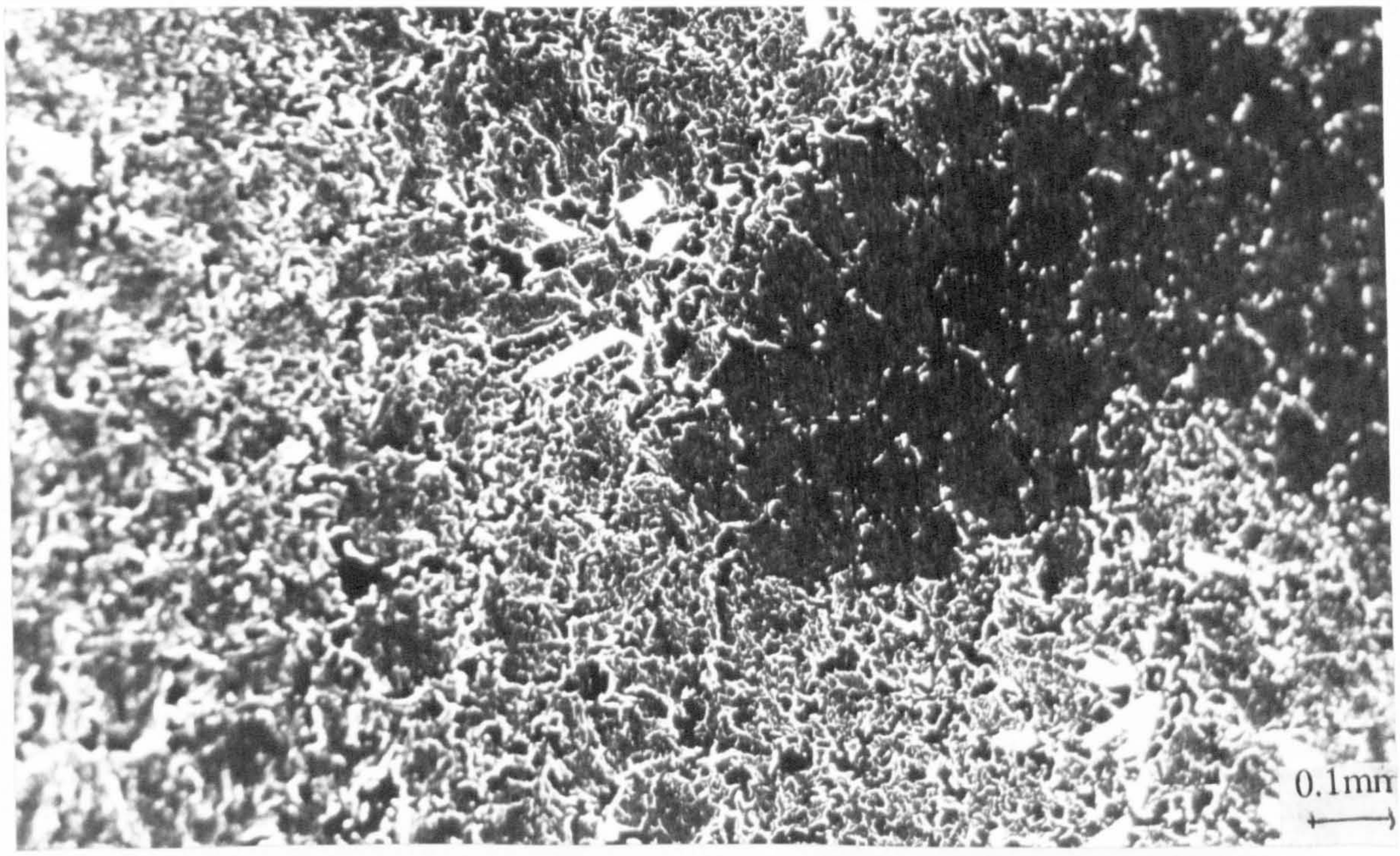

Fig. 7.21. Double layered film on UNS S31254 after 3 months and anodic polarisation

EPMA confirmed the presence of Fe and S in the adherent basal film, **F**, (and also significant amounts of the other alloying elements). On the UNS S32760 and the 25Cr duplex, this adherent film formed preferentially on the austenitic phase as shown in Figs 7.22. The darker phase is the austenite and the lighter matrix is the higher Cr and Mo-containing ferrite. Figure 7.23 shows the high S peak found on UNS S32760 from EPMA.

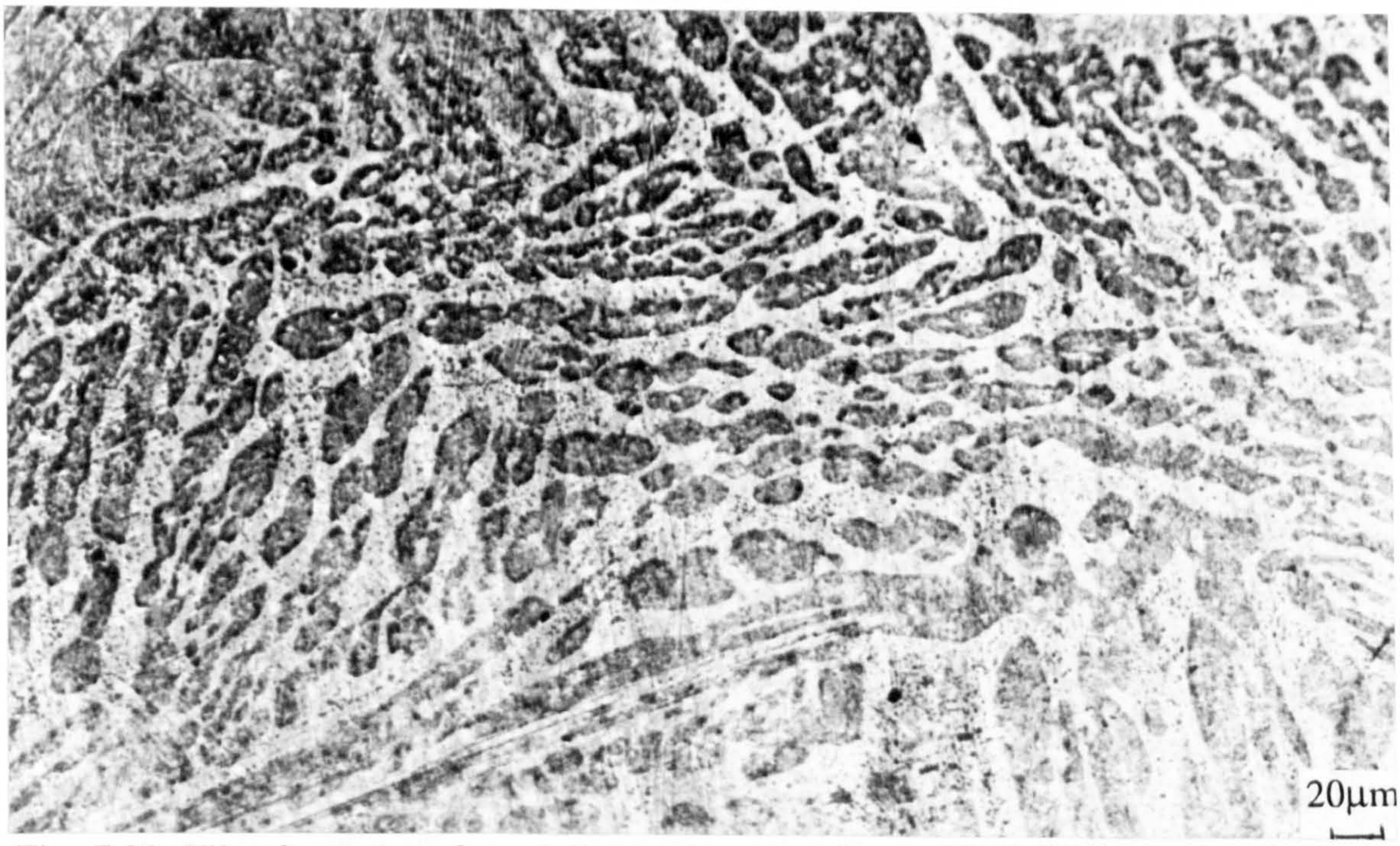

Fig. 7.22. Film formed preferentially on the austenite on UNS S32760 after 3 weeks and anodic polarisation

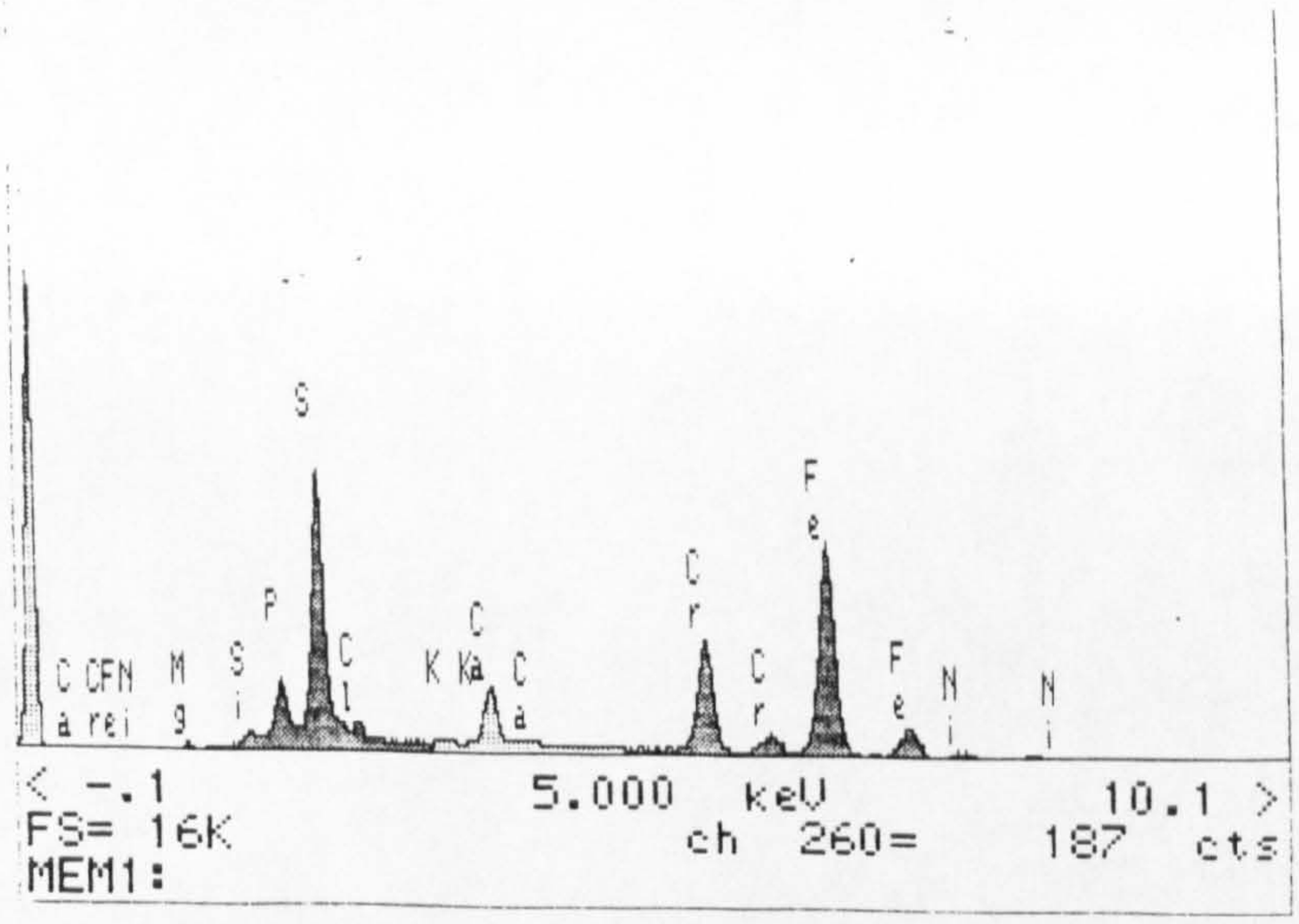

Fig. 7.23. EPMA trace from the austenitic phase after 3 weeks immersion and anodic polarisation on UNS S32760

The form of pitting attack after anodic polarisation in SRB on the 25Cr duplex and UNS S31603 was clearly distinct from that in SRB-free seawater. The morphology of the pits on 25Cr duplex changed from the regular symmetrical, usually circular form, observed in laboratory conditions in SRB-free seawater to complex pits where they appeared as a system of several pits coalesced. On initially removing the specimens from the SRB medium, the pits were easily located by black clusters of corrosion products as shown in Fig. 7.24 on 25Cr duplex after 3 weeks and anodic polarisation. On removing the corrosion products for examination, the complex series of pits was revealed as in Fig. 7.25.

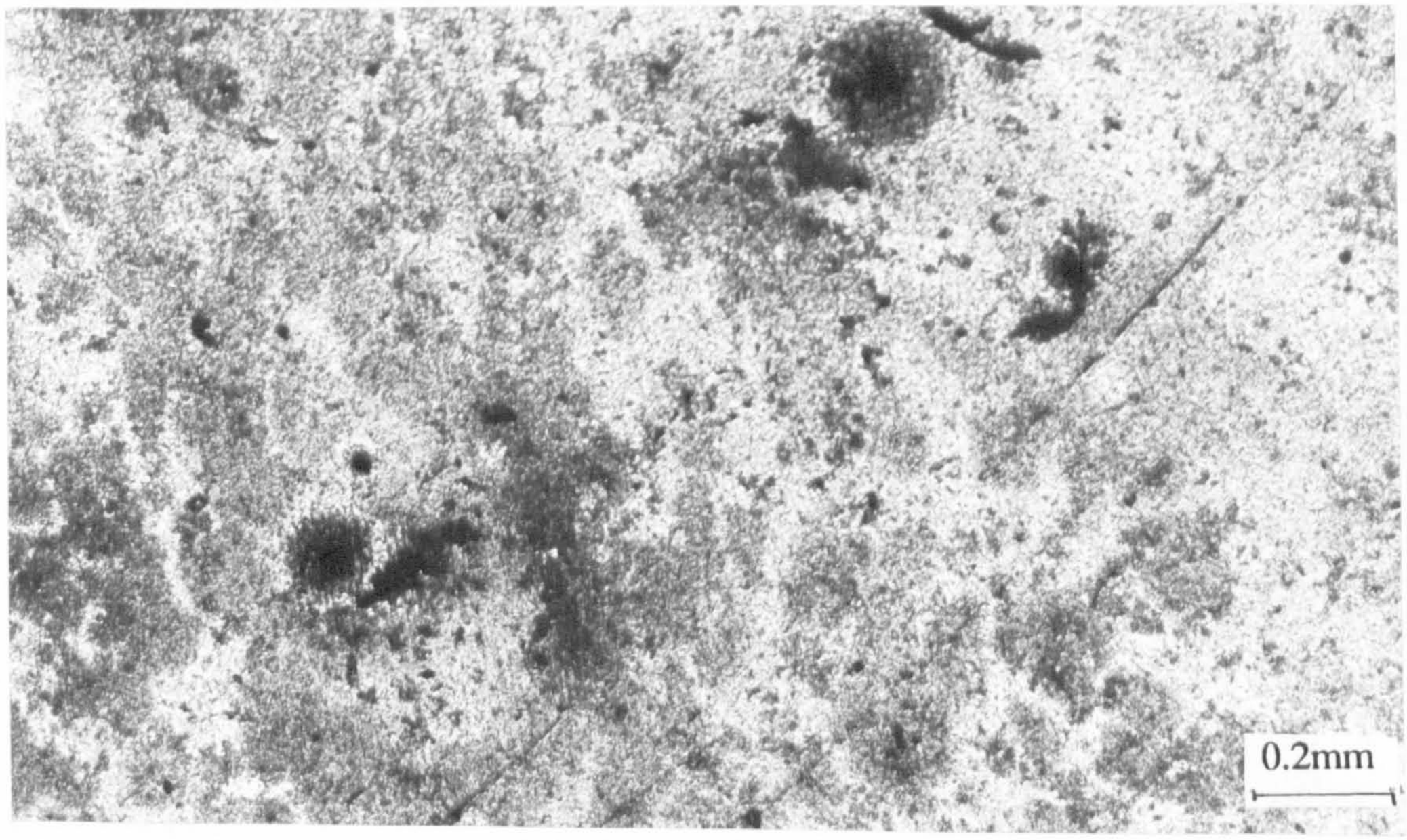

Fig. 7.24. As-removed specimen of 25Cr duplex showing the clear clusters of corrosion products resulting form pitting attack

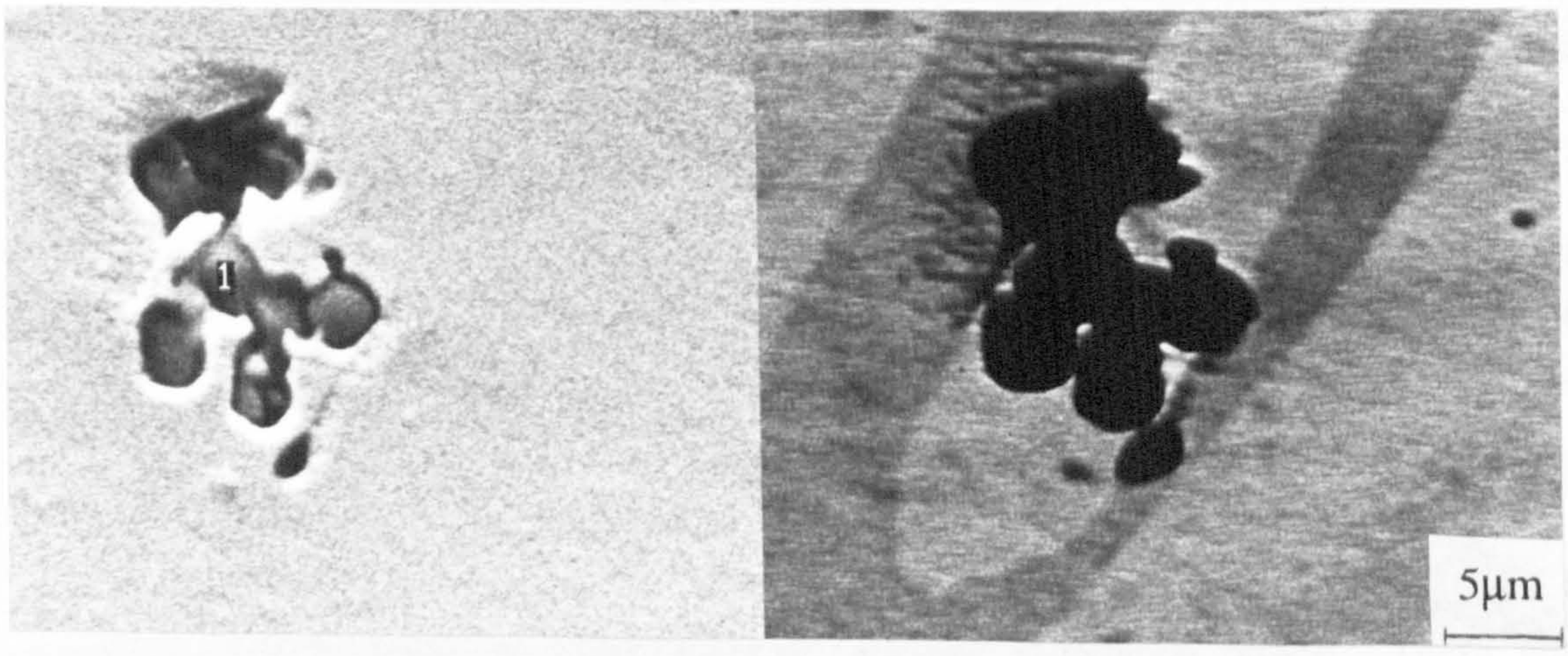

Fig. 7.25. Complex pitting formed after anodic polarisation in SRB on 25Cr duplex. 3 weeks immersion.

On UNS S31603, in SRB, pitting still appeared as regular and symmetrical on the surface, but on examination and by prodding the surrounding area with a sharp metal rod, hollow areas were revealed beneath the perforated surface. After 3 months in SRB and anodic polarisation, there was pitting attack on the free surface of UNS S31603 but the most severe attack was in the form of crevice attack at the resin/metal interface, as shown in Fig. 7.26.

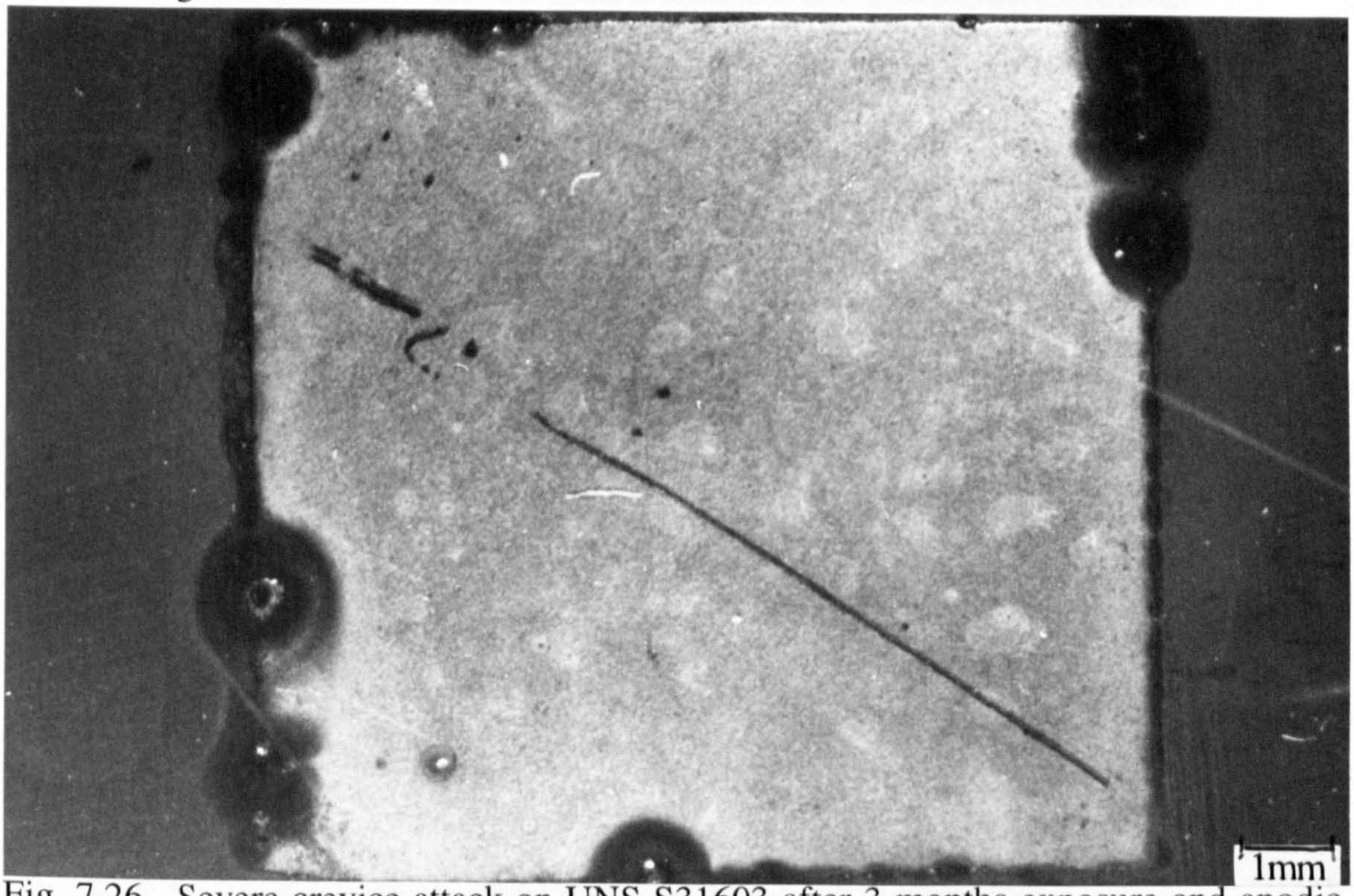

Fig. 7.26. Severe crevice attack on UNS S31603 after 3 months exposure and anodic polarisation

Prolonged exposure of 6 months and anodic polarisation facilitated pitting attack of significantly enhanced severity. Figure 7.27 shows one pit in the vicinity of an area of crevice attack in which. Examination inside the pit revealed the austenitic structure (Figs 7.28 and 7.29).

Analysis using energy dispersive EPMA showed that around the edge of the pitted sites on UNS S31603, a clear trace of sulphur was detected. Several of the pits were large enough to obtain an EPMA trace from the bottom of the interior of the pit. In none of the pits could any trace of sulphur be found.

Under free-corrosion conditions, UNS S31603 suffered pitting attack after a 1 week immersion period while the other materials resisted significant attack. There was evidence of initiation of crevice attack on the 25Cr duplex alloy. However, after 3

weeks immersion, the higher grade alloys, with the exception of UNS S31254, showed susceptibility to pitting attack as illustrated in Fig. 7.30 on UNS S32760.

Fig. 7.27. Pitting near the crevice after 6 months immersion

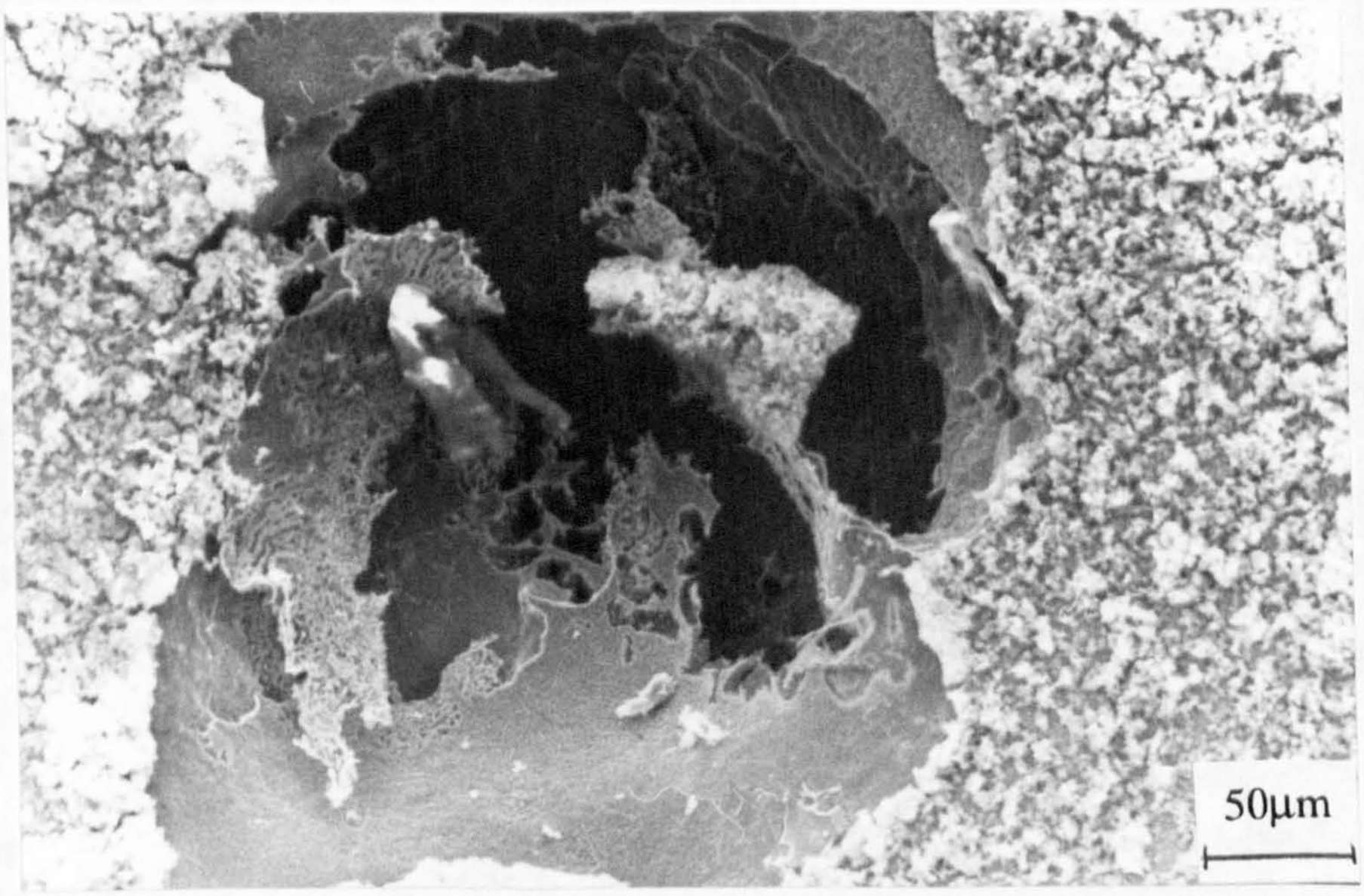

Fig. 7.28. Closer view of pitting and the austenitic structure

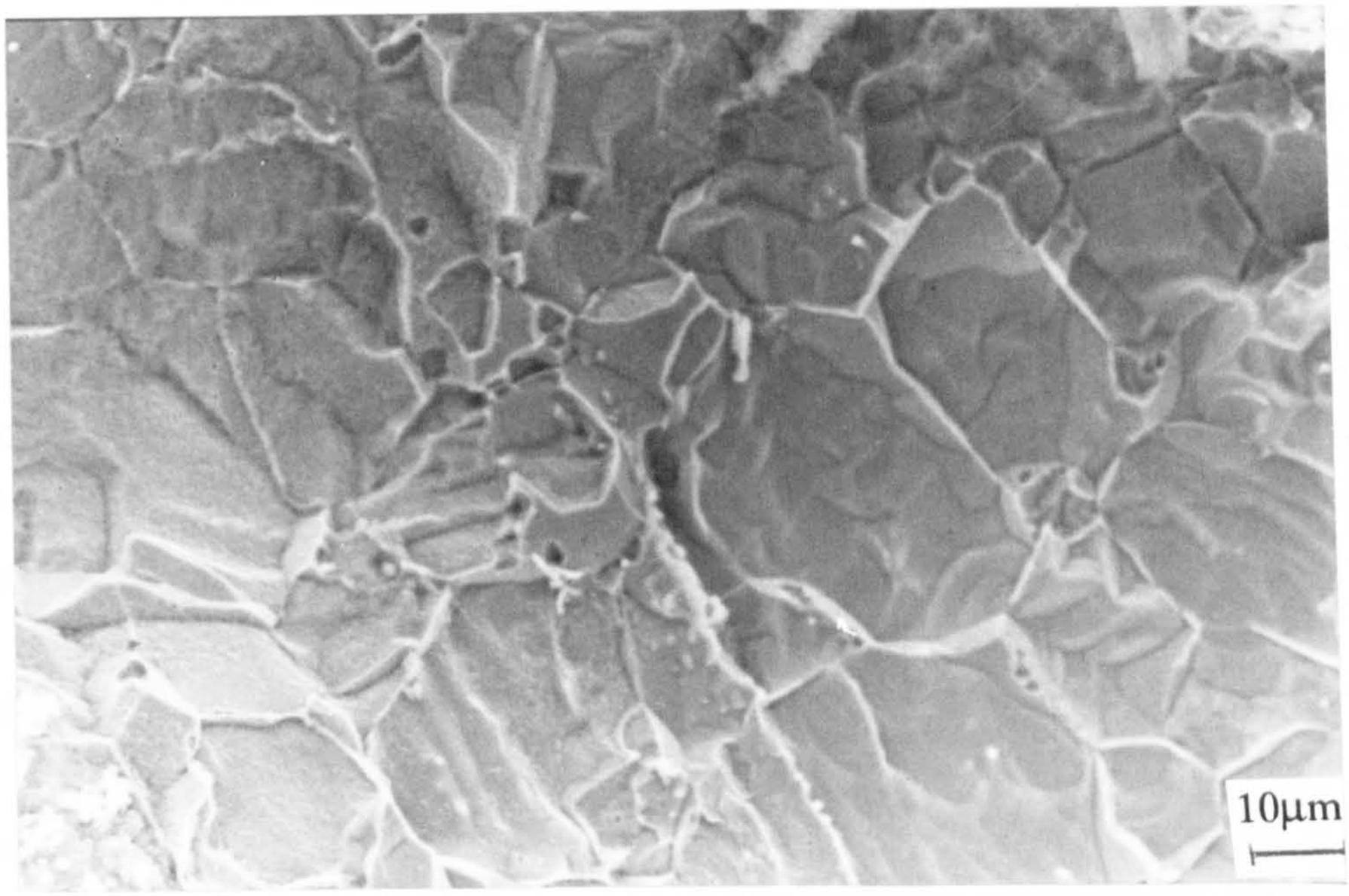

Fig. 7.29. Austenitic structure inside the pit

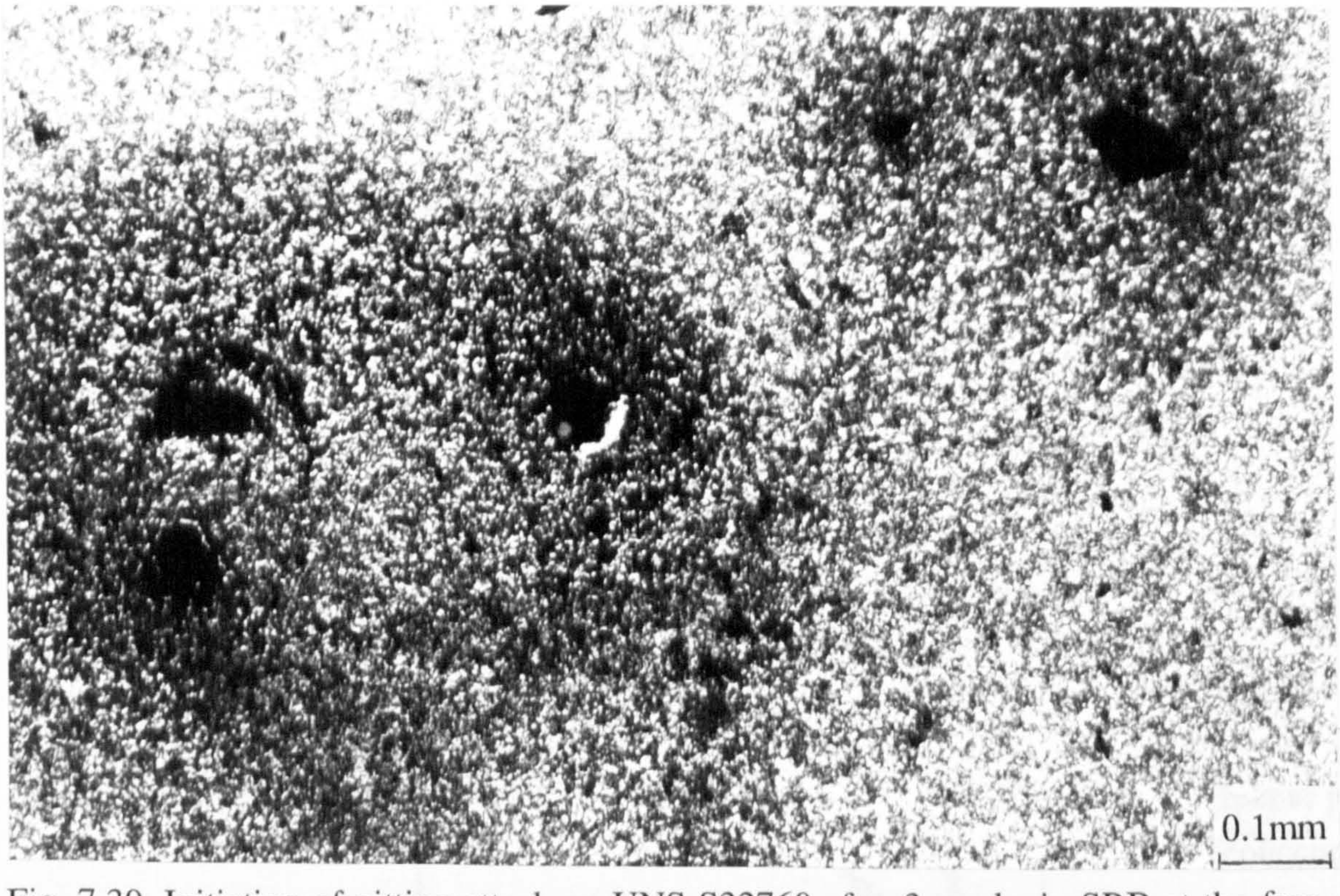

Fig. 7.30. Initiation of pitting attack on UNS S32760 after 3 weeks in SRB at the free corrosion potential

Three months immersion saw the initiation of pitting attack on the most resistant UNS S31254 alloy. Comparable immersion periods of these materials in natural seawater have failed to produce pitting attack (see chapter 8) indicating the ability of the severe environment to affect the localised integrity of the passive film.

Microscopical examination of the UNS S31603 specimen immersed for 3 weeks in SRB before anodic polarisation revealed severe crevice attack and an adherent basal film signifying mixed general and local mechanisms of attack. On Table 7.2, it is shown that the current trip value of 500μA was attained within the previously described anodic current transient and hence the current did not decrease to a steady value. Also on UNS S32760 after 3 months immersion, crevice attack and etching were observed when the same rise in current to 500μA occurred at the modest positive shift in potential from E_{corr}. Pit initiation was observed but was also evident on the freely corroded specimen.

Cathodic Polarisation

The emphasis in this study was on the effects of SRB on the mechanisms of attack and for this reason only limited cathodic polarisation tests were performed. These were concentrated on only selected materials.

As expected there were distinct differences in the cathodic polarisation characteristics in the deaerated SRB-containing seawater as opposed to the aerated seawater considered in previous chapters. Figure 7.31 shows for 1 hour immersion in aerated seawater and SRB containing seawater, the differences in the current-potential relationship. The H_2S content of the solution was 120ppm.

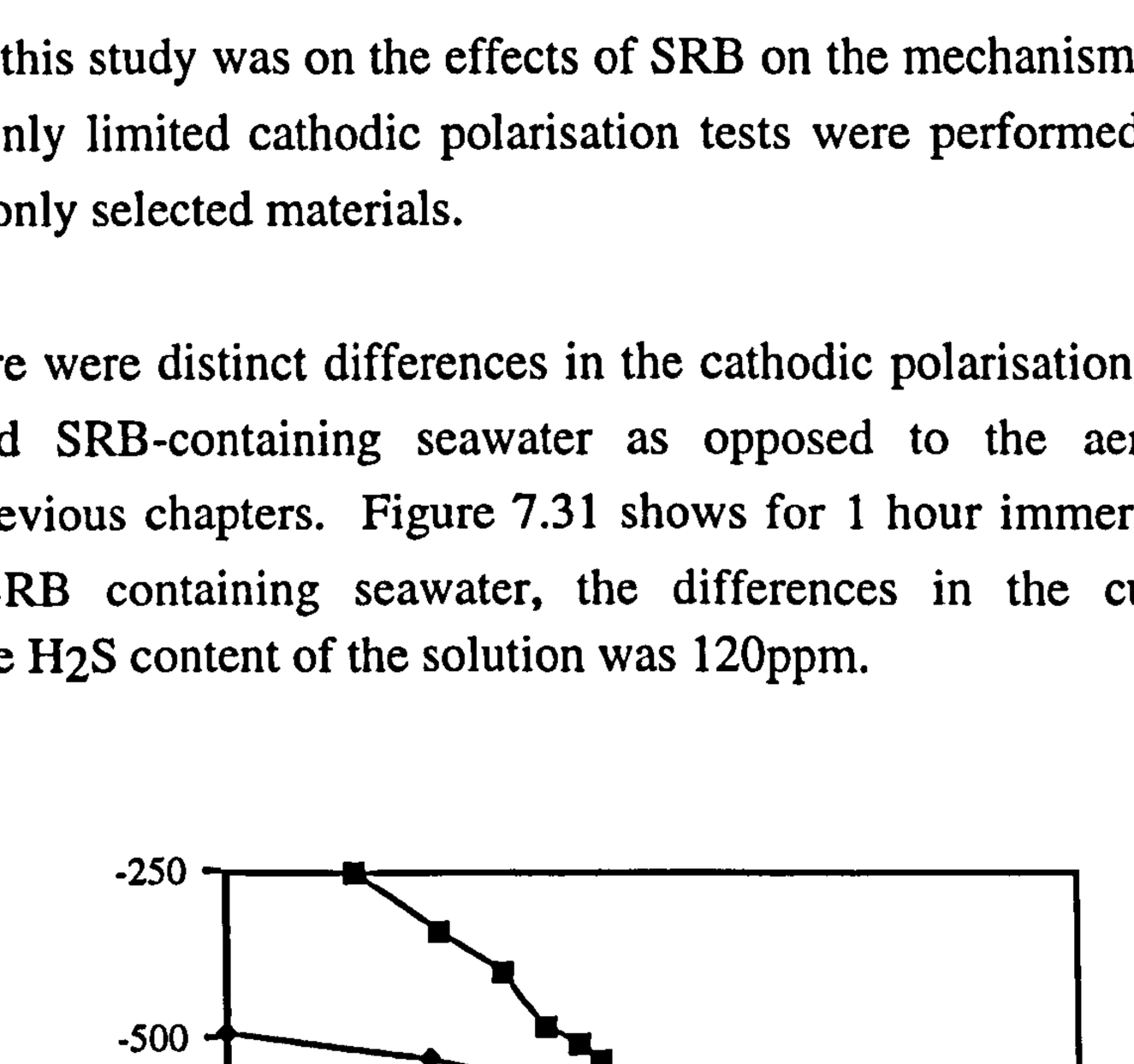

Fig. 7.31. Cathodic polarisation on UNS S32760 in SRB and in SRB-free seawater

There are concentration polarisation effects evident in the SRB polarisation curve but in contrast to the SRB-free case, the limiting currents are an order of magnitude greater and for the potential range from E_{corr} to -1100mV the reaction largely follows Tafel kinetics. The currents in the SRB-containing environment are lower in the small potential region nearest to E_{corr}

After immersion for 6 days in the same SRB container, cathodic polarisation on UNS S32760 yielded a higher limiting current as shown in Fig. 7.32. The H_2S level was measured at 140ppm and was therefore relatively stable for the total immersion period between 1 hour and 6 days.

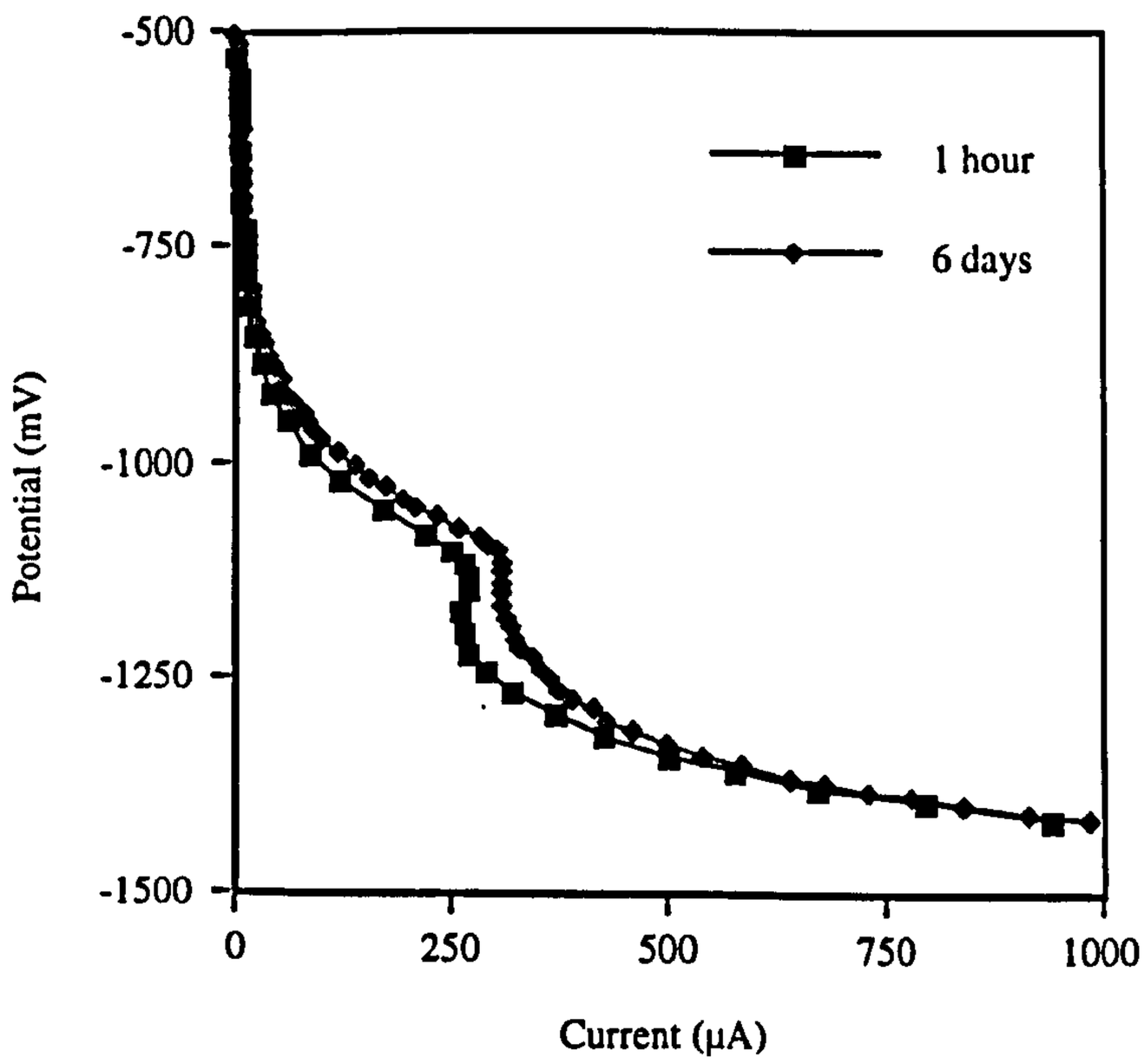

Fig. 7.32. Cathodic polarisation on UNS S32760 after 1 hour and 6 days in SRB

After 3 months in SRB, the concentration of H_2S was measured at 30ppm (much lower than in the aforementioned tests). Cathodic polarisation on a new specimen immersed for 1 hour at 30ppm showed a lower limiting current than for the same immersion period at 150ppm, possibly due to depletion of buffer capacity at the surface during hydrogen evolution. The effect of immersion time was still evident in that higher cathodic currents were obtained on the specimen immersed for 3 month (Fig. 7.33).

An anodic polarisation test was performed on UNS S32760 up to an anodic current of 7000μA and it was clear that the surface was partially covered by sulphide corrosion products. The specimen was left in SRB for 3-4 hours until E_{corr} had stabilised to near

it's original value. At that point the cathodic reaction characteristics were monitored through cathodic polarisation and it was found that the effect of this treatment was to depolarise the cathodic reaction to the extent shown in Fig. 7.34.

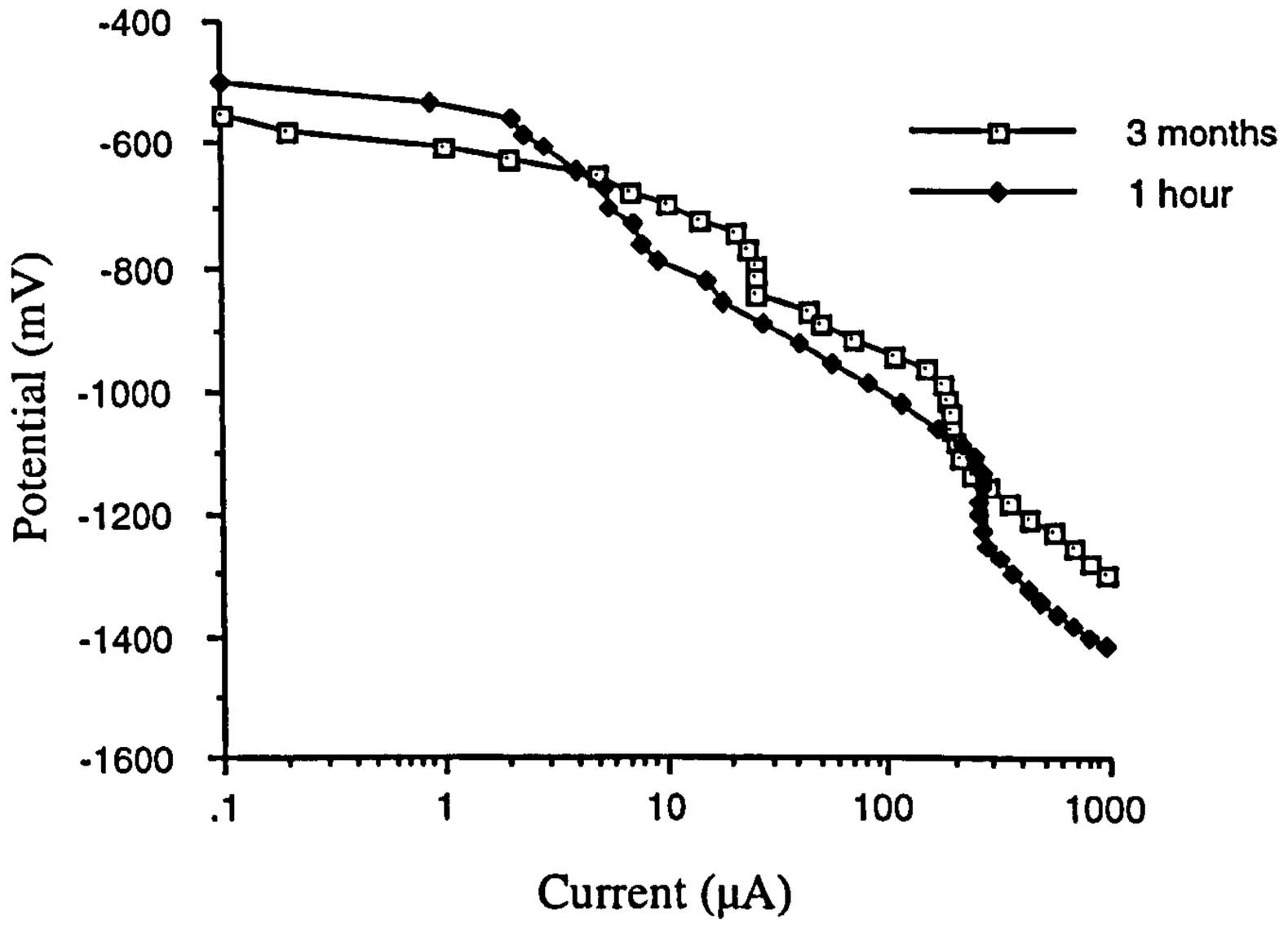

Fig. 7.33. Cathodic polarisation on UNS S32760 after 1 hour and 3 months in SRB

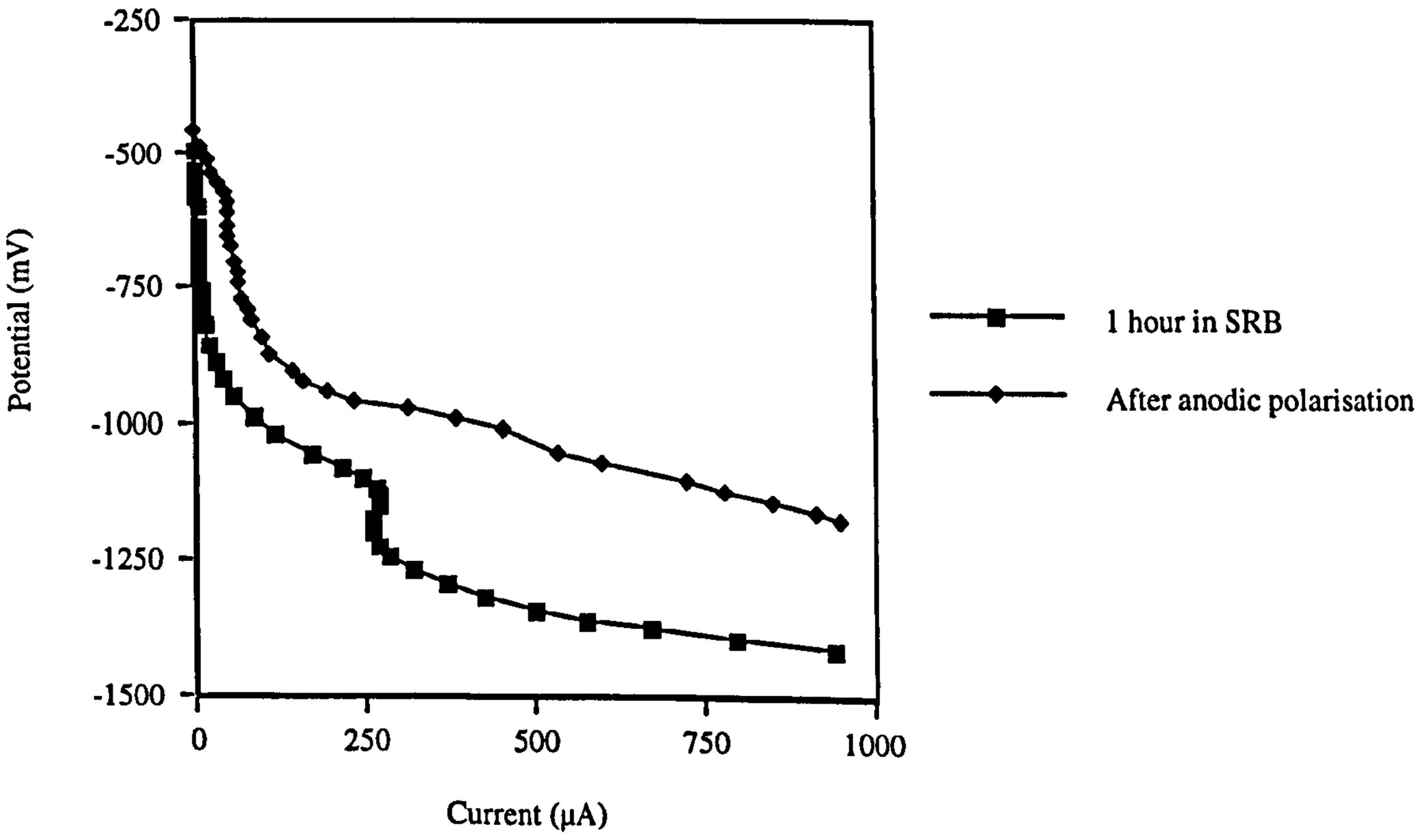

Fig. 7.34. Cathodic polarisation on a specimen containing an extensive covering of black sulphide corrosion products

Investigation of the Current Transient (I_a)

A series of tests was devised to investigate the electrochemical phenomena and the corrosion attack (if any) associated with the initial rise in current to I_a. Two types of test were performed: anodic polarisation tests to the peak current I_a at which point the specimen was removed from the SRB and examined and potentiostatic tests where the potential was scanned to reach the current peak I_a and then held constant with the current recorded as a function of time.

The potentiostatic tests were arbitrarily concentrated on two materials : 25Cr duplex and UNS S31254. After 2 days, 1 month and 6 months immersion the current in the potentiostatic test on 25Cr duplex immediately fell off to small values when the potential was held constant as shown in Fig. 7.35a,b and c. Even after 6 months when the initial current at I_a was substantially larger than after 2 days, the current still dropped rapidly to a very low value (<5μA).

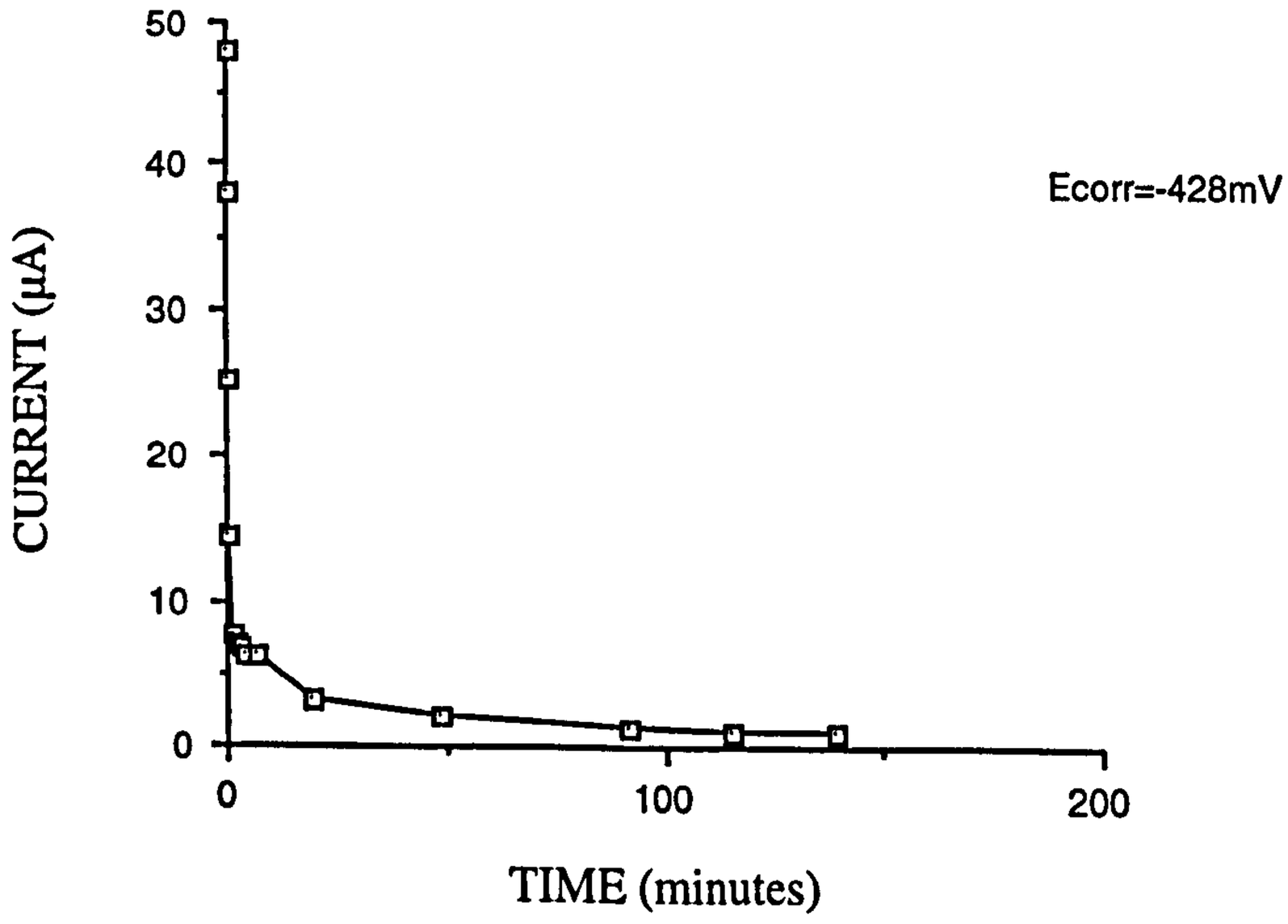

(a)

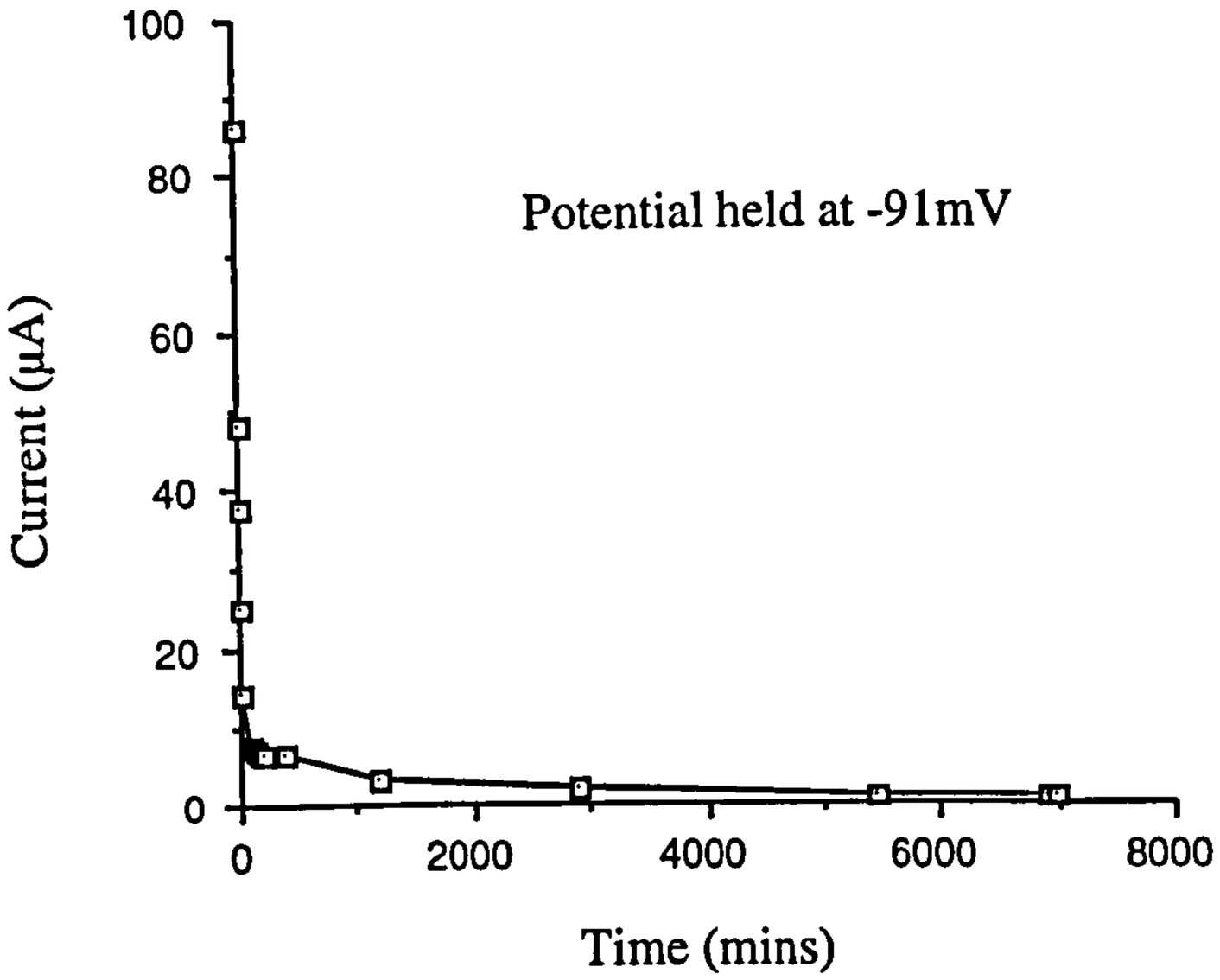

(b)

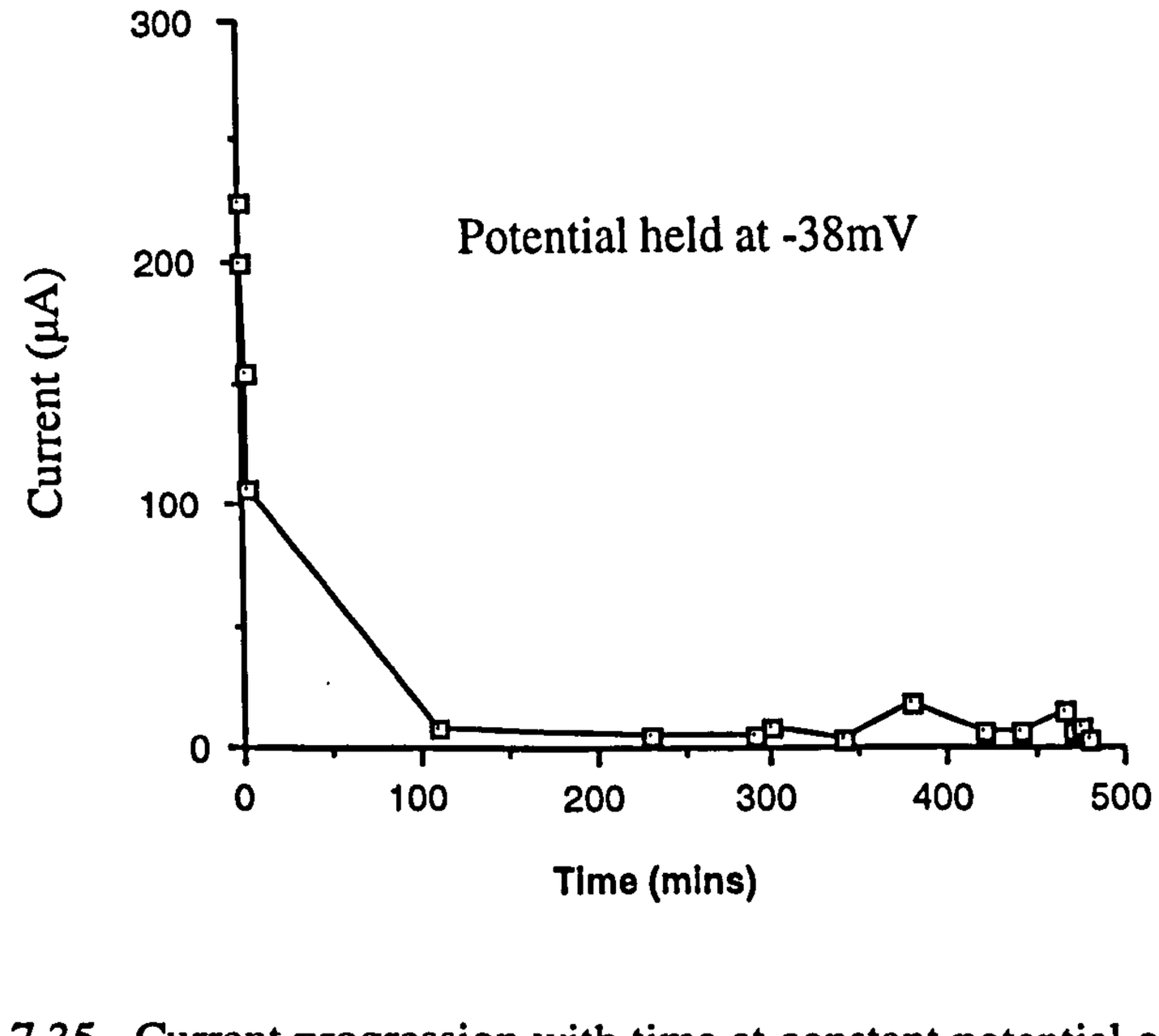

(c)

Fig. 7.35. Current progression with time at constant potential corresponding to I_a after (a) 2 days (b) 1 month and (c) 6 months

In all the potentiostatic tests, control samples were immersed which were not subjected to the increase in potential and after completion of the tests, both the polarised and unpolarised specimens were examined. Although in each potentiostatic test the current had fallen off, suggesting an immediate repassivation and minimal corrosion attack,

surprising evidence of extensive attack, not observed on the unpolarised specimens was recorded. After 1 month in SRB, there was severe etching, signifying attack at the grain boundaries over a significant area (approximately 25%) of the specimen. The attack was evident under a black sulphide film as was found on the unpolarised specimen. Figure 7.36 shows the loose film on the surface and underneath the areas where the outer surface layer has been removed to reveal an etched structure. In Fig. 7.37, the lower Cr and Mo austenitic -1 and 3, and ferritic regions-2 (identified by spot analyses) are shown and the patchy sulphide film surrounds the attacked area. The SEM backscattered image (Fig.7.38) shows clearly the areas at the grain boundaries lower in atomic number which were found to correlate to the areas rich in sulphur.

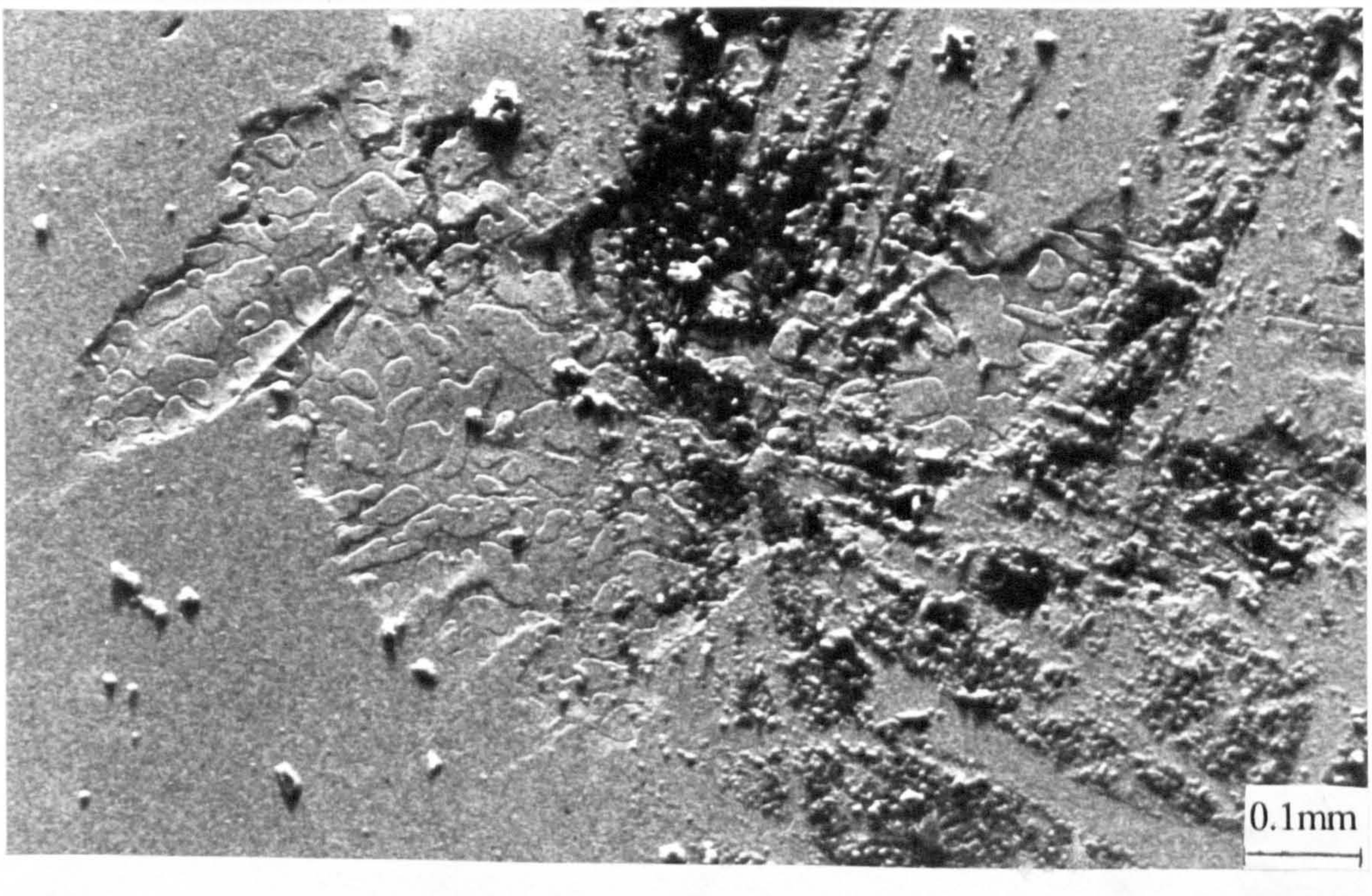

Fig. 7.36. Loose film and etching on the surface of 25Cr duplex after 1 month and the current taken to I_a

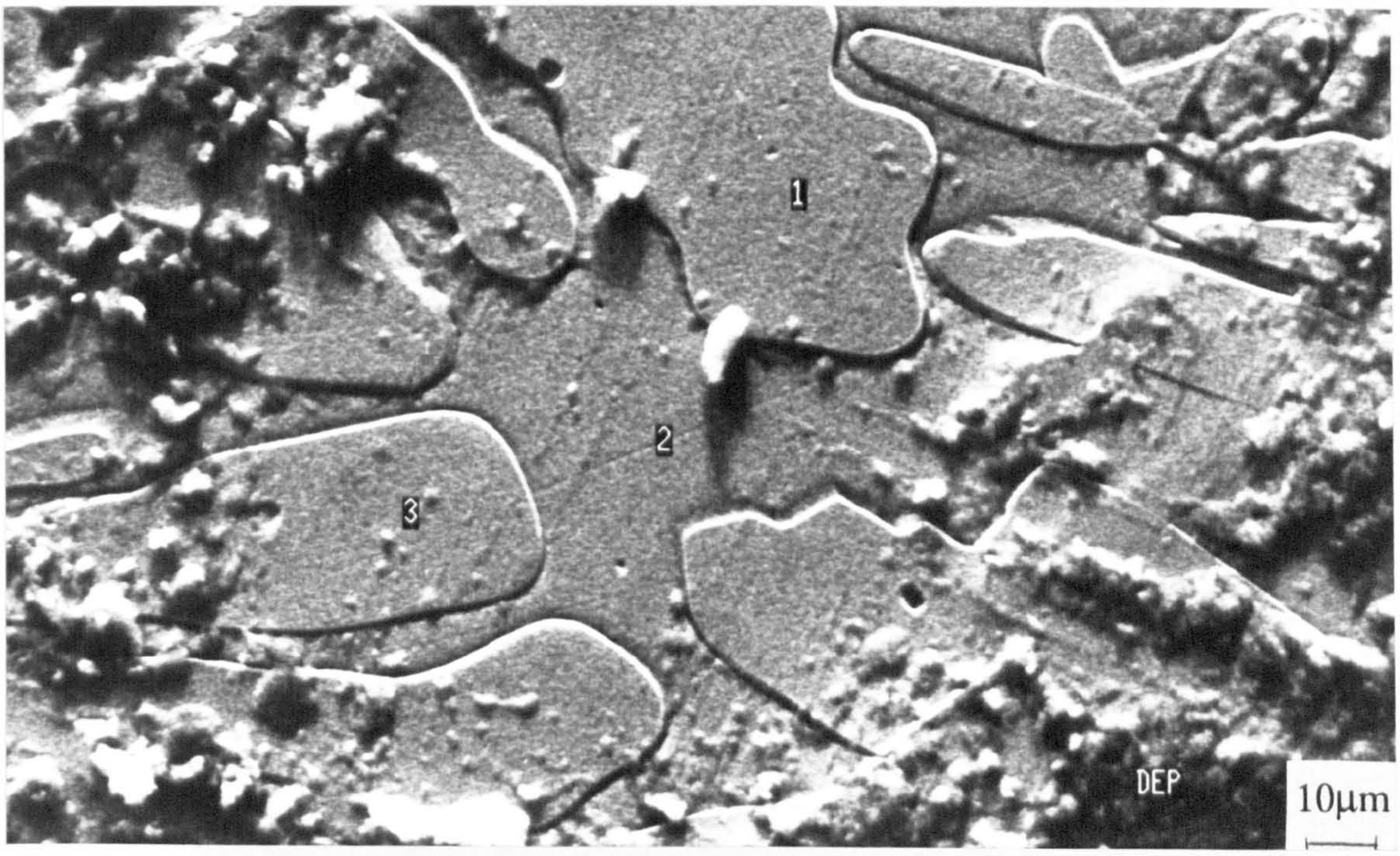

Fig. 7.37. Etching on the surface of 25Cr duplex after 1 month and the current taken to I_a

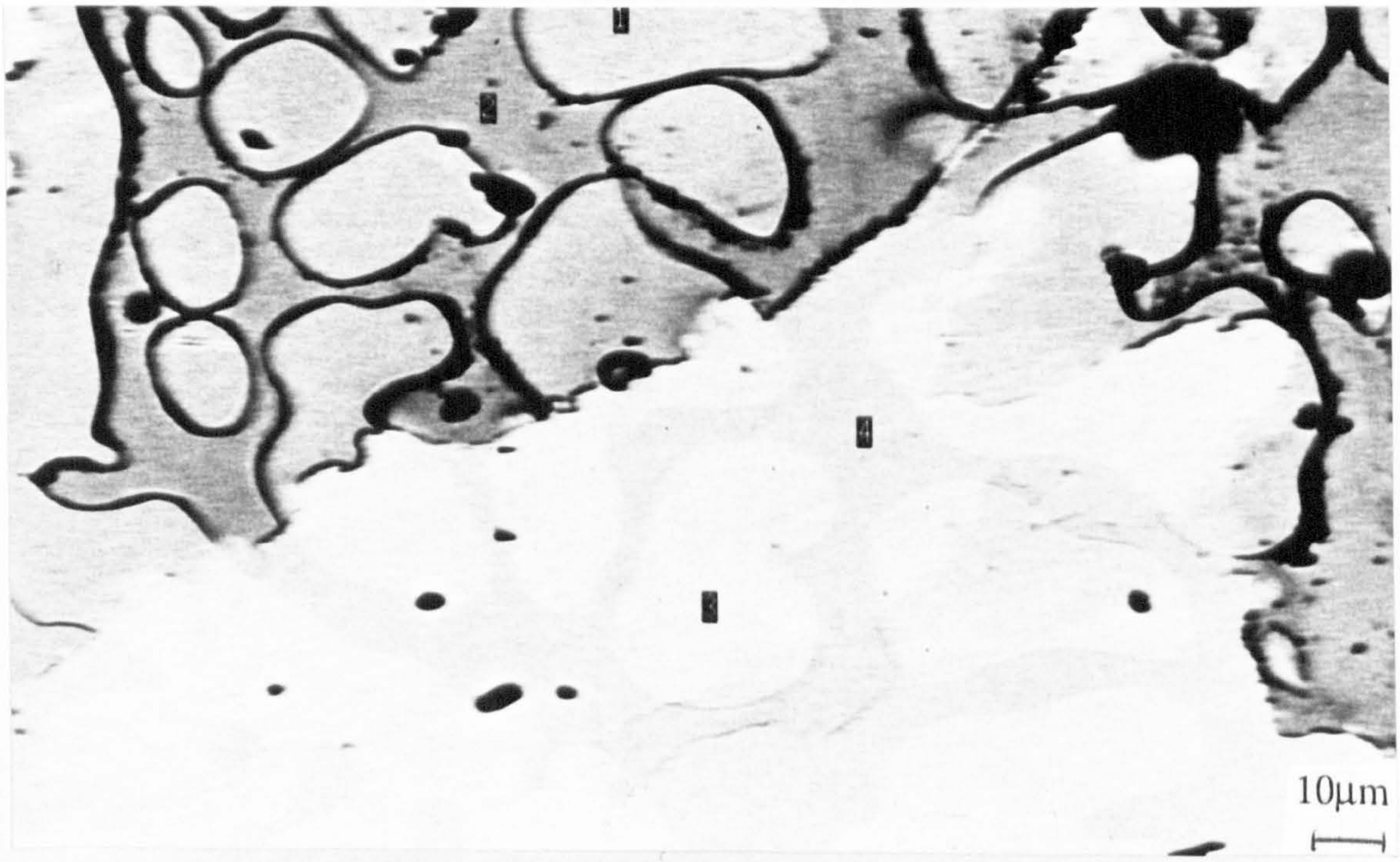

Fig. 7.38. Backscattered image of etching on the surface of 25Cr duplex after 1 month and the current taken to I_a

After 6 months immersion in SRB, it has already been stated that under free corrosion conditions the 25Cr duplex showed signs of crevice corrosion and etching with preferential sulphide formation on the austenite. After 6 months immersion, followed by the potentiodynamic sweep to -38mV and potentiostatic control, there was extensive attack visible which was not apparent on the unpolarised specimen. The attack was manifested in preferential removal of the austenite grains (Fig 7.39) to form pits as the voids which were left, coalesced (Figs 7.40a and b). There was evidence to suggest that the attack initiated at the grain boundaries and progressively encroached into the austenitic grains (Fig 7.41). The overall effect was to leave a surface extensively deteriorated by removal of one of the duplex phases (Fig. 7.42).

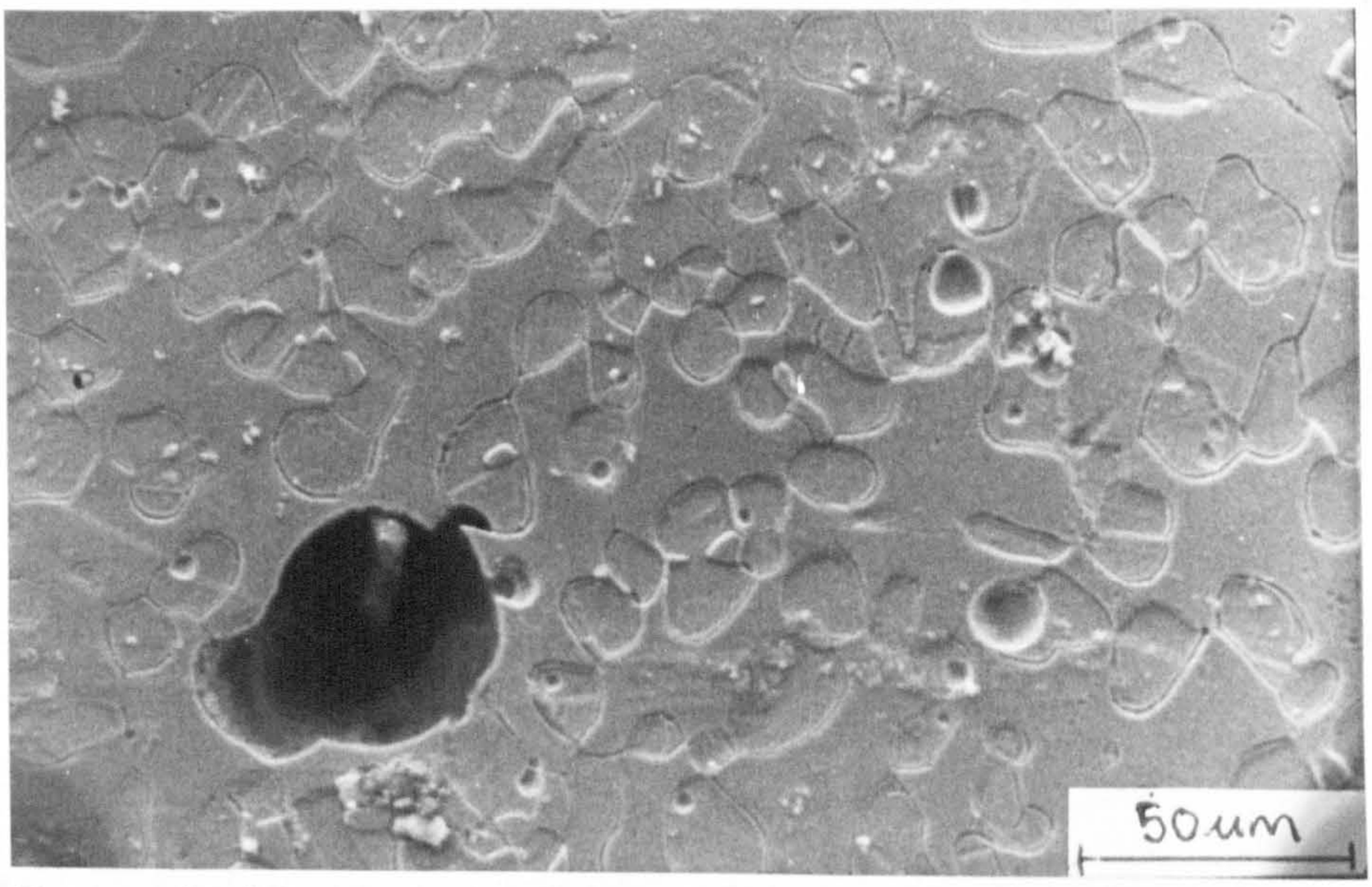

Fig. 7.39. Removal of the austenite phase of 25Cr duplex in SRB. Potential held at current transient peak.

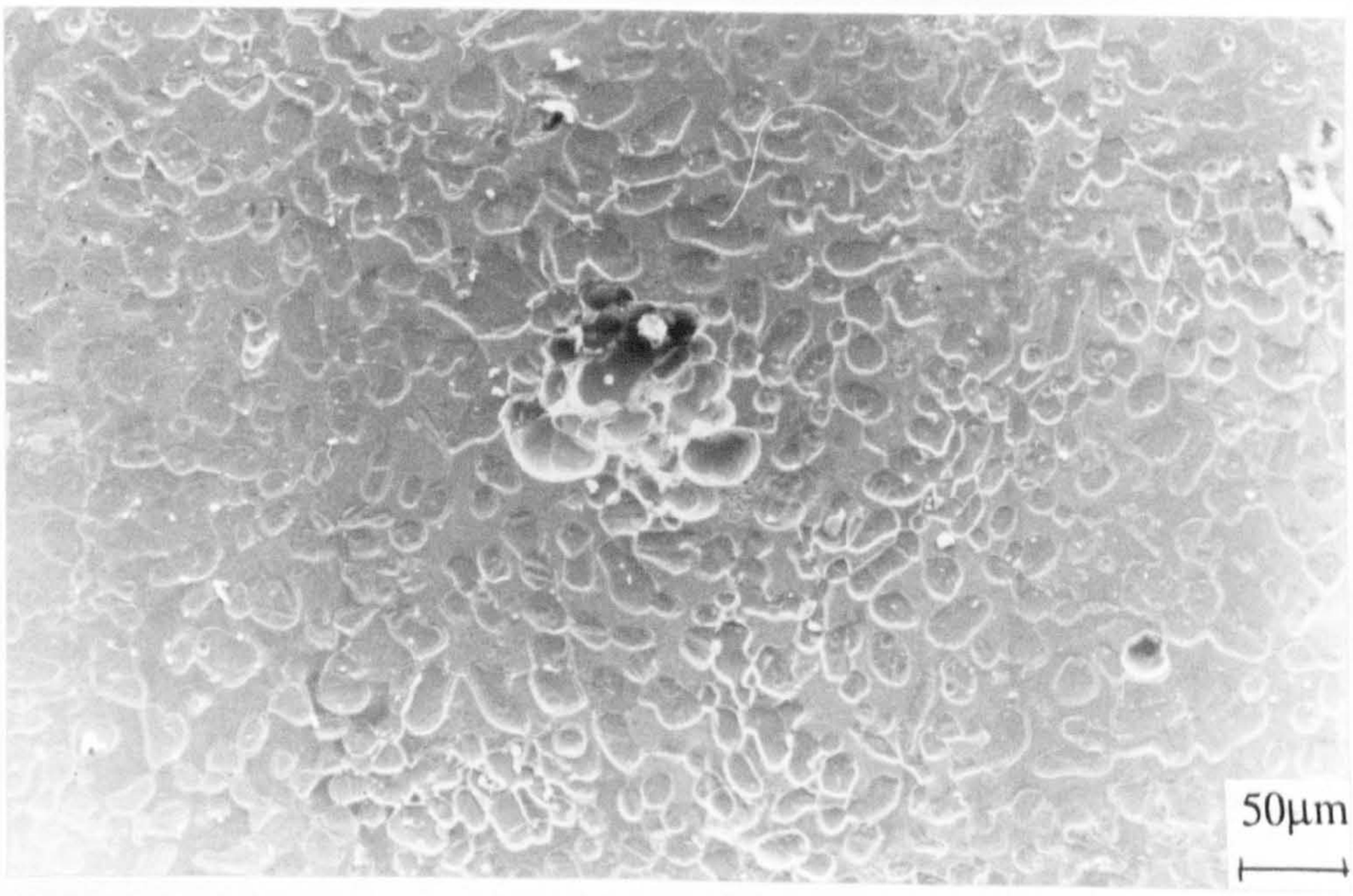

(a)

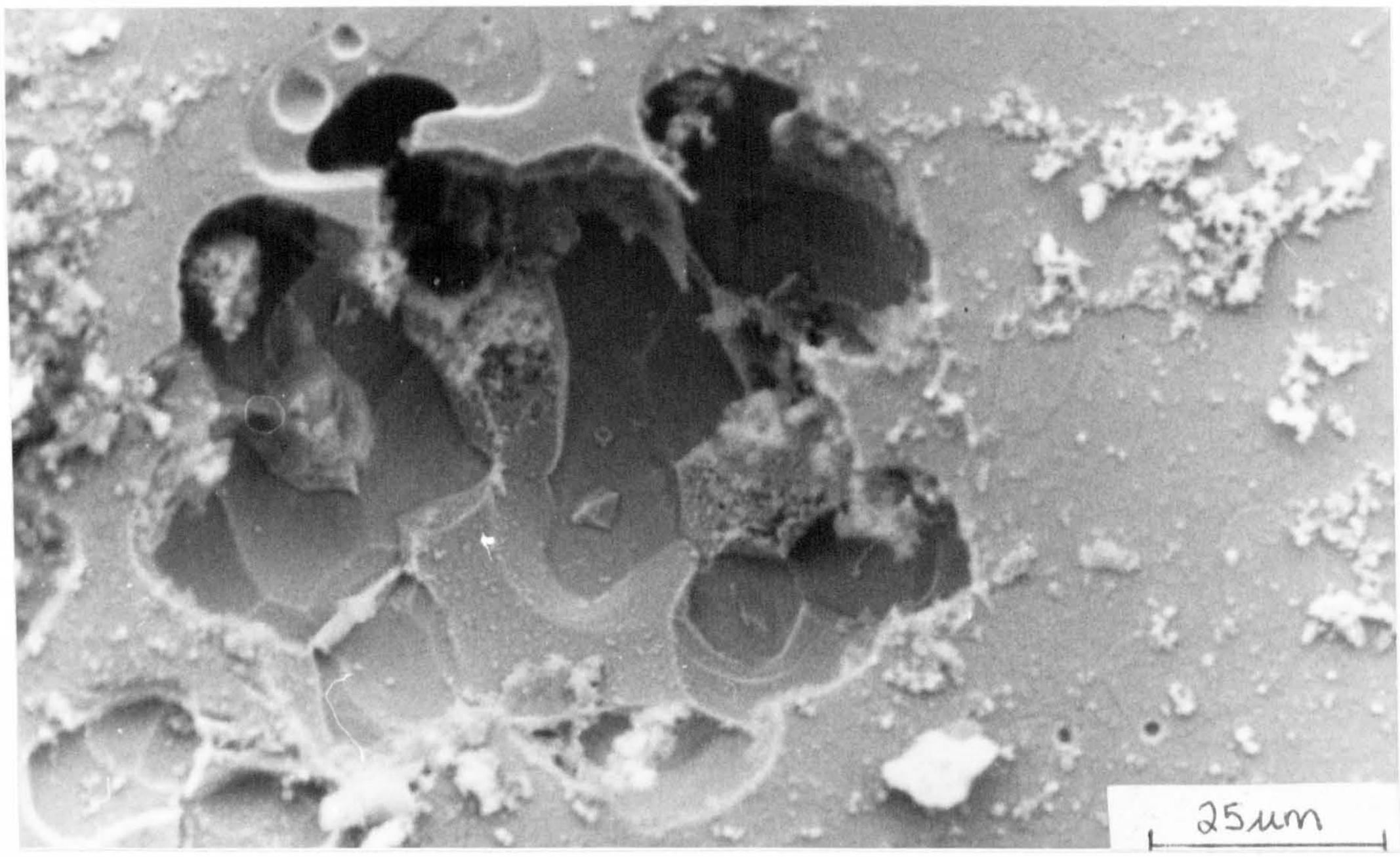

(b)

Fig. 7.40 (a). Pitting as the removed austenite areas coalesce and overall deterioration at pitted site and (b) duplex structure still evident within pit. Potential held at current transient peak.

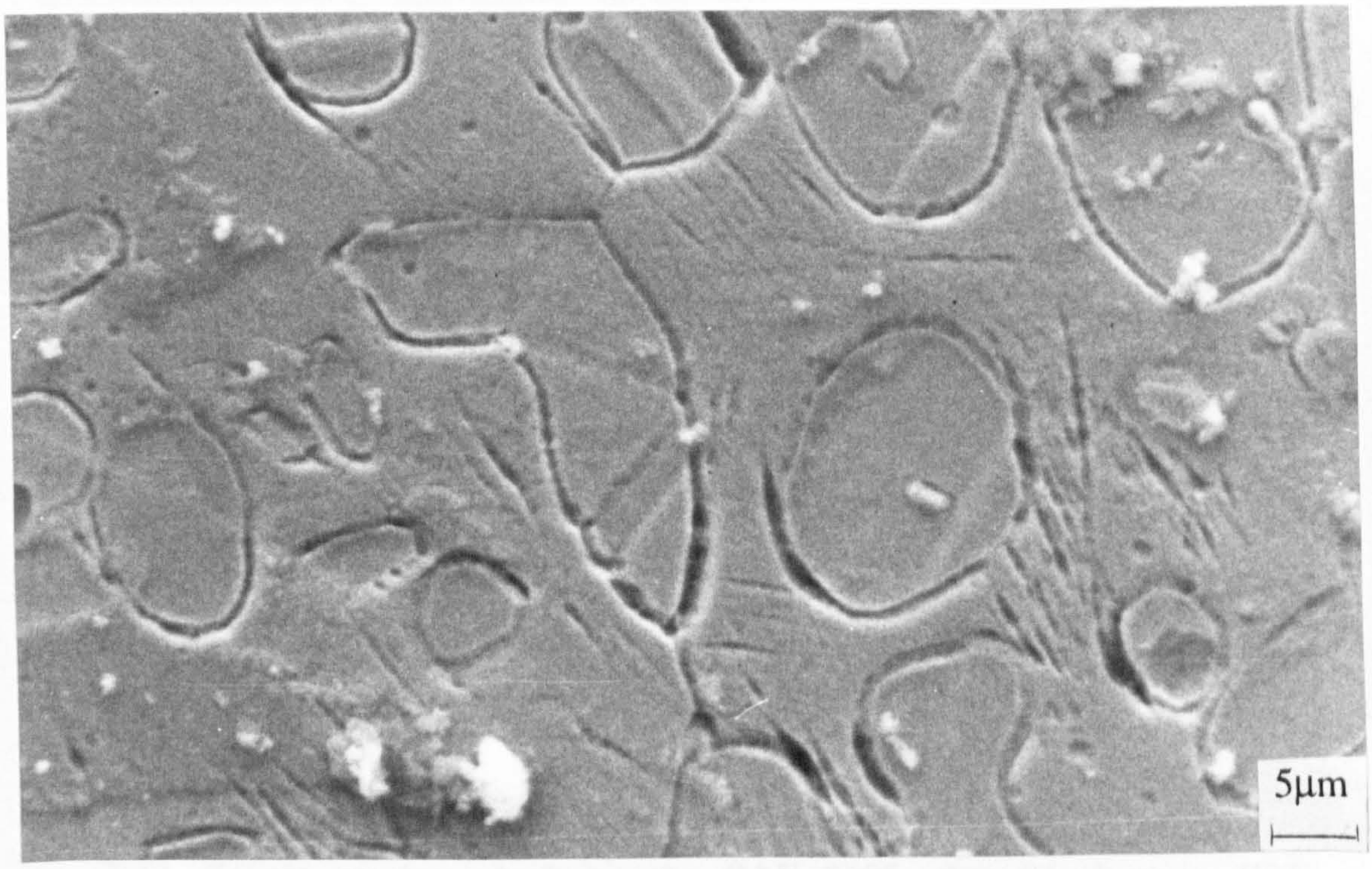

Fig. 7.41. Initiation of attack at the grain boundaries on 25Cr duplex

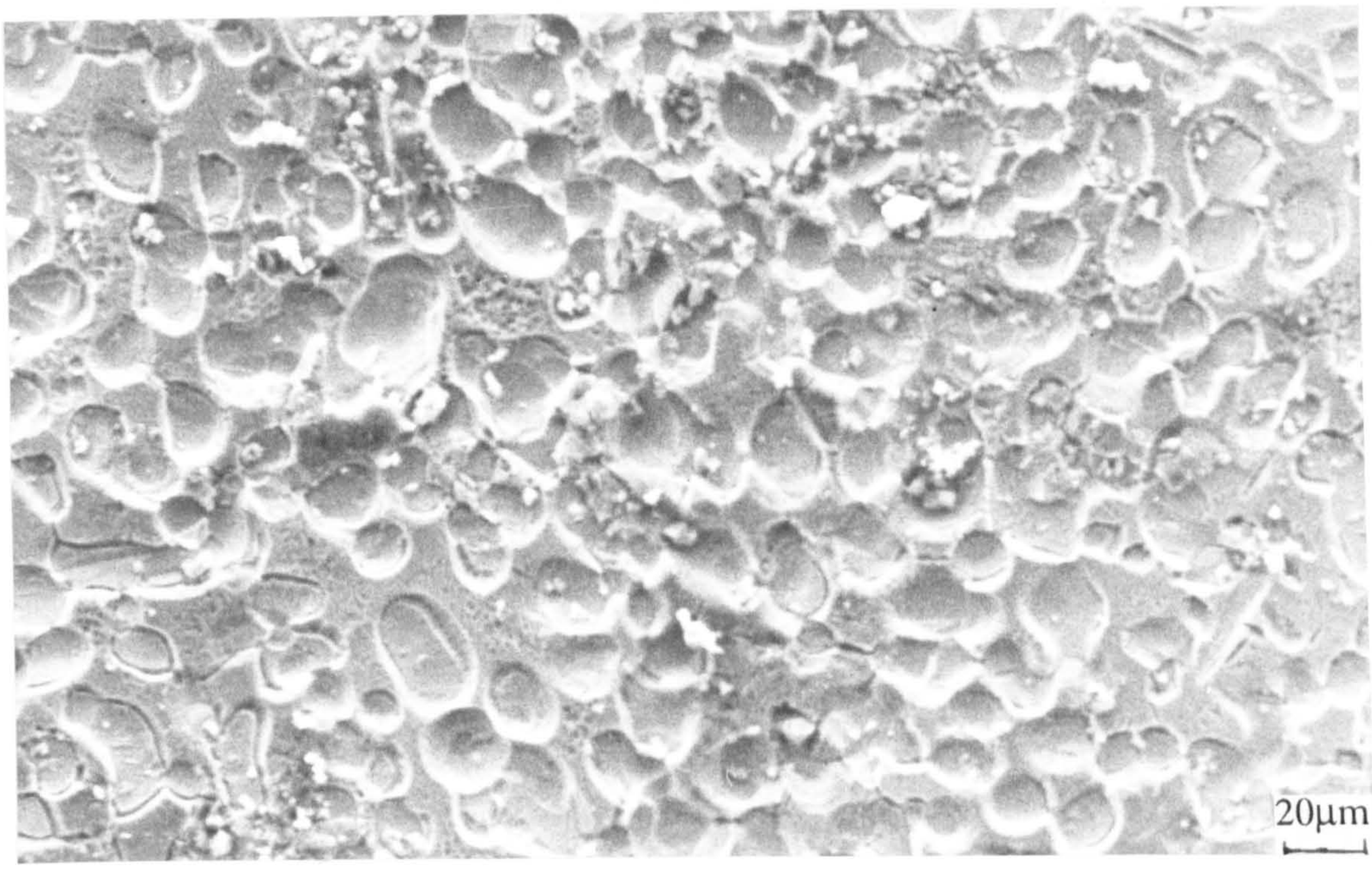

Fig. 7.42. Overall deterioration due to the preferential dissolution of austenitic phase

After 21 days in SRB at the free corrosion potential, SAF 2205 showed evidence of pit initiation in two small regions but otherwise was unattacked. However, after the same length of immersion (and the same concentration of H_2S) but with potentiostaic control at the end of the experiment at the current transient, severe crevice attack was visible at 3 of the 4 metal/resin interfaces (Fig. 7.43).

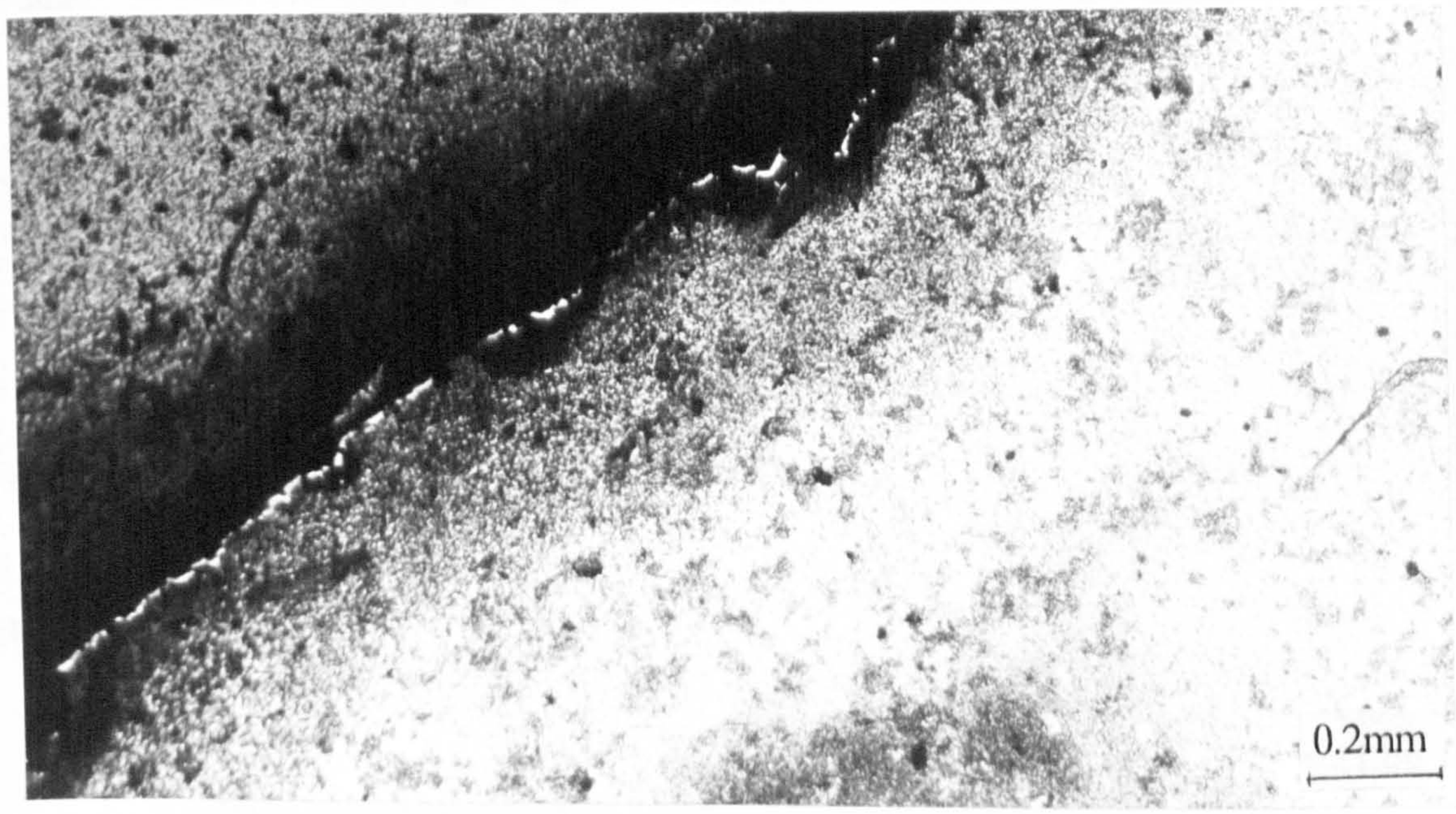

Fig. 7.43. Severe crevice attack on the SAF 2205 after 21 days in SRB and potentiostatic test up to the current transient peak.

UNS S31254 showed good resistance to localised corrosion initiation even after 6 months with only minor crevice attack observed. However, after a potentiostatic test for 3 hours at the current transient peak I_a (in which, like the 25 Cr duplex and the SAF 2205, the current dropped off immediately) distinctive attack was evident. Figure 7.44 shows signs of initiation of grain boundary attack at the austenite grain boundaries to reveal the UNS S31254 structure. The effect can be seen under the black film which had also formed on specimens after anodic polarisation (Fig. 7.44).

Further potentiostatic tests were performed on 25Cr duplex which involved taking the potential more positive than the current transient loop, to a potential of +385mV. The current logged as a function of time, in contrast to previous tests at the peak of the transient, increased as shown in Fig 7.45. No pitting attack was observed on the specimen but the characteristic etching and minor crevice attack were detected.

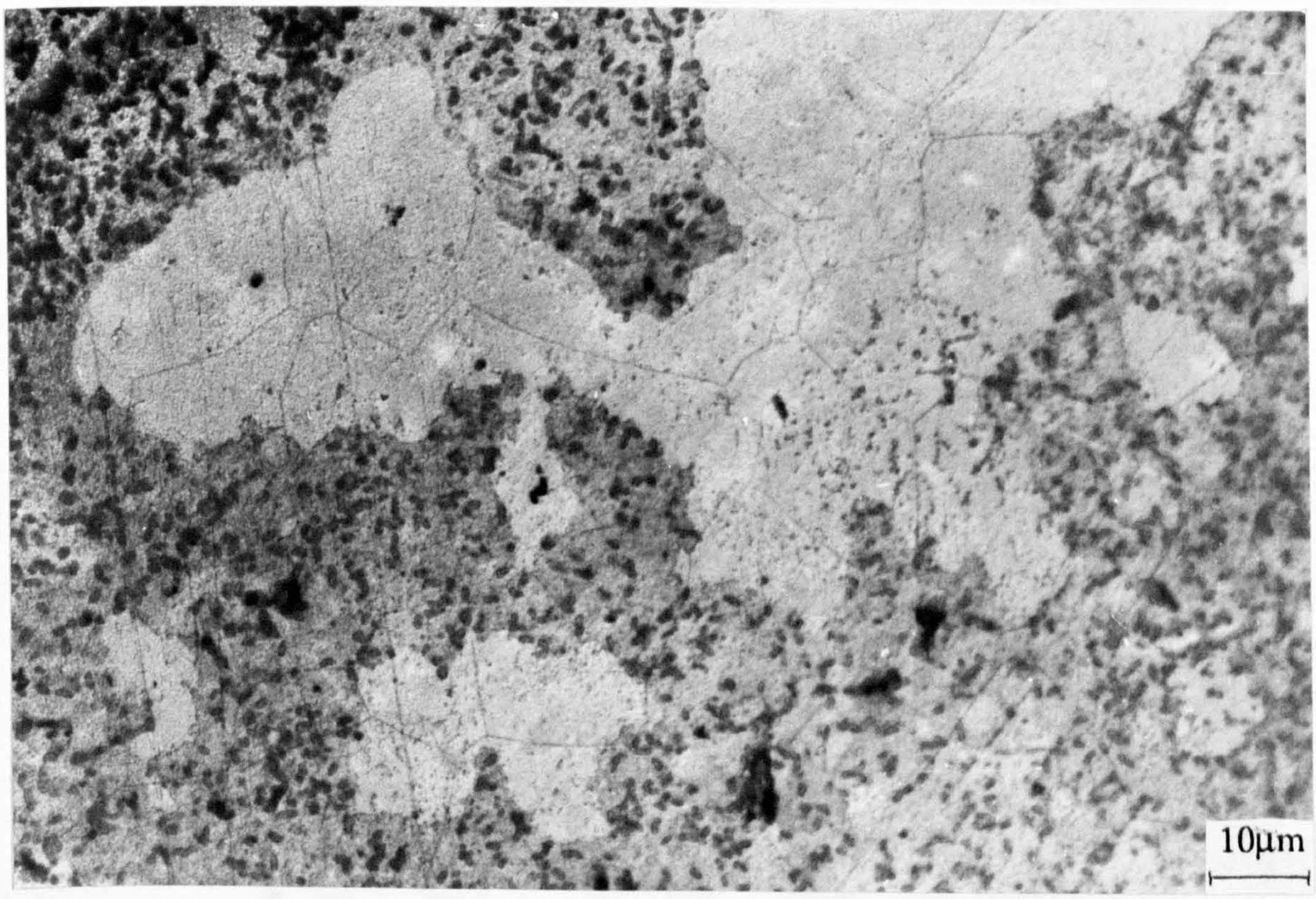

Fig. 7.44. Initiation of grain boundary attack on UNS S31254 under the sulphide film in SRB.

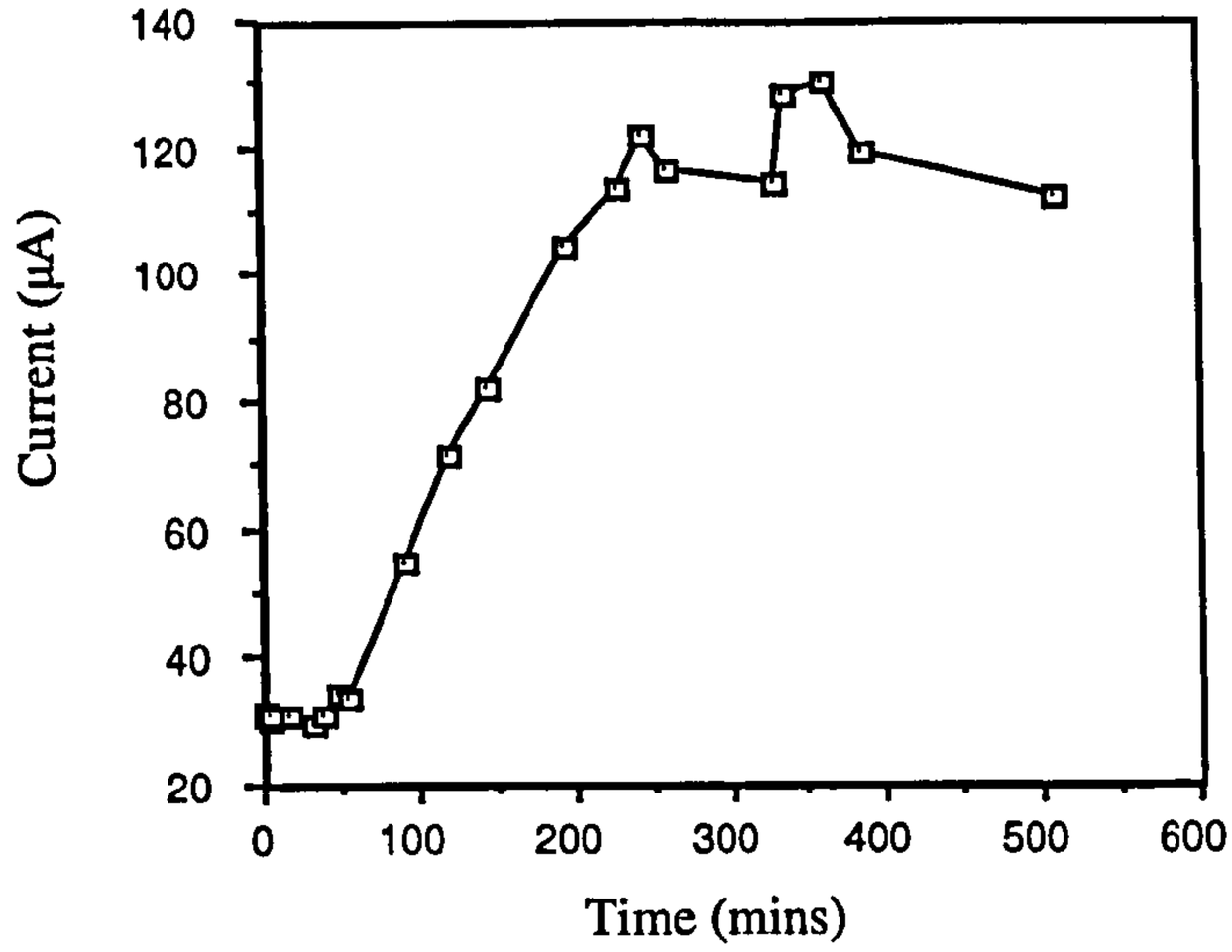

Fig. 7.45. Evolution of current versus time on 25Cr duplex at a potential of +385mV

Coupling Experiments

Specimens of 25Cr duplex were immersed simultaneously and coupled in SRB and the resulting currents were measured between them. As expected a very small current of 0.02μA was recorded. The specimen then acting as the anode (**A**) was then subjected to anodic polarisation to a high current of 5000μA and then immediately recoupled, the currents were again monitored. Specimen **A** was partially covered by black corrosion products whereas **B** which had not undergone any polarisation was virtually free from a surface deposit. Figure 7.46 shows the resulting currents recorded after the anodic polarisation of A. It is important to note that specimen **A** at all times acted as the couple *cathode.*

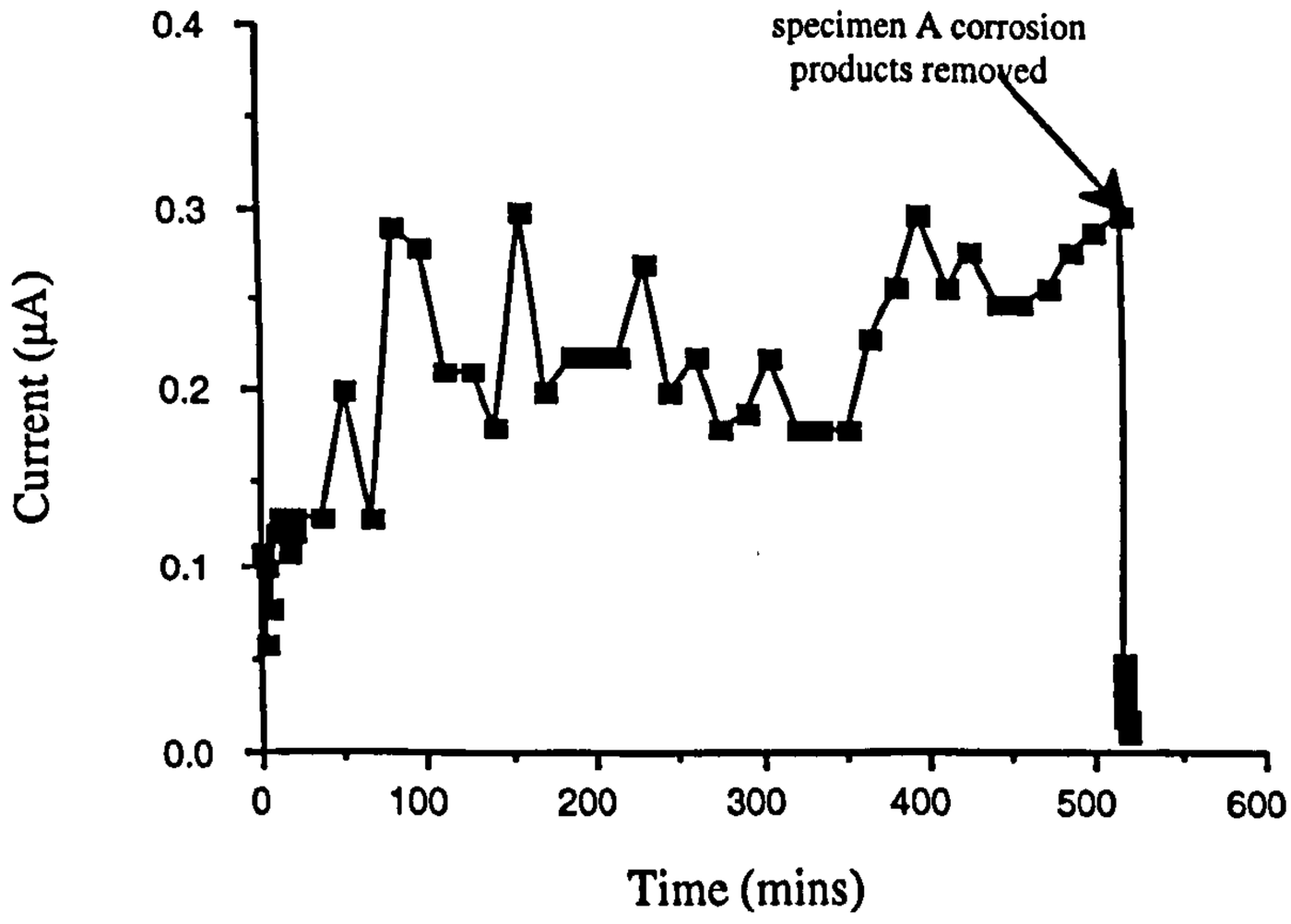

Figure 7.46. Currents monitored in the galvanic cell between **A** and **B**

After 520 minutes the corrosion products from specimen **A** were removed by a small cloth without disturbing the H_2S content which was 45ppm for the duration of the test. The current between the specimens was seen to fall to very small values.

Aerobic Bacteria - *Vibrio Alginolyticus*

Trends in E_{corr}

In the culture of aerobic bacteria, there was no systematic trend in E_{corr} over the immersion period of 10 weeks. An initial decrease in E_{corr} was observed for all materials with the exception of UNS S32760 as shown in Fig. 7.47.

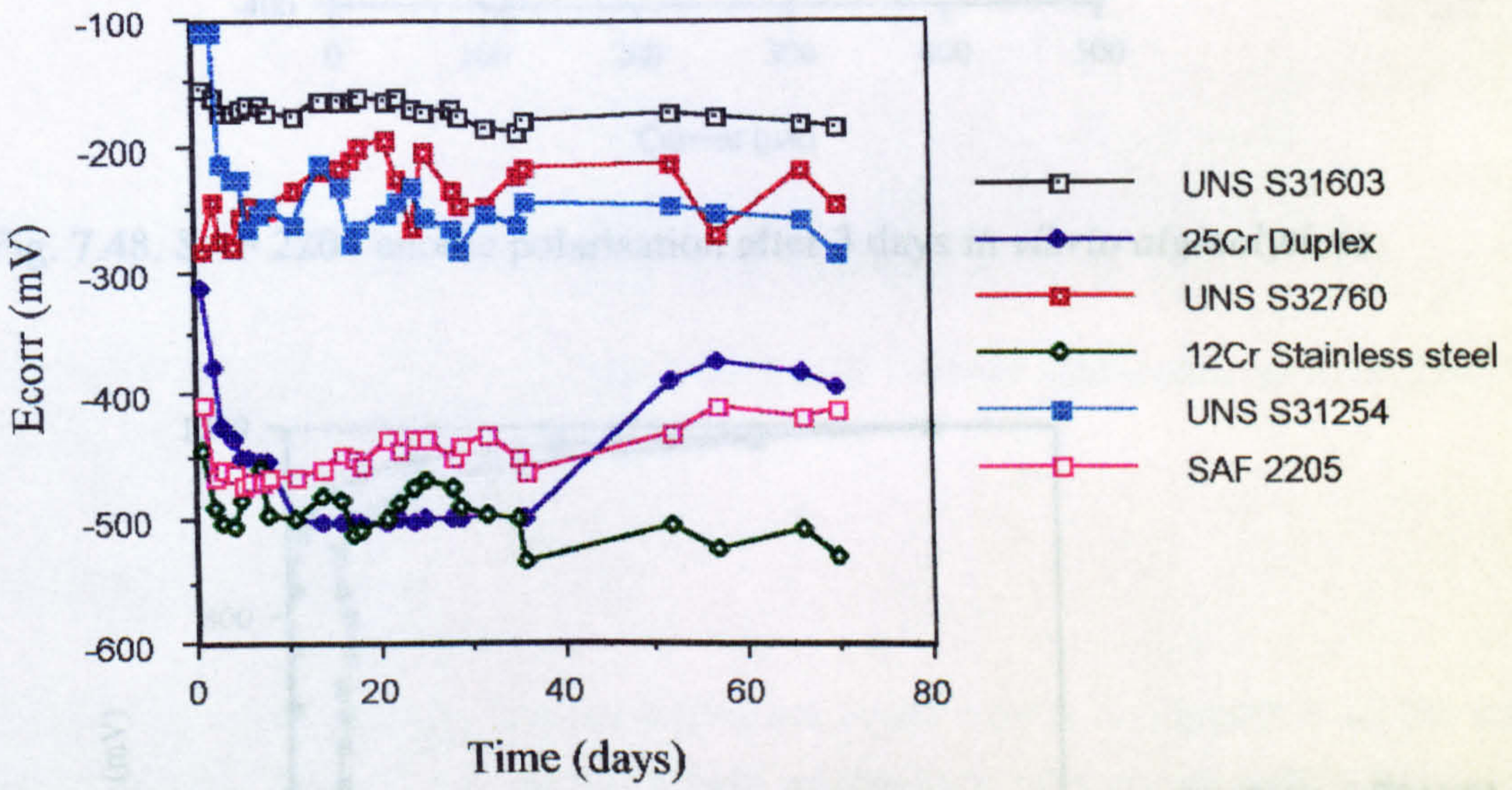

Fig. 7.47. Trends in E_{corr} during immersion in a culture of aerobic bacteria

Anodic polarisation

On the superduplex stainless steel UNS S32760 and the superaustenitic UNS S31254, the presence of the aerobic bacteria did not have any detrimental effect over the short immersion periods studied (up to 2 weeks). On SAF 2205 and the 25Cr duplex however, although the breakdown potential was not lowered by the bacterial inoculation, there were changes in the repassivation characteristics. After anodic polarisation scan reversal, the current dropped as if complete repassivation would occur but as shown in Figs 7.48 and 7.49 for SAF 2205 and 25Cr duplex respectively, the currents on the reverse scan remained much larger than in the forward scan of the 'passive' region. On UNS S31603, the only effect was to increase the current I_{max} from 1600μA to 2200μA.

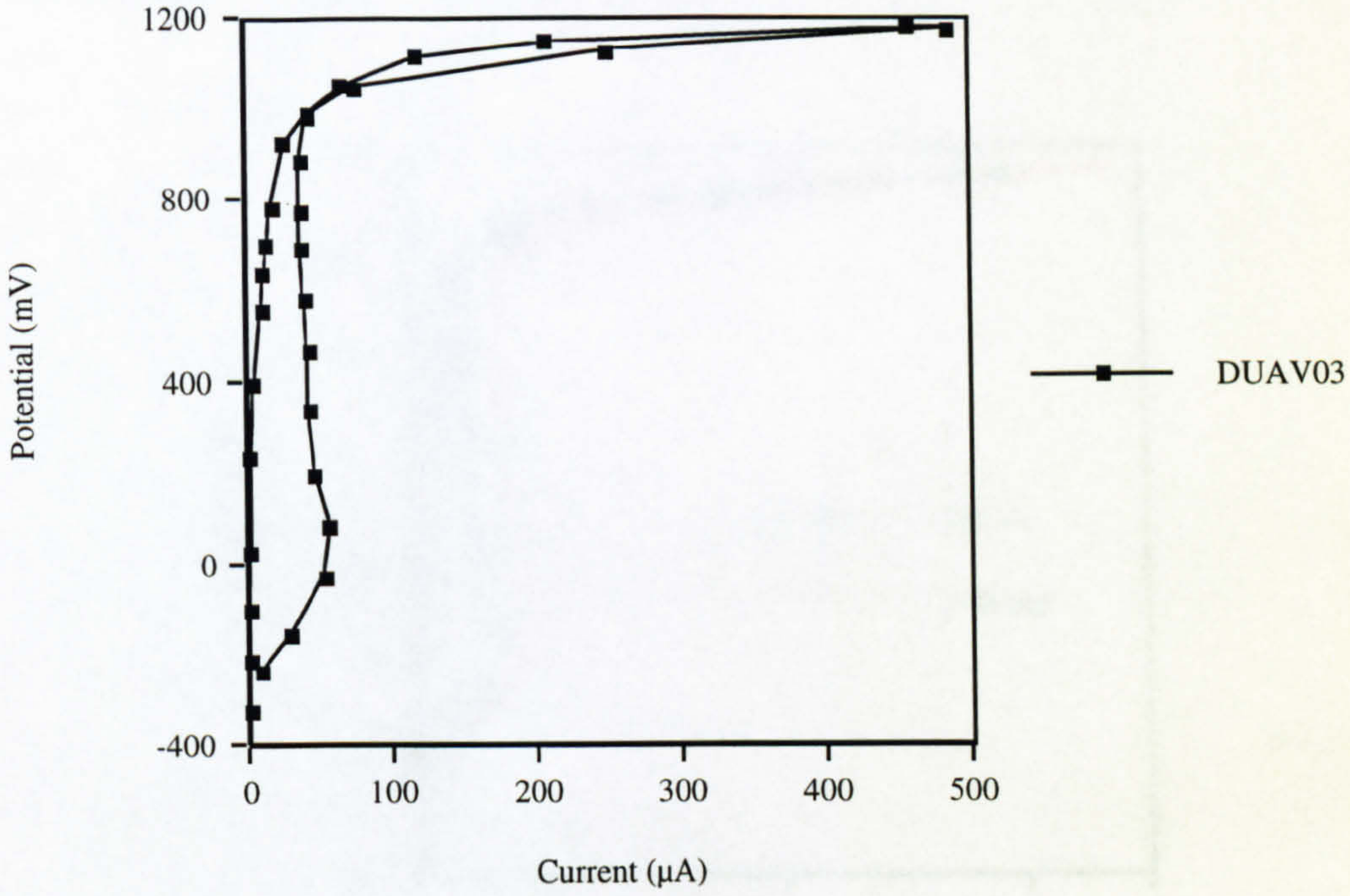

Fig. 7.48. SAF 2205 anodic polarisation after 3 days in *vibrio alginolyticus*

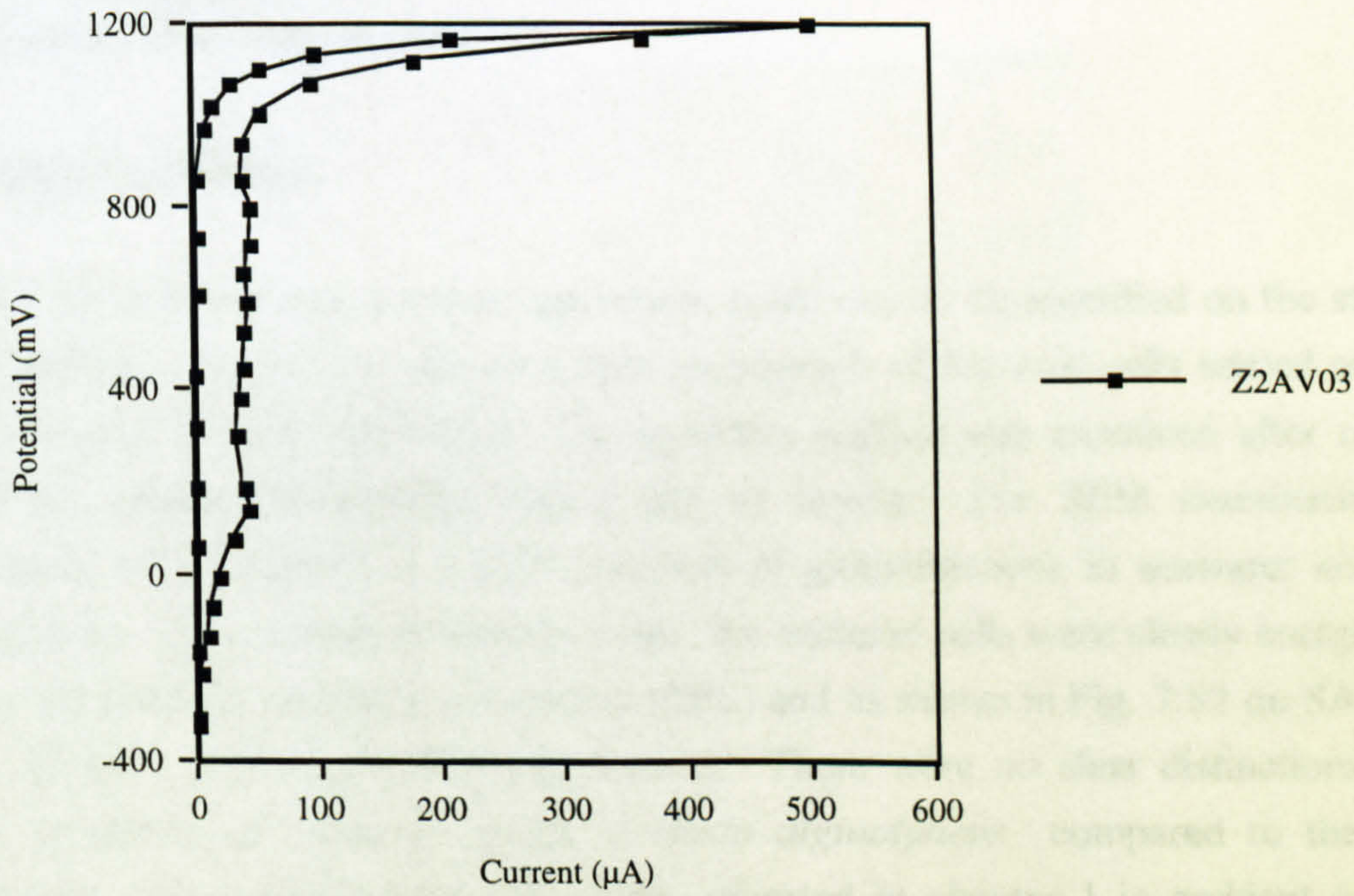

Fig. 7.49. 25Cr duplex anodic polarisation after 3 days in *vibrio alginolyticus*

The effect of prolonged immersion up to 3 weeks on the SAF 2205 and the 25Cr duplex was to further enhance the currents registered in the reverse scan region but no lowering of the breakdown potential was evident (Fig. 6.50). Up to 3 weeks immersion

anodic polarisation characteristics UNS S32760 and UNS S31254 remained unaffected by the presence of the *vibrio alginolyticus* .

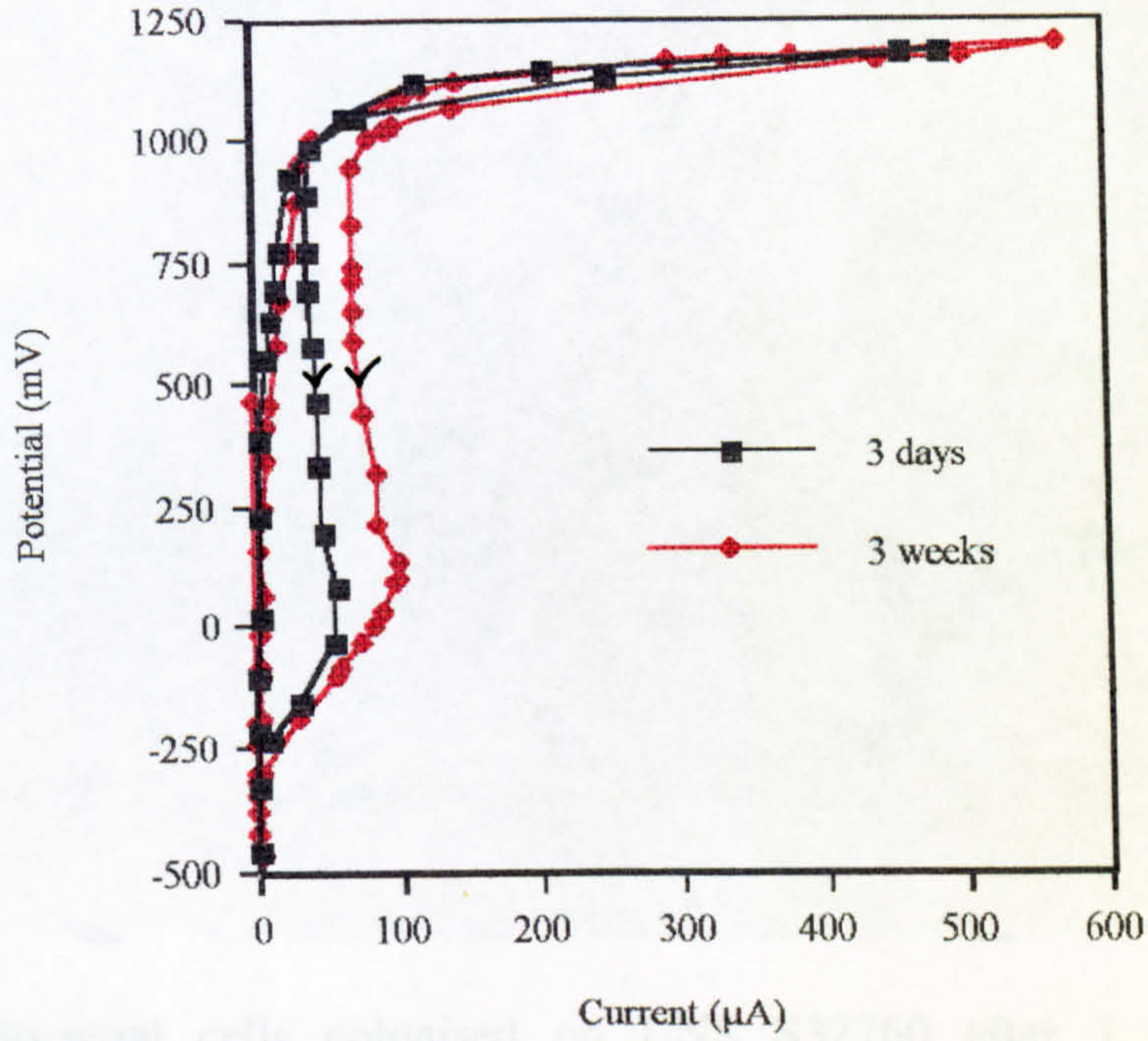

Fig. 7.50. Anodic polarisation after 3 days and 3 weeks immersion on SAF 2205 in the presence of *vibrio alginolyticus*

Specimen Examination

After 1 week immersion, bacterial settlement could clearly be identified on the stainless steel surfaces. Figure 7.51 shows a light micrograph of bacterial cells settled on UNS S32760 after 1 week immersion. The specimen surface was examined after removal from the culture followed by rinsing and air drying. For SEM examination, the specimens were retained in a 2.5% solution of gluteraldehyde in seawater and were freeze dried. After longer immersion times, the bacterial cells were clearly encapsulated in the extracellular polymeric substances (EPS) and as shown in Fig. 7.52 on SAF 2205 after 21 days, a patchy biofilm was formed. There were no clear distinctions in the types or extent of corrosion attack in *vibrio alginolyticus* compared to the sterile seawater. The localised forms of attack, reported in chapter 1 in ambient seawater (18°C) were comparable beneath the bacterial biofilm (Fig. 7.53).

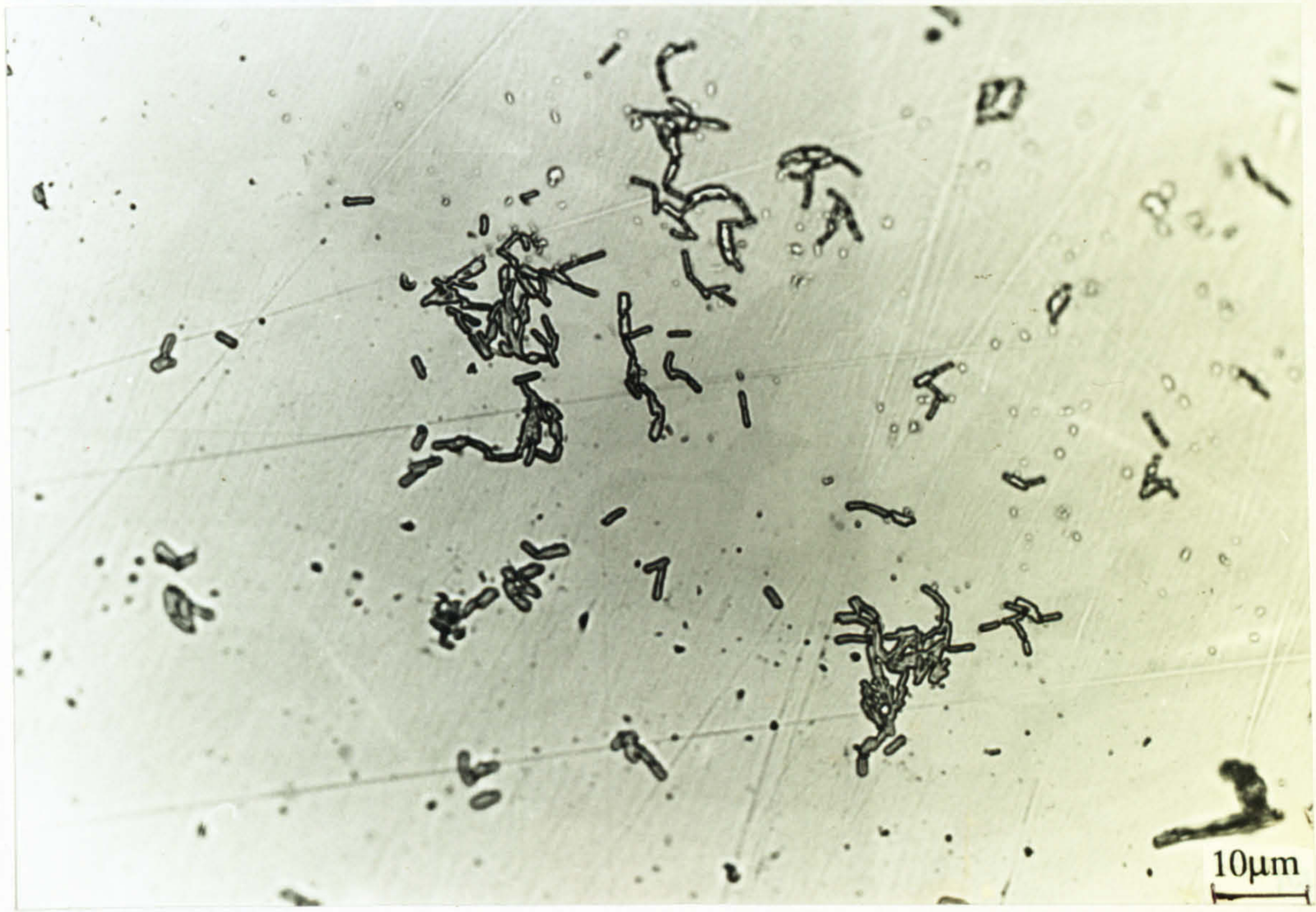

Fig. 7.51. Bacterial cells colonised on UNS S32760 after 1 week in *vibrio alginolyticus*

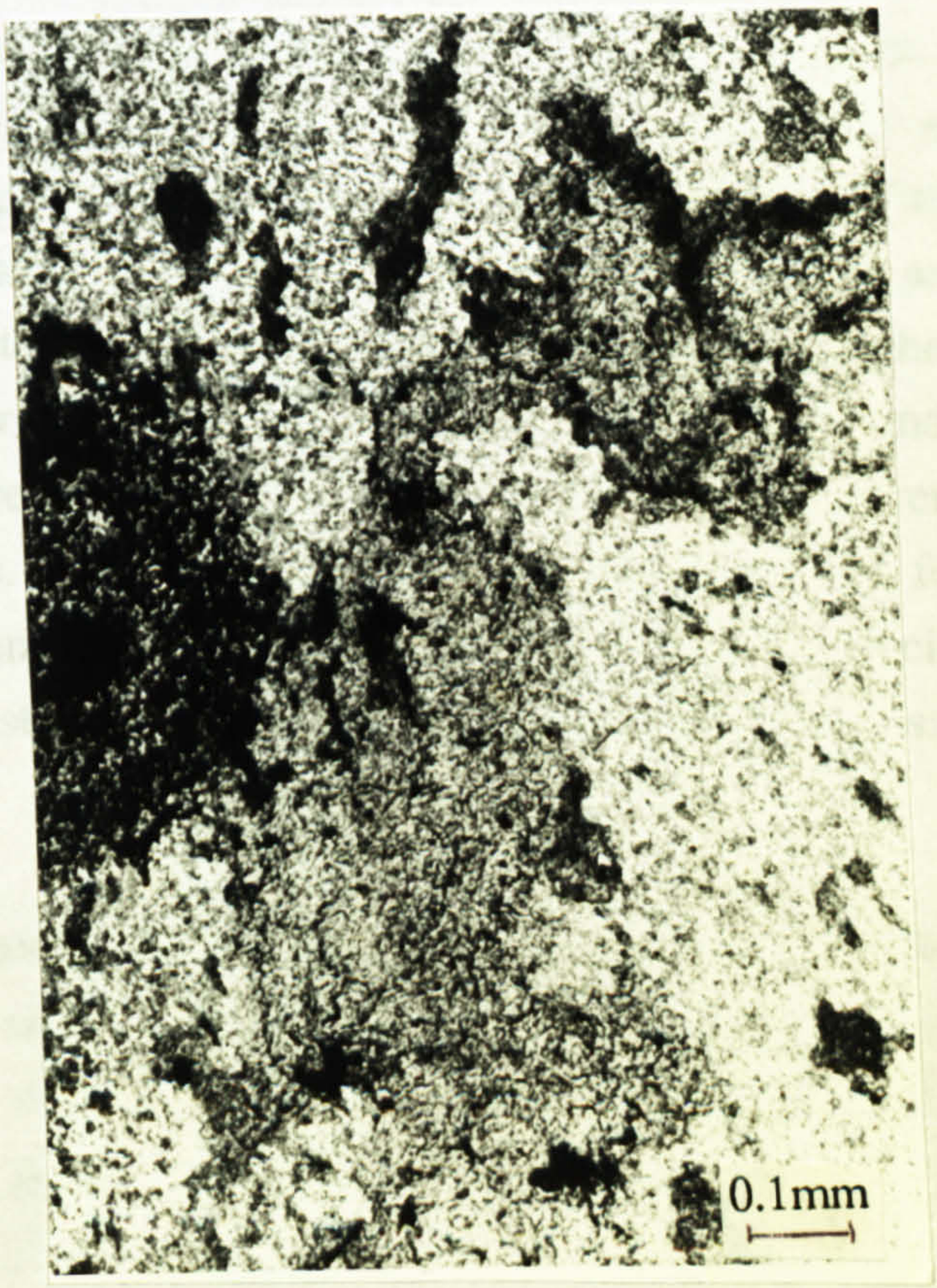

Fig. 7.52. Patchy biofilm on SAF 2205 after 3 weeks in *vibrio alginolyticus*

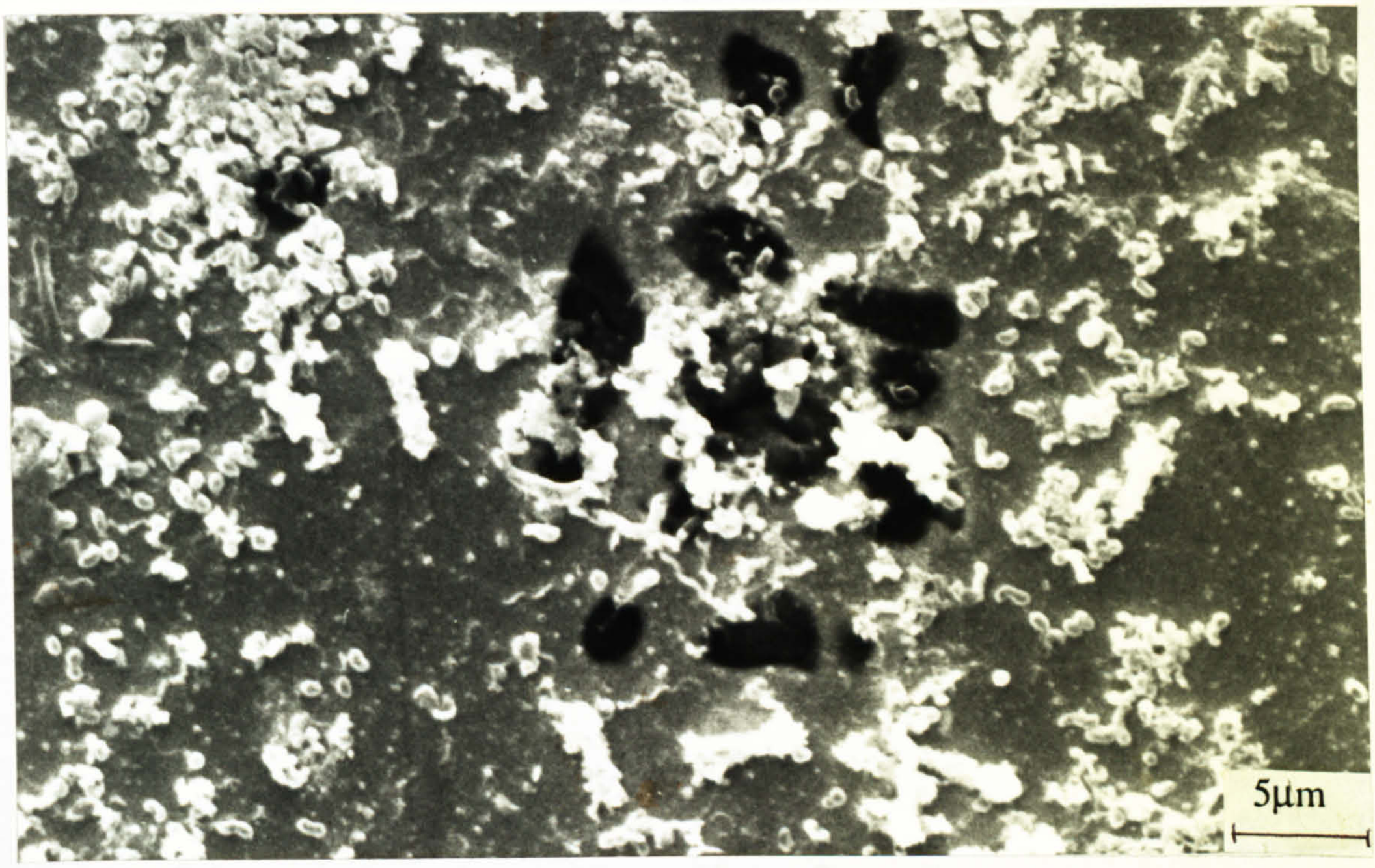

Fig. 7.53. Pitting attack on SAF 2205 after 21 days in *vibrio alginolyticus* followed by anodic polarisation

Aerobic Bacteria-Sterile and SRB-Sterile Coupling

In an attempt to assess in electrochemical terms, to what extent the presence of the anaerobic SRB or the aerobic *vibrio alginolyticus* affect the anodic and cathodic reactions, galvanic couples were set up between specimens of the same material in SRB-containing seawater conditions and sterile seawater and between *vibrio alginolyticus* and sterile conditions. The connection betwee the two compartments was an agar salt bridge. The specimens in the bacterial conditions were always assumed to be the resultant anode and therefore a positive current indicated that the assumption was true. Figure 7.54 shows the very small currents for the aerobic-sterile couple. The difference in free corrosion potential between specimens in the aerobic bacteria and in the sterile seawater on initial immersion was less than 100mV in all cases.

In the SRB-sterile couple there was a small difference between the currents registered on the lower grade austenitic UNS S31603 stainless steel and the higher-grade alloys which would agree with the anodic polarisation results obtained, which showed that even after a short period in SRB, the susceptibility of UNS S31603 to localised corrosion initiation is enhanced (Fig.7.55). The driving force for galvanic current flow was approximately 300-400mV and thus significantly greater than in the aerobic bacteria-sterile couple.

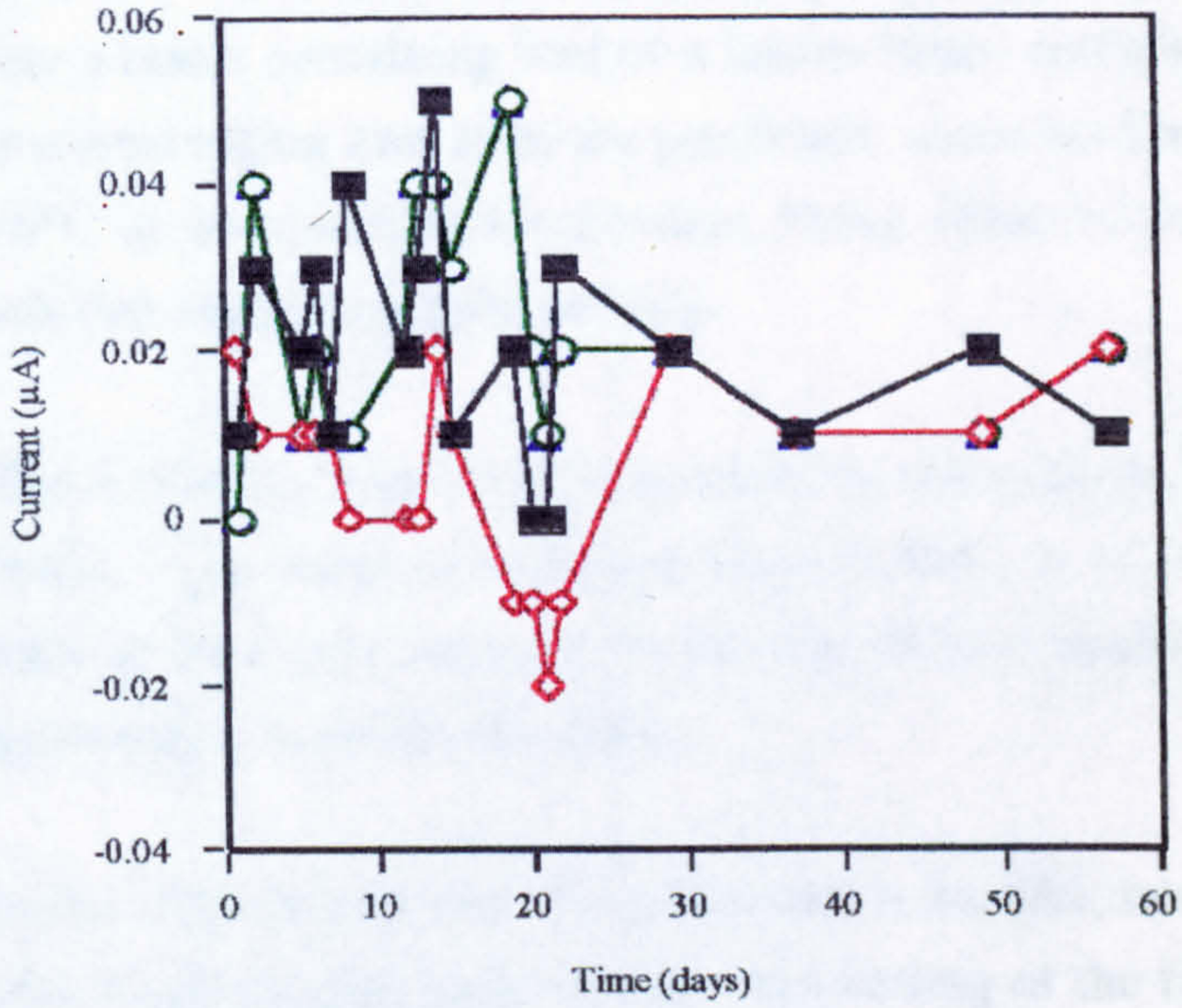

Fig. 7.54. Galvanic currents recorded in aerobic-sterile couple

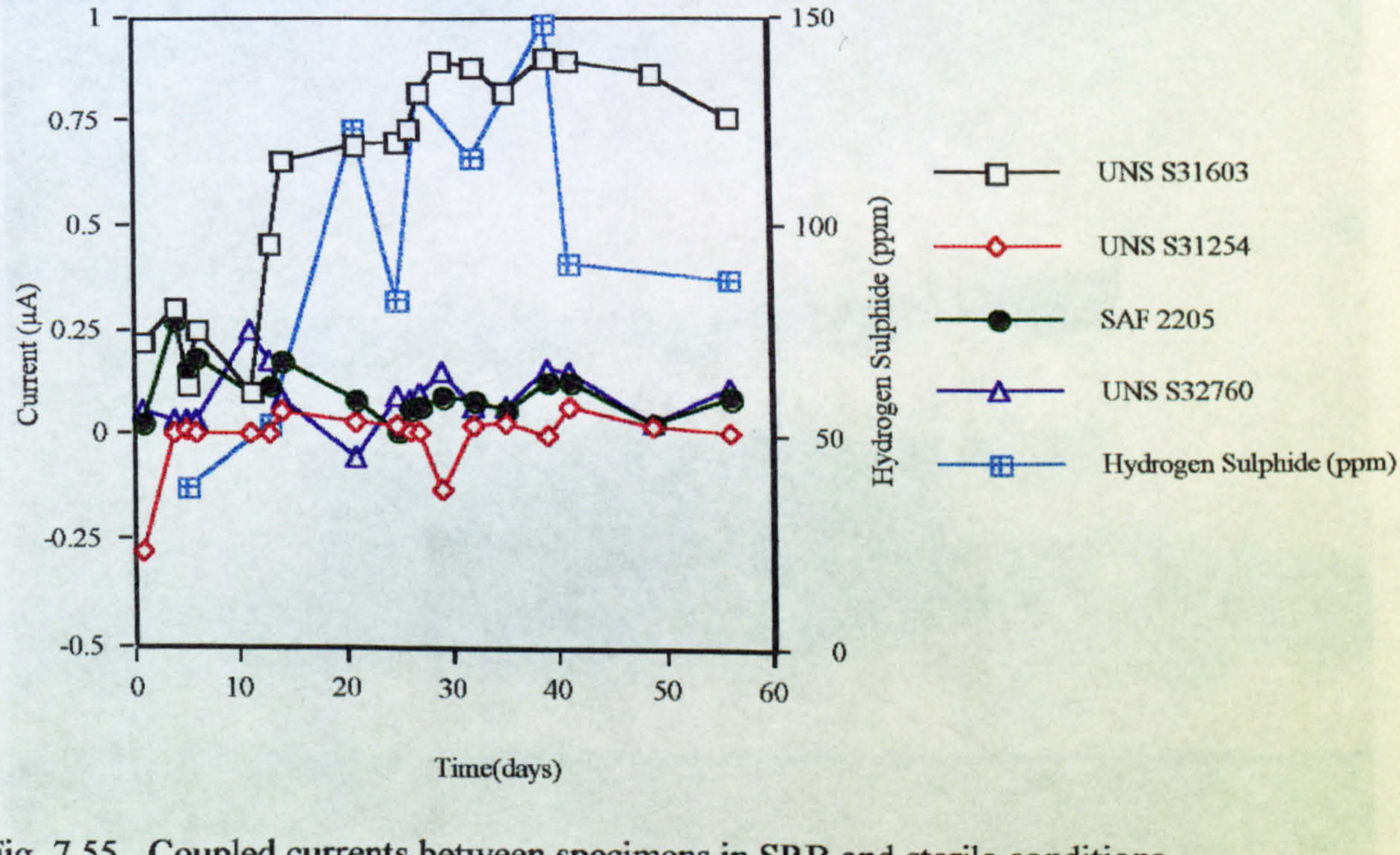

Fig. 7.55. Coupled currents between specimens in SRB and sterile conditions

Enumeration of SRB

The enumeration of viable cells in the SRB vessels was performed by the method developed by the American Petroleum Institute (API) and described in it's recommended practice No 38 (RPI-38).

A 1ml sample of the SRB-containing solution was drawn up in a syringe and injected into a bottle containing 9ml of a lactate based culturing medium. Progressive dilutions involved taking 1ml from the previously inoculated bottle. The bottles were retained at 16°C in an incubator for 28 days, being observed for characteristic blackening of the solution signifying SRB activity.

The method is based on the assumption that a single bacterium is required to blacken a bottle. The simplest interpretation of results is to consider that if one bottle blackens then at least one organism is present, if two blacken then 10 are present and so on, following a logarithmic pattern.

In the experiments over 3 months and 6 months, two tests were performed at 1 month and 4 months and each test gave blackening of the first 4 dilutions, interpreted as 10^3-10^4cells/ml present (Fig. 7.56).

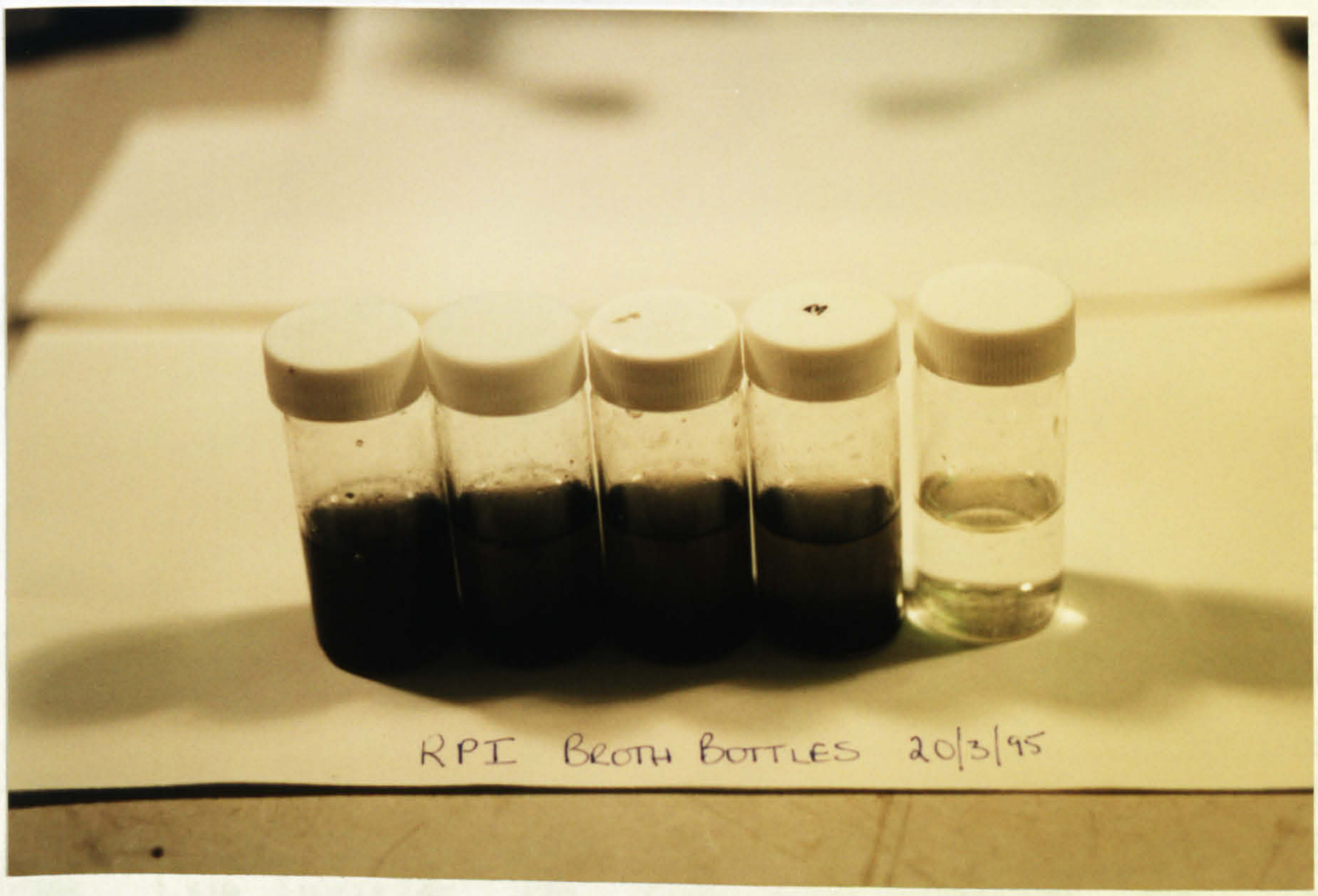

Fig. 7.56. Dilution technique for enumeration of SRB.

This test method has obvious disadvantages - not least the time delay of 28 days for detection. In this work the test method was used as a validation of the SRB activity but more precise monitoring of the H_2S level was performed to define the experimental conditions.

	< 1 Week					3 Weeks				
MATERIAL	**E_{corr}**	**E_b**	**I_a**	**I_s (I_p)**	**E_r**	**E_{corr}**	**E_b**	**I_a**	**I_s (I_p)**	**E_r**
UNS S32760	-606 (-222)	1000 (1080)	85 (-)	65 (8)	970 (910)	-521 (-460)	1000* (940)	30 (-)	50 (10)	990 (920)
25Cr duplex	-475 (-344)	1010 (1100)	74 (-)	45 (20)	960 (980)	-388 (-410)	1050* (800)	50 (-)	30 (15)	1040 (-200)
UNS S31254	-545 (-156)	1030 (1050)	90 (-)	66 (15)	1030 (950)	-709 (-260)	1050* (990)	310 (-)	100 (10)	-70 (940)
UNS S31603	-363 (-154)	290 (500)	73 (-)	50 (12)	-260 (10)	-452 (-450)	Ia reached 500µA (420)	(-)	(25)	(-320)
SAF 2205	-518 (-314)	1060 (1100)	110 (-)	65 (30)	1050 (1040)	-502 (-401)	1010* (980)	390 (-)	70 (10)	900 (800)
Dissolved H_2S (ppm)	Range 0-45ppm At time of polarisation 15-20ppm					Range 0-190ppm At time of polarisation 70ppm				

* denotes there was a significant rise in current before E_b was attained

Table. 7.2. Anodic polarisation electrochemical data after <1 week and 3 week immersion

	3 months					6 months				
MATERIAL	**E_{corr}**	**E_b**	**I_a**	**I_s (I_p)**	**E_r**	**E_{corr}**	**E_b**	**I_a**	**I_s (I_p)**	**E_r**
UNS S32760	-504 (-192)	Ia reached 500µA (1000)	(-)	(10)	(950)	-560	1000*	80	40	970
25Cr duplex	-537 (-164)	1000* (1020)	420 (-)	50 (25)	1000 (970)	-471 (-405)	1070* (1000)	100 (-)	80 (40)	1050 (990)
UNS S31254	-468	1090	300	85	970	-562 (-422)	1020* (950)	130 (-)	35 (10)	970 (920)
UNS S31603	-515 (-162)	325* (630)	180 (-)	160 (20)	-400 (-160)	-559 (-458)	380 (380)	140 (-)	50 (90)	-160 (-130)
SAF 2205	-519	1021*	60	40	-420	-557	1070*	70	45	140
Dissolved H_2S (ppm)	Range 0-90ppm At Time Of Polarisation 30ppm					Range 0-154ppm At Time Of Polarisation <2ppm				

Table. 7.3. Anodic polarisation electrochemical data after 3 months and 6 months immersion

	IMMERSION PERIOD			
MATERIAL	**< 1 WEEK**	**3 WEEKS**	**3 MONTHS**	**6 MONTHS**
UNS S32760	**P+E(f)**	**E(b)+P.i**	**C+E(b)+P.i**	**C+P.i+E(b)**
25Cr duplex	**F+E(b)+P**	**C**(severe)+ **P**(20 small)	**E(b)+P**	**C+F+E(b)**
SAF 2205	**C+P.i+E(f)**	**E(f)+C**(severe)	**C+E(f)**	**C+E(b)**
UNS S31254	**C**	**C**(severe)+**P.i** (4-5 areas)	**C+P.i+F**	**C**(minor)+**F**
UNS S31603	**C+F**	**C**(severe)+**F+P**	**C**(severe)+**P**	**C+P**(severe)+**F**

E(b)- Etching (black areas) **F**-Layer adherent to substrate

P.i.- Pit initiation **C**-Crevice attack

E(f)-Etching (faint microstructure) **P**-Pitting attack

Table 7.4. Mechanisms of attack detected during microscopical examination of anodically polarised specimens.

	IMMERSION PERIOD			
MATERIAL	**< 1 WEEK**	**3 WEEKS**	**3 MONTHS**	**6 MONTHS**
UNS S32760	No attack	**P.i**	**P.i**	**P.i+C**
25Cr duplex	**C** (minor)	**E(b)+P.i**	**C**(at thread)	**E(b)+C**
SAF 2205	No attack	**P.i**(2 areas)	**C**(severe)+**E(f)**	**C**(severe)+**E(f)**
UNS S31254	No attack	No attack	**P.i+C**(minor)	**C**(minor)
UNS S31603	**P.i** (1 area)	**C+P**	**C**(severe)+**F**	**C**(severe)+**P+F**

Table 7.5. Mechanisms of attack detected during microscopical examination of non-polarised specimens.

Discussion

The results of this study have shown that a wide range of duplex and austenitic stainless steels are susceptible to enhanced attack in seawater containing sulphate-reducing bacteria. The combination of electrochemical and microscopical techniques have demonstrated the occurrence of complex modes of general and localised corrosion of these materials when SRB are present. Over the short term experiments in marine aerobic bacteria, there were no detrimental effects on the superduplex and superaustenitic stainless steels but on the duplex stainless steels (SAF 2205 and 25Cr duplex) and the lower grade austenitic UNS S31603, the repassivation was retarded.

The observation that without exception, E_{corr} in SRB was more negative than in normal seawater is in agreement with work by Mansfeld and Little [37] and Gouda et al. [32]. The free corrosion potential in the culture of aerobic bacteria did not change significantly. Work in natural seawater by several groups has established that ennoblement of Ecorr often occurs which is not readily observed in sterile or synthetic seawater. This work has confirmed that in isolation, the influence of the common bacteria *vibrio alginolyticus* does not induce ennoblement of the free corrosion potential even although a biofilm of bacteria and EPS was evident on the specimen surface.

It has been shown in this study, via electrochemical anodic polarisation tests that after immersion periods of < 1 week (which in natural seawater would fail to detrimentally change the anodic polarisation curve) an anodic current transient was observed on all materials. It has been confirmed during this study that the occurrence of the initial rise in current at a small potential increase from E_{corr}, reported on lower-grade austenitic stainless steels [33] in sulphide environments, is a phenomenon apparent only once the SRB are active and represents an electrochemical feature connected with definite corrosion deterioration.

The findings of Gouda et al. [32], in agreement with the findings in this study, reported pitting corrosion associated with the 'active' loop found on anodic polarisation on 904L stainless steel. Also on Monel 400 (65.5%Ni/32.2%Cu), the sequence of electrochemical events in SRB was determined to be a fall in E_b, an acve peak formation and a reduction in the passive region. Confirmation of the validity of such laboratory findings was given by Scott and Davies [38] who reported, in polluted waters containing SRB, incidences of pitting and general etching.

The work reported in this chapter and elsewhere [39], is broadly in agreement with the aforementioned studies. The remainder of this discussion will focus on the detailed studies on the mechanisms of attack associated with the anodic current transient. Detailed behaviour of the range of high grade alloys covered in this study has not previously been reported.

Anodic polarisation up to I_a followed by potentiostatic control after 9 and 27 days resulted in general attack of the 25Cr duplex and SAF 2205 in the form of an etched microstructure. It was later confirmed after prolonged immersion up to 6 months that the austenitic phase of the duplex stainless steels is susceptible to preferential attack. Further substantiation was obtained when grain boundary attack was observed on UNS S31254 austenitic stainless steel which, in SRB-free seawater, has shown superior resistance to localised corrosion initiation and propagation (chapters 2 and 3).

Substantial crevice attack was observed on specimens polarised to I_a, not apparent on unpolarised specimens thus confirming the correlation between I_a and metal dissolution. The effect of immersion in SRB is therefore to eliminate, in the region after I_a, the extensive passive potential range exhibited by the high-grade alloys in normal aerated seawater (from E_{corr} usually to potentials near to +1000mV) and replace it with a region of stable current where corrosion attack has been found to occur. As a consequence, in SRB, passive behaviour is only exhibited in the very much restricted potential range between E_{corr} and the start of the anodic current transient. As with the full anodic polarisation scan, good correlation existed between the attack observed at I_a and that observed after longer immersion periods at the free corrosion potential. Further confirmation that the anodic current transient is an effect linked with corrosion deterioration came from peripheral tests carried out on commercially pure Titanium (I.M.I. 115) which failed to show the large increase in current to I_a but showed a modest increase of up to 5μA followed by a decrease in current to a steady passive value of 1-2μA. Examination of the specimen which did not lose general passivity up to a potential of +1400mV(SCE), at which the anodic polarisation was terminated, showed an area of minor crevice attack of <1mm length.

The potential range over which passive behaviour was exhibited was not reduced when immersed in seawater containing the aerobic bacteria *vibrio alginolyticus* . Interestingly there was a reduction in the ability of the second generation duplex stainless steels (SAF 2205 and 25 Cr duplex) to repassivate, manifested in an incomplete hysteresis and higher currents in the passive region of the reverse scan. Also on the lower grade UNS S31603, a higher Imax signified the propagation of corrosion after scan reversal, enhanced by the presence of bacteria. As expected, the

superduplex and superaustenitic stainless steels, which offered superior resistance to passivity breakdown in synthetic seawater at ambient temperature were not detrimentally affected.

Having obtained strong evidence that the anodic transient peak in SRB is associated with corrosive attack which is reproduced under unpolarised exposures, it is relevant to try to detect any factors governing, for instance, the magnitude of I_a. In agreement with the findings others [33] on a 904L austenitic stainless steel, tests in the present study on specimens in separate beakers (of varying H_2S concentrations) exposed for very short periods of up to 8 hours, demonstrated that higher sulphide concentrations (as H_2S or HS^-) at the time of the anodic polarisation yielded higher values of I_a. However, as Tables 7.2-7.5 reveal, over longer periods of exposure, no general correlation was evident between H_2S concentrations and the value of I_a. In other words, neither the length of immersion nor the concentration of H_2S could be directly related to the extent of the anodic current transient on a given material nor was any trend apparent on the materials likely to support the highest I_a. This supports the findings of work by Case [40] reported by Edyvean & Videla [41] which implies that the extent of corrosion in fouled systems where H_2S is present is not solely determined by the H_2S concentration in the bulk environment but rather that the controlling factor is what occurs within the colonies of bacteria and what the sulphide levels are on a more localised level at the substrate/solution interface. Hence after prolonged exposure to SRB where bacteria colonies and clusters of deposited sulphide compounds form on the surface, the relationship between the environmental conditions and the electrochemistry of the anodic reactions becomes dominated by the conditions nearer the substrate surface and would require the use of micro electrodes to define more precise correlations.

The presence of SRB has been demonstrated in this work to disrupt the passive behaviour of a range of stainless steels both under free corrosion conditions and under the influence of relatively modest anodic polarisation. The resulting corrosion attack has been observed to be complex and elucidation of the detailed corrosion mechanisms requires careful correlation of electrochemical test and precise microscopical and microstructural examination. Some progress has been made in this respect. One distinctive feature is the vulnerability of these materials to general surface attack (in the form of etching and/or film formation) at modest anodic overpotentials and even, in some cases, under free corrosion conditions. Thus, on UNS S31603 after 6 months, a complete basal film (noticeably thicker than on the duplex stainless steels) was observed, broken at only the sites of localised attack. On the higher-grade superaustenitic UNS S31254, such general attack was observed after anodic

polarisation but not under unpolarised conditions. On the duplex stainless steels, 25%Cr and UNS S32760, film formation was associated with selective attack on the underlying austenitic phase (found, as expected to be lower in Cr and Mo than the ferrite grains). This range of evidence confirms the important role of Cr and Mo in conferring resistance to passive film breakdown on SRB-containing environments. Enhanced localised attack has been observed in the presence of SRB in the field and several studies have focused on the causative environmental species. Newman [26] has postulated that the enhanced pitting observed on stainless steels in the presence of SRB is due to thiosulphate, perhaps as an intermediate in sulphate reduction. The production of thiosulphate is indicated by a decrease in the pH. In this work the pH remained relatively constant from the time of SRB culturing throughout the experiment between 7.8-7.9. However, it is possible that the thiosulphate could be present in local areas thus not affecting the bulk pH. Newman's model is based on the availability of an oxidising species (such as oxygen) to facilitate the production of thiosulphate, and is used to explain the much accelerated attack in SRB when there is air present nearby.

In relation to the mechanisms of local corrosion, it was apparent that the areas of pitting attack, previously described, were found at discontinuities in the biofilm and the observed changed morphology of these pits on 25Cr duplex was perhaps dominated by the non-uniformity of the conditions at the site and was rather a coalescing of several pits all initiated at local areas where the solution conditions (pH, chloride and sulphide content) under the biofilm reached a critical value. EPMA performed in the vicinity of the tunnelling pits observed on the austenitic stainless steel, UNS S31603, after 6 months in SRB and the results of anodic polarisation implied that compositional differences and distribution of sulphide corrosion products, around and inside the pit site, could lead to galvanic effects and promote pit propagation. Indeed analyses at the edge of pitted sites yielded a high concentration of S in the corrosion products whilst inside the pit there was no S detected.

One of the most important findings in this study was that in the absence of oxygen and, as such, an efficient oxygen cathode, significant corrosion was observed on even the superduplex and the superaustenitic stainless steels. In consideration of this observation and the compostional differences recorded around a localised corrosion site, it is postulated that the higher corrosion rates are stimulated, not by an oxygen cathode but by a depolarised cathodic reaction on the FeS corrosion products produced during localised dissolution.

A mechanism is proposed to relate the presence of the current transient peak to the stimulation of localised galvanic effects between active anodic sites and cathodic sites

induced by the production of corrosion products. The mechanism is based on the cathodic depolarisation produced by the presence of sulphides - the effects of which are apparent on a localised scale. It has been demonstrated that the current increase up to I_a at potentials shifted positive from E_{corr}, is associated with corrosion attack and therefore the release of metal ions into the solution. It is postulated that the formation of metal sulphides (primarily FeS) in the vicinity of the corrosion attack increases the rate of cathodic reaction on the substrate and therefore the stabilisation of the current to a lower value I_S, signifies a reduction in the *net* current at the electrode rather than a reduction of the anodic current.

Figure 7.57 is a schematic representation of the sequential events which interact to produce an effective fall in current which is correlated to enhanced corrosion attack.

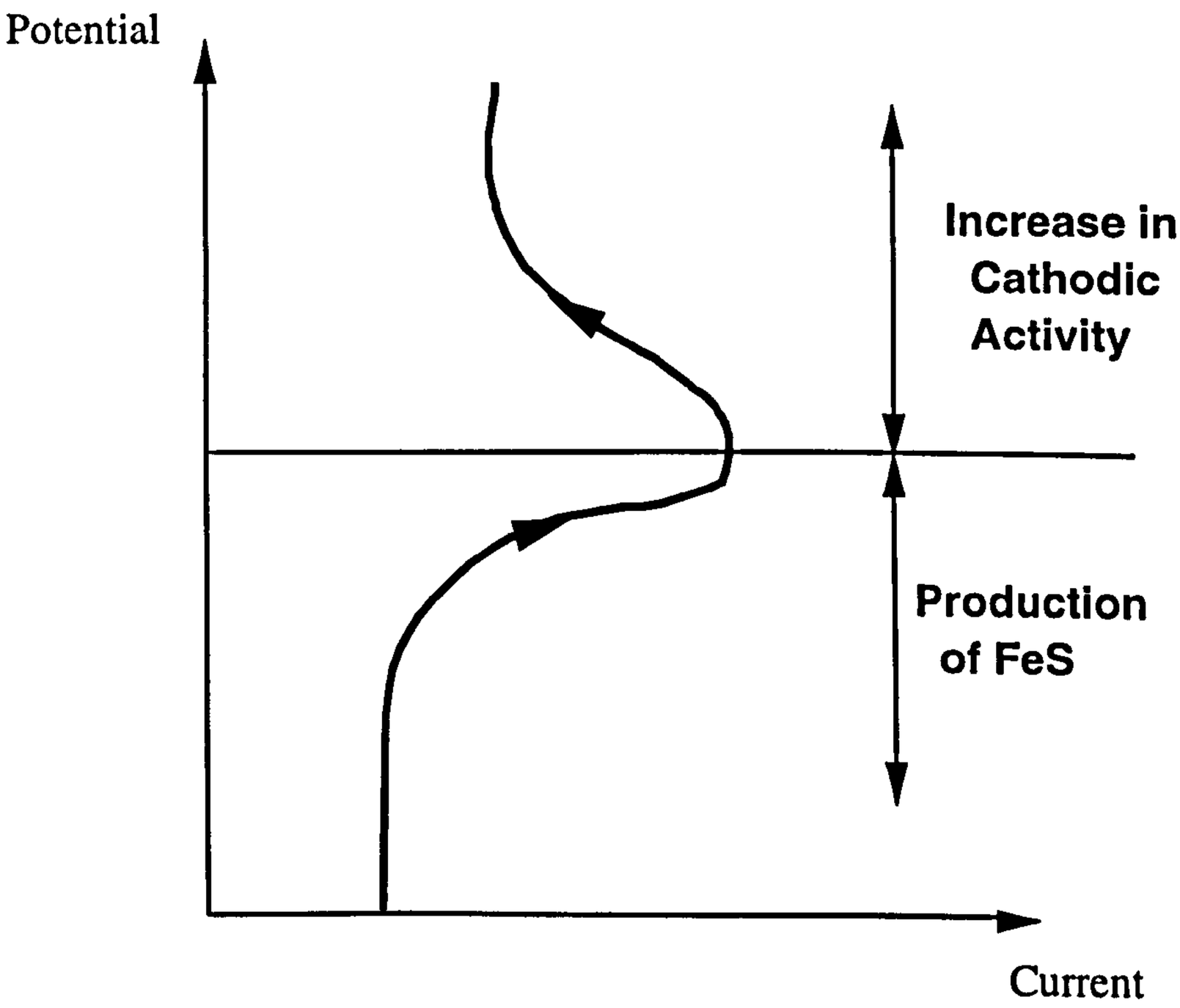

Fig. 7.57. Interaction of corrosion and enhanced cathodic activity related to the current transient I_a

On a localised scale, the anodic dissolution produces the metal ions to combine with the sulphides which result from bacterial sulphate reduction, the product of which enhances the cathodic activity. Through examination and EPMA, distinct regions of sulphide formation have been found at the mouth of deep pits on UNS S31603 with the inside of the active pit remaining free from sulphide. Hence there is an auto-catalytic effect as the amount of sulphide builds up and promotes a cathodically controlled

propagation rate. Moreover the good correlation of the visual examination between polarised and non polarised specimens provides strong evidence that the afore-mentioned mechanism is applicable to corrosion behaviour under free corrosion conditions.

The initiation of pitting attack and crevice corrosion has been shown to be enhanced in the presence of SRB and a small potential shift from E_{corr} yields relatively high anodic currents. It would therefore be expected that by coupling specimens in SRB to specimens in sterile seawater there would be a galvanic flow of current from the SRB specimen (i.e. the specimen in SRB being the anode). It was shown that although there was a small transfer of charge, the current oscillated about the zero current point on the duplex stainless steels (UNS S32760 and SAF 2205) and the superaustenitic (UNS S31254). Only on the UNS S31603 was the current consistently flowing in the direction to render the SRB specimen the anode. Hence it is inferred that in addition to the increased anodic activity, shown to exist in SRB, there is enhanced cathodic activity which shields the extent of the galvanic effect.

Indeed to substantiate the proposed mechanism, the cathodic reaction has been shown to be depolarised on an electrode containing a significant proportion of sulphides.

In conditions of aerated seawater where crevice attack is initiated and proceeds, it is generally accepted that the mechanism of self propagation is the creation of a differential aeration cell between the low oxygen shielded crevice area and the aerated area outside the crevice. An alternative mechanism to stimulate the propagation of crevice attack, so prominent in these, low O_2, SRB-containing experiments, involves the reduction of elemental sulphur, S^o, as proposed by Schaschl [34]. The elemental sulphur acts as the cathodic reactant for the reaction

$$S_o + H_2O + 2e^- \rightarrow HS^- + OH^-.$$

In the SRB cell this would require the presence of an oxidising reactant to facilitate the production of S_o from the FeS produced during corrosion, since from the Pourbaix S-H_2O system, it is apparent that the water alone cannot oxidise FeS to S^o [42]. The cathodic reaction, predominant in SRB must therefore involve some other species.

Indeed in SRB, the cathodic polarisation curve shows two activation-controlled regions suggesting two prominent cathodic reactions. Electrochemical calculations have shown that under these conditions, hydrogen production is thermodynamically possible

even at potentials in the vicinity of E_{corr}. However in the presence of high concentrations of H_2S, the most likely reaction at the potentials near to E_{corr} is the reduction of H_2S in the reaction

$$H_2S + e^- \rightarrow HS^- + 1/2H_2$$

as proposed by Costello [14], the thermodynamics of which are the same as hydrogen evolution. Although in this work, no evidence has been obtained to suggest that there is a correlation between the H_2S level and the rate of the H_2S reduction reaction, or the limiting current density, it may be postulated that in deposits created from the SRB activity, the local levels of H_2S will vary and as such there may be no direct correlation between the progression of the reaction to the bulk concentration. At the more negative potentials, once the overpotential is large enough to overcome activation barriers, hydrogen production is favoured.

Points of Practical Relevance

This study has demonstrated the effective use of accelerated electroochemical techniques in the determonation of the susceptibility of materials, over long and short term exposure to SR, to localised corrosion attack.

It has signalled the increased incidence of localised corrosion initiation on even the high grade superduplex and superaustenitic stainless steels in SRB. While it is evident that there are benefits to be gained in employing alloys with higher Cr and Mo to confer greater protection against localised corrosion, the benefits are less pronounced than in SRB-free environments.

It is of practical importance that the increased susceptibility to ocalised corrosion initiation is realised and as imortant is the realisation that even where there is no effective oxygen cathode, corrosion propagation can proceed by local cell action.

Conclusions

The susceptibility to complex modes of general and local attack of a range of duplex and austenitic stainless steels in conditions of high SRB activity has been demonstrated. Good correlation was found between the mechanisms of attack observed after the accelerated electrochemical tests and that observed after prolonged exposure at the free-corrosion potential thus emphasising the usefulness of accelerated test methods as a tool for predicting long term corrosion behaviour. Aerobic bacteria vibrio

alginolyticus, over the short term tests were shown to have little effect on the passivity breakdown potential of the stainless steels but did retard repassivation on the second generation duplexes.

Of particular importance is the observed general surface corrosion after relatively modest potential shifts from E_{corr} and also on non polarised specimens of both duplex and austenitic stainless steels in addition to the normal pitting and crevice corrosion suffered by stainless steels in normal seawater.

Mechanisms of corrosion in SRB are evidently much more complex than in normal seawater with the indication of interesting cathodic effects. The depolarisation of the cathodic reaction of hydrogen sulphide reduction on FeS has been postulated as the mechanism by which localised attack is self-propagated and accounts for the development of a current transient during anodic polarisation. More importantly, it provides a plausible mechanism to explain corrosion under free corrosion conditions.

Perhaps not surprisingly, there appears to be a similar role of the alloying elements Cr, Mo and N in conferring enhanced resistance to attack in SRB environments but is nevertheless clear that, even the higher-grade duplex and austenitic stainless steels are significantly more vulnerable to corrosion in seawater containing active SRB.

References

1. R. H. Gains, Bacterial activity as a corrosive influence in the soil, *J. Ind. Engng. Chem.*, 128 (1910)

2. D. E. Hill, S. V. Bross, E. R. Goldmann, The impacts of microbial souring of a North slope oil reservoir, *Proc. Int. Conf. on Microbiologically Induced Corrosion and Biodeterioration*, ed. N. J. Dowling, Knoxville, 1990

3. R. G. Edyvean, C. J. Thomas, I. M. Austen, in *Biological Induced Corrosion*, ed. S. C. Dexter, NACE 8, 1985

4. J. D. A. Miller, Metals, in *Economic Microbiology*, Vol. 6, ed. A. Rose, Academic Press, London 1981

5. G. J. Bass, J. Webb, P. F. Sanders, H. Lappin Scott, Influence of surfaces on hydrogen sulphide production, *Presented at the 9th Int. Conf. on Marine Corrosion and Fouling*, Portsmouth, July, 1995

6. C. A. Willingham, H. L. Quinby, Effects of hydrostatic pressure on anaerobic corrosion of various metals and alloys by sulphate-reducing marine bacteria, *Developments in Industrial Microbiology*, 12, 1971, p278

7. B. Little, P. Wagner, Indicators for sulfate-reducing bacteria in microbiologically influence corrosion, in *Biofouling and Biocorrosion in Industrial Water Systems*, eds. G. G. Geesey, Z. Lewandowski, H-C. Flemming, Lewis Publishers, 1994

8. W. A. Hamilton, Metabolic interactions and environmental microniches : implications for the modelling of biofilm processes, in *Biofouling and Biocorrosion in Industrial Water Systems*, eds. G. G. Geesey, Z. Lewandowski, H-C. Flemming, Lewis Publishers, 1994

9. H. R. Rosser, W. A. Hamilton, Simple assay for accurate determination of [^{35}S] sulfate reduction activity, *Appl. Environ. Microbiol.*, Vol. 45, 1983

10. W. A. Hamilton, S. Maxwell, Biological and corrosion activities of sulphate-reducing bacteria within natural biofilms, in *Biologically Influenced Corrosion*, NACE 8, ed. S. C. Dexter, 1986

11. J. F. D. Stott, What progress in the understanding of microbiologically induced corrosion has been made in the last 25 years? A personal viewpoint., *Corros. Sci.*, Vol. 35, Nos. 1-4, pp667-673, 1993

12. C. A. Von Wolzogen Kuhr, L. S. Van der Vlugt, Water, *Den Haag*, Vol. 18, (16), 1934

13. A. J. Krasna, Hydrogenase : Properties and applications, *Enzyme Microb. Technol.*, 1, 165, 1979

14. J. A. Costello, PhD thesis, *University of Cape Town*, South Africa, 1975

15. R. A. King, J. D.A. Miller, Corrosion by the sulphate redcing bacteria, *Nature*, Vol. 233, 1971

16. S. Daumas, Y. Massiani, J. Crousier, Microbiological battery induced by sulphate-reducing bacteria, *Corros. Sci.*, Vol. 28, No. 11, 1988, pp1041-1050

17. G. Kobrin, Corrosion by microbiological organisms in natural waters, *Mater. Perf.*, Vol. 15, July 1976

18. F. L. Laque, Corrosion and fouling, *Proc. 3rd Int. Conf. on Marine Corrosion and Fouling*, NBS, Vol. 2, 1972

19. P. R. Puckorius, Mater. Perf., December 1983

20. L. R. Brown, G. S. Pabst, *Proc. 3rd Int. Conf. on Biodegradation*, eds. J. M. Sharpley, A. M. Kaplan, pp875-882, Applied Scientific Publications, 1976

21. V. K. Gouda, W. T. Riad, S. Mansou, I. M. Banat,Premature failure of Monel 400 coolers in Arabian Gulf seawater applications, *Proc. 11th Int. Corros. Congr.*, Florence, Italy, p4281, 1990

22. V. K. Gouda, A. l-Hashem, *Advances in corrosion and Protection Conference*, UMIST, 1992

23. V. K. Gouda, W. T. Riad, S. Mansou, I. M. Banat, Microbial-induced corrosion of Monel 400 in seawater, *Corrosion/90*, NACE, Paper No. 107, 1990

24. J. Oudar, P. Marcus, Role of adsorbed sulphur in the dissolutio and passivation of nickel alloys, *Appl. Surf. Sci.*, Vol. 3, No. 48, 1979

25. P. Marcus, E. Protopopoff, Potential-pH diagrams for adsorbed species, *J. Electrochem. Soc.*,Vol. 137, p2709, 1990

26. R. C. Newman, W. P. Wong, A. Garner, A mechanism of microbial pitting in stainless steel, *Corrosion*, Vol. 42, No. 8, 1986

27. S. J. Mulford, D. Tromans, Crevice corrosion of nickel-based alloys in neutral chloride and thiosulphate solutions, *Corrosion*, Vol. 44, No. 12, 1988

28. R. C. Newman, Pitting of stainless steels in sulfate solutions containing thiosulfate ions,*Corrosion*, Vol. 41, No. 8, 1985

29. D. Tromans, L. Frederick, Effect of thiosulfate on crevice corrosion of stainless steels, *Corrosion*, Vol. 40, No. 12, 1984

30. B. J. Webster, R. C. Newman, A novel electrode assembly for studying corrosion of stainless steels by sulphate reducing bacteria, *Corros. Sci.*, Vol. 35, Nos. 1-4, pp 675-682, 1993

31. R. C. Newman, B. J. Webster, R. G. Kelly, *ISIJ Int.*, Vol. 2, 201, 1991

32. V. K. Gouda, H. M. Shalaby, I. M. Banat, The effect of sulphate-reducing bacteria on the electrochemical behaviour of corrosion-resistant alloys in sea water, *Corros. Sci.*, Vol. 35, Nos. 1-4, pp 675-682, 1993

33. D. A. Moreno, J. R. Ibars, C. Ranninger, H. . Videla, Use of potentiodynamic polarization to assess pitting of stainless steels by sulfate-reducing bacteria, *Corrosion*, Vol. 48, No. 3, 1992

34. E. Saschl, Elemental sulphur as a corrodent in dearated, neutral aqueous solutions, *Mater. Perf.*, July 1980

35. In T. R. Dado, J. E. P. Young (eds), *The national collections of industrial and marine bacteris : Catalogue of strains*, 1990

36. L. Barta, D. J. Bradley, Extension of the specific interaction model to include gas solubilities in high temperature brines, *Geochem. Cosmochim. Acta*, Vol. 49, p195-203

37. F. Mansfeld, B. Little, A technical review of electrochemcal techniques applied to MIC, *Corros. Sci.*, Vol. 32, No. 3, 1991, p247

38. P. J. B. Scott, M. Davies, *CORROSION/89*, NACE, Paper 86, 1989

39. A. Neville, T. Hodgkiess, A comparative study of the corrosion behaviour of duplex and austenitic stainless steels in marine environments containing sulphate-reducing bacteria, *Proc. of the Int. Conf. on Duplex Stainless Steels*, DUPLEX '94, Glasgow, 1994

40. L. C. Case, *Water problems in oil production : An operators manual*, 2nd edition, PPC books, 1979

41. R. G. J. Edyvean, H. A. Videla, Biofouling and MIC interactions in the marine environment : An overview, Microbial Corrosion, *European Federation of Corrosion Publications*, No.8, 1991

42. A. Pourbaix, L. E. Aguiar, A. Clarinval, Local corrosion processes in the presence of sulphate-reducing bacteria : measurements under biofilms, *Corros. Sci.*, Vol. 35, Nos. 1-4, 1993, p693-698

Chapter 8

A Study of the Effect of Micro and Macro-Fouling on the Short and Long Term Corrosion Behaviour of High-Grade Alloys

Introduction

The previous chapter dealt with the effects of the anaerobic sulphate-reducing bacteria on corrosion of high-grade alloys. This chapter presents a more general overview of the influence of marine fouling on corrosion through a programme of short and long term exposure experiments.

Long term immersion tests were carried out at the marine biology station at Millport, Isle of Cumbrae on the West coast of Scotland over a period of two and a half years. Specimens were situated in two different locations : a static tank containing renewed seawater and suspended from the Kibble Pier. The aim of the experiment was to follow the progress of fouling throughout the seasons via photographic records and to correlate the magnitude of fouling to observed corrosion characteristics.

A short term laboratory programme (up to 12 weeks) was conducted at the Ifremer research laboratory, Brest, France using DC-electrochemical techniques. It consisted of a two part study into the effect of micro and macro fouling on the electrochemical corrosion behaviour of stainless steels and related alloys and the mass transfer characteristics of oxygen at a rotating disk electrode.

Literature Review

The consequences of marine fouling can be costly and can be manifested in significant weight gain in marine structures due to extensive macrofouling, enhancement of localised corrosion attack, increased fluid frictional resistance in pipelines and reduced heat transfer efficiency in heat exchange systems. Microfouling, as the primary stage, represents the formation of a conditioning layer on the surface such as to control the latter stages of macrofouling (the settlement of barnacles, seaweed etc.).

The study of marine fouling has, in the main, been directed towards the early stages of fouling since it has been recognised that subsequent colonisation by macro-organisms is dependent on the initial biofilm. However, over recent years, studies have been carried out to characterise the behaviour of materials which, on the surface, contain a thick layer of fouling products.

It is widely accepted in the literature that metals immersed in a biologically active media such as seawater are exposed to a complex sequence of biological and inorganic changes that result in an important modification of the metal/solution interface [1]. The primary phase is focused around the formation of a layer of micro-organisms : the biofilm.

Biofilm Formation

The concept that biofilms are the predominant mode of bacterial growth in aquatic systems was initially realised through the work of Costerton et al. [2] in 1983. Prior to this, cell growth had been assumed to occur in the planktonic mode and as such biologist's studies reflected this.

The formation of a biofilm is a multistage process which commences by the absorption of organic substances which alter the electrostatic charge and wettablility of the surface [1,3]. This is followed by the settlement of the pioneer bacteria , the growth of which leads to the development of a biofilm. The biofilm consists, mainly of water, bacterial cells and their extracellular polymeric substances (EPS) responsible for bacterial adhesion [4]. In general, bacterial population develop rapidly, in some cases within hours of immersion, followed by the production and accumulation of EPS [5]. On metallic substrata, it has been estimated that bacterial colonisation occurs within 24-72 hours of immersion depending on the environment and material [1].

Biofilms alter the near-surface environment by affecting the bulk media and the growth surface. Within the biofilm/substrate system, there is a complex network of chemical reactions, the kinetics of which control the nature of the biofilm. Across the biofilm, each chemical constituent which is produced or consumed, forms a diffusivity-related concentration profile. The heterogeneous and anisotropic nature of the biofilm ensures that at localised locations, the rate of any one chemical reaction can be very different [6].

The use of ion-selective and gas-sensing microelectrodes has been heavily adopted in biofilm characterisation. Levandovski [6] measured the dissolved oxygen level across a biofilm with the aim of relating the information to the diffusivity of oxygen through the continuous layer.

A microbial 'slime' layer which develops after the initial bacterial colonisation forms a surface attractive to the larvae of macro-fouling organisms. Hence the progressive development of biological layer, reaching a thickness of a few centimetres, continues. The micro-environment developed within a fouling system, consisting of a primary biofilm layer and subsequent micro-algal and animal fouling layers has not been well characterised. Woolmington and Davenport [7] studied the local pH and oxygen content beneath fouling layers and concluded that low pO_2 can exist and that the pH is very much dependent on the fouling species.

Biological Aspects of Corrosion

The physical presence of microbial cells on a surface, in addition to their metabolic activities, modifies electrochemical processes. The sequence of inorganic changes (corrosion and passivation) occurs simultaneously with biofilm formation. Edyvean et al. [1] used the schematic representation as in Fig. 8.1 to describe the passivity process acting in the opposite direction to the biofilm (being produced from bulk solution towards the metal/solution interface).

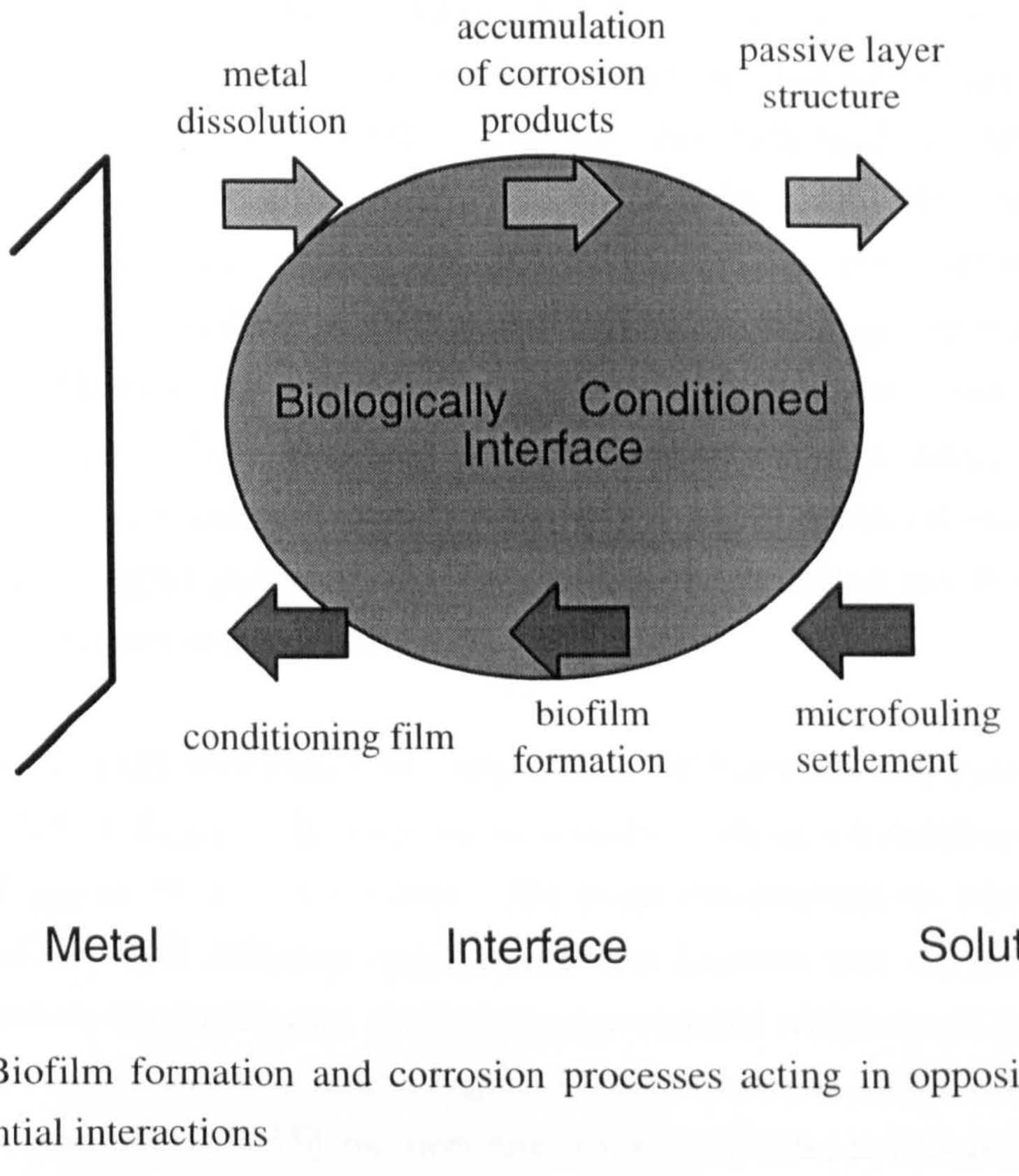

Fig 8.1. Biofilm formation and corrosion processes acting in opposite directions and their potential interactions

Electrochemical corrosion concepts in the study of corrosion in the presence of a biofilm must be adapted to consider the interactions between biofilm and passive layers. Indeed it was suggested in by Wallen [8] that the galvanic series of metals in seawater should take into consideration the microbial action of the environment. Several studies have ascertained that natural seawater is more corrosive than artificial seawater. The recent comprehensive study by Gallagher et al. [9] attempted to clarify the exact mechanisms by which microbes in the seawater affect the corrosion processes. In agreement with several independent studies [10], an ennoblement of the free-corrosion potential, E_{corr}, was observed in natural seawater, often not observed or to a lesser extent in artificial seawater. The authors concluded that increases in E_{corr} to values in the region of 350-450mV SCE would increase the probability of corrosion initiation.

The ennoblement of E_{corr} which has been consistently been observed in natural seawater and brackish water was explained by Mollica et al. [11] and Scotto et al. [12] to be the result of cathodic depolarisation of the oxygen reduction reaction due to bacterial influence. Combining the extensive studies into biofilm formation and related electrochemical changes, in which only sparse diatom settlement was found on ennobled surface, it was confirmed by Mollica [3] that the depolarisation was due to settlement of non-thermophilic bacteria alone. The findings were corroborated by observations that

the ennobling process could be slowed down by increasing the flow speed and reducing bacterial attachment. The effect of algal settlement was investigated by Mollica et al. [13] in which the chlorophyll 'a' content was measured in different illumination conditions. The increase in potential was found to be independent of algal presence and it was concluded that photosynthetic mechanisms are not contributing factors. In restricted light, Motoda et al. [14] found that although E_{corr} ennobled as in unshielded conditions, the rate was lower in the period up to 20 days immersion. After 20 days, no difference between light and dark conditions could be found, which is in contrast to the findings of Dexter and Zhang [10] where the E_{corr} in darkened seawater was found to increase to a higher potential than in light conditions, implying that the probability of localised initiation is increased.

Scotto et al. [12] confirmed the importance of bacterial respiration in facilitating a positive shift in E_{corr}. The addition of sodium azide as a respiratory inhibitor caused a shift in E_{corr} in the active direction. The exact mechanisms by which the bacterial and diatom slime could enhance oxygen-reduction kinetics was not confirmed. However depolarisation due to enzyme catalysis was postulated which could result in an increased exchange current density of the oxygen-reduction reaction. This was supported in work by Johnson and Bardal [15] and later confirmed by Dexter and Gao [16].

Two mechanisms of cathodic depolarisation were examined by Mollica [3,17]. Local acidification by the biofilm, initially proposed by Dexter et al. was disputed in this study. Depolarisation of the oxygen reduction reaction was verified by potentiostatic methods and was described as an autocatalytic process, the rate of reaction increasing as the instantaneous cathodic current increases.

Recent evidence has emerged to substantiate the theory that ennoblement is, in part, due to a local decreases in pH. However Chandrasekaram and Dexter [18] acknowledged that the substantial ennoblement of E_{corr} must be due to other contributing factors in addition to pH decrease. They proposed a novel mechanism for ennoblement, based on a synergism between pH decrease and production of hydrogen peroxide as a bacterial by-product. The relatively noble thermodynamic equilibrium potential of peroxide reduction compared to oxygen-reduction is considered to contribute to ennoblement [18, 19].

Although it is generally agreed that the ennoblement of E_{corr} is substantially due to a depolarisation of the cathodic reaction, it has recently been suggested that the thickening of a passive film on passive alloys could play an additional role [20]. This finding is not

in isolation since workers in France have observed significant changes in the passive film characteristics due an ageing effect in natural seawater [21]. Hence there are implications that ennoblement, to some extent, could be affected by changes in anodic reaction kinetics.

Since localised corrosion is a stochastic process, factors which affect it's probability have to be considered. The ennoblement of E_{corr} is significant since it is often assumed that the likelihood of pitting and crevice corrosion initiation is enhanced as the free corrosion potential approaches the pitting or breakdown potential. However, Holthe et al.[22] found that the biological aspect of seawater has little or no influence on the initiation phase of crevice corrosion. The kinetics of propagation are affected by the depolarisation of the oxygen-reduction reaction which facilitates effective cathodic activity in a corrosion cell developed between aerated and low oxygen areas within the intermittent biofilm.. Large decreases in corrosion potential are associated with initiation of localised corrosion. Scotto et al. [12] correlated the measured weight loss of samples exposed to natural seawater to the length of time that the E_{corr} remained at a value below a defined critical potential (0mV SCE). Dexter and Gao [16] observed localised corrosion on stainless steel specimens which exhibited active E_{corr} values.

Measurement of E_{corr} is the easiest electrochemical test. Mansfeld and Little [23] warn against over-interpretation of E_{corr} data. Since E_{corr} is a mixed potential, complex interactions of anodic and cathodic partial reactions can occur especially over a non-homogeneous biofilm-covered surface. E_{corr} cannot therefore be assumed to come about due to a single mechanism affecting only one reaction. Traditional DC-electrochemical techniques have proved successful in the interpretation of MIC in aerobic environments [24] and in particular the employment of dual-cell techniques in the study of microbial corrosion has advanced the understanding of anodic and cathodic processes and how biofilm formation affects their reaction kinetics [23].

Hydrodynamic Study of the Biofilm

The characterisation of biofilms has traditionally involved the use of microscopical techniques and biological assays such as acridine orange staining. Disadvantages of such methods are the inherent risks of interrupting the biofilm during the surface preparation and, as such, techniques which can monitor biofilm formation in-situ are of fundamental interest.

The rotating disk electrode has been extensively used to characterise the mass transport of a species through a solution by diffusion processes and also to study hydrodynamic effects on corrosion processes. Extension of classical hydrodynamic theory by Levich [25] has led to the development of a model to determine the mass transfer characteristics of a chemical species through a porous layer covering an electrode surface [26] and this model has recently been employed to represent the events during biofilm formation on gold electrodes [27]. The method is based on a model in which the biofilm must be considered as a porous non-reacting layer covering the metallic interface as shown in Fig. 8.2. The theory states that the diffusion rate of any chemical species through the layer is retarded once the biofilm forms. This method, utilising the defined hydrodynamics at a rotating disk electrode (RDE) allows the characteristics of oxygen transport through the biofilm to be elucidated.

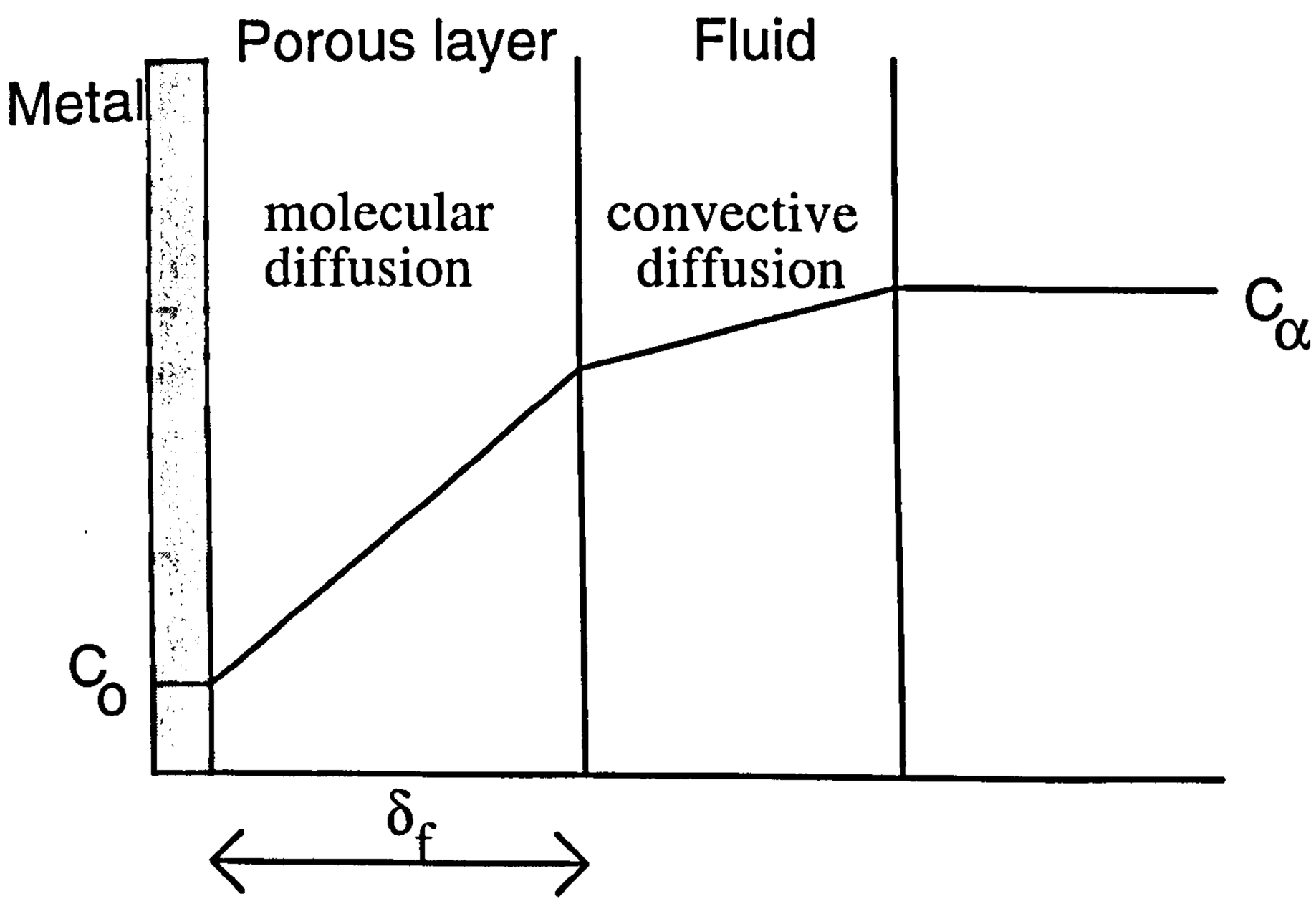

Fig. 8.2. Schematic representation of the biofilm/substrate interface

In the fluid layer in Fig 8.2, the concentration distribution is governed by convective diffusion of oxygen to the biofilm/fluid interface. In the biofilm, the transport of oxygen is governed by molecular diffusion. The steady state oxygen reduction current, I_o, can be analytically determined from a relationship of the form

$$I_0^{-1} = I_L^{-1} + I_K^{-1} + I_{\Omega-\infty}^{-1} \qquad (1)$$

I_L is the limiting diffusion current at the electrode surface, before any biofilm has formed and when the rotation speed is Ω. I_L is determined by the Levich relationship in which I_L^{-1} varies linearly with $\Omega^{-1/2}$ via the relationship

$$I_L^{-1} = K\Omega^{-1/2} \qquad (2)$$

where the Levich constant $K = 0.62nFS\sqrt{\frac{2\Pi}{60}}^{2/3} D^{\frac{2}{3}}\nu^{-1/6}C_\infty$ (3)

In (3), C_∞ is the concentration of dissolved oxygen in the solution in mole/cm^3, ν is the kinematic viscosity of seawater in cm^2/s, F is the Faraday constant and S is the electrode area in cm^2.

I_K in equation (1) represents the kinetic current assuming that mass transfer is infinitely fast and that the current varies via the relationship

$$I_K = kC\infty\exp(b\eta) \qquad (4)$$

where k is a constant, b is the Tafel constant for oxygen reduction in mV/decade, and η is the overpotential in mV.

$I_{\Omega-\infty}$ in (1) is the limiting current when the entire concentration gradient is located within the porous layer and there is no convective diffusion concentration boundary layer at the fluid/porous layer interface. $I_{\Omega-\infty}$ is represented by the expression

$$I_{\Omega-\infty} = \frac{nFSD_fC_\infty}{\delta_f} \qquad (5)$$

where D_f is the diffusion coefficient of oxygen through the porous biofilm and δ_f is the thickness if the biofilm.

By considering reciprocal quantities, as is often done for processes occurring in series, an experimental plot of I_o^{-1} against $\Omega^{-1/2}$ must be a straight line parallel to the linear Levich variation.

Determination of the cathodic current as a biofilm forms has been performed on gold electrodes [27] through a series of potentiostatically controlled experiments. A series of

cathodic polarisation curves were attained at different disk rotation speeds to determine the potential range of the diffusion plateau (i.e. the region of the diffusion limited process). On the diffusion limited plateau, the contribution to I_0 from kinetic factors, I_K, can be neglected since the process is mass transfer controlled. The rotating disk electrode potential was held at a predefined constant value of -900mV and cathodic current against rotation speed were plotted. The recorded cathodic current included a proportion due to hydrogen evolution at the electrode, I_H, and as such, the total current, I, could be represented by

$$I = I_H + I_0 = I_H + \frac{1}{I_L^{-1} + I_{\Omega-\infty}^{-1}} \qquad (6)$$

On stainless steels, previous workers have established that the well-defined diffusion plateau found on gold does not occur and therefore the kinetic factors in equation (6) can not be neglected as for gold.

This steady state analysis of the cathodic current gives the magnitude of the porous layer permeability, $\mathbf{D_f/\delta_f}$, once $I_{\Omega-\infty}$ is determined. However, additional use of transient techniques is required in order to determine actual values of the porous layer (biofilm). Development of transient Electro Hydrodynamic Impedence (EHD) techniques gives the diffusion time constant $\mathbf{\delta_f^2/D_f}$ which when combined with the steady state solution $\mathbf{(D_f/\delta_f)}$ can give absolute values of the diffusion rate through the film and the actual film thickness.

EHD involves analysis of the frequency response of the disk electrode to a perturbation of the angular speed (Ω). The technique is discussed fully in [28,29].

Experimental Methods - PART I

In this work, a short-term (up to 12 weeks) study was carried out in natural seawater in the marine laboratories of the Institut Francais de Recherche pour l'Exploitation de la Mer (Ifremer), Brest. Two materials were studied : UNS S31603 (a standard austenitic stainless steel) and UNS S32760 (a superduplex stainless steel). The study consisted of two phases. The initial immersion and DC-electrochemical monitoring were performed at Ifremer between the period of July and October, followed by a programme of microscopical examination at the University in Glasgow.

Specimens of the two materials were immersed in two glass cells : one clear and one darkened glass as shown in Fig. 8.3.

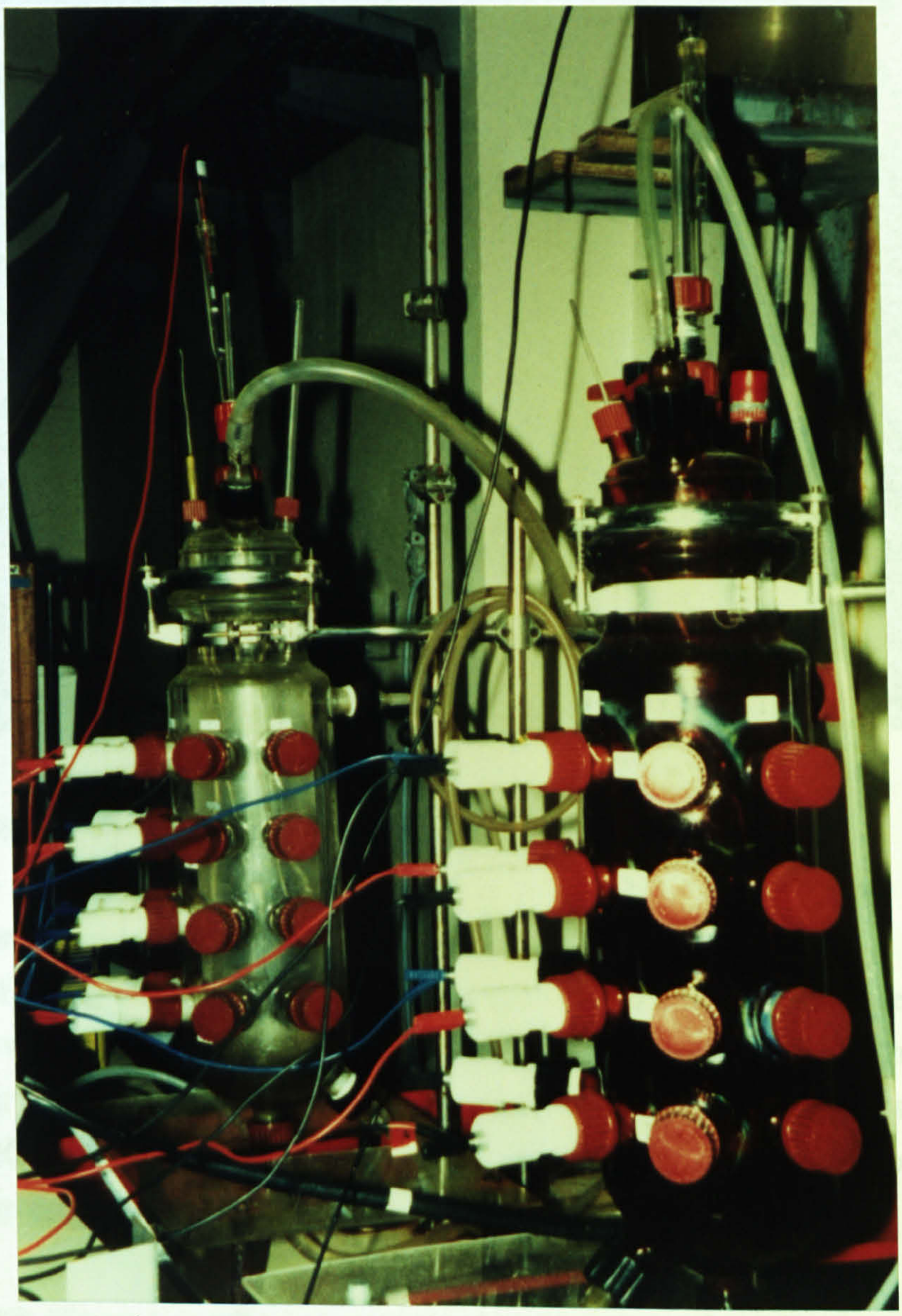

Fig. 8.3. Glass cells containing replenished natural seawater

The specimen holder consisted of a PTFE tube, into which the specimen was inserted (marked 1 on Fig. 8.4) and a metal rod (2 in Fig. 8.4) which formed the electrical contact between the specimen (3 in Fig. 8.4) and the electrochemical apparatus. The specimens were then inserted into the vessel so that the continually replenished seawater was flowing parallel to the surface.

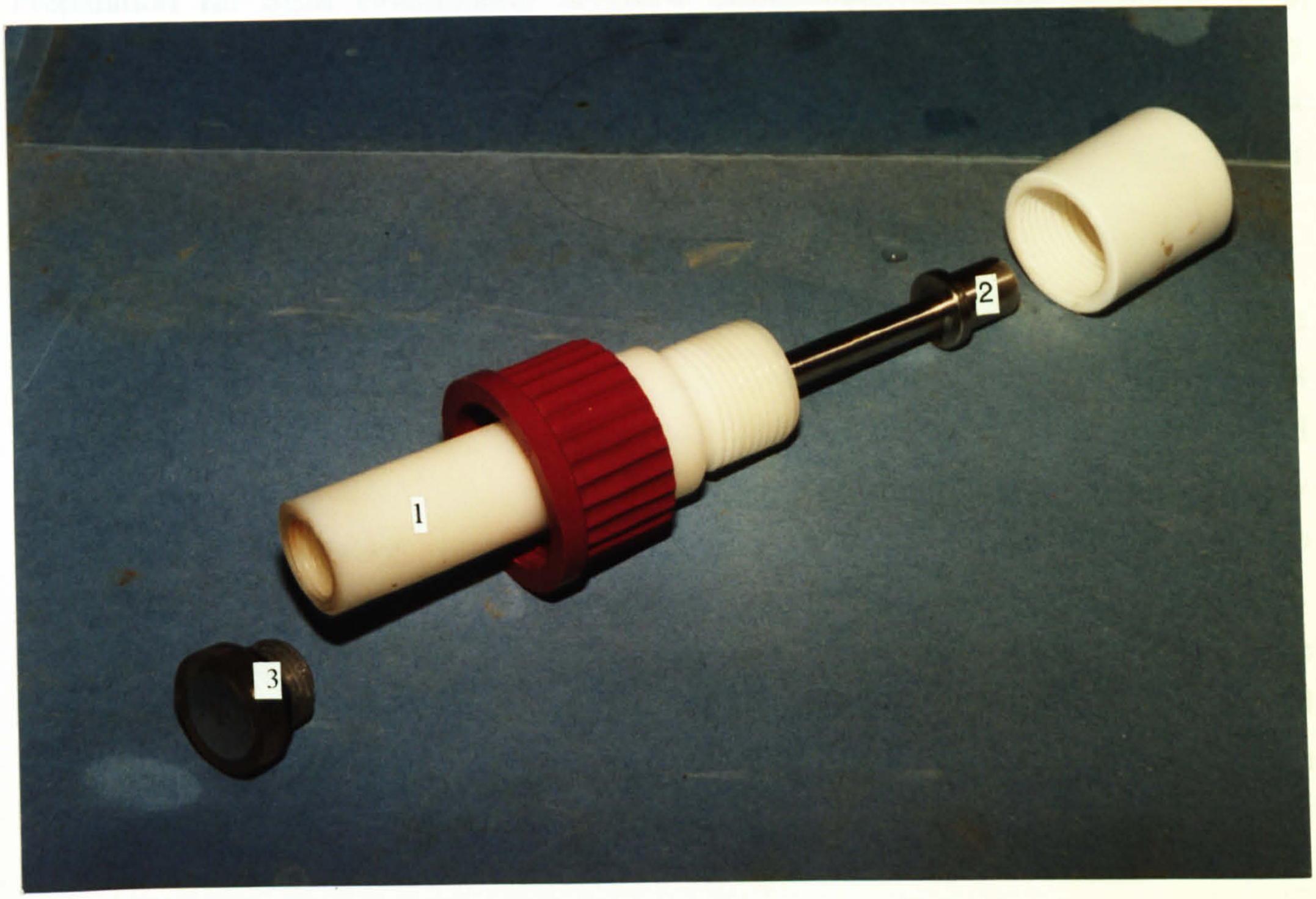

Fig. 8.4. Specimen holder and electrical connecting arrangement

Specimen preparation was carried out with the main intention to eliminate the possibility of crevice corrosion at the metal/resin interface. The specimens in this part of the work were not of the form previously used but were circular with a stem rather than a soldered wire to enable electrical contact to be made. This was embedded in Araldite 2020 epoxy resin in a rubber mould which could then be removed to leave a threaded stem, able to be inserted into the PTFE cylinder.

Setting the specimens in resin was conducted in two parts. Initially the specimens were put in the rubber moulds, half full of resin, for 45 minutes within a vacuum flask. After 45 minutes, all the air bubbles were at the surface of the resin and the moulds were then completely filled with the remaining resin. By removing the air from the resin at the specimen surface, a good adherent bond is achieved at the interface. In this chapter these specimens will be denoted 'Type I'. Whether the preparation does eliminate crevice corrosion can only be established on examination of the specimens after testing. The specimens were abraded to a 1200 grit finish after which they were cleaned ultrasonically in distilled water for 15 minutes. The exposed surface area of each specimen was $2cm^2$.

Preparation for SEM examination involved maintaining the entire specimen in a solution of 2.5% gluteraldehyde in filtered seawater immediately after removal from the test cell. After a maximum of 6 weeks the specimens were freeze dried and retained in a dessicator. Finally after light microscopy was complete the specimens were carbon coated for SEM work.

The programme lasted 12 weeks and consisted in the main part of following the progression of the free corrosion potential, DC-anodic and cathodic polarisation tests and a limited number of potentiostatic tests. Free corrosion potential was recorded automatically at 5 minute intervals in the initial 24 hours followed by half-hourly intervals. The polarisation tests were performed, on separate specimens (with duplicate tests performed at each time interval in each cell), immediately on immersion, after 1 week, 2 weeks, 4 weeks and 8 weeks in each cell. Duplicate polarisation tests were performed and two specimens for each immersion period were removed from the cell for examination without polarisation. The water flow rate in the cells was 1000ml/min which could be equated to a velocity of approximately 0.1m/s.

For comparative purposes, a parallel study of the electrochemical behaviour of the same materials was conducted on specimens of the type used for the rest of the programme, containing a more apparent crevice at the metal/resin interface. For the remainder of this chapter, these will be referred to as Type II specimens. Anodic and cathodic polarisation tests were only performed after 1, 2 and 4 weeks but as for the 'crevice free' specimens some were left for examination without polarisation. The free corrosion potential was recorded manually twice daily. These specimens were immersed in a tank containing seawater which was entering the tank at a rate of 1000ml/min.

The seawater salinity was relatively constant throughout the experiment at between 34,940 and 35,021ppm. Dissolved oxygen remained between 7.9mg/l and 8.2mg/l and the temperature varied between 16.5°C and 20.5°C.

PART II

Over a period of two and a half years, specimens were immersed in natural seawater at the University Marine Biological Station Millport (UMBSM). The main aim of this experiment was to look at the macro-fouling of the specimens and ultimately how thick layers of marine fouling affect the electrochemical characteristics of the materials. To this aim, the fouling was studied by means of a photographic record followed by

electrochemical tests and microscopical examination. Anodic polarisation tests were mainly carried out after periods of 1 month, 2 months, 6 months and 18 months. Cathodic tests were carried out after relatively short periods since the main aim of these tests was to establish how the biofilm, formed after the first few days affects the oxygen reduction reaction.

A small study to investigate the effect of barnacle settlement on the corrosion of stainless steels was set up involving plate specimens of UNS S31603 and SAF 2205. Artificially cultured barnacle larvae was crushed and placed on the plate surface before the barnacle settlement season and then the specimens were immersed in the natural seawater and fresh barnacles settled. After 18 months and no polarisation, these specimens were examined.

The conditions at UMBSM were significantly different from Ifremer. UMBSM is an estuarine location, the seawater being of much lower salinity (between 28,000-30,200ppm) and the temperature varied only between 6°C and 12°C.

PART III

This work aimed to follow the initial formation of the biofilm in terms of oxygen reduction characteristics by use of a rotating disk electrode. There were two main aims of the project which was carried out during a short study visit to the Ifremer marine laboratories. The principal aim was to validate the rotating disk/oxygen diffusion technique to assess the characteristics of biofilm formation, already developed on gold, on stainless steel alloys. As will be reported in the Results section, there were changes made to the assumptions and the experimental; analysis to account for the different material characteristics. The second aim, which depended on the outcome of the validation process, would be to calculate values of the parameter (D_f/δ_f), the layer permeability, which could directly give a quantitative measure of how the biofilm is changing the accessibility of the surface to diffusing oxygen.

The experimental procedure is described in the following paragraphs. Speed control of the rotating disk electrode was achieved by means of a tachometer and the speed variation was imposed by a ramp input signal. Two materials were studied here, namely UNS S31603 and UNS S32760. The specimens were made from 8mm diameter rod and were machined to a smaller diameter at the end to be secured in the RDE chuck. The exposed face area was therefore 0.5cm^2. The electrode was covered with a shrink fit insulating sleeve along it's length and this left only the front face exposed (Fig. 8.5).

Care was taken to ensure that at the sleeving/electrode interface there were no air gaps and that good adherence was attained.

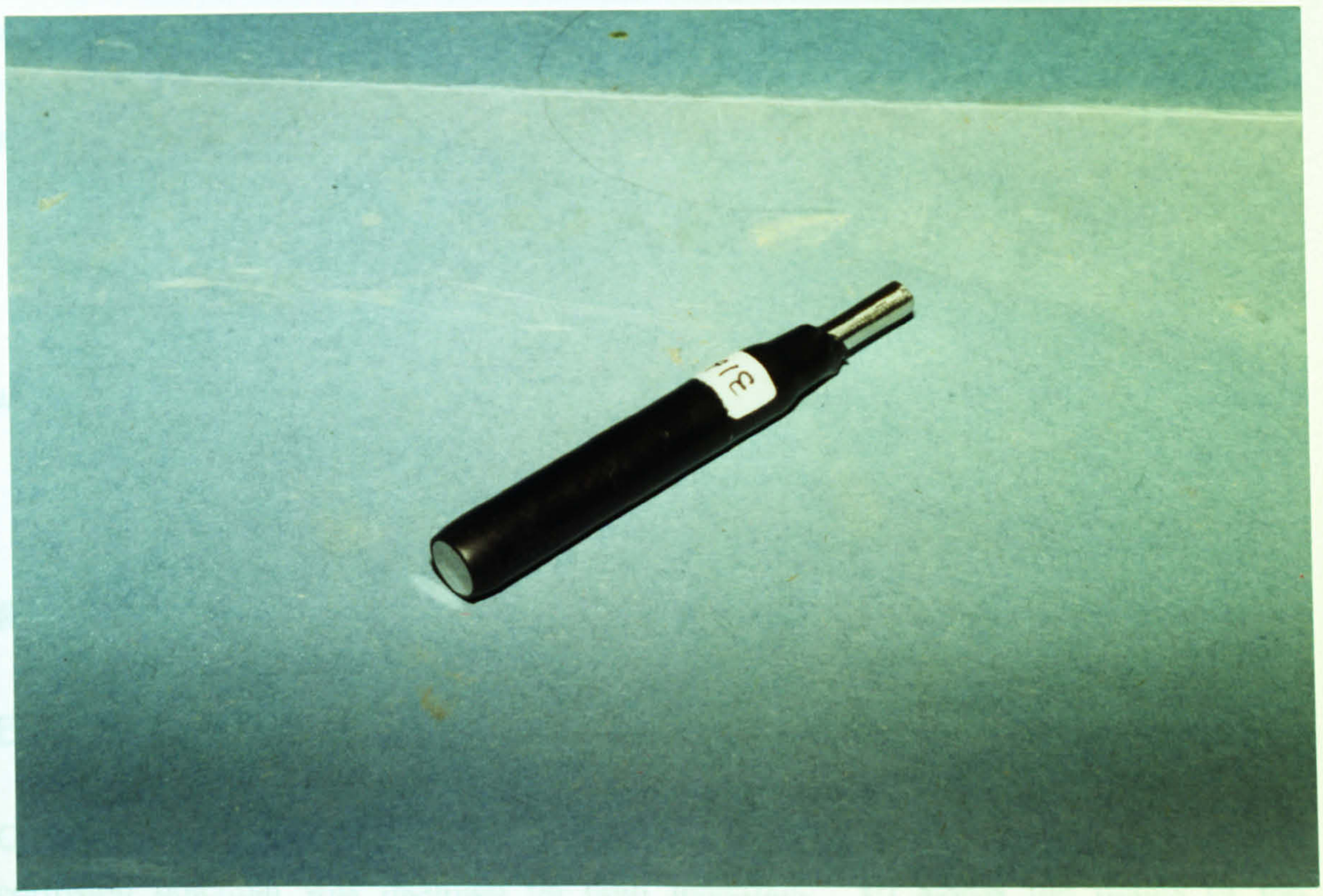

Fig. 8.5. Rotating electrode

Preliminary cathodic polarisation experiments were carried out at different rotational speeds to characterise the form and the current stability in the oxygen reduction diffusion plateau. The scan rate used was 5mV/min, slower than in previous potentiodynamic scans, in order to model quasi-stationary behaviour. Previous work on stainless steels [30] had shown that in contrast to the oxygen reduction reaction on gold electrodes, the current in the diffusion controlled region can often increase significantly. The intention of the initial cathodic polarisation curves was to find a potential at which the current would be relatively stable (i.e. form a flat diffusion region).

Continuation of the work involved using potentiostatic control to analyse the steady state response of the system to an increase, followed by a decrease, of disk rotational velocity. The current as a function of angular velocity was then plotted (I versus Ω). The angular velocity was increased from 99rpm to 1188rpm, the complete cycle taking three and a half minutes. Four cycles were performed on each electrode and the data points taken from the fourth cycle, in which the forward scan and the reverse scan were coincident, were used in the data analysis.

This procedure was carried out on three electrodes of the two materials each day for a period of 9 days after immersion. Data points were then inserted into a curve fitting package to yield values of the parameters A, B' and C in equation (7), developed from equation (6), representative of the relation between the current and the rotational velocity ;

$$I = A + \frac{1}{B' + C\Omega^{-0.5}} \quad \text{----------} \quad (7)$$

where $A = I_H$

$B' = I_K^{-1} + I_{\Omega-\infty}^{-1}$

$C = K^{-1}$

Results - PART I

Free Corrosion Potential

On the Type 1 specimens, in the light and the dark cells, an ennoblement of the free corrosion potential was recorded on both materials. To assess the trends of the ennoblement, the following parameters were used : the incubation period ($\mathbf{t_{inc}}$) denoting the time after immersion before the ennoblement commenced, the potential at time of immersion ($\mathbf{E_o}$), the rate of increase of potential (**dE/dt**), in mV/hour and the maximum potential attained ($\mathbf{E_{max}}$).

The free-corrosion potential of the duplex stainless steel UNS S32760 was consistently more negative on immersion than the austenitic UNS S31603. The extent of the ennoblement on UNS S32760 was typically greater then UNS S31603.

Significant differences were observed in the evolution of E_{corr} in the dark and the clear vessels. In the dark vessel, both materials exhibited a substantially longer t_{inc} than in the clear vessel. In addition, the maximum potential attained in the clear cell was generally, more noble than in the darkened conditions.

Figure 8.6a shows the evolution of E_{corr} of four specimens of UNS S31603 in the first two weeks of immersion in the clear cell and Fig. 8.6b. shows the same data in the dark cell. From Fig. 8.6a it is clear that one sample exhibited erratic E_{corr} behaviour, attaining an extremely noble E_{corr} (400mV) followed by a substantial decrease after 145 hours. After two weeks immersion, this specimen was removed for examination

severe crevice corrosion (Fig. 8.7) was observed. Apart from one sample in the light cell, the specimens E_{corr} all followed the same trend. To monitor these trends, average values were calculated of the parameters above and are tabulated (Tables 8.1-8.3) for the three immersion periods starting on the dates shown.

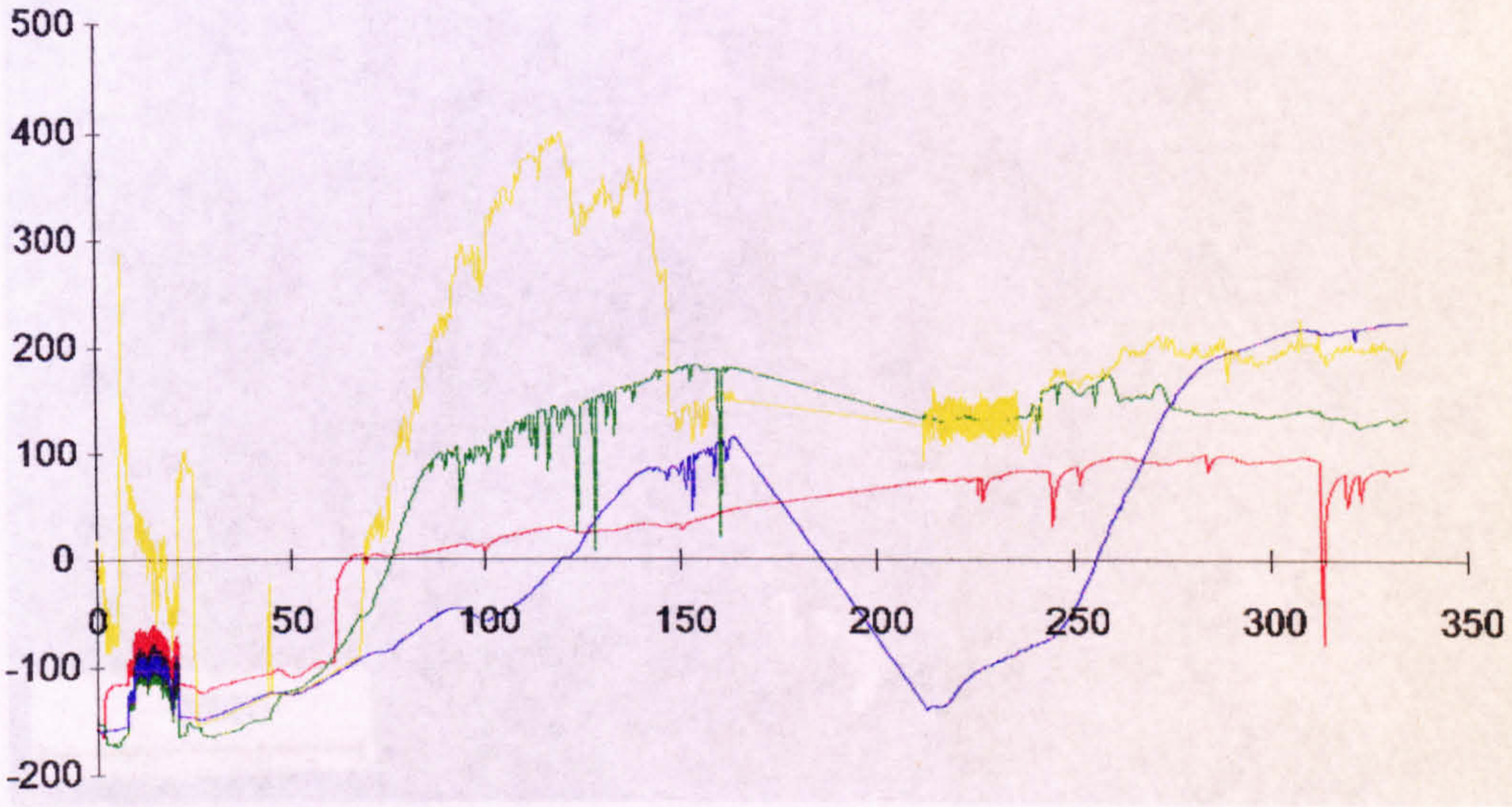

Fig. 8.6a. Free corrosion potential of UNS S31603 in light cell

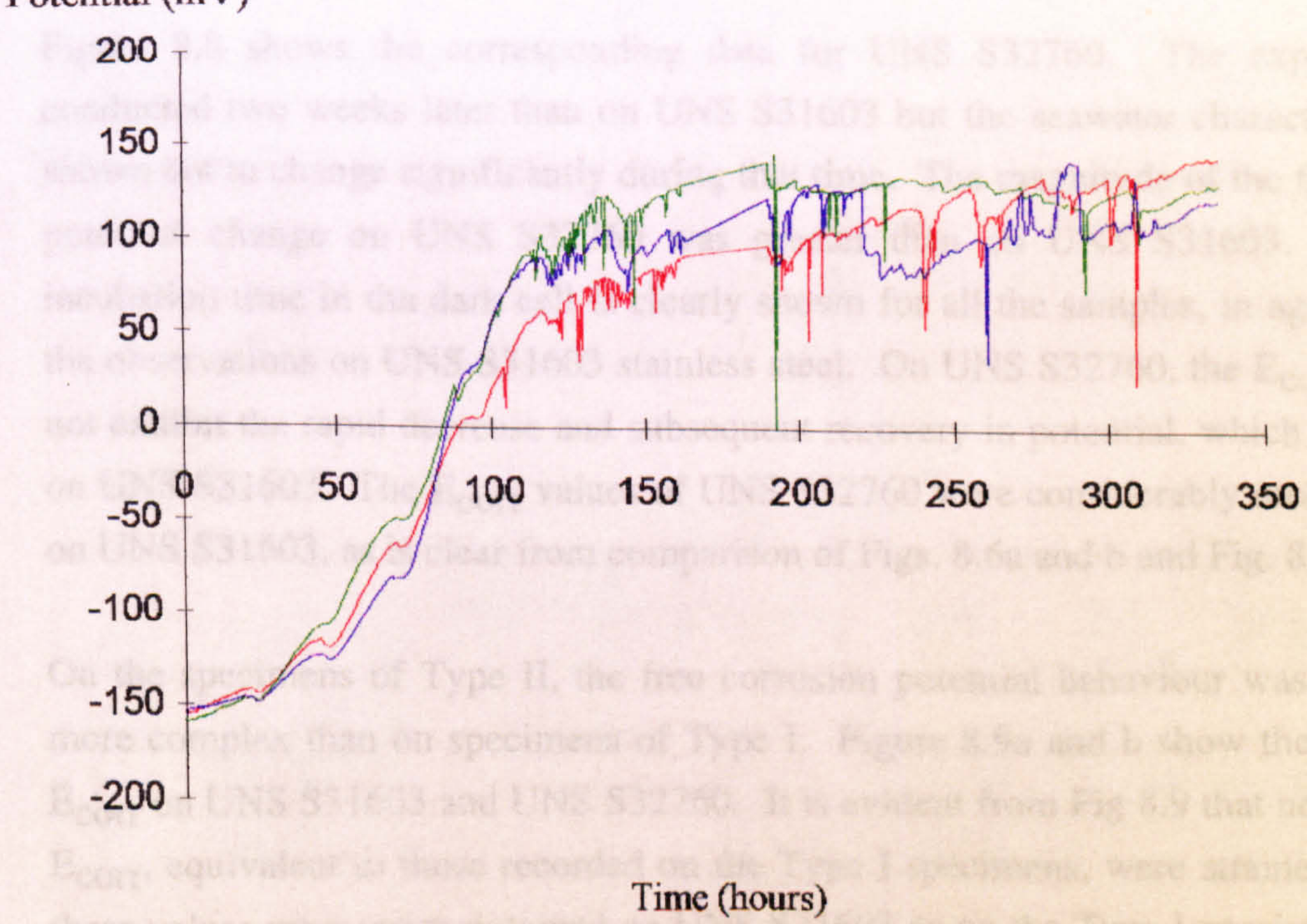

Fig. 8.6b. Free corrosion potential of UNS S31603 in dark cell

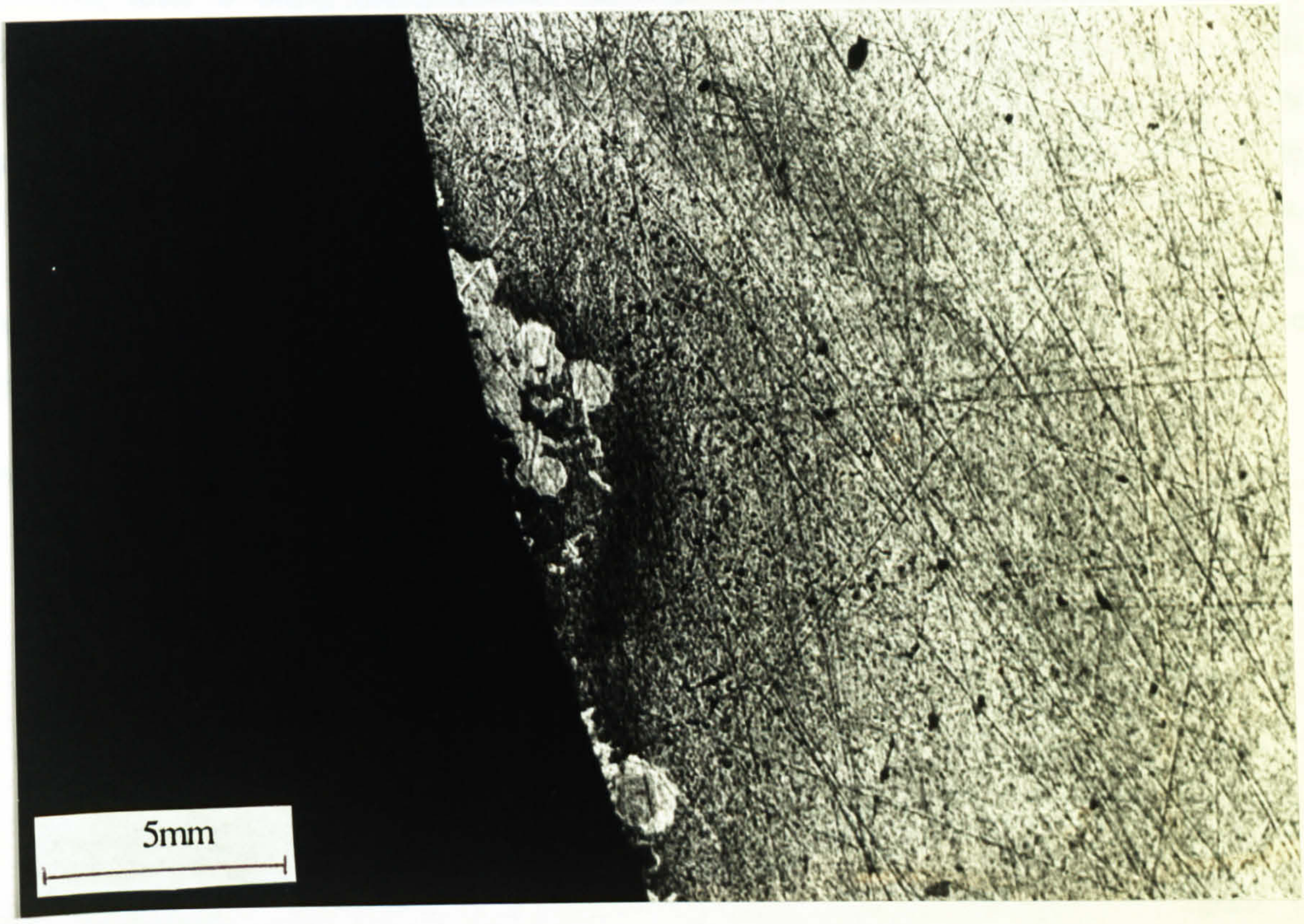

Fig. 8.7. Crevice corrosion on UNS S31603 in the light cell after immersion for 2 weeks and no polarisation

Figure 8.8 shows the corresponding data for UNS S32760. The experiment was conducted two weeks later than on UNS S31603 but the seawater characteristics were shown not to change significantly during that time. The magnitude of the free corrosion potential change on UNS S32760 was greater than on UNS S31603. The longer incubation time in tha dark cell is clearly shown for all the samples, in agreement with the observations on UNS S31603 stainless steel. On UNS S32760, the E_{corr} values did not exhibit the rapid decrease and subsequent recovery in potential, which were evident on UNS S31603. The E_{corr} values of UNS S32760 were considerably more stable than on UNS S31603, as is clear from comparison of Figs. 8.6a and b and Fig. 8.8.

On the specimens of Type II, the free corrosion potential behaviour was significantly more complex than on specimens of Type I. Figure 8.9a and b show the evolution of E_{corr} on UNS S31603 and UNS S32760. It is evident from Fig 8.9 that noble values of E_{corr}, equivalent to those recorded on the Type I specimens, were attained. However, these values were not maintained on UNS S31603 as on the Type I specimens and after 12 days the free corrosion potential consistently registered negative values. On UNS

S32760, after 8 days, the potential had significantly ennobled and this trend was maintained for up to 60 days. On both materials, it was clear that in the period between 150-175 hours, the scatter in the free corrosion potential values was greatest followed by a region of more stable values on all three specimens. After 14 days, examination of the UNS S31603 stainless steel specimens showed that on each of the four specimens, crevice corrosion had initiated. In contrast, the UNS S32760 remained unattacked. After 47 days, one of the four specimens of UNS S32760 showed signs of crevice corrosion on one edge.

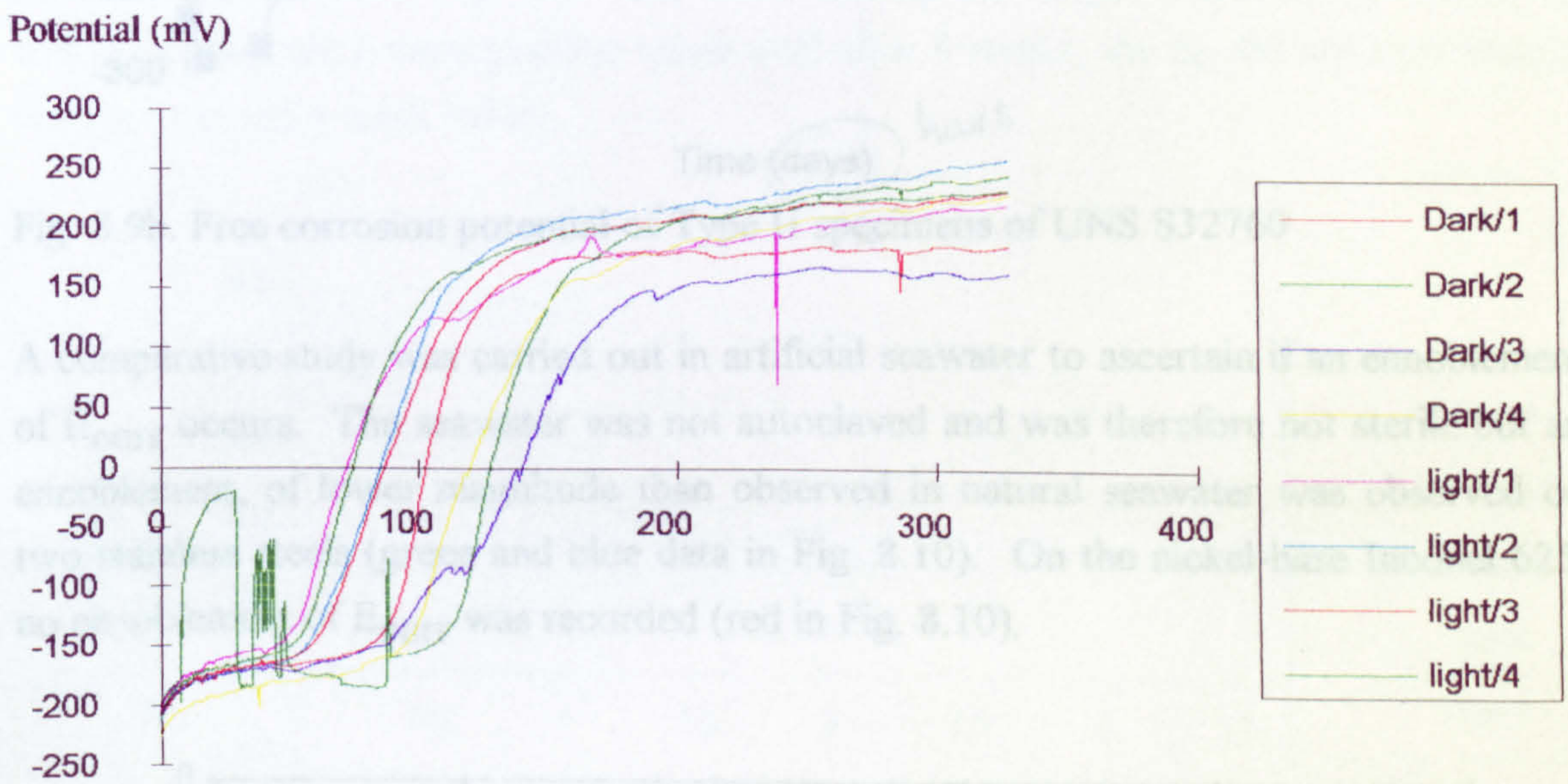

Fig. 8.8. Free corrosion potential evolution on UNS S32760 in the light and the dark cell

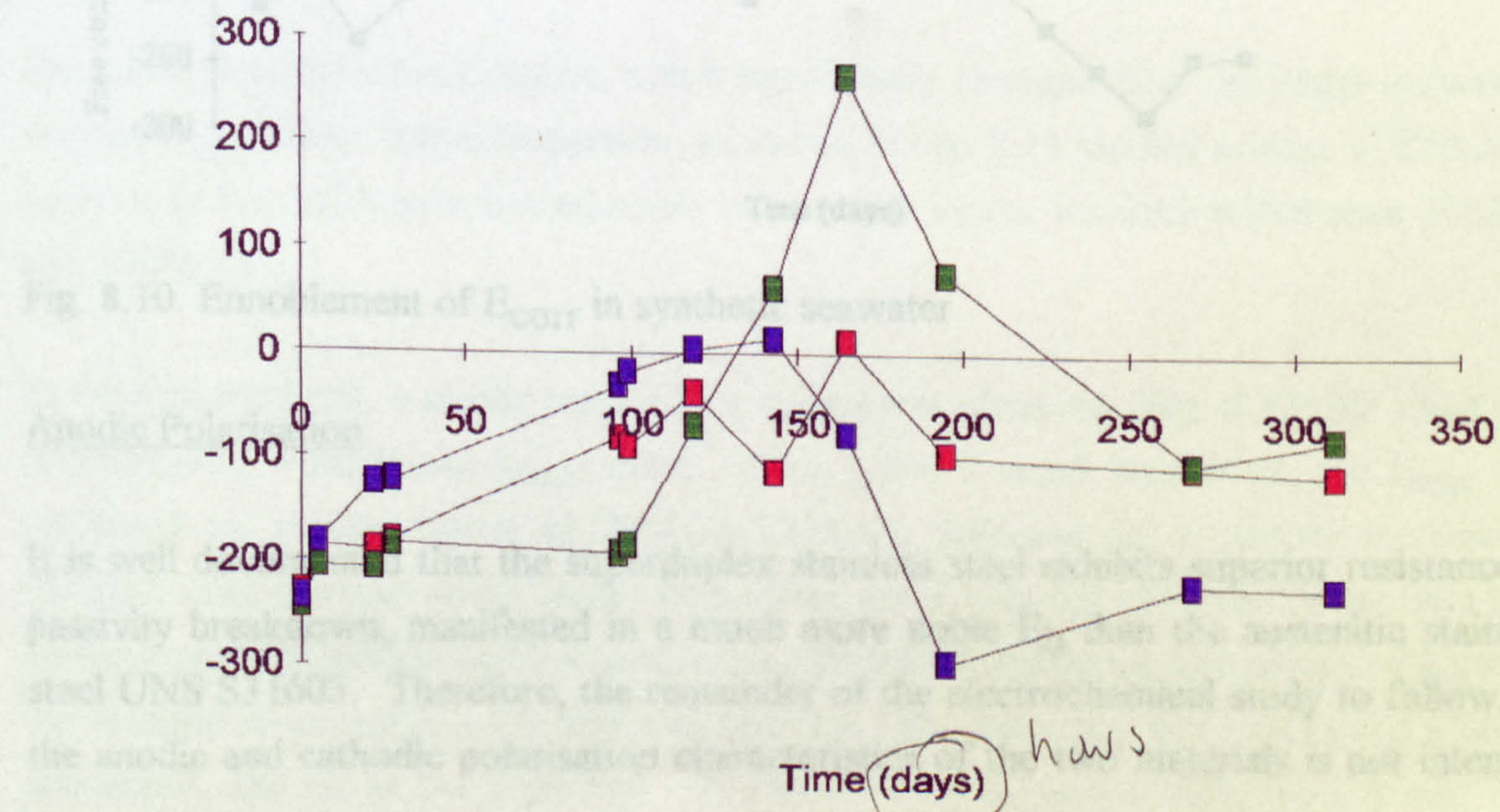

Fig. 8.9a. Free corrosion potential on Type II specimens of UNS S31603

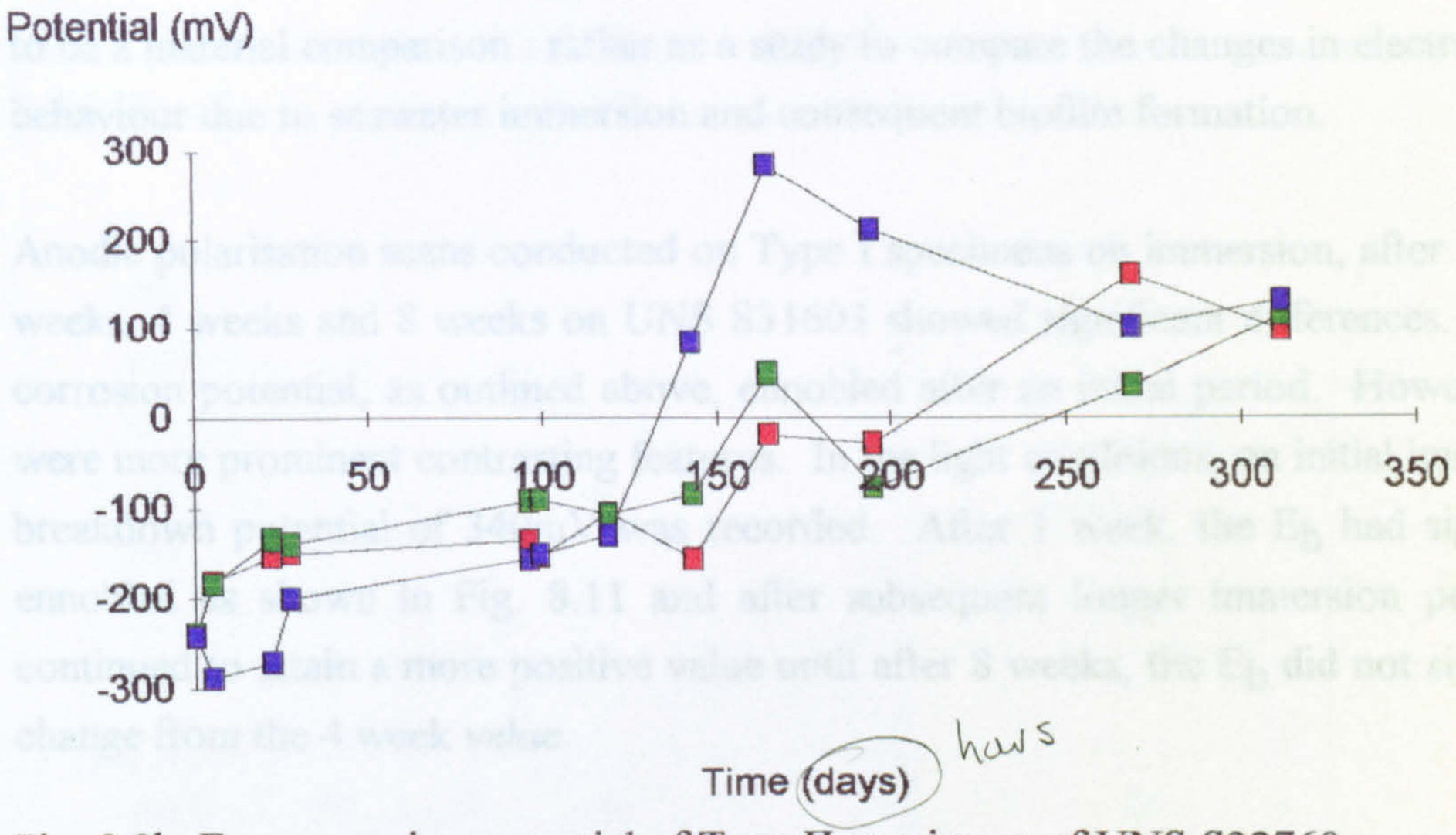

Fig. 8.9b. Free corrosion potential of Type II specimens of UNS S32760

A comparative study was carried out in artificial seawater to ascertain if an ennoblement of E_{corr} occurs. The seawater was not autoclaved and was therefore not sterile but an ennoblement, of lower magnitude than observed in natural seawater was observed on two stainless steels (green and blue data in Fig. 8.10). On the nickel-base Inconel 625, no ennoblement of E_{corr} was recorded (red in Fig. 8.10).

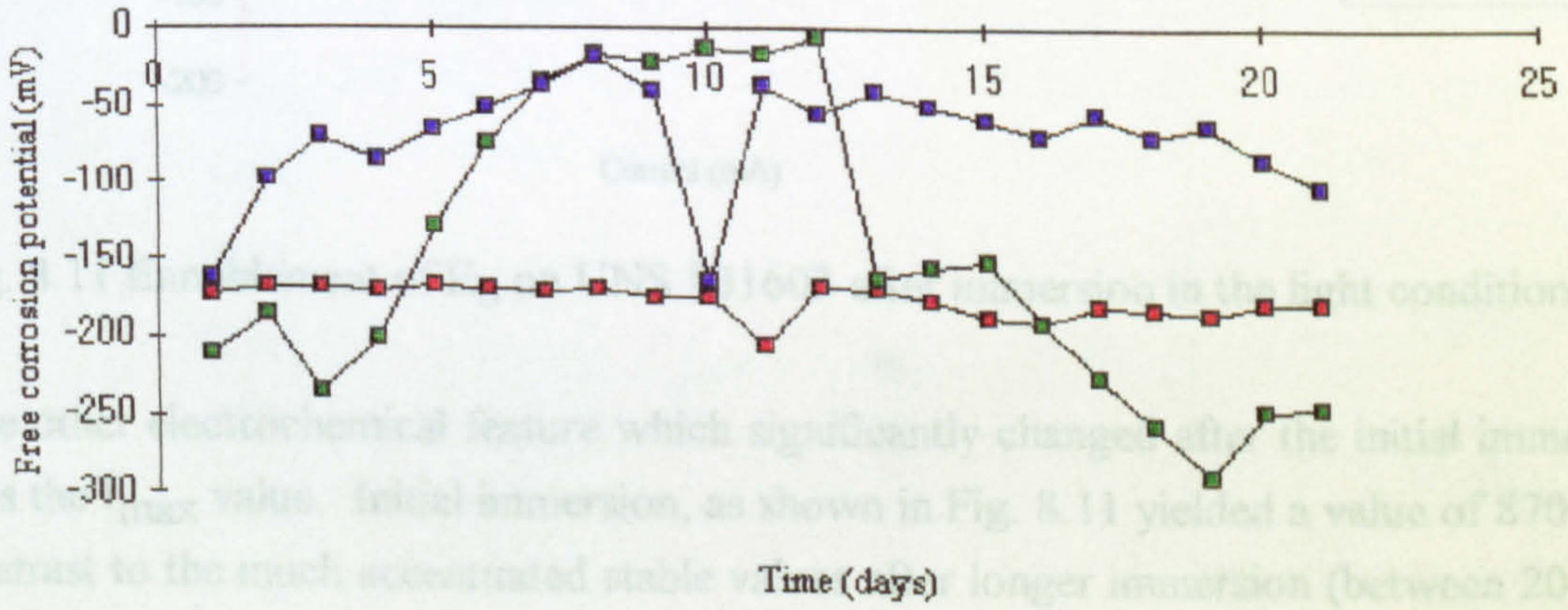

Fig. 8.10. Ennoblement of E_{corr} in synthetic seawater

Anodic Polarisation

It is well documented that the superduplex stainless steel exhibits superior resistance to passivity breakdown, manifested in a much more noble E_b than the austenitic stainless steel UNS S31603. Therefore, the remainder of the electrochemical study to follow, on the anodic and cathodic polarisation characteristics of the two materials is not intended

to be a material comparison : rather as a study to compare the changes in electrochemical behaviour due to seawater immersion and consequent biofilm formation.

Anodic polarisation scans conducted on Type I specimens on immersion, after 1 week, 2 weeks, 4 weeks and 8 weeks on UNS S31603 showed significant differences. The free corrosion potential, as outlined above, ennobled after an initial period. However, there were more prominent contrasting features. In the light conditions, on initial immersion, a breakdown potential of 340mV was recorded. After 1 week, the E_b had significantly ennobled as shown in Fig. 8.11 and after subsequent longer immersion periods, E_b continued to attain a more positive value until after 8 weeks, the E_b did not significantly change from the 4 week value.

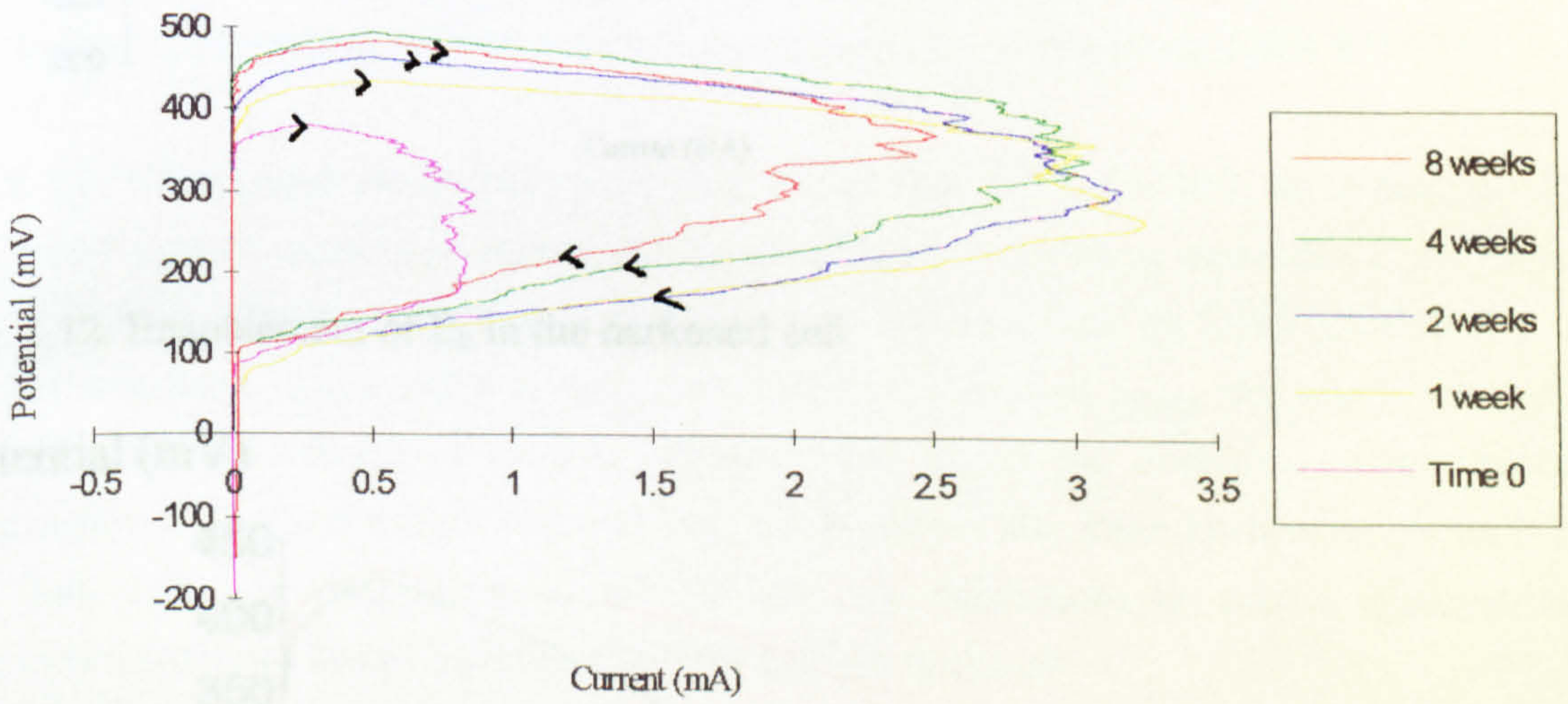

Fig. 8.11 Ennoblement of E_b on UNS S31603 after immersion in the light conditions

The other electrochemical feature which significantly changed after the initial immersion was the I_{max} value. Initial immersion, as shown in Fig. 8.11 yielded a value of 870μA in contrast to the much accentuated stable values after longer immersion (between 2000μA and 3000μA).

In the darkened cell, a similar trend in E_b values was observed (Fig. 8.12) but there was a contrasting trend in the I_{max} value. After 1 and 2 week immersion, the I_{max} was increased to, in the region of 2000μA-2800μA, followed by a further increase to 3800μA after 4 weeks and 8 weeks immersion which was not observed in the light cell. In the immersion period up to 4 weeks, no substantial difference was observed between the breakdown potential in the light cell and dark cell. However, at 4 weeks and 8 weeks immersion, the E_b in the darkened cell was consistently more noble than in the light conditions albeit by a small margin (50-60mV). Figure 8.13a shows the comparative

anodic polarisation curves in the light and dark cell after 1 week immersion and in Fig. 8.13b the corresponding graphs after 4 weeks immersion are shown.

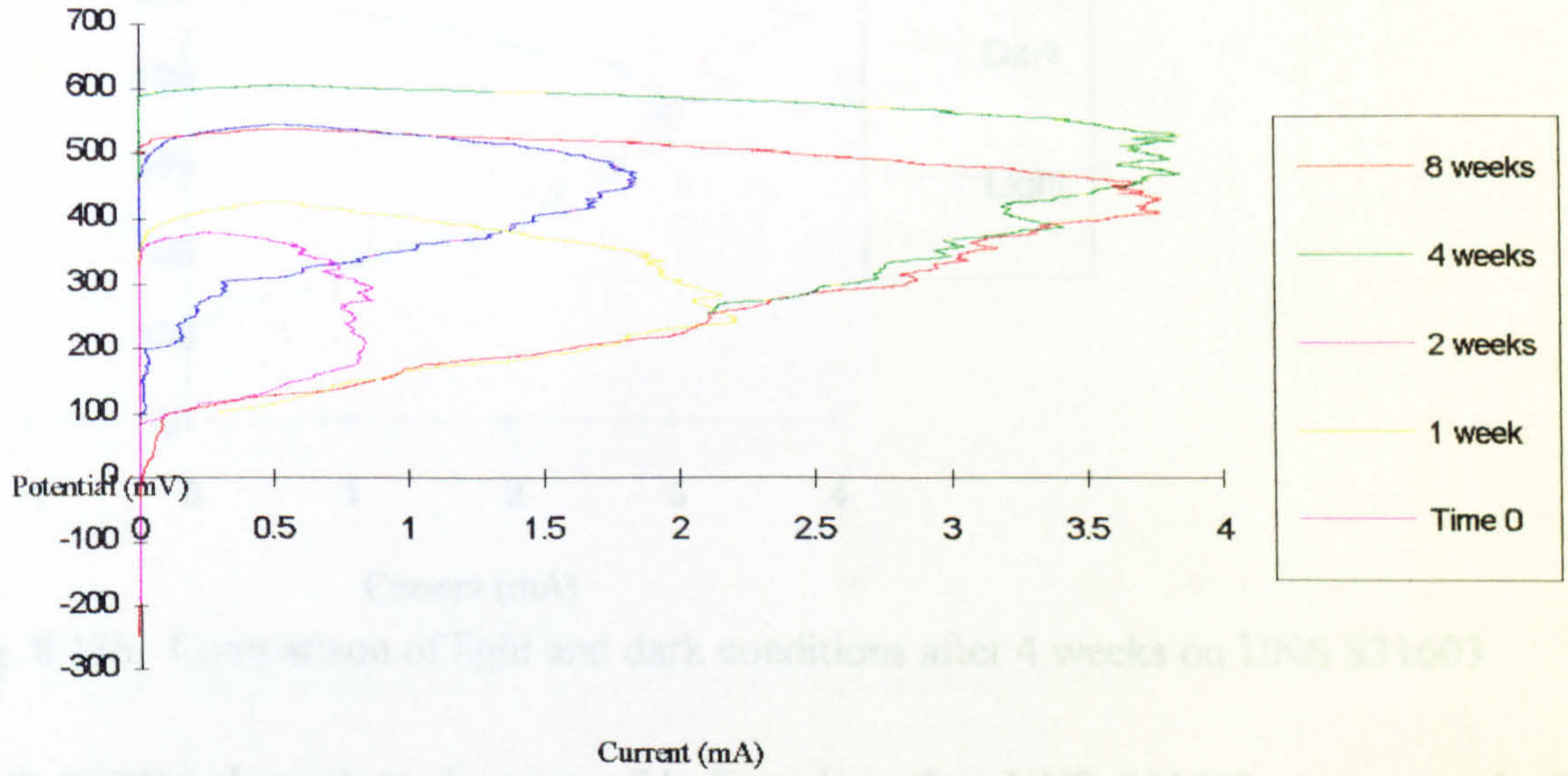

Fig. 8.12. Ennoblement of E_b in the darkened cell

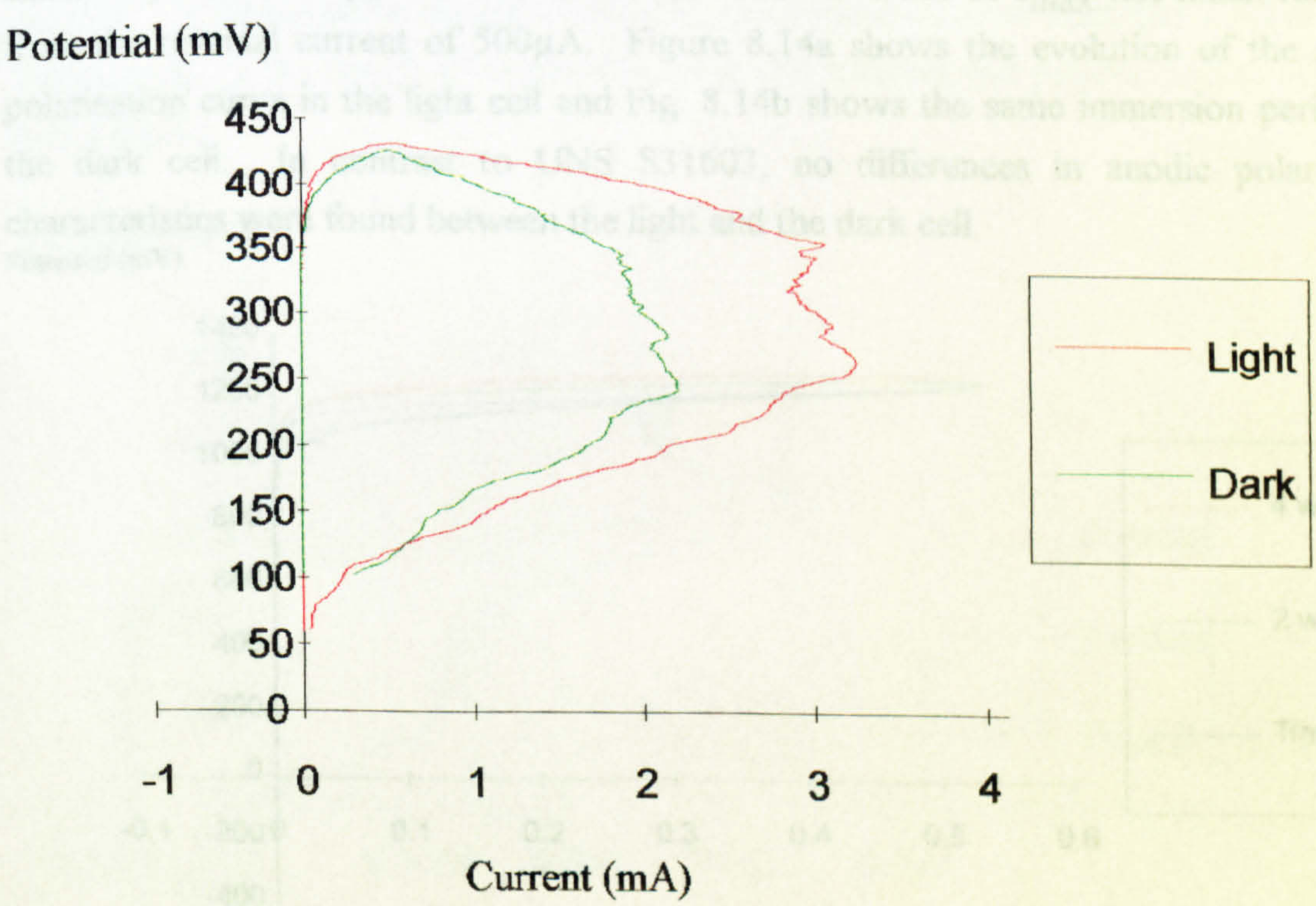

Fig. 8.13a. Comparison of light and dark conditions after 1 week on UNS S31603

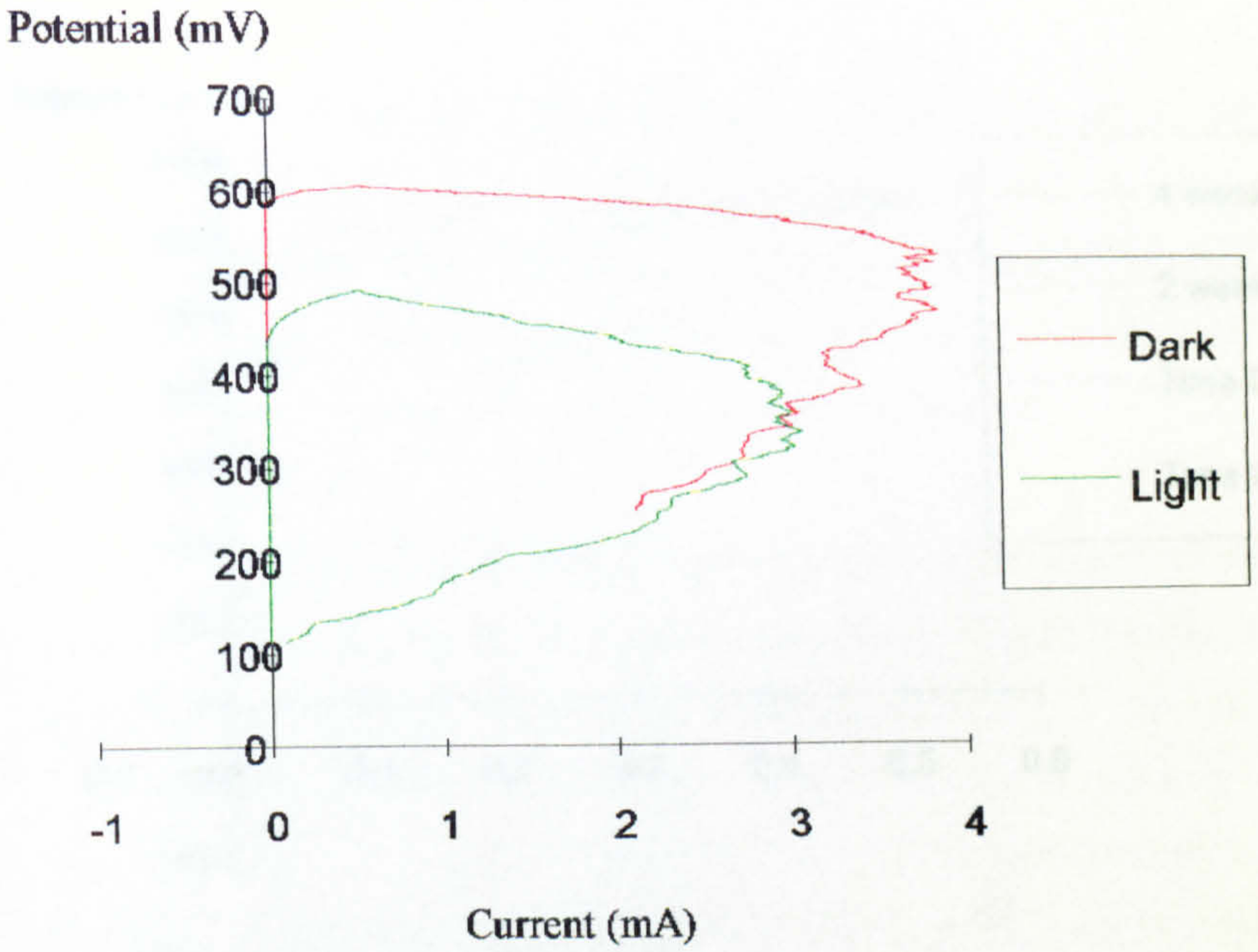

Fig. 8.13b. Comparison of light and dark conditions after 4 weeks on UNS S31603

UNS S32760 showed much more noble E_b values than UNS S31603, as expected. In the period up to 4 weeks immersion, the E_b ennobled but not by as extensive a margin as UNS S31603. The repassivation was much more efficient than on UNS S31603 (i.e. a smaller hysteresis loop) and was also manifested in values of I_{max} not much removed from the reversal current of 500µA. Figure 8.14a shows the evolution of the anodic polarisation curve in the light cell and Fig. 8.14b shows the same immersion periods in the dark cell. In contrast to UNS S31603, no differences in anodic polarisation characteristics were found between the light and the dark cell.

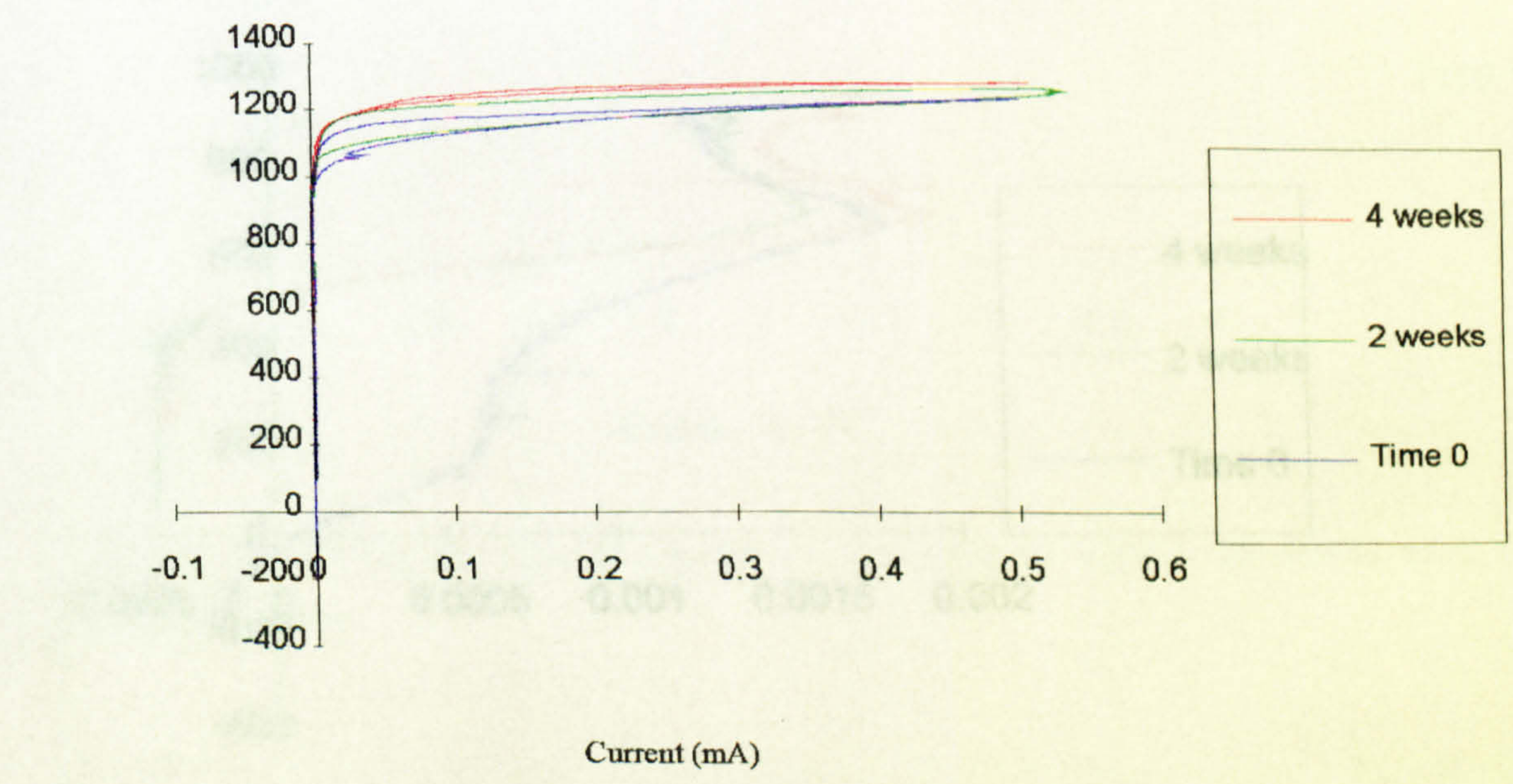

Fig. 8.14a. Ennoblement of E_b in the light cell on UNS S32760

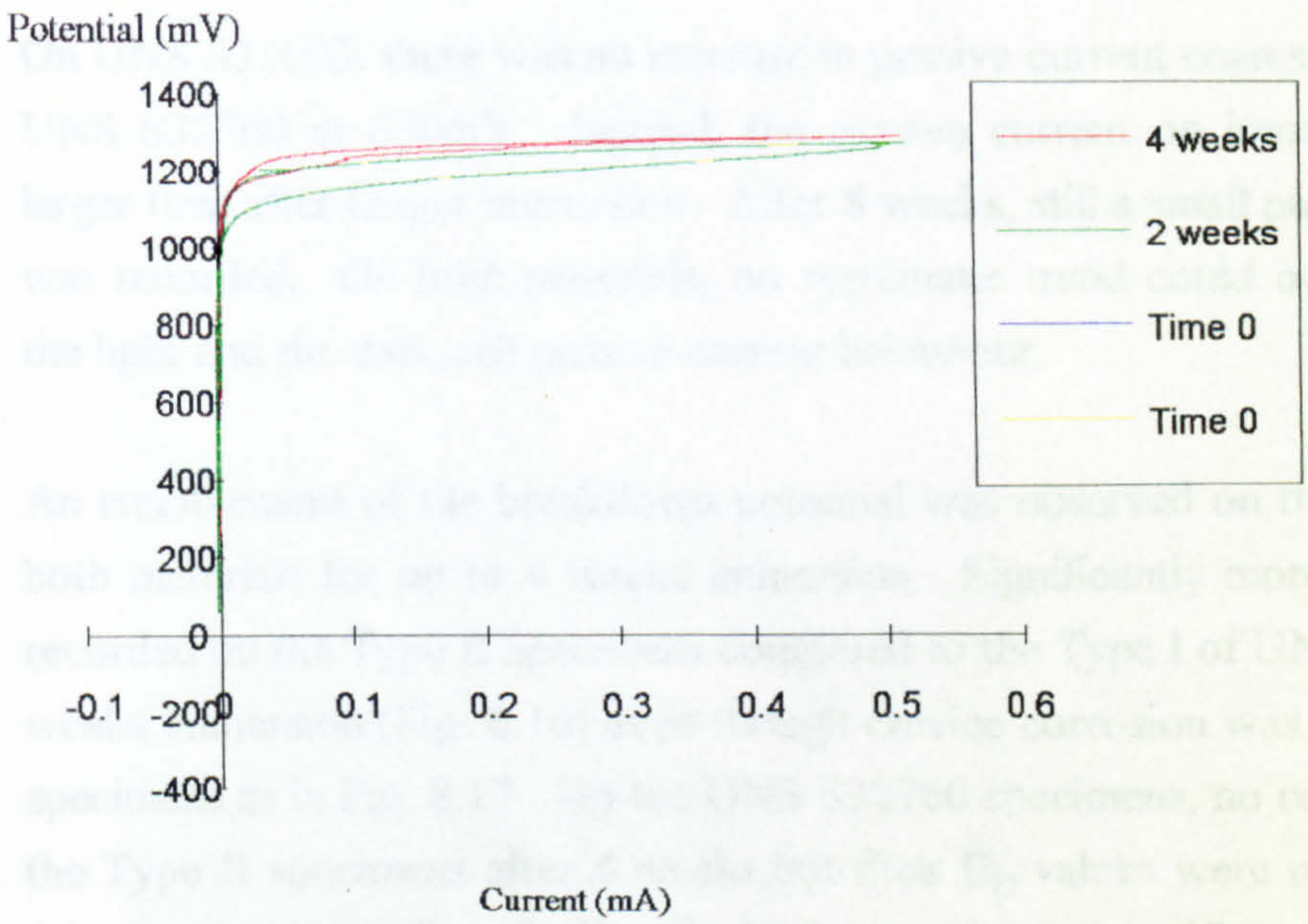

Fig. 8.14b. Ennoblement of E_b on UNS S32760 in the dark cell

A feature of interest, observed on anodic polarisation of UNS S32760 was the higher passive current in the potential range between E_{corr} and 600mV immediately after immersion, which after 1 week had diminished to a value stable for the longer immersion periods. At potentials in excess of 600mV, the passive current exhibited a value almost independent of the length of immersion. Fig. 8.15 shows the passive region after 0, 2 and 4 weeks.

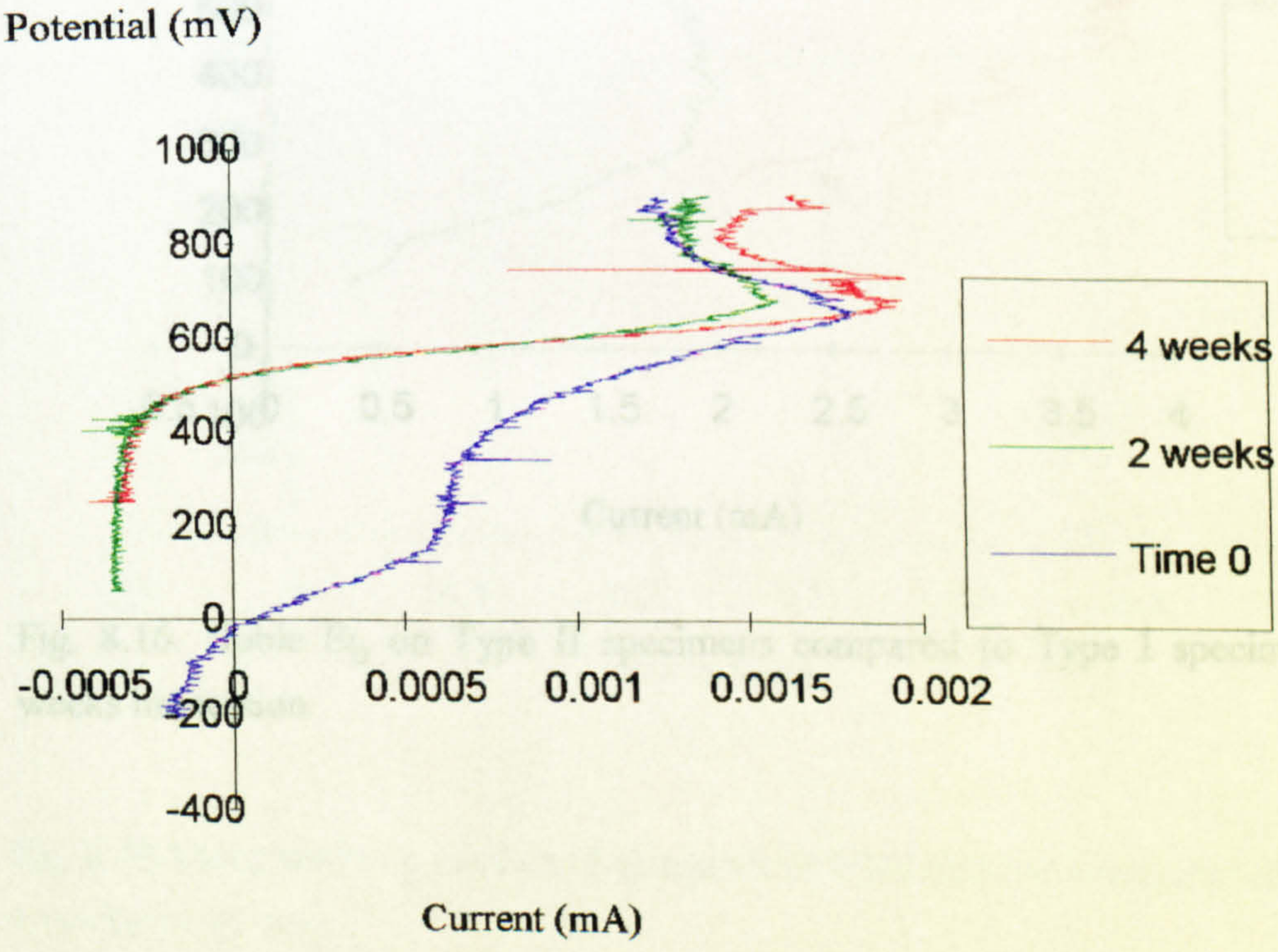

Fig. 8.15. Passive region on UNS S32760 after 0, 2 and 4 weeks immersion

On UNS S31603, there was no increase in passive current corresponding to that seen on UNS S32760 at 600mV. Instead, the passive current on immediate polarisation was larger than after longer immersion. After 8 weeks, still a small passive current of <0.2μA was recorded. On both materials, no systematic trend could be distinguished between the light and the dark cell passive current behaviour.

An ennoblement of the breakdown potential was observed on the Type II specimens of both materials for up to 4 weeks immersion. Significantly more noble E_b values were recorded on the Type II specimens compared to the Type I of UNS S31603 after 2 and 4 weeks immersion (Fig. 8.16) even though crevice corrosion was clearly visible on all the specimens as in Fig. 8.17. On the UNS S32760 specimens, no corrosion had initiated on the Type II specimens after 4 weeks but their E_b values were noticeably lower than on Type I specimens (Fig. 8.18). On both materials, a significant increase in the passive current was evident on all the Type II specimens compared to Type I for the same period.

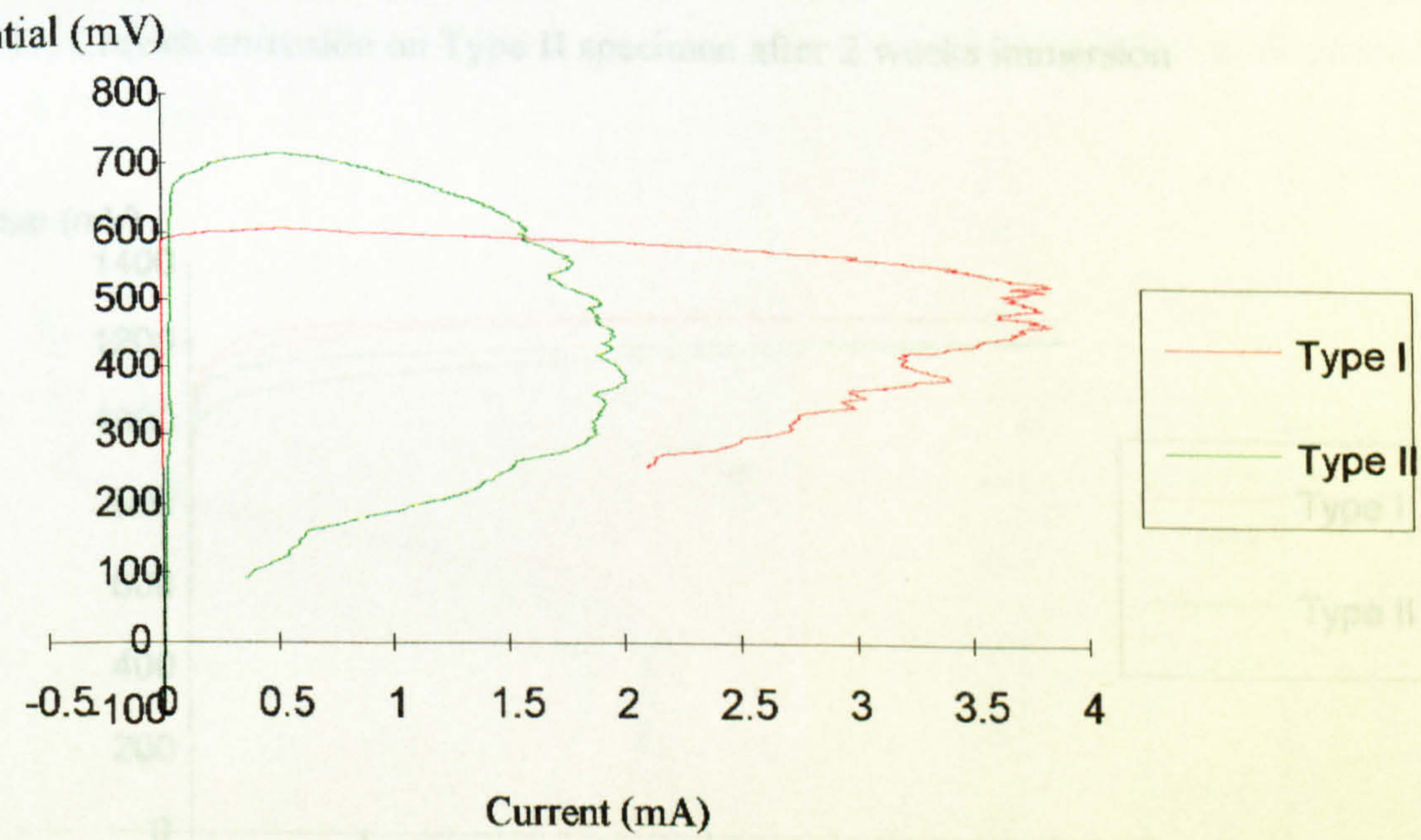

Fig. 8.16. Noble E_b on Type II specimens compared to Type I specimens after two weeks immersion

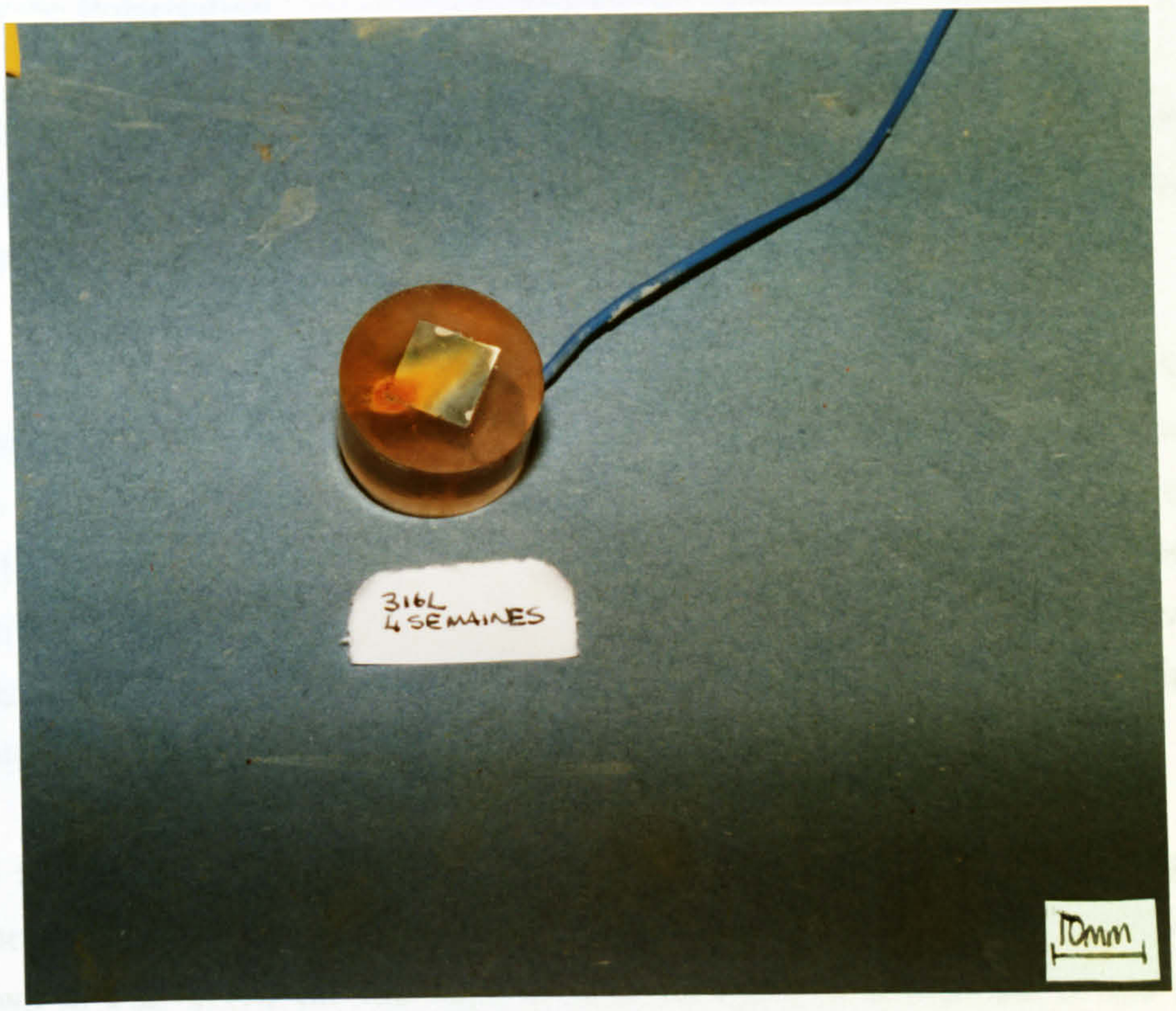

Fig. 8.17. Crevice corrosion on Type II specimen after 2 weeks immersion

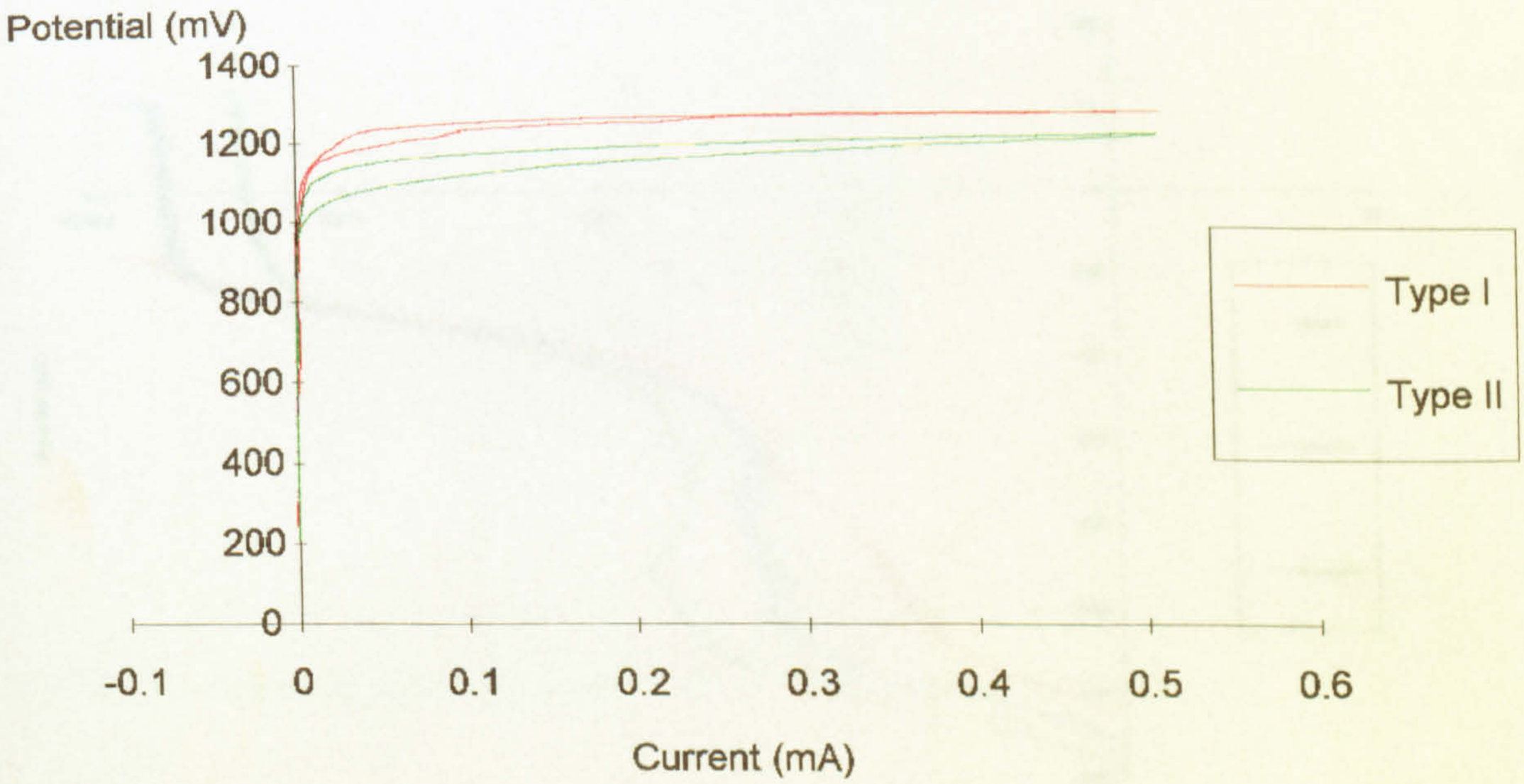

Fig. 8.18 More noble E_b on Type I specimen of UNS S32760 compared to Type II after 4 weeks immersion

Cathodic Polarisation

Cathodic polarisation tests on Type I specimens were performed as in previous chapters but once a cathodic current of 1mA was attained, the cathodic scan was reversed and the return scan to the free corrosion potential was traced.

The form of the cathodic scan was similar to those referred to in chapters 1 and 2. Without exception, the cathodic polarisation scans commenced at a more noble potential than in chapters 1 and 2. The initial increase in current at point E_T (where T denotes the Tafel region of oxygen reduction) was followed by a stabilisation of the current to a relatively constant value until a potential was reached at which hydrogen evolution could progress. The diffusion controlled region corresponding to the limiting current is compared for the two materials after different immersion periods.

The first important observation was that on initial immersion, the limiting current was higher than after 1 week, 2 weeks, 4 weeks and 8 weeks immersion for UNS S31603. As shown in Fig. 8.19a for the light conditions, there is a decrease in the current in the diffusion controlled region as the immersion period increases and similarly for the dark conditions (Fig. 8.19b). This trend was also observed for the UNS S32760 as illustrated in Figs. 8.20a and b.

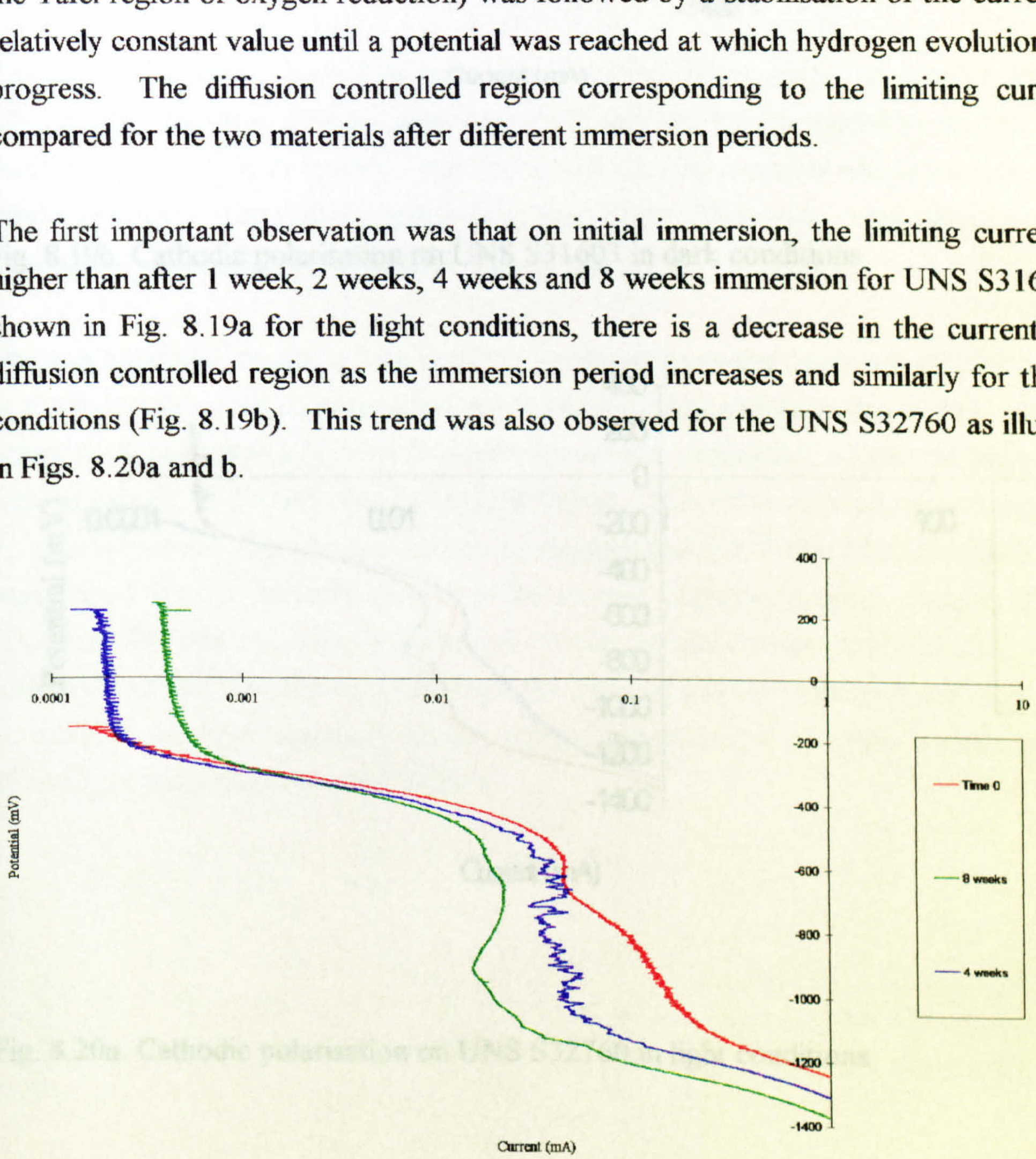

Fig. 8.19a. Cathodic polarisation on UNS S31603 in light conditions

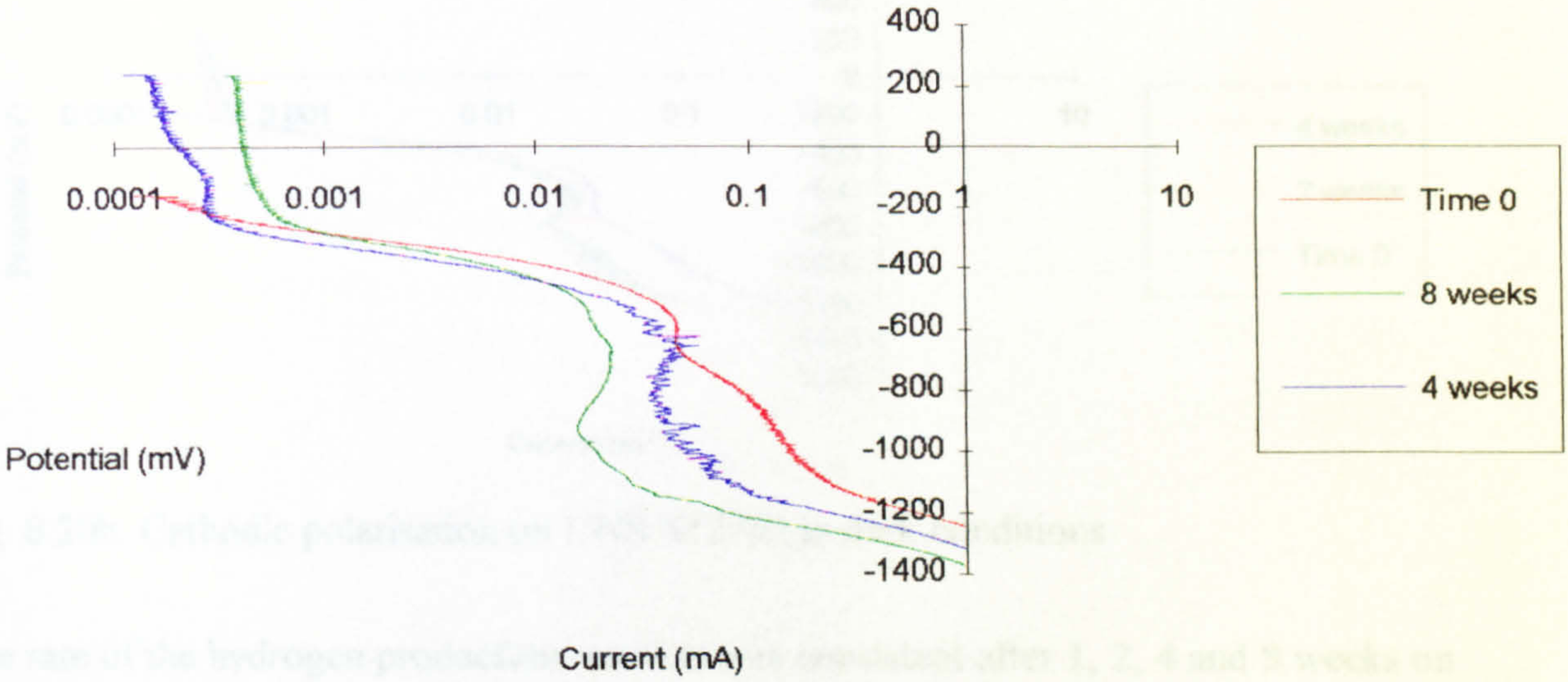

Fig. 8.19b. Cathodic polarisation on UNS S31603 in dark conditions

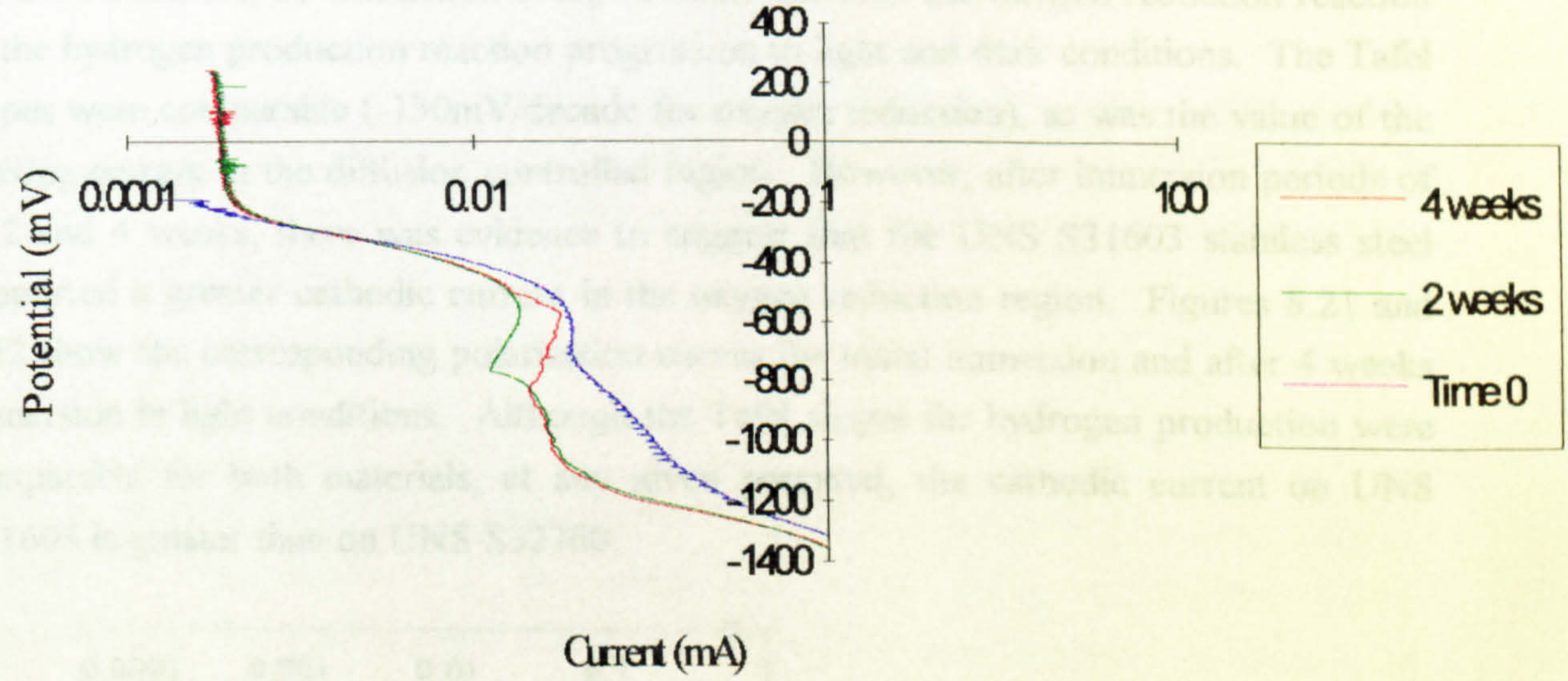

Fig. 8.20a. Cathodic polarisation on UNS S32760 in light conditions

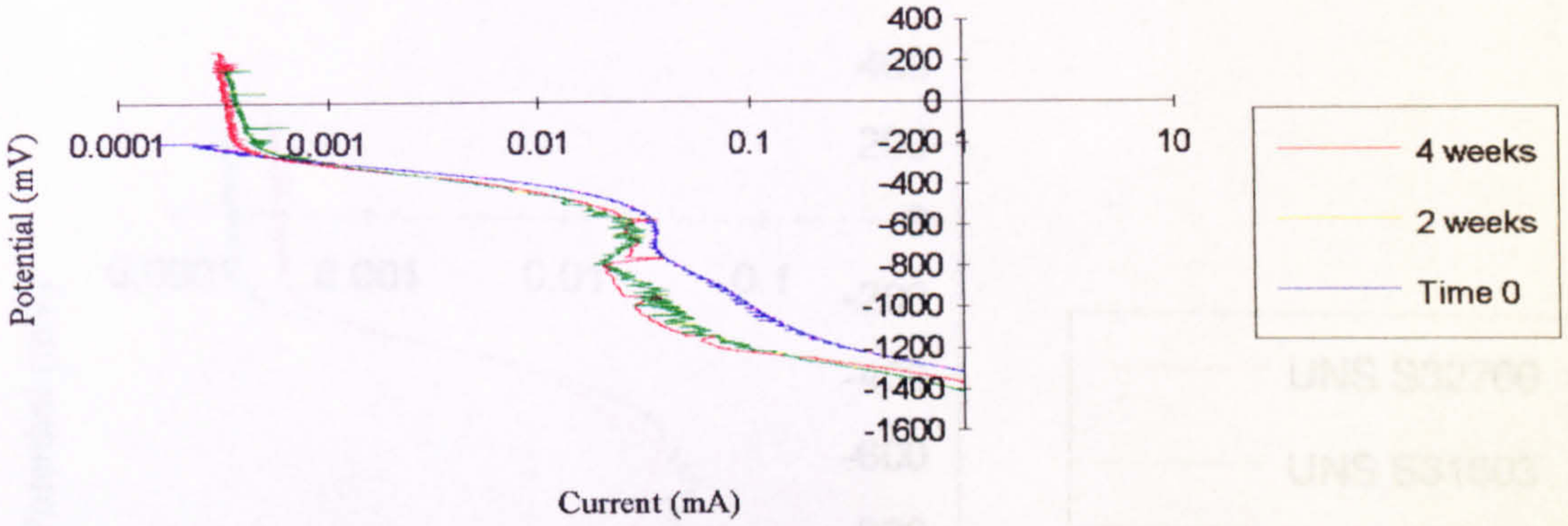

Fig. 8.20b. Cathodic polarisation on UNS S32760 in dark conditions

The rate of the hydrogen production reaction was consistent after 1, 2, 4 and 8 weeks on UNS S31603 and after 2 and 4 weeks on UNS S32760, but compared to the reaction on initial immersion, the Tafel slope was less steep (i.e. the reaction rate enhanced after an initial period). On initial immersion the Tafel slope was approximately -230-240mV/decade compared to -180mV/decade thereafter.

On both materials, no distinction could be made between the oxygen reduction reaction or the hydrogen production reaction progression in light and dark conditions. The Tafel slopes were comparable (-130mV/decade for oxygen reduction), as was the value of the limiting current in the diffusion controlled region. However, after immersion periods of 0, 2 and 4 weeks, there was evidence to suggest that the UNS S31603 stainless steel supported a greater cathodic current in the oxygen reduction region. Figures 8.21 and 8.22 show the corresponding polarisation curves for initial immersion and after 4 weeks immersion in light conditions. Although the Tafel slopes for hydrogen production were comparable for both materials, at any given potential, the cathodic current on UNS S31603 is greater than on UNS S32760

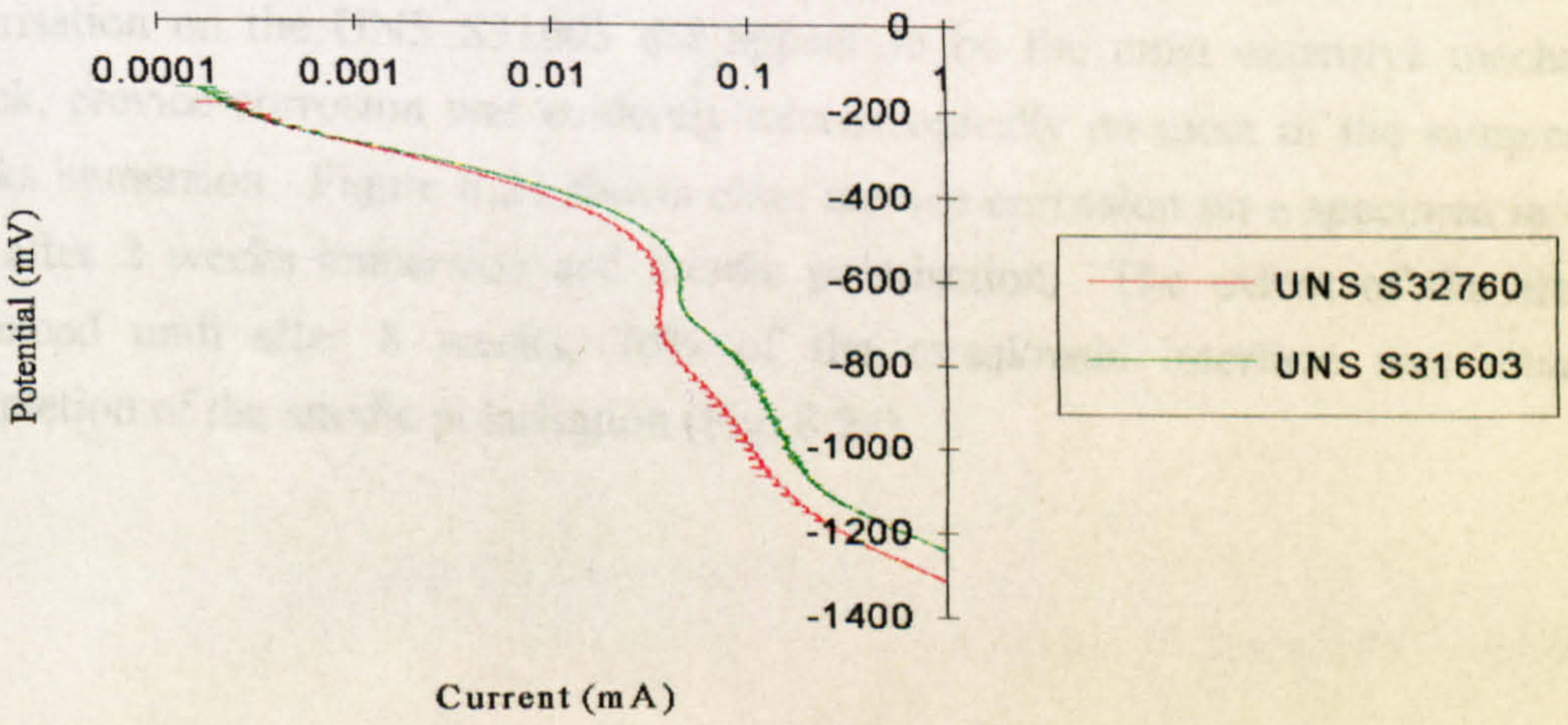

Fig. 8.21. Cathodic polarisation on UNS S31603 and UNS S32760 on initial immersion.

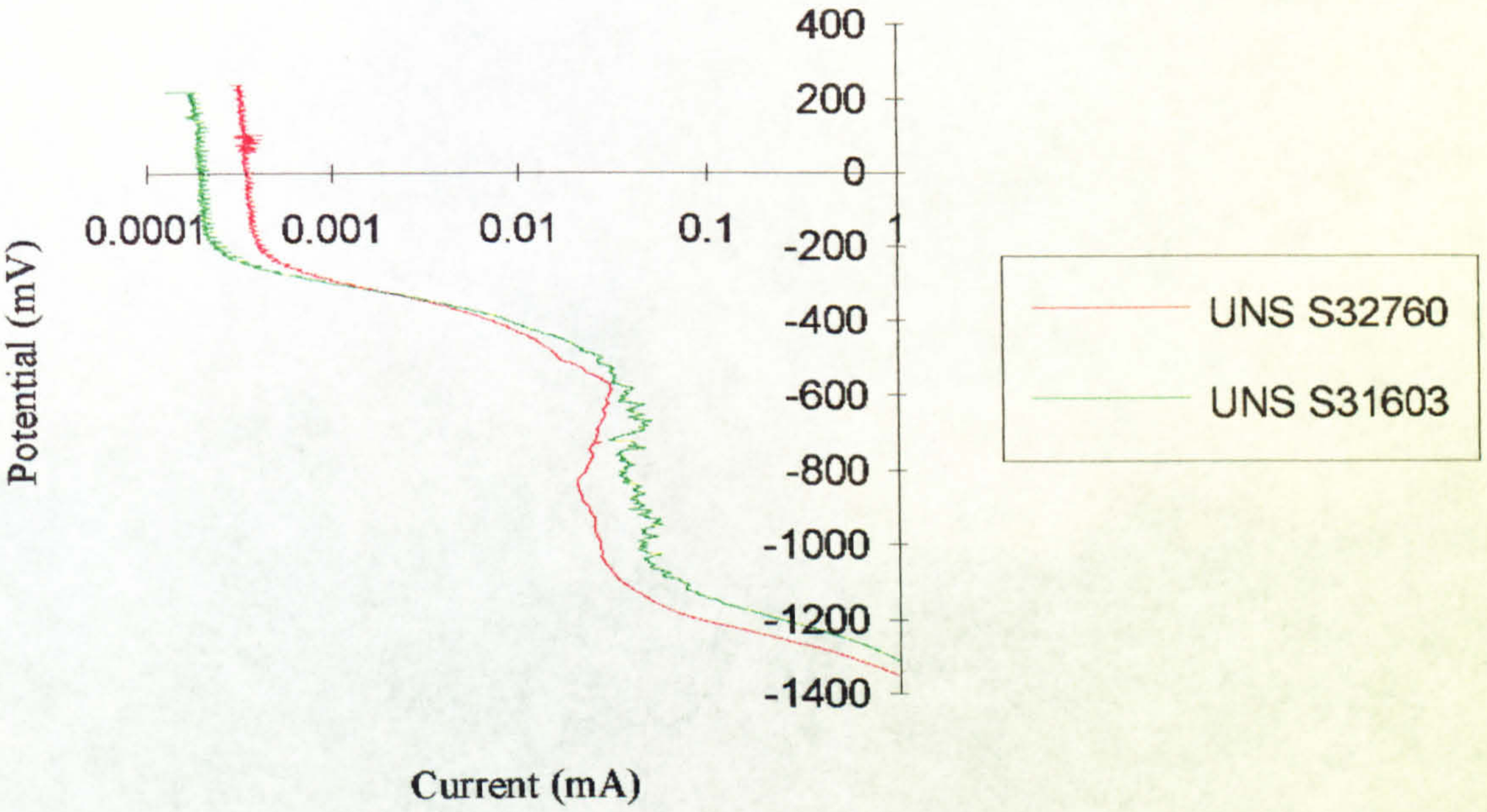

Fig. 8.22. Cathodic polarisation on UNS S31603 and UNS S32760 after 4 weeks in light conditions.

Larger anodic currents in the passive region were detected on the Type II specimens as previously reported. Similarly the cathodic currents were greater on the Type II specimens of both materials and in addition, much more fluctuation was observed in the diffusion limited region.

Visual Examination

Although the Type I specimens were produced with the main aim of preventing crevice corrosion, it was confirmed in this study that whilst pitting attack after anodic polarisation on the UNS S31603 did appear to be the most extensive mechanism of attack, crevice corrosion was evidently microscopically on most of the samples after 2 weeks immersion. Figure 8.23 shows clear crevice corrosion on a specimen in the clear cell after 2 weeks immersion and anodic polarisation. The extent of the attack was enhanced until after 8 weeks, 70% of the metal/resin interface was attacked on completion of the anodic polarisation (Fig. 8.24).

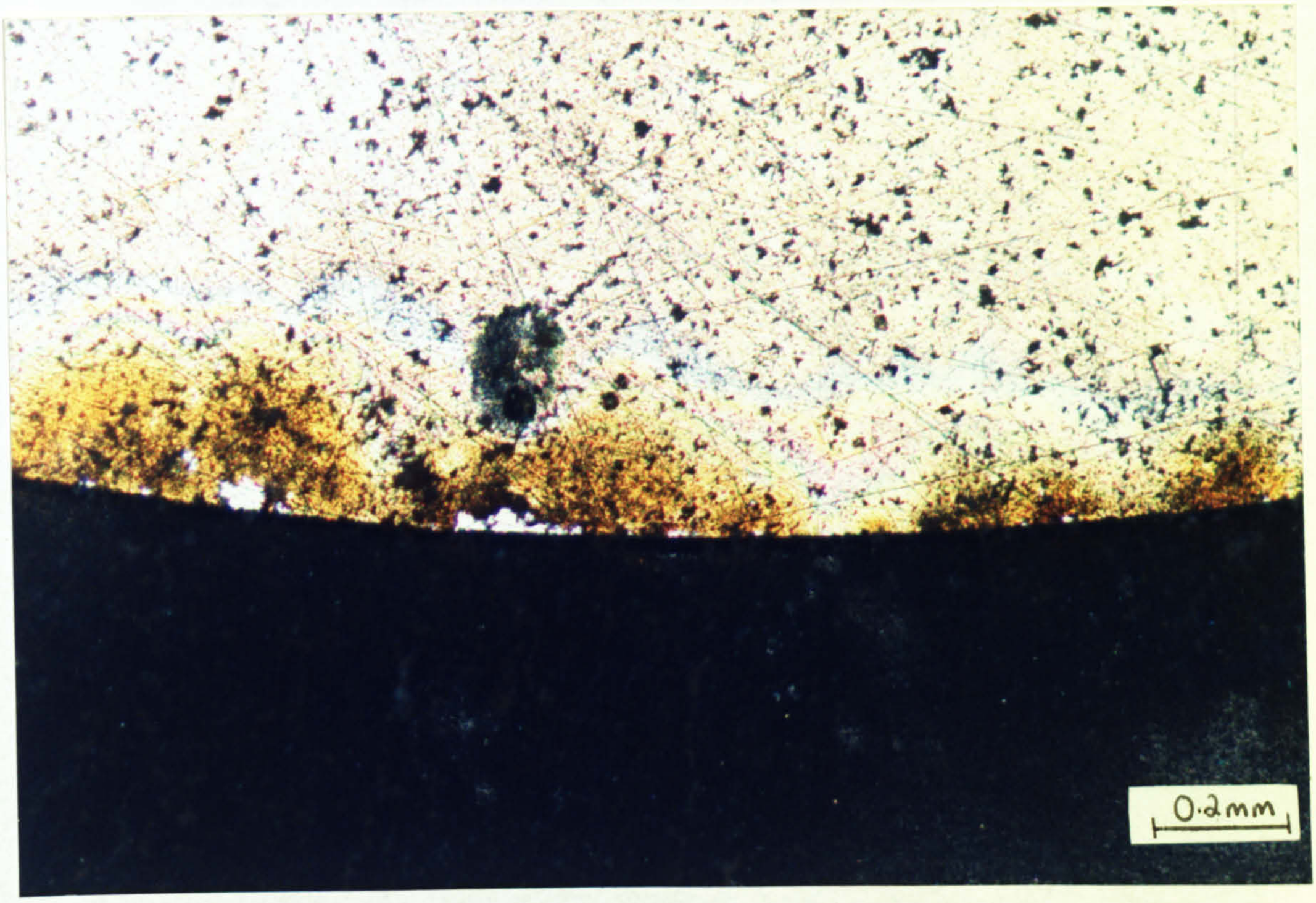

Fig. 8.23. Crevice corrosion on UNS S31603 after 2 weeks immersion and anodic polarisation

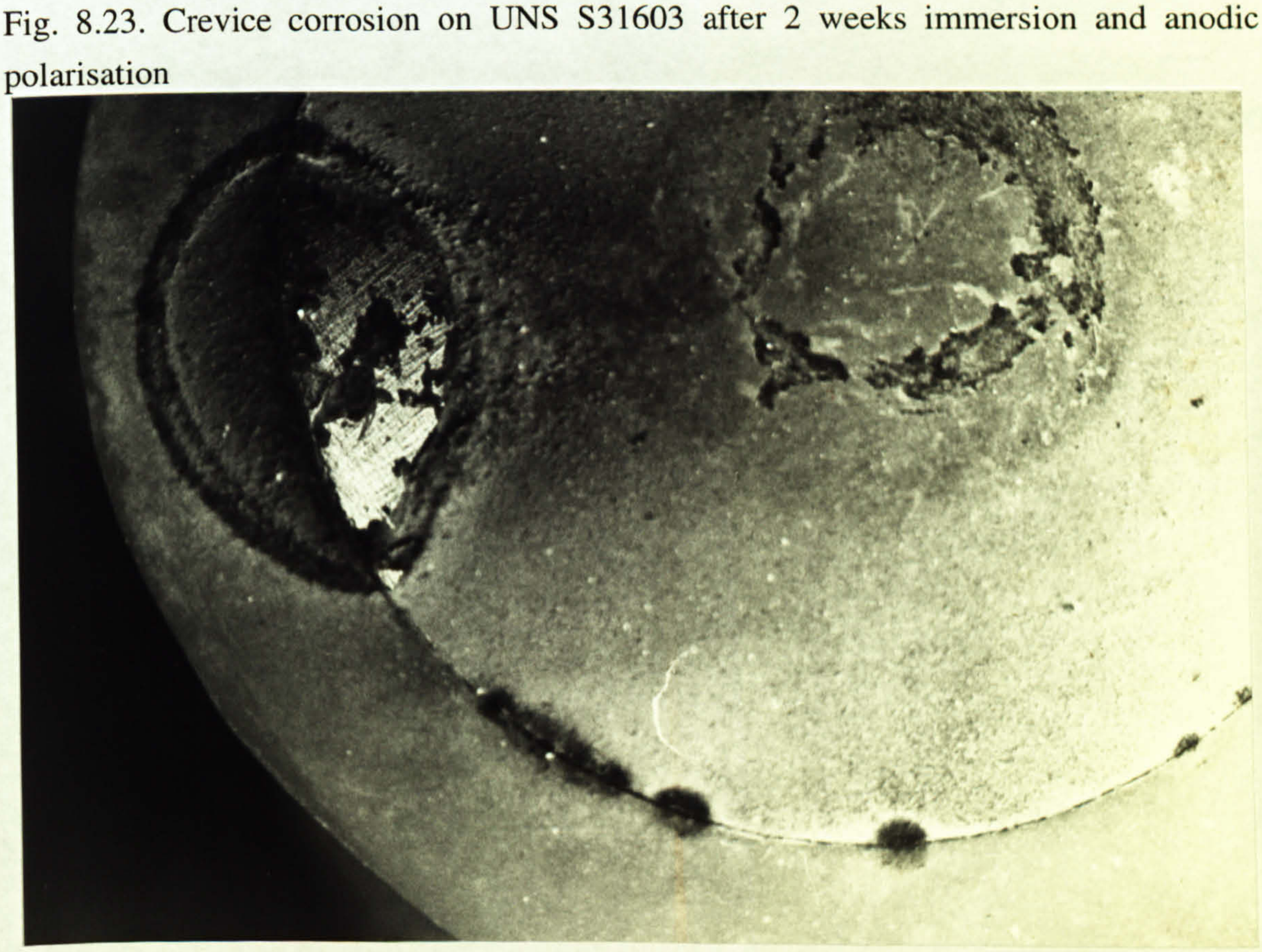

Fig 8.24. Attack at the crevice after 8 weeks immersion and anodic polarisation on Type I specimen.

Pitting attack on UNS S31603 appeared as a system of localised surface perforations under which the pit developed. Figure 8.25 shows one such pit, formed after 8 weeks immersion in light conditions where the central area has caved in to form an open pit. The biofilm settlement around the pit can be clearly seen. Figure 8.26 shows a line of pits, caved in, on UNS S31603 after 4 weeks immersion in natural seawater and anodic polarisation.

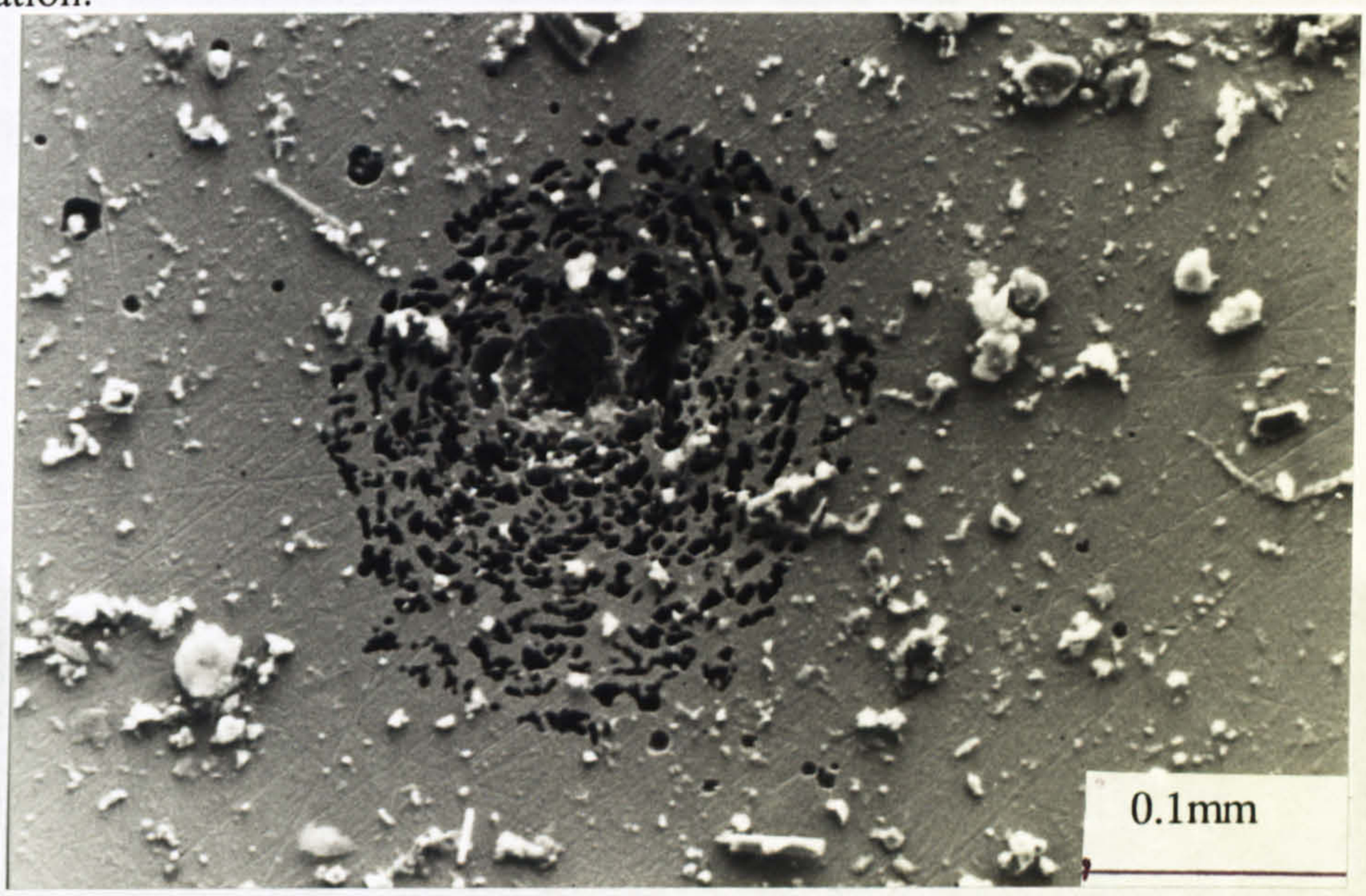

Fig. 8.25. SEM micrograph of the perforated area around the pitted site and the biofilm formation in the pit vicinity

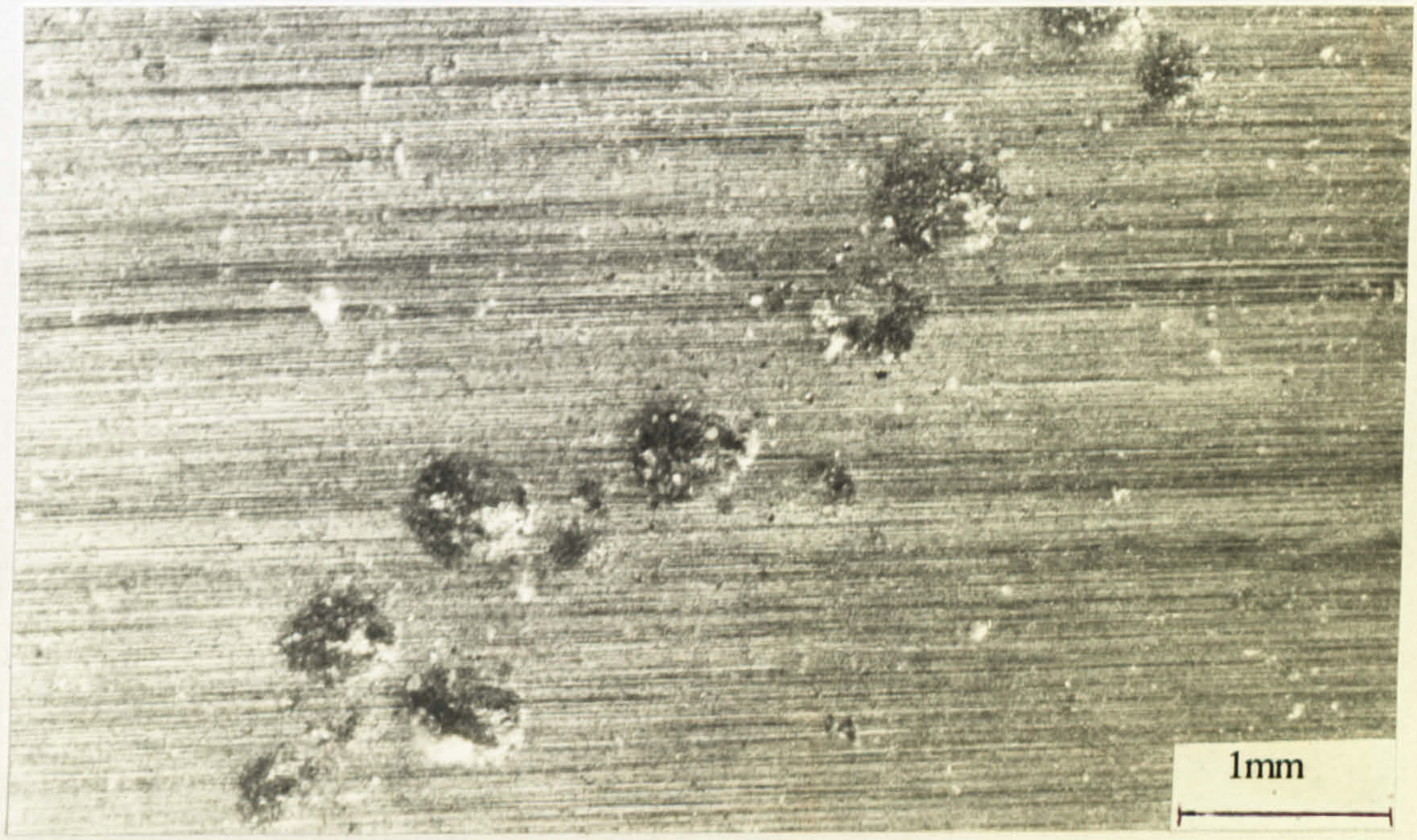

Fig. 8.26. Line of caved in pits formed on UNS S31603 after 4 weeks immersion and anodic polarisation

As expected, the corrosion attack on UNS S32760 was significantly less severe than on UNS S31603 as shown in Tables 8.5 and 8.6. However, it was of interest to note that although the study was intended to investigate the 'pitting potential' changes after immersion in natural seawater, in fact only pitting in the initiation stage was observed on UNS S32760. The main attack that could be identified was crevice attack, which in most cases was not extensive. After 4 weeks immersion without polarisation, there were traces of crevice corrosion initiating as shown in Fig. 8.27. Other significant attack which could be identified was the small etched area (Fig. 8.28) after 4 weeks immersion in the light cell. However this was only observed on one sample.

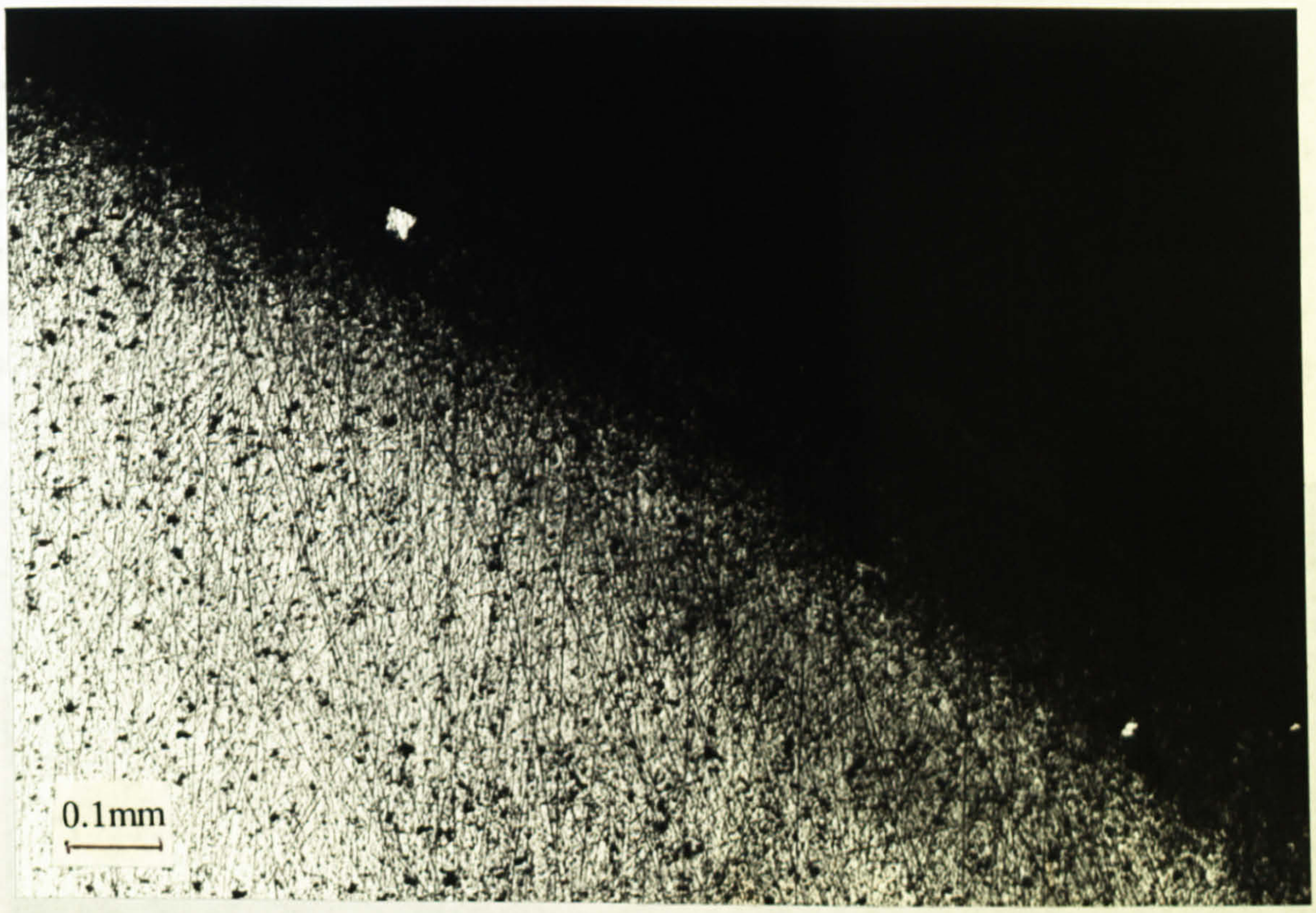

Fig. 8.27 Crevice corrosion initiation on UNS S32760 after 4 weeks immersion and no polarisation

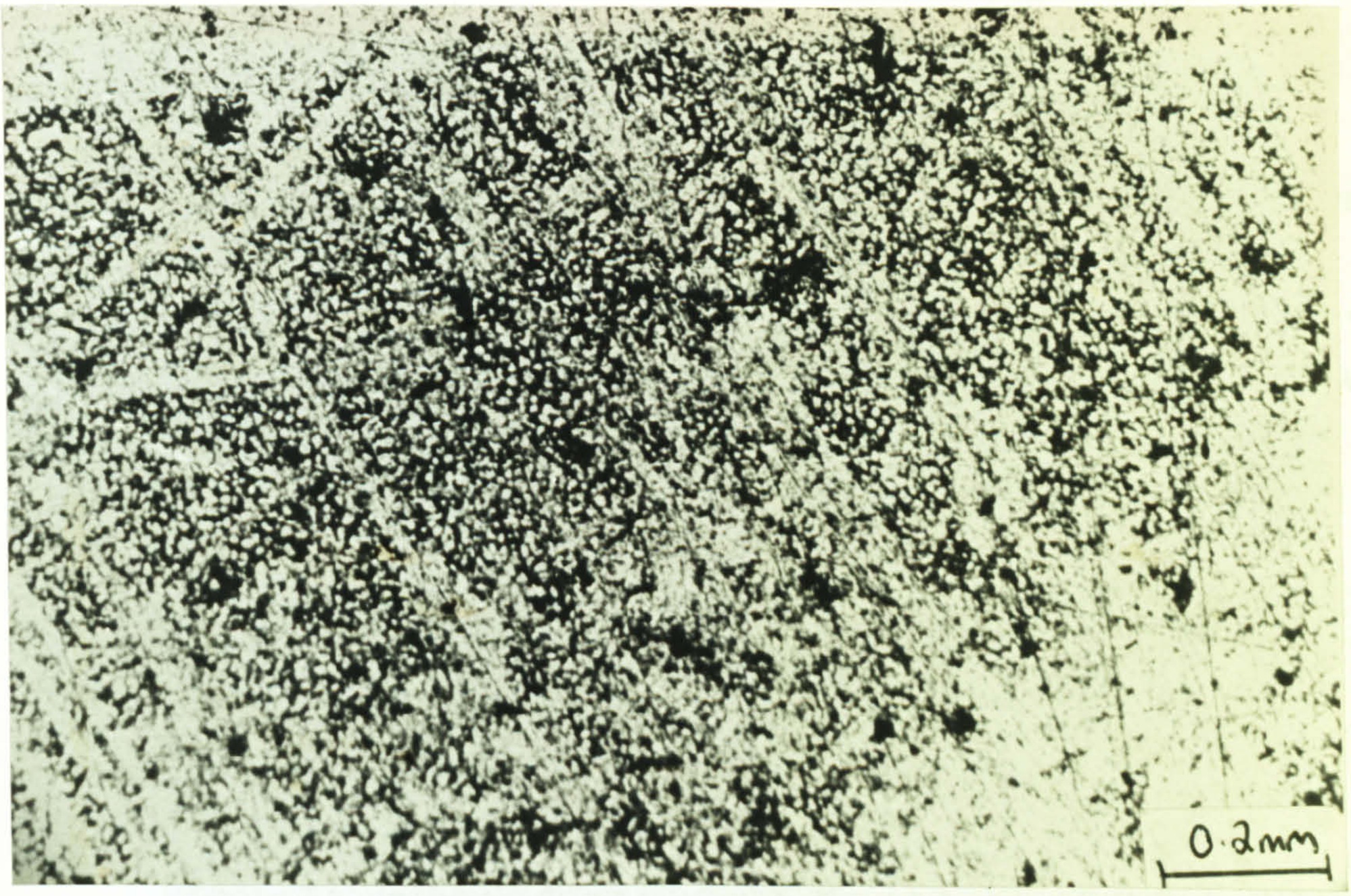

Fig. 8.28. Etched area on free surface of UNS S32760 after 4 weeks immersion and no polarisation.

As mentioned previously, Type II specimens of the austenitic UNS S31603 immersed at the free corrosion potential resisted crevice attack only over the first two weeks immersion and thereafter every specimen showed signs of attack at the metal/resin interface. In contrast, UNS S32760 after 4 weeks showed no signs of crevice attack but after 8 weeks, 1 of the 4 specimens was clearly attacked at one edge (Fig. 8.29). After anodic polarisation UNS S32760 showed signs of pitting attack, much reduced from the large tunnelling pits on UNS S31603.

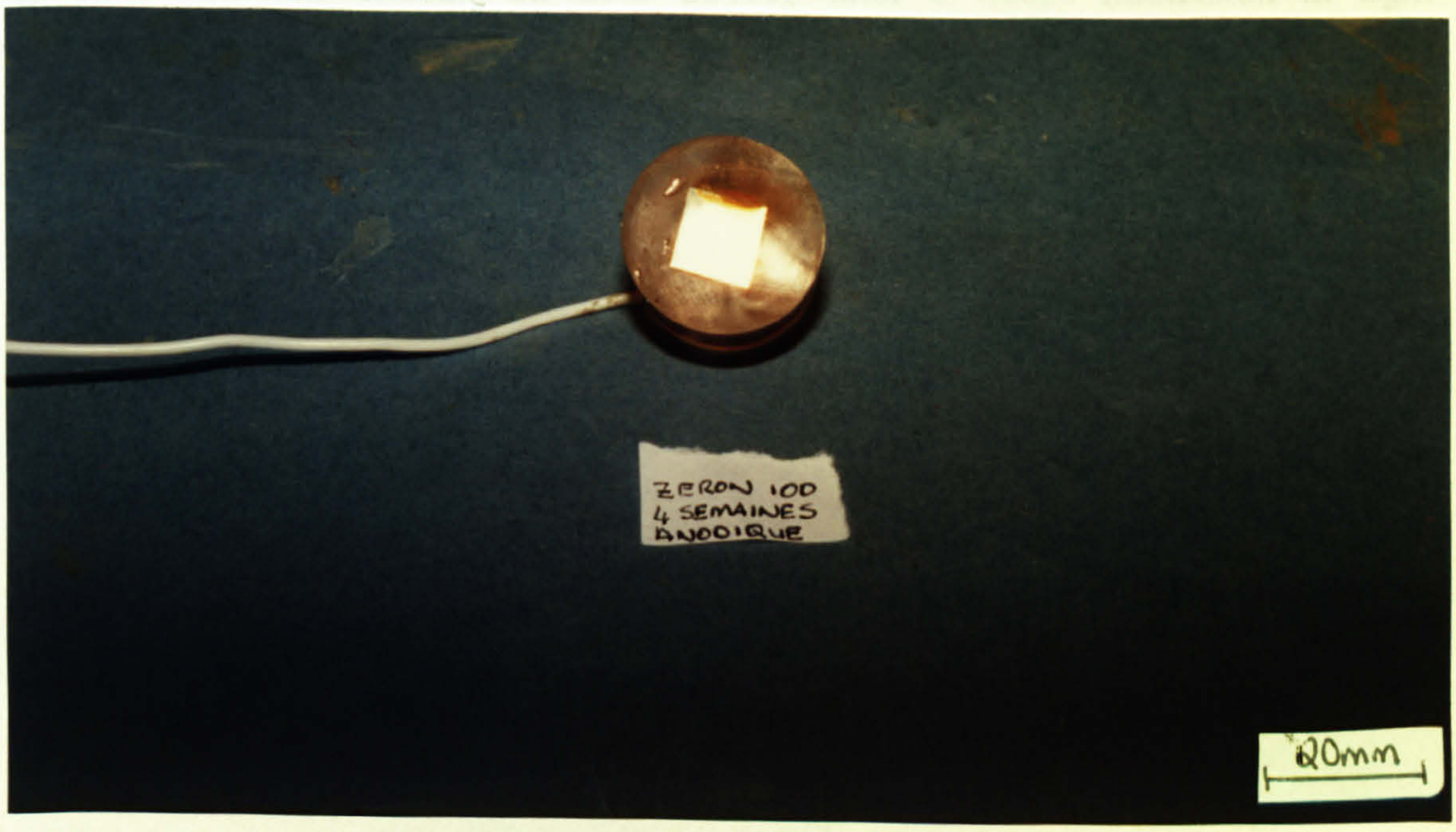

Fig. 8.29. Crevice attack on UNS S32760 after 4 weeks at the free corrosion potential in natural seawater

After 1 week immersion, a non-evenly distributed, sparse biofilm formed. Not until a two week period had elapsed, was diatom settlement observed on both materials. The number of diatoms did not significantly increase between the 2 week and the 8 week immersion. Figure 8.30 shows pennate diatoms settled on UNS S31603 after 8 weeks immersion in the light cell.

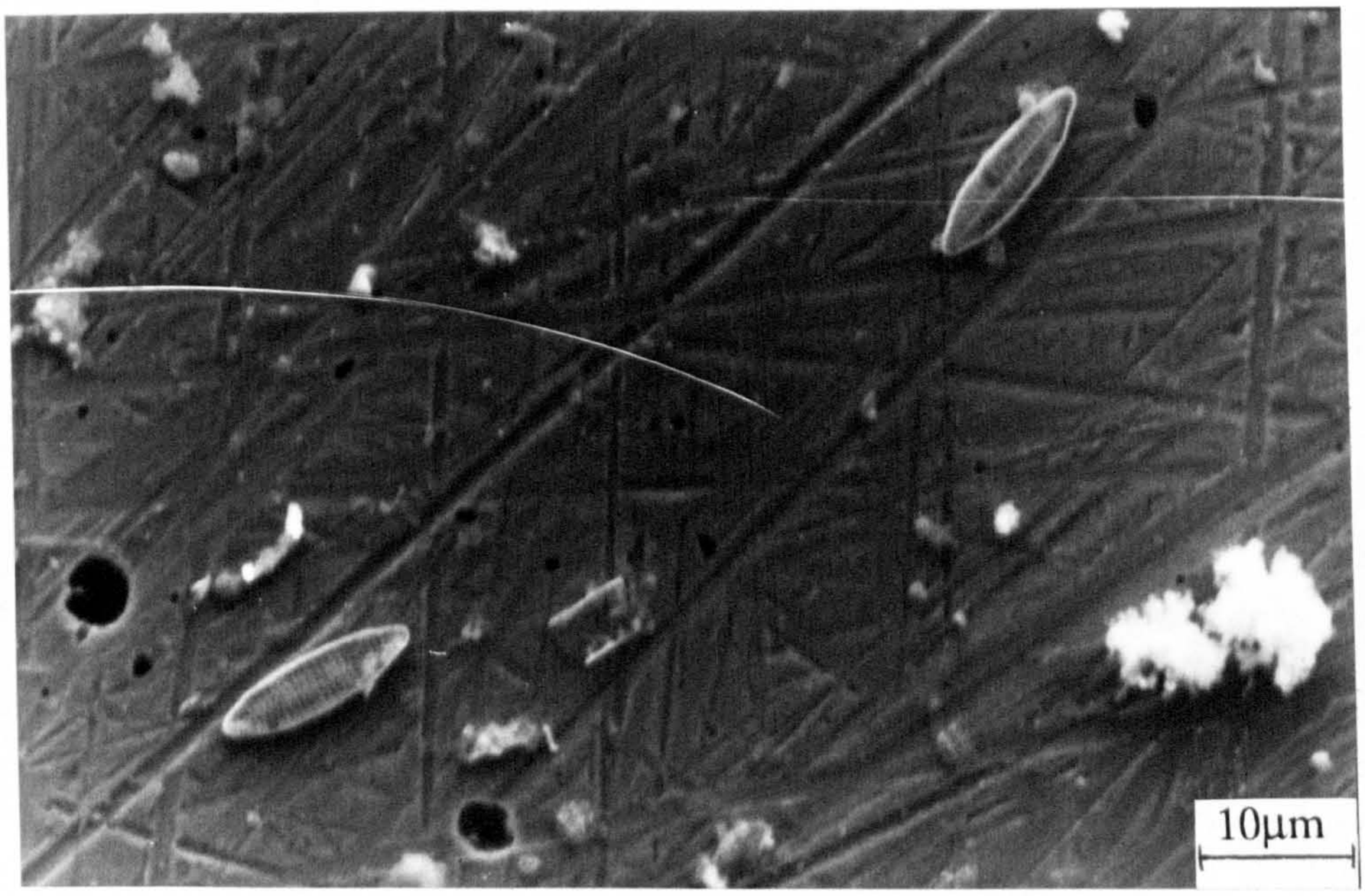

Fig. 8.30. Pennate diatoms on UNS S31603 after 8 weeks immersion in light conditions.

No distinction could be made between the diatom settlement or biofilm formation in the dark and the light cell. However, on comparing UNS S31603 with UNS S32760, there was an indication that more bacterial settlement occurred on UNS S32760. However this effect was not extensive as shown in Figs. 8.31a and b for UNS S31603. The comparative settlement on UNS S32760 is shown in Figs. 8.31c and d after 4 weeks immersion and no polarisation. No algal settlement was observed on any material, even after the longest exposure of 8 weeks.

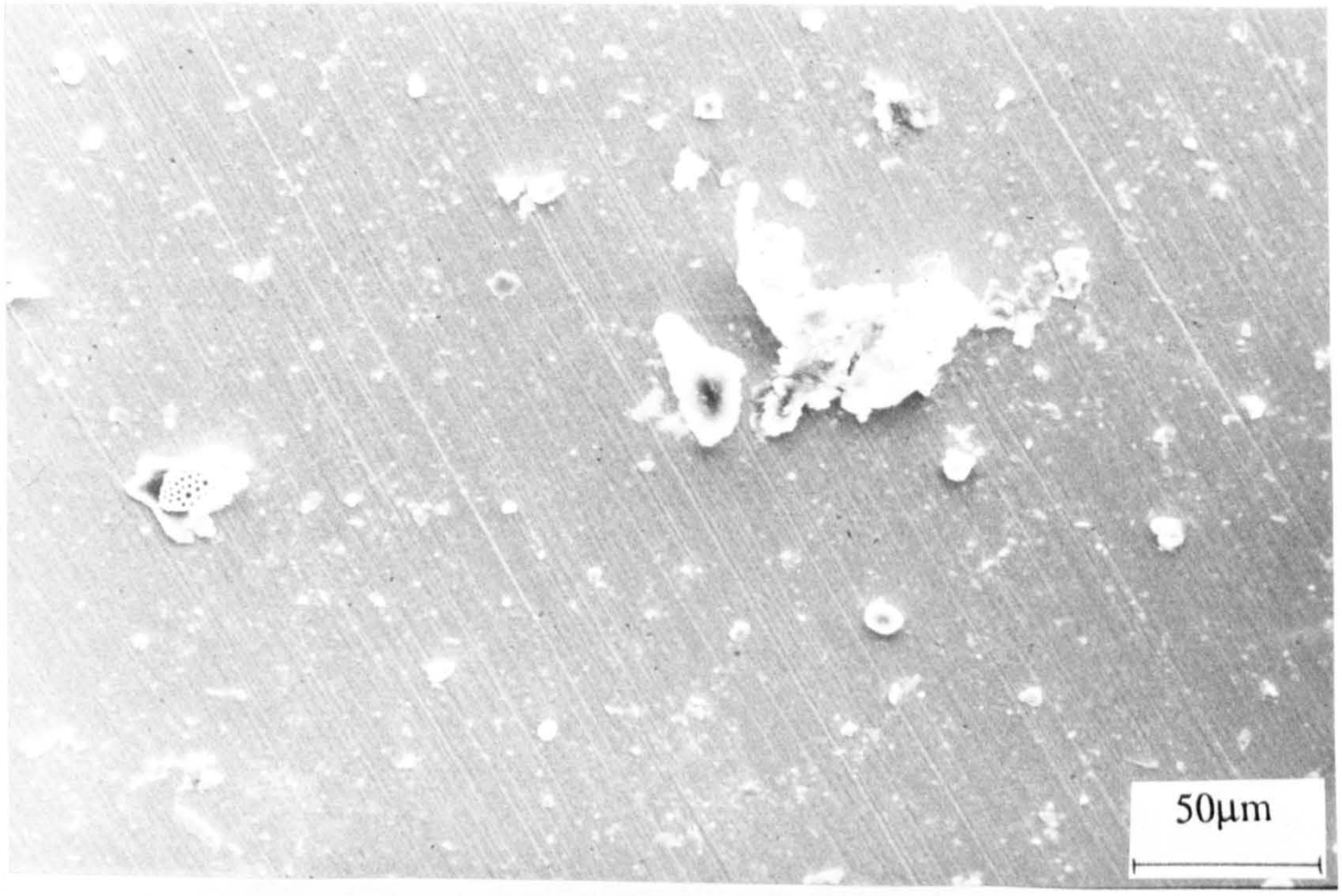

(a)

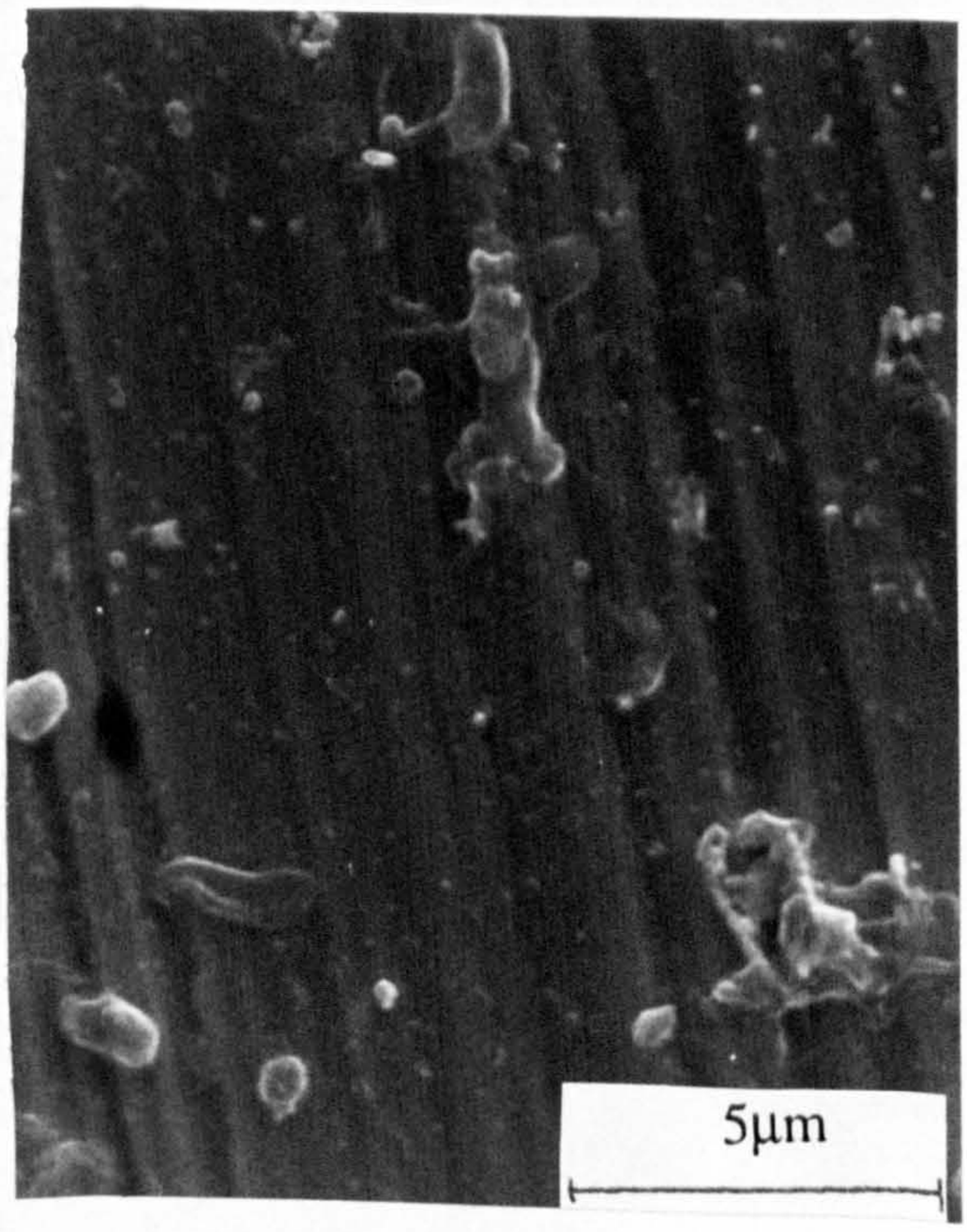

(b)

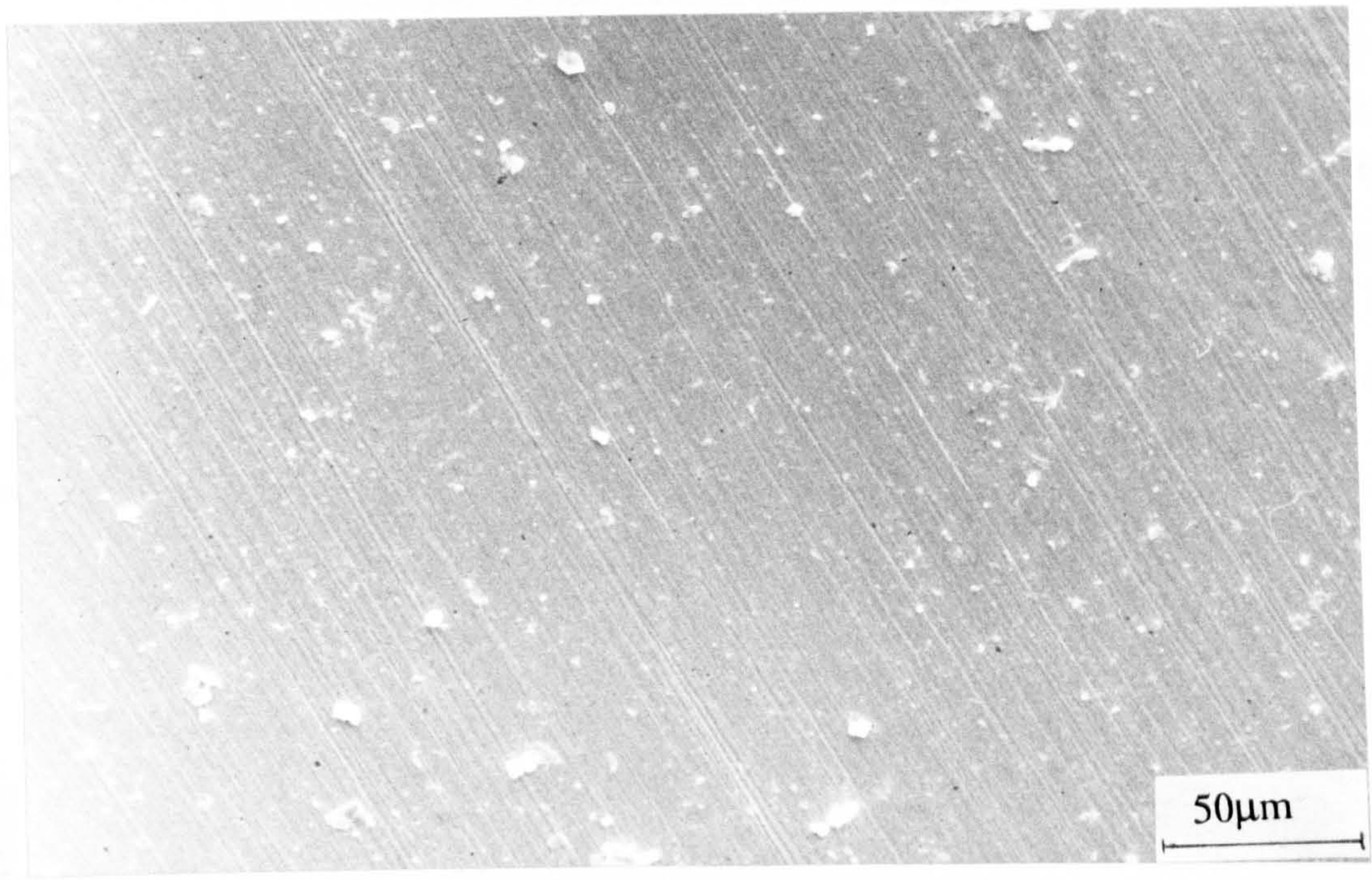

(c)

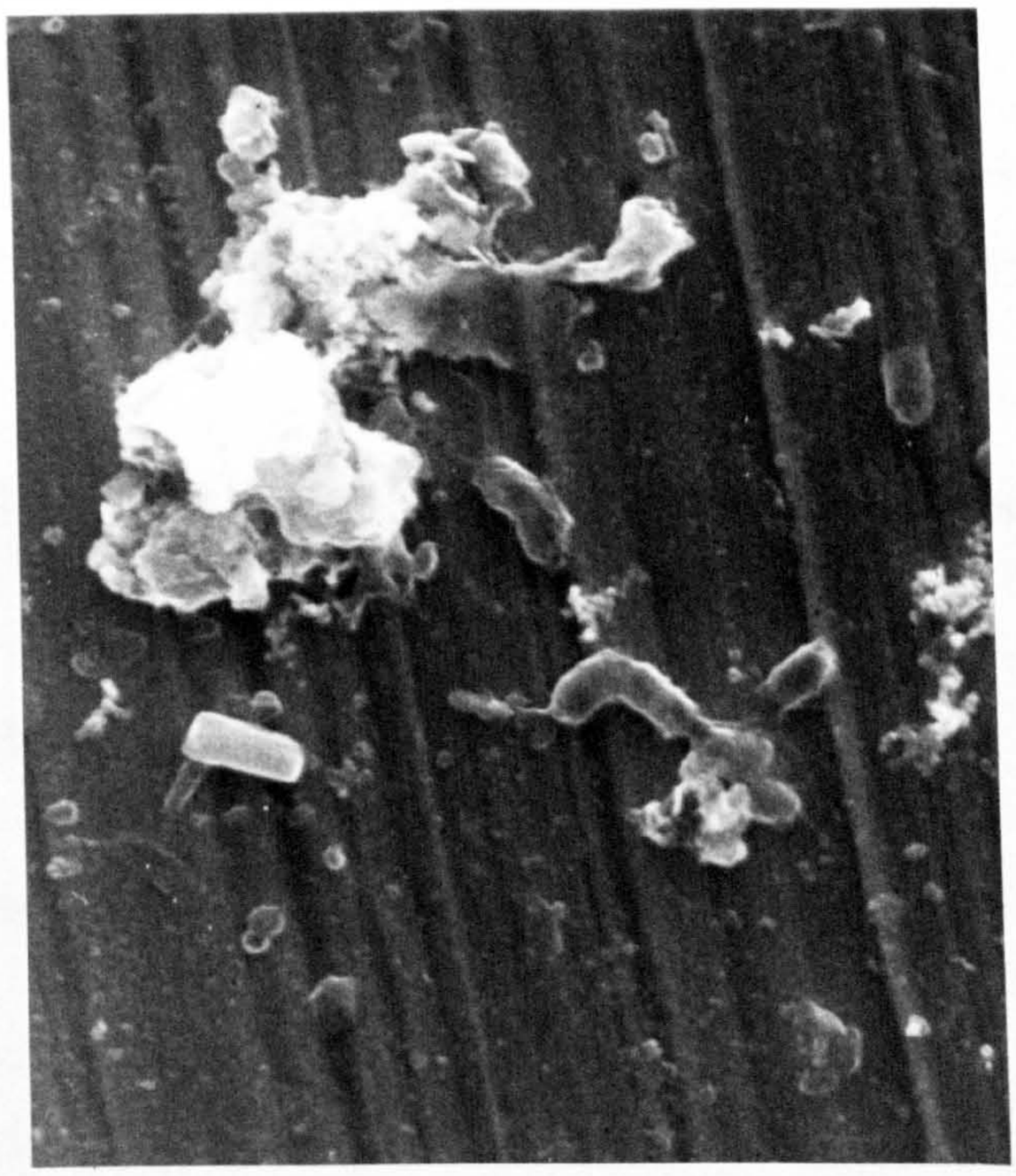

(d)

Fig. 8.31. a and b. Biofilm on two specimens of UNS S31603. c and d. Formation of biofilm on UNS S32760 after 4 weeks immersion

Potentiostatic Test

An experiment on UNS S31603 under potentiostatic control was carried out at -600mV(SCE) and the resulting cathodic current plotted as a function of time. From an initial current of 176A the current was found to decrease consistently over a 6 day period as shown in Fig. 8.32. Hence no depolarisation of the cathodic reaction, as is often used to explain the ennoblement of E_{corr} was found. However, in the same conditions, an ennoblement of E_{corr} to almost +300mV was recorded.

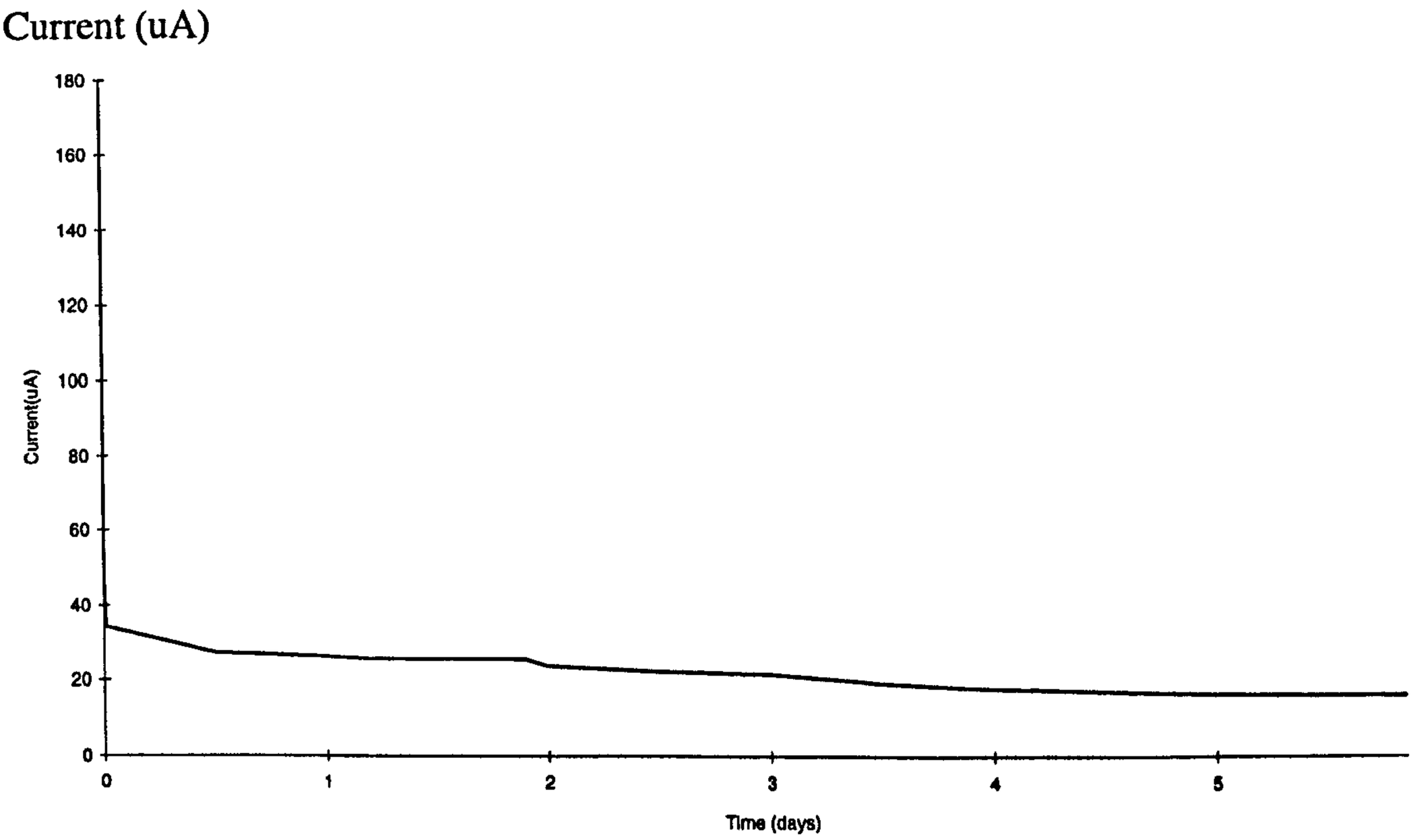

Fig. 8.32. Current progression with time under potentiostatic control at -600mV (SCE) on UNS S31603

Results - PART II

Free corrosion potential

The evolution of free corrosion potential of the specimens immersed at UMBSM over a 1 year period took the form as shown in Fig. 8.33. The data was not collected automatically and therefore the data points are less frequent than for the specimens immersed at Ifremer. However, it is clear from Fig. 8.33 that on all specimens, ennobled values of the free corrosion potential were recorded, comparable with those found at Ifremer. After approximately 25 days the free corrosion potential tended in the

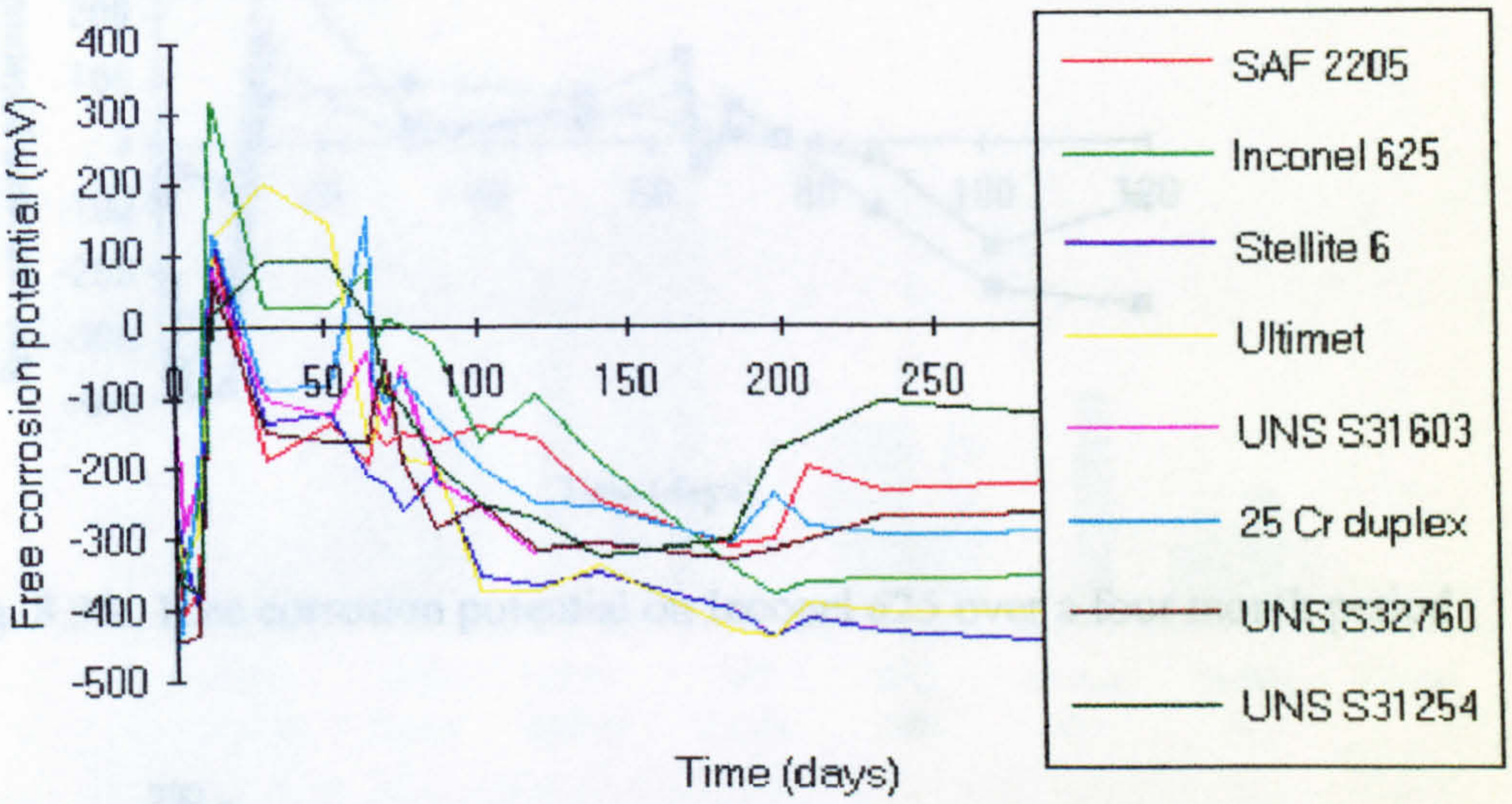

Fig. 8.33. Free corrosion potential over a one year period on all material included in the study

Figure 8.33 shows the free corrosion potential on one specimen of each material but values of 3 or 4 of each material were recorded. The distribution of E_{corr} was in some cases as large as 300mV but figures 8.34, 8.35 and 8.36 show, on UNS S31603, Inconel 625 and 25Cr duplex respectively, the trend of E_{corr} with time and that the scatter tended to reduce as the consistently less positive values were recorded.

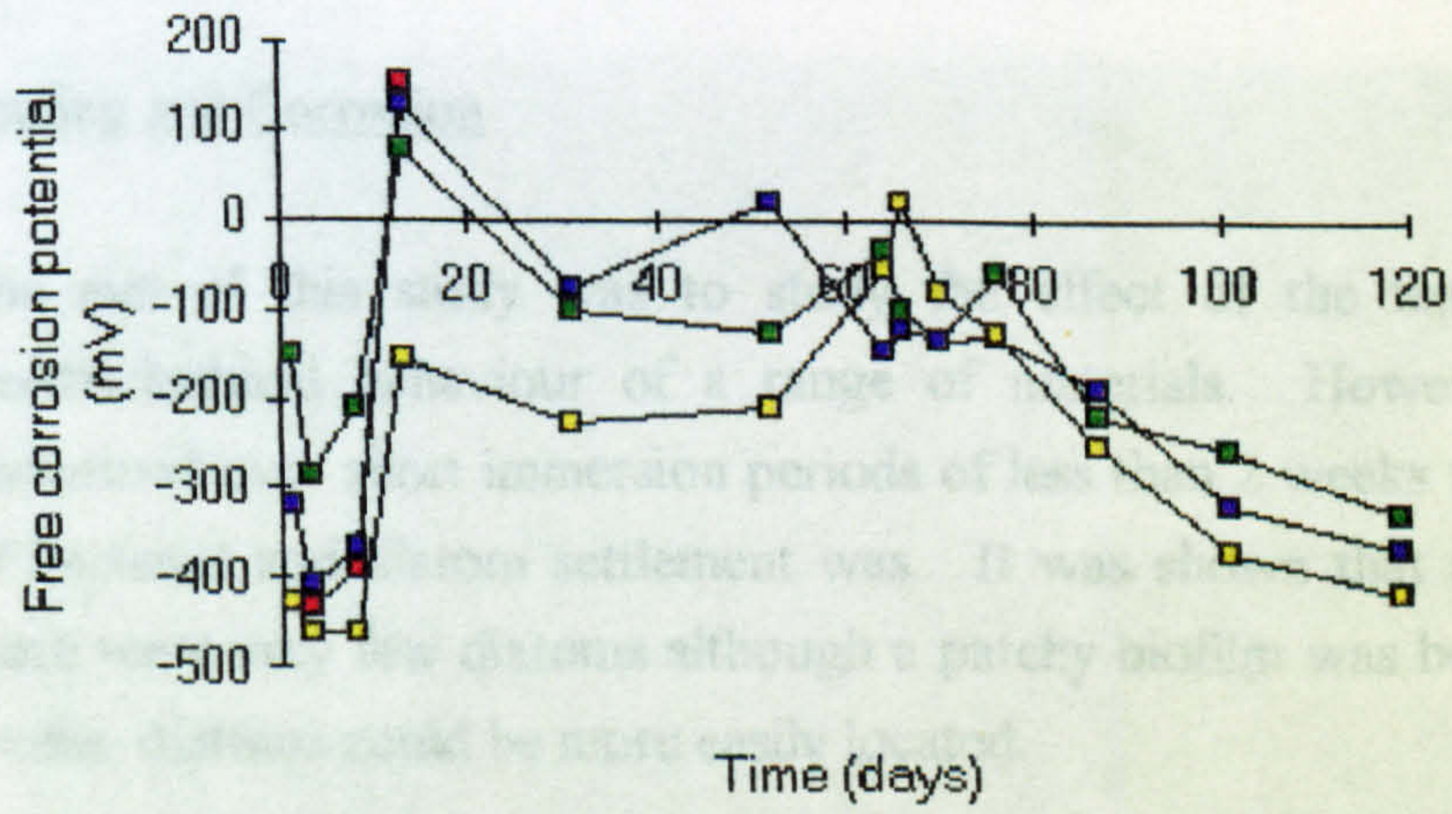

Fig. 8.34. Free corrosion potential on UNS S31603 over a four month period

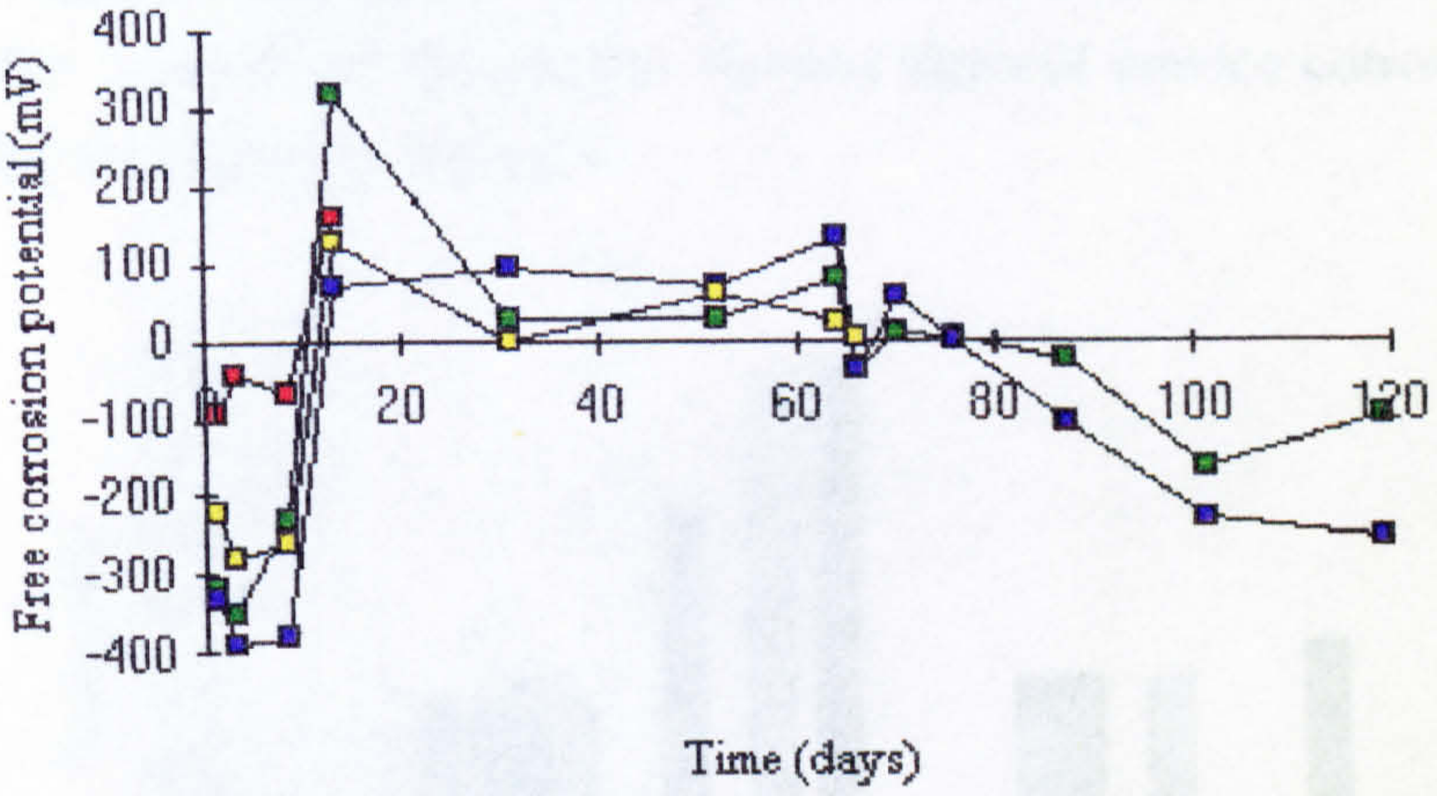

Fig. 8.35. Free corrosion potential on Inconel 625 over a four month period

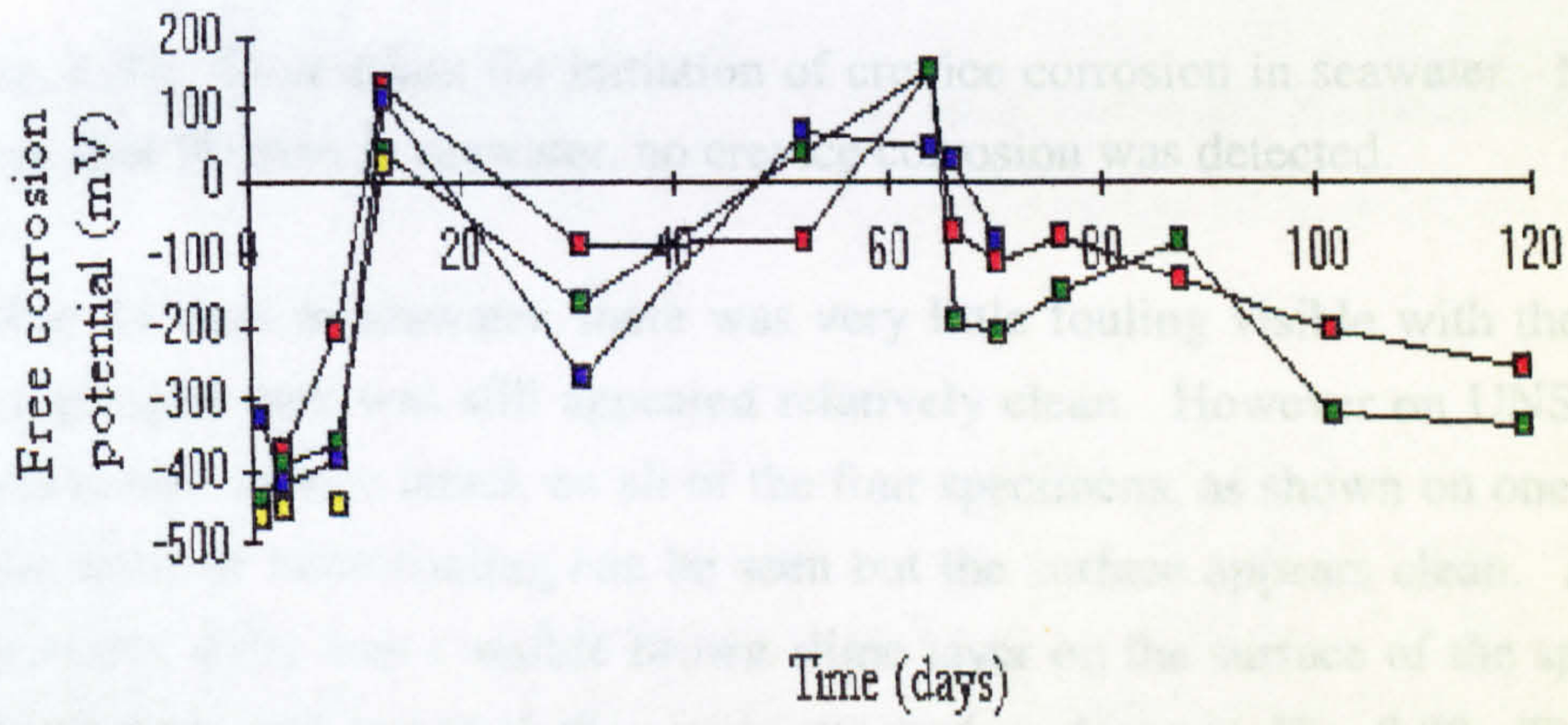

Fig. 8.36. Free corrosion potential on 25Cr duplex over a four month period

Fouling and Corrosion

The aim of this study was to study the effect of the macrofouling layers on the electrochemical behaviour of a range of materials. However, an initial study was performed over short immersion periods of less than 2 weeks to ascertain what the level of bacterial and diatom settlement was. It was shown that after 1 week in seawater, there were very few diatoms although a patchy biofilm was beginning to form. After 2 weeks, diatoms could be more easily located.

Over a period of 3 months, the specimens were visually examined (before any polarisation) for signs of crevice corrosion, the localised form of attack which, on most alloys, is the most readily initiated. Relative resistance to crevice corrosion was based on the number of samples out of the four of each material under test showing signs of attack and on the amount of time taken for the attack to initiate. Figure 8.37 shows that in

in agreement with the literature, the resistance to initiation of UNS S31603 is poor and after 2 weeks all the samples showed signs of crevice corrosion. Poor resistance was also exhibited by Stellite 6.

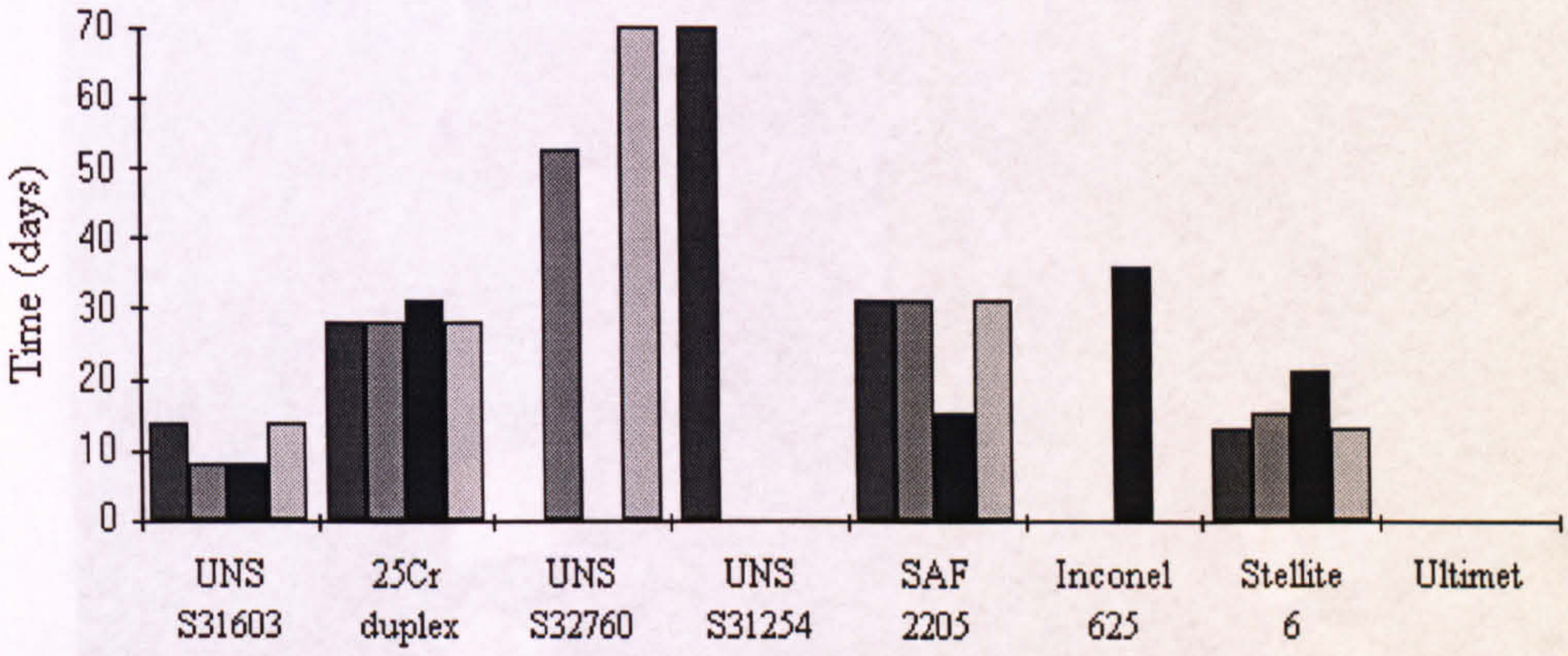

Fig. 8.37. Time taken for initiation of crevice corrosion in seawater. No result means that after 90 days in seawater, no crevice corrosion was detected.

After 14 days in seawater, there was very little fouling visible with the naked eye and the perspex rack was still appeared relatively clean. However on UNS S31603, there was severe crevice attack on all of the four specimens, as shown on one in Fig. 8.38. A few areas of microfouling can be seen but the surface appears clean. After 21 days in seawater, there was a visible brown slime layer on the surface of the specimens and on the perspex rack to which they were attached as shown in Fig. 8.39. There is clearly no crevice attack visible at the metal/resin interface on either UNS S31254 (top) or 25Cr duplex (bottom).

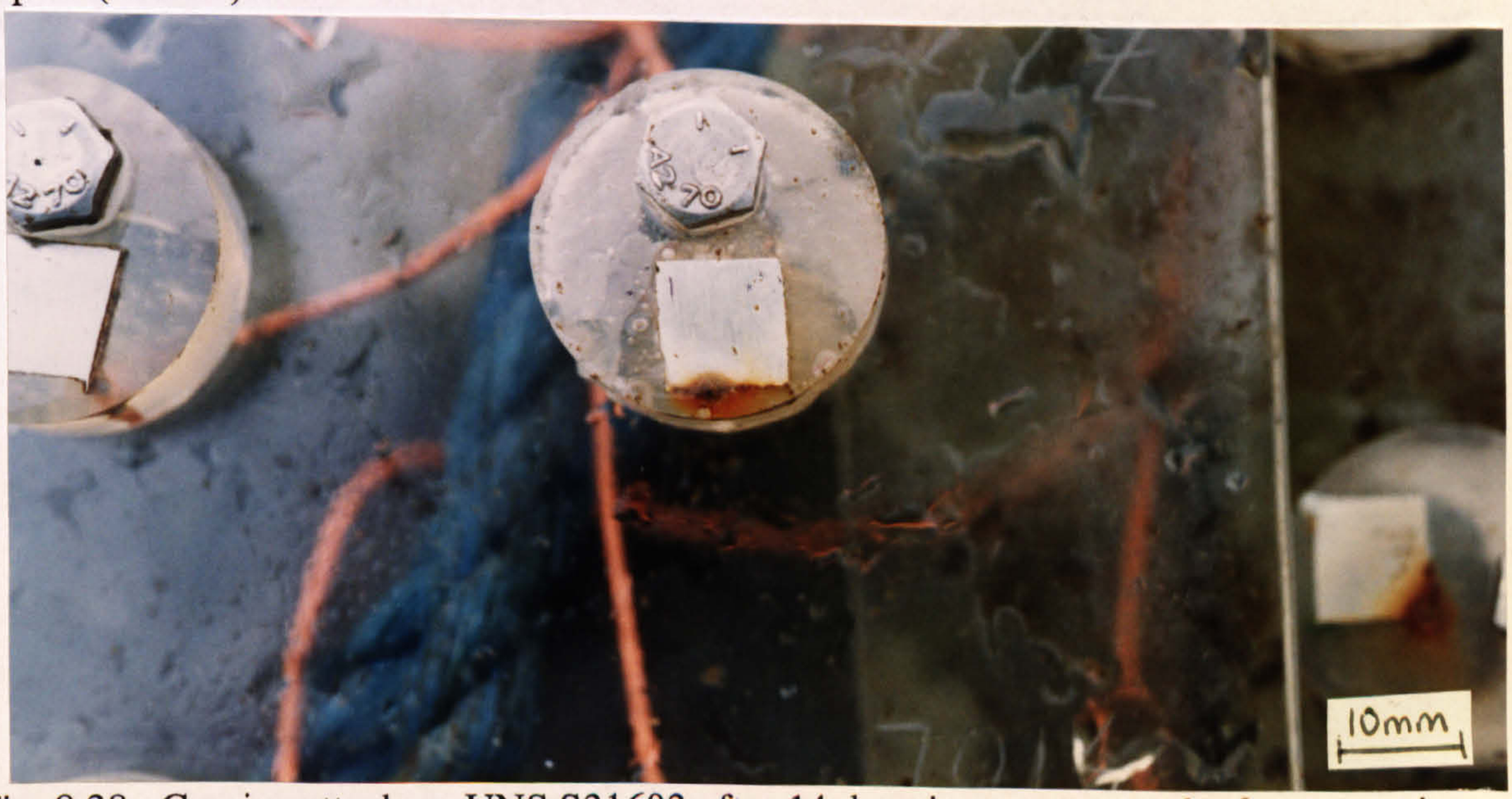

Fig. 8.38. Crevice attack on UNS S31603 after 14 days in seawater at the free corrosion potential

Fig. 8.39. Early stages of fouling in the form of a brown slime covering on UNS S31254 (top) and on 25Cr duplex (bottom)

Cathodic polarisation over the period of 1 month on UNS S32760 followed the trend shown in Fig. 8.40a where it can be seen that there is very little change in the polarisation characteristics. There is a small increase in the magnitude of the limiting current after one month immersion. On UNS S31603, the limiting current density increased from 15 days immersion to 34 days by a small amount but a significant decrease was observed after 119 days immersion (Fig 8.40b). The decrease corresponded to a discontinuous fouling layer being observed on the specimens but covering a significant proportion of the surface as in Fig. 8.41.

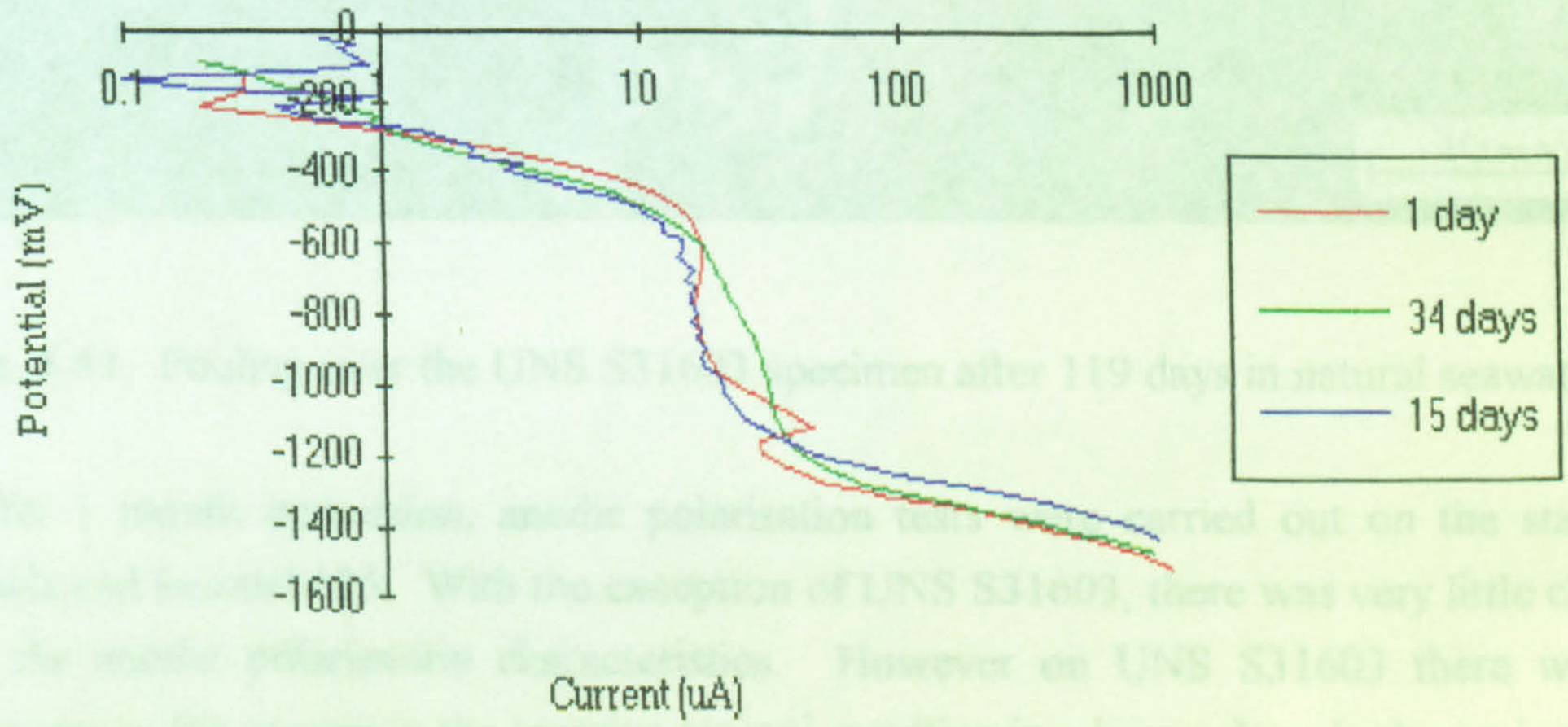

(a)

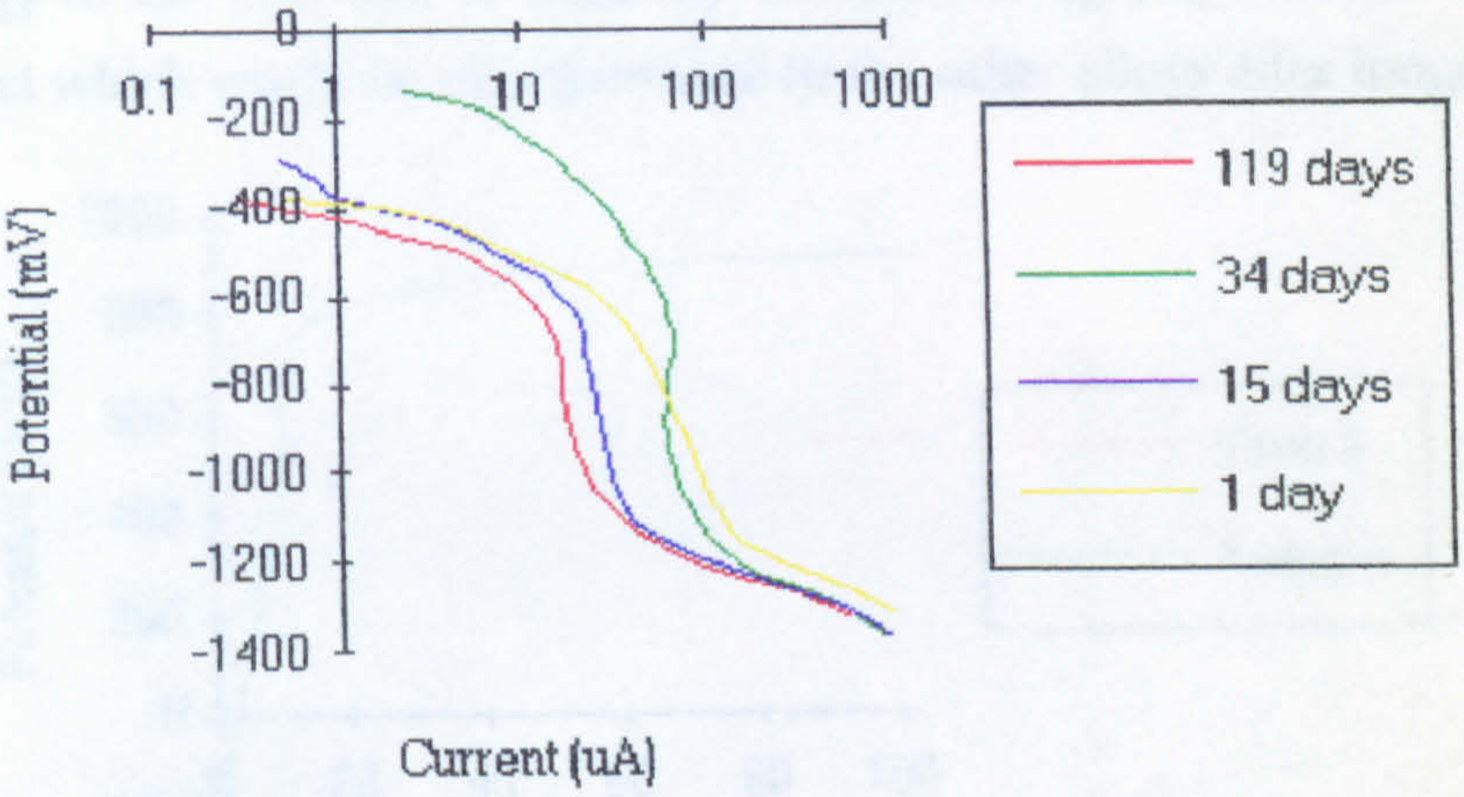

(b)

Fig. 8.40. Cathodic polarisation in natural seawater on (a) UNS S32760 and on (b) UNS S31603

Fig. 8.41. Fouling over the UNS S31603 specimen after 119 days in natural seawater

After 1 month immersion, anodic polarisation tests were carried out on the stainless steels and Inconel 625. With the exception of UNS S31603, there was very little change in the anodic polarisation characteristics. However on UNS S31603 there was an increase in the current in the 'passive region' resulting in a lower slope in the region from

E_{corr} to the potential of passivity breakdown E_b (Fig. 8.42). This result signified an effect which would be of importance to the other alloys after longer immersion periods.

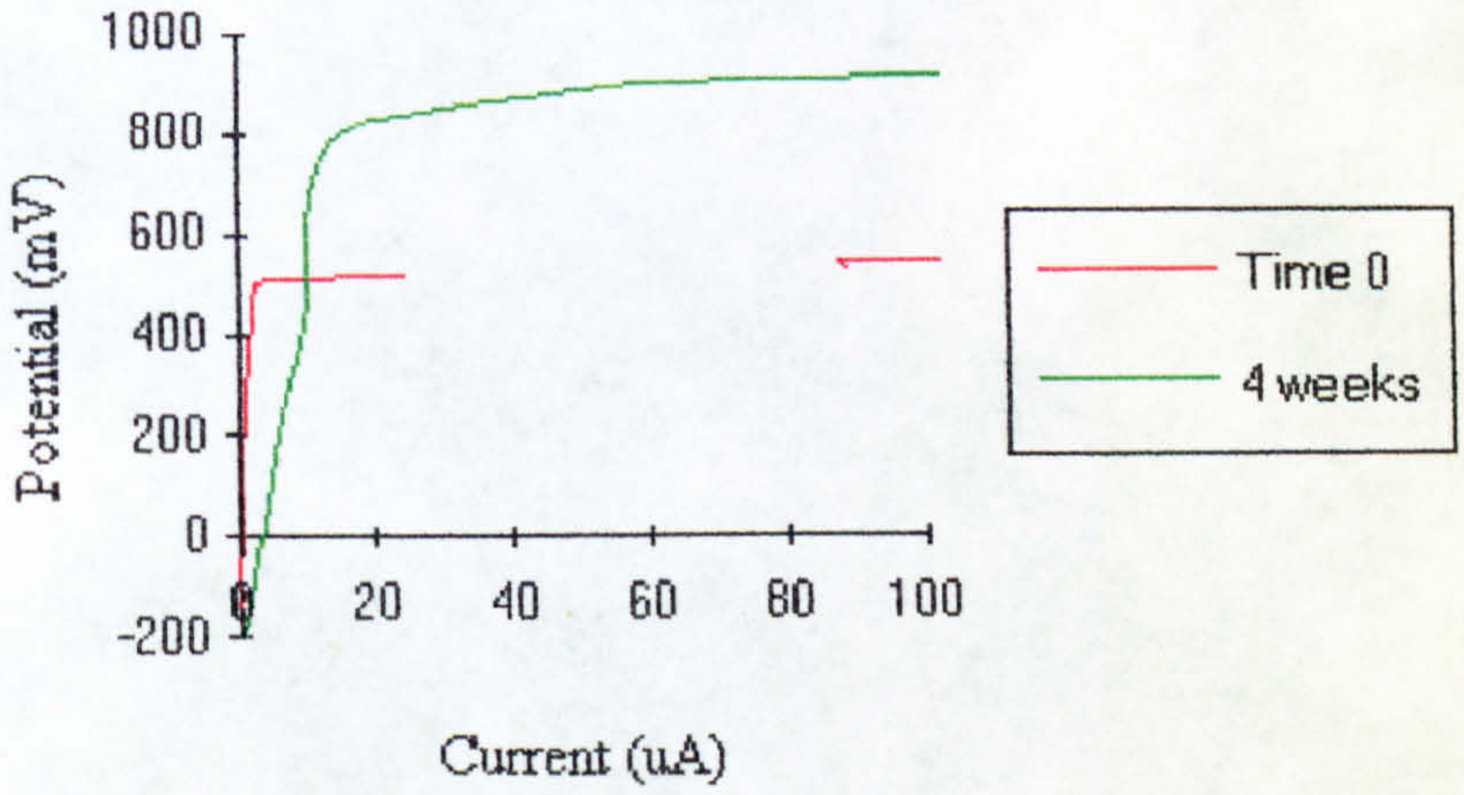

Fig. 8.42. Higher anodic currents in the passive region on UNS S31603 after 1 month immersion in natural seawater

Two months immersion yielded significant changes in the anodic polarisation characteristics and will be discussed in due course. In considering the surface fouling before the anodic polarisation tests were carried out, there was a clear patchy biofilm on the specimens shown in Figs 8.43a and b. It is clear that in the area shown in Fig. 8.41a, there is a high percentage of surface coverage in contrast to the more sparsely fouled area on the same specimen (Fig. 8.43b). Macroscopically the fouling was enhanced from the 21 day specimens but still consisted of a discontinuous fouling layer. With the exception of Ultimet, at least one of the 4 samples of each material had shown signs of crevice corrosion initiation (Fig. 8.37). Fig. 8.44 shows the severe attack on SAF 2205 (left) with the patchy fouling and in contrast, 2 of the 3 unattacked specimens of Inconel 625 (right). There were signs of green algae on the surface as can be seen on Stellite 6 in Fig. 8.45, in addition to the extensive attack at the metal/resin interface.

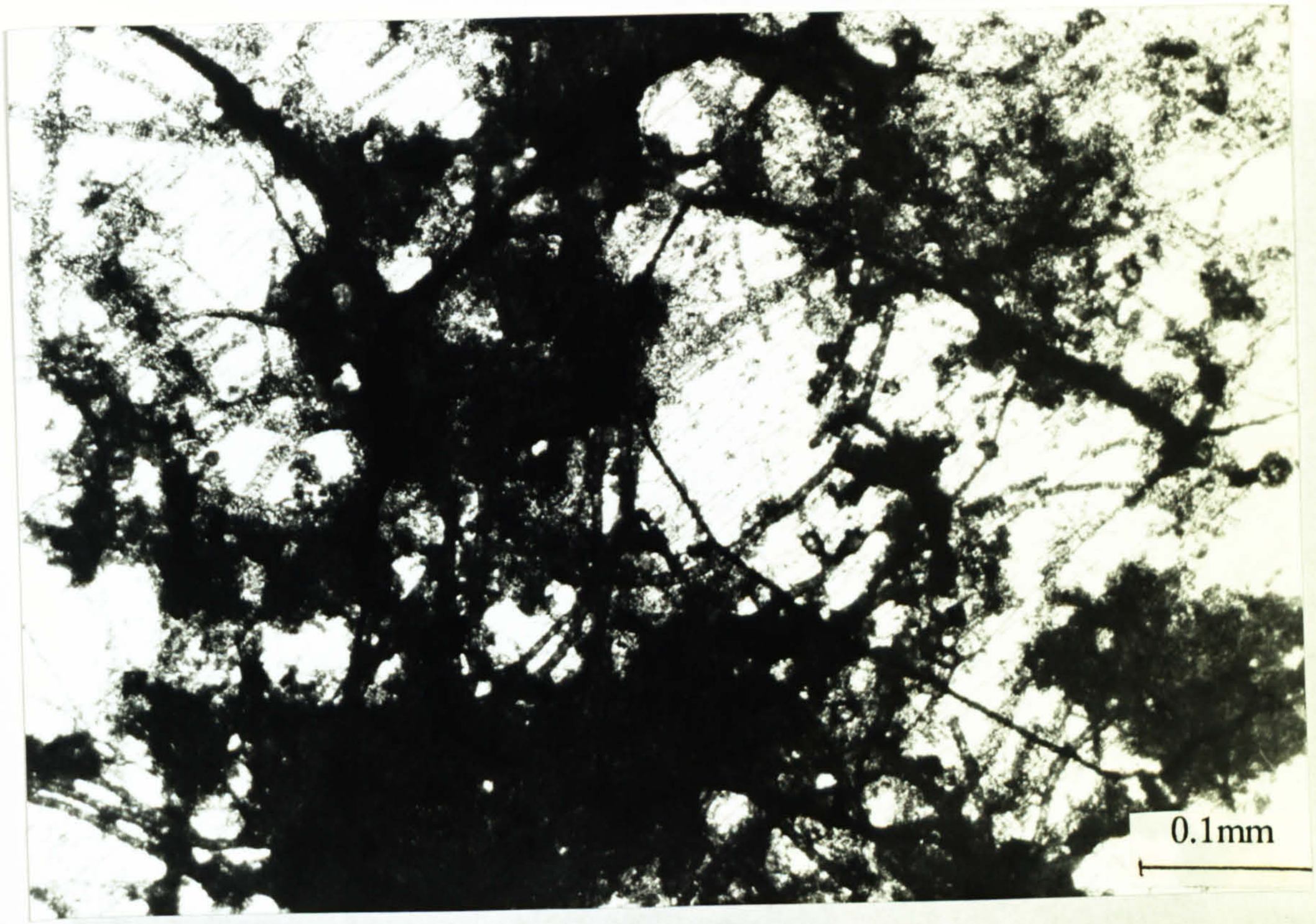

(a)

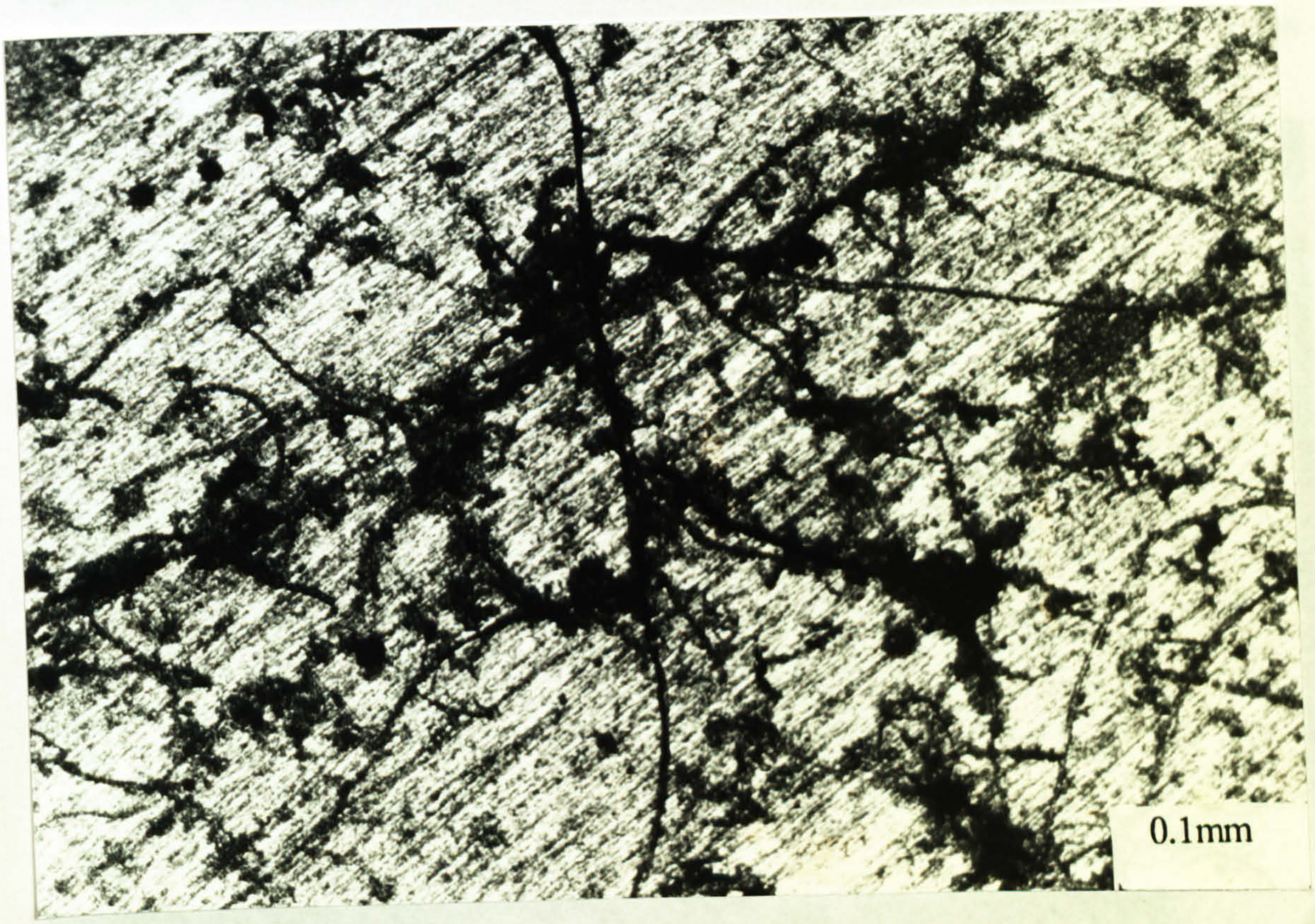

(b)

Fig. 8.43. Fouling on UNS S32760 after 2 months on (a) a significantly covered area and (b) on a sparsely fouled area

Fig. 8.44. Severe attack on SAF 2205 (left) with patchy fouling and in contrast, 2 of the 3 unattacked specimens of Inconel 625 (right). After 2 months in natural seawater at the free corrosion potential.

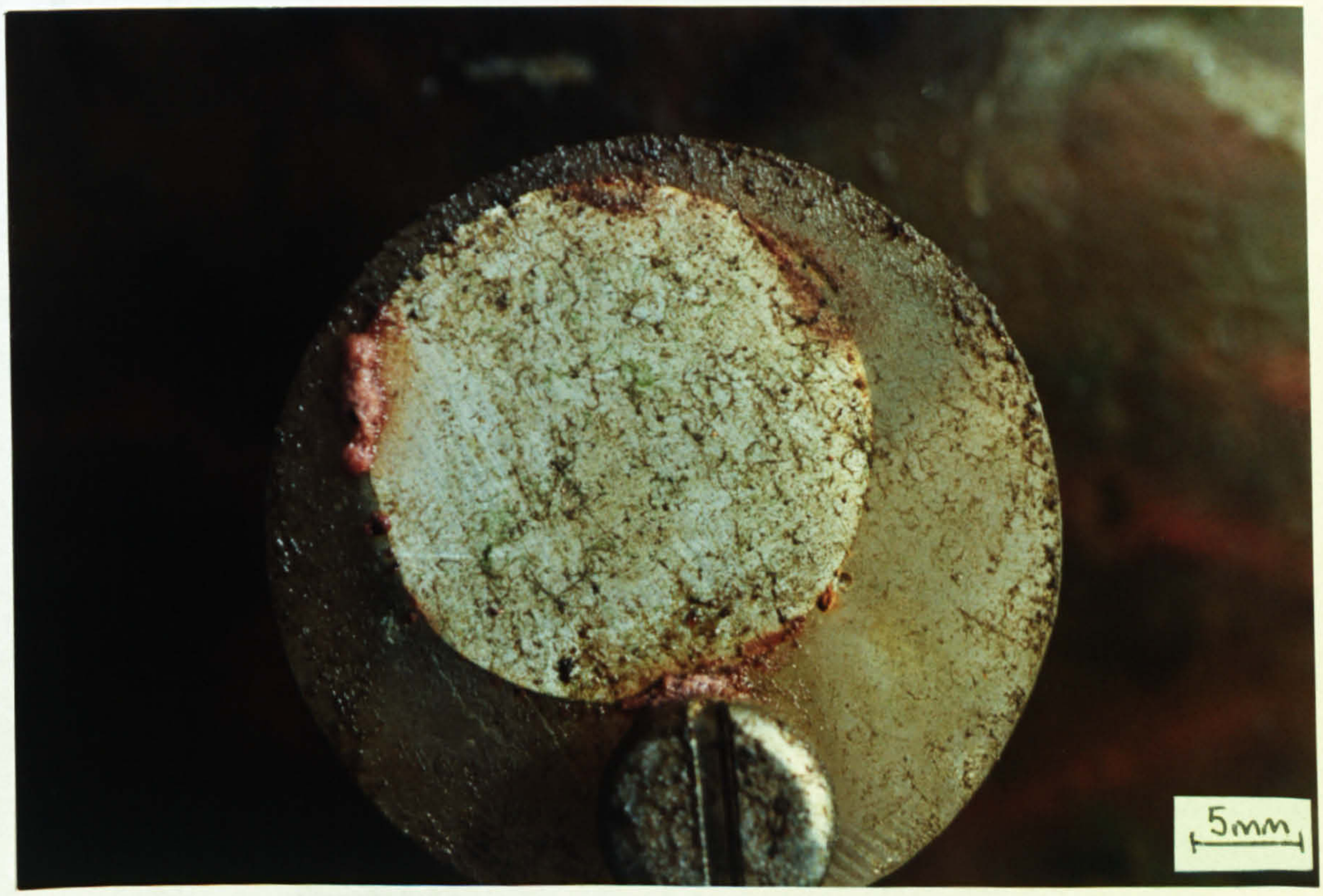

Fig. 8.45. Green algae on the surface of Stellite 6 in addition to the extensive attack at the metal/resin interface after 2 months in natural seawater at the free corrosion potential.

Anodic polarisation tests were carried out after 2 months on Inconel 625, 25Cr duplex, UNS S31254 and on UNS S32760. With the exception of UNS S31254, the anodic plots displayed a higher passive current than on immediate immersion. The effect was much less pronounced on Inconel 625 than on 25Cr duplex and on UNS S32760, the extent of the effect appeared to be dependent on whether crevice corrosion had initiated or not. In Figs. 8.46 and 8.47 the enhanced currents are shown for 25Cr duplex and UNS S32760 respectively. It is apparent from Fig. 8.47 that the specimen with the crevice corrosion supports a higher passive current than the specimen which appears unattacked. Figure 8.48 shows the comparably smaller increase on the Inconel 625 specimen on which, examination after the test showed no trace of crevice corrosion. It is evident from the following figures that there was no significant change in the breakdown potential after the 2 months immersion.

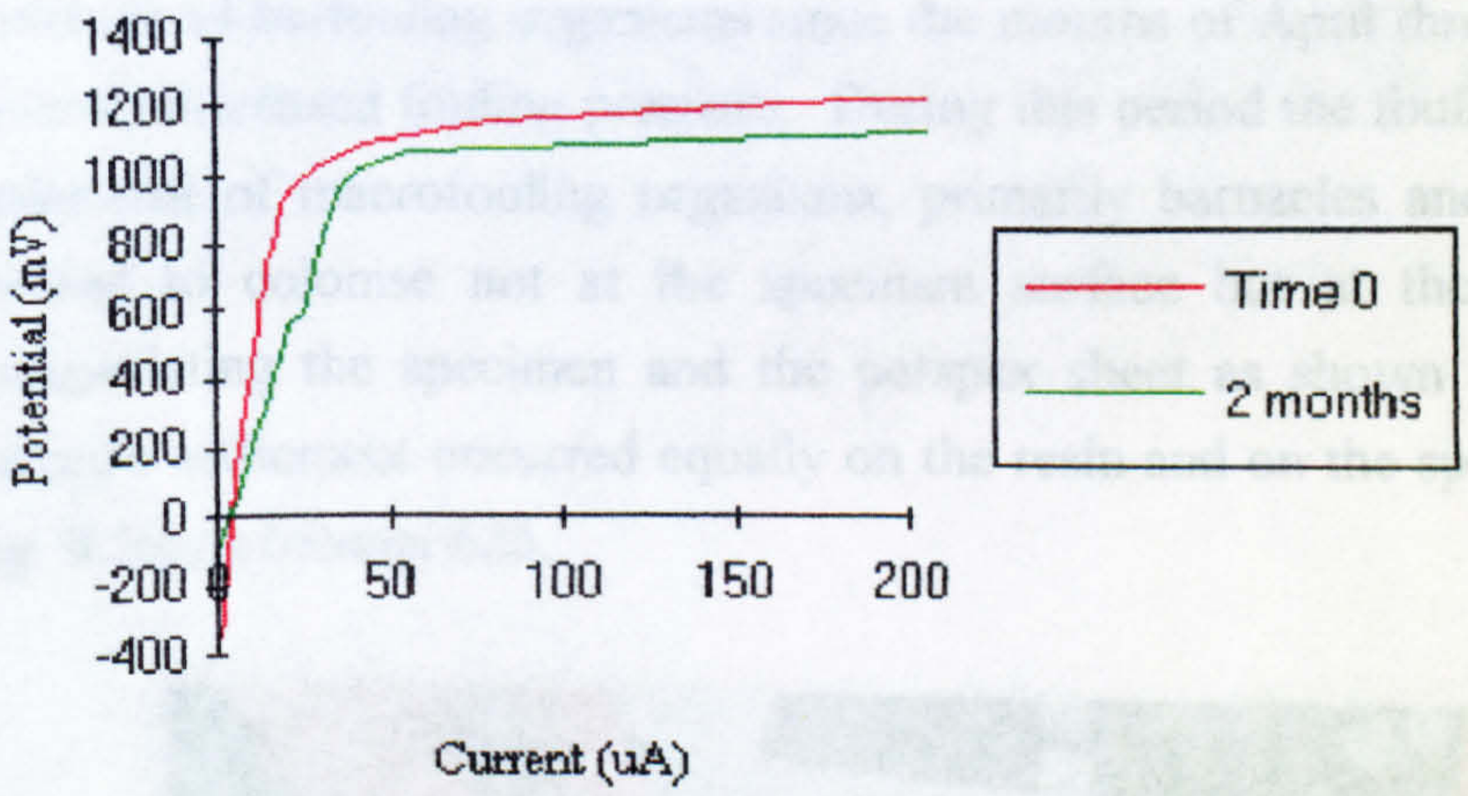

Fig. 8.46. Increase in passive current during anodic polarisation on 25Cr duplex after 2 months immersion

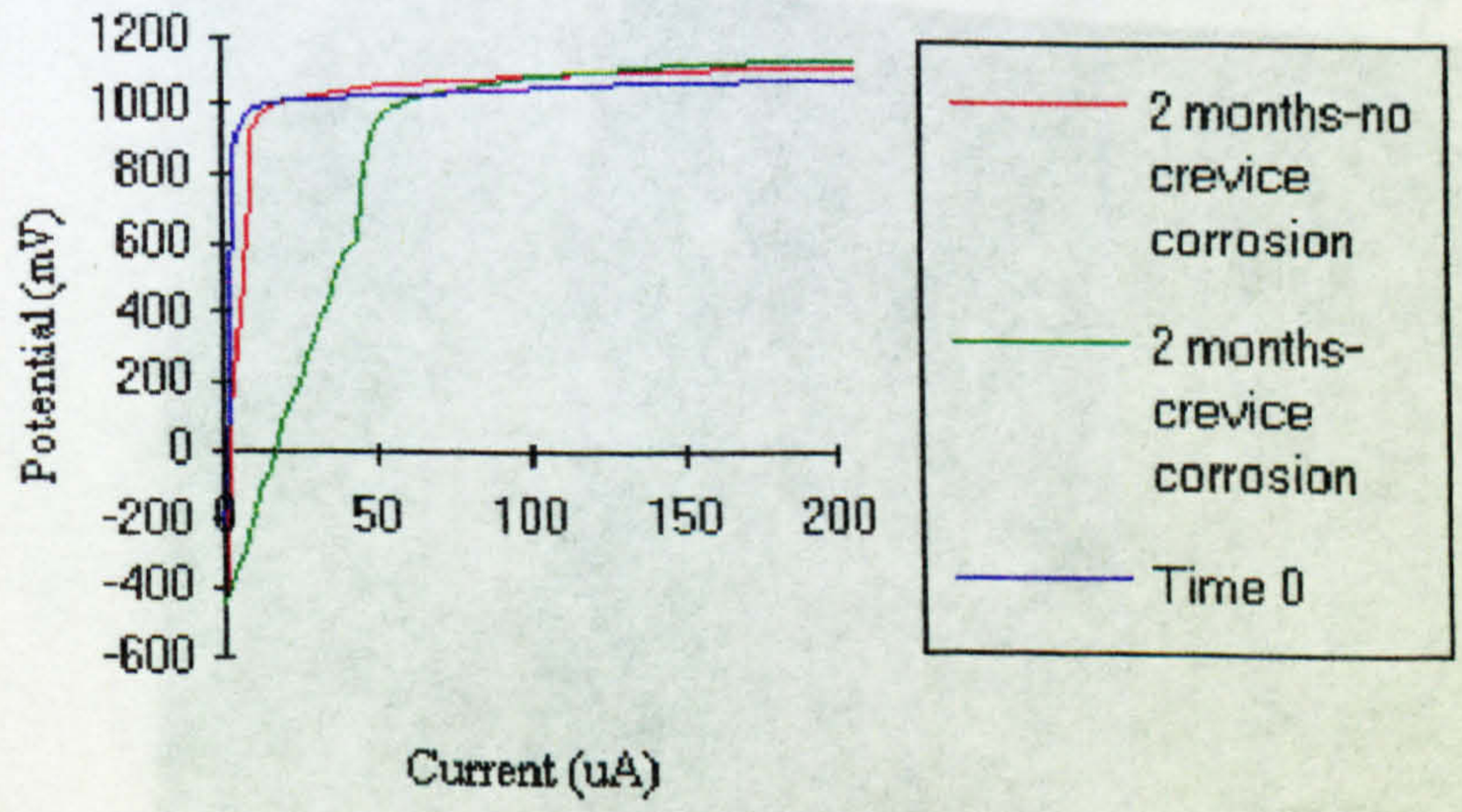

Fig. 8.47. Anodic polarisation on UNS S32760 after 2 months immersion showing increased passive currents on specimen with crevice corrosion

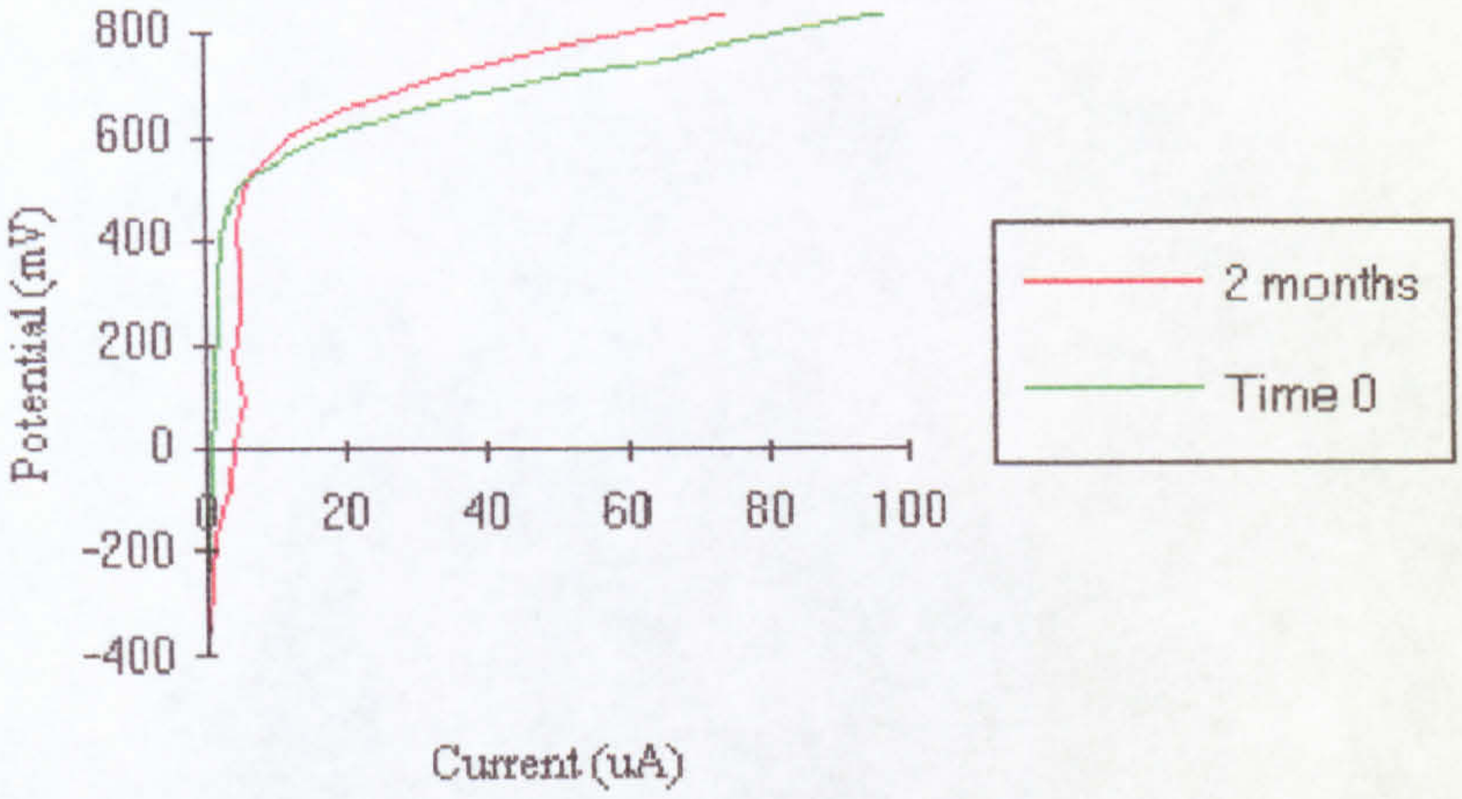

Fig. 8.48. Anodic polarisation on Inconel 625 after 2 months immersion

Progression to 6 months in natural seawater led to significantly increased surface coverage of biofouling organisms since the months of April through June tend to invoke severely increased fouling pressure. During this period the fouling was manifested in the settlement of macrofouling organisms, primarily barnacles and mussels. The mussels seemed to colonise not at the specimen surface but at the join between the resin encapsulating the specimen and the perspex sheet as shown in Fig. 8.49. However, barnacle settlement occurred equally on the resin and on the specimen surface, shown in Fig. 8.50 on Inconel 625.

Fig. 8.49. Mussels developing around the resin moulds after 6 months in seawater. Anodic polarisation.

Fig. 8.50. Barnacle settlement on Inconel 625 after 6 months immersion.

The presence of the more dense macrofouling fouling layer after 6 months, was associated with further enhancement of the passive current on the afore-mentioned materials, again with the exception of UNS S31254, even though no distinction could be made between the level of fouling. On UNS S31603 there was an added effect in that the breakdown potential E_b was significantly reduced thus signifying a loss in the material's resistance to passivity breakdown (Fig. 8.51). However, the polarisation tests were carried out on only one specimen for the 6 month immersion period. On UNS S31254, an interesting feature was observed at the metal/resin interface after anodic polarisation : the presence of a dense colony of diatoms dispersed amongst the corrosion products. The diatoms were concentrated around the site of the crevice corrosion and were not evenly distributed over the entire surface (Fig 8.52).

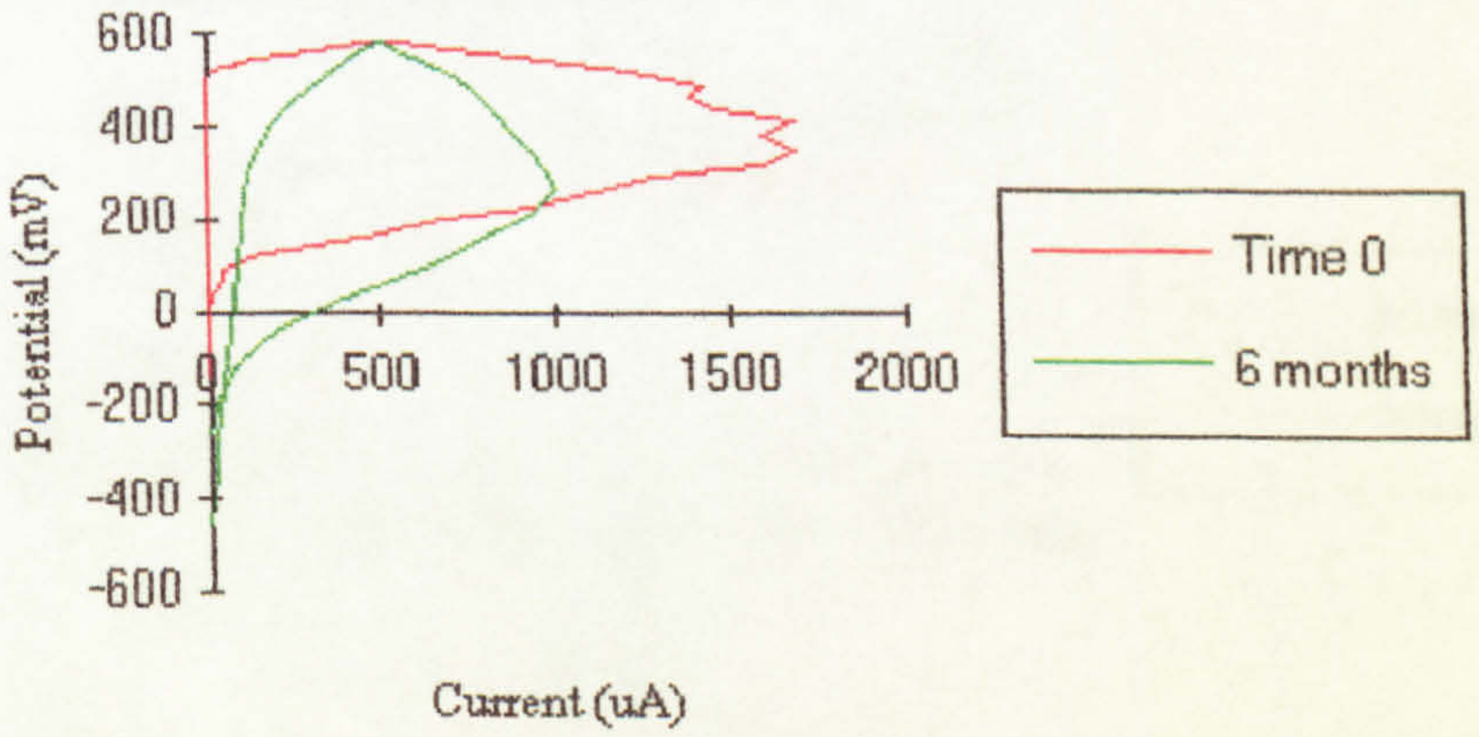

Fig. 8.51. Passivity resistance detrimentally affected on UNS S31603 after 6 months in seawater

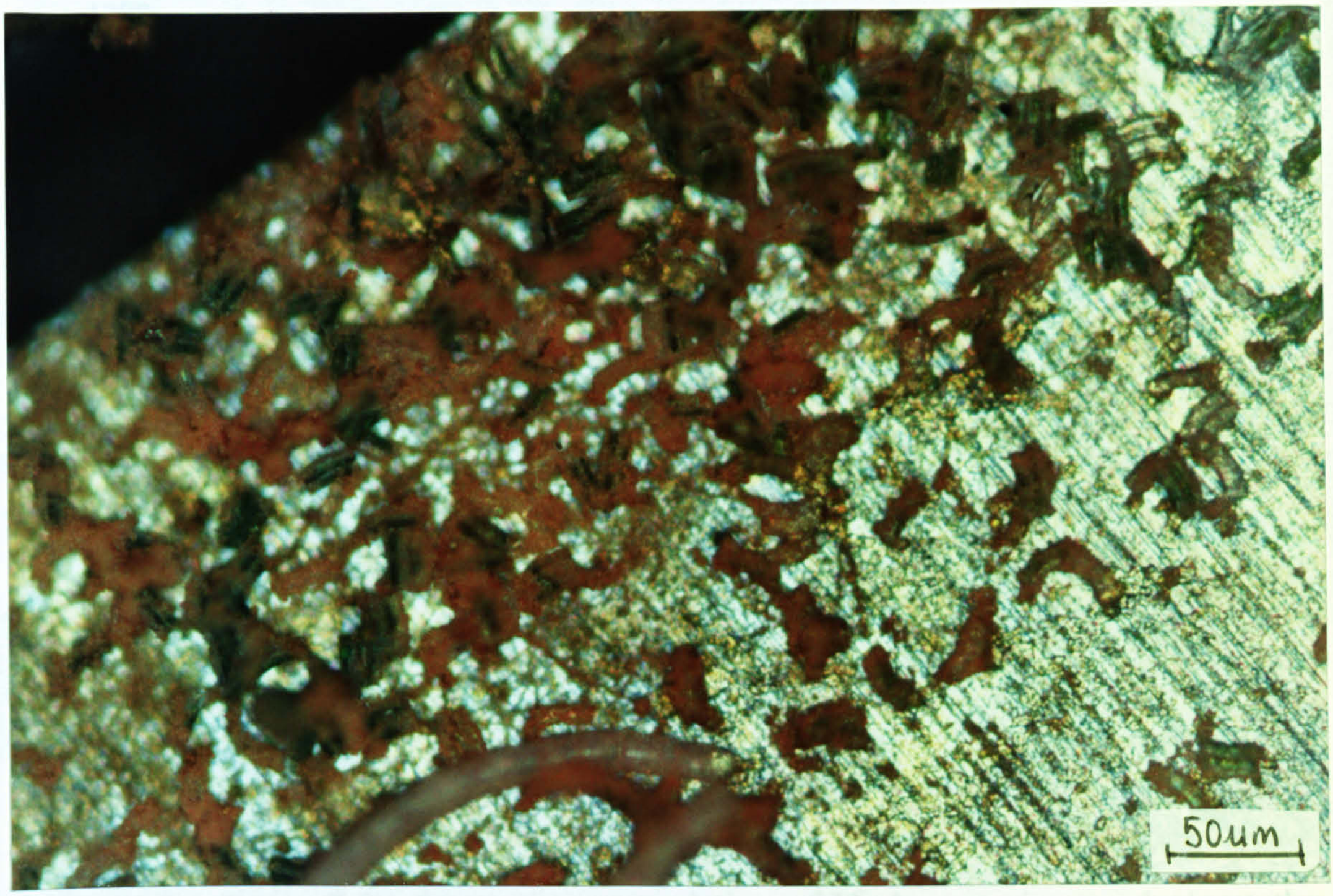

Fig. 8.52. Diatoms at the site of crevice corrosion on UNS S31254 after 6 months in seawater and anodic polarisation.

The longest immersion period, after which anodic polarisation test were performed was 18 months and it occurred that it was after this period that the most interesting results were obtained. The anodic polarisation characteristics continued to change through the increase of the anodic currents in the passive region and in addition, there was also a reduction in the E_b noted on all the stainless steels and Inconel 625 except the superduplex and the superaustenitic although both materials showed increased passive currents. In Figures 7.53 and 7.54, the lower E_b in conjunction with the higher currents in the 'passive' region as shown.

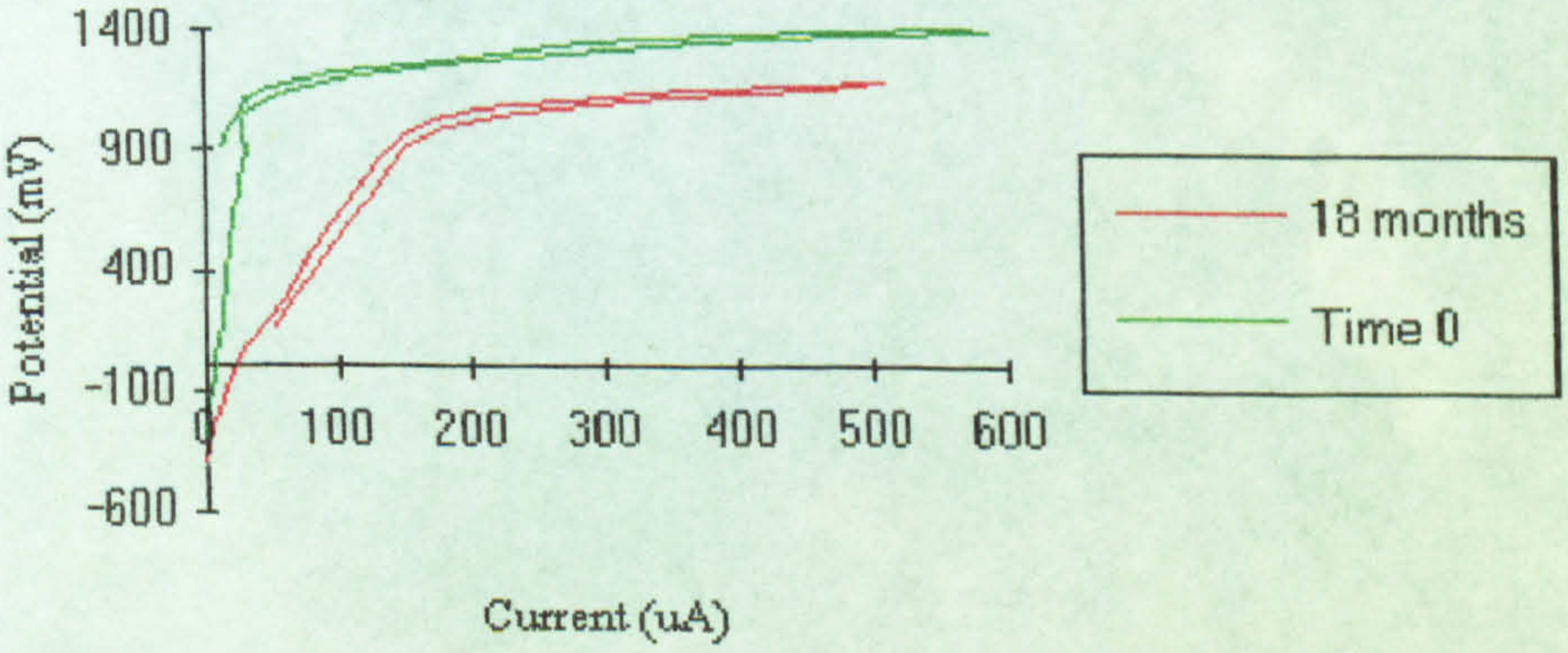

Fig. 8.53. Fall in E_b and enhanced passive currents after 18 months in natural seawater on SAF 2205

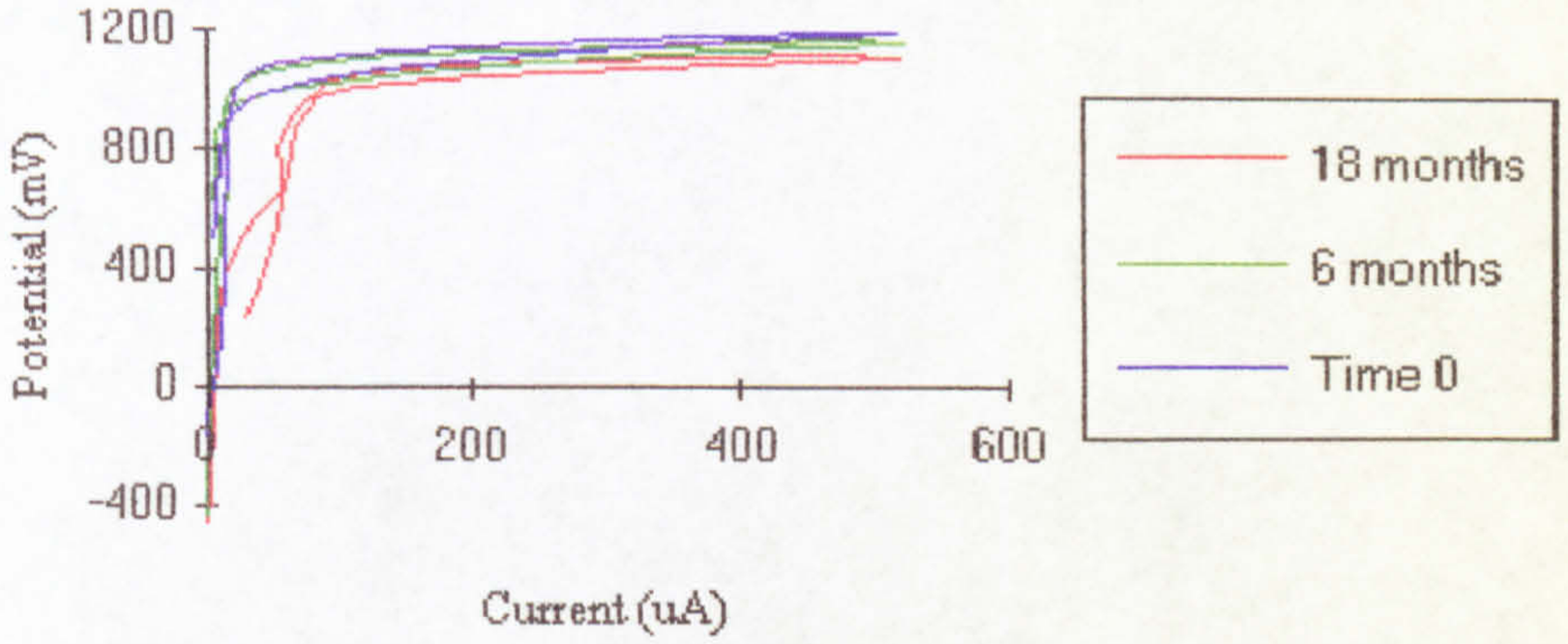

Fig. 8.54. Enhanced passive currents after 18 months in natural seawater on UNS S31254

On removing the specimens from the seawater after anodic polarisation, it was observed that there were black corrosion products present and in addition there was a pungent smell which could be compared to that encountered in the SRB cultures (chapter 7). The black corrosion products were primarily observed around the base of the barnacles on SAF 2205, Inconel 625 and UNS S31254 which had all been subject to anodic polarisation. Figure 8.55 shows the accumulation of black corrosion products at the barnacle base of SAF 2205. A similar effect was seen on UNS S31254 on which there were no complete barnacles but the debris of fouling and the remains of barnacles were surrounded by black corrosion products as shown in Fig. 8.56 on UNS S31524. On removing the UNS S32760 specimen from the perspex rack, the fouling was found to be loosely adherent and was removed. However, as shown in Fig. 8.57, there were still black corrosion products at the metal/resin interface.

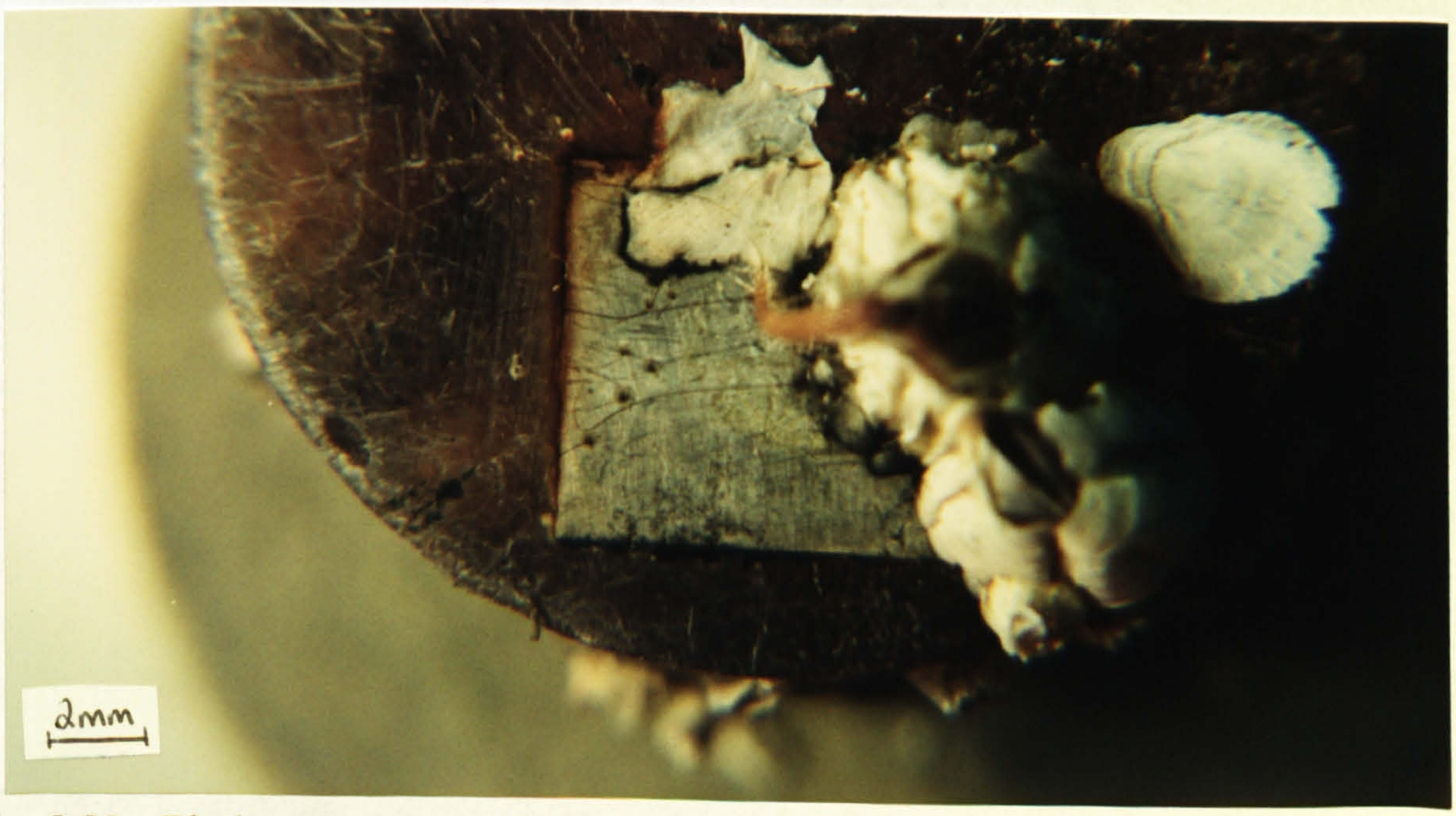

Fig. 8.55. Black corrosion products at the base of a barnacle on SAF 2205 after 18 months immersion and anodic polarisation

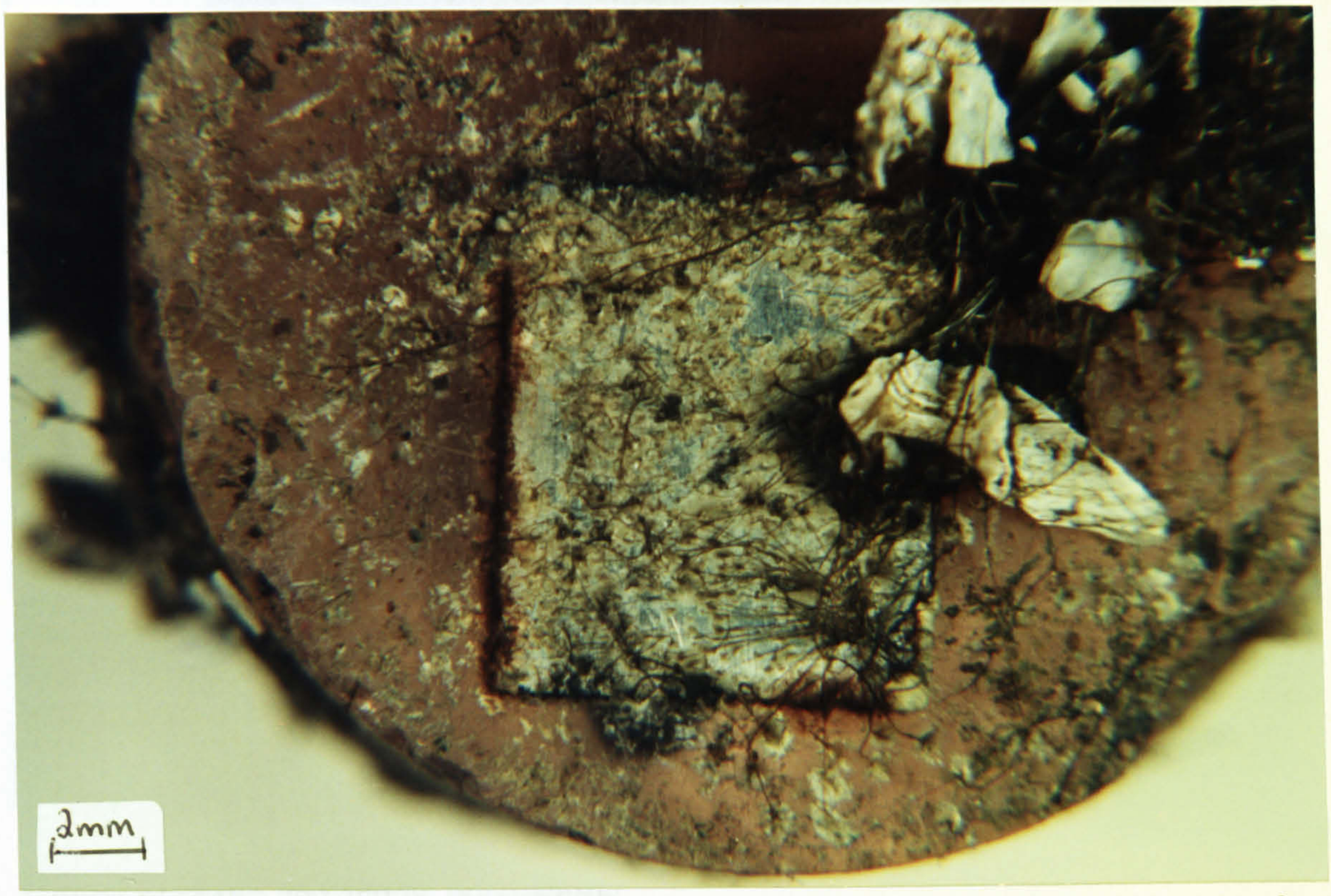

Fig. 8.56. Black corrosion products at the remains of a barnacle on UNS S31254 after 18 months immersion and anodic polarisation

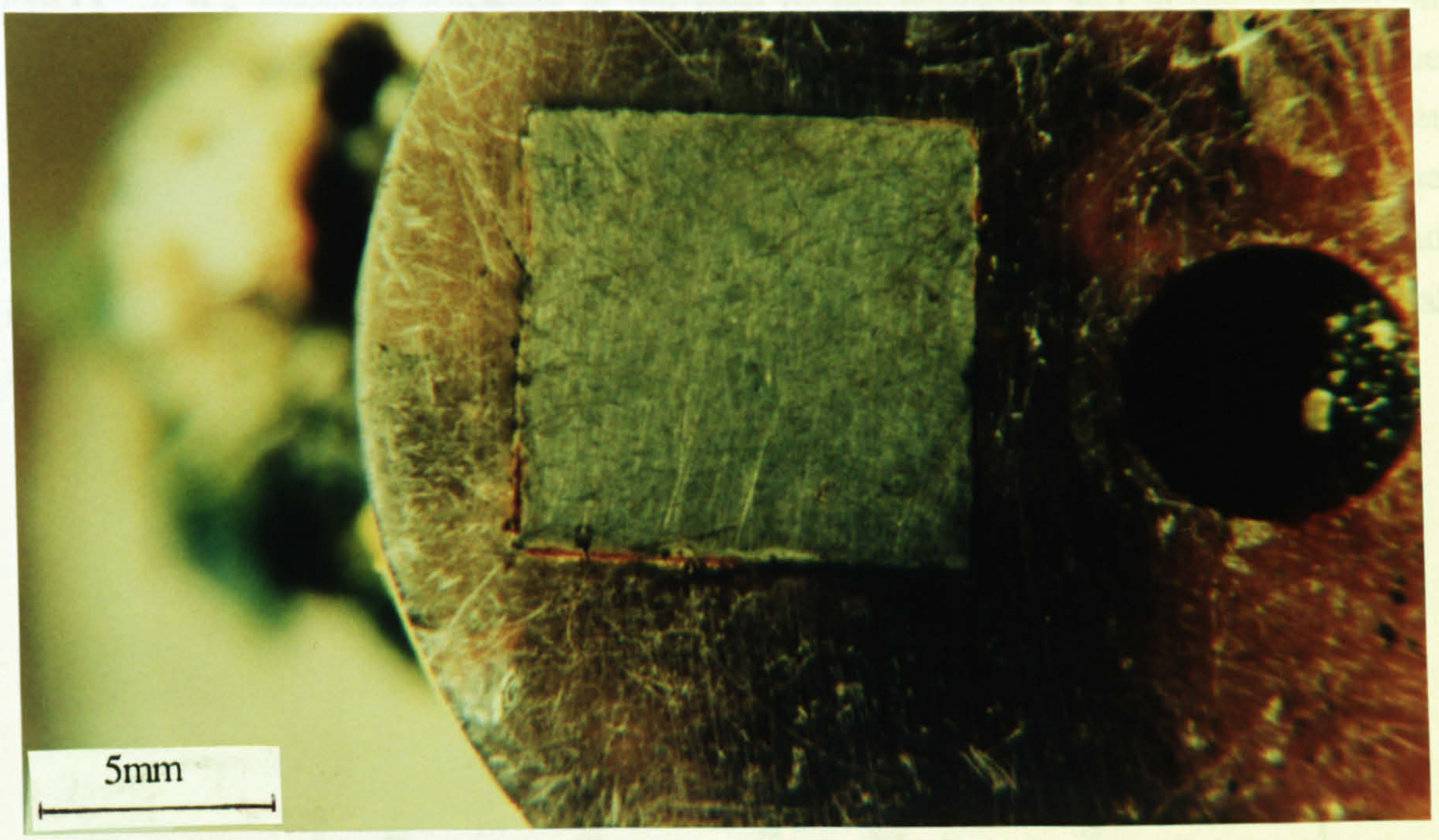

Fig. 8.57. Black corrosion products at the metal/resin interface after 18 months on UNS S32760 immersion and anodic polarisation

On Stellite 6, there was the distinction that, in addition to black corrosion products, there were traces of green corrosion products at the outer edges of the barnacle scar as shown in Fig. 8.58.

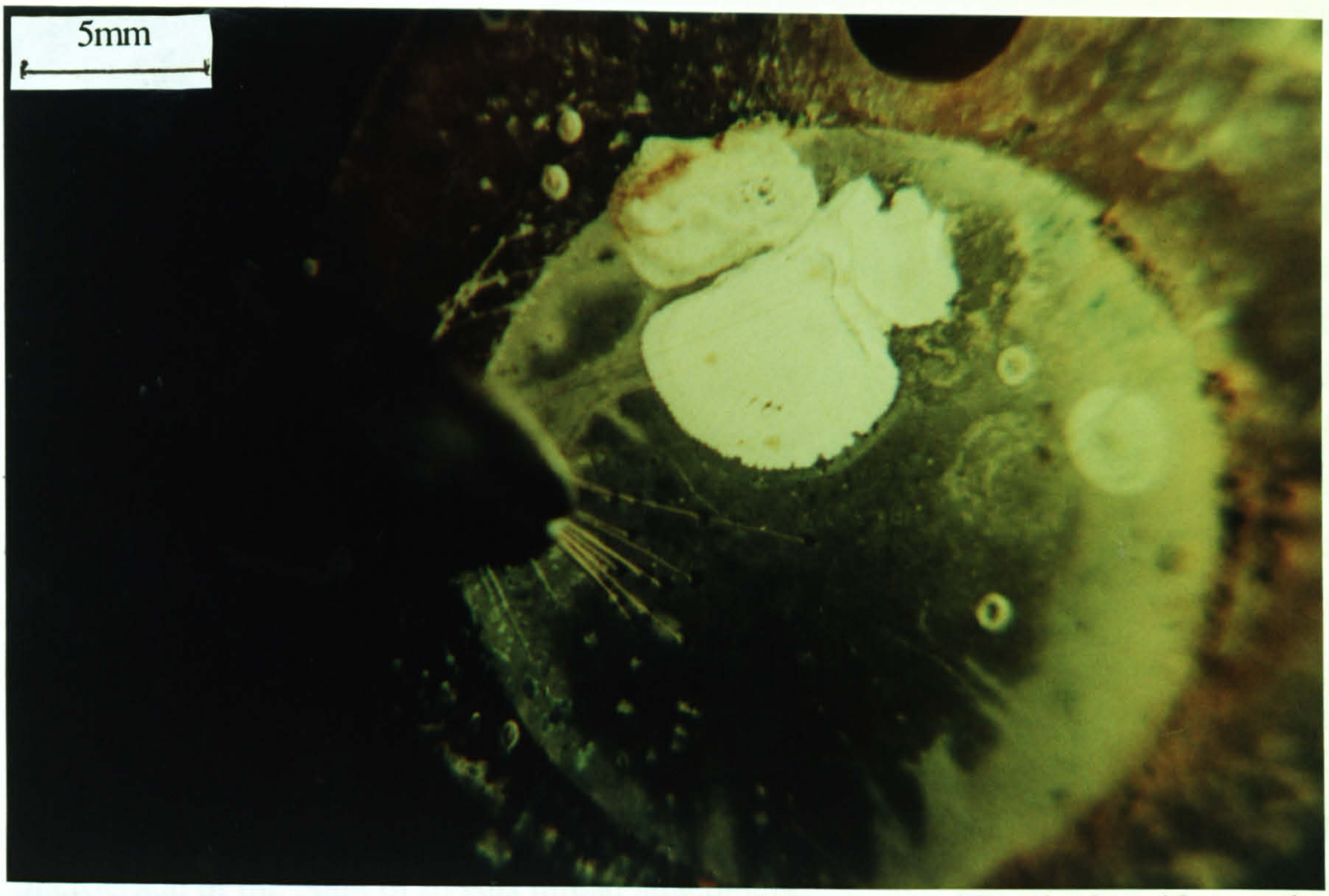

Fig. 8.58. Corrosion products at the barnacle scar on Stellite 6 after 18 months in natural seawater and anodic polarisation.

EPMA on the corrosion products at the base of the barnacles and at the metal/resin interface confirmed the presence of a sulphur (Fig. 8.59) and therefore inferred the activity of SRB in the vicinity of the corrosion at the barnacle base and the crevices set up at the metal/resin interfaces. It was observed that after several hours exposed to the atmosphere, after removal from the seawater, the black corrosion products had invariably turned white (perhaps indicating the oxidation of sulphides to elemental sulphur) but the green corrosion products on Stellite 6 still remained.

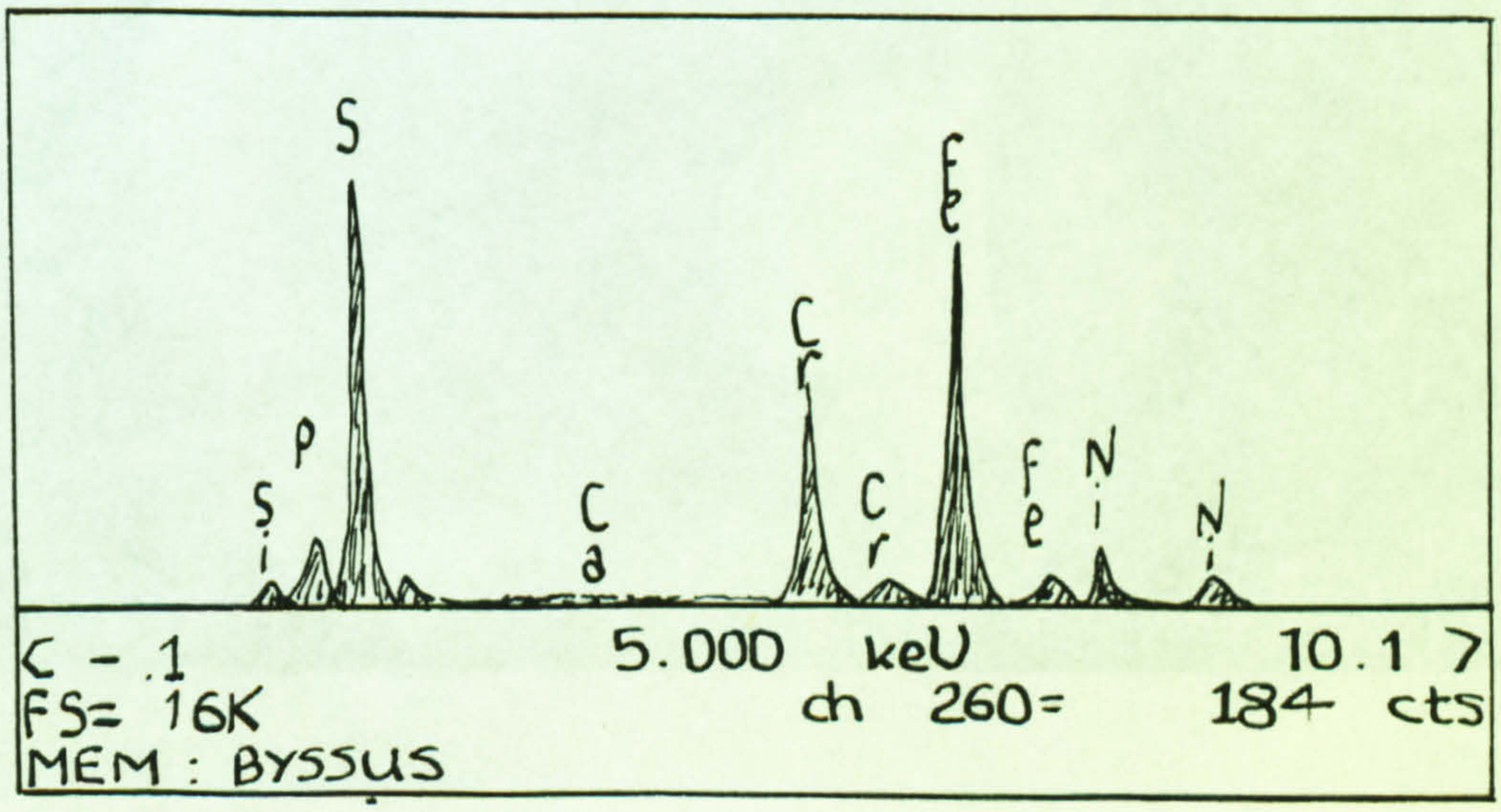

Fig. 8.59. Presence of S in corrosion products on UNS S31254 after 18 months in natural seawater and anodic polarisation .

The association of sulphate reducing bacteria with barnacles was initially inferred by Laque [31] and indeed other authors [32,33] have observed corrosion due to SRB under barnacles. However, the presence and activity of SRB has, to date, been associated with dead barnacles. In this work the barnacles were alive as confirmed by the movement of the species on removal from the seawater. A finding not reported previously was made in that that pockets of S-containing corrosion products were detected at the base of their byssus threads attaching the mussels to the surface. Figure 8.60 shows a light micrograph of the point of attachment on Stellite 6 where the mussel and the threads originating from it can be seen. It can be clearly seen that at the point where the thread attaches to the surface there is a small black area. Fig 8.61. shows the interface of the barnacle with the surface of SAF 2205 and also on the surface are extensive black corrosion products and byssus threads. The localised area of black S-containing substance is shown in Fig. 8.62 on SAF 2205 in the high magnification SEM micrograph of the point of byssus thread attachment.

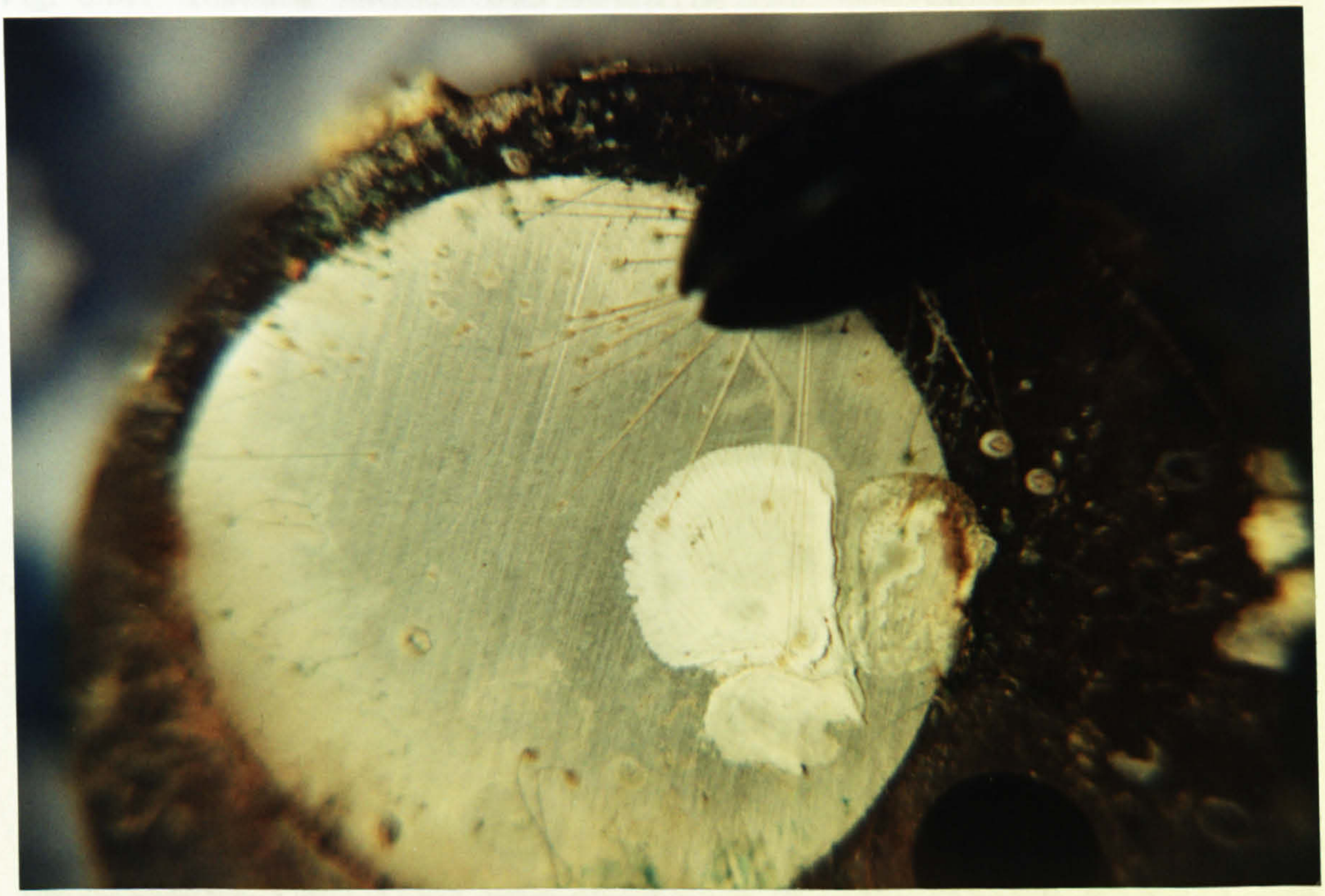

Fig 8.60. Byssus threads, attaching the mussel to the Stellite 6 substrate. Small black areas associated with attachment point. 18 months immersion in natural seawater and anodic polarisation.

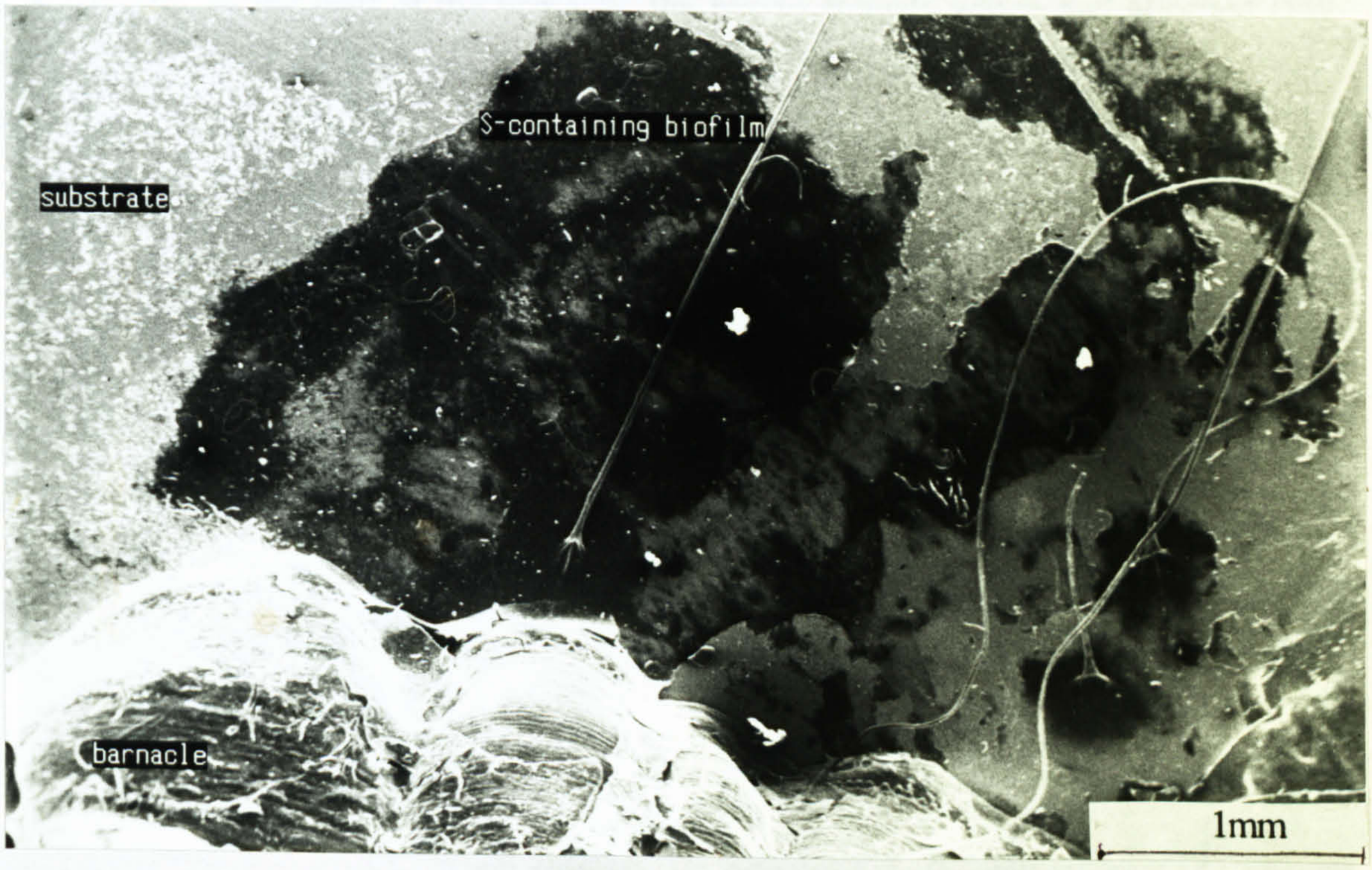

Fig. 8.61. Barnacle interface with surface of SAF 2205 and the associated black corrosion products after 18 months in natural seawater and anodic polarisation

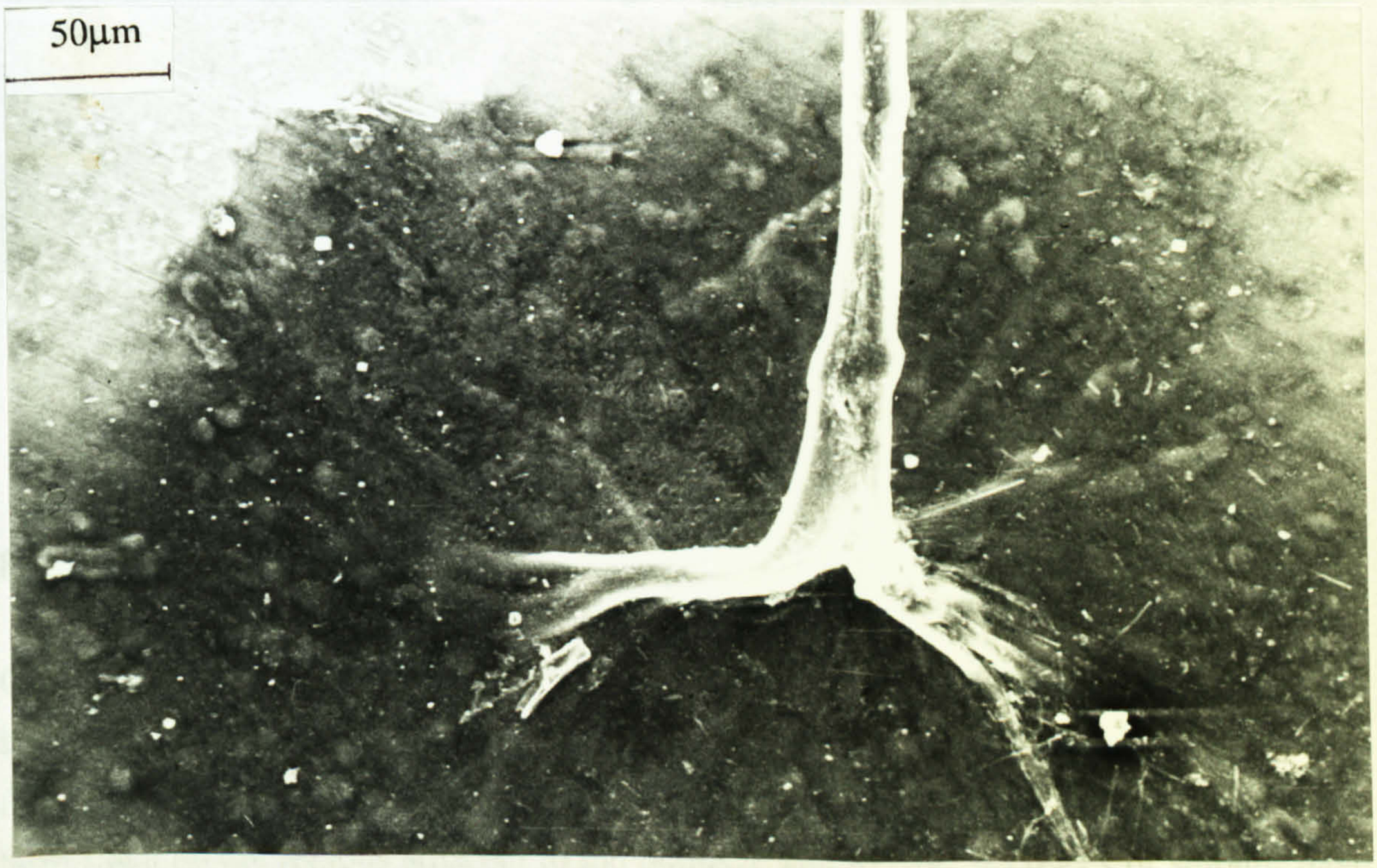

Figure 8.62. SEM micrograph of the byssus threads attaching to the surface and the associated ring of very localised S-containing products.

Interestingly, on the wall of the barnacle, the byssus threads which had attached (Fig. 8.63) also contained trace of S, detected by EPMA. However there were no visible black products associated with these sites.

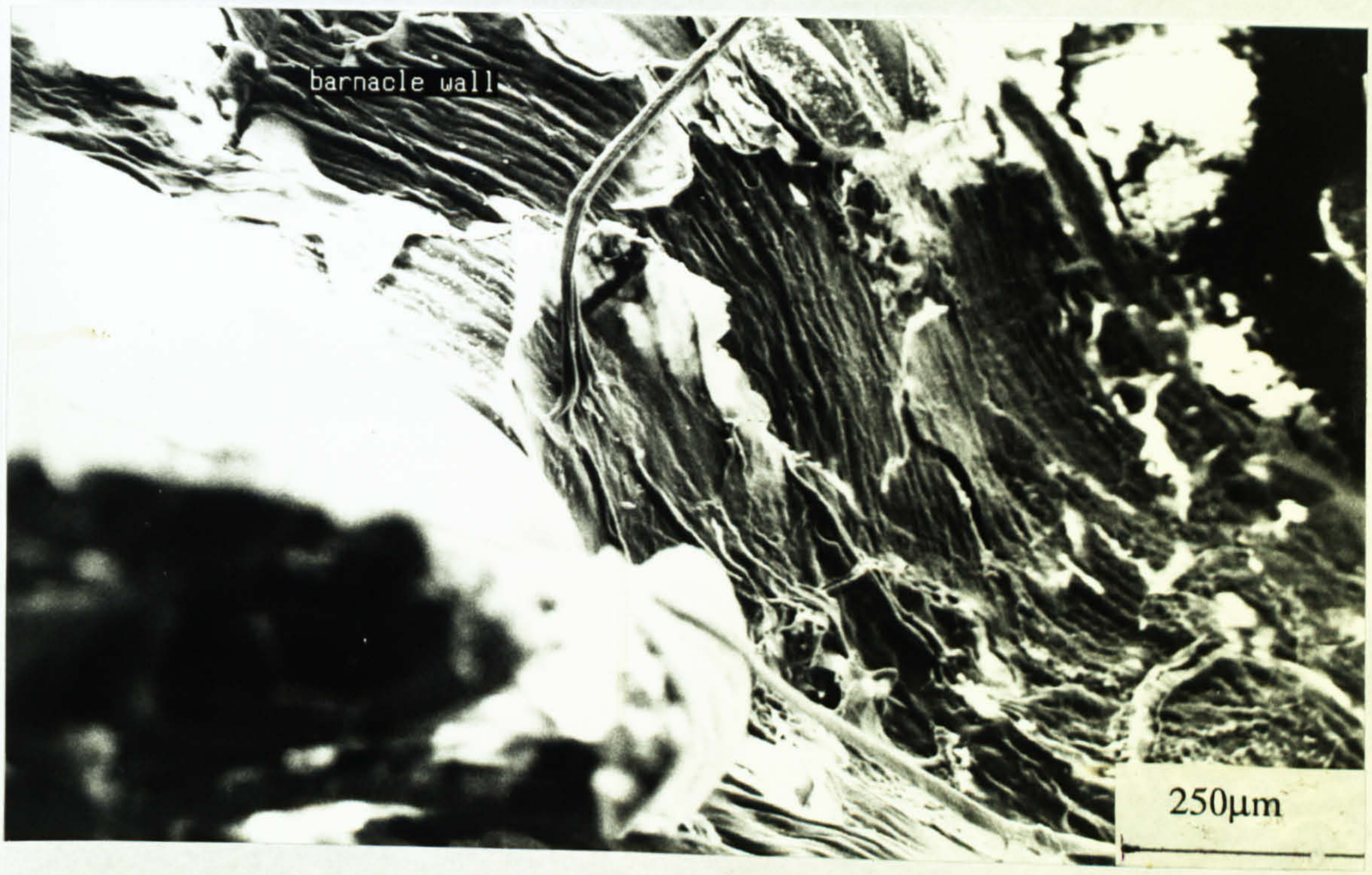

Fig. 8.63. Byssus threads attached to the wall of the barnacle

On the plate specimens, immersed for 18 months in natural seawater at Millport with barnacles cultured on the surface, there was a thick biofilm of bacteria and diatoms (Figs. 8.64 and 8.65) and the settlement of barnacles (Fig. 8.66). Several analyses were performed on the regions adjacent to the barnacle and to date, no traces of sulphur have been found. At one site on UNS S31603, there was evidence to suggest that the presence of the barnacle had initiated crevice corrosion, as shown in Fig. 8.67. No such attack was evident on SAF 2205.

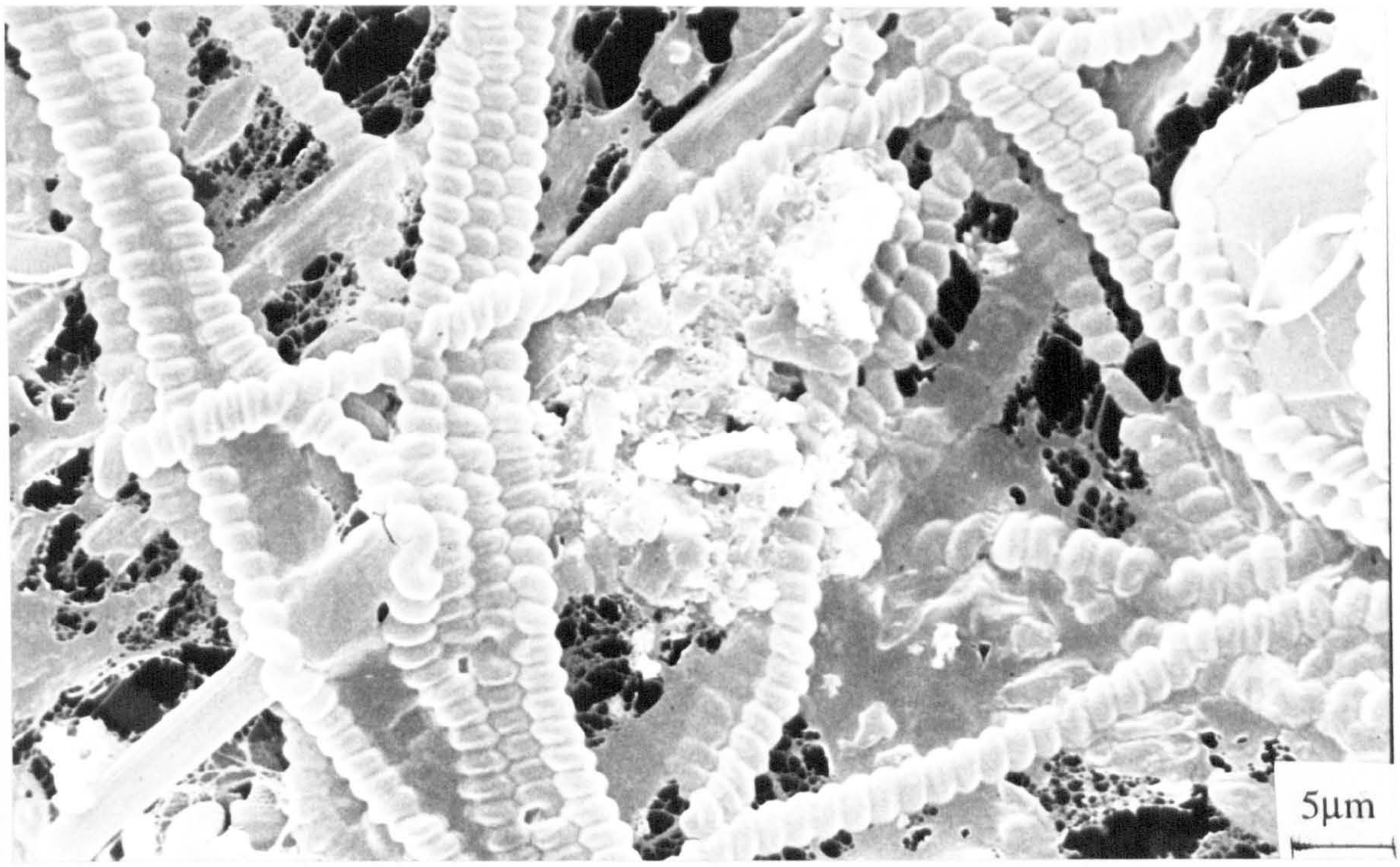

Fig. 8.64. Thick biofilm on UNS S31603 after 18 months in natural seawater at the free corrosion potential

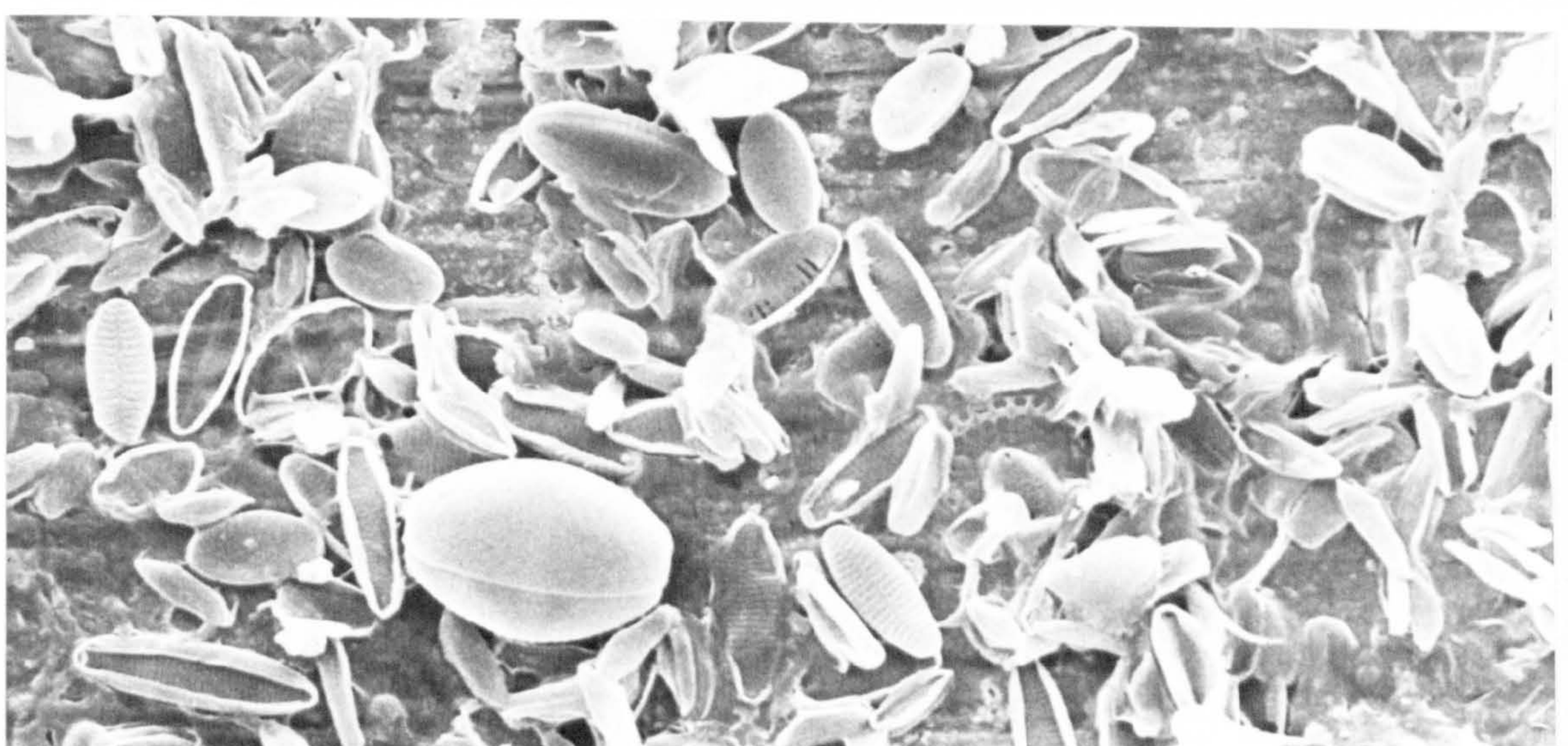

Fig. 8.65. Thick biofilm on SAF 2205 after 18 months in natural seawater at the free corrosion potential

Fig. 8.66. Barnacle settlement on UNS S31603 after 18 months in natural seawater

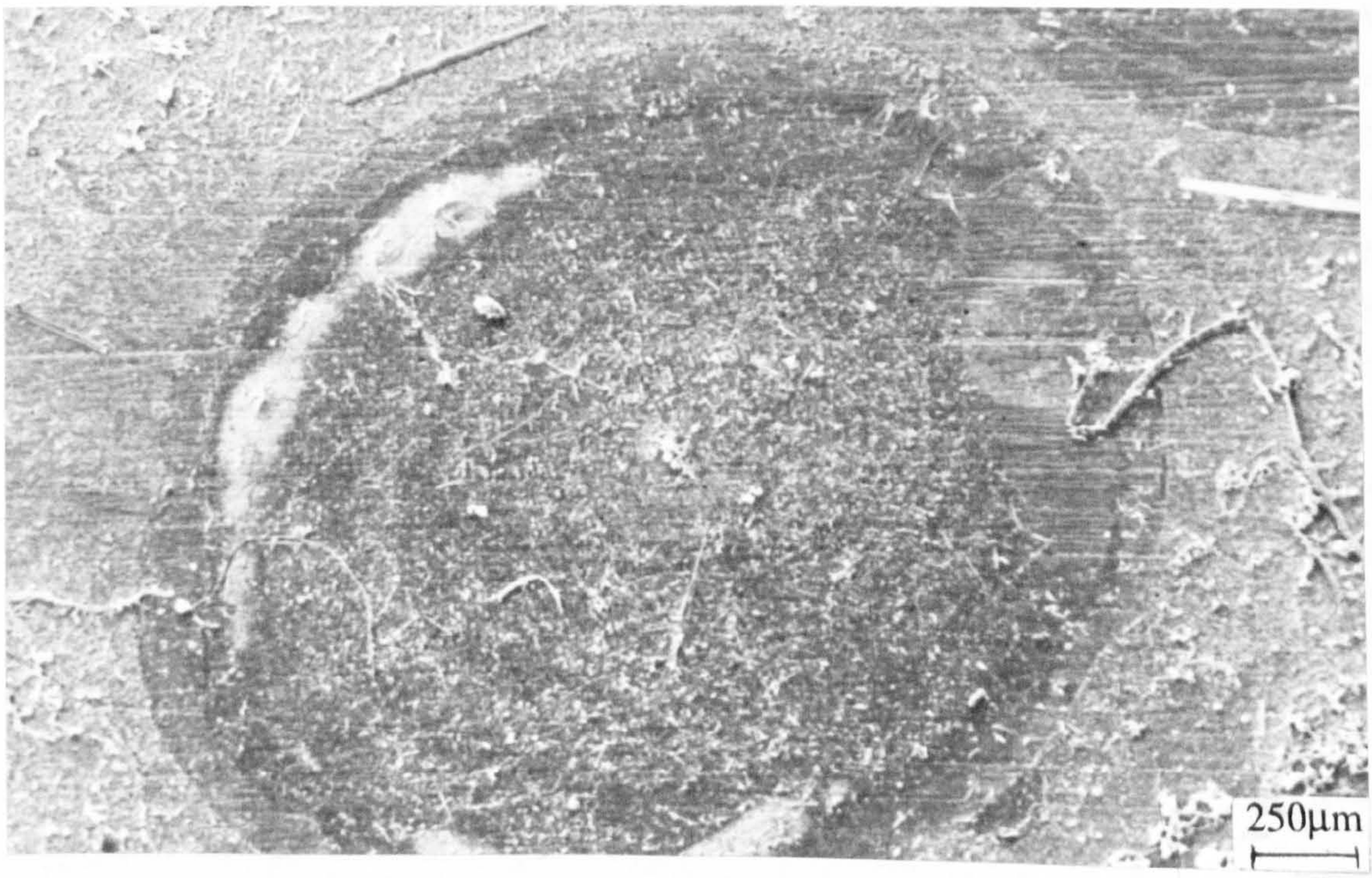

Fig. 8.67. Crevice corrosion on UNS S31603 after 18 months in natural seawater

Material Ranking

In chapters 2 and 4, the use of electrochemical techniques in association with microscopy enabled the relative resistance to corrosion initiation and propagation to be considered and ranking lists to be established for the alloys under investigation. In agreement with the ranking in static seawater at ambient temperature, this study in natural seawater has shown that the alloy UNS S31603 has much increased susceptibility to crevice corrosion than the superduplex and superaustenitic alloys as expected. However, the duplex stainless steels (25Cr and SAF 2205) were shown to have poor resistance to crevice corrosion initiation, which would agree with the suggested vulnerability of the passive film to localised breakdown inferred by the performance at high temperature. Also in agreement with the study in synthetic seawater, the alloys, Ultimet and Inconel 625 were found here to resist initiation of attack until longer periods than the other alloys.

Results - PART III

The results of preliminary tests to determine the potential at which the cathodic current is stable and forms the oxygen diffusion plateau are shown for UNS S32760 in Fig. 8.68. Cathodic polarisation curves at 300rpm, 600rpm and 1200rpm show the increase in current as the disk angular velocity increases. However there is not a well-defined diffusion plateau as found on gold electrodes by other authors [27]. Preliminary work on stainless steel by the same group also found that a well defined plateau was not obtained on stainless steels [30]. On UNS S31603, a better diffusion plateau was observed as shown in Fig. 8.69 for the same rotational velocities. Hence on stainless steels, the cathodic current can not be represented by purely diffusional characteristics and the increase in current due to increasing overpotential must be accounted for. This factor has been termed the kinetic factor, I_K [30]. More precisely, it represents the current factor which accounts for non-diffusional components of the current. At time 0, when no biofilm is present, the model gives the parameter I_K since $I\Omega - \infty$ is zero. This non-diffusional component has been assumed to be constant over immersion time [30] and in this work the same approach had to be taken. However, through studies of the cathodic reaction in seawater over different periods, it is apparent that there are significant changes over time and to assume that these are purely due to the biofilm is not wholly justified. Indeed tha question as to whether the oxide film on the surface changes with immersion time and how this affects the progression of the cathodic reaction must be addressed. Depolarisation of the cathodic reaction in the absence of a

Specimens were left in natural seawater over a period of 7 days at E_{corr} to follow the characteristics of the cathodic polarisation curve and to ascertain whether a more prominent diffusion controlled region is obtained after prolonged immersion. After 7 days, cathodic polarisation at 600rpm still failed to show a clear stable region.

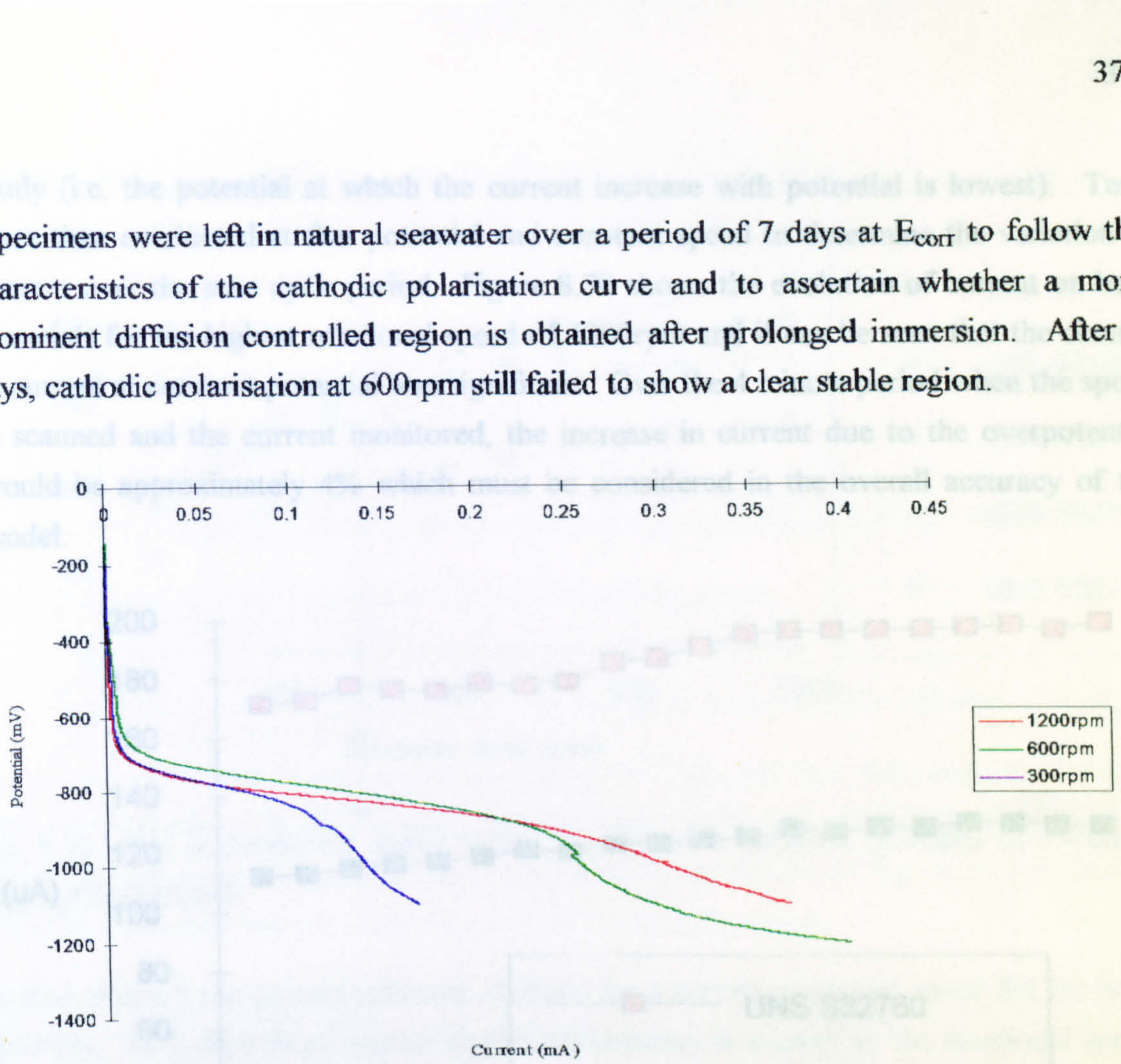

Fig. 8.68. Cathodic polarisation on UNS S32760 at different rotational velocities

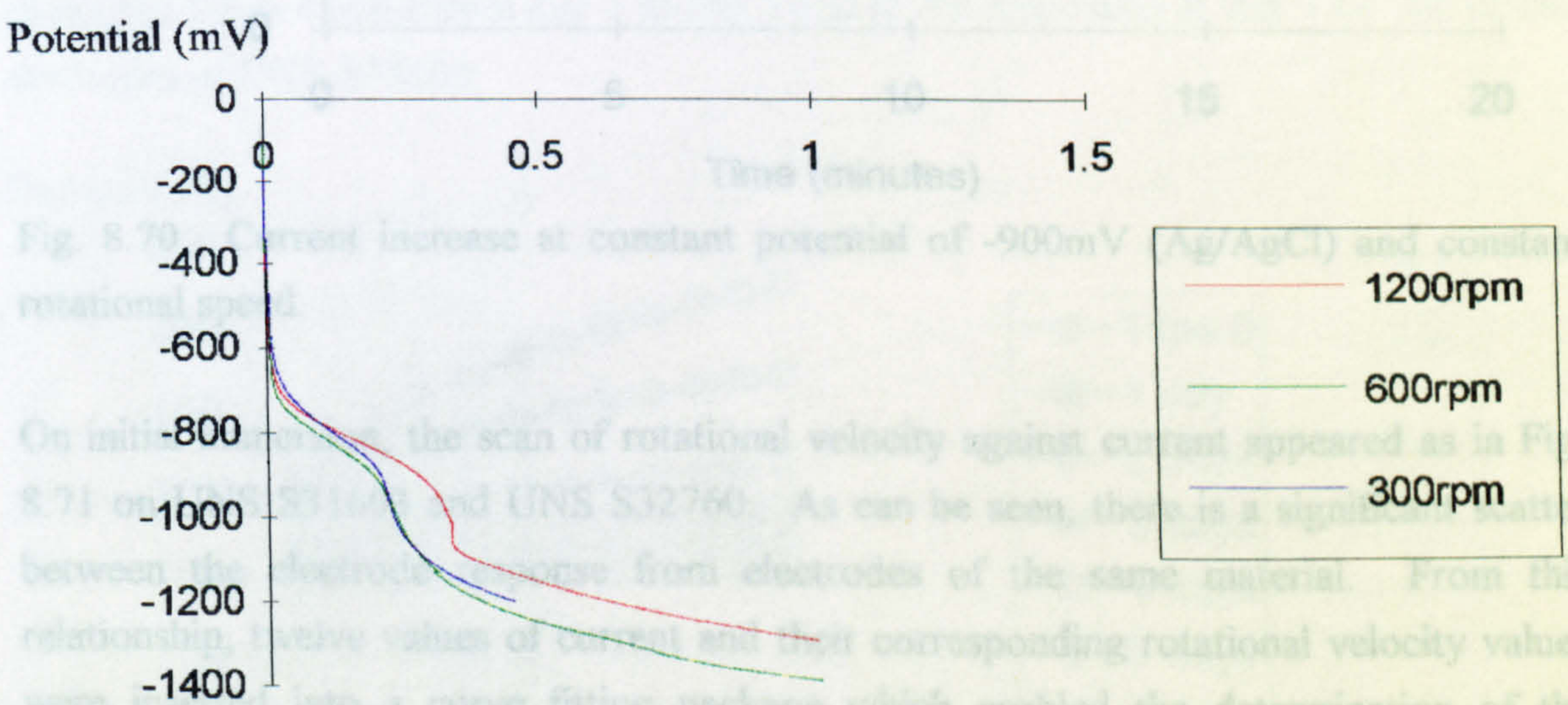

Fig. 8.69. Cathodic polarisation on UNS S31603 at different rotational velocities

Through analysis of the potentiodynamic cathodic polarisation data, the potential of -900mV (Ag/Ag/Cl) was chosen to be the most appropriate for the oxygen diffusion

study (i.e. the potential at which the current increase with potential is lowest). Tests were then conducted at that potential and constant speed to determine the variation of current over the scan cycle period. Figure 8.70 shows the evolution of current on both materials for the highest rotational speed of 1200rpm and it can be seen that the change in current at constant potential was significant. Over the 4 minute period when the speed is scanned and the current monitored, the increase in current due to the overpotential would be approximately 4% which must be considered in the overall accuracy of the model.

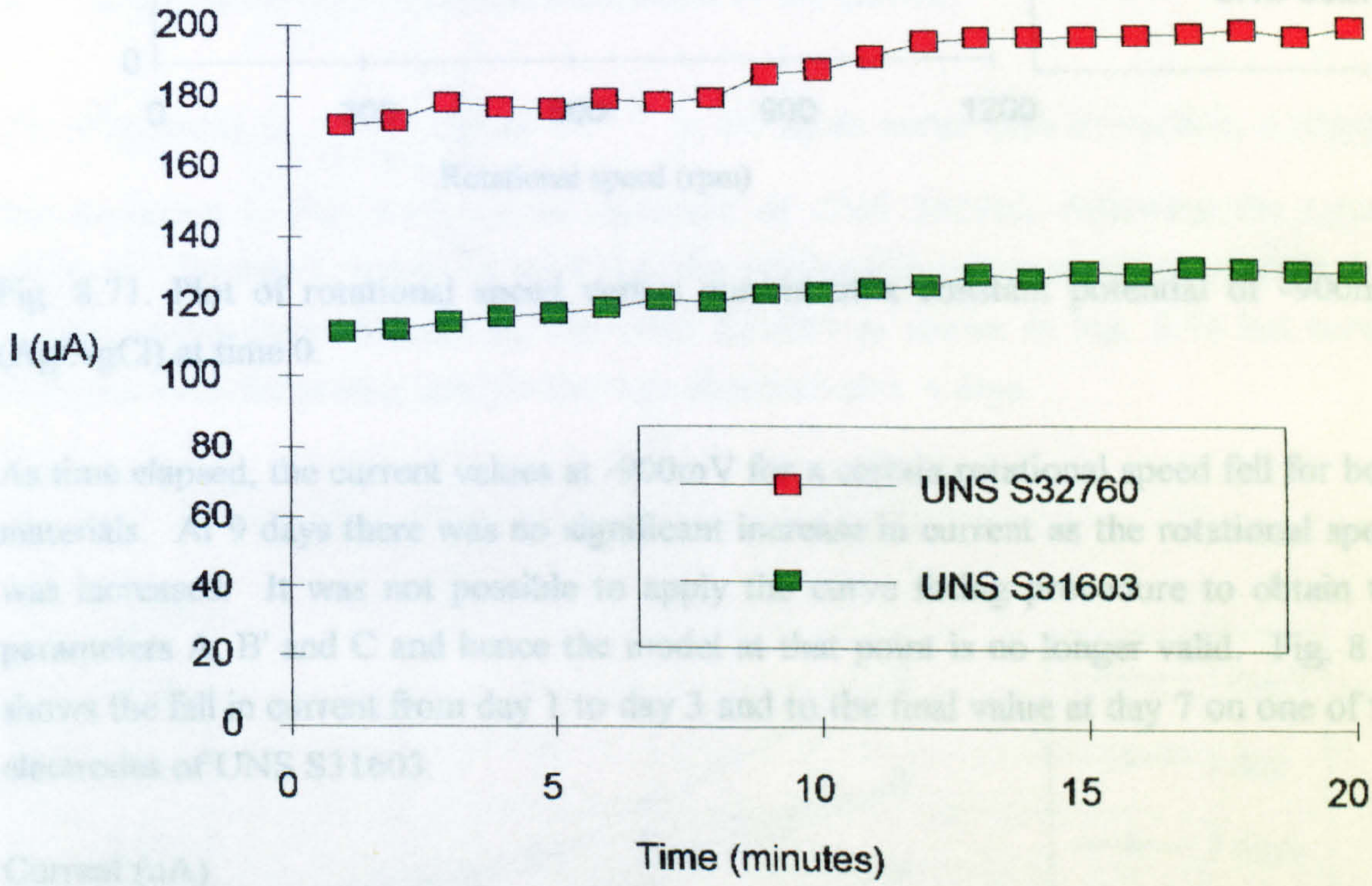

Fig. 8.70. Current increase at constant potential of -900mV (Ag/AgCl) and constant rotational speed.

On initial immersion, the scan of rotational velocity against current appeared as in Fig. 8.71 on UNS S31603 and UNS S32760. As can be seen, there is a significant scatter between the electrode response from electrodes of the same material. From this relationship, twelve values of current and their corresponding rotational velocity values were inserted into a curve fitting package which enabled the determination of the parameters A, B' and C from equation 8. Only three values are required for the fitting procedure and then the package checks whether the remaining experimental values fit well with the curve fit. If the experimental data does not fit well with the data for each point an error message invalidates the data set.

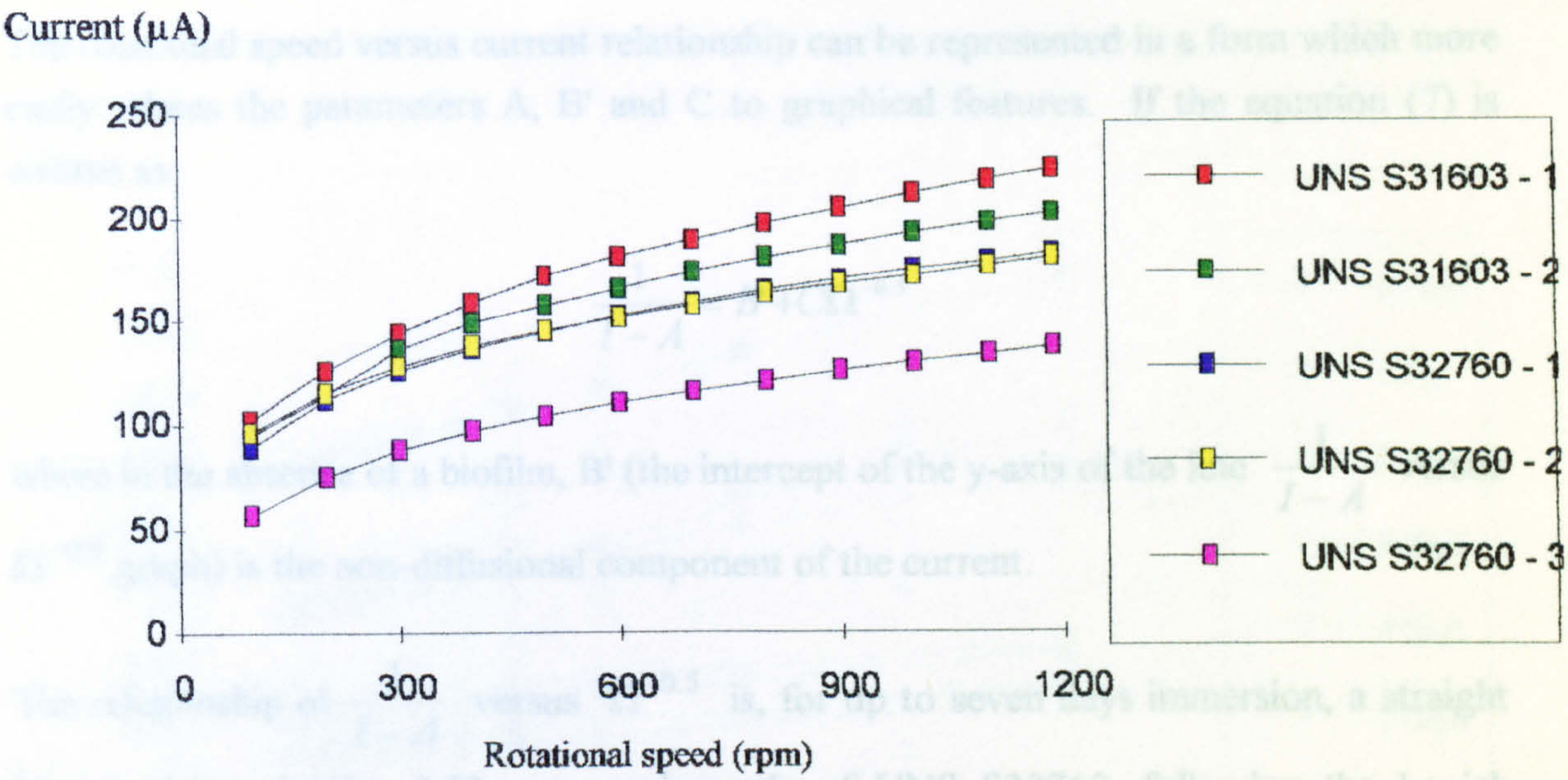

Fig. 8.71. Plot of rotational speed versus current at a constant potential of -900mV (Ag/AgCl) at time 0.

As time elapsed, the current values at -900mV for a certain rotational speed fell for both materials. At 9 days there was no significant increase in current as the rotational speed was increased. It was not possible to apply the curve fitting procedure to obtain the parameters A, B' and C and hence the model at that point is no longer valid. Fig. 8.72 shows the fall in current from day 1 to day 3 and to the final value at day 7 on one of the electrodes of UNS S31603.

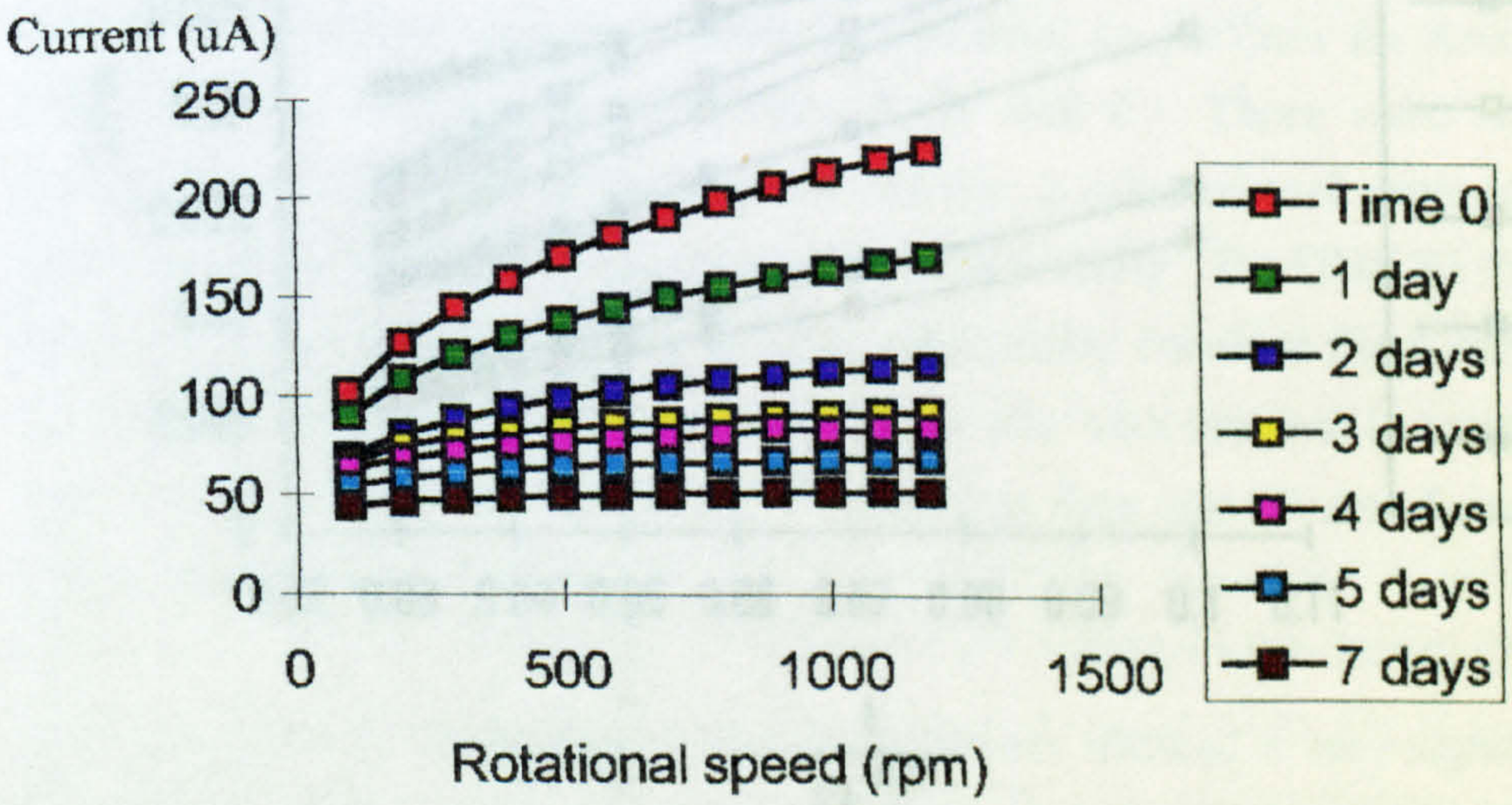

Fig. 8.72. Current decrease as time progresses on UNS S31603

The rotational speed versus current relationship can be represented in a form which more easily relates the parameters A, B' and C to graphical features. If the equation (7) is written as

$$\frac{1}{I-A} = B' + C\Omega^{-0.5}$$

where in the absence of a biofilm, B' (the intercept of the y-axis of the line $\frac{1}{I-A}$ versus $\Omega^{-0.5}$ graph) is the non-diffusional component of the current.

The relationship of $\frac{1}{I-A}$ versus $\Omega^{-0.5}$ is, for up to seven days immersion, a straight line as shown in Fig. 8.73, on an electrode of UNS S32760, following the Levich variation. On day 7, it can be seen that the relationship is not a perfect straight line. Similar results were obtained for the UNS S31603 as shown in Fig. 8.74 but here a deviation from the perfect straight line was observed after 4 days.

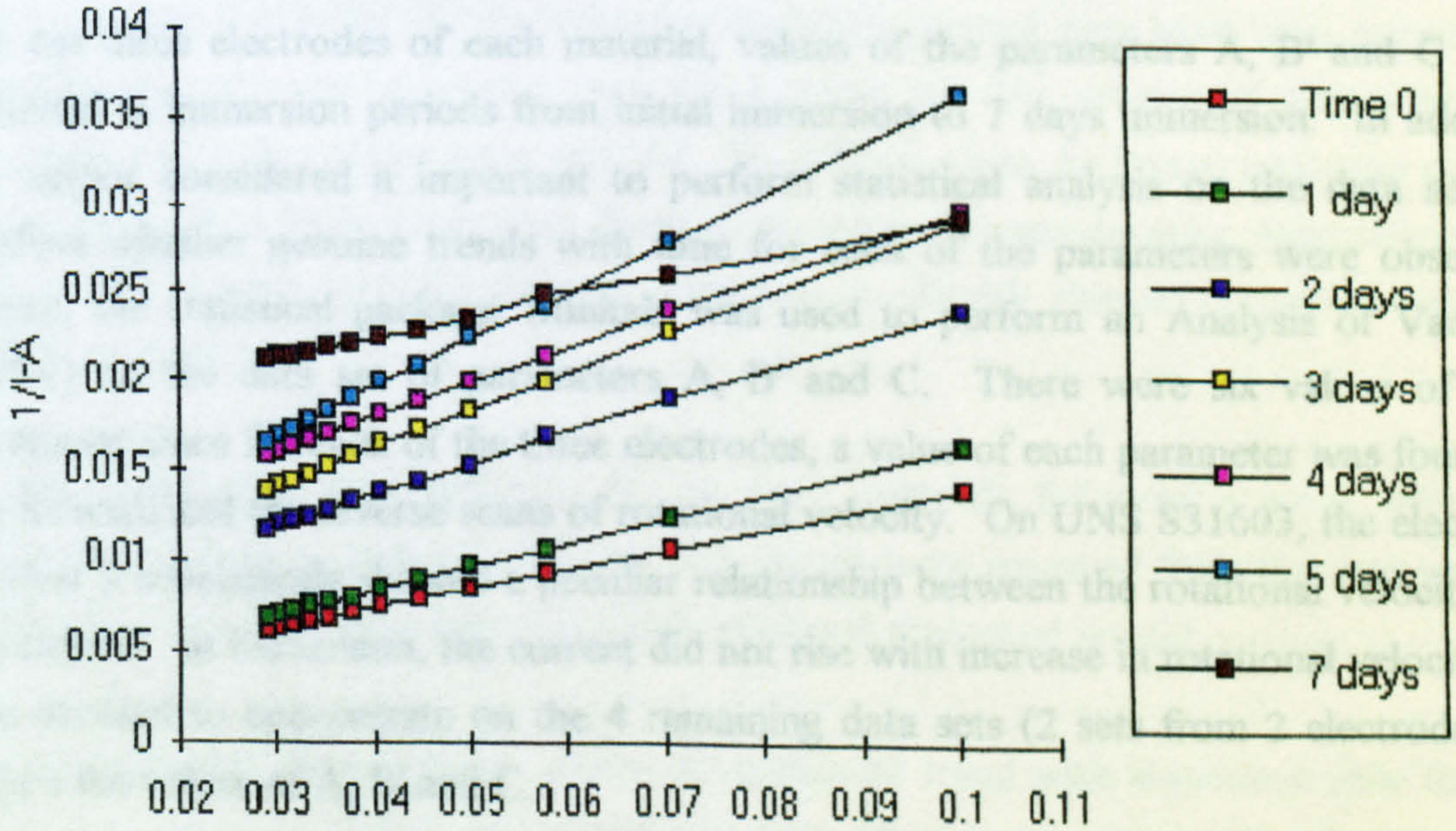

Fig. 8.73. Up to 7 days immersion on one UNS S32760 electrode

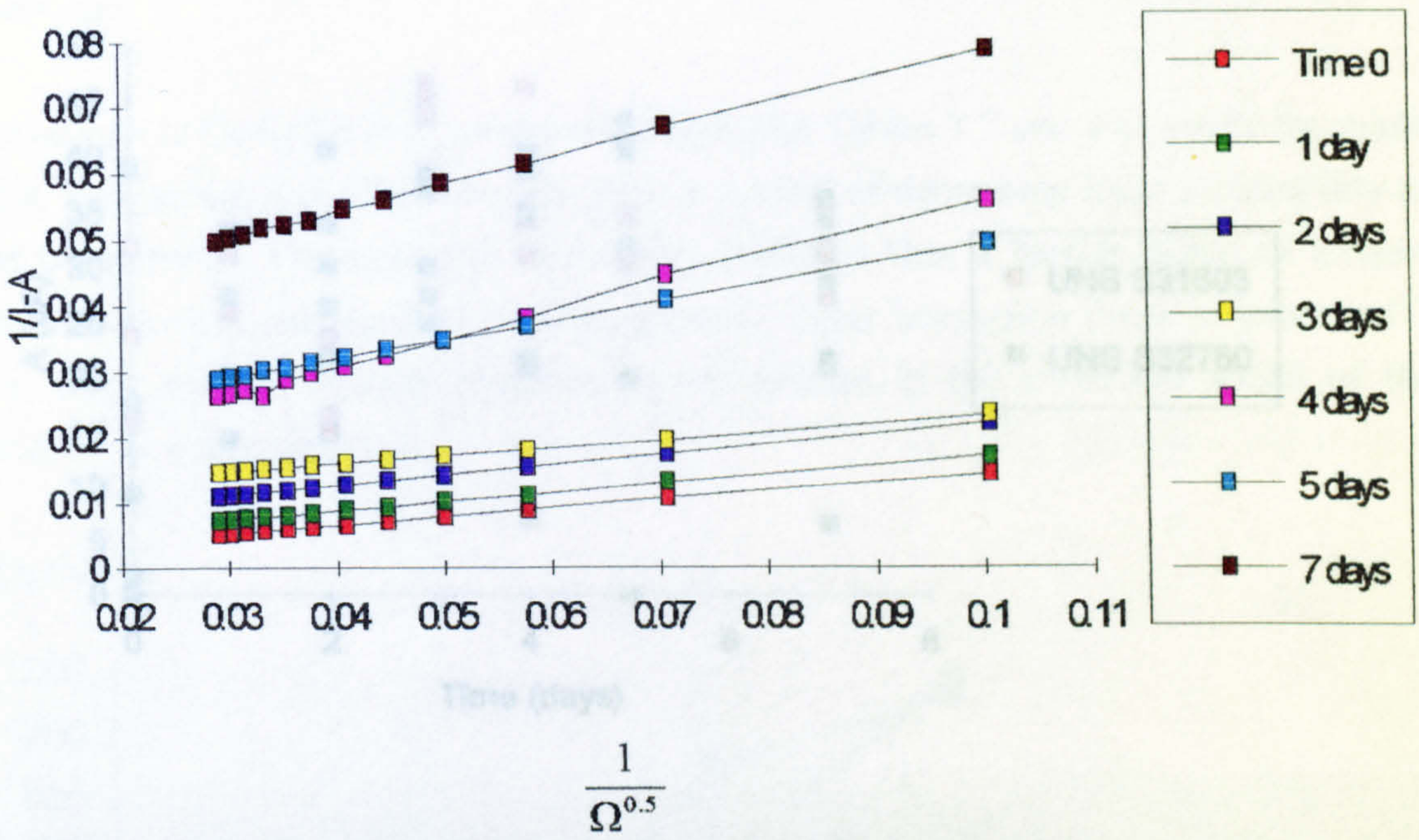

Fig. 8.74. Up to 7 days immersion on one electrode of UNS S31603

For the three electrodes of each material, values of the parameters A, B' and C were obtained at immersion periods from initial immersion to 7 days immersion. In addition the author considered it important to perform statistical analysis on the data set to confirm whether genuine trends with time for each of the parameters were observed. Hence, the statistical package 'Minitab' was used to perform an Analysis of Variance (AOV) on the data set of parameters A, B' and C. There were six values of each parameter since for each of the three electrodes, a value of each parameter was found on the forward and the reverse scans of rotational velocity. On UNS S31603, the electrode number 3 consistently showed a peculiar relationship between the rotational velocity and the current : at immersion, the current did not rise with increase in rotational velocity. It was decided to concentrate on the 4 remaining data sets (2 sets from 2 electrodes) to obtain the values of A, B' and C.

The parameter A, the hydrogen evolution current showed a very significant scatter. On UNS S32760, the scatter was more significant than on UNS S31603. For UNS S32760, the AOV results implied that the hydrogen evolution current could not conclusively be related to the immersion time and that no specific trend in evolution of A could be evaluated. The AOV was based on 95% confidence limits such that $p>0.05$ implied that

all data points were from the same population and no trend with time was detectable. The calculated values of A can be seen in Fig. 8.75.

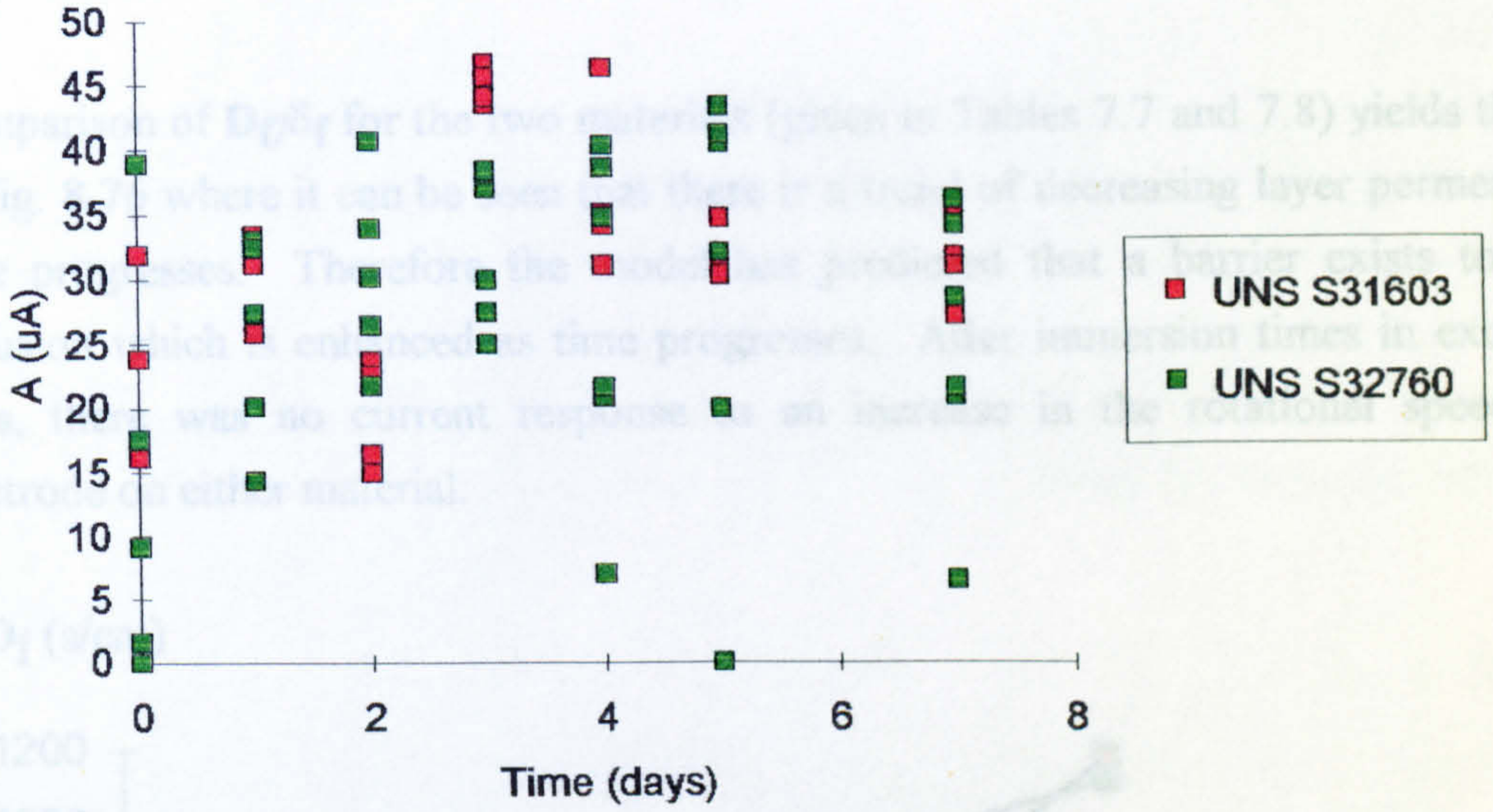

Fig 8.75. Values of parameter A for the two materials as a function of time

Although the parameter A, the hydrogen evolution current may have been expected to remain constant over immersion time, the concern was the amount of scatter between different electrodes of the same material. In addition, these hydrogen evolution currents could be up to 4 times larger than those measured in potentiodynamic polarisation tests. In potentiodynamic tests the currents registered at -900mV showed consistent values on different specimens.

It was found that the parameter B' on both materials followed a trend with time. However, it must be remembered that two values were removed from the data set from UNS S31603 which would have certainly rendered that trend invalid.

The parameter C was found to follow no particular trend with immersion time for both materials. This in itself is not unrealistic since there is no reason why the convective diffusion, of which C is a measure, should be dependent on the surface condition. However, previous work [30] used parameter C to calculate S from the Levich constant. This author regarded the factor D_f/δ_f (the layer permeability) to be indicative of any surface coverage effect in reducing the availability of reactive area. For this work therefore, the surface area for the seven day experiment was taken to be constant as the actual electrode area, $0.5cm^2$. In support of this, use of the determined value of C to calculate S at time 0 gave an initial active area of $0.35cm^2$ which is not possible since the

surface is assumed to be free from any biofilm. The use of an initial S of 0.5cm2 has implications on the value of the dissolved oxygen content and it was decided that the initial value be calculated from the Levich constant. This value was used throughout the experiment.

Comparison of $\mathbf{D_f/\delta_f}$ for the two materials (given in Tables 7.7 and 7.8) yields the graph in Fig. 8.76 where it can be seen that there is a trend of decreasing layer permeability as time progresses. Therefore the model has predicted that a barrier exists to oxygen diffusion which is enhanced as time progresses. After immersion times in excess of 7 days, there was no current response to an increase in the rotational speed of the electrode on either material.

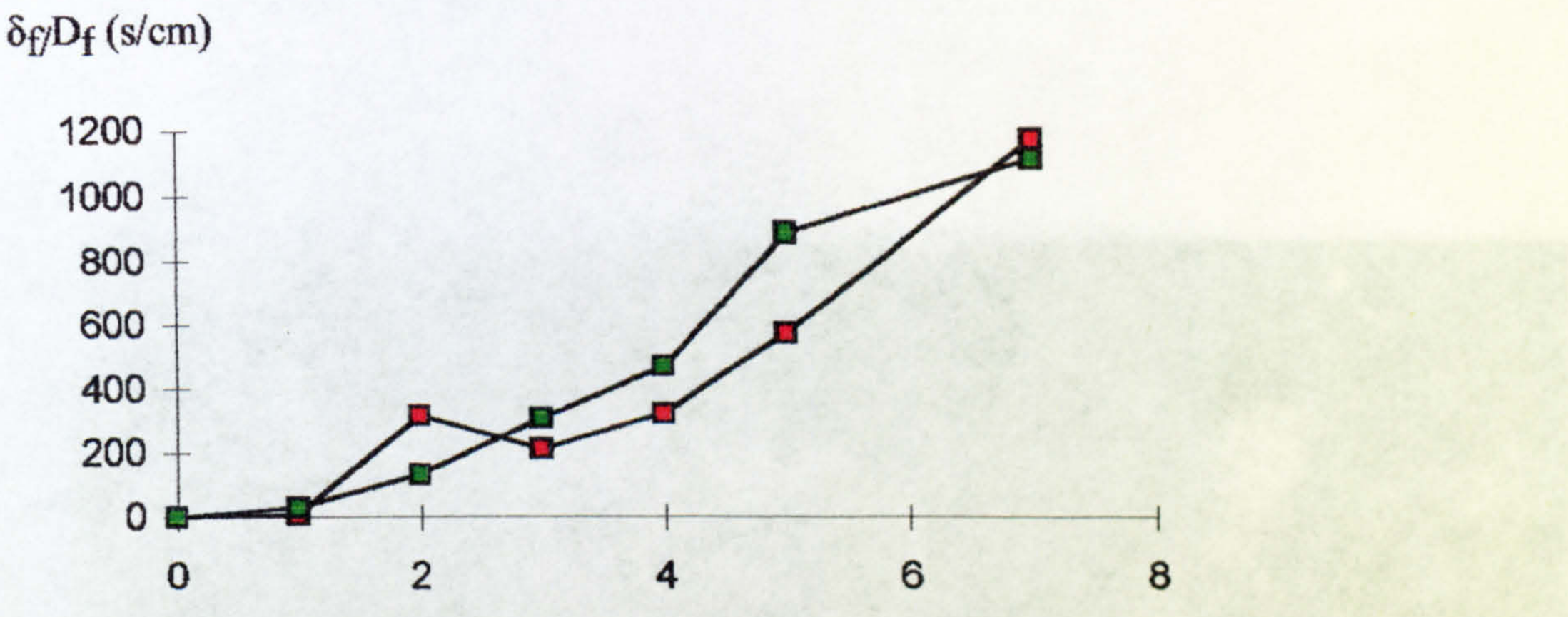

Fig. 8.76. Graph of inverse of layer permeability (δ_f/D_f) of the two materials as a function of time

In another experiment, continuing with the same electrodes of UNS S32760 after 9 days, they were immersed in the biocidal sodium hypochlorite to see if by killing any organisms on the surface, the current response would increase. After 24 hours in 500ppm $NaOCl^-$, there was still no current response. The electrodes were then cleaned ultrasonically for 15 minutes in distilled water, the result being still no increase in current. Finally, one of the electrodes was wiped clean with a soft cloth and this enabled the current to increase as the velocity increased. However the response did not reflect that observed after initial immersion but was instead intermediate between the 5 and 7 day response, indicating that the surface was not restored to it's initial, newly exposed state.

Visual Examination

The instinctive explanation for the reduced permeability, decreasing the availability of oxygen to the electrode surface, is the formation of a biofilm and indeed previous work has dwelled on that assumption. However on examination of the specimens of UNS S31603 (not included in final part of experiment involving ultrasonic bath and OCl^-), it was found that sporadic traces of a white deposit, which was confirmed to be rich in Ca, existed on the surface. Figure 8.77 shows the deposit and the associated trace from EPMA is shown in Fig. 8.78. It is postulated that the deposit is $CaCO_3$. Although in this region the deposit seems relatively dense, there was not a uniform covering on the surface as shown in Fig. 8.79.

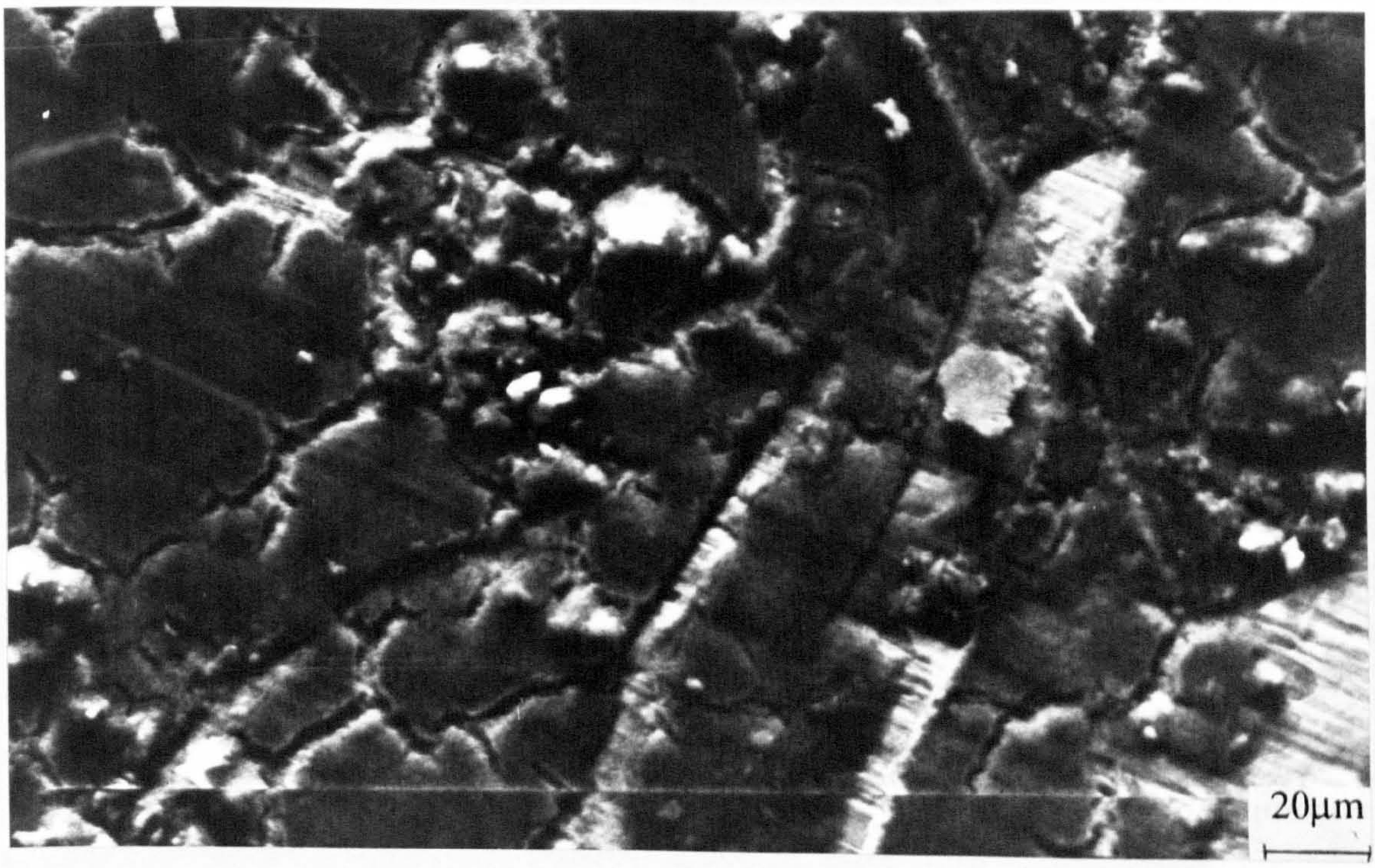

Fig. 8.77. Deposit on the surface of the electrode of UNS S31603 after 9 days in natural seawater and polarised to -900mV for approximately 40 minutes each day.

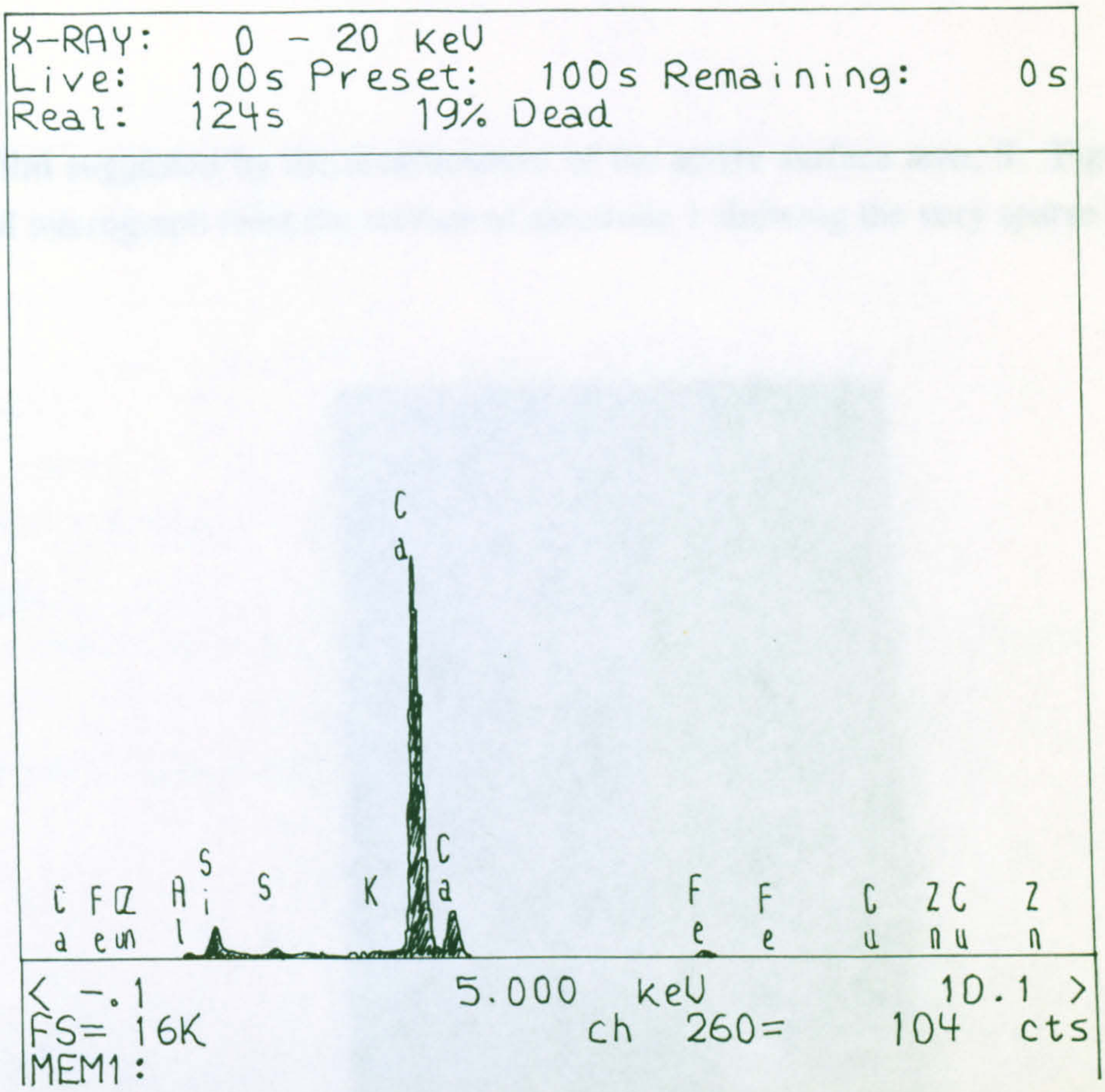

Fig. 8.78. EPMA trace showing the high Ca level in the deposit.

Fig. 8.79. Overall rotating disk electrode showing small areas of deposition

On the specimens of UNS S31603 which had not been immersed in NaOCl on the 9th day, there were signs of bacterial colonisation but there was not an evenly distributed biofilm. Comparison of the level of bacterial settlement with the specimens from the immersion tests in Part I suggested that in the experiments involving the rotating disk there was notably less settlement and indeed there was not the level of coverage by

biofilm suggested by the measurement of the active surface area, S. Figures 8.80 is an SEM micrograph from the surface of electrode 1 showing the very sparse biofilm.

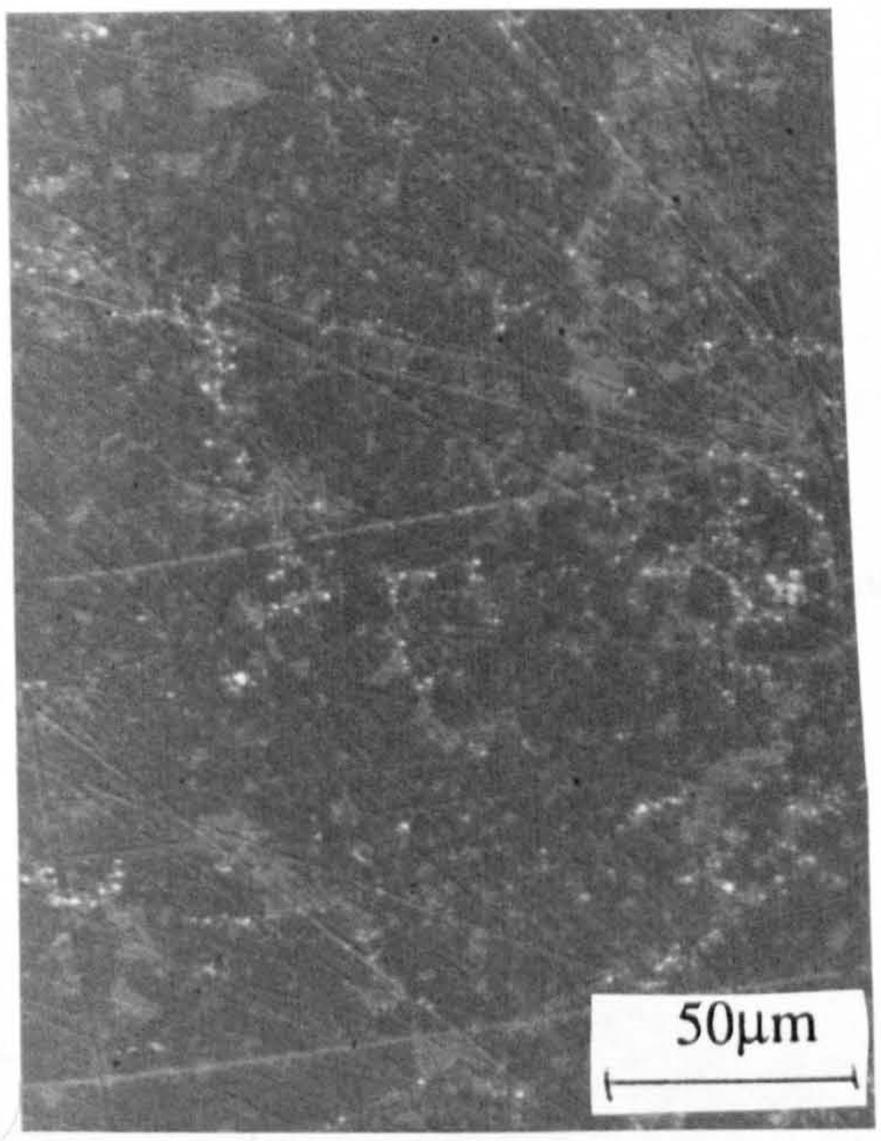

Fig. 8.80 Surface of the electrode showing very little biofilm

It should be pointed out that there is continual concern regarding the methods used for surface preparation for SEM analysis. It could therefore be implied that the very sparse biofilm is an artefact due to the preparation. In answer to this, it is stressed that the plate specimens and indeed all the Ifremer specimens were freeze dried and carbon coated using an identical procedure and as such the author is confident that the bulk of the surface would remain as it was removed from the environment.

	Light	**Dark**
E_o (mV)	-154	-154.4
t_{inc} (hour)	62	49.5, 71.5
dE/dt (mV/hour)	1.42, 3.43, 1.54	2.75, 5.1
E_{max}	150.9	128

Table 1.1. E_{corr} parameters for UNS S31603, starting 26th July

	Light	Dark
E_o (mV)	-150	-152
t_{inc} (hour)	60	72
dE/dt (mV/hour)	2.26, 6.26*	1.57, 2.94
E_{max}	158.3	124

* two results indicates two different slopes in increasing potential region

Table 8.2. E_{corr} parameters for UNS S31603, starting 3rd August

	Light	Dark
E_o (mV)	-146	-158
t_{inc} (hour)	46.5	81.5
dE/dt (mV/hour)	4.72	2.43
E_{max}	234	226

Table 8.3. E_{corr} parameters for UNS S31603, starting 23rd August

	Light	Dark
E_o (mV)	-209	-211
t_{inc} (hour)	54.5	88.5
dE/dt (mV/hour)	6.12	6.3
E_{max}	234	191

Table 8.4. E_{corr} parameters for UNS S32760, starting 30th August

	1 week	2 weeks	4 weeks	8 weeks
Light - anodic	21 pits minor crevice attack 2 diatoms	25-30 pits minor crevice attack 5-10 diatoms	>30 pits 15% crevice attack 10 diatoms	27-30 pits 70% crevice 10-15 diatoms
Dark - anodic	23 pits no crevice attack no diatoms	30 pits 15% crevice attack no diatoms	20-30 pits minor crevice attack <5 diatoms	57 pits minor crevice attack 10-15 diatoms
Light - cathodic	no pits no crevice attack no diatoms	no pits 50-60% crevice 5-6 diatoms	no pits minor crevice attack 5 diatoms	7 pits minor crevice attack <10 diatoms
Dark - cathodic	no pits no crevice attack no diatoms	no pits minor crevice attack no diatoms	no pits no crevice attack <5 diatoms	4-5 pits minor crevice attack <10 diatoms
Light - No Polarisation		0 pits severe crevice attack no diatoms	2-3 pits minor crevice attack <10 diatoms	4 pits 1mm crevice attack 10-15 diatoms
Dark - No Polarisation		0 pits no crevice attack no diatoms	0 pits minor crevice attack 2-3 diatoms	2 pits no crevice attack 12 diatoms

Table 8.5. Observations of corrosion attack and diatom settlement on UNS S31603, Type I specimens

	2 weeks	4 weeks	8 weeks
Light - anodic	no pits minor crevice attack 5-10 diatoms	no pits 5% crevice attack 10-15 diatoms	
Dark - anodic	1 pit minor crevice attack <5 diatoms	pit initiation minor crevice attack 10-15 diatoms	
Light - cathodic	0 pits no crevice attack <5 diatoms	0 pits no crevice attack 5-10 diatoms	
Dark - cathodic	0 pits no crevice attack <5 diatoms	0 pits no crevice attack 5-10 diatoms	
Light - No Polarisation	small etched area no crevice attack 5-10 diatoms	small etched area no crevice attack 5-10 diatoms	0 pits minor crevice attack 10-15 diatoms
Dark - No Polarisation	0 pits minor crevice attack 5-10 diatoms	0 pits minor crevice attack 5-10 diatoms	

Table 8.6. Observations of corrosion attack and diatom settlement on UNS S32760, Type I specimens

Time (days)	B' (μA^{-1})	B (μA^{-1}) no kinetic effects	C ($rpm^{0.5}(\mu A)^{-1}$)	δ_f/D_f (s/cm)
0	0.00312	0	0.1158	0
1	0.00332	0.0002	0.1214	6.7
2	0.01260	0.00948	0.3589	315
3	0.00949	0.00632	0.1807	210
4	0.01274	0.00962	0.2188	320
5	0.02041	0.01729	0.2161	575
7	0.03832	0.0352	0.2050	1171

Table 8.7. Evolution of the ratio δ_f/D_f (the inverse of the layer permeability) over the 7 days immersion - based on mean values of parameter B' - on UNS S32760 stainless steel.

Time (days)	B' (μA^{-1})	B (μA^{-1}) no kinetic effects	C ($rpm^{0.5}(\mu A)^{-1}$)	δ_f/D_f (s/cm)
0	0.001952	0	0.11319	0
1	0.002790	0.000838	0.12996	27.9
2	0.005887	0.003935	0.13799	130
3	0.011168	0.009216	0.19382	306
4	0.016070	0.014118	0.39358	469
5	0.028475	0.026523	0.24981	882
7	0.035315	0.033363	0.45517	1108

Table 8.8. Evolution of the ratio δ_f/D_f (the inverse of the layer permeability) over the 7 days immersion - based on mean values of parameter B' - on UNS S31603 stainless steel.

Discussion

E_{corr} and E_b ennoblement

There have been numerous reported incidences of ennoblement of E_{corr} on passive alloys in natural seawater. The exact mechanism by which the marine environment ennobles E_{corr} is not yet elucidated although there have been several attempts to explain the phenomena. In this work the ennoblement of E_{corr} was observed and in the following discussion an attempt will be made to correlate the trend in E_{corr} to other observations (electrochemical and microscopical).

The most widely accepted explanation of E_{corr} ennoblement is the depolarisation of the cathodic reaction by bacteria metabolism [16]. In this work, the cathodic reaction was investigated over the first 8 weeks of immersion at Ifremer. During this time it was found that the situation was not one of a simple depolarisation of the oxygen reduction cathodic reaction. In contrast a complex system of changes was observed. On initial immersion, the oxygen reduction reaction proceeded via Tafel kinetics to reach a limiting current. In contrast, after 1 week, 2 weeks and up to 8 weeks immersion, the reaction proceeded from E_{corr}, starting at a higher current, but was severely polarised until a potential was reached at which oxygen reduction proceeded following the same kinetics as on a newly immersed specimen. The changes observed in E_{corr} and in the cathodic polarisation curves were observed on specimens in which biofilm formation was very sparse. Although bacteria were observed, there was not a uniform covering. This perhaps suggests that as postulated by Johnsen and Bardel [15], the most important factor is a primary conditioning layer of organic macromolecules of thickness 80-100A which alter the surface properties. The so-called primary film has the very important property of being able to bind heavy metal ions which increases the exchange current density for oxygen reduction. In agreement with Johnsen and Bardel, in this work, the effect of immersion was to increase the current in the region near to E_{corr} and also to reduce the limiting current density in the diffusion controlled region. However, more importantly, the current did not increase significantly with increasing overvoltage indicating that the reaction from E_{corr} to the start of the Tafel oxygen reduction reaction was severely polarised. In addition, under potentiostatic control, at a potential where hydrogen evolution is not thermodynamically possible, no increase in the cathodic oxygen-reduction current was observed with time.

Hence an explanation for the severely polarised cathodic reaction from E_{corr} to a potential of approximately -200mV is required. Work by Compere et al. [21] has recently established that during immersion in natural seawater, an ageing effect is observed in the passive film on stainless steel which is manifested in an enrichment of Cr in the inner layer. Malik and Fozan [20] attributed the ennobled E_{corr} values to a healing or thickening of the passive film but Compere did not observe a change in film thickness. It is therefore possible that changes in the structure and composition of the passive film could reduce the transfer of charge across it and increase the overpotential required for oxygen reduction to proceed. Further evidence to relate the observed electrochemical behaviour to a passive film is obtained in Vetter [34] in which the cathodic reduction of the oxide layer (or chemisorption layer) is shown, during cathodic polarisation, as small currents in the region from E_{corr}. He also stated that the oxide layer thickens to a maximum stable value which is in accordance to the results obtained which show no further changes after the first week of immersion. In this respect, the comparison between cathodic polarisation in light and dark conditions is important. Increases in E_{corr} were recorded in dark conditions comparable with light conditions, albeit after a longer t_{inc} in dark conditions. It is therefore evident that photosynthetic organisms are not wholly responsible for the ennoblement and as such, the modification of the passive film may provide a viable explanation. This is in contrast to the findings of some other workers.

The theory postulated by Chandrasekaran and Dexter [18] requires the presence of H_2O_2, produced by a biofilm which is in turn used as a cathodic reactant in H_2O_2 reduction. The E^o in H_2O_2 reduction is more noble than O_2 reduction and can therefore induce an ennoblement of the free corrosion potential. The theory states that a synergistic effect between decrease in pH and H_2O_2 production exists to ennoble E_{corr}. On a bare and biofilmed platinum electrode Chandrasekaran and Dexter [18]. observed two Tafel regions, the first of which he postulated to be representative of H_2O_2 reduction and the second to the reduction of oxygen. Since in the biofilm, the concentration of H_2O_2 is limited, the reduction reaction quickly exhibits concentration polarisation. At a higher overpotential, the reduction of oxygen proceeds. This theory could be utilised to explain apparent polarised reaction near to E_{corr} since in this work, the presence of a mature biofilm was not verified via microscopy and it must therefore be assumed that the extent to which the pH under the biofilm is reduced and H_2O_2 is produced will be restricted. The steep current-potential relationship near to E_{corr} may therefore be due to concentration polarisation effects on the H_2O_2 reduction reaction, reflecting the rapid depletion of the cathodic reactant produced during sparse biofilm formation. The Tafel region is therefore representative of the oxygen reduction reaction

which proceeds until it becomes diffusion controlled, in agreement with Chandrasekaran [19]. The decrease in the limiting current density over the entire 8 week period, theoretically could be due partly to the reduced oxygen within the biofilm and also the increased diffusion barrier imposed by the settlement. However, in this case the biofilm was very sparse indicating a minimal effect on the diffusion. Hence other mechanisms are sought to explain this phenomenon.

If the progression of the cathodic reaction in natural seawater is dependent, in the region near to E_{corr} on the amount of H_2O_2 produced by the organisms within the biofilm, then it is difficult to envisage that in such a short time, there can be differences in the surface condition on two stainless steels which are illustrated by the larger cathodic currents consistently recorded on the UNS S31603.

The ennoblement of E_{corr} is therefore a complex phenomena, involving theories focused on the biological nature of the biofilm and also on the structure of the passive film. Indeed Mansfeld and Little in a recent publication implied that it is not possible to ascertain the cause of the ennoblement from E_{corr} data alone [23]. Often no account is taken of the anodic reaction and the mechanism by which it can affect the free corrosion potential. Scotto et al. [12] stated that the same passive currents were observed in natural and artificial seawater and as such the ennoblement is due to cathodic effects. Some evidence has been obtained in this work, in agreement with some other workers that in artificial seawater, E_{corr} ennoblement can occur and in this work, an ennoblement of lower magnitude than in natural seawater was observed on two stainless steels.

Effects on the passive region have been observed which could effectively shift E_{corr} in the positive direction. With reference to Fig. 8.15, there is an obvious steepening of the anodic polarisation curve in the region positive from E_{corr} to +600mV after the initial immersion. As time progresses, only minor changes are observed. The system of anodic and cathodic reactions determine the free corrosion potential of the electrode. It is mostly assumed that cathodic depolarisation ennobles E_{corr} but there is direct evidence here to suggest that polarisation of the anodic reaction in the passive region could contribute to the effect.

Consideration of the anodic reaction poses an additional question with regard to the small but sharp increase in current at approximately +600mV seen on all specimens after initial immersion.. It can be seen that initially, progression up to the passive current of 0.2μA is steady from E_{corr} but after the initial period, a different behaviour is

exhibited. The problem can be addressed from two different approaches: the biological effect of the biofilm and the modification of the passive film (which incidentally could be partly due to a biofilm). With relation to the proposed oxide film modification, it is suggested that the inner enrichment of Cr [21], reported after 1 week immersion, could form a more effective barrier to charge transfer and thus reduce the anodic current. On initial immersion the steady increase in current could be due to the establishment of the passive film. After initial immersion, no further change was observed in the passive characteristics in the potential region from E_{corr} to +400mV.

The anodic reaction at +400mV was postulated to be the evolution of oxygen which, at currents of 1.5μA suffers concentration polarisation. However, the magnitude of currents in the concentration polarisation region of oxygen evolution are sown to be an order of magnitude smaller than in the cathodic reduction of oxygen. This is perhaps indicative of the passive film, which is reduced on cathodic polarisation and therefore allows the passage of larger currents.

Study of the complete anodic polarisation curve on the superduplex stainless steel UNS S32760 and the austenitic stainless steel revealed that the breakdown potential progressively increased as a function of time. This is in agreement with the work of Compere et al., on stainless steel UNS S31603 [21]. Improved resistance to passivity breakdown, observed also on Type II specimens, on which crevice corrosion had initiated, suggests that during the immersion, the condition of the passive film has altered, by an ageing effect. However, once the material has been depassivated, it has been demonstrated that after longer immersion the pitting corrosion severity is enhanced, as illustrated by the higher I_{max} as time progresses. This finding contradicts the postulated theory that ennoblement of E_{corr} increases the risk of passivity breakdown by moving the potential nearer to the breakdown potential. What is clear is that on the less resistant material UNS S31603, there are sharp potential drops, followed by increases at a comparable rate, over the immersion period which can be correlated to the initiation of crevice corrosion. However, even after the 8 weeks immersion, the sites can quickly repassivate and via anodic polarisation, it is clear that the material overall passivity is not detrimentally affected. Mansfeld and Little [23] stated that the ennoblement of E_{corr} does not directly signify the enhanced susceptibility to localised corrosion and this has been shown here on the two materials.

It is evident that the crevice formed on specimens at the metal/resin interface is crucial in the stability of the free corrosion potential, since on specimens of Type II, ennoblement was observed but to a much lesser extent than on the Type I specimens and

this is attributed to the ability of the Type II specimens to initiate and sustain crevice corrosion.

Long Term Immersion

During immersion off the West coast of Scotland in the Clyde estuary, the characteristic free corrosion potential ennoblement was observed but as on Type II specimens at Ifremer, a steady E_{corr} value was not maintained. Again this was attributed to the facilitation of crevice corrosion which, as reported by previous authors leads to a much more negative E_{corr}.

The progression of the anodic polarisation curve after different immersion periods showed no detrimental effect on E_b up to 6 months immersion. At 6 months, there was a significant decrease in the E_b of UNS S31603, and after 18 months even the most resistant superaustenitic and superduplex alloys showed a decreased in E_b.

The most apparent effect, after 2 months immersion, on all alloys was the enhancement of anodic passive currents. The effect seemed to be accentuated if crevice corrosion, manifested in a very negative E_{corr} was recorded. These increased currents were postulated to be attributed to the occurrence of crevice corrosion : more specifically to the IR-drop within the crevice. After 6 months in natural seawater and in conjunction with the settlement of barnacles on the surface, further enhanced anodic currents were observed. It was after 18 months that during anodic polarisation, the high currents were followed by the production of black sulphide-containing corrosion products at the barnacle base and at the metal/resin interface.

An important finding has been the observation of black corrosion products underneath the rim of the barnacles on several of the materials in this study. Although there is a general feeling that conditions under barnacles might support SRB activity, very little direct evidence of this has been reported. High counts of SRB have been found under heavy marine fouling [31] and have been associated with the formation of sulphides under barnacles [33]. The presence of SRB itself is not indicative of the environment severity - the SRB must be in the active state and capable of producing toxic metabolic products : primarily H_2S. This study has identified that by anodically polarising the specimens, the formation of sulphide corrosion products occurs. Since analysis under barnacles on specimens which have not been subject to anodic polarisation, failed to yield traces of sulphur, it is therefore assumed that the anodic polarisation has some

direct or indirect mechanism of stimulating SRB. Two possible mechanisms are suggested. The first is that the production of small quantities of Fe^{2+} ions during the initial stages of anodic polarisation, facilitates the growth of the SRB culture due to the provision of an iron-based energy source. Further dissolution of metal enables the production of metal sulphide corrosion products. Alternatively, the SRB are already actively reducing the sulphate in the seawater and it is only by accelerating the production of metal ions by anodic polarisation that the formation of sulphides can occur. In this respect the anodic polarisation could act as an effective indicator for SRB activity under fouling encrustations.

Another significant (and hitherto unreported finding), is the formation of sulphide-containing corrosion products under the microscopic cell produced by the attachment of the byssus threads from mussels to the specimen surface. This observation is important to illustrate that even in circumstances where the surface is not heavily fouled, very local pockets of SRB can exist on the smallest scale. Comparing the laboratory simulation of SRB to the present situation in natural seawater, it is evident that there is no characteristic transient in current which is invariably observed in laboratory conditions. The distinction in natural seawater is that the cell consists essentially of an anaerobic anodic area and a larger aerated cathodic area [35]. In contrast, in the laboratory set-up, both the anodic and cathodic sites are anaerobic. As discussed in chapter 7, the presence of the current transient is associated with the effectiveness of FeS in stimulating cathodic activity. Since in these conditions the cathodic reaction will be the reduction of oxygen, since locally the potential will be more positive, there is not the scope for stimulated cathodic activity which would form the reduced current section on the anodic polarisation curve.

Hydrodynamic Study of the Biofilm

The use of the rotating disk electrode in studies under controlled hydrodynamics has been applied to the investigation of mass transfer characteristics in several contexts including erosion-corrosion studies. In this study the mass transfer of dissolved oxygen through a porous layer, representative of the biofilm formed on stainless steel was investigated. The theory defines a region - the diffusion plateau - where the mass transfer of oxygen is diffusion controlled and variation of the rotational speed enables the characteristics of mass transfer in the diffusion layer to be established. The Levich relationship [25] states that in a diffusion controlled reaction, the flux of current must be proportional to the square root of the rotational velocity.

As time progressed, the current at the constant potential (-900mV) decreased which was documented [27] to be due to the action of the porous layer in forming a diffusion barrier. On the three electrodes of each material, the variation of the current with rotational speed was significant but relatively, the current on each electrode decreased with time.

Since at time 0 there is no biofilm, the parameter B' is due only to kinetic factors. The assumption was made that over the experimental period, the non-diffusional component of current was constant. There is no clear evidence to suggest that this assumption is justified and indeed from other parts of this work it has been implied that the reaction kinetics of the cathodic reaction are dependent on the surface condition.

Using these assumptions, it was found that there is a trend of increasing (δ_f/D_f), perhaps signifying the enhancement of biofilm thickness. However, the detection of a deposit of $CaCO_3$ would strongly suggest that there is a very significant effect of this formation on the diffusional characteristics, and as such the layer permeability. This is substantiated by the finding that there was a very sparse settlement of micro-organisms.

The main objective of this study was to validate the rotating disk electrode techniques as a method for determining permeability of oxygen through the surface layer to the electrode surface. The experimental results in several aspects gave cause for concern, not least in the large degree of scatter which is in agreement with previous work on stainless steels. The result obtained on gold electrodes [27] have shown to be more consistent. It is suggested that the formation of $CaCO_3$ on the surface of the stainless steels could be avoided by the use of a new electrode for each day of immersion. However, this would not eradicate the wide scatter obtained even on initial immersion, when there would be no deposition of a biological or crystalline nature.

Conclusions

This study has shown that in natural seawater, ennoblement of E_{corr} can occur in the presence of a very sparse biofilm. Attempts have been made to elucidate the mechanisms by which this ennoblement occurs and more importantly what effect it has on the performance of materials with respect to localised corrosion. The main conclusions are: while it is accepted that there is some constituent in natural seawater which ennobles E_{corr}, the ennoblement was also observed to a lesser extent in artificial seawater. It is therefore concluded that the modification of the passive film has some effect, and a contributing factor to this modification could be the biological organism

presence. In relation to the observed electrochemical observations, it is concluded that ennoblement does not directly increase the susceptibility of the material to passivity breakdown and indeed the reverse was the case. Perhaps this points to a more effective passive film presence.

The theoretical model of biofilm diffusion characteristics is based on very well defined hydrodynamics and although the mass transfer characteristics on a bare electrode can be interpreted, it is more difficult on a non homogeneous surface. On stainless steel there is the additional complication of deposition of $CaCO_3$. The model must therefore be confirmed via examination and biological assays and to this aim the current study would not confidently confirm the results.

Long term exposure has shown the very important presence and activity of SRB under barnacles and at the crevices formed at the metal/resin interface, identified by performing anodic polarisation on specimens. Under free corrosion conditions, crevice attack at the barnacle/metal interface has been found. Perhaps most importantly, it has been shown that on a very small scale, the local activity of SRB, under the byssus of mussels can produce an electrochemical cell and the production of sulphides.

References

1. R. G. J. Edyvean, H. A. Video, Biofouling and MIC interactions in the marine environment : an overview, *Proceedings of the 2nd AFC workshop*, European federation of corrosion publications, No. 8.

2. J. W. Costerton, G. G. Geese, K. J. Cheng, How bacteria stick, *Sci. Am.* 238, 86, 1978.

3. A. Mollica, Biofilm and corrosion on active-passive alloys in seawater, *International Biodeterioration and Biodegradation*, 29, (1992), 213-219

4. W. G. Characklis, K. C. Marshall, Biofilms : a basis for an interdisciplinary approach, in *Biofilms*, Characklis and Marshall, Eds., Wiley-Internscience, New York, 1990, chap. 1

5. H. A. Videla, Biocorrosion of nonferrous metal surfaces, *in Biofouling and corrosion in industrial water systems*, Eds. Geesey, Lewandowski & Flemming, Lewis publishers, chap15.

6. Z. Lewandowski, Dissolved oxygen gradients near microbiologically colonized surfaces, in *Biofouling and corrosion in industrial water systems*, Eds. Geesey, Lewandowski & Flemming, Lewis publishers, chap 11

7. A. D. Woolmington, J. Davenport, pH and pO2 levels beneath marine macrofouling organisms, *J. Exp. Mar. Biol. Ecol.,* 1983, Vol. 66, p113-124

8. B. Wallen, Some factors affecting stainless steel corrosion in seawater, *Avesta Corrosion Management,* No. 9, 1990

9. P. Gallagher, R. E. Malpas, E. B. Shone, Corroson of stainless steels in natural, transported and artificial seawater, Brit. Corr. J., 1988, 4, 23

10. S. C. Dexter, H. J. Zhang, Effect of biofilms sunlight and salinity on corrosion potential and initiation, *Proceedings of the International Congress on Microbiologically*

Influenced Corrosion, Eds. N. J. Dowling, M. W. Mittleman, J. C. Danko, October 1990.

11. A. Mollica, A. Trevis, E. Traverso, G. Ventura, G. De. Carolis, R. Dellepiane, Cathodic performance of stainless steels in natural seawater as a function of microorganism settlement and temperature, *Corrosion*, Vol. 45, No. 1, January, 1989.

12. V. Scotto, R. Di. Cintio, G. Marcenaro, The influence of marine aerobic microbial film on stainless steel corrosion behaviour, *Corros. Sci.*, Vol. 25, No. 3., pp185-194, 1985.

13. A. Mollica, A. Trevis, E. Traverso, G. Ventura, V. Scotto, G. Alabiso, G. Marcenaro, U. Montini, G. De Carolis, Interaction between biofouling and oxygen-reduction rate on stainless steels in seawater, *Proc. 6th Int. Congress on marine Corrosion and Fouling*, p269-81, 1984

14. S. Motoda, Y. Suzuki, T. Shinohara, S. Tsujikawa, The effect of marine fouling on the ennoblement of electrode potential for stainless steels, *Corros. Sci.*, Vol. 31, pp515-520, 1990

15. R. Johnsen, E. Bardal, Cathodic properties of different stainless steels in natural seawater, *Corrosion*, Vol. 41, No. 5, May 1985

16. S. C. Dexter, G. Y. Gao, Effect of seawater biofilms on corrosion potential and oxygenreduction of stainless steel, *Corrosion*, Vol. 44, No. 10, October 1988

17. A. Mollica, G. Ventura, E. Traverso, On the mechanism of corrosion induced by biofilm growth on active-passive alloys in seawater, *Proceedings of the International Congress on Microbiologically Influenced Corrosion*, Eds. N. J. Dowling, M. W. Mittleman, J. C. Danko, October 1990.

18. P. Chandrasekaran, S. C. Dexter, Mechanism of potential ennoblement on passive metals by seawater biofilms, *CORROSION/93*, NACE, paper 493

19. P. Chandrasekaran, Factors affecting ennoblement of passive metals due to biofilms in seawater, *Presented at the 12th Int. Corrosion Congress*, Vol. 5B, NACE, 1993

20. A. U. Malik, S. A. Fozan, Localised corrosion of AISI 316L S.S. in Arabian Gulf seawater, *Proceedings of the World Conference on Desalination and Water Treatment*, Vol 1, Japan, November 1993

21. C. Compere, P. Jaffre, D. Festy, Ageing of 316L stainless steel in natural seawater. Statistical study of the relationship between open-circuit potential, exposure and pitting potential, *CORROSION/95*, NACE 1995

22. R. Holthe, E. Bardal, P.O. Gartland, Time dependence of cathodic properties of materials in seawater : stainless steel, titanium, platinum and 90/10 Cu/Ni, *Mat. Perf.*, June 1989

23. F. Mansfeld, B. Little, A technical review of electrochemical techniques applied to microbiologically influenced corrosion, *Corros. Sci.*, Vol. 32, No. 3, P247-272, 1991

24. S. Dexter, D. J. Duquette, O. W. Siebert, H. A. Videla, Use and limitations of electrochemical techniques for investigating microbiological corrosion, *Corrosion*, Vol. 47, No. 4, April 1991

25. V. G. Levich, *Physicochemical hydrodynamics*, Prentice Hall, Englewood Cliffs, NJ (1962)

26. C. Deslouis, B. Tribollet, M. Duprat, F. Moran, Transient mass transfer at a coated rotating disk electrode, *Journal of the Electrochemical Society*, Vol. 134, No. 10, October 1987

27. A. Ambari, B. Tribollet, C. Compere, D. Festy, E. L'Hostis, Detection and characterisation of biofilms in natural seawater by analysing oxygen diffusion under controlled hydrodynamic conditions, *Proc. 3rd European Federation of Corrosion Workshop on Microbial Corrosion*, Estoril, Portugal, 1993

28. D. Festy, F. Mazeas, M. E. Rhazi, B. Tribollet, Characterisation of the bio-film formed on a steel electrode in seawater by analysing the mass transport of oxygen, *Proceedings of the 12th International Corrosion Congress*, NACE, 1993, Houston, Texas

29. B. Tribollet, Etude de la reduction de l'oxygene dissous sur l'acier inoxydable en l'eau de mer a l'aide de l'impedance electrohydrodynamique (EHD), Contrat Universitaire, 91 2 34 24 24, Laboratoire de l'Universite Pierre et Marie Curie

30. B. Tribollet, C. Compere, F. Darrieux, D. Festy, Determination of biofilm on stainless steel in seawater as a function of seasons by analysing the mass transport of oxygen, *CORROSION/94*, NACE, Houston, 1994

31. F. L. Laque, Corrosion and Fouling, *Proc. 3rd Int. Congress on Marine Corrosion and Fouling*, Maryland USA, 1973, 2-13

32. M. Eashwer, G. Subramanian, P. Chandrasekaran, K. Bulkrishnam, Mechanism for barnacle induced crevice corrosion in stainless steels, *Corrosion*, Vol. 48, No. 7. 1992

33. A. Mollica, A. Trevis, E. Traverso, G. Venture, G. De Carolis, R. Dellepiane, *Corrosion*, Vol. 44, No. 4, 1987, p194

34. K. J. Vetter, *Electrochemical Kinetics*, Academic Press, 1967, London

35. B. Little, P. Wagner, F. Mansfeld, An overview of microbiologically influenced corrosion, Geochim. Acta., Vol. 37, No. 12, pp2185-2194, 1992

Chapter 9

The Effect of High Concentrations of Sodium Hypochlorite on the Corrosion Behaviour of High-Grade Alloys

Introduction

Marine fouling on engineering structures and components can cause severe operational problems such as reduced flow efficiency in seawater handling pipe networks, increased weight on oilfield structures and enhanced corrosion due to SRB proliferation and local acidification under fouling layers.

This work addresses an engineering application in which biocidal distribution systems are required to handle concentrations of the biocide, sodium hypochlorite, well in excess of the level required to effectively curb fouling. A series of tests has been performed in high levels of free chlorine (up to 600ppm) with the main objective of determining the behaviour the superduplex stainless steel, UNS S32760, and assessing it's suitability for the particular application. Parallel tests were conducted on lower grade duplex stainless steels and austenitic stainless steels.

Literature Review

Background

One of the first known uses of chlorine as a disinfectant was in the form of hypochlorite which, in 1850, was used to disinfect the Broad Street Pump water supply in London after an outbreak of cholera [1].

Today, seawater injection is used in secondary oil production systems to increase the recovery of oil by maintaining pressure and sweeping oil from injection wells to production wells. Oxygen is removed from the injection stream through vacuum degassing to reduce corrosion of carbon steel components [2]. However, this process increases the incidences of microbial corrosion by the sulphate-reducing bacteria. Ineffective biocidal control systems have been reported to increase the corrosion rate by a factor of ten times [3]. Although in this application the problematical organisms are the sulphate-reducing bacteria, biocide treatments are widely used in seawater applications to reduce the harmful effects of bacteria, the aim being to prevent surface colonisation by bacteria of all types and other biofouling species.

Sterilisation of waters by oxidising biocides such as free chlorine has been used for many years in industrial applications and are often used in conjunction with biocidal dosing of non-oxidising species such as gluteraldehyde or the quaternary ammonium compounds [2]. Chlorination can be achieved principally by one of two processes: electrochlorination and chlorine dosing. Electrochlorination involves the electrolysis of seawater to produce Cl_2 at the anode in an electrochemical cell and is used extensively in MSF desalination plants [4]. There has been much research into the process parameters for electrochlorination, namely, at what levels the Cl_2 should be maintained, whether the process should be continuous or intermittent and if intermittent, at what frequency should the chlorination be applied. Alternatively, addition of a biocide can be via compound containing the hypochlorite ion, normally sodium hypochlorite (NaOCl).

It has recently been reported [5] that, in the Trondeim fjord, Norway, a residual chlorine level of 0.1-0.2ppm is sufficient to reduce the microbial activity on a stainless steel surface to almost zero. Intermittent chlorination required 1ppm for 30 minutes each day to achieve the same effect. In Genua, a Mediterranean water, 0.1ppm was found to be sufficient [6] to completely control micro and macro fouling.

Chemistry of Chlorination

When chlorine dissolves in water, it hydrolyses rapidly, according to

$$Cl_2 + H_2O \rightarrow HOCl + H^+ + Cl^-$$

to form hypochlorous acid. Hypochlorous acid can then partially dissociate in water to form the hypochlorite ion as follows [1,2],

$$HOCl \rightarrow OCl^- + H^+$$

The principal chlorine containing species in chlorinated seawater is strongly dependent on the pH, TDS and the temperature. From the distribution curve in Fig. 9.1 (for 20°C in 0.6MCl^- solution), the proportion of each species can be determined at a given pH.

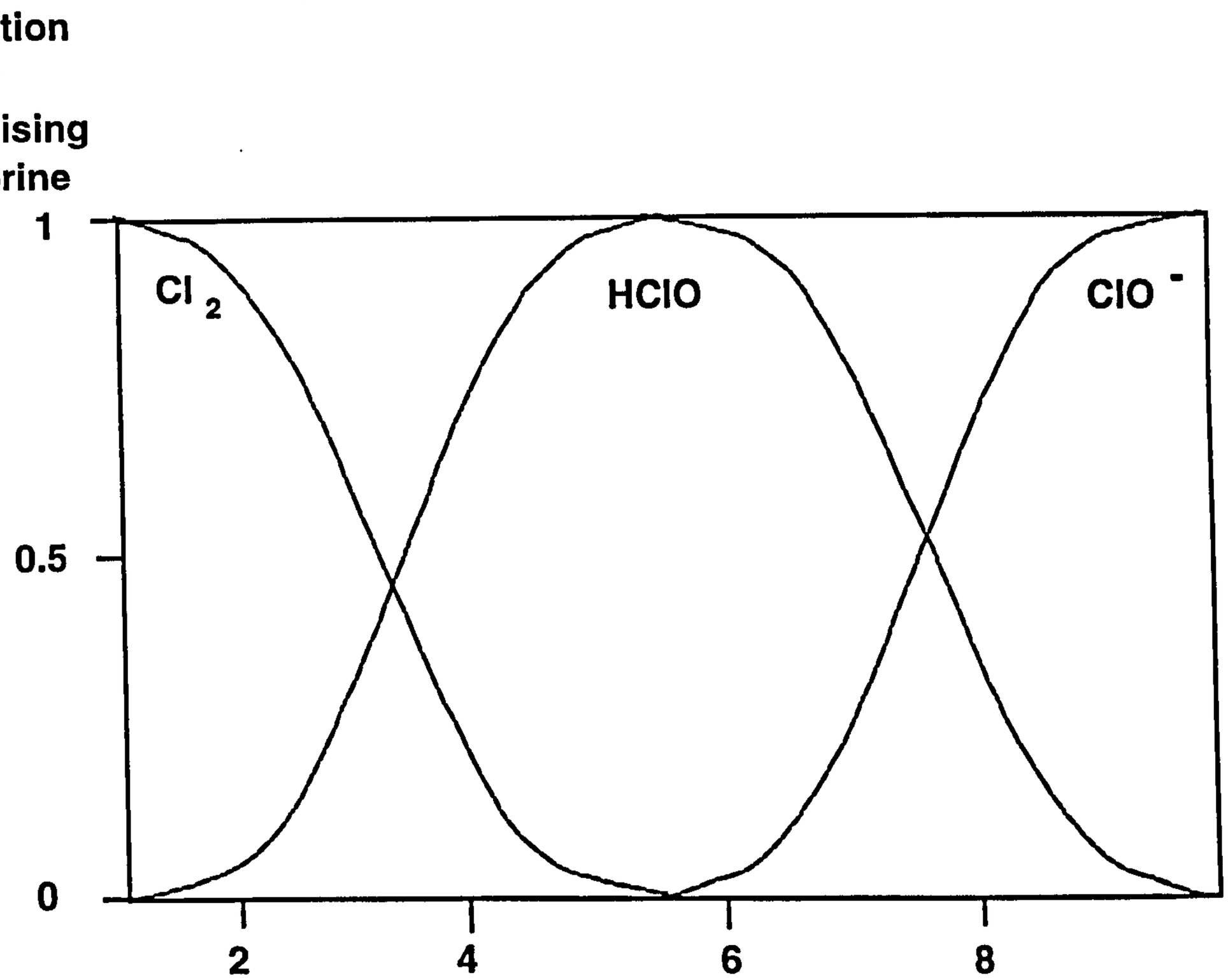

Fig. 9.1. Distribution curve for chlorine species as a function of pH.

Hypochlorous acid (HOCl) is the active agent in chlorinated solutions and is up to 80 times more biocidally active than the OCl^- ion due to it's ability to penetrate cell membranes [2]. In seawater of near neutral pH, it can be seen from Fig. 9.1 that the

prominent species are OCl- and HOCl and also the presence of Cl_2 to act as a biocide is negligible.

The presence of 70ppm bromide in natural seawater results in the reduction of Cl^- containing species and the oxidation of Br^- to hypobromous acid. The reaction goes almost to completion. Therefore in seawater systems at neutral pH, most of the residual halogen content is present as hypobromous acid and the hypobromite ion as represented in Fig. 9.2. In the presence of ammonia, the formation of chloro- and bromo-amines is promoted. Decomposition of these compounds to form hypobromous acid has been used to explain general corrosion on stainless steels [4]. Whether the active halide is Cl or Br from the point of view of this work is not crucial since the chemistry of Cl and Br is very similar [7].

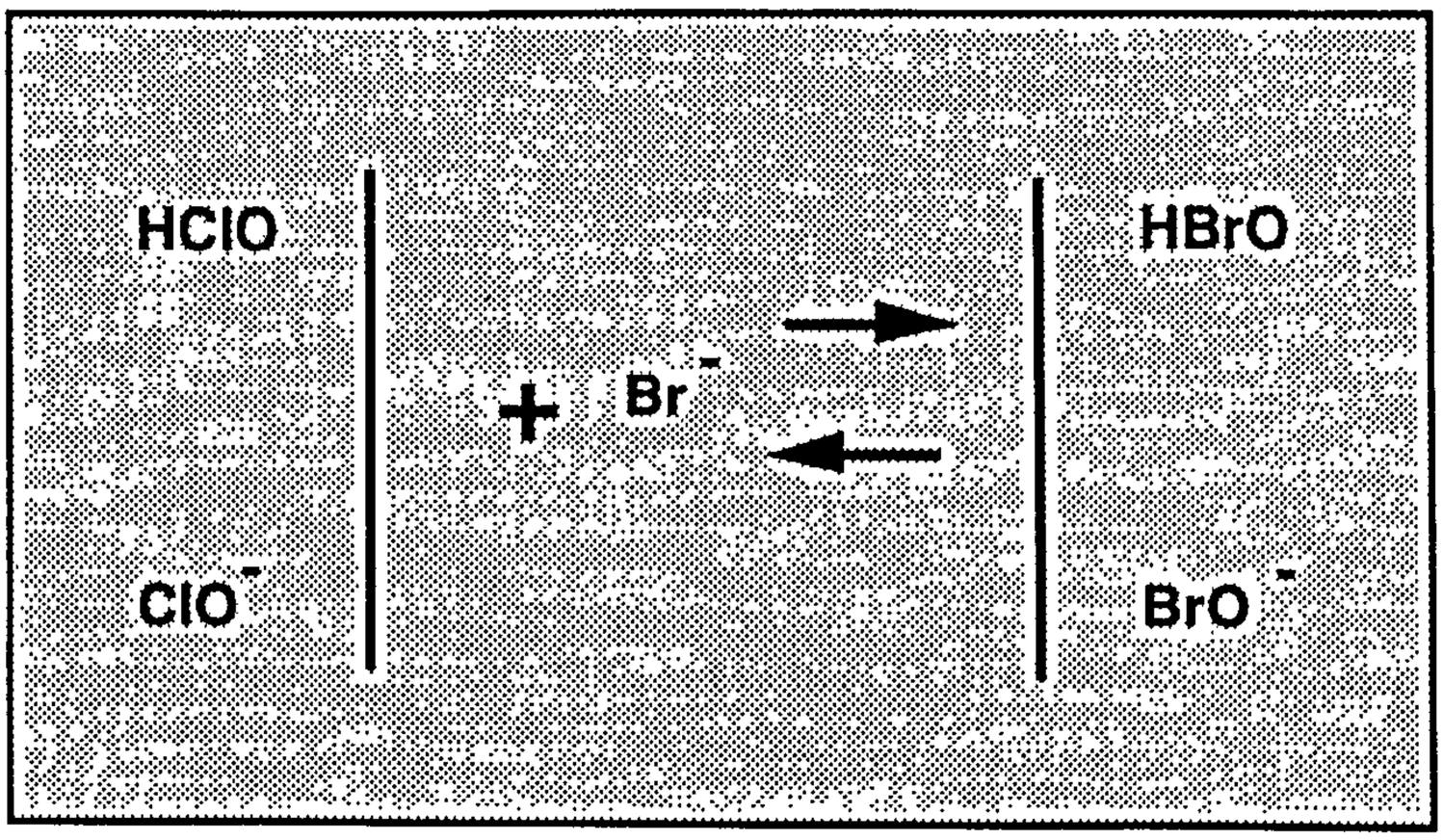

Fig. 9.2. Formation of bromine compounds in the presence of chlorine species in seawater.

Corrosion Considerations

Although chlorination, whether achieved by electrochlorination or by hypochlorite dosing, is an effective biocide, being a powerful oxidising agent, it can be responsible for corrosive attack of metals.

Chlorination of seawater in small concentrations has been shown by several authors [2, 5, 8] to push the free corrosion potential of passive alloys in the positive direction. Final potentials are considerably more positive than in unchlorinated seawater [5]. In chlorinated seawater there are alternative cathodic reactions to compete with oxygen reduction, all of which have significantly higher equilibrium electrode potentials [7] as represented below.

prominent species are OCl- and HOCl and also the presence of Cl_2 to act as a biocide is negligible.

The presence of 70ppm bromide in natural seawater results in the reduction of Cl^- containing species and the oxidation of Br^- to hypobromous acid. The reaction goes almost to completion. Therefore in seawater systems at neutral pH, most of the residual halogen content is present as hypobromous acid and the hypobromite ion as represented in Fig. 9.2. In the presence of ammonia, the formation of chloro- and bromo-amines is promoted. Decomposition of these compounds to form hypobromous acid has been used to explain general corrosion on stainless steels [4]. Whether the active halide is Cl or Br from the point of view of this work is not crucial since the chemistry of Cl and Br is very similar [7].

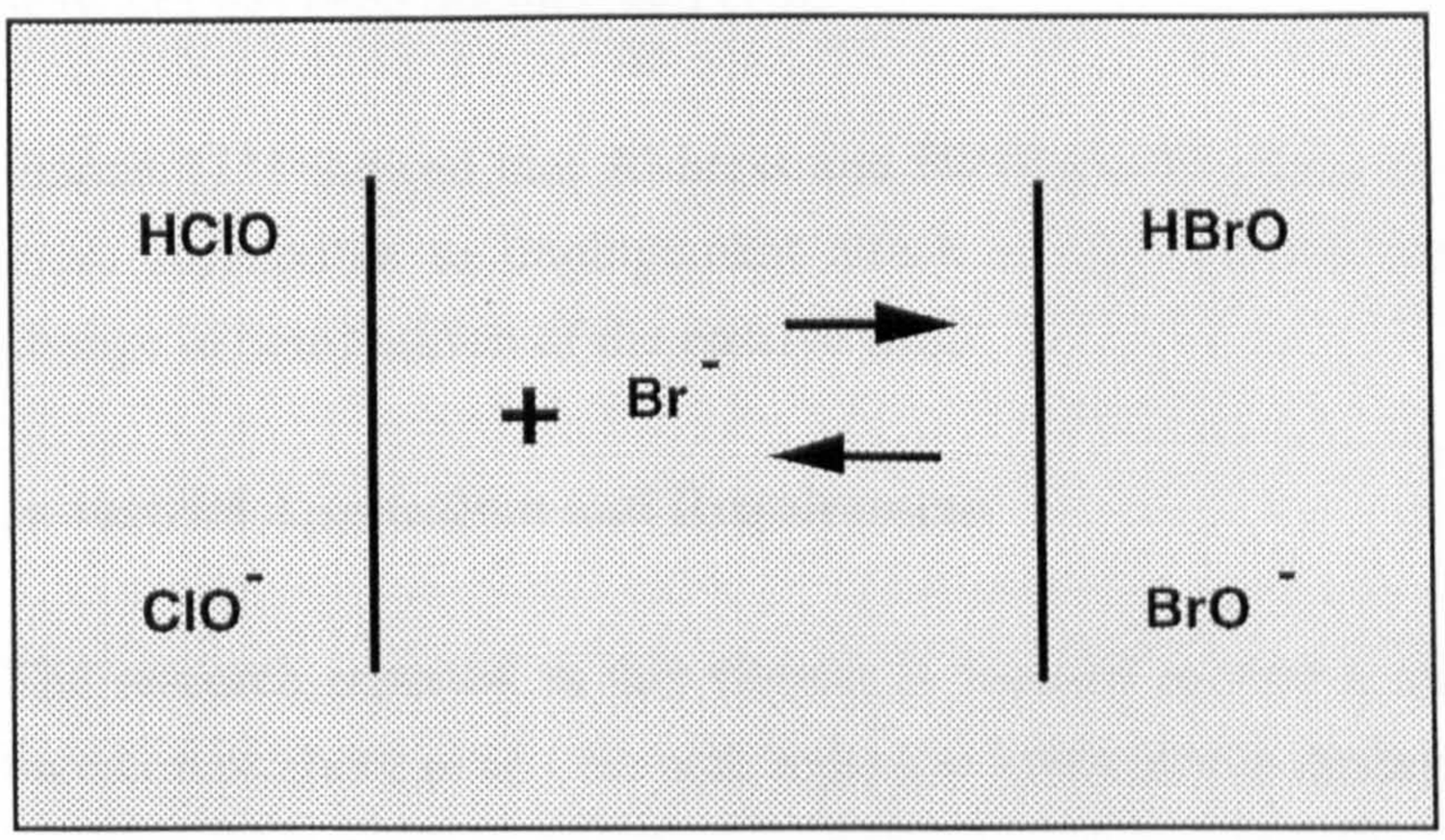

Fig. 9.2. Formation of bromine compounds in the presence of chlorine species in seawater.

Corrosion Considerations

Although chlorination, whether achieved by electrochlorination or by hypochlorite dosing, is an effective biocide, being a powerful oxidising agent, it can be responsible for corrosive attack of metals.

Chlorination of seawater in small concentrations has been shown by several authors [2, 5, 8] to push the free corrosion potential of passive alloys in the positive direction. Final potentials are considerably more positive than in unchlorinated seawater [5]. In chlorinated seawater there are alternative cathodic reactions to compete with oxygen reduction, all of which have significantly higher equilibrium electrode potentials [7] as represented below.

$$Cl_2 + 2e \rightarrow 2Cl^- \qquad E_0^0 = 1.395V$$

$$HClO + H^+ + 2e \rightarrow H_2O + Cl^- \qquad E_0^0 = 1.494V$$

$$ClO^- + 2H^+ + 2e \rightarrow 2OH^- + Cl^- \qquad E_0^0 = 1.715V$$

One author has suggested that higher anodic currents in chlorinated seawater contribute to the enhanced ennoblement [9]. Cathodic reactions in chlorinated seawater (reduction of OCl or Cl_2) produce Cl^- ions, the result of which can be a weakening of the passive film and enhanced localised corrosion. The susceptibility of even the highest grade superaustenitic stainless steels to crevice corrosion in chlorinated seawater has been documented [10].

Francis [11] showed that Al-brass and 90/10 Cu/Ni alloys in chlorinated seawater are more susceptible to impingement attack as the chlorine level increases due to the change in composition of the passive film.

Industrial Application and Requirement

The research reported in this chapter is focused around a material selection problem faced on offshore platforms with regard to hypochlorite dosing to control biofouling.

Seawater lift pumps are hung on the end of column pipes (2m length of flanged pipe of 8"-14" o/d). The pumps are positioned inside the caissons to protect them from damage and the fresh seawater reaches the pump via holes in the caisson, well below the water line. Fouling control is achieved by chlorination which involves taking some of the seawater from the discharge branch of the pump and feeding it through a bank of chlorination cells. The concentrated solution produced in this stage can range from 100mg/l and 1500mg/l chlorine at a temperature of 5-15°C.

The concentrated solution is then injected into the system via a pipe fastened to the inside of the caisson and terminating several metres below the pump mouth (in an attempt to dilute the solution before entering the pump).

It is for the hypochlorite pipe that a suitable material is sought. Because it is very long, the material must be very strong and easily attached to the caisson. Normally when such high levels of corrosive hypochlorite are involved, the materials used would be

titanium or plastics (e.g. GRP). However, in this application these are unsuitable since GRP is not mechanically strong enough and to obtain the required mechanical strength from titanium, thick walled piping would be required and hence the costs would be excessive. In the past, carbon steel has been used with a coating and a design allowance for corrosion. However, when the coating is locally ruptured (by the pump, for example, when it is raised and lowered for maintenance) severe problems of rapid metal dissolution can be encountered.

The requirement therefore is to assess the corrosion behaviour of the superduplex stainless steel (UNS S32760) in highly chlorinated seawater and perhaps establish the limitations on it's performance in terms of localised corrosion initiation and propagation.

Experimental Methods

A series of tests was conducted in static conditions and in flowing seawater, at 1.6m/s, containing different levels of free chlorine up to 600ppm. Free chlorine measurements were made using a Lovibond coulometric test kit.

The central part of the work was the assessment of the girth weld in a superduplex stainless steel pipe (manufactured by powder metallurgy) which was inserted into the flow loop, and it's free corrosion potential monitored over test periods of 35 days. The welding was carried out by the stainless steel manufacturer. PVC flanges were adhesively bonded to the pipe (Fig 9.3) and these were then bolted to the sections in the flow rig. After the 35 day test, the pipe was cut along it's axis and the welded area and the heat affected zone were examined for corrosion initiation. A sharp, hardened steel was used to probe the surface to reveal any sub-surface corrosion. Multiple crevice assembly specimens (MCAs) of UNS S31603, SAF 2205 and UNS S32760 were immersed in the reservoir tank in the flow loop and the free corrosion potential logged with time. The crevice washers which were in contact with both sides of the plate were made from polyacetal and consisted of 30 grooves and so on each sample there were 60 potential sites for crevice corrosion initiation. The washers were tightened to a constant torque of 10Nm. In addition, specimens of three duplex stainless steels (UNS S32760, SAF 2205, 25Cr duplex), two austenitic stainless steels (UNS S31603 and UNS S31254), Stellite 6 and Inconel 625 were immersed in the flow rig, flush with the pipe wall and with the flow parallel to the exposed face. Wires were attached to enable electrochemical monitoring and electrochemical polarisation tests were performed.

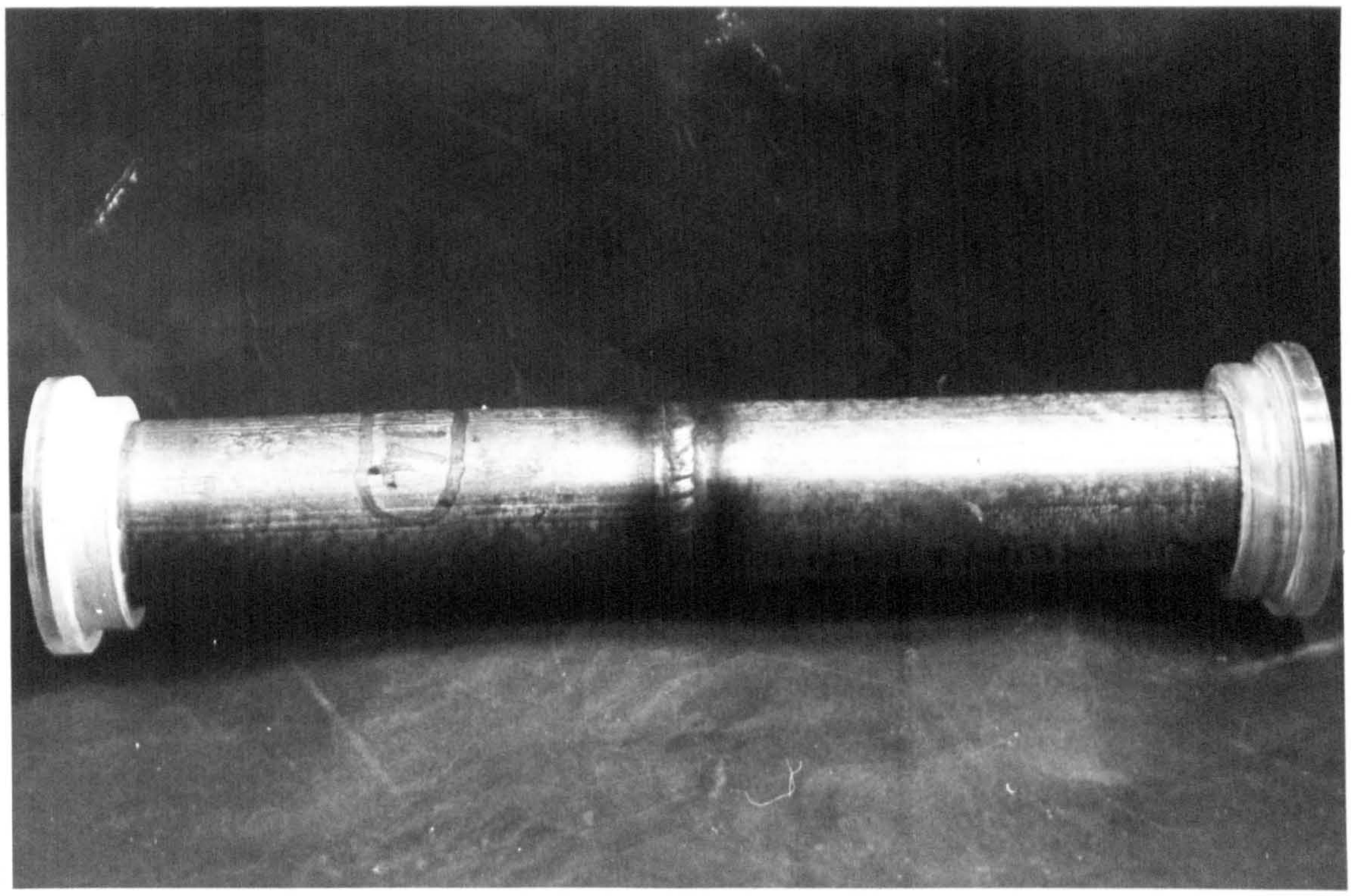

Fig. 9.3. Welded pipe and adhesively bonded flanges before insertion into the flow loop

The flow rig in Fig. 9.4 consisted of:

(a) a removable section into which the welded pipe could be inserted

(b) ports to accommodate metal coupons with electrical connections

(c) salt bridges to connect the reference electrodes

(d) feeder tank in which the MCAs were immersed.

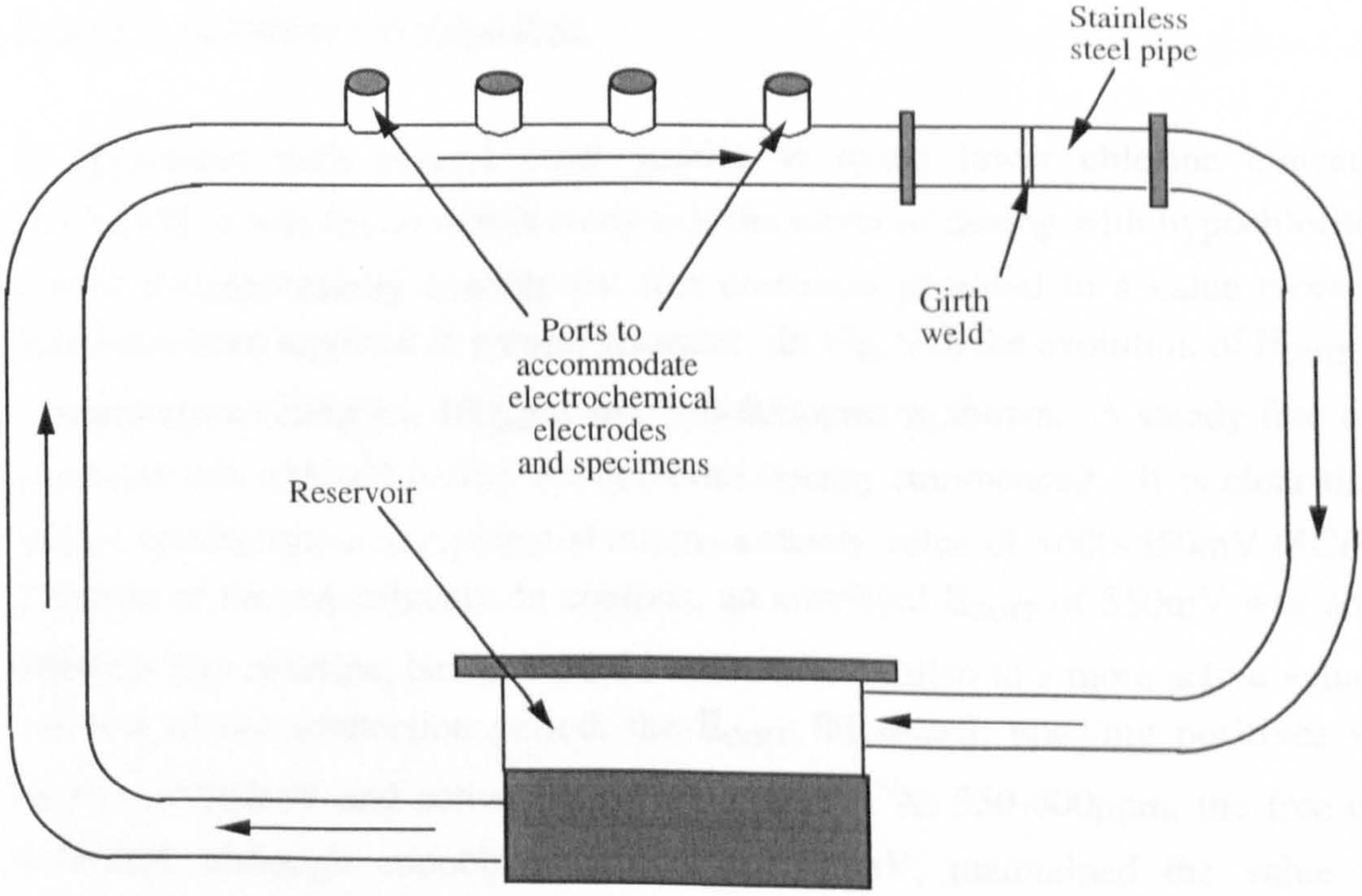

Fig. 9.4. Schematic representation of the flow loop

In static tests, samples were immersed in a sealed container containing a reference electrode (connected via a salt bridge) and an auxiliary electrode. Immersion tests followed by microscopy were performed with the free corrosion potential being followed over the immersion period. The anodic and cathodic polarisation characteristics were followed as a function of free chlorine concentration and of immersion time. Anodic polarisation tests were conducted in concentrations of 200ppm and 550-600ppm total available chlorine (as determined by the coulometric kit) after 4 hours immersion and after 50 days immersion. Cathodic polarisation tests were conducted after a four hour immersion period but only at the lower concentration of 200ppm free chlorine.

Anodic and cathodic polarisation tests were conducted under flow conditions after four hours in the low concentration of hypochlorite. For all polarisation tests in static conditions three replicate specimens were used whilst in flowing conditions duplicate experiments were performed. The crevice washer results are from consecutively run, duplicate experiments at each concentration. At 200ppm, two experiments were conducted on the pipe but at 400ppm and 550-600pm, only one 35 day test was run.

The pH was measured throughout the test period and was found to be relatively stable at 8.3-8.4. The temperature was below 16°C for all the entire test period.

Results

$\underline{E_{corr}}$ Ennoblement - Welded Pipe

In agreement with several other studies in much lower chlorine concentrations [10,12,13], it was found in this study that the effect of dosing with hypochlorite was to almost instantaneously ennoble the free corrosion potential to a value more positive than have been reported in natural seawater. In Fig. 9.5, the evolution of E_{corr} for each concentration (200ppm, 400ppm and 550-600ppm) is shown. A steady free corrosion potential was attained before hypochlorite dosing commenced. It is clear that at the lowest concentration, the potential attains a steady value of +600-650mV (SCE) for the duration of the experiment. In contrast, an ennobled E_{corr} of 550mV was attained in 400ppm free chlorine, but after 30-35 hours it had fallen to a more active value and for the rest of the immersion period, the E_{corr} fluctuated, reaching positives values in excess of 500mV and active values of -200mV. At 550-600ppm, the free corrosion potential, although ennobling initially to 500mV, maintained the value for only approximately 24 hours before a sharp fall in the potential was recorded. For the

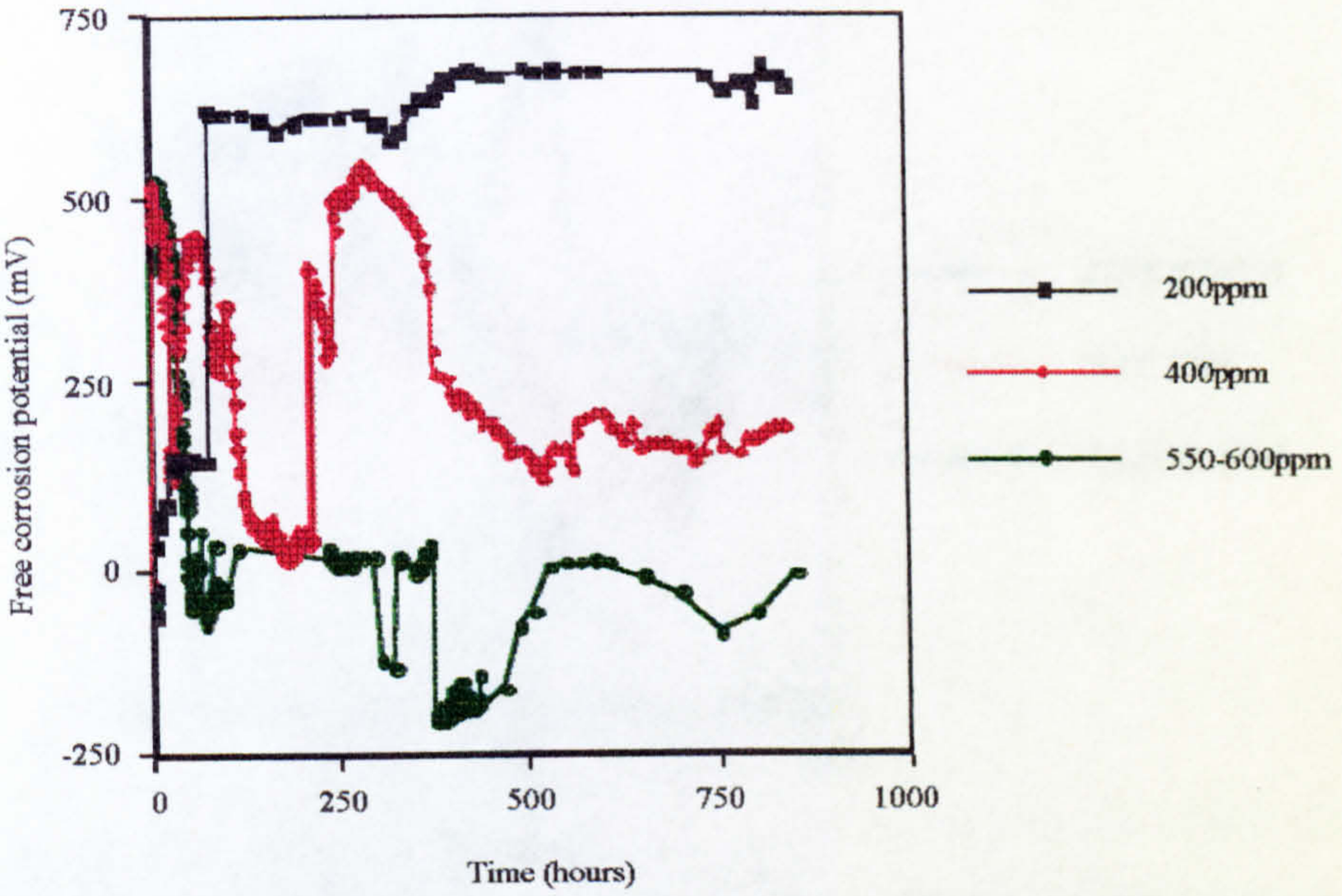

Fig. 9.5. E_{corr} evolution on the welded pipe (UNS S32760) at different concentrations of hypochlorite dosing

Multiple Crevice Assemblies (MCAs)

Ennoblement of E_{corr} on the MCAs was also recorded at 200ppm (Fig. 9.6) but the magnitude of the shift in E_{corr} was significantly less than on the welded pipe, although the starting potential of the UNS S32760 MCA was comparable with the pipe E_{corr}.

At 550-600ppm free chlorine, the only crevice assembly specimen to exhibit a positive free corrosion potential was the superduplex UNS S32760. As shown in Fig. 9.7, the other two materials showed an ennoblement but only of 100-200mV.

Specimens for Electrochemical Monitoring

The specimens embedded in resin with wires attached, for anodic and cathodic polarisation, displayed very similar trends in E_{corr} to the MCAs. Ennoblement of the E_{corr} of the superaustenitic UNS S31254, 25Cr duplex, Stellite 6 and Inconel 625 was also observed at the two concentrations as shown for UNS S31254 in Fig. 9.8 and tabulated for the other materials in Table 9.1. It was shown consistently at both concentrations that the degree of ennoblement of E_{corr} was greater on the Stellite 6 (Co-base) and Inconel 625 (Ni-base) alloys

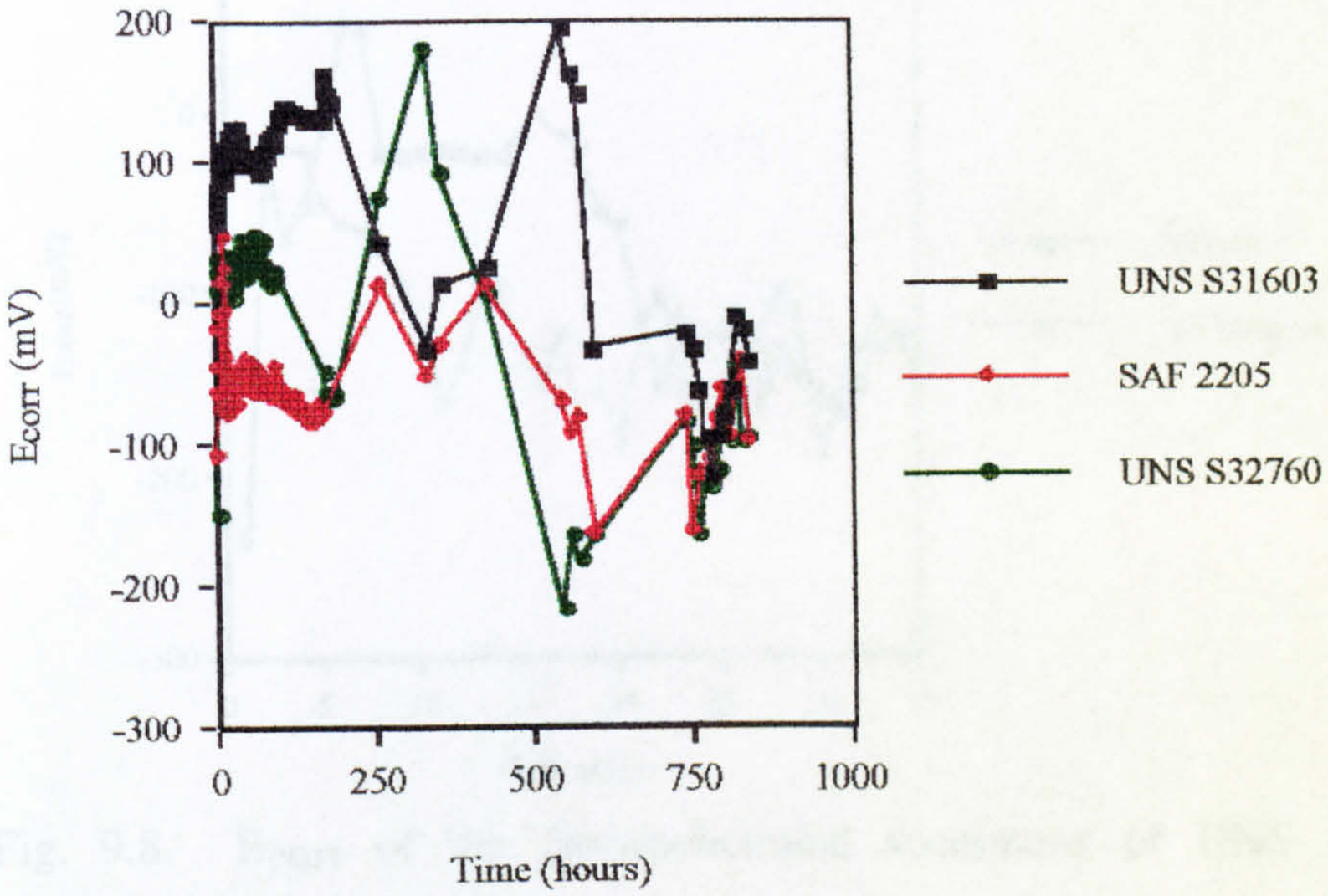

Fig. 9.6. E_{corr} of the MCAs at the lowest concentration of free chlorine (200ppm)

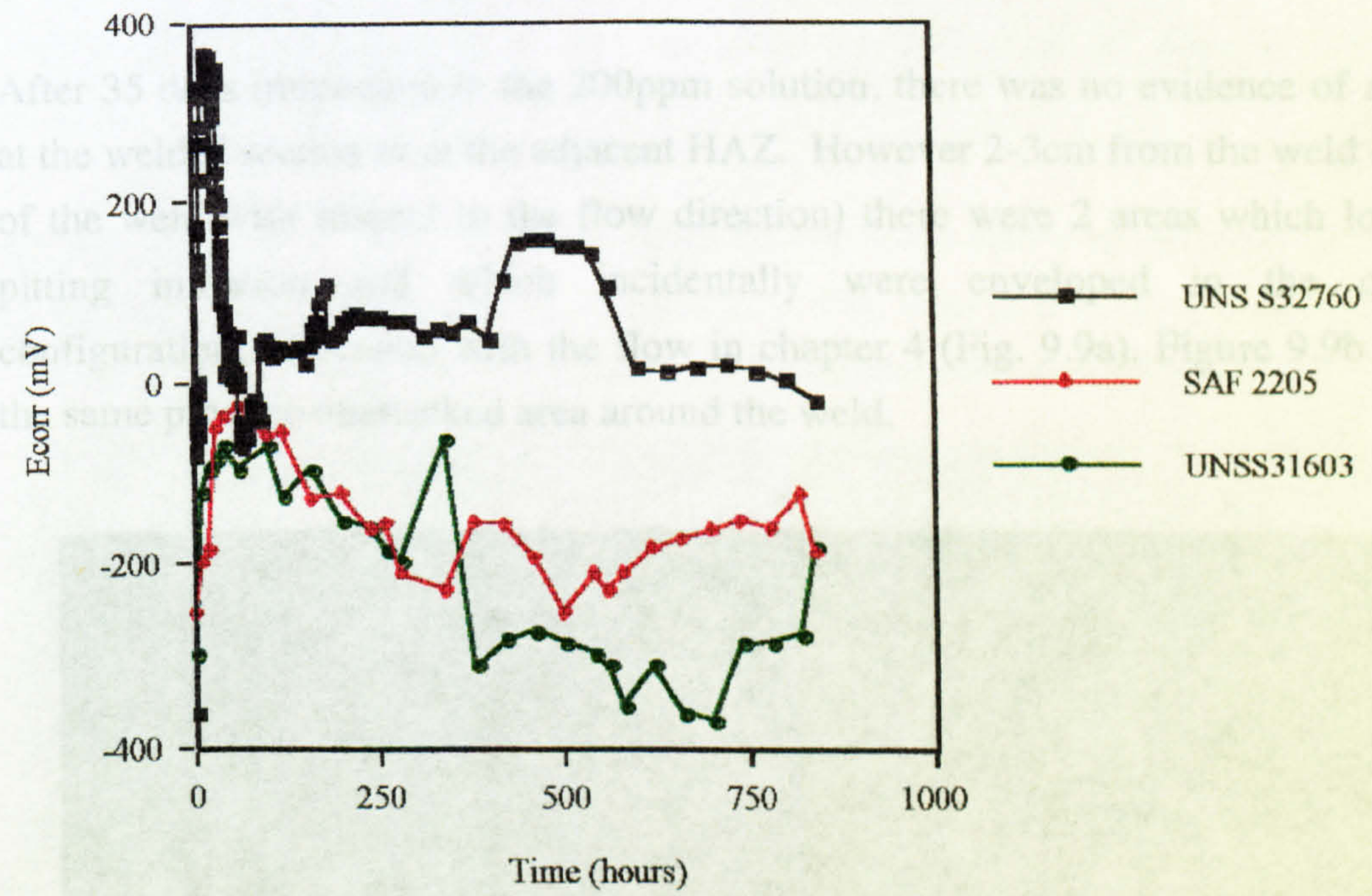

Fig. 9.7. E_{corr} of the MCAs at the higher concentration of free chlorine (550-600ppm)

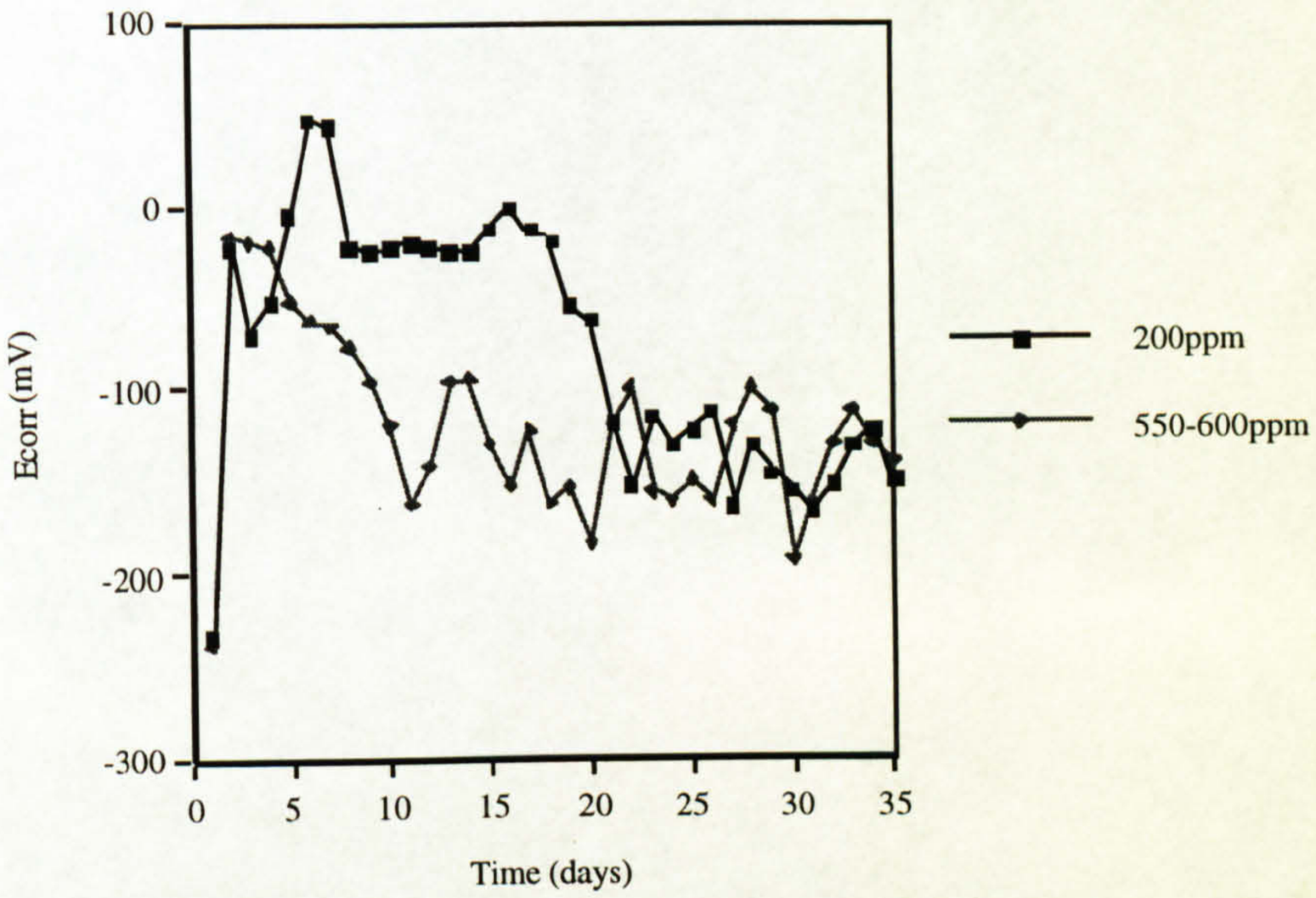

Fig. 9.8. E_{corr} of the electrochemical specimens of UNS S31254 at the two concentrations of free chlorine.

Attack Mechanisms - Welded Pipe

After 35 days immersion in the 200ppm solution, there was no evidence of any attack at the welded section or at the adjacent HAZ. However 2-3cm from the weld (upstream of the weld with respect to the flow direction) there were 2 areas which looked like pitting initiation and which incidentally were enveloped in the comet-like configuration, associated with the flow in chapter 4 (Fig. 9.9a). Figure 9.9b shows on the same pipe the unattacked area around the weld.

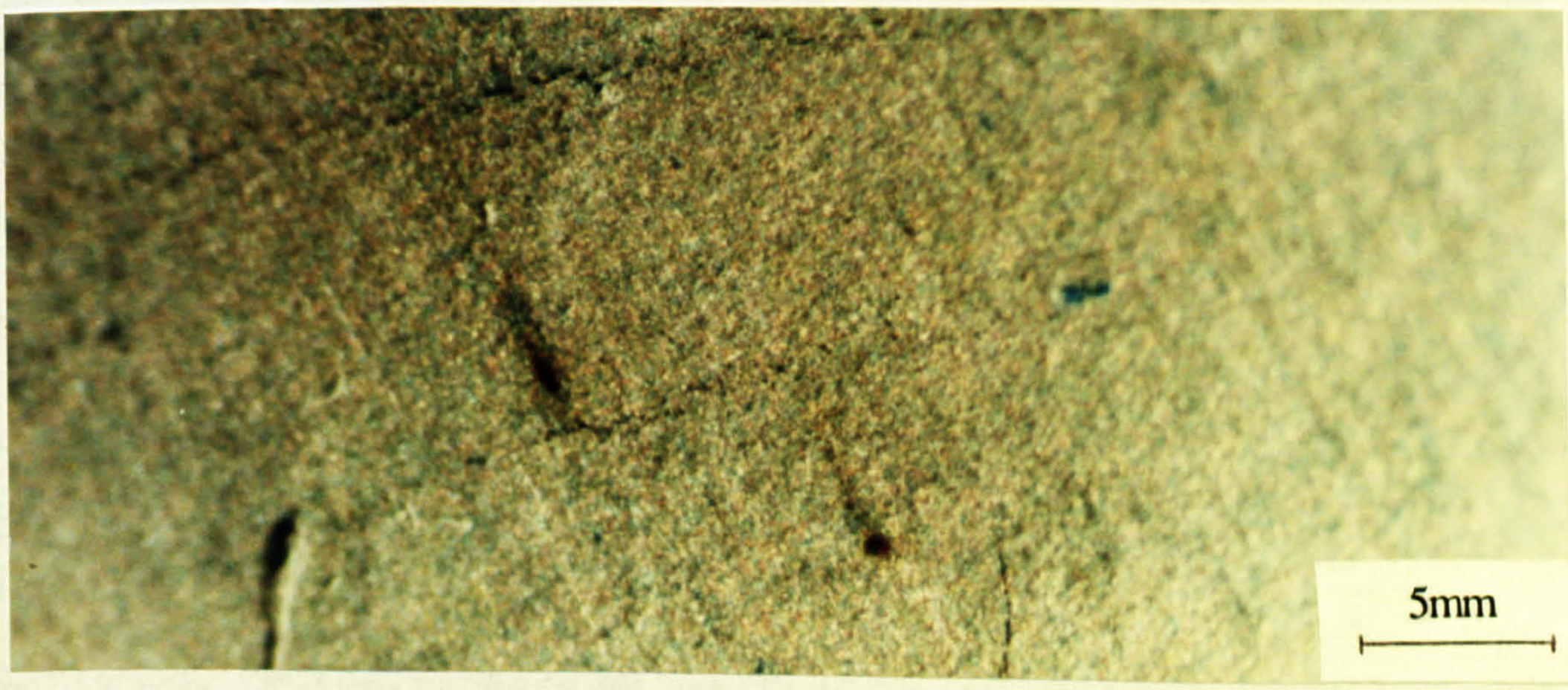

Fig. 9.9a. Suspected pit initiation away from the weld on the pipe in 200ppm free chlorine flow at 1.6m/s

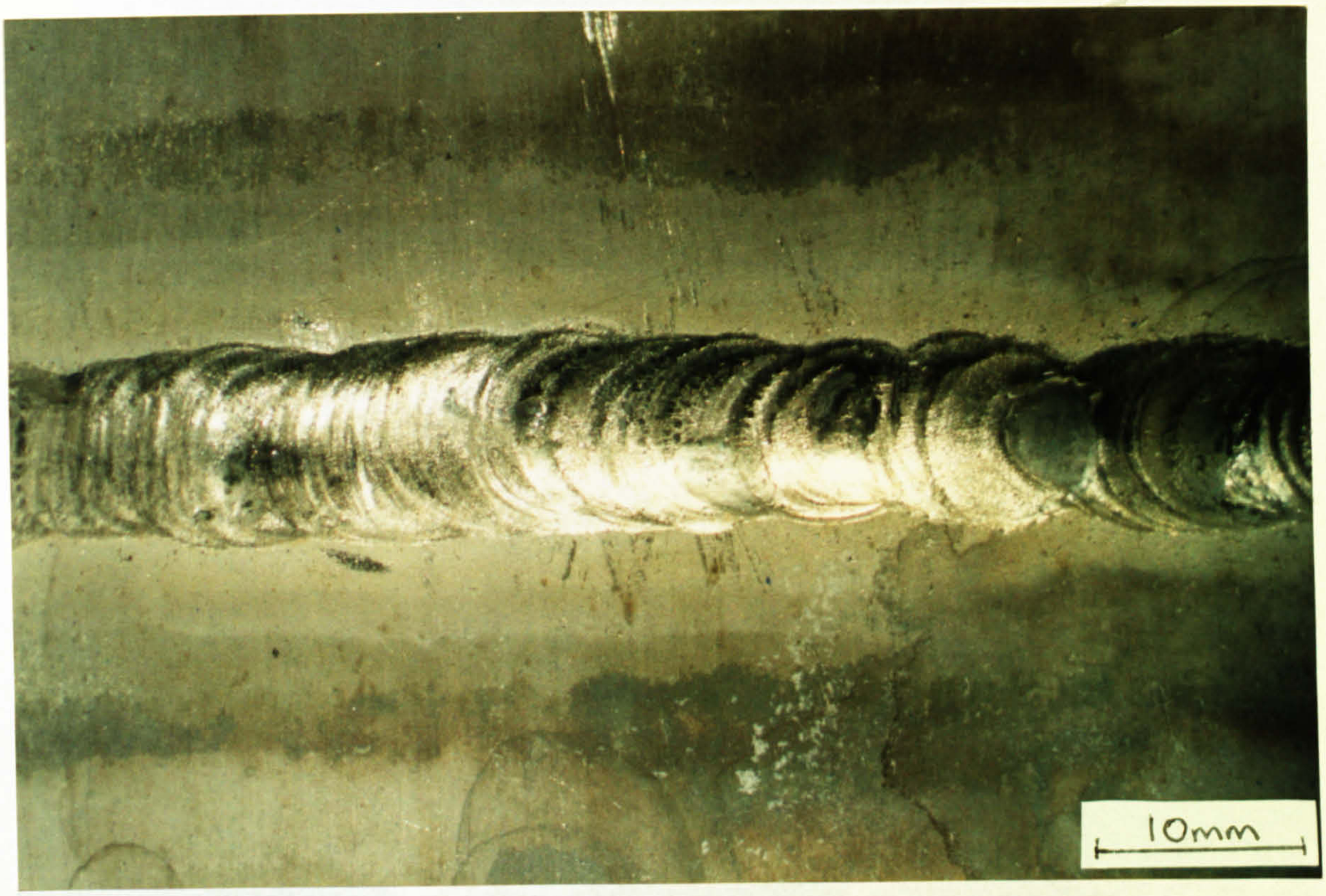

Fig. 9.9b. Unattacked weld area on UNS S32760 after 35 days in 200ppm free chlorine.

At the intermediate concentration, again no corrosion could be detected in the vicinity of the weld but a small number of areas as in Fig. 9.9a in the lower concentration were identified as shown in Fig. 9.10, again upstream from the welded area.

Fig. 9.10. Pit initiation away from the weld on the pipe in 400ppm free chlorine flow at 1.6m/s

The highest concentration of free chlorine induced significantly enhanced corrosion attack, not at the weld but at the artificial crevice set up between the pipe and the adhesively bonded flange. Almost the entire interface could be seen to be attacked as shown in Figs. 9.11 and 9.12. There was no such attack at the pipe/flange interface after 35 days in the lower (200ppm) concentration solution.

Fig. 9.11. Crevice corrosion at the pipe/flange interface at 550-600ppm free chlorine

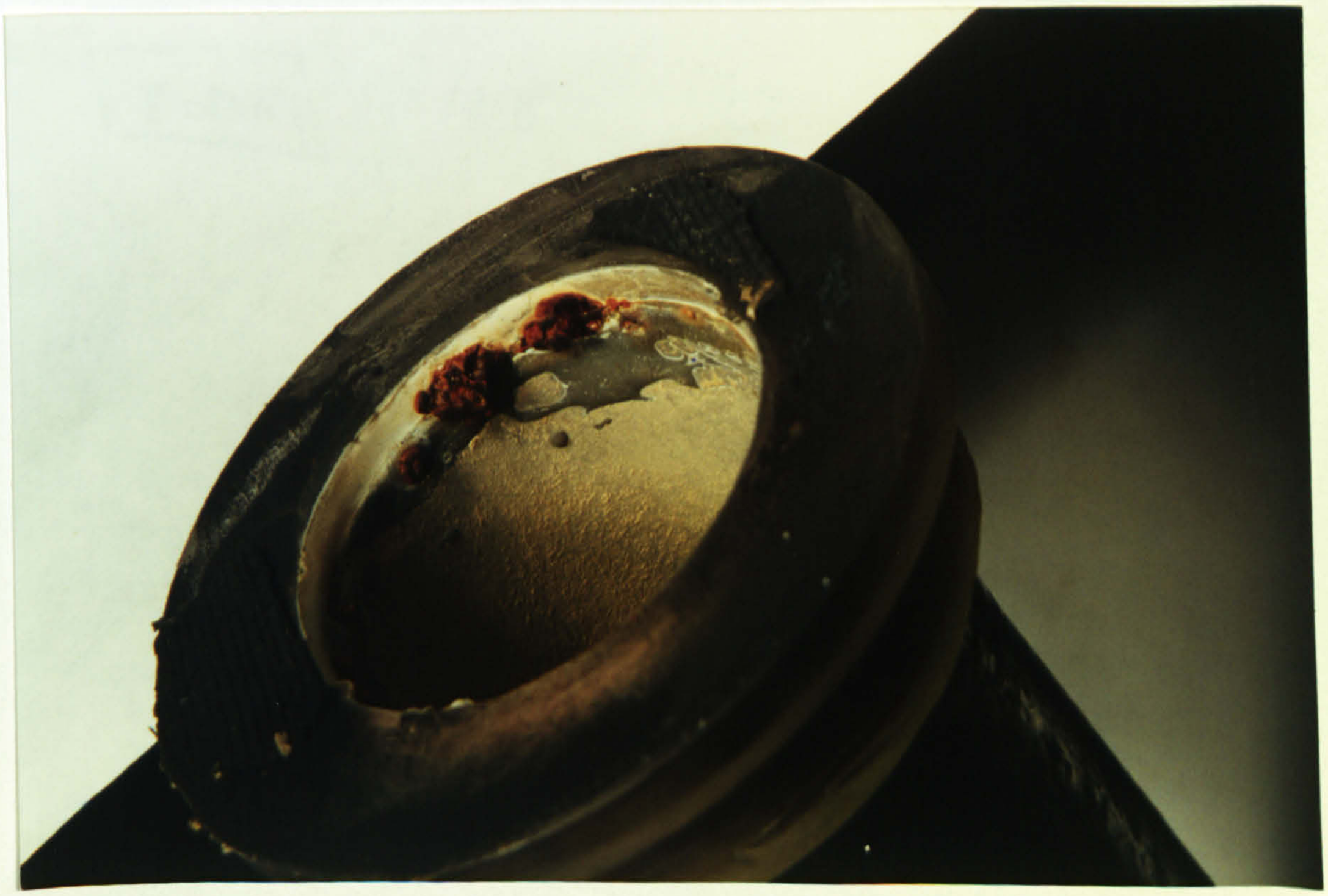

Fig. 9.12. Crevice corrosion at the pipe/flange interface at 550-600ppm free chlorine.

It was noted that even at the lowest concentration of hypochlorite, after 2-3 days, there was a cream/yellow substance deposited on the welded pipe and which, after 35 days was relatively thick (Fig. 9.13). The deposit was found to rich in Ca (Fig. 9.14).

Fig. 9.13. Deposit on the inside of the welded pipe after 35 days in lower concentration flow

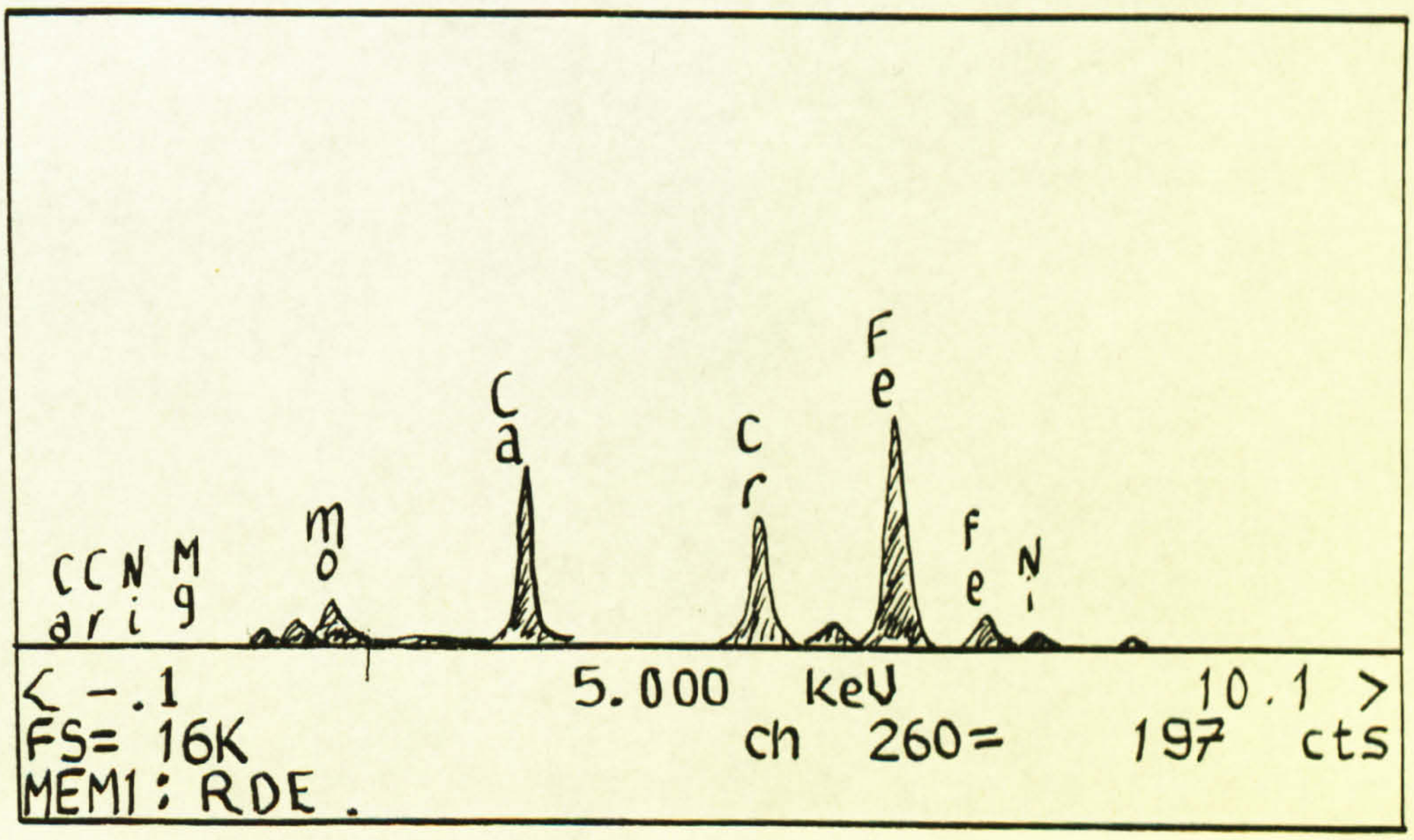

Fig. 9.14. EPMA trace showing high concentration of Ca in the deposit

MCAs

The attack on the MCAs was complicated by the attachment of the wire to enable E_{corr} measurement. The resin/metal interface facilitated the initiation of crevice corrosion attack which had to be considered in analysis of the overall severity of attack. A final experiment in 550-600ppm free chlorine was performed without wires attached and the depth of penetration measured at the crevice washer alone. The extent of attack measured at the site of the wire attachment and at the crevice assembly is recorded for each sample in Table 9.2. In Table 9.3, the depth of penetration of attack at the site of the crevice assembly is recorded.

At 550-600ppm, the UNS S32760, as expected, proved to be the most resistant to attack via crevice corrosion as shown in Fig. 9.15 where virtually no depth of penetration can be detected at the crevice washer and no depth of attack is observed at the metal/resin interface. In contrast, at both regions, the SAF 2205 and the UNS S31603 showed signs of severe crevice attack (Figs 9.16 and 9.17). The exposed faces of the MCA specimen plate can be seen to be covered by a black deposit which was found to be rich in Cl.

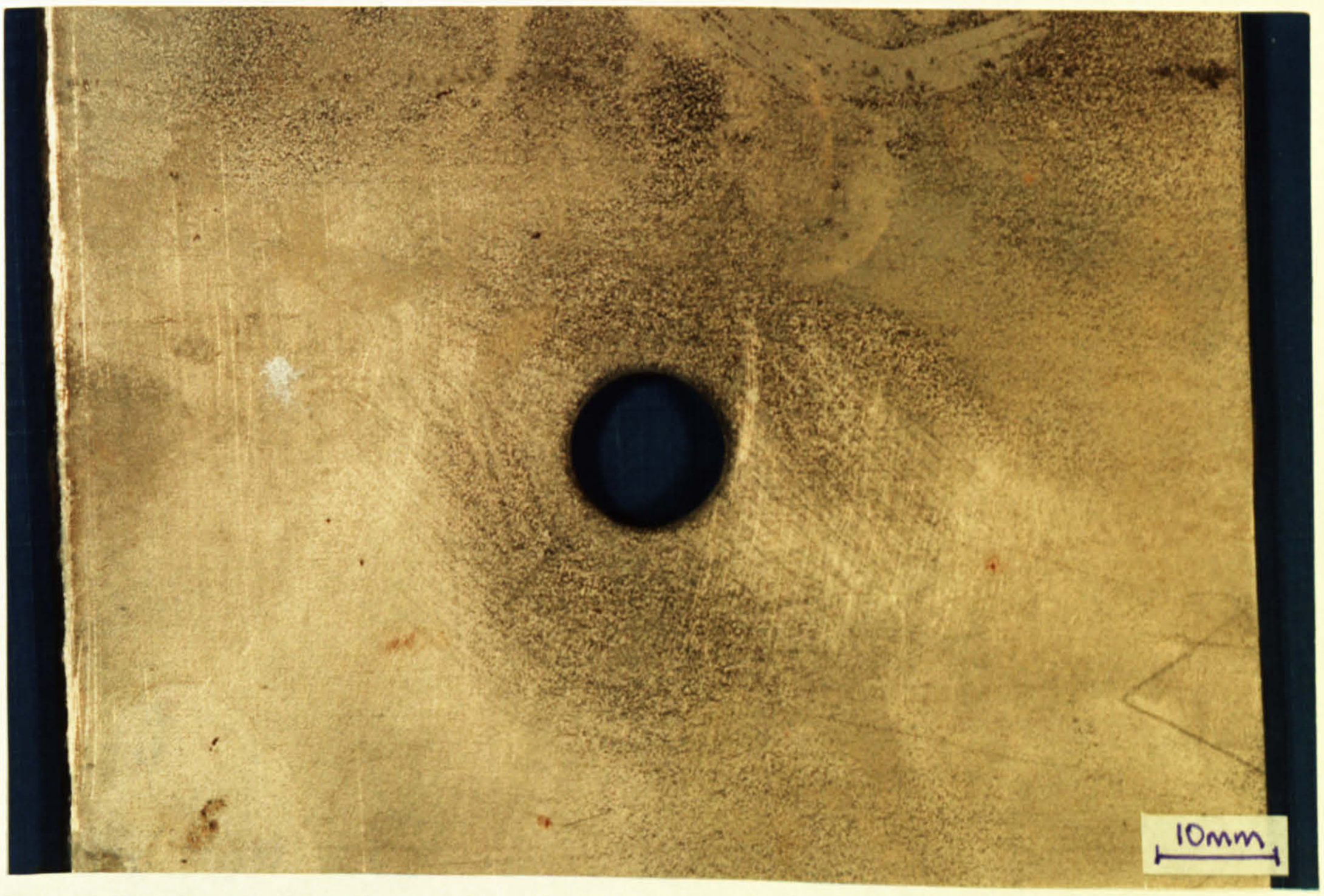

Fig. 9.15. Virtually unattacked crevice region on UNS S32760 at 200ppm free chlorine in static conditions.

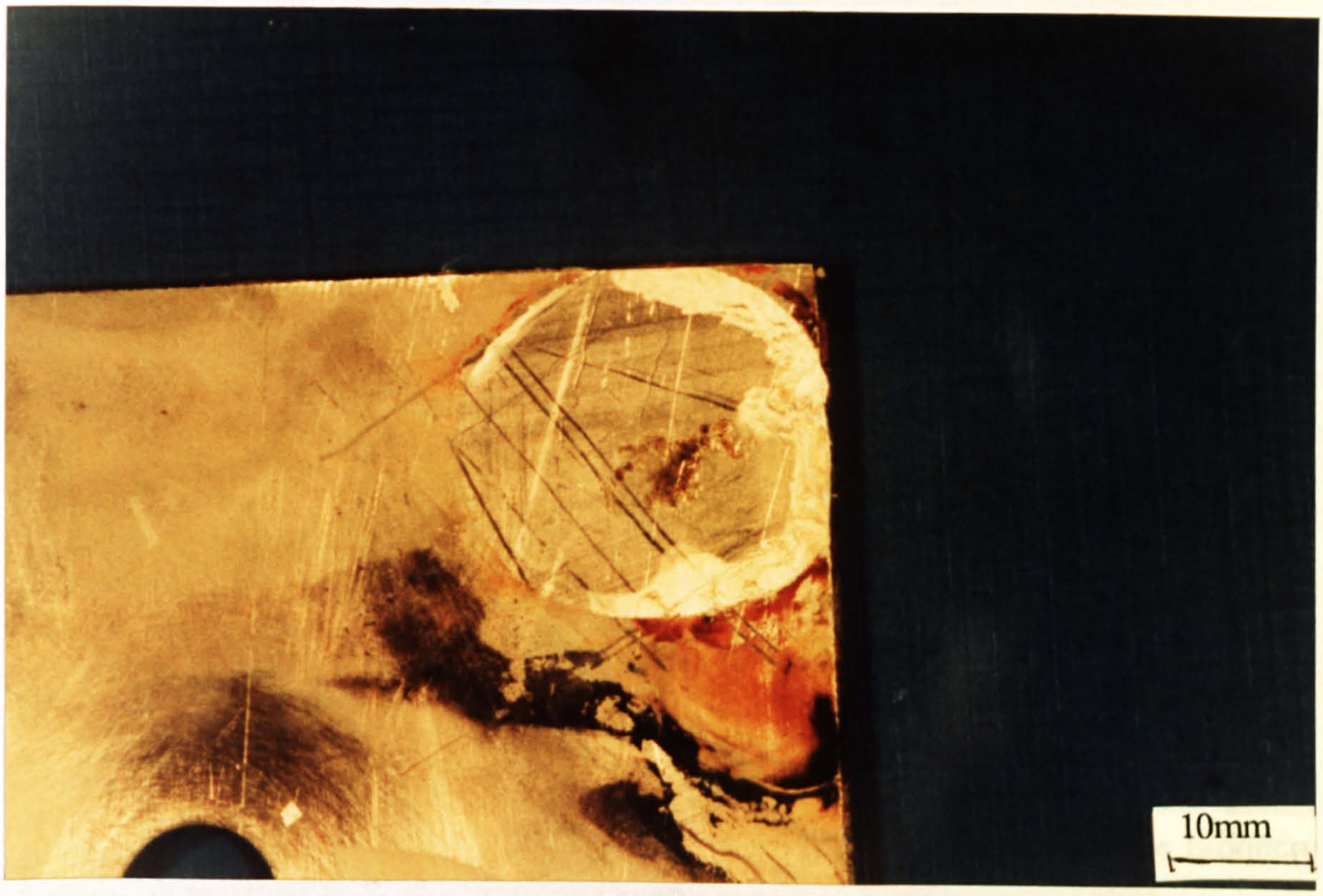

Fig. 9.16. Severe attack at the metal/resin interface on UNS S31603 after 35 days in 200ppm free chlorine in static conditions

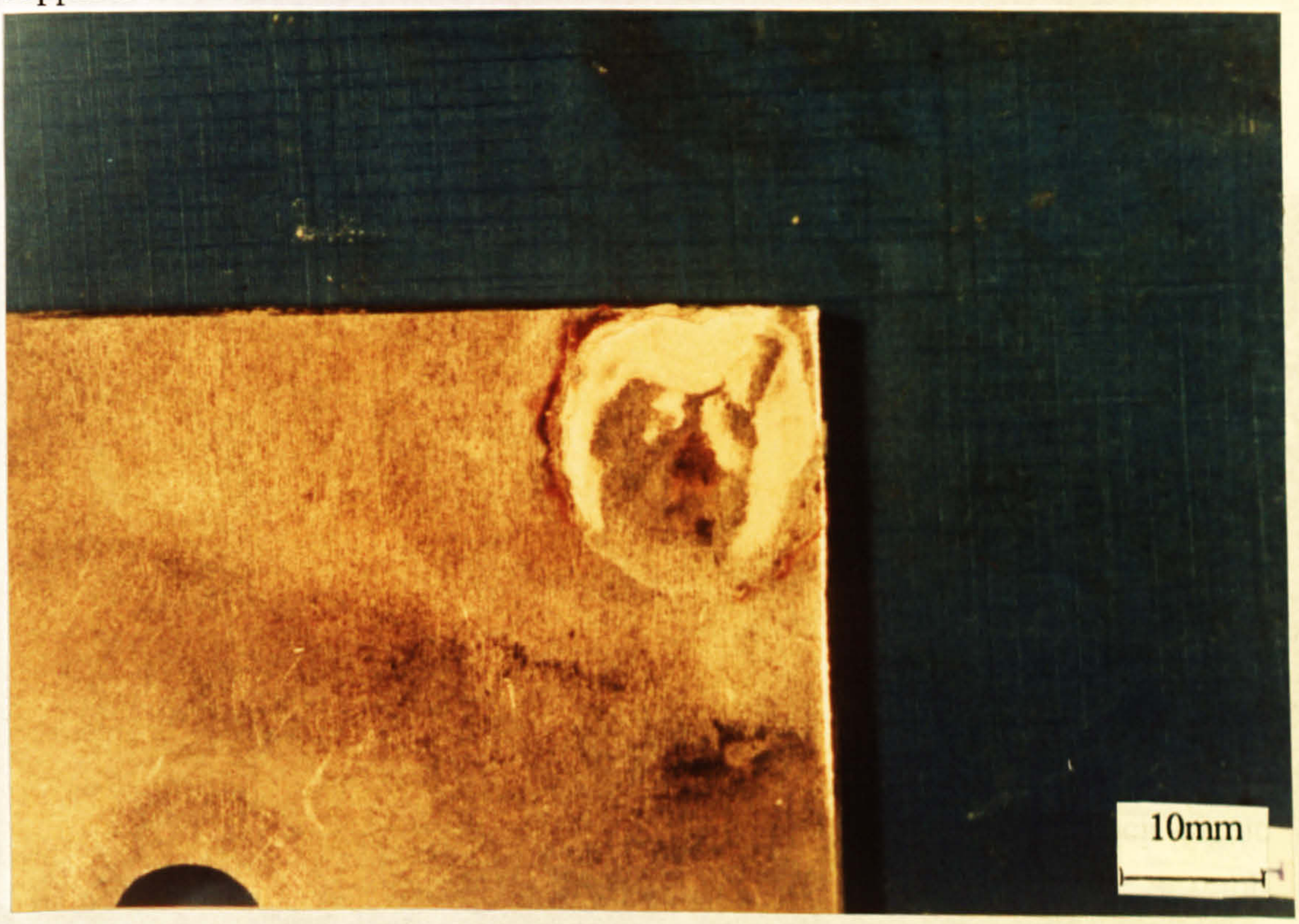

Fig. 9.17. Severe attack at the metal/resin interface on SAF 2205 after 35 days in 200ppm free chlorine in static conditions

Increased concentration of free chlorine to 550-600ppm consistently increased the maximum depth of penetration of crevice corrosion at both the resin/metal interface and at the crevice sites of the crevice washers. In addition, the number of grooves under which crevice corrosion had initiated was increased such that at every site on each material, crevice corrosion could be observed to have initiated. Figures 9.18a and b and 9.19 show the severe attack at every groove on UNS S31603 and SAF 2205. Consistent with the attack at the lower concentration of 200ppm, the depth of attack on UNS S32760 was substantially less than on the other 2 materials, although at every site, crevice corrosion had initiated (Figs. 9.20a and b).

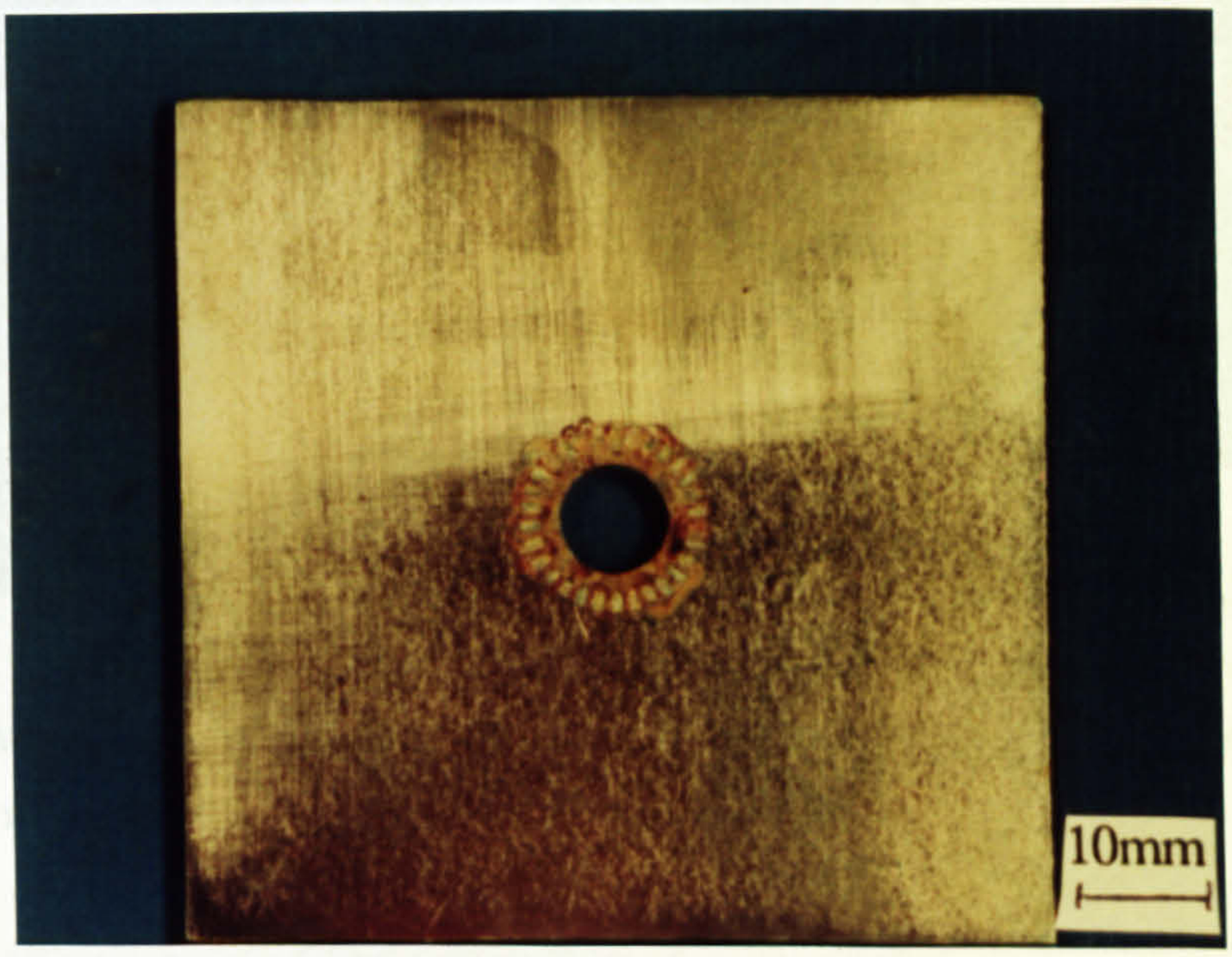

(a)

Fig. 9.18a. Severe crevice attack at every groove at the crevice assembly on UNS S31603 after 35 days in static conditions (a) view of overall assembly (b) attacked region

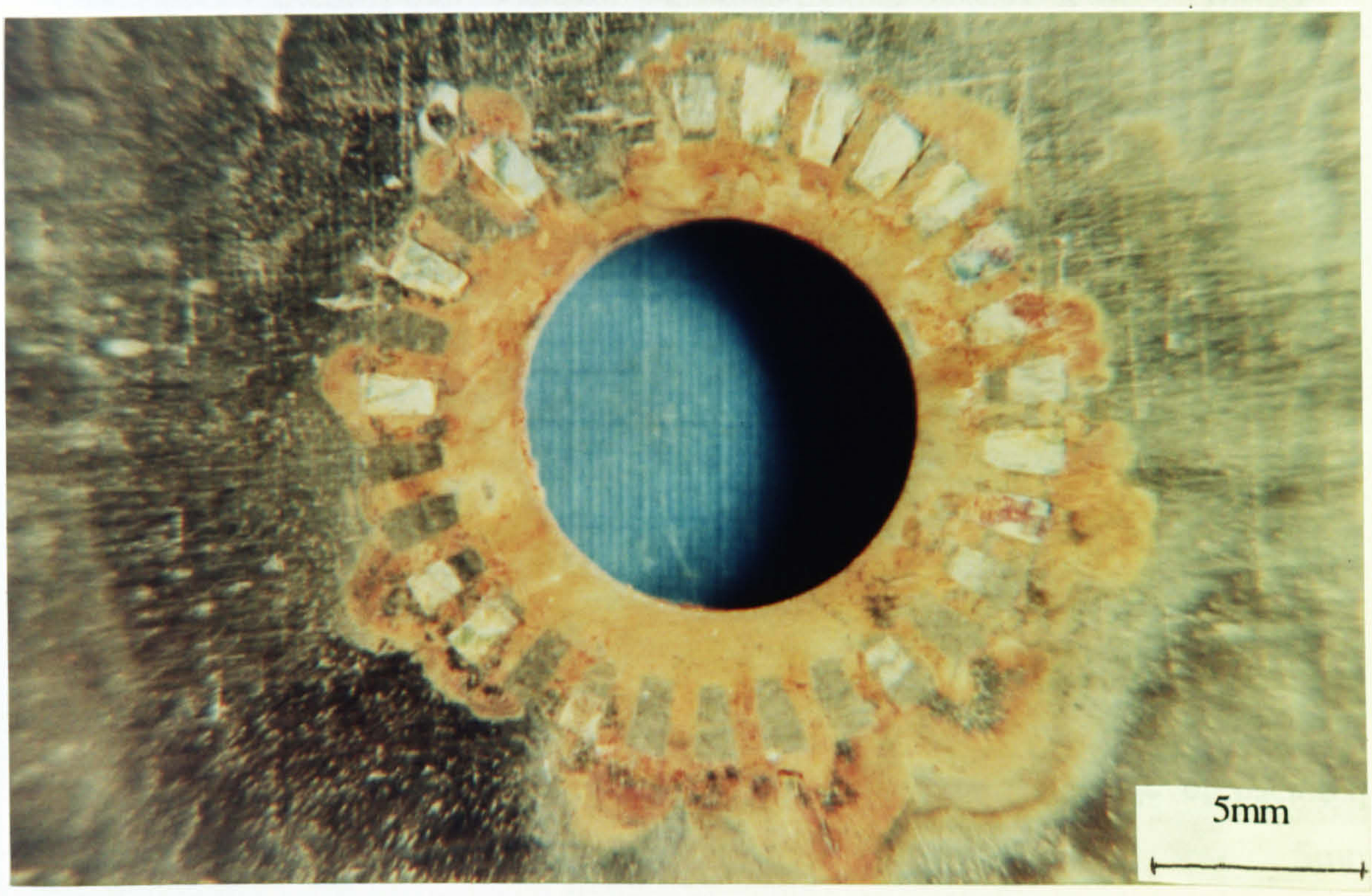

Fig. 9.19. Severe crevice attack at every groove at the crevice assembly on SAF 2205 after 35 days in static conditions at 550-600ppm

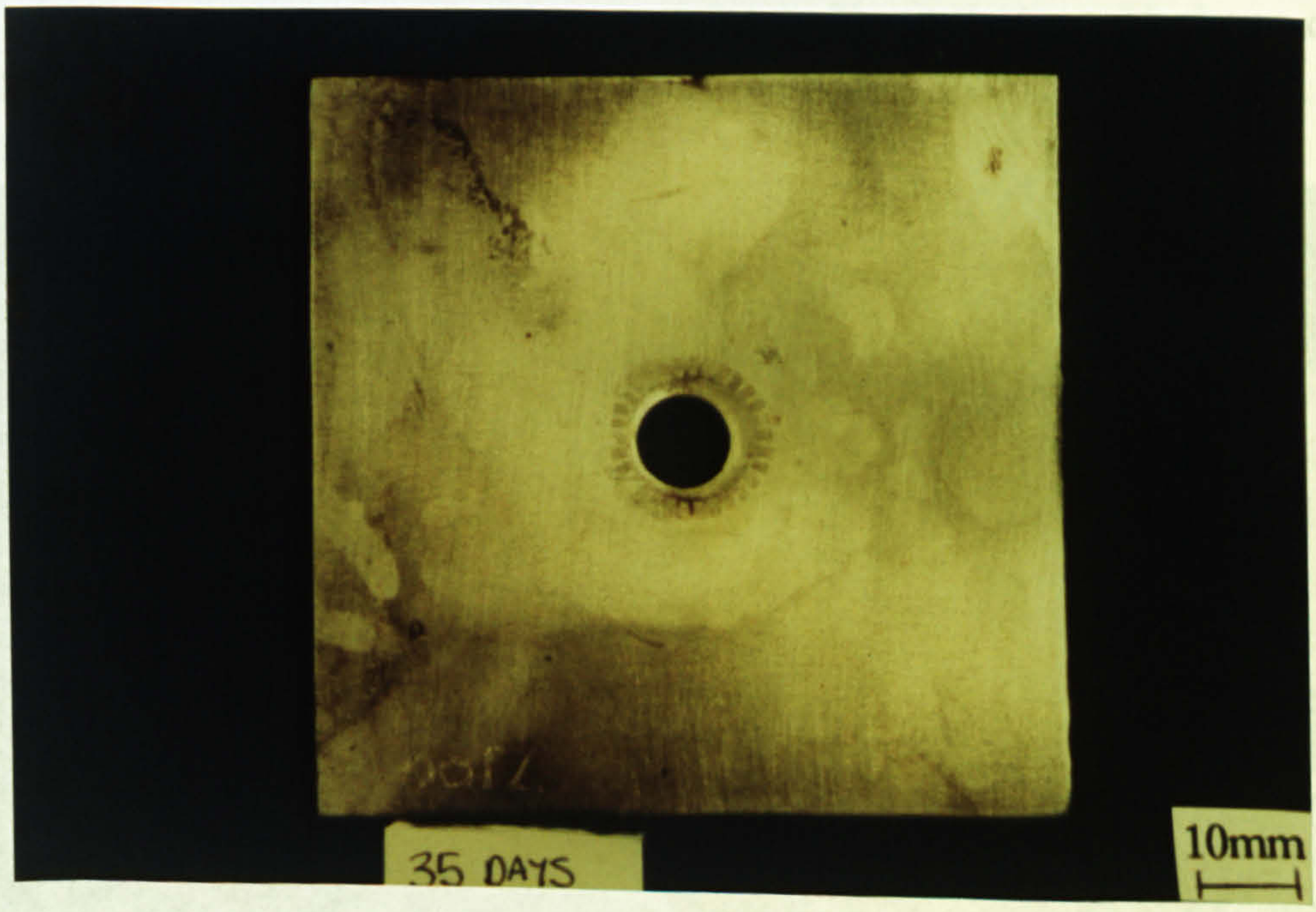

(a)

(b)

Fig. 9.20. Crevice attack on UNS S32760 after 35 days in static conditions at 550-600ppm (a) showing overall assembly and (b) showing shallow depth of penetration

At 550-600ppm, in the absence of any electrical connection (no wire attached) the crevice corrosion was concentrated at the crevice washer and as such the maximum depth of penetration was greater on every material. Figure 9.21a and b shows on UNS S31603 the perforation of the through thickness of the material after 35 days in 550-600ppm of free chlorine.

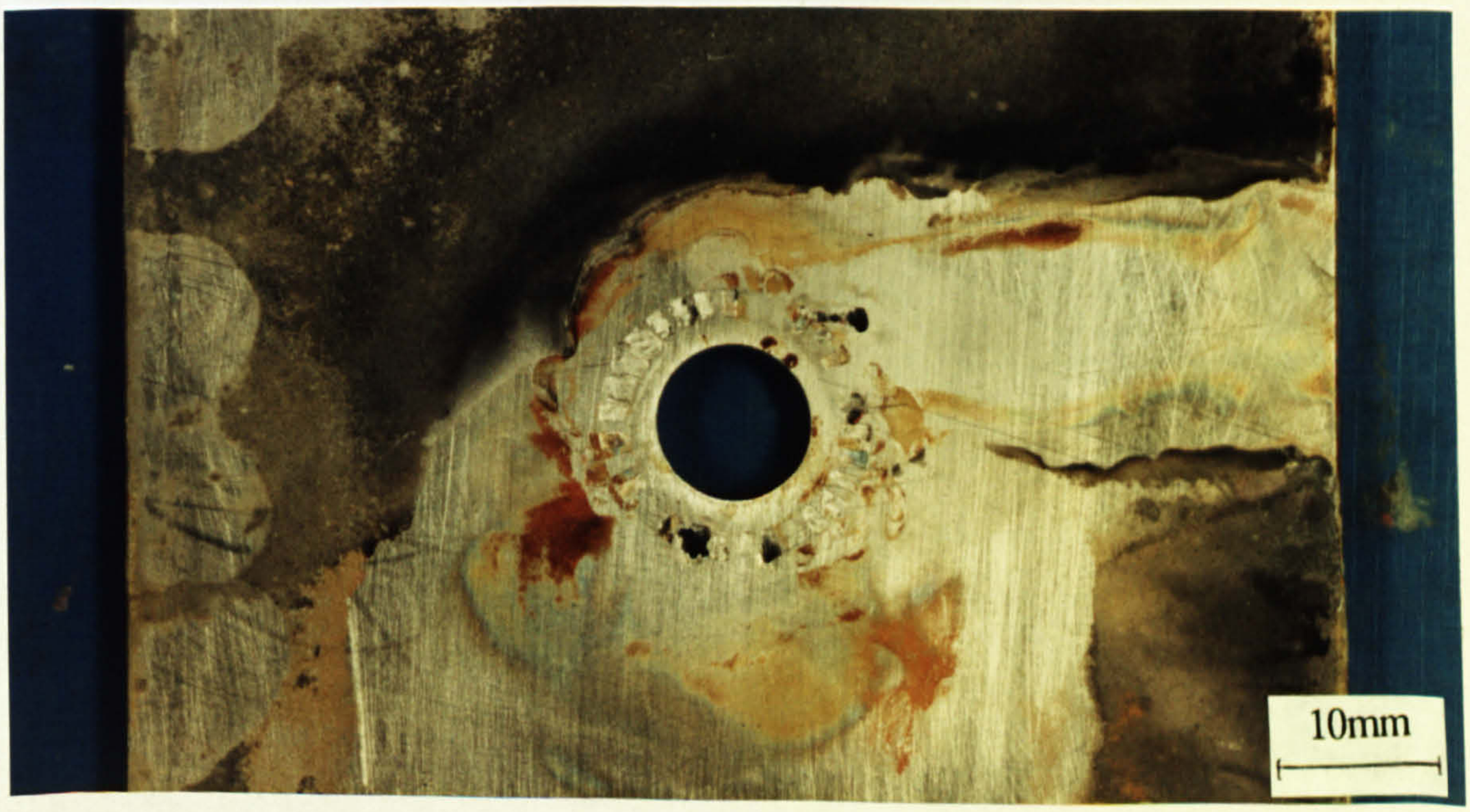

(a)

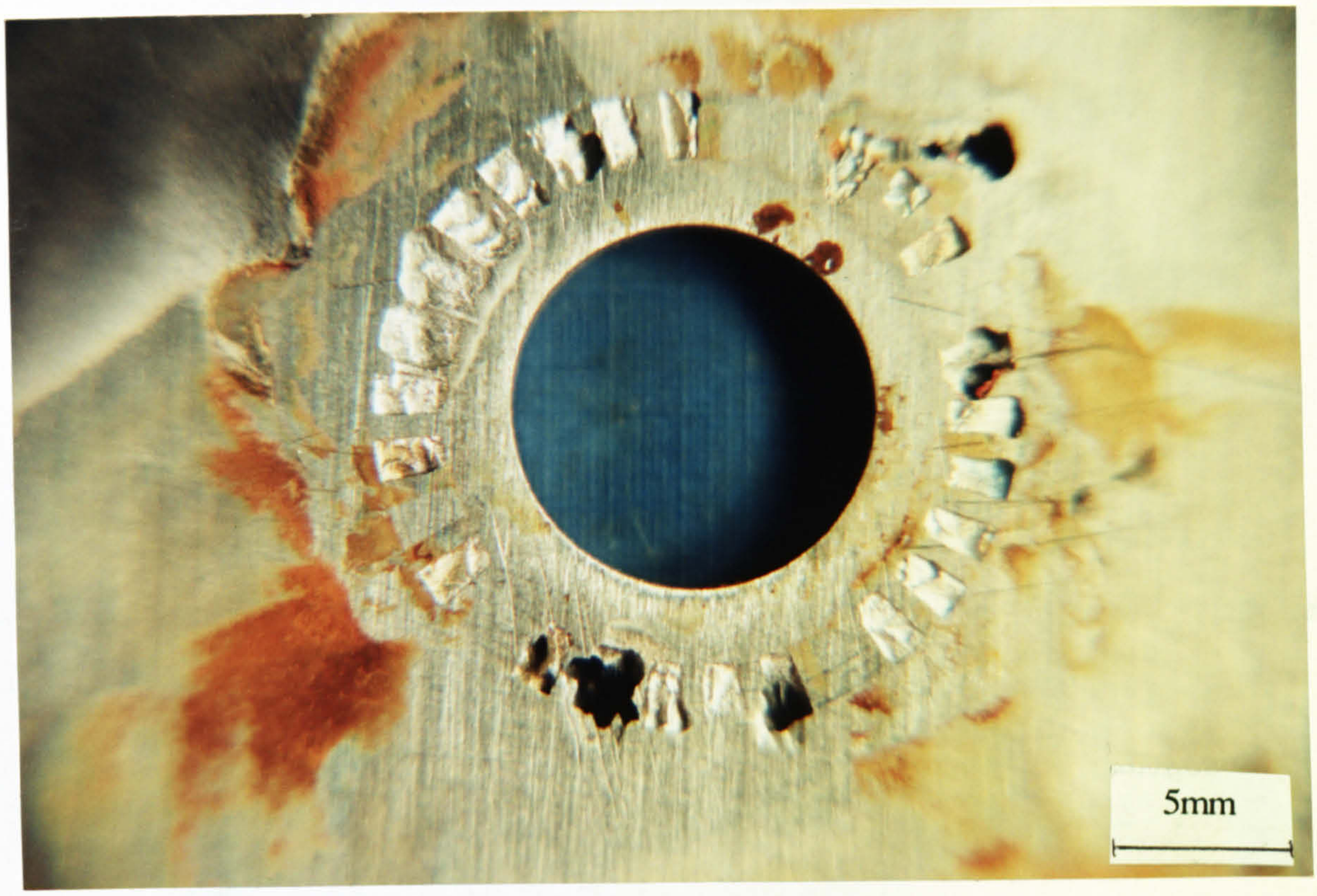

(b)

Fig. 9.21. Perforation of the sheet UNS S31603 after 35 days in 550-600ppm of free chlorine (a) overall view of assembly and black corrosion products and (b) closer view of perforated region

Anodic Polarisation - Static Conditions

Immersion in chlorinated seawater at the lower concentration (200ppm free chlorine) did not significantly affect the anodic polarisation parameters (E_b, I_{max}, E_r etc.) on any of the materials in the study when the anodic polarisation was carried out on initial immersion although a slight lowering of Eb (50mV) was observed consistently. Prolonged exposure (to 35 days) at 200ppm also failed to cause any significant effect on the resistance to passivity breakdown (monitored by E_b) on any of the materials as illustrated in Figs. 9.22 and 9.23 for SAF 2205 and 25Cr duplex respectively.

At the higher concentration (550-600ppm) there was a significant decrease in E_b on initial immersion, compared to hypochlorite-free seawater, on several of the materials as illustrated in Fig. 9.24. It should be noted that the two materials which showed least resistance to passivity breakdown in unchlorinated seawater (UNS S31603 and Stellite 6) are here affected least by the addition of high concentrations of hypochlorite.

The interesting feature at the higher hypochlorite concentration was the apparent 'recovery' of the breakdown potential after longer immersion on all materials, with the

exception of Inconel 625, as shown in Fig. 9.25, but the effect was more pronounced on the higher-grade duplex and austenitic alloys. Full anodic polarisation curves, illustrating this effect are shown in Fig. 9.26.

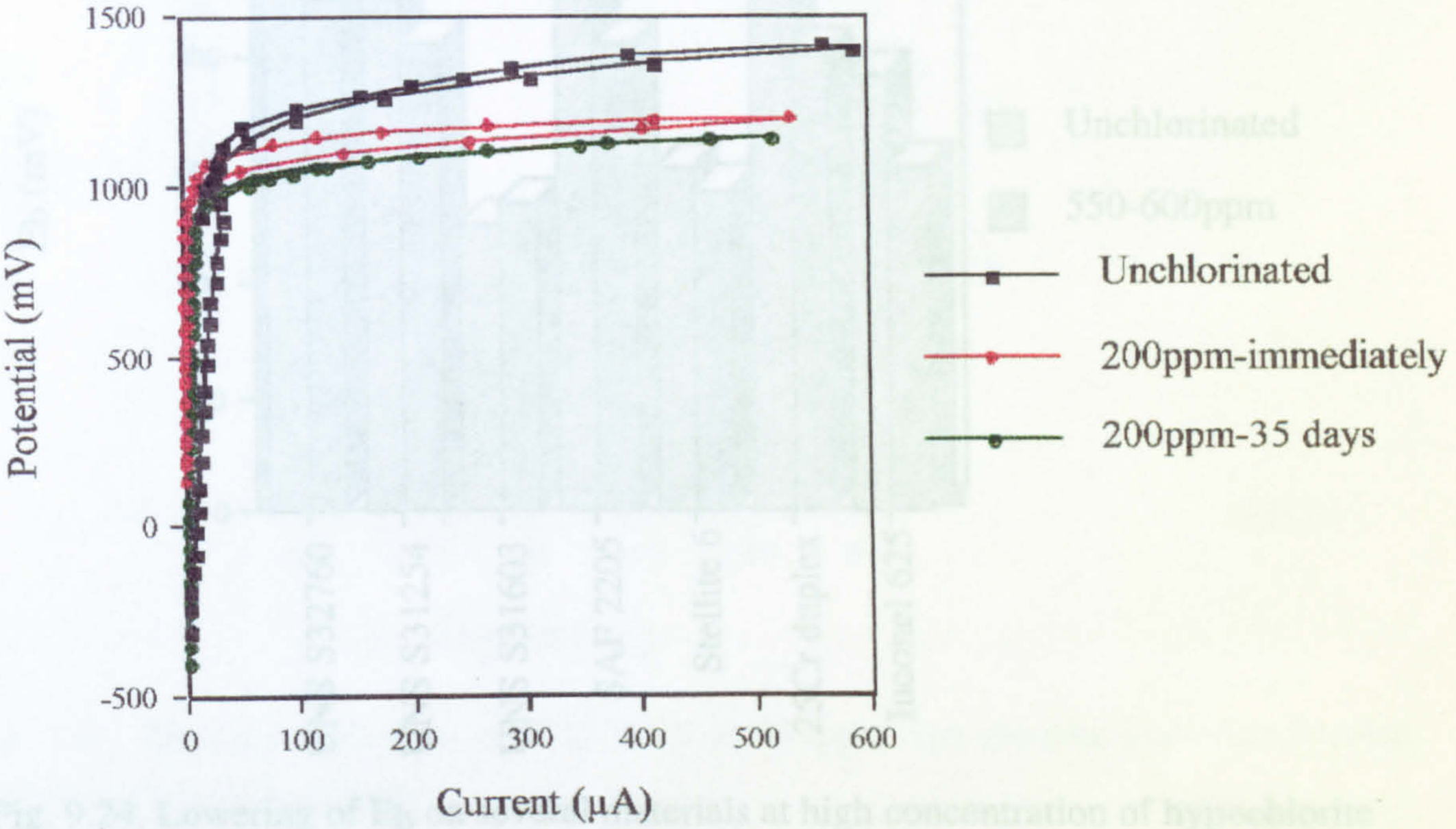

Fig. 9.22. Anodic polarisation on SAF 2205 in 200ppm free chlorine immediately after immediate and after 35 days immersion

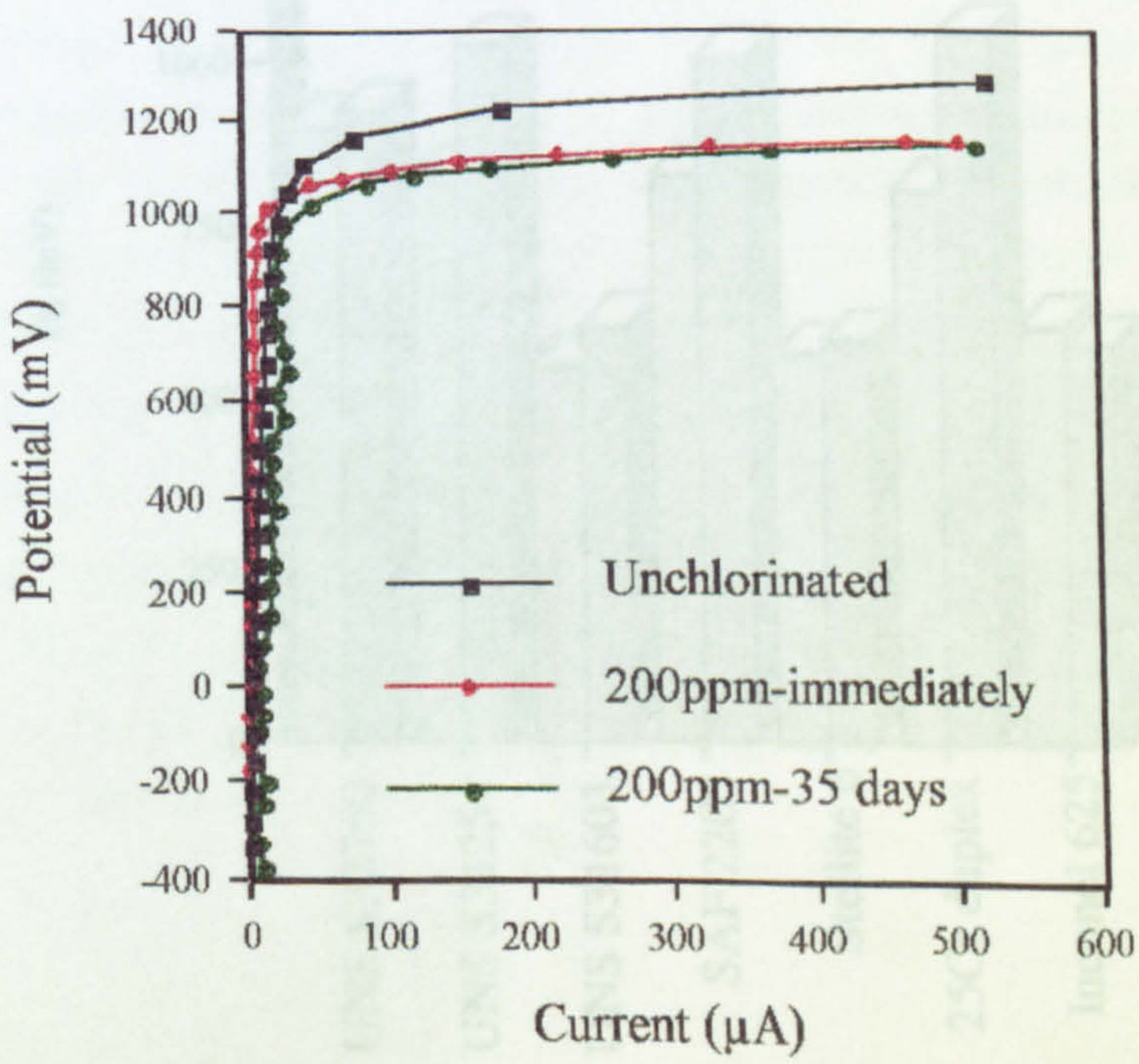

Fig. 9.23. Anodic polarisation on 25Cr duplex in chlorinated seawater (200ppm free chlorine) on immediate immersion and after 35 days.

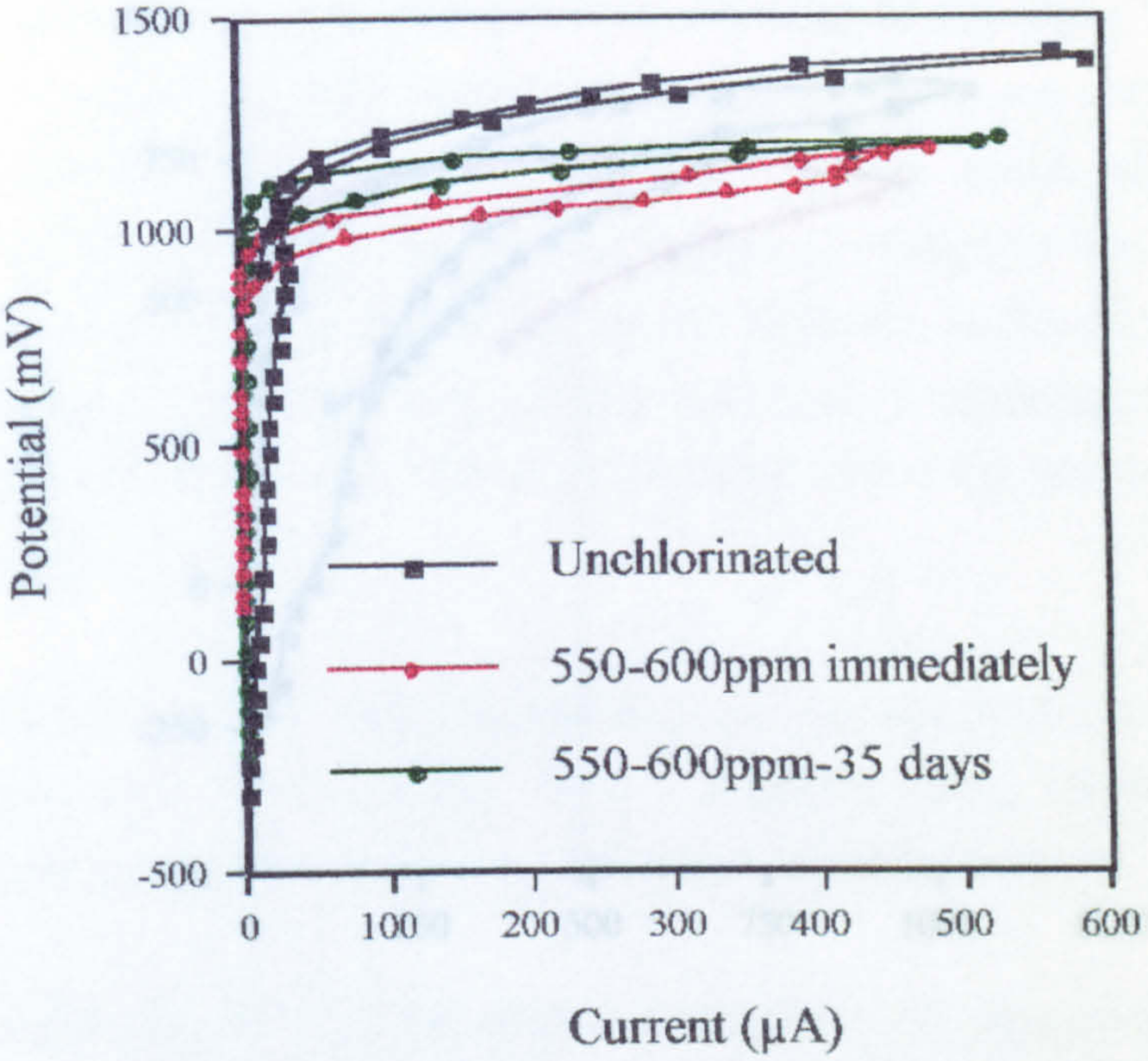

Fig. 9.26. Anodic polarisation on SAF 2205 in 600ppm free chlorine immediately after and after 35 days immersion

Inconel 625, the nickel-base alloy, was consistently shown to have a free corrosion potential more noble than the stainless steels. The potential range over which the material exhibited passive behaviour was therefore very much reduced in chlorinated seawater at both concentrations. On Stellite 6, the passive range was very short on immediate immersion (Fig. 9.27) but the situation was reversed after longer immersion in that a greater passive range was observed at both concentrations. This was due almost entirely to the decrease in E_{corr} (perhaps due to localised corrosion initiation) after longer immersion periods since E_b was not significantly different. Figure 9.28 compares the passive range (E_b-E_{corr}) in chlorinated seawater and unchlorinated seawater for Stellite 6 and Inconel 625. After 35 days immersion, Stellite 6 had a much larger passive range than Inconel 625; the free corrosion potential of Inconel 625 tended in the positive direction whilst the breakdown potential lowered with time. However, it was apparent on examination of the specimens that the attack on Stellite 6 was significantly more severe.

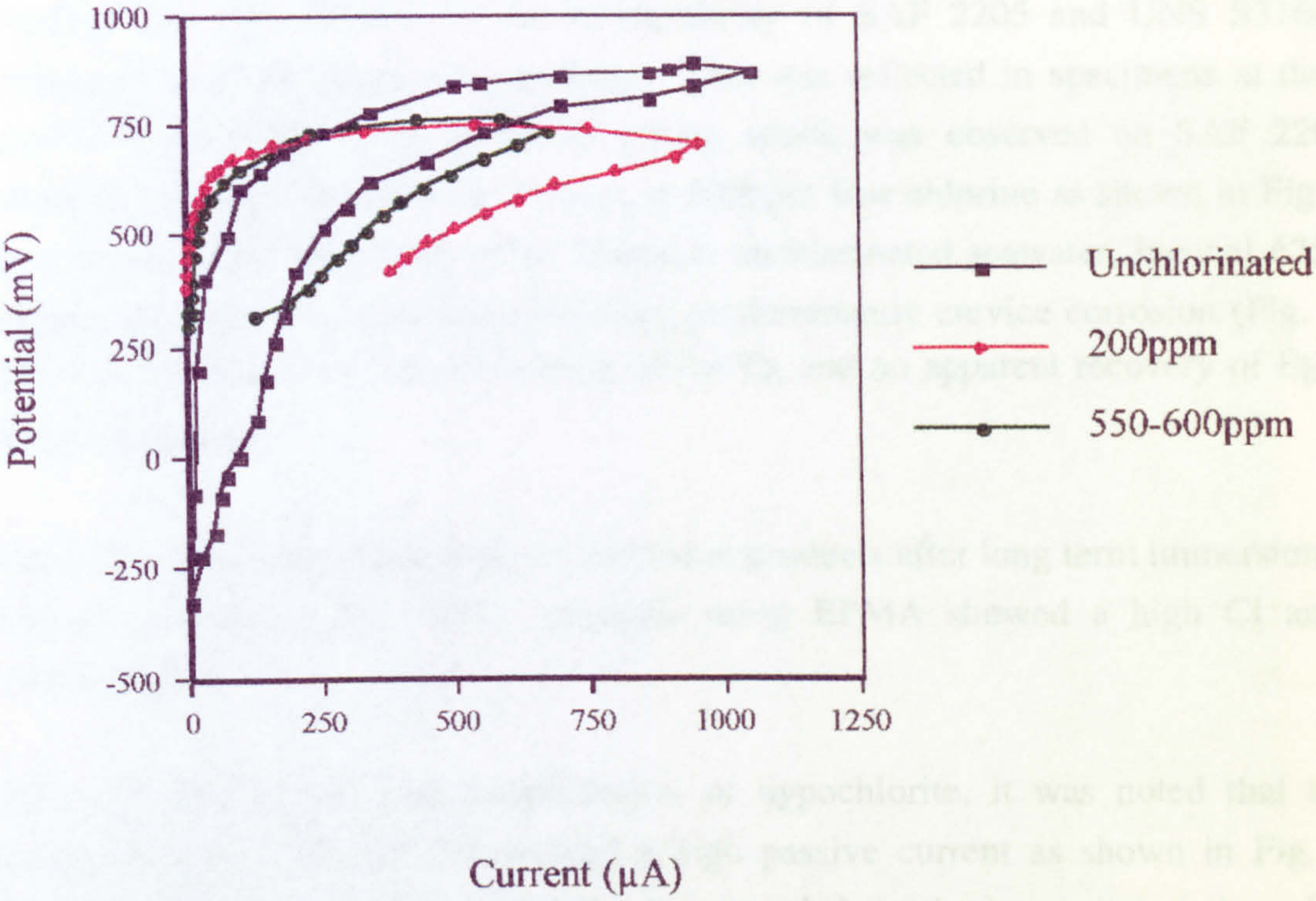

Fig. 9.27. Stellite 6 anodic polarisation on immediate immersion showing a smaller passive range than in unchlorinated seawater.

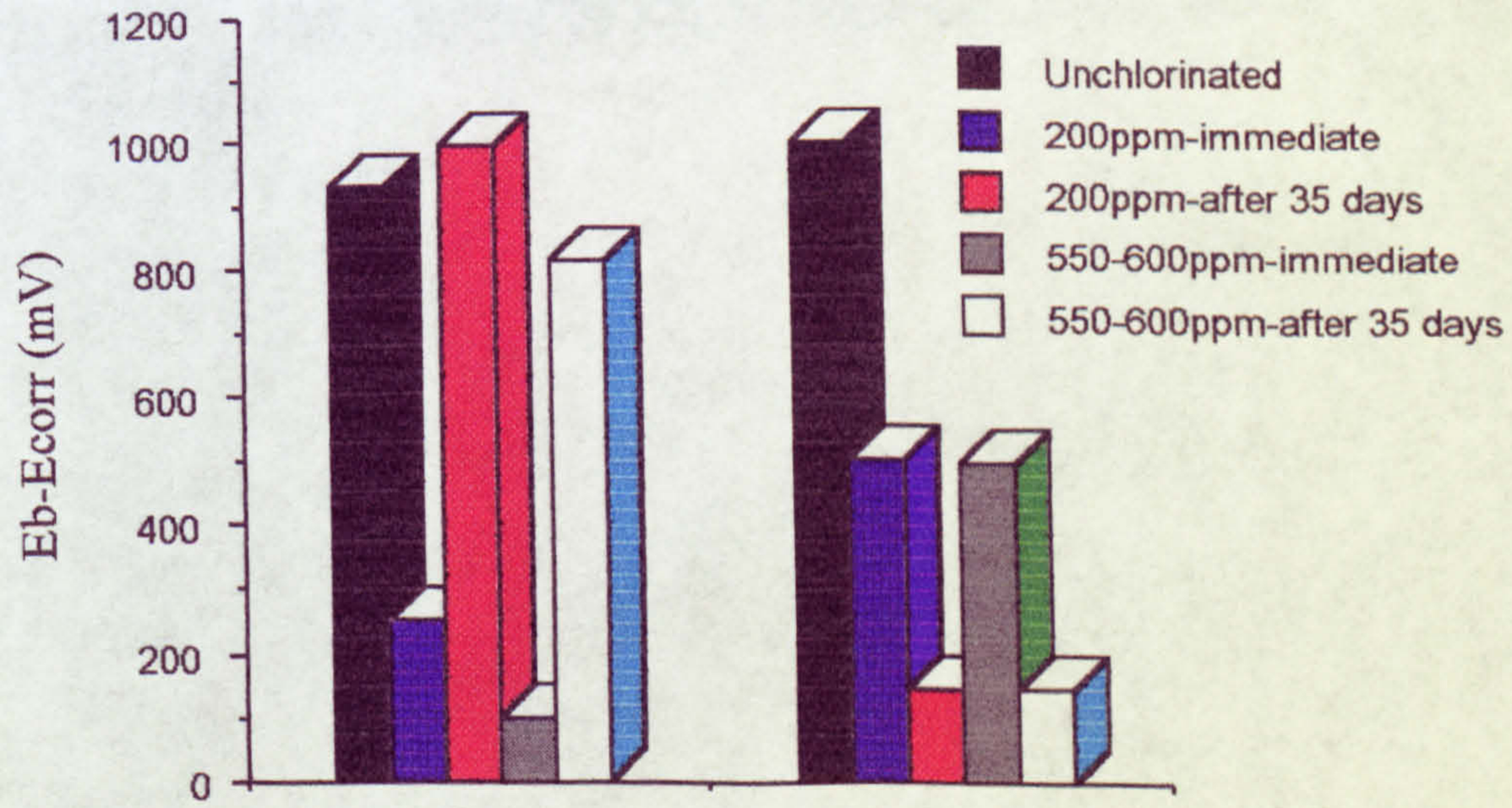

Fig.9.28. Passive potential range on Inconel 625 and Stellite 6 in chlorinated and unchlorinated seawater.

The mechanisms of attack are listed in Tables 9.4-9.7 with the anodic polarisation parameters. In agreement with previous work in unchlorinated seawater at elevated temperatures (see chapter 2), the susceptibility of SAF 2205 and UNS S31603 to enhanced localised attack was apparent. This was reflected in specimens at the free corrosion potential where extensive pitting attack was observed on SAF 2205 in addition to crevice attack after 35 days in 600ppm free chlorine as shown in Fig.9.29. In contrast to the behaviour of the alloys in unchlorinated seawater, Inconel 625 was shown to be prone to localised corrosion, predominantly crevice corrosion (Fig. 9.30) and this was manifested in a lowering of the E_b and no apparent recovery of E_b after longer immersion.

On the Co-base alloy. Stellite 6, the corrosion products after long term immersion were black as shown in Fig. 9.31. Analysis using EPMA showed a high Cl and Co concentration.

After 35 days in the high concentration of hypochlorite, it was noted that anodic polarisation on UNS S31254 yielded a high passive current as shown in Fig. 9.32. Examination of the specimen after the test revealed crevice corrosion as the principal form of attack (Fig. 9.33). On he duplex and superduplex stainless steels, this high passive current was not observed.

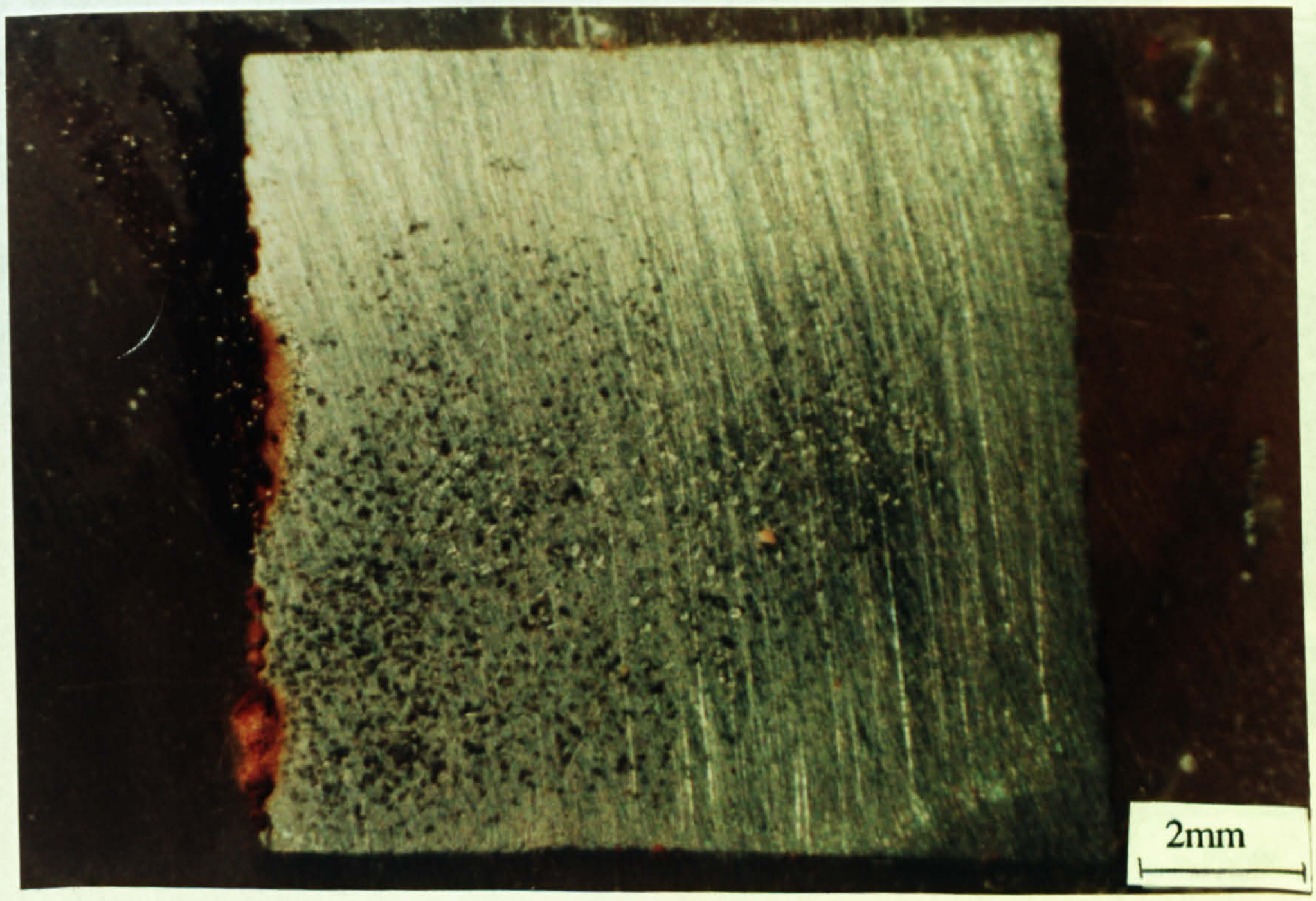

Fig. 9.29. Pitting and crevice corrosion on SAF 2205 after 35 days in 600ppm free chlorine at the free corrosion potential

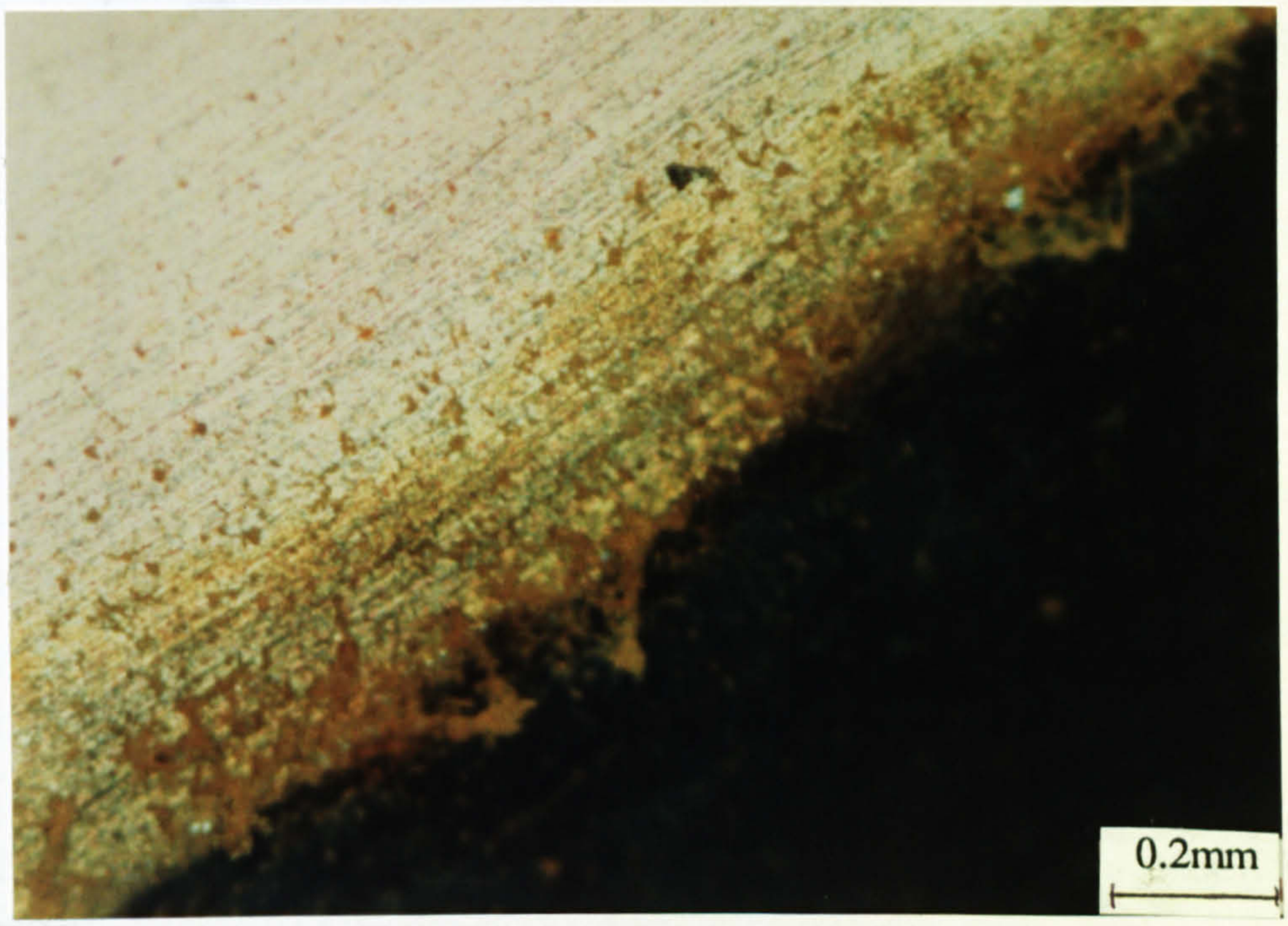

Fig. 9.30. Crevice corrosion on Inconel 625 after 35 days in 600ppm free chlorine at the free corrosion potential

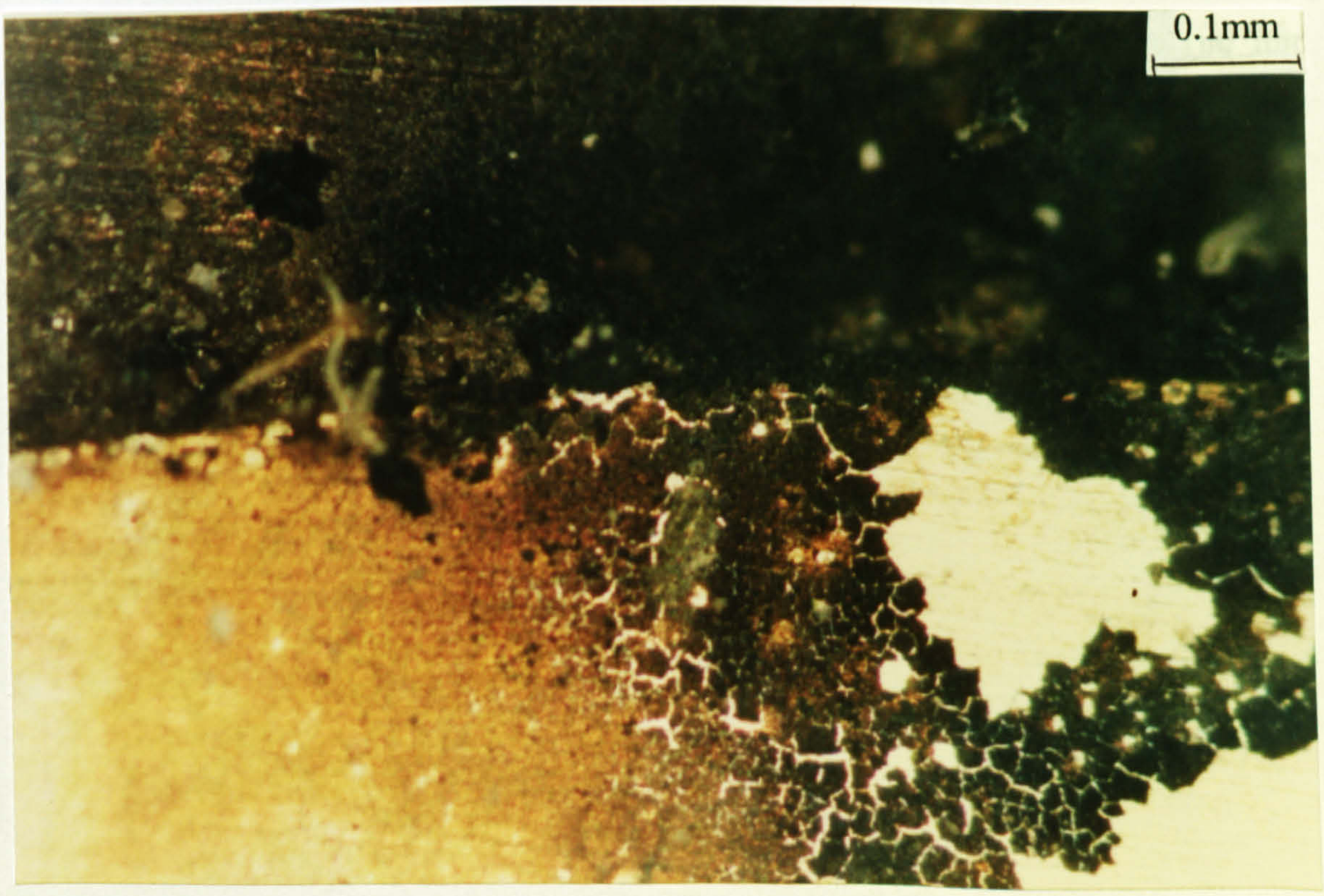

Fig. 9.31. Black corrosion products on Stellite 6 after 35 days immersion at 200ppm free chlorine.

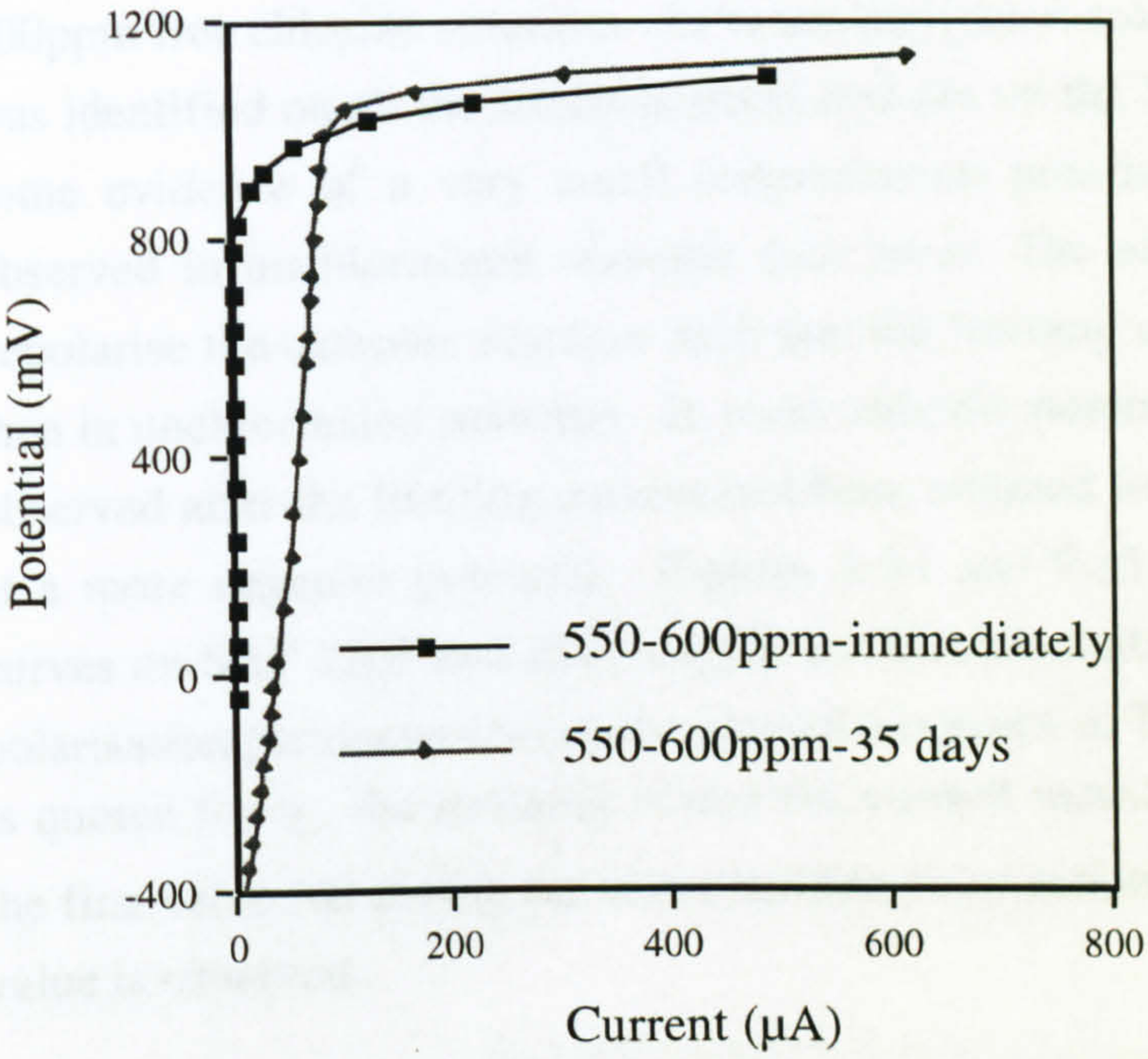

Fig. 9.32. Higher passive currents on UNS S31254 in chlorinated seawater after longer immersion

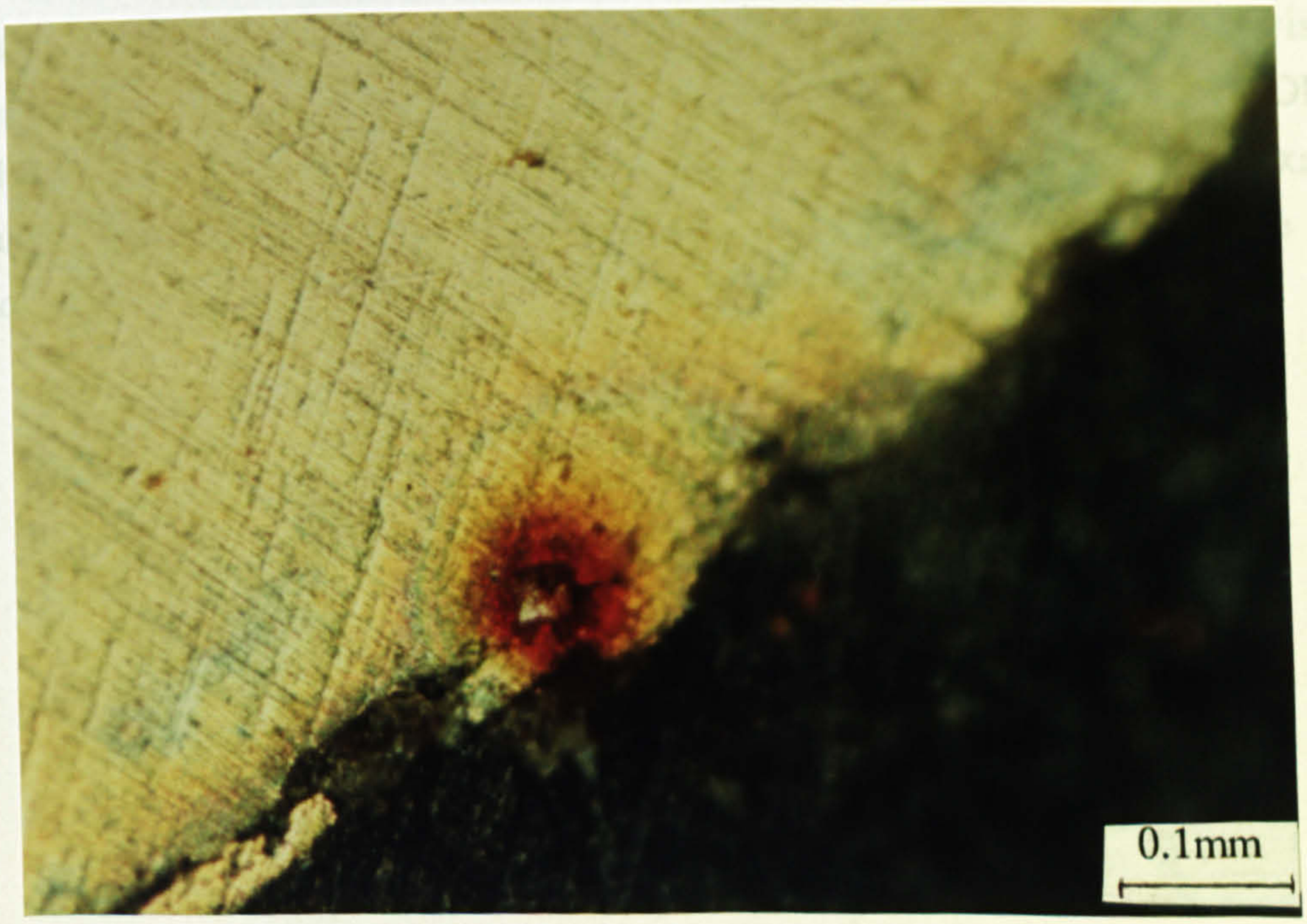

Fig. 9.33. Crevice corrosion observed after 35 days at 550-600ppm free chlorine.

Cathodic Polarisation

Cathodic polarisation tests were only carried out after 4 hours immersion in the 200ppm free chlorine solution. As in unchlorinated seawater, a limiting current density was identified on all the stainless steels and not on the Ni-base Inconel 625. There was some evidence of a very small concentration polarisation region on Stellite 6, not observed in unchlorinated seawater (see later). The effect of the hypochlorite was to depolarise the cathodic reaction such that the limiting current was several times greater than in unchlorinated seawater. In most cathodic polarisation tests, a fall in current was observed after the limiting current had been attained followed by a further Tafel region at a more negative potential. Figures 9.34 and 9.35 show the cathodic polarisation curves on SAF 2205 and 25Cr duplex in chlorine-containing seawater and the cathodic polarisation parameters for each material are given in Table 9.8. Where a current range is quoted for i_L, the meaning is that the current increases in the initial Tafel region to the first value but during the concentration polarisation region, a decrease to the second value is observed.

An interesting feature observed on all the stainless steels after cathodic polarisation in chlorinated seawater at both concentrations was the presence of a white scale, identified to contain Ca (probably as $CaCO_3$). It should be emphasised that the cathodic polarisation test parameters were consistent with those in previous chapters (i.e. in static seawater at elevated temperature, in SRB etc) and only under the conditions of hypochlorite dosing has this been observed to the extent that the scaling is visible with the naked eye (Fig. 9.36a), probably due to the enhanced production of OH^- by the depolarised cathodic reaction and resulting increased surface pH. SEM examination revealed on several of the specimens, an almost continuous layer over the specimen surface (Fig. 9.36b).

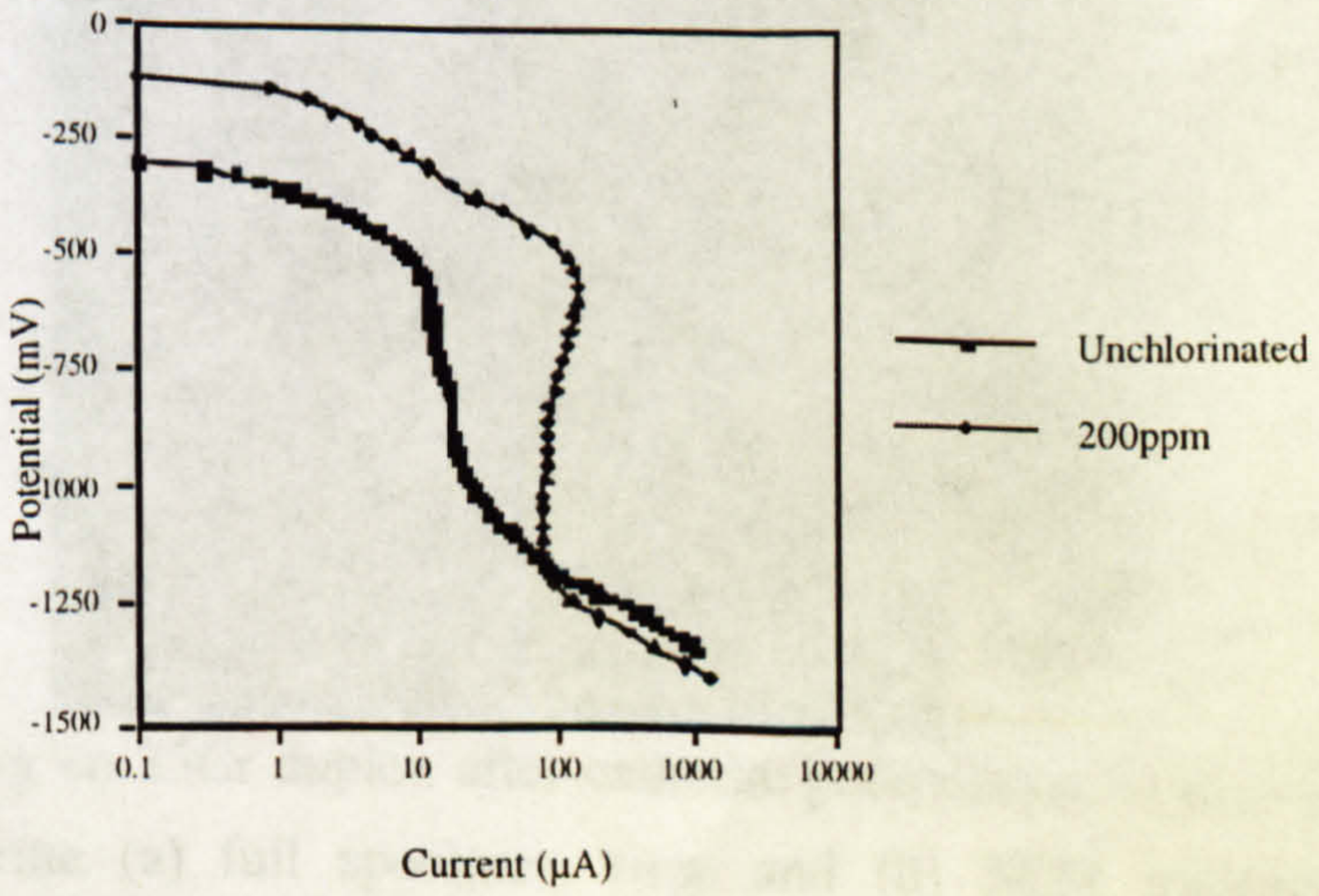

Fig. 9.34. Cathodic polarisation on SAF 2205 in unchlorinated and chlorinated seawater

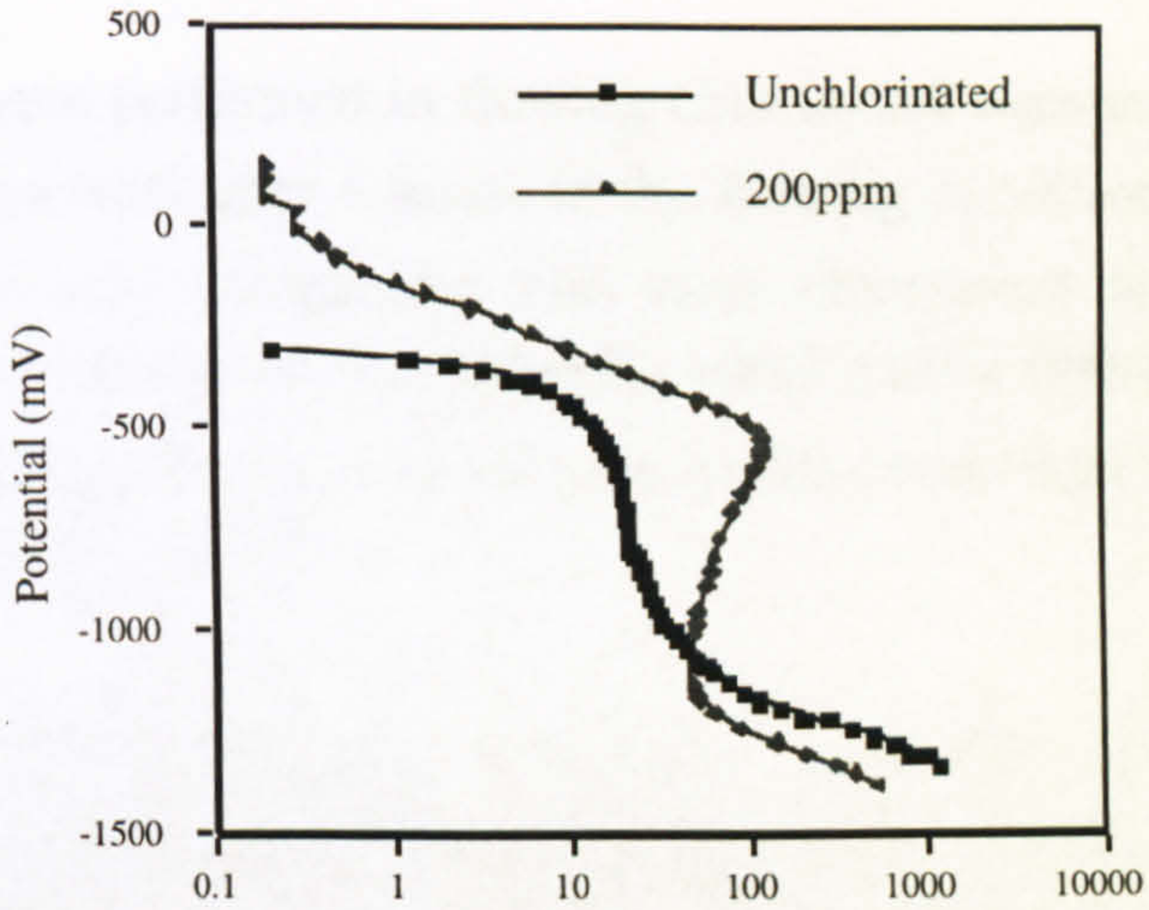

Fig. 9.35. Cathodic polarisation on 25Cr duplex in unchlorinated and chlorinated seawater

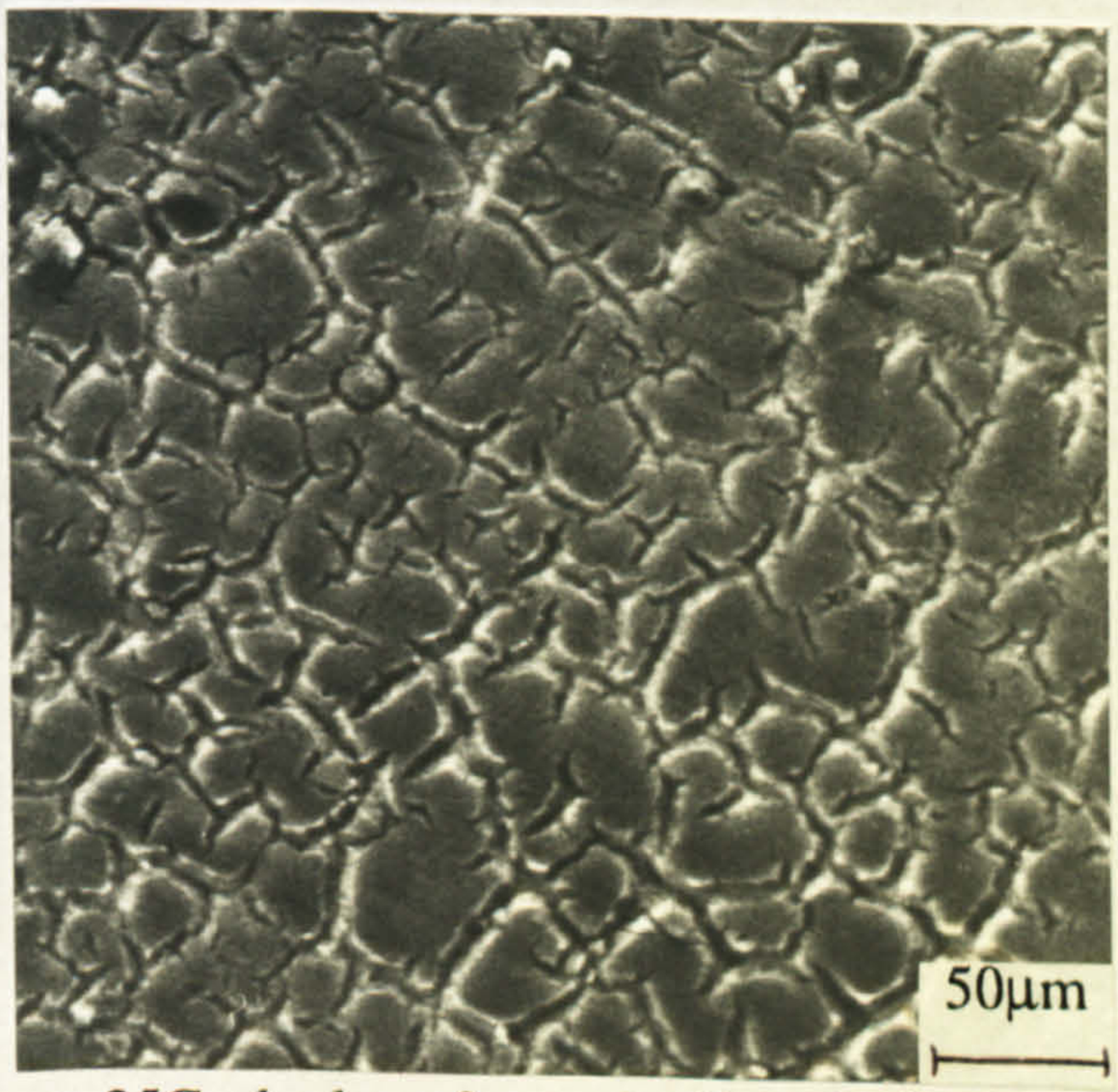

Fig. 9.36a. Scaling on 25Cr duplex after cathodic polarisation in seawater containing 200pm free chlorine (a) full specimen view and (b) SEM micrograph showing continuous layer of $CaCO_3$ scale .

Flow Conditions - Anodic Polarisation Tests

No long term tests were performed in flowing chlorinated seawater and the results of the anodic polarisation tests after 4 hours in the flowing conditions indicated that the anodic characteristics were comparable with static chlorinated seawater of the same concentration. Comparison of the parameter E_b which can be indicative of the integrity of the material to resisting passivity breakdown, yielded very little variation from static conditions as shown in Fig. 9.37.

The mechanism of attack were also comparable, with SAF 2205 showing severe crevice attack (Fig. 9.38) and extensive pitting being observed under corrosion products on UNS 31603 (Fig. 9.39). Black corrosion products at the crevice on Stellite 6 were also observed

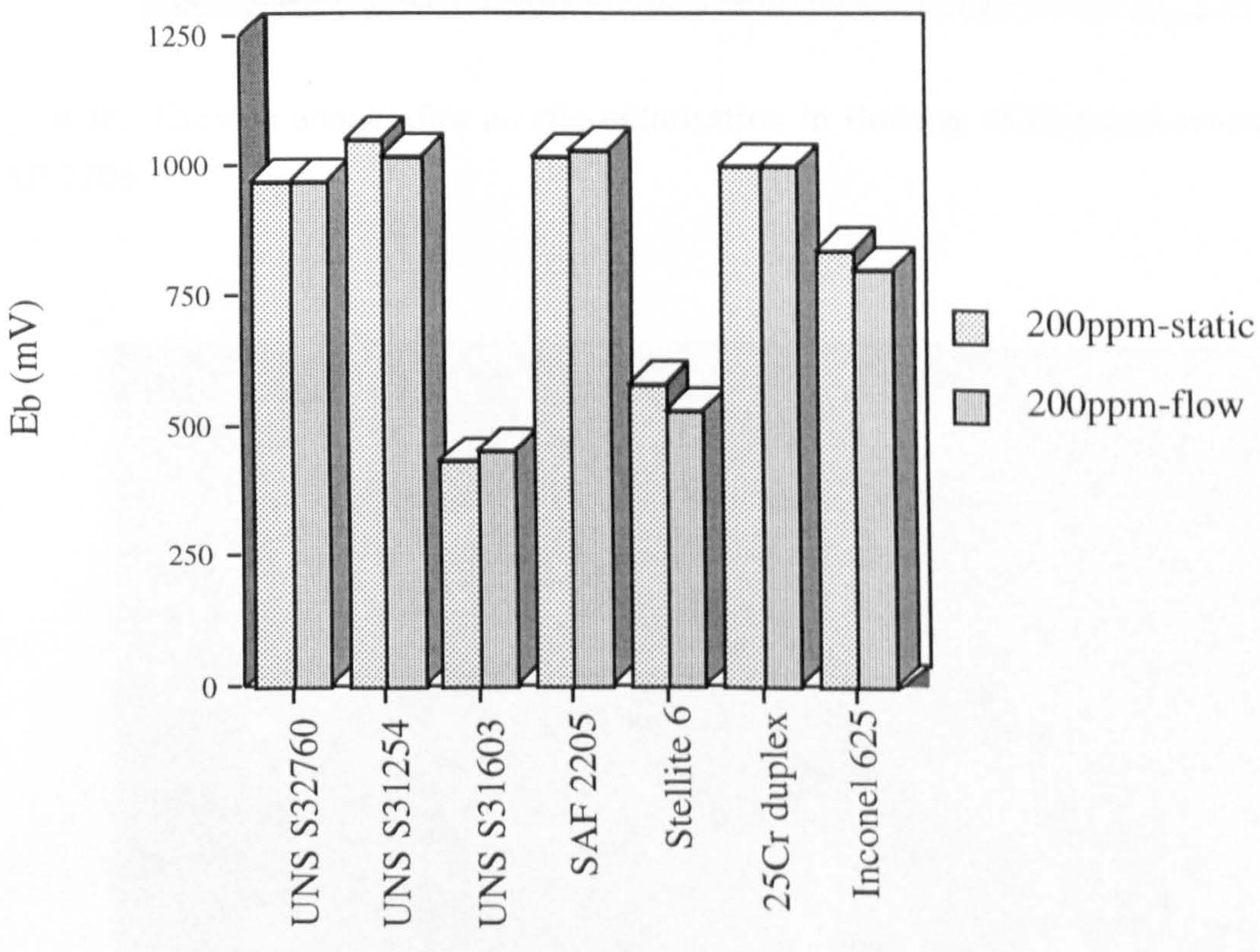

Fig. 9.37. Changes in E_b in flowing chlorinated seawater compared to static chlorinated seawater.

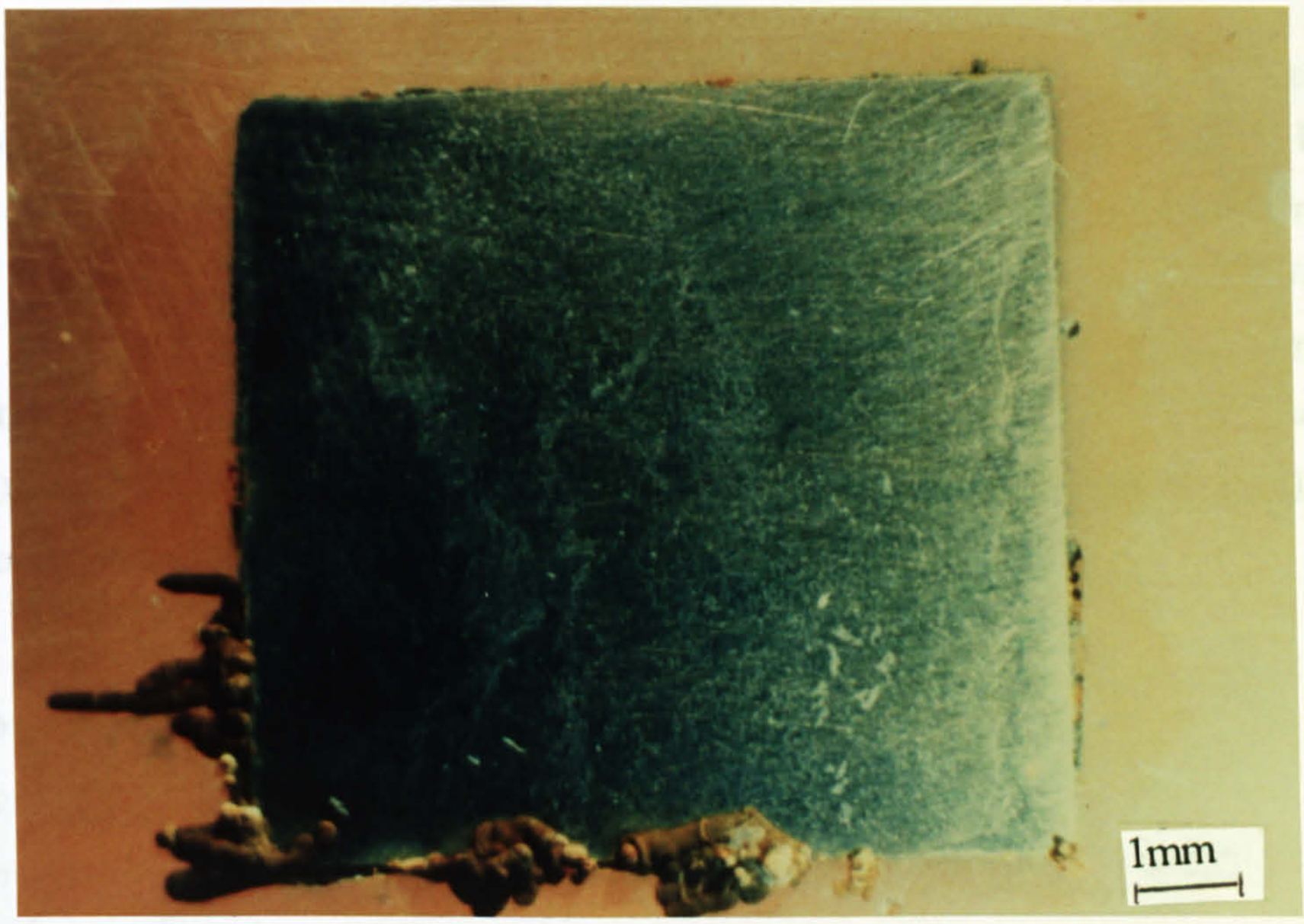

Fig. 9.38. Crevice attack after anodic polarisation in flowing chlorinated seawater on SAF 2205

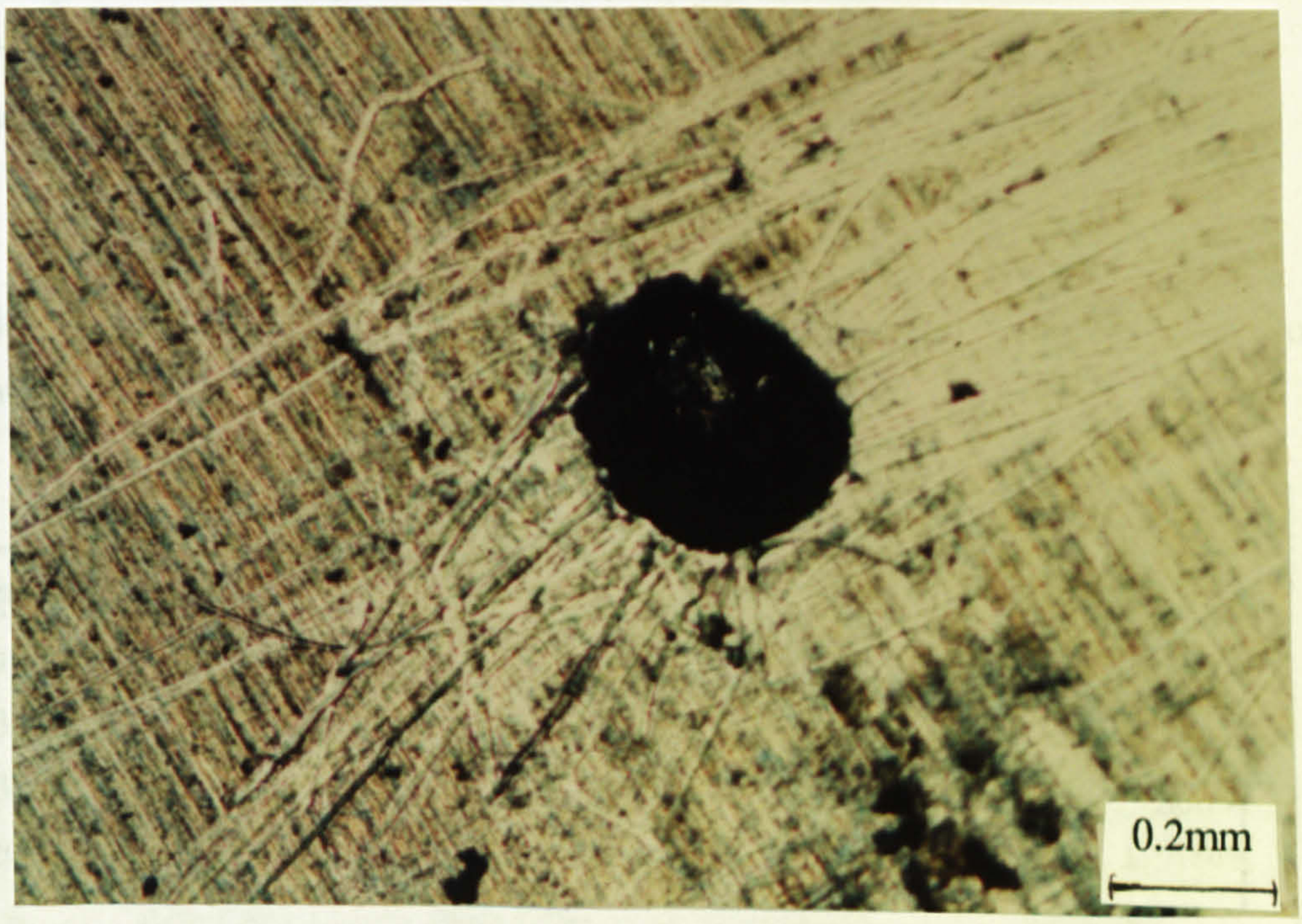

Fig. 9.39. Pitting corrosion after corrosion products are removed from the mouth of the pit on UNS S31603 after anodic polarisation in flowing chlorinated seawater

Cathodic Polarisation

It was not surprising to note that under flowing conditions, the effect on the cathodic reaction on all the stainless steels was to enhance the magnitude of i_L since by the nature of diffusion controlled processes, the effect of flow is to increase the rate of supply of reactants to the surface. The increase was of the order of 20-40μA/cm^2. However, the effect of flow on Stellite 6 was more surprising in that a very prominent concentration polarisation region was present displaying a value of i_L of 100μA/cm^2 (Fig. 9.40). As in static conditions, two Tafel regions were observed in flowing seawater on Inconel 625 and no concentration polarisation.

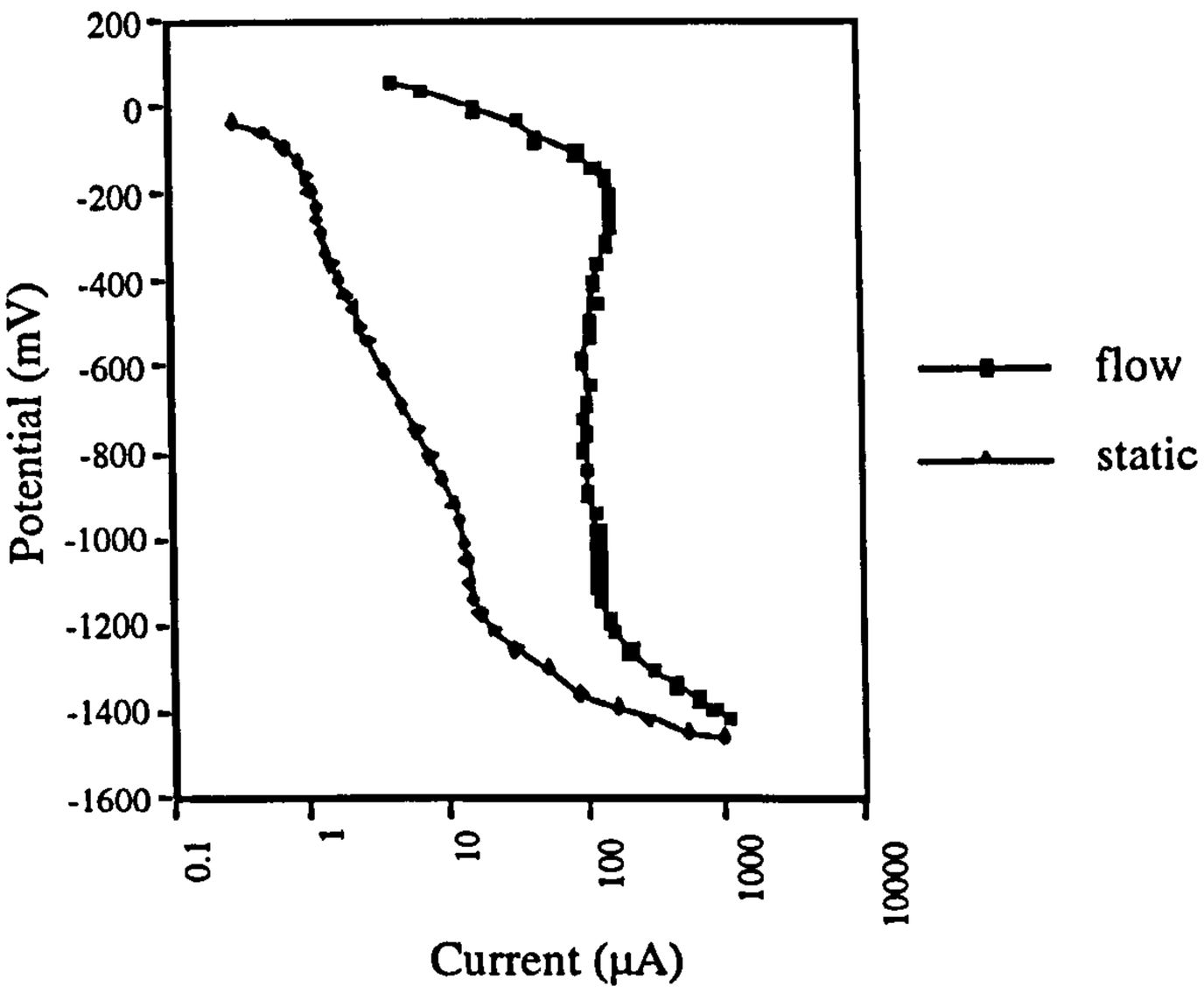

Fig. 9.40. Cathodic polarisation characteristics on Stellite 6 in static and flowing chlorinated seawater.

	200ppm		550-600ppm	
Material	E_{corr} start	Ennoblement	E_{corr} start	Ennoblement
25Cr duplex	-132mV	185mV	-148mV	255mV
UNS S31603	-277mV	195mV	-179mV	228mV
UNS S32760	-162mV	230mV	-213mV	304mV
SAF 2205	-204mV	178mV	-259mV	275mV
Stellite 6	-212mV	480mV	-327mV	620mV
Inconel 625	-211mV	550mV	-321mV	740mV

Table 9.1. Initial value of E_{corr} of the specimens for electrochemical monitoring and the magnitude of the ennoblement at the two different concentrations

	200ppm		550-600ppm	
Material	Depth at crevice assembly	Depth at resin	Depth at crevice assembly	Depth at resin
SAF 2205	30µm	1mm	50µm	1.2mm
UNS S31603	100µm	1.1mm	212µm	1.5mm
UNS S32760	12µm	-	88µm	50µm

Table 9.2. Maximum depth of crevice attack after 35 days immersion in chlorinated seawater

	550-600ppm - no wire
Material	Depth at crevice assembly
SAF 2205	144µm
UNS S31603	6mm
UNS S32760	21µm

Table 9.3. Maximum depth of crevice attack at the crevice assembly after 35 days in chlorinated seawater

Material	E_{corr} (mV)	E_b (mV)	E_r (mV)	I_{max} (µA)	Mechanisms of attack
25Cr duplex	-122	1000	900	500	C+G
UNS S31603	-312	430	-110	4500	G+C+P
UNS S32760	69	970	840	500	C(1-2mm)+G
SAF 2205	128	1020	1000	520	C+G
Stellite 6	179	580	-	900	G+C+P*
Inconel 625	337	837	820	500	G
UNS S31254	30	1050	990	600	P.i.+G

* denotes presence of black corrosion products

Table 9.4. Anodic polarisation characteristics in static chlorinated seawater (200ppm) on initial immersion

Material	Ecorr (mV)	Eb (mV)	Er (mV)	Imax (μA)	Mechanisms of attack
25Cr duplex	-366	980	990	550	C+G+P
UNS S31603	-154	500	-100	3000	C(severe)+G+P
UNS S32760	-123	970	955	500	C+G+P.i
SAF 2205	-407	900	880	500	P(severe)+G+C
Stellite 6	-445	600	-200	550	C+G+P*
Inconel 625	442	590	590	500	C+G
UNS S31254	-371	970	960	500	P.i.+G

* denotes presence of black corrosion products

Table 9.5. Anodic polarisation characteristics in static chlorinated seawater (200ppm) after 35 days immersion

Material	Ecorr (mV)	Eb (mV)	Er (mV)	Imax (μA)	Mechanisms of attack
25Cr duplex	98	800	1090	510	P+C
UNS S31603	-160	540	0	2500	G+C(severe)
UNS S32760	-137	900	900	550	G+P.i
SAF 2205	16	820	1000	510	C+G
Stellite 6	295	560	-	640	C+C+P*
Inconel 625	107	600	900	700	G+P.i
UNS S31254	-39	820	810	500	C+G

* denotes presence of black corrosion products

Table 9.6. Anodic polarisation characteristics in static chlorinated seawater (550-600ppm) on initial immersion

Material	Ecorr (mV)	Eb (mV)	Er (mV)	Imax (μA)	Mechanisms of attack
25Cr duplex	-366	1040	990	540	C+G+P
UNS S31603	-104	600	0	3200	C(severe)+G+P
UNS S32760	-496	920	900	510	C+G+P.i
SAF 2205	-214	1000	900	500	P+G+C(severe)
Stellite 6	-228	580	260	680	C+G+P*
Inconel 625	422	570	860	500	C+G+P.i
UNS S31254	-519	1020	940	620	P.i.+G

Table 9.7. Anodic polarisation characteristics in static chlorinated seawater (550-600ppm) after 35 days immersion

Material	E_{corr} (mV)	1st Tafel slope (mV/decade)	i_L ($\mu A/cm^2$)	E_h (mV)	2nd Tafel slope (mV/decade)
25Cr duplex	136	-190	120-65	-1200	-180
UNS S31603	-143	-180	85-95	-1140	-200
UNS S32760	-161	-190	50	-1160	-190
SAF 2205	-120	-200	130-80	-1180	-170
Stellite 6	-37	-500	-	-1200	-110
Inconel 625	-38	-460	-	-940	-190
UNS S31254	249	-180	120-70	-1150	-180

Table 9.8. Cathodic parameters on immediate immersion in chlorinated seawater at a level of free chlorine of 200ppm

Discussion

Control of micro and macro fouling has, for decades, posed a serious operational problem in seawater systems and, as such, there have been numerous research programmes and initiatives dedicated to the development of novel anti-fouling substances for a range of applications. However, in seawater applications, still one of the principal fouling control practices is biocide dosing using the oxidising biocide sodium hypochlorite.

During the past decade, there have been several studies reporting the effects of low concentrations of residual chlorine (0-2ppm) on the corrosion behaviour of stainless steels and related alloys [10,12,13]. In contrast, this study has approached a different aspect of the biocidal water treatment involving the effect of very high concentrations of residual chlorine, typical of those encountered at the distribution point of oilfield pumping systems. In the following section, comparisons between aspects of the low concentration and high concentrations will be made and the resulting implications for future material selection will be discussed.

The ennoblement of E_{corr} to potentials in excess of those reported in unchlorinated seawater has consistently been reported in numerous studies in low concentrations of chlorine (up to 10ppm). Unlike the situation in biological systems (reported in chapter 8) the mechanisms of E_{corr} ennoblement in chlorinated systems are known to be due to

the different predominant cathodic reactions which have much higher equilibrium potentials than oxygen reduction and can therefore impose a potential rise in E_{corr}. The cathodic reaction progression in chlorinated systems and the importance of the changed cathodic kinetics will be discussed later.

Since the cause of E_{corr} ennoblement is well established, the questions which remain to be answered concern the effect of ennoblement on corrosion initiation. In particular, does the ennoblement of E_{corr} to values often near to the breakdown potential of passive materials induce an enhanced susceptibility to initiation?

In this study, rapid ennoblement of E_{corr} was observed on dosing with hypochlorite, the extent of which was dependent on the material type and on the specimen form (i.e. crevice assembly, electrochemical specimen or pipe). A study by Gartland [7] reported E_{corr} values of +600mV (SCE) on the superaustenitic stainless steel (UNS S31254) at 10ppm chlorine which is more noble than the E_{corr} recorded in our study on this material but is comparable with the E_{corr} on the superduplex pipe.

Although E_{corr} ennobled in all experiments in this study, on only the superduplex pipe were the high values obtained initially maintained for the duration of the 35 day experiment. In contrast, on the MCAs, the electrochemical specimens and on the pipe at higher concentrations, the E_{corr} fluctuated and tended to decrease over the immersion period. This points to a situation where there are conflicting effects determining the trend in free corrosion potential. Crevice corrosion initiation will tend to pull the free corrosion potential in the active direction as reported in other work [10] whereas the presence of the oxidising biocide will tend to ennoble E_{corr}. Indeed on the superduplex pipe, the unstable more negative values recorded at higher concentrations of free chlorine were associated with crevice attack at the metal/flange interface. Recorded E_{corr} values are therefore heavily dependent on two main factors : the chlorine concentration (the high concentration in this work causing the higher ennoblement) and the initiation of crevice corrosion. The rate at which E_{corr} ennobles, whether due to formation of a biofilm or by chlorination has been suggested to determine the probability of the initiation of localised attack [9]. Faster ennoblement of E_{corr} in hypochlorite has been reported to be more severe than the slower ennoblement observed in natural seawater [9] and this is in agreement with present findings.

Ennoblement of E_{corr} is a concern when the breakdown potential is approached and localised corrosion can occur. During anodic polarisation tests, the effect of hypochlorite dosing at 200ppm was not apparent in a significant lowering of the

breakdown potential, although a slight lowering was observed on all materials. Even after 35 days immersion, when the E_{corr} had invariably fallen to active values, the breakdown potential was maintained. Some previously reported work by Gartland [7] demonstrated the beneficial ageing of the material passive film in chlorinated seawater such that longer immersion periods can induce a strengthening of the passive film and reduce susceptibility to breakdown.. From his work, it was suggested that the initial immersion is crucial and that by progressively increasing the hypochlorite level, the material ages and can tolerate higher levels than would be possible if initial immersion was at the higher concentration. Although his work referred to much lower levels of free chlorine (10ppm), there is some evidence to suggest that in higher concentrations, analogous effects exists.

Much higher crevice corrosion rates were measured in chlorinated seawater than have been reported in unchlorinated seawater. Hodgkiess et al. [14] reported crevice corrosion depth of 1.4mm on UNS S31603 after five and a half months whereas after 35 days in 550-600ppm free chlorine, the plate of 6mm thickness had perforated. Since the anodic polarisation data on this alloy implied that the overall passivity is not significantly affected by immersion in chlorinated seawater, the evidence points towards a propagation process controlled by the progression of the cathodic reaction rather than the inability of the passive film to repair once broken down locally which would have been shown during anodic polarisation by a higher I_{max} and a wider hysteresis. No such effects were observed. It has been demonstrated in this study that extensive depolarisation of the cathodic reaction occurs in chlorinated systems with cathodic reactions other than oxygen reduction being favoured.

Since at the neutral pH in this study, the concentration of the chlorine species Cl_2 is very low, the most probable cathodic reaction is the reduction of OCl^- (or equivalent Br species) at E_{corr} and negative to E_{corr} (1st Tafel slope) since the equilibrium electrode potential for this reaction is more noble than for HOCl reduction, although at E_{corr} and potentials more negative both reactions are thermodynamically possible As such the recorded current could be representative of a composite cathodic reaction. The OCl^- and HOCl concentrations in chlorinated seawater are very much higher than the concentration of dissolved oxygen in aerated seawater and the equilibrium potential is much more noble, hence there is scope for extensive depolarisation. The sharp concentration polarisation region may be due to the depletion of one of the species (most probably HOCl since at pH 8.2, it is less abundant than OCl^-) and analogous to oxygen reduction in aerated seawater, the reaction rate changes. In this case, a decrease in the current is often observed.

An important observation was made in that scaling (identified as CaCO3) was present after a cathodic polarisation test taken to a maximum current of 1mA (which in unchlorinated seawater failed to produce a visible deposit). This is indicative of the production of (OH) ions on a larger scale in the initial cathodic OCl reduction reaction which would increase the local surface pH and hence favour deposit formation. This observation has been made by other workers [5] and explained the lower galvanic current measured.

One of the main aims of this study was to assess the suitability of the superduplex alloy UNS S32760 in high hypochlorite concentrations and in particular assess the performance of the girth weld in the pipe. The findings have demonstrated that the limiting factor for the use of the superduplex in these conditions would be it's resistance to crevice corrosion which is in agreement with other work on lower grade duplex alloys [10]. After 35 days at 550-600ppm, severe crevice attack on the pipe was observed. However, the performance of the superduplex was superior in every respect to any of the other alloys in the study and at lower concentrations, it is suggested that there would be no major limitations in it's use. The welded zone resisted attack in all circumstances which is evidence that a properly made weld does not neccessarily provide a site with increased corrosion susceptibility.

From a material selection point of view, the present study has illustrated that the important factor in chlorinated seawater is crevice corrosion resistance which further restricts the use of type UNS S31603 alloys which are prone to crevice corrosion in unchlorinated seawater. This study suggests that even the duplex stainless steels (SAF 2205 and 25Cr duplex) will present problems due to crevice attack at 200ppm free chlorine. Once initiated, crevice corrosion has been shown to propagate rapidly and the superduplex has been shown significantly enhance resistance. In unchlorinated seawater the nickel-base Inconel 625 and the superaustenitic stainless steel UNS S31254 offered excellent resistance to localised attack, even at elevated temperature but in this study both materials have been show to be prone to crevice attack, much less severe than on Stellite 6, 25Cr duplex, UNS 31603 and SAF 2205, but to a greater extent than the UNS S32760.

Conclusions

For the application to which this study was directed, it has been demonstrated that the superduplex alloy has the required resistance to weld attack and performed well with respect to crevice corrosion at the lower concentrations (200 and 400ppm). Only at high concentrations of 550-600ppm free chlorine was severe crevice corrosion

observed. Alternative materials were not identified in this study, the main limitations being the enhanced crevice corrosion of even the Ni-base and the superaustenitic materials.

Mechanistically, it has been demonstrated that the propagation of crevice corrosion is very much enhanced, probably due to the severely depolarised cathodic reaction in chlorinated systems. This finding has implications for applications where cathodic protection is used in conjunction with chlorination.

References

1. G. C. White, *The handbook of chlorination and alternative disinfectants*, 3rd ed., Van Nostrand Reinhold, 1992

2. P. F. Sanders, D. L. Robinson, Corrosion control using continuous residual chlorine in water injection systems, *Proc. 2nd Int. European Federation of Corrosion Workshop on Microbial Corrosion*, 1990

3. P. F. Sanders, Monitoring and control of sessile microbes : cost effective ways to reduce microbial corrosion, *Microbial Corrosion 1*, eds. C. A. C. Sequeira, A. K. Tiller

4. J. W. Oldfield, B. Todd, Corrosion of stainless steels caused by bromine emission from chlorinated seawater, *European Federation Of Corrosion Publications*, No. 10, Marine Corrosion of Stainless Steels : Chlorination and Microbial Effects, 1993

5. B. Wallen, Some factors affecting stainless steel corrosion in seawater, *Avesta Corrosion Management,* No. 4, 1990

6. A. Mollica, E. Traverso, G. Ventura, *Proc. 11th Int. Corrosion Congress*, Vol. 4, Florence, Italy, 1990

7. P. O. Gartland, Aspects of testing stainless steels for seawater applications, *European Federation Of Corrosion Publications*, No. 10, Marine Corrosion of Stainless Steels : *Chlorination and Microbial Effects*, 1993

8. M. B. Ives, Y. C. Lu, J. L. Luo, Cathodic reactions involved in metallic corrosion in chlorinated saline environments, *Corros. Sci.*, Vol. 32, No. 1., pp 91-102, 1991

9. E. Bardal, J. M. Drugli, P. O. Gartland, The behaviour of corrosion resistant steels in seawater, A review., *Corros. Sci.*, Vol. 35, Nos. 1-4, p675-682, 1993

10. B. Wallen, S. Henrikson, Effect of chlorination on stainless steels in seawater, *Werkstoffe und Korrosion*, Vol. 40, pp 602-615, 1989

11. R. Francis, The effects of chlorine on the properties of films on copper alloys in seawater, *Corros. Sci.*, Vol. 26, No. 3, 1986, p205-212

12. P. Gallagher, A. Nieuwhof, R. M. J. Tausk, Experiences with seawater chlorination on copper alloys and stainless steels, *European Federation Of Corrosion Publications*, No. 10, Marine Corrosion of Stainless Steels : Chlorination and Microbial Effects, 1993

13. G. Ventura, E. Traverso, A. Mollica, Effect of NaClO biocide additions in natural seawater on stainless steel corrosion resistance, *Corrosion*, Vol. 45, No. 4, 1989

14. T. Hodgkiess, A. Asimakopoulos, Studies of the localised corrosion behaviour of some stainless steels, Incoloy 825 and titanium in seawater, *Desalination*, 38,(1981), p247-256

Chapter 10

Concluding Remarks and Recommendations for Future Work

This final chapter, because of the diversity of the study, is intended to summarise the important findings in each section and identify areas to which further research should be directed. Where relevant, conclusions will be drawn with regard to findings from more than one chapter.

Material selection for marine applications where seawater at elevated temperature is handled has been shown to be significantly more complex than at low temperature where much data exists to accurately define the alloy behaviour and limitations. Increase in temperature in static seawater, as expected, increased the susceptibility of all the materials in the study to localised corrosion initiation and propagation. However, of primary importance is the finding that the extent to which the temperature affects the electrochemical behaviour and the attack mechanisms is different for each material. The result of this is that there is a significant effect on the relative performance of materials and the material choice must account for this.

This study has shown that in static conditions, the superaustenitic alloy resisted severe localised attack in the complete temperature range, as did the Nickel-base Inconel 625. Although, in agreement with several studies, the superduplex alloy was demonstrated to have superior corrosion resistance at ambient temperature (18°C), limitations in it's performance with regard to crevice corrosion have been elucidated, such that at temperatures in excess of 40°C the susceptibility to attack is significantly increased. Although at ambient temperature, the duplex stainless steels (SAF 2205 and 25Cr duplex) exhibit significantly better corrosion resistance than the austenitic stainless steel UNS S31603, as predicted by PRE formulae, temperature increase in the range up to 60°C has demonstrated that this superiority no longer exists. The 25Cr duplex still exhibits marginally better performance than UNS S31603 but both electrochemical considerations and visual examination have shown the SAF 2205 to be more susceptible to attack than UNS S31603. Thus the benefits of increased Cr and Mo concentrations, apparent at lower temperature are not maintained as the temperature is increased.

In conjunction with increased temperature an increase in seawater concentration to a solution of almost four times normal seawater concentration was found to have no additive effect on the material performance.

The kinetics of the cathodic oxygen-reduction reaction have been shown to be dependent on material and in particular differences in the cathodic characteristics of the Co-base and Ni-base alloys have been identified. No concentration polarisation regions were identified on these alloys in static seawater at ambient temperature. However, compared to the other alloys the reaction was not depolarised in the potential region from E_{corr} to the start of hydrogen evolution. On the stainless steels, there were two concentration polarisation regions identified suggesting a two step oxygen reduction cathodic reaction which has been postulated by several previous authors. Since it would be expected that the kinetics of oxygen diffusion would be independent of electrode surface, it is postulated in this work that the initial region of low current at potentials near to E_{corr} comes about due to the presence of an oxide film and, as such, there is a barrier to charge transfer at the surface.

An impinging seawater jet, free of solids, was found to impart only minor changes in the electrochemical behaviour of the high-grade alloys at ambient temperature and no mechanical effects could be seen on the surface after up to 8 days impingement. On the lower grade austenitic stainless steel, there was a slight lowering of the breakdown potential. However increasing the temperature the susceptibility of all the stainless steels increased and an interesting feature of a rise in anodic current at a potential significantly reduced potential from E_b was observed which was found to be associated with pit initiation and the formation of a coloured film. Although the effect of increased temperature on Inconel 625 and Ultimet was to decrease the parameter E_b, it was apparent that the effect was much less than on the stainless steels thus they seemed to have he ability to maintain the corrosion resistance under the impinging jet. Indeed the resistance of these two materials was shown to increase under the impinging jet. Most adversely affected was the Co-base Stellite 6 alloy which under liquid erosion at increased temperature (50°C) actually exhibited active corrosion behaviour and high dissolution rates were recorded.

As expected the increased fluid turbulence at the electrode surface under the impinging jet had the effect of eliminating concentration polarisation effects of the oxygen reduction cathodic reaction. Instead the reaction was heavily depolarised, and oxygen reduction, proceed following Tafel kinetics. The initial region where lower currents were observed in static conditions was not apparent but instead the reaction proceeded quickly from E_{corr}. However, the reaction rate changed at a lower potential, again suggesting a two step reaction. Whether the initial currents (higher than in static conditions) could be due to the reduction of a thicker oxide in impinging conditions is not clear. Indeed the precise mechanisms of oxygen reduction on an oxide covered surface needs further attention.

A transition from passive corrosion behaviour to active corrosion behaviour was evident on the stainless steels, Co-base Ultimet and Ni-base Inconel 625 on subjecting them to an impinging two phase, liquid-solid, flow. Even at the much reduced free stream velocity of 25m/s compared to 100m/s in the liquid erosion tests, the impacting particles had sufficient kinetic energy to transfer the passive materials into an active corrosion regime. The consequences of the interaction between mechanical effects and electrochemical corrosion effects were manifested in high rates of metal loss being measured, even on the hard (Stellite 6, Ultimet and Inconel 625) alloys. The work under these conditions therefore considers the performance of the alloys while in the active corrosion domain and this concept was shown to introduce some interesting effects. It has identified that in these conditions, galvanic effects between materials which would normally not pose a serious problem could be significant.

A significant proportion of the total material loss was identified as being due to the direct and indirect effect of corrosion and this led to the definition of a synergistic factor which has been similarly defined in other work. There is often confusion as to what this factor physically represents but in this work the definition has been given as the effect of *corrosion* on the *erosion* process. Thus it represents the addition of weight loss when corrosion effects are present.

The overwhelming component of weight loss was found to be that due to pure mechanical erosion which accounted for between 70 and 80% of the total weight loss on the 'passive' materials. Although the pure corrosion component of weight loss as calculated from electrochemical tests was calculated to be less than 5%, the synergistic component ensured that the indirect effects meant that corrosion could actually contribute to approximately 20% of the material loss. The Co-base alloys and the Ni-base alloys displayed the lowest total material loss but in general, the proportion of weight loss due to corrosion was higher than the stainless steels. It was found that although the rate of deterioration of the duplex stainless steels was less than UNS S31603, the corrosion component was less on UNS S31603.

Tests on cast iron and C-Mn steel which exhibit poor corrosion resistance in static conditions as expected resulted in the highest dissolution rates. Interesting effects of removal of material due to corrosion attack at the graphite flake/matrix interface and subsequent mechanical removal on cast iron were identified which illustrated the interactive effects between the two processes. Although corrosion was found to have a significantly increased effect on the determination of the rate of metal deterioration on the C-Mn steel and cast iron, it was still evident that the process was still governed by

the erosion rate, constituting more than 50% of the weight loss. However, it was important to note that under liquid erosion, the process turned to one dominated by corrosion in that the synergy became the dominant factor. Hence in the absence of corrosion, the mechanical erosion rate by the liquid jet was very much reduced.

Damage of the materials showed effects due to angle of impact which suggest that in any one system, there is a complete range of impinging angle. Studies of impingement angle should therefore not be confined to altering the nominal jet angle since by consideration of the flow pattern and diversion as it approaches the surface and after initial impact with the surface can yield information on the types of damage associated with high and low angle impingement.

From a practical viewpoint as well as identifying for the range of materials the relative resistance to materials loss, this study has also shown that the benefits of applying cathodic protection in an erosion-corrosion environment can be significant, especially on materials such as cast iron and C-Mn steel. This could perhaps signal application of CP to reduce not only corrosion but erosion when the two factors are interacting. The logistics and practicalities of this will need significant further research.

The effect of the marine organism settlement and on the biocides used to deter settlement is a major issue in marine systems from the point of view of environmental factors and economic considerations regarding material replacement due to irreversible fouling. Ennoblement of Ecorr is consistently shown to occur and has been attributed to the effect of marine settlement of pioneering bacteria on the electrochemical processes at the electrode surface. This study has importantly shown that in the absence of a significant biofilm, ennoblement has still been shown to occur. The mechanisms have not fully been elucidated but via a combination of results from anodic polarisation tests which show an increase in the resistance to passivity breakdown with time in natural seawater and no observed depolarisation of the cathodic reaction, current opinion is that the process is controlled by the passive film and it's ability to polarise the anodic reaction and reduce passive currents near to E_{corr}. The nature of the passive film and it's evolution with time is a topic which requires significant further attention.

The effect of the sulphate-reducing bacteria on corrosion of steel has, for decades, been the focus of research and in recent years the effect on stainless steels has been targeted. In this work, their effect has been studied from two different aspects : in completely anaearobic conditions, set up within a laboratory and in natural seawater conditions which occur under a thick macro fouled layer. In the laboratory experiment, it has been

shown that the effect of an active culture of SRB is to promote material dissolution at anodic potentials moderately shifted from E_{corr}. The presence of an anodic current rise at relatively low potentials, has been shown by potentiostatic and potentiodynamic tests to be associated with real corrosion attack and the implications from this with respect to the probability of initiation is obvious. What the evidence points to is that significant attack can occur on even the most resistant stainless steels in a completely anaerobic system. The efficient oxygen cathode, often referred to as a requirement for SRB corrosion, is not always necessary.

In the natural seawater conditions, after long term immersion, it has been shown that by performing anodic polarisation, the presence of SRB under macrofouling can be identified. The appearance of black corrosion products at the rim of barnacles and at the edge of barnacle scars has inferred the activity of SRB. The process by which this occurs is not fully understood but it is thought that the anodic polarisation simply produces the metal ions which can readily form metal sulphides and are traced by their characteristic black colour (i.e. iron sulphide). This finding alone substantiates the often implied existence and activity of SRB in conditions of low oxygen under barnacles. However, of greater importance is the finding of SRB activity and associated high levels of sulphur under the minute attachment points of mussel byssus threads at the metal surface and this has not previously been reported.

Biocide addition and the consequent effect on corrosion was the focus of this investigation. In contrast to much previous work, this study investigated concentrations two orders of magnitude greater than is normal for fouling control. studies of such high levels have not previously been reported. It was found that although welded zones on duplex stainless steels are thought to represent susceptible areas for corrosion attack in high levels of hypochlorite, a properly made weld on the superduplex stainless steel UNS S32760 can withstand concentrations of up to 600ppm free chlorine. The limitation on the performance is not dictated from the weld but is due to crevice corrosion resistance and at concentrations of free chlorine in excess of 400ppm, there is evidence to suggest that the resistance of this material severely affected. On the anodic polarisation characteristics and visual examination, it was found that there was a slight effect of ageing observed in that the resistance to passive film breakdown seemed to increase after longer immersion.

In conclusion, this work represents a broad study of several related and unrelated aspects of corrosion in marine environments. From a material selection point of view it has emphasised the point that in any marine system, there are several factors which can dictate a material's performance and the interactions between such factors are often

significant. Through experimental studies of the type reported here and actual field test, these factors can be elucidated and efficient materials selection and future material development can be achieved.